

AD _____

Award Number: W81XWH-05-1-0330

TITLE: A Biophysico-Computational Perspective of Breast Cancer Pathogenesis and Treatment Response

PRINCIPAL INVESTIGATOR: Valerie Weaver

CONTRACTING ORGANIZATION: University of California, San Francisco
San Francisco, CA 94103 -4249

REPORT DATE: March 2011

TYPE OF REPORT: Annual

PREPARED FOR: U.S. Army Medical Research and Materiel Command
Fort Detrick, Maryland 21702-5012

DISTRIBUTION STATEMENT: Approved for public release; distribution unlimited

The views, opinions and/or findings contained in this report are those of the author(s) and should not be construed as an official Department of the Army position, policy or decision unless so designated by other documentation.

REPORT DOCUMENTATION PAGE

Form Approved
OMB No. 0704-0188

Public reporting burden for this collection of information is estimated to average 1 hour per response, including the time for reviewing instructions, searching existing data sources, gathering and maintaining the data needed, and completing and reviewing this collection of information. Send comments regarding this burden estimate or any other aspect of this collection of information, including suggestions for reducing this burden to Department of Defense, Washington Headquarters Services, Directorate for Information Operations and Reports (0704-0188), 1215 Jefferson Davis Highway, Suite 1204, Arlington, VA 22202-4302. Respondents should be aware that notwithstanding any other provision of law, no person shall be subject to any penalty for failing to comply with a collection of information if it does not display a currently valid OMB control number. **PLEASE DO NOT RETURN YOUR FORM TO THE ABOVE ADDRESS.**

1. REPORT DATE (DD-MM-YYYY) 01-03-2011		2. REPORT TYPE Annual		3. DATES COVERED (From - To) 1 Mar 2010 - 28 Feb 2011	
4. TITLE AND SUBTITLE A Biophysico-Computational Perspective of Breast Cancer Pathogenesis and Treatment Response				5a. CONTRACT NUMBER	
				5b. GRANT NUMBER W81XWH-05-1-0330	
				5c. PROGRAM ELEMENT NUMBER	
6. AUTHOR(S) Valerie Weaver E-Mail: weaverv@surgery.ucsf.edu				5d. PROJECT NUMBER	
				5e. TASK NUMBER	
				5f. WORK UNIT NUMBER	
7. PERFORMING ORGANIZATION NAME(S) AND ADDRESS(ES) University of California, San Francisco San Francisco, CA 94103 -4249				8. PERFORMING ORGANIZATION REPORT NUMBER	
9. SPONSORING / MONITORING AGENCY NAME(S) AND ADDRESS(ES) U.S. Army Medical Research and Materiel Command Fort Detrick, Maryland 21702-5012				10. SPONSOR/MONITOR'S ACRONYM(S)	
				11. SPONSOR/MONITOR'S REPORT NUMBER(S)	
12. DISTRIBUTION / AVAILABILITY STATEMENT Approved for Public Release; Distribution Unlimited					
13. SUPPLEMENTARY NOTES					
14. ABSTRACT The extracellular matrix (ECM) regulates breast homeostasis and is corrupted in breast cancers. We showed that the breast ECM progressively reorganizes into large bundles and stiffens due to high activity of ECM remodeling and cross-linking enzymes such as lysyl oxidase (LOX). The functional relevance of this was revealed through in vitro and in vivo work which revealed that ECM stiffness enhances breast cell growth, survival, migration and regulates treatment responsiveness by promoting integrin adhesions and signaling to enhance tumorigenesis and metastasis and compromise treatment efficacy. More recently, we also found that ECM stiffness induces inflammation and angiogenesis and we are exploring how this effect may regulate metastasis and treatment response by determining if this is mediated through direct effects on vascular endothelial cells and immune cells or indirectly by modulating growth factor and chemokine levels. To clarify how ECM remodeling modulates breast cell survival we identified a novel mechanism elicited through ECM dimensionality and that promotes Arf6-dependent breast cell survival. We are now exploring the clinical relevance of these findings through a comprehensive molecular and biophysical characterization of freshly excised human breast tissues.					
15. SUBJECT TERMS Extracellular matrix, stiffness, mechanical, force, apoptosis, resistance, Bioengineering, invasion, computational, tumor progression					
16. SECURITY CLASSIFICATION OF:			17. LIMITATION OF ABSTRACT	18. NUMBER OF PAGES	19a. NAME OF RESPONSIBLE PERSON
a. REPORT	b. ABSTRACT	c. THIS PAGE			19b. TELEPHONE NUMBER (include area code)
U	U	U	UU	263	

Table of Contents

Introduction.....	4
Body.....	5-53
Key Research Accomplishments.....	6-7, 15-16, 19- 20, 23, 45-47, 49-53
Reportable Outcomes.....	53-57
Conclusions.....	57-58
References.....	59-63
Appendices 1-11.....	64-onwards

INTRODUCTION:

Apoptosis resistance regulates the pathogenesis, and treatment response of breast tumors. Despite concerted effort towards understanding the molecular basis for apoptosis resistance in breast tumors, progress in this area has been frustratingly slow. Lack of advancement may be attributed in part to the current cell autonomous view of breast cancer etiology and treatment responsiveness. What we now know is that the organ microenvironment can and does regulate the therapeutic responsiveness of metastatic tumors^{1,2}, and that stromal-epithelial interactions influence mammary gland development, tissue homeostasis and breast tumor progression³. Alterations in the mammary gland ECM correlate with changes in mammary differentiation, involution (apoptosis) and tumor progression, and culture experiments clearly show that the stromal ECM can modulate mammary epithelial cell (MEC) growth, differentiation and survival and alter apoptotic responsiveness^{2,4,5}. **How the stroma promotes apoptosis-resistant breast tumors remains unclear.**

We have been studying the role of integrin ECM receptors as key regulators of mammary tissue behavior as well as malignant transformation and metastasis. We have been exploring the molecular mechanisms whereby the ECM can regulate mammary tissue homeostasis, invasion and apoptosis responsiveness. We found that integrin expression, organization and activity are consistently altered in breast tumors and that perturbing integrin expression and activity can drive malignant behavior of non-malignant and pre-malignant MECs, and that normalizing integrin activity represses expression of the malignant breast phenotype in culture and in vivo^{3,6}. We also determined that integrins regulate cell survival and modulate the apoptotic responsiveness of mammary tissues to a diverse array of exogenous stimuli including various chemotherapies and immune receptor activators^{2,7}. We found that integrin-dependent apoptosis resistance and survival are intimately linked to many of the biochemical pathways and mechanisms that regulate tissue organization and specifically tissue polarity. For example, we found that $\alpha6\beta4$ integrin directs mammary epithelial cells to assemble polarized mammary tissue structures that display apoptosis resistance to a wide spectrum of apoptotic insults. We are now exploring the underlying mechanisms whereby integrin expression and/or function becomes altered in breast tumors, how integrin modulate the survival of nonmalignant and transformed mammary epithelial cells, what the molecular link could be between integrin-dependent survival and tissue polarity and the clinical relevance of these findings.

We found that prior to malignant transformation the mammary gland exhibits a 'desmoplastic' response that is associated with an incremental and significant increase in global elastic modulus (stiffness) of the gland and elevated/altered expression of integrins and integrin adhesions⁸⁻¹⁰ (unpublished data). Consistent with results from other laboratories we determined that externally-applied mechanical force regulates the behavior and phenotype of multiple cell types including endothelial, fibroblasts, neurons, and MECs¹¹⁻¹³. Although the mammary gland is not traditionally viewed as a mechanically-regulated tissue, MECs within the ductal tree and alveolus experience passive (isometric) and active mechanical force throughout the lifetime of the mammary gland most notably during development, lactation and involution^{9,14}. Similar to other solid tumors, the mammary gland also becomes appreciably stiffer in association with its malignant transformation and mammary epithelial cells within the tumorigenic mammary gland experience an array of additional compression and stress and interstitial associated forces^{15,16}. During the process of metastasis and once at the metastatic site breast tumor cells also encounter an array of external mechanical forces that could conceivably influence their behavior and alter their response to treatment. For example, many of the common metastatic sites for breast cancer differ appreciably with respect to their stiffness and biochemical compositions than a normal mammary gland such as bone (very stiff, high vitronectin), in the vasculature (high pulsatile pressures, high fibronectin and fibrin), pleural cavity (very compliant with high fibrin composition but also adjacent fibrotic lung could be quite stiff with a high amount of elastin).

Because physical forces so profoundly influence cell proliferation, survival and differentiation of multiple cell types, we maintain that it is critical to understand how mechanical cues could influence mammary tissue behavior and apoptosis responsiveness.

Accordingly, we predict that the physical organization of the ECM (which contributes to its mechanical properties) constitutes an independent regulator of mammary epithelial behavior and apoptosis resistance. Delineating the molecular basis for this phenotype will likely have important consequences for tumor therapy. To rigorously test this idea we are in the process of achieving the following specific aims:

Specific Aim 1. Engineer tractable 3D organo-typic model systems that recapitulate the biophysical properties of primary and metastatic breast tumor tissues, and then use these models to dissect candidate molecular stress-response mechanisms whereby ECM stiffness could regulate apoptosis resistance in culture and in vivo.

Specific Aim 2. Develop xenograft and transgenic mouse models to test whether ECM stiffness regulates apoptotic responsiveness of mammary epithelia in vivo.

Specific Aim 3. Build a computational model that can predict how changes in ECM compliance could influence integrin-dependent apoptosis responsiveness of mammary epithelia and query this model with clinical data.

Specific Aim 4. Develop non-invasive imaging tools that could be used to monitor changes in ECM stiffness or stiffness-induced changes in mammary tissue phenotype.

Summary of Achievements - Proposal Body:

We are now conducting studies in this grant proposal on a "no cost" extension basis. The no cost extension occurred for the following reasons:

1. We encountered several months delay (4 months duration approximately) in processing and acquiring the original funds from the DOD when the award was first initiated at the University of Pennsylvania. The consequence of this delay was an unexpended carry over from the first year of funding that was approximately 25-35% -equal to an amount reflecting the delayed start date.

2. Secondly, in the midst of the second year of funding my group relocated to the University of California, San Francisco. Despite initiating appropriate grant transfer procedure through DOD and University of Pennsylvania - the funds transfer was delayed significantly - primarily due to difficulty with the University of Pennsylvania administration. Consequently we could not use the DOD grant at UCSF for almost one full year. Thus, expenditures on the grant were frozen for approximately 10 months. Rather than lay off individuals supported by the Scholar grant I instead chose to use my allocation of UCSF "start up" funding (i.e. funds provided to me by UCSF Department of Surgery to support my laboratory relocation. It was however not possible to use funds to hire new personnel required to carry out many of the animal study and human tissues directed goals/tasks outlined in the proposal. Only once funding and spending had been approved was I then permitted to proceed with recruitment and hiring. This further delayed work on the project because there is a 3-6 month delay between advertising for personnel, interviewing and hiring. Therefore, progress and spending on the project were further delayed. The total delay here amounted to close to 1.5 years. However, once the

new personnel were hired and trained progress on the project accelerated greatly. Thus, my group has been able to make excellent progress on many other facets of the project as indicated by publications, achieved goals and tasks completed in annual progress reports.

3. Due to the relocation to UCSF and the delay in the hiring of new personnel there was a significant delay in initiating and executing the animal experiments and the human tissue analysis due to need to submit and obtain approval for animal work and human studies. Thus, there was a delay in the preparation, submission and procurement of the IRB application generation and human tissue project initiation. In addition, IACUC paperwork and approval and animal procurement, breeding and transgenic generation were substantially delayed.

All of these setbacks have now been addressed and work is proceeding well and goals are being achieved. Thus, despite all of these setbacks as soon as funding became available and my group was again re established at UCSF and new personnel were hired we began work on project goals in earnest. IRBs and IACUCs were procured for the project and transgenic animals bred, experiments conducted and transgenics generated and consequently progress on animal studies has been proceeding at an excellent pace these past few years. Nevertheless, due to these unexpected delays we are behind our stated schedule and have been carrying forward unexpended funds.

Thus, last year we asked for and were awarded a two year no cost carry over during which time our objective has been to continue to generate new transgenic animals for pre clinical trials, to complete many of the animal studies initiated at the University of Pennsylvania and to move forward on our human tissue studies to address translational relevance of our findings. Our goal has also been to translate our findings into published articles and obtain extramural funding to continue with our project(s). We have been making excellent progress towards all of these stated goals such that we have also initiated a few exploratory projects that expand the scope of the original work and assist with our objective of eventually translating our findings to the clinic.

Task 1: Engineer tractable 3D organo-typic models that recapitulate the biophysical properties of primary and metastatic breast tumor tissues, and use these models to dissect candidate molecular mechanisms whereby ECM stiffness could regulate breast tumor behaviors including treatment responsiveness in culture and in vivo.

PART A Development of natural 3D ECM models that recapitulate the biophysical properties of primary normal and malignant and metastatic breast tissues.

Achievements as listed per Revised Statement of Work

In this first year of our no cost extension we have continued to develop and elaborate 3D organotypic models.

a. Complete studies to measure mechanical properties of natural biomaterials as well as mouse tissues using newly developed micro indenter device¹⁷ as well as nano AFM indentation with CFP-tagged mouse models as well as fluorescence tagged DEXTRAN to mark the vasculature. If/when possible we will also attempt to orient stiffness measurements in the context of infiltrating immune cells. Objectives will include normal and various stages of malignant progression of breast cancer in mouse models including but not restricted to PyMT mouse model, Her2/neu model and p53 +/- mice. We will also examine physical changes/properties of liver, brain, bone and lungs to determine whether cellular metastasis is also mediated in part by compatibility changes in tissue biophysical

properties. This analysis will include a comprehensive biochemical analysis of the state of collagen processing and cross-linking in these tissues. (Months 0-24) **Partially completed.**

Towards this work goal we have successfully used a micro indenter device¹⁷ to measure the materials properties of mammary gland tumors that developed in PyMT mice with and without inhibition of the lysyl oxidase cross-linking enzyme. We could show that mammary glands stiffen as they progress towards malignancy so that invasive breast tumors are significantly stiffer than normal glands. We could also demonstrate that inhibiting collagen cross-linking using the pharmacological inhibitor of LOX (BAPN) reduces stiffness towards that of a premalignant breast. This work was reported in last year's progress report and therefore we have not included those data again here. Rather what became evident to us through those studies, was that those mechanical measurement approaches do not have the resolution needed to distinguish whether altered stiffness of the tissue relates to changes in epithelial behavior, ECM remodeling or an altered vasculature. Accordingly, in the past few years we have been working to develop a novel cryo preservation technique. In the past year this technique has now been perfected and a summary of our results are now included in this report for review. This new technique permits us to conduct high resolution Atomic Force Microscopy (AFM) force indentation on mouse and human breast tissue. Our work shows that using freshly excised tissue we are able to measure regions in the tissue using AFM and demonstrate that tumors are stiffer than normal tissue (Lopez et al., J Integ Biol; Attachment 1; figure 1). However, using this approach it became rapidly evident that it is not clear what precisely we are probing when we poke fresh tissue. Therefore we obtained transgenic mice in which the epithelium is genetically marked with CFP so that we could be sure that AFM indentation of green cells in fact was probing the mechanical characteristics of the mammary epithelium. Moreover, to determine the mechanical integrity of the tissue associated with the vasculature we injected the animals with Rhodamine lectin just prior to sacrificing them. This strategy marks the vasculature. Using this technique we could show that the vasculature associated with breast tumors also progressively stiffens and moreover that not all vessels exhibit similar stiffness characteristics. Thus, vessels within the core of the tumor are significantly stiffer than those at the invasive front suggesting that the nature of the vessels might be different in these different regions (Lopez et al., J Integ Biol Attachment 1; figure 2). To address the issue of ECM stiffness contribution to tumor stiffness we developed a novel cryopreservation approach (Lopez et al., J Integ Biol, Attachment 1; figure 3). Using this approach we could show that the ECM progressively stiffens as breast tissue advances from normal through pre malignant to invasive lesions (Lopez et al., J Integ Biol Attachment 1; figure 4). In fact, our conclusion is that the epithelium, the blood vessels and the ECM simultaneously stiffen as a function of tumor evolution but that the ECM appears to show the most profound increase in rigidity. Together all of these components therefore account for the altered mechanical behavior of breast tumors.

In our last report we discussed our studies using the Her2/neu model and our peer reviewed article published in Cell Journal in late 2009;¹⁸. That article was discussed in our last progress report and therefore will not be discussed here in this new report. Instead, we report here on current studies aimed at exploring the interplay between ECM tension and breast tumor metastasis. Thus, we have used carry over funding to complete two additional mouse studies with the PyMT mouse model. As shown in figures 1-6 included in the body of this document, these studies illustrate that analogous to the Her2/neu mouse model of breast cancer the PyMT mice show increased integrin adhesion activity during the early stages of breast tumor progression i.e. commencing at week 8 when pre malignant MIN lesions have developed in virtually all mammary glands of these mice. Thus, distinct from the Her2/Neu mouse model of breast cancer the PyMT mice develop multi focal lesions very very quickly in ALL mammary glands and these lesions progress quickly to invasive lesions by 11-12 weeks and then metastasize by 14 weeks in 100% of the mice (Figure 1A). Associated with this increase in integrin adhesion activity there is a progressive elevation in the levels of expression of LOX which becomes evident and significant by 8 weeks of age (Figure 1B). Importantly, inhibition of LOX activity using the pharmacological inhibitor

BAPN delayed the formation of tumors in these mice by as much as 2-3 weeks as illustrated in Figure 1C. Yet, eventually all mice eventually developed palpable lesions and their histophenotype did not appear to be markedly different as shown in the images below Figure 1C. Yet, significantly, we noted that while the majority (greater than 60%) of the animals treated with the LOX inhibitor did not develop lung tumors (Figure 1D and 1E) untreated animals all uniformly developed lung metastasis by 14 weeks of age and the metastatic lesions that did form in the BAPN treated mice were markedly smaller than those formed in the control untreated animals.

We were naturally curious to understand how LOX inhibition could be regulating breast tumor metastasis. Therefore, we looked carefully at their histophenotype and also measured their stiffness using the micro indenter. Although we did not note any obvious differences in the histophenotype of the 14 week old mammary glands treated with LOX inhibitor (Figure 2A) we did measure a significant reduction in the stiffness of the tissue both at 8 and 14 weeks of age (Figure 2B) suggesting that LOX inhibition did in fact reduce collagen cross-linking and prevent tissue stiffening. We are now interested in understand whether the altered tissue stiffness could account for the reduced tumor metastasis and how. Moreover, in the next year of support from this no cost extension we will be conducting AFM indentation studies to assess specifically the physical properties of the ECM associated with the lesions +/- BAPN treatment. We will also be conducting carefully cross-linking analysis studies.

Thus far to explore potential molecular mechanisms we have been exploring potential effects on tissue inflammation and changes in immune function. We did not observe any obvious difference in CD45 positive cells (which mark immune infiltrate) between BAPN treated and nontreated PyMT mice. However, we did note that there was a marked increase in infiltrating CD45+ immune cells in 14 week old BAPN treated PyMT mice (Figure 3A). Upon further analysis we noted that there was an increase in B220+CD3-: B cells, CD3+CD8+: cytotoxic T cells, and CD3+CD4+: helper T cells and lower CD11b+F4/80+: Macrophages in the BAPN treated PyMT tumors at 14 weeks. Although quite preliminary these data do suggest that perhaps there is less inflammation and a more productive T cell response which could explain the reduced tumor metastasis we have been consistently observing (Figure 3B). To address this possibility we profiled the chemokine/cytokine profile of PyMT tumors from mice +/- BAPN treatment. We were encouraged to note that at 8 weeks of age BAPN treated mice had reduced levels of these chemokines/cytokines - (Figure 4 bottom bar graphs) yet by 14 weeks of age the levels were now higher than quantified in the 8 week old animals suggesting the animals had in fact caught up and compensated with elevated levels of all of the soluble factors we tested including TNF alpha and TGF beta etc, at least at the RNA level. Whether the RNA in fact truly reflects the activity levels of these factors is not clear and is something we are now exploring (Figure 4 top bar graphs).

Tumor metastasis is also very tightly regulated by the state of tissue hypoxia. Therefore, we examined the status of vascular integrity and infiltration of blood into the BAPN treated and non-treated tumors. We found that the BAPN treated animals appeared to have greater vascular density and also that upon perfusion there was a higher diffusion noted in the mice suggesting there should be reduced hypoxia (Figure 5). These results actually make a lot of sense considering the fact that we noted that the BAPN treated tumors were less stiff and that the tumors appears morphologically more integrated with ECM stroma. This phenotype is consistent with the idea that BAPN treatment reduces ECM cross-linking and potentially reduces interstitial pressure permitting efficient vascularization and perfusion of the tissue. This in turn would reduce hypoxia and permit efficient immune cell infiltration of the tissues -

Figure 1. LOX enzymatic activity is implicated in PyMT-induced mammary carcinoma and metastasis.

A) Immunohistochemistry images of $\beta 1$ -integrin and FAKp^{Y397} in the mammary glands of MMTV-PyMT mice as a function of tumor progression. B) Bar graphs of qPCR levels of Lysyl Oxidase (LOX) expressed in PyMT mice as a function of tumor progression. Data illustrate that while LOX levels are low to nonexistent in the mammary glands of control and 4 week old PyMT mice that expression of the enzyme increases dramatically by 8 weeks and remains quite high even at 14 weeks of age. C) (top) Line graphs indicating delayed mammary gland tumor formation in PyMT mice following inhibition of LOX activity. (bottom) H&E images of mammary glands from 14 week old MMTV-PyMT animals treated with and without BAPN treatment D) (top) Bar graphs indicating that up to 40-60% of PyMT treated with BAPN remained metastasis free (left) and that the total number of metastasis to the lungs was significantly reduced in the BAPN treated mouse cohort (right). (bottom) H&E micrographs of the lungs from PyMT mice treated with or without BAPN. Images reveal that even when lung metastasis developed in the BAPN-treated animals the lesions were significantly smaller.

Figure 1

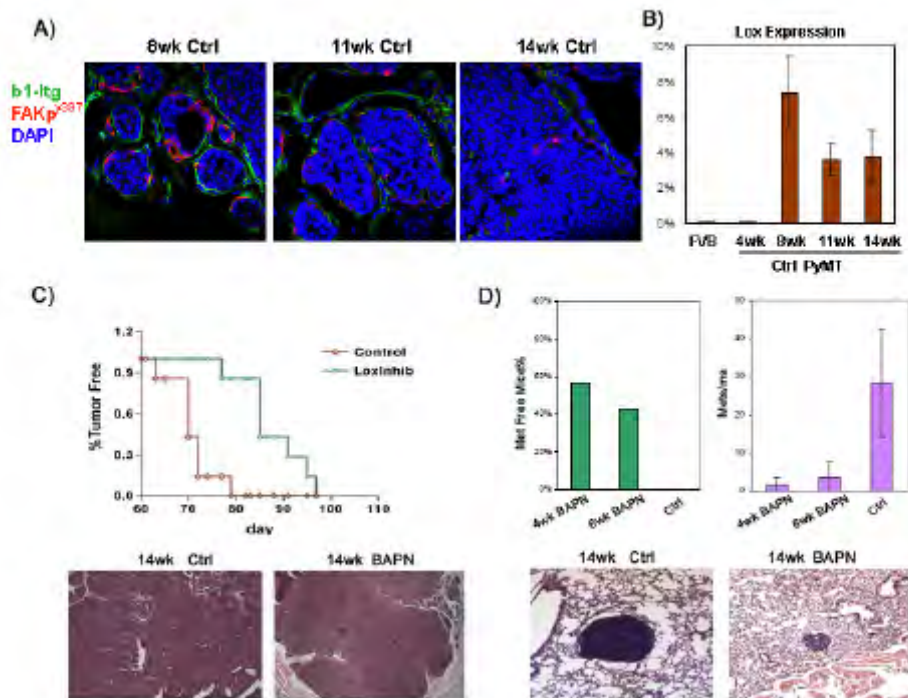


Figure 2. Histophenotype, Immune Infiltrate markers and Mechanical Testing of Mammary Glands from 8, 11 and 14 week old PyMT mice following treatment with the LOX inhibitor BAPN.

A) Micrographs showing H&E images from 8, 11 and 14 week old mammary glands from PyMT mammary tumors with and without inhibition of LOX activity using the pharmacological inhibitor BAPN. Note that the mammary glands of both non treated (ctl) and BAPN treated (BAPN) animals have abundant levels of infiltrated leukocytes. B) Bar graphs showing tissue indenter measurements of the materials properties of the mammary glands of PyMT mice treated with and without BAPN inhibitor at 8 and 14 weeks. Data show that mice treated with BAPN had greatly reduced mammary gland stiffness.

Figure 2

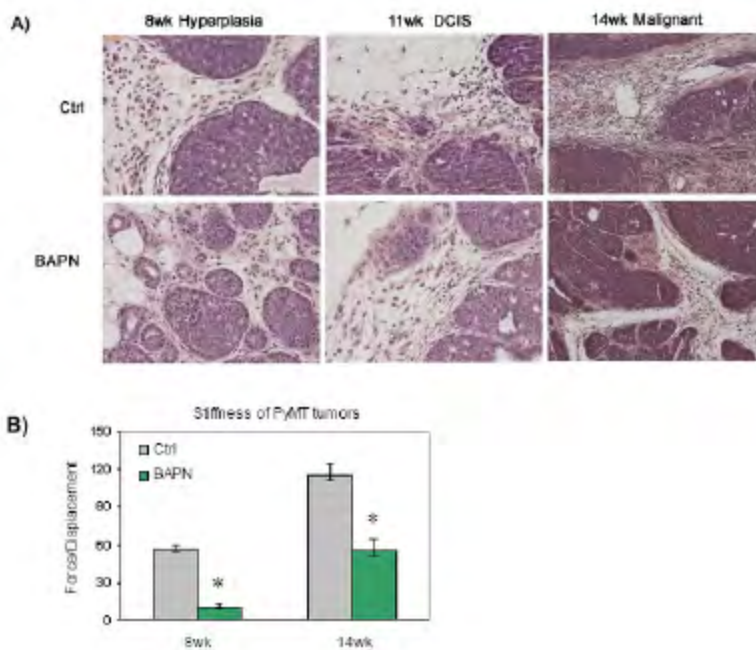


Figure 3. FACS analysis of immune cell infiltrate in PyMT mice treated with BAPN.

A) Scatter graph showing flow cytometric analysis of total leukocytes in the mammary tumors from 11 and 14 week old PyMT mice treated with and without BAPN. The results show that while the fraction of total hematopoietic cells (CD45 positive) is similar in the mammary glands of the 11 week old mice there is a significant increase in immune cell infiltration in the 14 week old mammary glands of mice treated with BAPN. B) Bar graphs depicting the nature of the leukocyte populations infiltrating the mammary glands of 11 and 14 week old mice with and without BAPN treatment. Flow cytometric analysis of leukocyte population was achieved using 25 cell surface markers specific for various subpopulations of Thymocytes, B lymphocytes, Natural Killer cells, macrophages, dendritic cells, and monocytes. Data indicate that the levels of CD11b+Ly6G+ granulocyte cells is increased in the 11 week old mammary glands of PyMT BAPN treated tumors, and reduced levels of CD11b+Ly6C+ Monocytes and CD11b+F4/80+ macrophage fractions in the 14 week old mammary glands of PyMT BAPN-treated tumors. .

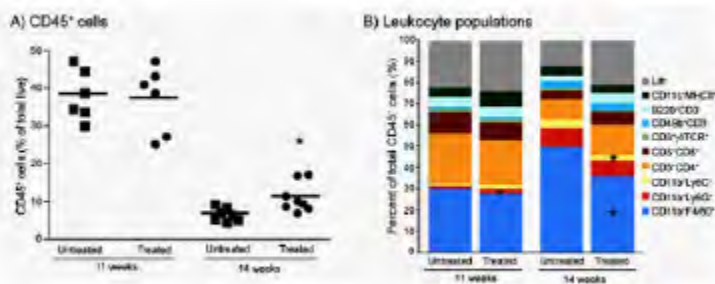
Figure 3

Figure 4. Reducing mammary gland stiffness through inhibition of LOX activity modifies the immune cytokine profile of the tissue.

A) (top graphs) Bar graphs showing qPCR analysis of the expression of M1 and M2 macrophage cytokines in the primary tumors from 14week-old mice. Data indicate that there is no difference in the levels of M1 or M2 cytokines in the mammary glands of mice treated with BAPN by 14 weeks. These results suggest that while initially the BAPN might reduce levels of these cytokines at least at the RNA level there is a compensatory rise in levels so that by 14 weeks of age the difference is negligible. B) (bottom graphs) Bar graphs showing qPCR analysis of the expression of M1 and M2 macrophage cytokines in the primary tumors from 8 week-old mice. Results suggest that the expression of M2 cytokines is lower in the mammary glands of mice treated with BAPN.

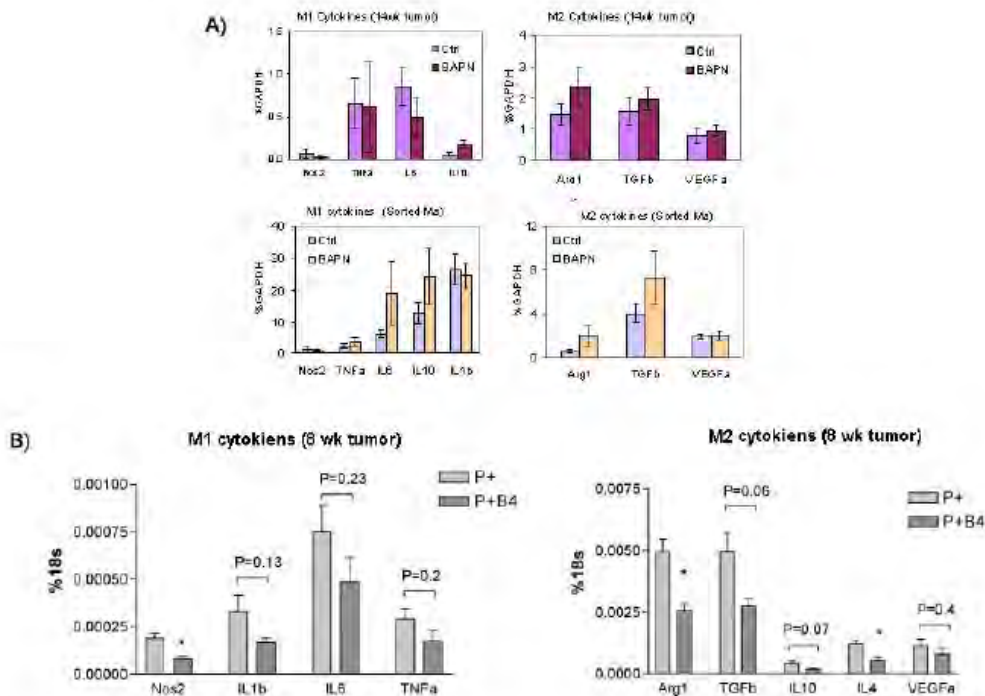


Figure 5. Reducing mammary gland stiffness through treatment with BAPN delays in infiltration of immune cells into the mammary gland of PyMT mice.

A) Images showing immunohistochemistry of the total macrophages (F4/80 Positive) and total CD206 positive M2 macrophages associated with 11 (right) and 14 (left) week old mammary tumors in the BAPN treated and untreated animals. Data indicate that BAPN treatment significantly reduces the total number of macrophages infiltrating the mammary gland at 11 weeks of age. Nevertheless, by 14 weeks of age the difference has disappeared and the density of macrophages appears to be greater. This is likely due to the fact that the BAPN treated mammary glands are softer and hence more penetrable by immune cells. B) Bar graphs quantifying the density of M2 and total macrophages in the mammary glands of 11 and 14 week old mice treated with and without BAPN.

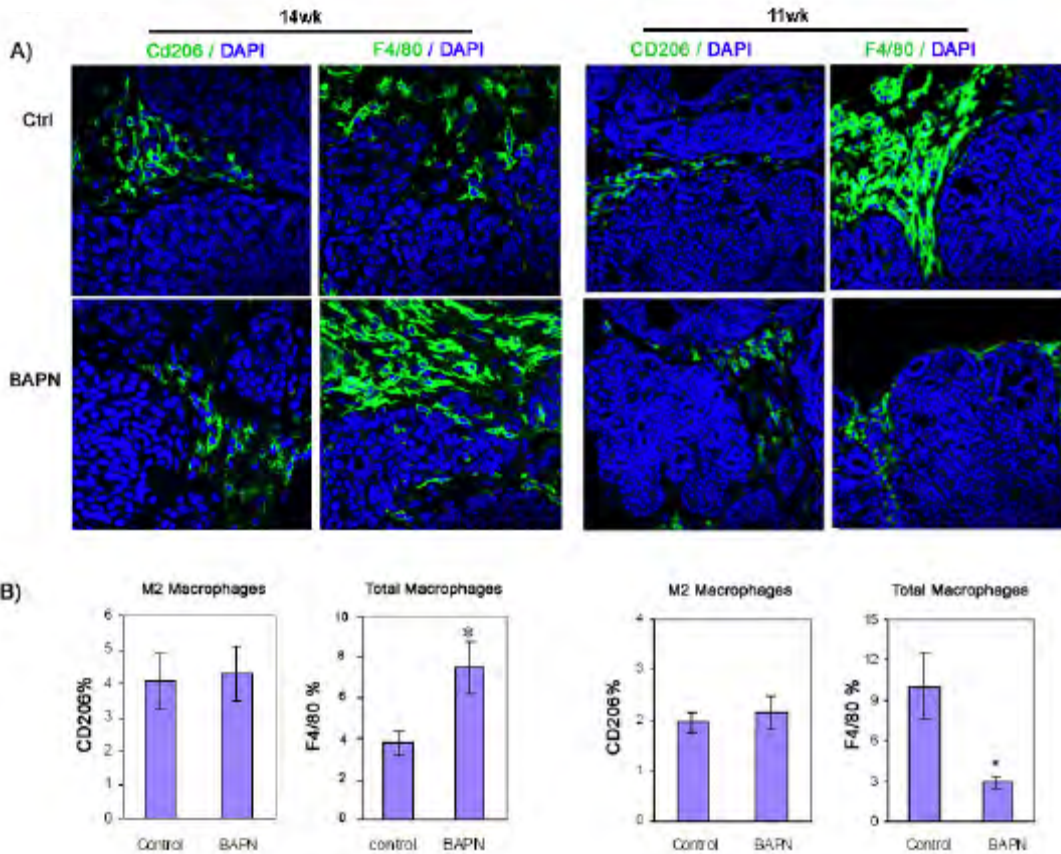
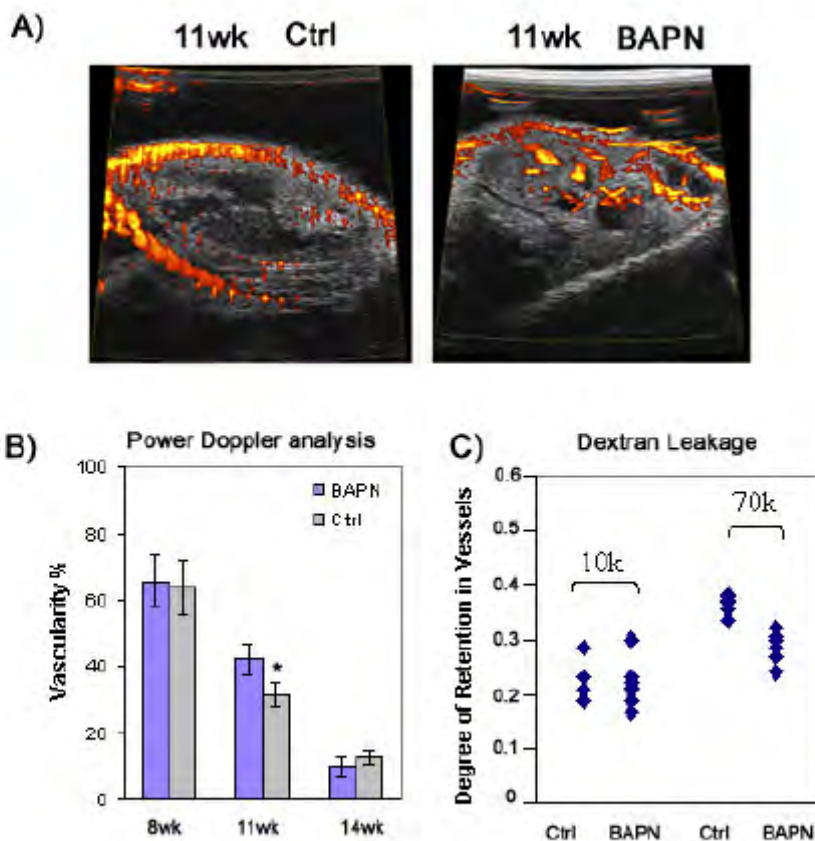


Figure 6. BAPN treatment reduces mammary gland stiffness and facilitates vascularization of PyMT breast tumors.

A) Doppler images of mammary glands from PyMT mice with and without BAPN treatment. Images suggest that the mammary glands of the BAPN-treated animals have increased vascular density and penetration. B) Bar graphs showing quantification of Doppler images taken from the mammary glands of PyMT mice at 8, 11 and 14 weeks of age with and without BAPN treatment. Data indicate that as tumors evolve and grow larger and more advanced their perfusion decreases dramatically. However, BAPN treatment which reduces tissue stiffness delays this effect. C) Bar graphs quantifying the amount of 10kDalton Dextran versus 70kDalton Dextran vascular leakage into the mammary glands of PyMT mice treated with and without BAPN. Data suggest that the mammary glands of animals treated with BAPN are significantly leakier than nontreated animals.

Figure 6



something immunohistochemistry suggested when we examined the immune infiltrate status of these treated mammary tumors (Figure 6). In the next several months we intend to explore this possibility further through analysis of interstitial pressure and hypoxia analysis. We hope to complete additional mouse studies using the PyMT mouse model.

We are also in the process of initiating a set of collaborative studies with members of Georgia Technical institute who have developed a novel technique that permits a comprehensive analysis of the visco elasticity of the lungs of mice. Using this approach we hope to examine whether PyMT animals that have been treated with LOX inhibitors exhibit lower levels of lung metastasis because there is reduced cross-linking and stiffening of the lung tissue. This would suggest that circulating LOX could condition the metastatic niche thereby fostering metastasis formation.

Moreover, to further examine the interplay between collagen cross-linking and tissue stiffening (ECM stiffening) and breast tumor metastasis we have initiated collaborations with the Moses group. The Moses group is assessing the effect of TGF beta and its effects on tissue inflammation and recruitment of immature myeloid progenitor cells on breast tumor metastasis. Dr. Moses and colleagues showed that analogous to human tumor that harbor loss of expression or mutations in the TGF beta receptor II PyMT mice lacking this receptor develop tumors that are twice as aggressive as normal and these animals develop lung metastasis after only 8 weeks! Intriguingly these mice show very strong myeloid infiltration that precedes and is critical for this accelerated metastasis because inhibiting myeloid cell recruitment prevents tumor metastasis. Our preliminary studies suggest that these myeloid cells secrete high amounts of TGF beta into the tissue. Because TGF beta is a potent inducer of LOX expression we are now assessing whether the accelerated tumor metastasis exhibited by these mice is linked to elevated LOX mediated collagen cross-linking.

- b. Write up experimental findings on biomaterial characteristics of primary and metastatic murine tissues as a function of tumor type and stage and submit for publication in peer reviewed journal. (Months 0-12) [Completed](#).**

This work was summarized and submitted for publication to the journal of Integrative Biology in July 2010. We received our reviews back from the journal in the fall of 2010. The work received favorable comments however, several additional experiments were suggested. We therefore spent the fall and this past winter conducting additional animal studies and AFM measurements on intact tissue as well as isolated breast tumor cells. The work was resubmitted for consideration and we have received informal communication that the work has now been accepted for publication (see Lopez et al., J Integrative Biol Accepted; Attachment 1). We summarized our findings in this publication above and attach the article for assessment in this report.

In addition to these in vivo studies we have also completed a comprehensive series of studies our studies on characterization of self assembling peptide polymer gels. These studies include comprehensive demonstration that analogous to collagen hydrogels (Miroshnova et al., J Physical Biology; attachment 2; figure 1), SAPs gels can be stiffened through increasing their concentration (Miroshnova et al., J Physical Biology, attachment 2; figure 2). Importantly, compliant SAPs and collagen gels incorporating laminin 111 are able to support tissue morphogenesis and polarity (Miroshnova et al., J Physical Biology; attachment 2; figure 3) and increasing SAP gel stiffness perturbs mammary tissue morphogenesis (Miroshnova et al., J Physical Biology; attachment 2; figure 4). However, high collagen concentrations simultaneously increase ligand binding sites, and reduce pore size. By contrast SAPs gels with high concentration that are stiffer do not demonstrate changes in pore size, nor do they vary ligand binding since they are synthetic. Thus, EM analysis showed that stiff collagen gels have greatly diminished pore size and larger fibrils whereas stiff SAPs gels exhibit topologies strikingly similar to

compliant SAPs (Miroshnova et al., J Physical Biology; attachment 2; figure 2). The physiological relevance of this is illustrated by the fact that a stiff SAPs gel promotes MEC invasion whereas a stiff collagen gel does not - something we are now exploring in greater detail. These studies demonstrate for the first time that ECM stiffness per se may be sufficient to promote an invasive phenotype in human breast tissue.

The results from this set of studies were summarized in the fall of 2010 and the manuscript was submitted to the Journal of Physical Biology for consideration. We received favorable reviews back in mid December 2010. After additional experiments were conducted to address reviewer suggestions, we revised the article and sent it back to the journal. Recently, we received official email notification that the article was accepted for publication. This week we received the galley proofs demonstrating that the article went to press and should be published shortly. Therefore, we have attached the uncorrected galley proofs as attachment 2 in this report. We expect that the article will be published either in the April or May issues of the journal 2011 (Miroshnova et al., Journal Physical Biology 2011, In Press; attachment 2).

- c. **Assay using nano AFM, imaging methodologies and biochemical assessment the physical and biochemical properties of human breast tissue as a function of breast tumor stage.** This will include an analysis of normal breast tissue, noninvasive breast lesions that have a pathological phenotype consistent with nonprogression and those with an "aggressive" phenotype and invasive early stage ductal carcinomas. (Months 0-24). [We have secured IRB approval to conduct these studies and have been working with clinicians, surgeons and pathologists at UCSF to acquire a repository of snap frozen human breast tumor specimens from surgical discard tissue. Accordingly, these studies are well in progress.](#)

We recently submitted our renewal for the IRB to conduct these studies and received approval. We were able to complete the development of approaches with which to spatially map the materials properties of these human surgically biopsied tissues and mastectomy tissue. tissues using AFM combined with second generation harmonics, PS staining, IHC and H&E. This permits us to determine the precise spatial relationship between changes in cell and ECM stiffness (AFM), remodeling and topological features of the ECM and invasive behavior of the cellular fraction and tumor stage and progressive nature. Thus far, in the past year we have been able to collect a range of normal adjacent, noninvasive/premalignant/fibrotic and invasive breast tissue. See attached table of specimens (Table 1). We have been systemically analyzing the physical properties of the ECM associated with these developing lesions. Surprisingly, we determined that the visco elasticity of the normal human breast mirrors that we measured in mouse tissue. Moreover, preliminary data suggest that the epithelial architecture and region of the human breast dictates or is dictated by differences in ECM organization, concentration and visco elasticity. In our next years report we hope to have completed a set of studies so that we can make more definitive conclusions. We are also continuing to collect additional specimens for our analysis. Thus far our preliminary data suggest that the human breast ECM in noninvasive fibrotic lesions is significantly stiffer than that of the normal breast and that invasive tumors stiffen further. Indeed, we noted that the invasive regions of human breast ECM are considerably stiffer than normal breast ECM and significantly stiffer than that associated with a noninvasive, non-progressive breast lesion (see Figure 7). Our goal for the upcoming year is to continue with our analysis of our banked tissue specimens and to extend this work to different histophenotypes of breast tumors and different stages of breast cancer versus non-progressive disease. Specifically, we are interested in determining whether there is a difference in ECM rigidity between ER/PR positive and ER/PR negative invasive breast lesions.

TABLE 1

HUMAN BREAST SPECIMENS ACQUIRED FOR EXECUTION OF MECHANICAL ANALYSIS OF MAMMARY GLANDS

Samples collected (sex/age)	Benign	DCIS			Invasive		
		I	II	III	I	II	III
F/36	✓						
F/36			✓		✓		
F/39	✓						
F/46				✓		✓	
F/51						✓	
F/54							✓
F/57			✓		✓		
F/58					✓		
F/60			✓			✓	
F/61		✓				✓	
F/61		✓				✓	
F/66						✓	
F/73						✓	

- d. **Write up experimental observations on human breast tissue** including novel protocol to measure "in situ" human breast tissue and to build correlative spatial maps of invasive behavior. (Months 18-24). [This work is still in progress.](#)

Some time this coming year we hope to be in a position to begin to assemble a paper with data compiled throughout the winter and spring of 2011 so that by the end of the summer/early fall we will be able to write a small article for a clinical journal. Dr. Weaver has been invited to present her findings at the Annual San Antonio Breast Cancer meeting in December 2011 and hopes to be in a position to present a completed body of work at the conference coincident with submission of an article for publication. Dr. Weaver believes that disseminating these findings at this clinical meeting will greatly assist with clinical translation of our work/ideas.

- e. **Continue to develop novel approaches to manipulate the stiffness of collagen and basement membrane gels and apply new technology to modulate and re create the biophysical AND biochemical properties of ECM microenvironment of the normal, pre malignant and malignant breast.** This will involve continued work with ribose cross-linkers but will also extend to photo-activatable cross-linkers and incorporation of methods to orient collagen fibrils and potentially to modulate their fibril architecture. Key parameters to be assessed will be morphogenesis, proliferation, survival and invasive phenotype of nonmalignant epithelial cells but also of pre malignant mammary epithelial cells (i.e. those with oncogenic/tumor suppressor modifications typically found in DCIS or fibrotic human breast tissues (Her2, EGFR amplification, altered myc, reduced BRCA1) (Months 0-24). [These studies are still in progress.](#)

Quantitative Assay of Collagen Cross-links in Mammary Tissue Thus far we have found that intermolecular cross-links between tissue collagens represent an excellent means to increase the overall mechanical rigidity of tissues without in principal increasing the overall collagen content. To this end we identified lysyl oxidase (LOX) as a major enzyme that regulates intermolecular collagen and elastin cross-links. We showed previously that reducing LOX activity increased stiffened the tissue and inhibiting LOX activity reduced tissue stiffening. We then worked closely with collaborators to biochemically assay the level and nature of the collagen and elastin cross-links present in tissues as they progressively transformed and following LOX enzyme inhibition. In the past year we familiarized ourselves with protocol to analyze collagen cross-linking in mouse and human tissue. Therefore, by assaying accurately the tissue collagen content and numbers and types of collagen cross-links in normal and tumorigenic mammary tissues we will be in a position to be able to determine if there is a positive correlation with mammographic density in normal glands and whether collagen content/cross-links are positively associated with tumor progression/histotype in murine models and human tumors and whether there are positive correlations with other orthogonal metrics of tissue mechanics (ex AFM measurements of tissue rheology).

To this end we have now begun applying previously published methods¹⁹ to sensitively identify and quantify both tissue collagens and cross-links by HPLC of acid tissue hydrolysates. We have successfully set up and validated both an assay for collagen content and that for both of the known divalent cross-links in normal murine and human mammary glands, as well as human normal and transformed tissue. Briefly, this technique involves using excised fresh or frozen tissues that have been delipidated by extraction in chloroform:methanol, rehydrated, homogenized and then reduced by treatment with sodium borohydride to stabilize divalent cross-links to acid hydrolysis. Following reduction tissue homogenates are freeze-dried and then hydrolyzed to constituent amino acids by treatment with 6N HCl for 24 hours at 110°C. After drying by evaporation amino acids cross-links are redissolved in water and the sample is divided for assay of collagen content and the larger portion for collagen cross-links. The smaller portion is used for assay of hydroxy-proline (OH-Pro) content by

HPLC fractionation on a strong cation exchange column with post column derivatization using ninhydrin and detection in an online flow through UV/Vis detector by absorbance at 440 nm. Integration of the OH-Pro peak relative to a standard of known concentration allows conversion to molar content of OH-Pro and molar collagen tissue content using the well established relationship of 14% mole fraction of collagen as OH-Pro. Figure 8 shows baseline separation of OH-Pro peaks from Asp in purified standards (Figure 8A), purified collagen I (Figure 8B) and in virgin murine mammary glands (Figure 8C) validating the specificity of the assay and establishing sensitivity of detection in our hands of (estimated from 4 week old virgin mouse mammary gland #4) of 1-2 mg wet weight of tissue (~0.5% of the total gland). The larger portion of tissue acid hydrolysate is pre-fractionated on a column of fibrous cellulose (CF-1) that enriches for cross-linked amino acids (that are adsorbed) and free (uncross-linked) amino acids that flow through the column. Adsorbed cross-links are eluted in water, concentrated by centrifugal evaporation and analyzed by HPLC fractionation on a strong cation exchange column with post column derivatization using phthaldialdehyde and detection of the resulting derivatives in an online flow through fluorometric detector with excitation of 334 nm and emission of 425 nm. Figure 9 shows enrichment and excellent separation of the collagen cross-links hydroxyl-lysinonorleucine (HLKNL) and dehydro-hydroxylysinonorleucine (Δ -HLNL) in CF-1 fractionated fresh frozen human normal and mammary tumor acid hydrolysates. Validation of peak assignments (Figure 9A) is based on analysis of demineralized bone (HLKNL > Δ -HLNL), relative orders of elution (HLKNL before Δ -HLNL), similarity to published chromatograms¹⁹, and most importantly peak loss in the absence of reduction prior to acid hydrolysis (both HLKNL and Δ -HLNL are destroyed in the latter case). Unlike in demineralized bone presumptively vascular elastin cross-links (isodesmosine and desmosine; incompletely resolved and tentatively assigned based on published chromatograms¹⁹ are also detected in normal and tumor mammary glands (Figure 8B). Figure 8A (Inset) also shows the improvement in detection sensitivity realized using phthaldialdehyde and fluorometric detection vs ninhydrin and absorbance detection as described by Avery et al.¹⁹. As a result estimated sensitivities of detection for HLKNL and Δ -HLNL are at about the level of 10 mg wet weight of tissue (human mammary gland) corresponding to a cubic volume of tissue estimated at a 2-3 mm on each side. These sensitivities are reliably below the size of tumor samples available to our laboratory. Current work is now focusing on increasing assay throughput and expanding the number of analyzed samples.

- f. **To continue to manipulate and calibrate bioreactor device** to apply a calibrated mechanical force (compression) to 3D cellular organoids for the study of effects of force on tissue behavior - in particular treatment responsiveness. (Months 0-18). [These studies are still in progress.](#)

We have on hand a force reactor and have been working with our colleagues from the University of Pennsylvania to use HA gels to test the effect of 10-20% compression loading (constant versus cyclical) on mammary tissue integrity. We have successfully calibrated this device and as reported in last years summary we could show that 15% cyclical compression loading stress is sufficient to modify MEC acini stability. These results have already been reported. However, one of the issues we have encountered with the current device is that long term studies are problematic in that the current system does not permit fluid exchange. Moreover, the gel size is quite small and therefore gene expression studies and protein analysis is quite challenging. Therefore, as outlined below to address this issue we are in the process of obtaining design drawings to build an in house set of compression loading devices with easy fluid exchange capabilities. This will not only permit long term studies with excellent cell feeding capabilities but will also permit us to conduct periodic samples of conditioned media. This should help us to determine whether compression loading alters the expression and secretion of active factors e.g. pro inflammatory chemokines and cytokines that could promote tumor evolution and progression as well as modify treatment response.

Figure 8. HPLC Assay for Tissue Collagen Content (Hydroxy-Proline).

Line graphs showing two buffer gradient HPLC fractionation of amino acids from standard mixture (A.) or acid hydrolysates of purified mouse collagen I (B.) and mouse mammary gland #4 (equivalent to 1 mg wet weight of tissue) on a strong cation exchanger (4.3 mm x 25 mm column) detected by absorbance of post column ninhydrin derivatives with a timed programmed detector change from 440 nm (secondary amines OH-Pro and Pro) and 570 nm (primary amines) to enhance sensitivity of detection. Peak corresponding to OH-Pro standard is circled in red and the corresponding peak in collagen (B.) or mouse mammary gland samples (C.) is indicated.

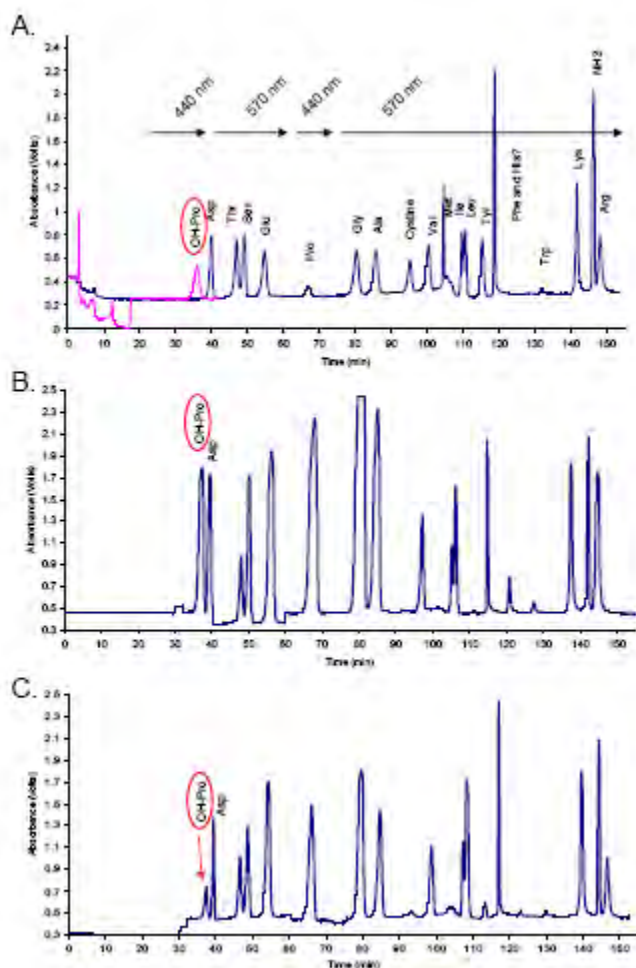
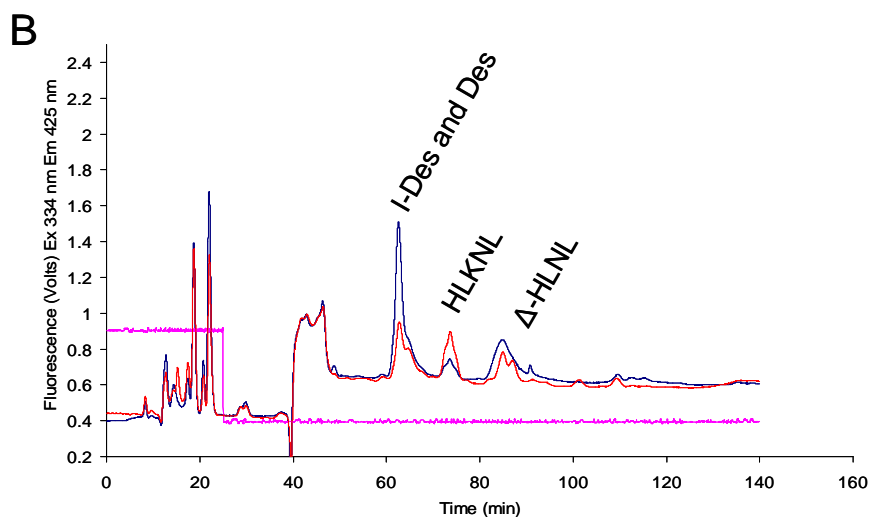
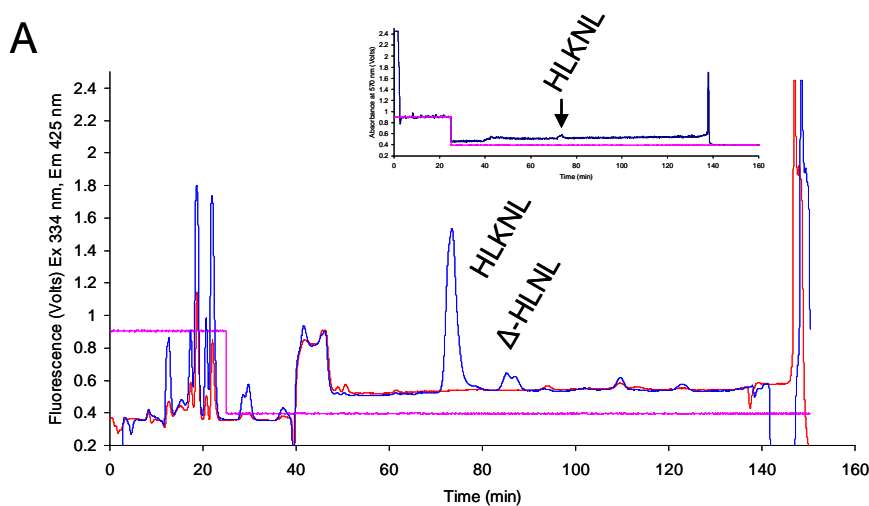


Figure 9. HPLC Assay for Tissue Collagen (and Elastin) Cross-links. Collagen cross-links detected and resolved in a CF-1 bound fraction of acid hydrolysates from demineralized bone (A.) and human normal (prophylactic mastectomy of contralateral breast, Brca2+; blue trace) and human tumor (Invasive Ductal Carcinoma, grade II; Ductal Carcinoma In Situ, grade I, ER+/PR+, Her2+, Brca1/2-; red trace) (B.) by HPLC on a strong cation exchanger (4.3 mm x 25 mm column). A. Identification of peaks corresponding to HLKKNL (hydroxy-lysinoketonorleucine) and Δ -HLNL (dehydro-hydroxylysinonorleucine) by comparison of identical samples of demineralized bone hydrolyzed with (blue trace) or without (red trace) sodium borohydride reduction prior to acid hydrolysis. Both HLKKNL and Δ -HLNL are destroyed by acid hydrolysis if not reduced and are lost from the trace. HLKKNL is more abundant than Δ -HLNL in bone and is expected to elute before Δ -HLNL under these conditions leading the indicated assignments. The same quantity of reduced sample of demineralized bone detected with post column derivatization with Ninhydrin and detection of absorbance at 570 nm is shown in the inset in A. as compared to the larger trace showing fluorescent detection of pthalaldialdehyde derivatives indicating the large increase in sensitivity obtained using fluorescent detection. B. Peaks with identical retention times to those indicated in samples from demineralized bone are identified as HLKKNL and Δ -HLNL in samples of human normal and tumor breast tissue. Presumptive elastin cross-links, isodesmosine (I-Des) and desmosine (Des) (tentative identification based on elution positions of cross-links in published chromatograms assayed under identical conditions and incompletely resolved) are also indicated.



- g. **To modify the existing bioreactor so that it encompasses a fluid exchange system** that will allow us to change media and maintain longer term culture conditions. We are also keen to try to assess the effects of hypoxia AND mechanical changes in microenvironment together since these two characteristics so often are changed in tandem in human breast. Both conditions are known to drive/modulate treatment responsiveness. Thereafter, once the bioreactor has been developed we will assess short term and long term consequences of modulating mechanical force on mammary epithelial cell morphogenesis, proliferation, survival and invasiveness - in breast cells that are nonmalignant and those that harbor pre malignant oncogenic and tumor suppressor changes (see above). (Months 12-24). [We are in the process of obtaining CAD CAM blueprints from our collaborators at Olin Engineering College to build our modified device at UCSF.](#)
- h. **Using new generation of biocompatible materials assess the responsiveness of nonmalignant and oncogenically/tumor suppressor modified breast cells to chemotherapeutic agents** including doxorubicin, etoposide, paclitaxel and gamma radiation as well as immune receptor activators such as TNF α and TRAIL. This will be deduced through viability assays, apoptosis analysis and clonogenic survival curves and will encompass dose dependency assessment as well as time course analysis. (Months 12-24). [These studies are now in process.](#)

Our SAP studies illustrated that we could use these self assembling peptide polymer gels provided they were spiked with small quantities of purified laminin or reconstituted basement membrane to generate mammary acini that recapitulate that achieved using reconstituted basement membrane gels or collagen gels spiked with basement membrane (see Miroshnova et al., J Physical Biology 2011; attachment 2; figure 1 & 2). We also determined that increasing the concentration of the SAPs gels increased their stiffness and this was sufficient to destabilize mammary epithelial tissue architecture. Importantly, we noted that while increasing ECM stiffness by elevating collagen concentration simultaneously reduced pore size, altered ECM fiber diameter and increased ligand binding sites in the range of stiffness we used for the SAPs gel experiments none of these compounding effects were observed. This means that we now have for the first time ever a tractable system with which to manipulate ECM stiffness independently and study effects on tumor progression and treatment response. Indeed, independently increasing ECM stiffness using the SAPs gels also suggested that ECM stiffness per se might be sufficient to induce breast cell invasion EVEN in the absence of overt oncogenic changes! We also worked out methods to conduct immunohistochemistry and monitor gene expression. These studies illustrated that not only does ECM stiffness change the morphology of mammary epithelial tissues but stiffness additionally modifies gene expression towards that found in breast tumors including increasing total fibronectin gene and protein expression and elevating levels of the epidermal growth factor receptor (see Miroshnova et al., J Physical Biology 2011; attachment 2; figures 3 & 4).

- i. **Complete revisions required to publish articles** identifying a novel repressor mechanism that inhibits efficient treatment responsiveness in breast tumors that is mediated through N-CoR2/HDAC3. [This work is STILL in PROGRESS and we now hope that after further modifications we should be finally able to have the article accepted for publication in a sufficiently high profile journal.](#)

This article was previously submitted to Nature Medicine and last year we were optimistic that we would finally have word that the article was accepted and would be published. However, this task is more challenging than originally anticipated. The article showed that Nuclear co-repressor 2 (NCoR2/SMRT) is part of the epigenetic mechanism which enhances cell survival by inhibiting pro-apoptotic and pro-inflammatory genes and through which tumors resist treatment (see Tsai et al., revision Nature Medicine; attachment 3). NCoR2/SMRT (Silencing Mediator of Retinoid and Thyroid

hormone receptors) and NCoR (Nuclear hormone receptor-Co-Repressor) were originally identified as co-repressors for nuclear receptors however we and others now have demonstrated that the molecule works as a more generic scaffolding molecule that can equally inhibit and stimulate gene expression^{20,21}. We found much to our surprise that the molecule was significantly up-regulated in treatment resistance breast tissues. When we generated an NCoR2 gene regulation signature we could demonstrate that this gene expression signature had profound prognostic power. (Months 0-12)

Last year we finally received reviews back from Nature Medicine that requested extensive new experiments. Therefore to address reviewer's comments and editorial suggestions we extensively revised the article and extended our original findings to identify a novel bystander mediated death regulatory mechanism. This was illustrated by demonstrating that NCoR2 interacts with and modifies the activity of a key transcription factor that regulates inflammation and death induction in breast cells by outcompeting CBP (see Tsai et al., revision Nature Medicine; attachment 3; figure 6). The article was therefore resubmitted for consideration late fall 2010. However, despite the fact that these data are highly significant a new set of reviewers again sent back a long list of comments and suggested experiments. The reviewers remain unconvinced by some of the findings. This has more to do with the fact that conventional wisdom views tumor cell survival as essentially a cell intrinsic mechanism dictated primarily by a balance of pro apoptotic and anti apoptotic signaling as well as regulated autophagy. Our data instead posit that treatment responsiveness is contingent upon initiating a tissue wide amplification that depends upon up-regulation of pro inflammatory pro death secreted gene/factors. This fact is based upon clinical observations and recent findings that virtually all therapies in tissues respond through up regulation of factors such as TRAIL which can stimulate death induction in surrounding cells. Yet, the main stream research community takes time and intensive experimental evidence before they will accept such a new idea.

My group has been studying the role of cell and tissue context in tumorigenesis of the breast and treatment responsiveness. We are highly committed to exploring this important issue so despite such difficulties in publishing our findings we intend to continue the work until such time as it has been accepted. Thus reviewers requested the addition of yet more experiments in animals and additional molecular manipulations. Another critique has to do with clinical relevance. Although we could definitively show that an NCoR2 gene signature could accurately predict treatment resistance and patient disease recurrence and mortality the reviewers insist upon further studies. They could not believe that NCoR2 could be a conserved mechanism that elicits resistance to treatment. In particular, with such a strong trend emphasizing personalized medicine and signaling pathway or oncogene involvement they are insisting that we identify whether this pathway is enriched in tumor initiating or stem like cells or is more represented in one sub class of breast tumors. Accordingly, we are now in the midst of conducting experiments to address these newest concerns. We are in the process of determining whether NCoR2 regulated genes might prove useful for predicting non-responsiveness in high grade non-responsive triple negative human breast tumors. This is being done through access of additional micro array data sets as well as by collaborations with Laura Esserman and Laura Van Der Veer at UCSF with the ongoing clinical trials for triple negative breast cancer as well as collaborations with Alana and Bryan Welm at the Huntsman Cancer Clinic, University of Utah in Salt Lake City, Utah. These next 4-6 months will be dedicated to completing new studies and resubmitting the manuscript either back to Nature Medicine or else to another suitable high profile Cancer related journal.

In addition to these ongoing studies we have been exploring additional mechanisms by which NCoR2 could influence breast tumor aggression and treatment resistance. Both NCoR2 and NCoR1 make direct contact with their nuclear receptor partners and then recruit additional components of a large corepressor complex that includes HDACs, TBL1, TBLR1 and GPS2²²⁻²⁵. NCoR and NCoR2 also mediate transcriptional regulation by variety of other factors, such as NF-kB²⁶, serum response factor²⁷, AP-1

proteins²⁷, Smads²⁸, RBP-Jk/CBF-1²⁹, c-Myb³⁰, PLZF, BCL-6³¹, PBX/Hox proteins³², ETO-1 and ETO-2³³, and MyoD³⁴ among others.

Our earlier work showed that NCoR2 enhances cell survival of mammary epithelial cells by recruiting and activating histone deacetylase 3 (HDAC3), which prevents the expression of key apoptotic mediators including the death receptor ligand tumor necrosis factor-related apoptosis-inducing ligand (TRAIL) (Tsai manuscript in revision, attachment 3). Three regions of the co-repressors mediate the interaction with HDAC3, the most N-terminal of these regions (deacetylase activation domain, DAD) not only binds HDAC3, but also activates the enzyme, which is otherwise inert^{35,36}. In addition to HDAC3 (class I HDAC), NCoR2 interacts with class II HDACs: HDAC4, HDAC5 and HDAC7, but in vitro experiments showed that these HDAC proteins do not possess intrinsic enzymatic activity and moreover they are inactive in the context of the NCoR2-HDAC3 complex and do not contribute to its enzymatic activity, which suggests that class II HDACs regulate transcription by bridging the enzymatically active NCoR2/NCoR-HDAC3 complex and select transcription factors independently of any intrinsic HDAC activity^{37,38}. In contrast to class I HDACs, which are ubiquitously expressed in most cell types, class II HDACs are expressed in tissue specific manner and have been implicated in the regulation of muscle and cardiomyocyte differentiation and in the processes of thymocyte maturation^{39,40}. Class II HDACs have been shown to physically interact with several tissue-specific transcriptional factors, among others with myocyte enhancer factor 2 (MEF2) transcription factors⁴¹⁻⁴³. MEF2D and MEF2C members of the MEF2 family of transcription factors also directly bind HDAC3 (class I HDAC). The interaction between HDAC3 and MEF2 proteins is mediated through MADS box, a domain contributing to DNA-binding properties of MEF2 factors⁴⁴. The MEF2 region responsible for binding to HDAC4/5/7/9 is the second part of the DNA-binding domain localized away from the MADS domain⁴³. Moreover, in-vitro experiments showed that HDAC3, but not the other HDACs interacting with MEF2D deacetylated and thus modulated its transcriptional activity. MEF2D also directly interacted with full-length NCoR2 protein, which proved that MEF2D, HDAC3 and NCoR2 form a trimeric complex and that NCoR2 cooperates with HDAC3 to repress MEF2-dependent transcription⁴⁴.

The function of MEF2D and its interacting HDAC7 has been further studied in the context of thymocyte maturation. HDAC7 is highly expressed in CD4+, CD8+ double-positive thymocytes, where it inhibits the expression of Nur77, an orphan receptor involved in apoptosis and negative thymocyte selection, via the transcription factor MEF2D. In resting thymocytes, the complex of MEF2D-HDAC7 is nuclear and functions as transcriptional repressor. HDAC7 plays a critical role in determining the threshold level at which a developing T cell undergoes positive versus negative selection, modulating the apoptotic response of developing thymocytes in response to T-cell receptor (TCR) activation. Upon TCR activation, HDAC7 is exported from the nucleus leading to Nur77 expression and TCR-mediated apoptosis^{40,45}. HDAC7 is exported to the cytoplasm by a calcium-independent signaling pathway after TCR activation. PKD1, a serine/threonine kinase, which is activated after TCR activation⁴⁶ interacts with HDAC7 and phosphorylates three serine residues at its N-terminus leading to the export of HDAC7 from the nucleus⁴⁷. Later after TCR activation myosin phosphatase specifically interacts and dephosphorylates HDAC7, which leads to nuclear import of HDAC7. In the nucleus HDAC7 interacts with MEF2D and they cooperatively repress Nur77 expression and thus inhibit the apoptosis⁴⁸. HDAC7 has been also reported a subject of nucleocytoplasmic shuttling in response to VEGF. VEGF plays a key role in angiogenesis by regulating proliferation, migration and survival of endothelial cells. VEGF induces phosphorylation of HDAC7 via protein kinase D, which promotes nuclear export of HDAC7 and activation of VEGF-responsive genes in endothelial cells⁴⁸.

Although NCoR2 and its interacting HDACs have been mostly studied in the context of thymocyte maturation and muscle differentiation epigenetic regulation of gene transcription is becoming particularly interesting in the cancer field. The result of epigenetic alterations can be aberrant

transcriptional regulation that leads to change of expression pattern of genes involved in cellular proliferation, survival and differentiation^{49,50}. Data suggest that deregulation of acetylation and deacetylation leads to abnormal gene expression in some forms of cancer⁵¹. For example, histone hypoacetylation associated with abnormal recruitment of HDACs to promoter of tumor suppressor genes has been shown to be related to the initiation and progression of acute promyelocytic leukemia⁵². Consistent with this observation, HDACs are overexpressed in prostate, colon and breast cancers⁵³⁻⁵⁷, which makes them promising anti-cancer drug targets⁵⁸.

We observed that HDAC-interacting NCoR2 protein was significantly elevated in 3D organotypic cultures of mammary epithelial cells and this elevated NCoR2 expression endowed them a resistance to cytotoxic drugs and radiation (Tsai, manuscript in revision; attachment 3), a phenotype similar to the multidrug resistance phenotype found in human cancers^{59,60}. While elevated NCoR2 expression level is associated with tumor progression and treatment resistance in breast cancers, the NCoR2 is also relatively broadly expressed in normal tissue. This observation indicates that NCoR2 has probably different functions in normal and tumor tissue. It is believed that the level of NCoR2 expression, as well as binding of NCoR2 to different proteins contributes to different functions of NCoR2 in normal and transformed epithelial cells. Accordingly we have been focusing on the identification and characterization of other proteins, which are part of the epigenetic NCoR2-HDAC complex in the context of normal and tumor breast tissue.

Although MEF2D transcription factor has been shown to interact with HDAC3 and through other HDACs with NCoR2 in maturing thymocytes^{40,45} and during muscle differentiation⁶¹, there is not much known whether MEF2D or other MEF2 factors play a role in tumor progression and treatment responsiveness. In vitro data suggest that up-regulated MEF2C levels possibly play a role in the invasiveness of myeloid leukemia cells^{62,63}. Since MEF2 transcription factors have never been systematically studied in the processes of breast cancer tumor progression and treatment we have been examining whether MEF2 proteins play a role in breast tumorigenesis and breast tumor cell survival and if so whether this role is mediated through their interaction with epigenetic complex NCoR2-HDACs.

In vertebrates MEF2 family of transcription factors comprises of four members: MEF2A, MEF2B, MEF2C and MEF2D⁶⁴. MEF2 proteins contain a highly conserved MADS-box and adjacent MEF2 domain, which together mediate binding to DNA and interaction with protein partners. They exhibit partially overlapping expression patterns in during embryogenesis and in the adult tissues, with the highest expression in cardiac and skeletal muscles and in the brain⁶⁵. MEF2 proteins play a role in many processes: in cardiac and skeletal muscle growth and differentiation⁶⁶⁻⁶⁸, T-cell apoptosis during thymocyte maturation^{40,45}, control of neuronal differentiation and survival⁶⁹⁻⁷¹. Interestingly, MEF2C protects differentiating neurons from apoptotic death, which is in contrast with the pro-apoptotic role of MEF2D during thymocyte development.

Breast malignancy is associated with reduced MEF2C expression

To determine the expression levels of MEF2 genes we performed quantitative RT-PCR analysis in normal breast tissue and in samples from primary breast tumors. The analysis showed that levels of MEF2C transcript were significantly reduced in ER+/PR+ (~46%) and ER-/PR- (~59%) primary mammary tumors compared to normal breast tissue (see Figure 10A). Similar analyses of MEF2A and MEF2D transcription levels did not show statistically significant results.

Analysis of the level of expression MEF2C from the NKI-295 data set⁷² representing patients with and without metastasis.

The NKI-295 data set contains gene expression profiles of breast cancer biopsies collected from 295 patients with primary invasive breast carcinoma. The Student's t-test with equal variance showed that MEF2C expression was significantly reduced in patients with metastasis compared to non-metastatic patients ($p=0.023$) (Figure 10B). These results are at least consistent with the notion that reduced MEF2C expression is associated with breast malignancy and it is more pronounced in patients with more aggressive disease, such as in patients with distant metastasis.

Low MEF2C expression is associated with decreased survival and shorter disease-free period in breast cancer patients

We next examined whether the low or high expression level of MEF2A, MEF2B, MEF2C and MEF2D genes was associated with survival and occurrence of metastasis in breast cancer patients. To answer this question we used publicly available NKI-295 data set of gene expression microarray data of breast tumor biopsies and their accompanying clinical outcome data⁷². The NKI-295 data set was obtained from Rosetta Inpharmatics (<http://www.rii.com/publications/2002/nejm.html>). This data set contains gene expression profile of 24,496 genes in breast cancer biopsies collected from 295 patients with primary invasive breast carcinoma and clinical data with the outcomes from patients of the same cohort. The expression levels of MEF2A (NM_005587), MEF2B (NM_005919), MEF2C (NM_002397) and MEF2D (NM_005920) were set as dichotomous variables with "high" expression defined to be more than 1.2 times the average expression level for all patients in the cohort. All other patients were classified as having "low" expression of the particular gene. The statistical analyses, which included Kaplan-Meier estimates, log-rank test, Cox-proportional hazards model and unpaired Student's t-test was performed in statistical software STATA. The log-rank analyses were used to correlate high and low expression of MEF2 genes with patient survival. These analyses showed that only MEF2C expression levels, but not the levels of other MEF2 genes correlated with patient's survival. The log-rank test showed statistically significant difference between high and low MEF2C expression and patient's survival ($p=0.02$). The corresponding Kaplan-Meier (K-M) curves documented that low MEF2C expression is associated with decreased survival in breast cancer patients (Figure 11A). The Cox-proportional hazards model of the high and low MEF2C expression and patient survival showed statistically significant result (HR=0.57; $p=0.023$; 95%CI 0.35 to 0.92). This result indicates that the risk of death is 43% lower for person with high MEF2C expression than for person with low MEF2C expression. As expected, the Cox-regression analyses of MEF2A, MEF2B and MEF2D expression and patient survival did not show statistically significant results.

We then examined whether the expression level of MEF2 genes correlated with the recurrence of the disease defined by diagnosis of metastasis. Similarly to survival analysis, only MEF2C was significantly correlated with remaining disease-free ($p=0.003$). The K-M curves showed that low level of MEF2C expression is associated with shorter disease-free period in breast cancer patients (Figure 11B). The Cox-proportional hazards model of MEF2C expression and remaining metastasis-free showed that the hazard of developing metastasis is 47% lower for patients with high MEF2C level than for patients with low MEF2C level and this result was statistically significant (HR=0.53; $p=0.004$; 95%CI 0.34 to 0.81). We also performed subgroup analyses to assess whether MEF2C level can predict survival in patients with lymph node positive/negative and estrogen receptor positive/negative subgroups. Neither the result of the log-rank analysis of MEF2C level and patient survival in the patients with lymph node positive status ($p=0.18$) nor the result of the analysis of MEF2C level and patient survival in the patients with lymph node negative status ($p=0.06$) showed statistically significant result, although the result of the lymph node negative subgroup was approaching the level of statistical significance. The log-rank analyses of MEF2C expression and patient survival in estrogen receptor 1 (ER1) positive and ER1 negative subgroups showed dramatically different results. While the high level of MEF2C expression was highly correlated with increased survival in patients with ER+ tumors ($p=0.007$) (Figure 11C), the

level of MEF2C expression was not correlated with patient survival in ER- subgroup ($p=0.56$) (Figure 11D). These data at least are consistent with the idea that the level of MEF2C transcription factor might be used to predict metastatic dissemination and survival in breast cancer patients. Low expression level of MEF2C transcription factor significantly correlates with shorter patient survival and with higher occurrence of metastasis. Interestingly, the subgroup analysis revealed that perhaps the level of MEF2C gene is strongly associated with survival only in patients with estrogen receptor positive, but not in patients with estrogen receptor negative tumors which differ from results obtained using the NCoR2 signature which suggests a stronger relationship to triple negative breast tumors. This work is very preliminary however and will require extensive experimentation. We also need to assess relationship to NCoR2 and HDAC3 expression and function that associate with MEF2C.

MEF2C modulates survival of mammary epithelial cells

To explore the relationship of MEF2C expression and tumor cell grade, we examined the effect of MEF2C loss on survival and tissue differentiation of mammary epithelial cells. We found that MEF2C is moderately expressed in non-malignant mammary epithelial cell line MCF10A and were essentially undetectable in the ER-, basal-like breast cancer cell line MDA-MB-231 (data not shown). The status of MEF2C in a panel of breast tumor cell lines is under way.

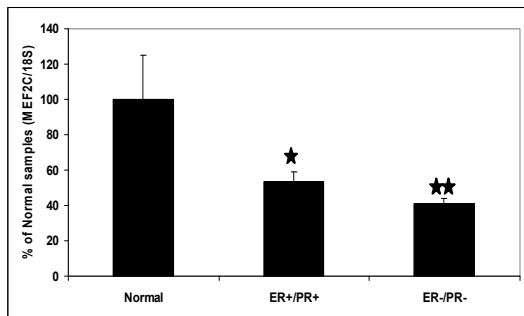
Nevertheless, to address the functional significance of MEF2C and to determine if the molecule regulates breast cell survival we used siRNAs to knock-down MEF2C levels in MCF10A cells. We obtained a variety of MEF2CshRNA lentiviral clones to knockdown the gene and determined that one clone (#15813, Sigma) was quite effective at reducing overall steady state MEF2C levels.

After verifying efficient MEF2C knockdown we assayed for effects on mammary tissue morphogenesis using the reconstituted basement membrane assay. We could show that loss of MEF2C had little to no effect on basal polarity and cell-cell junction formation as indicated by the ability of the breast cells to deposit an endogenous basement membrane indicated by laminin 5 immunostaining at their basal domains and to localize beta catenin at cell-cell junctions (Figure 12, top). However, and most provocatively and consistent with its association with HDAC3 and NCoR2 MEF2C loss led to retardation of lumen formation and reduced apoptosis induction induced in the breast epithelial cells located within the central region of the mammary spheroids. Thus, the mammary colonies with reduced levels of MEF2C failed to clear their lumens even after 3 weeks of culture within reconstituted basement membrane (see Figure 14 for quantification) and this was likely due to reduced apoptosis induction through loss of basement membrane interactions as indicated by lower levels of activated caspase 3 (see Figure 13). These observations indicate that MEF2C interactions with NCoR2/HDAC3 may be regulating breast epithelial cell survival. In the next year we will complete these studies and write and submit an article for publication. We are anxious to determine if MEF2C co association with NCoR2/HDAC3 might provide additional insight into the molecular function of NCoR2 in normal versus breast tumor cells.

Breast malignancy is associated with reduced MEF2C expression.

Figure 10 MEF2C expression is significantly reduced in breast cancer compared to normal breast tissue.

10A



10B

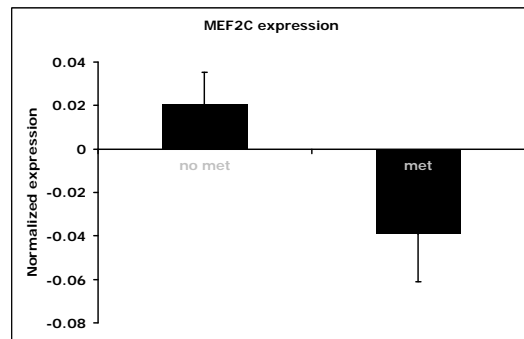
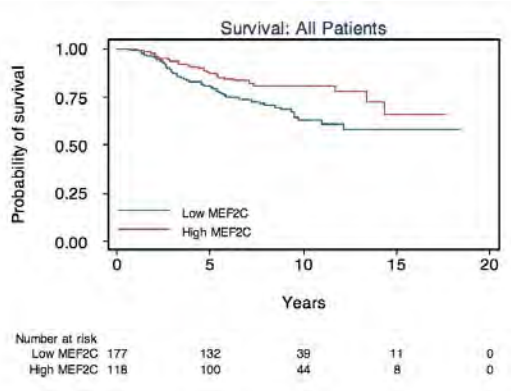


Figure 10A: MEF2C mRNA levels (normalized to 18S) are decreased in ER+/PR+ (N=10; p=0.013) and in ER-/PR- (N=15; p=0.005) primary mammary tumors compared to non-malignant tissue (N=5).

Figure 10B: MEF2C expression* is reduced in samples from patients with metastasis (met, N=101) compared to patients without metastasis (no met, N=194; p=0.023) in the NKI-295 dataset (* in logarithmic scale normalized to the mean intensity for all samples).

Fig.11 Low MEF2C expression is associated with decreased survival and shorter disease-free period in breast cancer patients. The NKI-295 data set [van de Vijver 2002] was obtained from Rosetta Inpharmatics. The predictor-intensity of gene expression was dichotomized with “high” expression defined to be more than 1.2 times the mean expression level for all patients in the cohort.

11A



11B

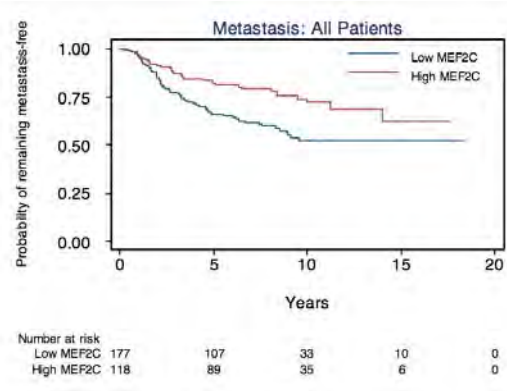
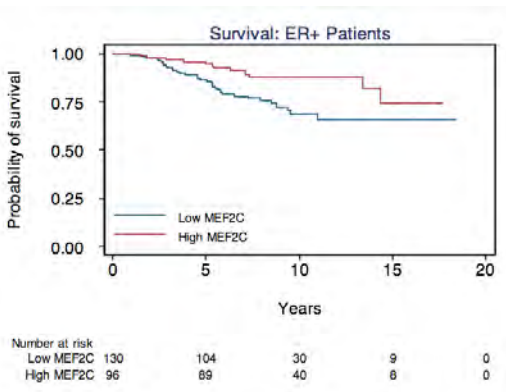


Figure 11A: Low MEF2C expression is associated with decreased survival in breast cancer patients (p=0.02).

Figure 11B: Low MEF2C expression is associated with shorter disease-free period in breast cancer patients (p=0.003).

11C



11D

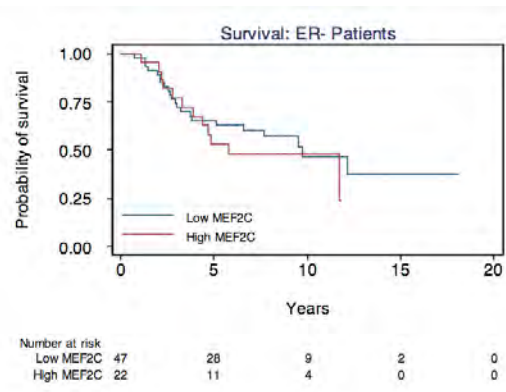


Figure 11C, 11D: Subgroup analysis: low MEF2C level is associated with shorter survival only in estrogen receptor 1 positive (ER+) (N=226; p=0.007), but not in ER- (N=69; p=0.56) patients.

Fig. 12 Immunofluorescence images of β -catenin (red), β 4 integrin (green), laminin-5 (green) and nuclei (blue) in non-malignant MCF10A colonies and in colonies of MCF10A cells expressing MEF2C shRNA. The cells have been cultured for 21 days in matrigel (scale bar=20 μ m).

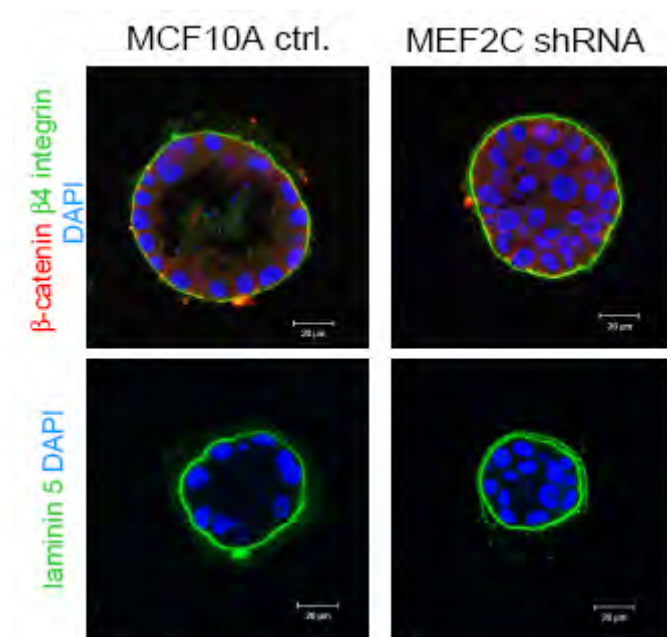


Figure. 13 Immunofluorescence images of caspase-3 (red), phalloidin (green) and nuclei (blue) in non-malignant MCF10A colonies and in colonies of MCF10A cells expressing MEF2C shRNA. The cells have been cultured for 14 days in matrigel (scale bar=20 μ m).

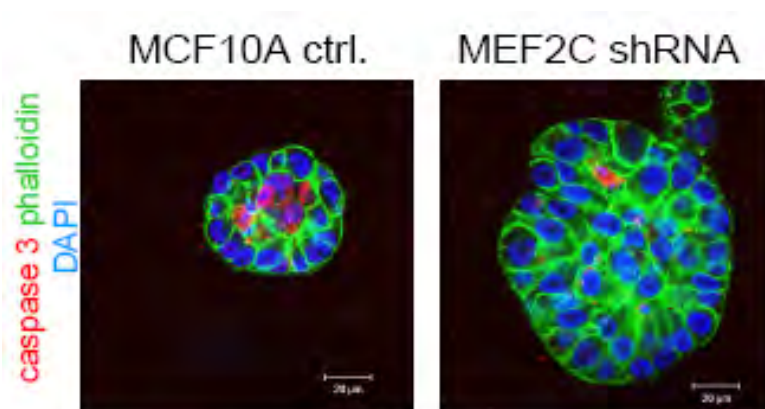
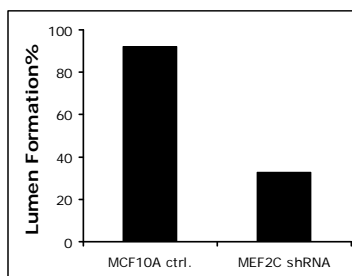


Figure 14 Bar graph quantifying lumens observed in MCF10A colonies (N=100) and in colonies of MCF10A cells expressing MEF2C shRNA (N=100) that have been cultured in matrigel for 21 days.



Extracellular Matrix Context Dictates Cell Survival

In addition to these studies on MEF2C we have begun to explore why cells encountering a matrix in three dimensions and not two dimensions exhibit such a profound enhancement of their survival phenotypes. This has led us to explore in more detail the role of ECM topology in cell survival.

Apoptosis resistance plays a key role in malignant transformation, metastasis and development of multi-drug resistance in breast cancer⁷³. In mammalian cells, growth and apoptosis programs can be switched by either promoting or preventing cell spreading⁷⁴. Cell spreading is mediated by interaction and binding of integrins in the plasma membrane to the extracellular matrix and integrin adhesion is considered to promote cell survival. Furthermore, earlier work from our lab showed that in non-spread mammary epithelial cells (MEC) grown in 3D to form acinis, cell survival is directed by $\alpha 6\beta 4$ integrin binding to laminin and requires Rac1 and NF κ B^{7,75,76}. However it is not known how non-spread single cells survive in 3D before dividing and forming multicellular structures.

The third dimension promotes survival in the absence of spreading.

To address this issue of non-spread cell survival in 3D, we generated laminin-1 coated micro-fabricated matrices with defined surface area to restrict MEC spreading while maintaining laminin-ligation of integrin receptors constant⁷⁷. Consistent with what has been previously reported for endothelial cells on fibronectin coated surfaces⁷⁴, we observed that cell spreading is also critical for MEC viability in 2D (Figure 15A and 15B). Spreading surface had to be higher than a square of 25 μ m size to exhibit similar survival rates as cells spread on unpatterned surfaces, without spreading limitations. MECs viability was also severely compromised when we plated MECs on compliant (140-400 Pascals) 2D basement membrane or laminin-1 conjugated polyacrylamide gels (PA gels) (Figure 15C) where MECs do not spread. This was in striking contrast to the continued maintenance of growth and viability observed in 2D cultures of MECs plated on basement membrane-conjugated stiff gels which support cell spreading¹⁰.

To determine whether dimensionality could account for the enhanced viability in non-spread MECs embedded within reconstituted basement membrane gels, we overlaid the non-spread MECs plated either on the micro-fabricated laminin-coated surfaces (8, 12 and 17 μ m squares) or on the soft basement membrane-conjugated PA gels with either 200 μ g/ml of reconstituted basement membrane (Matrigel) or purified laminin-1 (150 μ g/ml) (Figure 15C and 15D). In both instances, application of three dimensional laminin extracellular matrix was able to significantly rescue cell viability.

Laminin binding to $\alpha 6\beta 4$ integrin mediates spreading independent survival in the third dimension.

To further characterize the components of the extracellular matrix and its integrin ligand needed to maintain cells alive in 3D, fibronectin or collagen was applied as overlay at 150 μ g/ml each on micro-fabricated with the 8 μ m square pattern. None of those two matrices was able to restore cellular viability to non-spread MECs, suggesting that cell viability of MECs in 3D depends upon a laminin extracellular matrix (Figure 16A). The two major receptors for laminin known in MECs are integrin $\alpha 3\beta 1$ and $\alpha 6\beta 4$ ⁷⁸. We showed that integrin $\alpha 6\beta 4$ binding to autocrine laminin-5 is essential for anchorage-independent survival in a 3D matrix of mammary epithelial tumor cells⁷⁵. However, the MECs cells used in this study (MCF-10A and HMT-3522 S1) are non-malignant mammary epithelial cells. To identify the potential binding partner, we blocked integrin $\beta 1$ or $\beta 4$ receptors with function blocking antibodies for 24 hours in cells grown in 3D with a laminin overlay on micro-fabricated surfaces with a pattern of 8 μ m side length and determined effects on cell viability. Compared to cells in a 3D laminin overlay with or without IgG as controls, in these short term cultures, only blocking $\beta 4$ integrin compromised the

viability of non-spread MEC cells in 3D (Figure 16B), corroborating that spreading independent survival in 3D is mediated by $\beta 4$ integrin. To directly determine if $\beta 4$ integrin is necessary for MEC survival, we knocked down $\beta 4$ integrin using lentiviral shRNA. After validating that $\beta 4$ integrin levels were significantly reduced, viability of MECs in 3D laminin extracellular matrix was assayed. In accordance to what we saw with $\beta 4$ integrin function blocking antibodies, knocking down $\beta 4$ integrin significantly compromised the survival of 3D non-spread MECs (Figure 16C). Furthermore, to verify that survival is not merely due to more binding of integrin $\alpha 6\beta 4$ to laminin in 3D, we used HMT-3522 S1 over-expressing integrin $\beta 4$. The over-expressed protein was properly located at the plasma membrane as shown by FACS sorting in Figure 16D. By performing an integrin-laminin cross linking assay in 2D, we showed that these cells have more integrin $\beta 4$ -laminin bonds than the parental HMT-3522 S1 cell line (Figure 16E). However, over-expressing integrin $\beta 4$ in those cells did not rescue the apoptotic phenotype in 2D on soft substrate (Figure 16F). All together, these results strongly suggest that $\alpha 6\beta 4$ integrin is critical for the viability of non-spread MECs, and that viability is not driven by more integrin $\beta 4$ -laminin bonds in 3D.

Survival in the third dimension is supported by $\alpha 6\beta 4$ integrin-dependent Rac1 activation.

It is well established that binding of integrin $\beta 4$ to laminin can induce the activation of multiple signaling cascades⁷⁹. Signaling through the cytoplasmic tail of $\beta 4$ leads to anchoring-independent survival in 3D of mammary tumor cells by activation of the small GTPase Rac1⁷⁵, invasion and survival via PI 3-kinase⁸⁰ and mediates proliferation through a Ras-MAP kinase/ERK pathway⁸¹. Additionally, in non-malignant MEC grown in 3D to form spheroids, resistance to apoptosis is supported by elevated $\alpha 6\beta 4$ integrin-dependent Rac1-Pak signaling⁷⁶. However, it is unknown if Rac1 activation is involved in the initial cell survival, before the single MEC grown in 3D divides to give rise to spheroids. To investigate which $\beta 4$ integrin dependent signaling pathway is involved in survival of non-spread cells in 3D, we used pharmacological inhibitors for PI 3-kinase (LY29002), for the MEK1 and MEK2 (U0126) (leading to downstream inhibition of ERK) and for the GTPase Rac1 (NSC237766). Only the inhibition of Rac1 activation compromised viability of MECs in 3D (Figure 17A), suggesting that activation of Rac1 by integrin $\beta 4$ is responsible for the survival phenotype. To verify the role of Rac1 in survival, we assayed cells grown for 24 hours on soft polyacrylamide gels of 150 Pa in 2D and 3D for Rac1 activation. The level of active GTP-bound Rac1 was increased by a 2.5 fold in 3D non-spread MECs compared to 2D non-spread cells (Figure 17B). The direct role of $\beta 4$ integrin on Rac1 activation in MECs was verified in HMT-3522 S1 cells over-expressing $\beta 4$ integrin at the plasma membrane (Figure 17C). In these cells, Rac1 activation was increased by a 10 fold compared to control HMT-3522 S1 cells (Figure 17C). However, over-expression of the constitutively active mutant Rac1V12 in non-spread MECs did not rescue cell death in 2D, suggesting that a tight regulation of the signaling pathway induced by laminin binding to $\beta 4$ and Rac1 activation is necessary for survival (Figure 17D).

p21-activated kinase 1 activity downstream of Rac1 activation is necessary for survival in the third dimension

Rho GTPases activate signaling pathways through effector proteins⁸². The p21-activated kinase (Pak) family of serine/threonine kinases are effectors for Rac and Cdc42, and have been involved in cellular processes such as cell morphology, cell migration, survival, gene transcription, apoptosis and hormone signaling⁸³. From earlier work, we know that $\alpha 6\beta 4$ integrin activates Rac-dependent Pak1 to drive NF- κ B-dependent resistance to apoptosis in 3D mammary acini⁷⁶. We now show that levels of phosphorylated Pak (as read-out of activated Pak) are increased in 3D non-spread MECs, compared to 2D non-spread cells (Figure 17E). Apoptosis of 2D non-spread MECs was also partially rescued when

we over-expressed Pak1 WT, indicating again that Pak 1 is part of the signaling pathways promoting non-spread MEC survival (Figure 17F).

Matrix dimensionality regulates MEC survival by inhibiting MMP activity.

Because Rac has a plethora of cellular effector targets - which can either promote or inhibit cell death we wondered whether dimensionality could be restricting Rac effector actions. Consistently, we noted that non-spread MECs in 2D produced high levels of ROS and that V12Rac greatly enhanced this effect. In contrast, non-spread MECs in 3D had greatly diminished ROS levels and V12Rac only modestly increased ROS in these cells (Figure 18A). Indeed, when we treated 2D non-spread MECs with a few general ROS scavengers we observed a marked increase in cell survival (Figure 18B). Similarly, and more importantly, when we expressed a V12 Δ insert Rac which fails to interact with NADPH and therefore cannot increase NADPH-dependent ROS we were able to fully rescue the viability of 2D non-spread MECs (Figure 18B). A number of studies (reviewed in⁸⁴) have shown a direct link between ROS production and activation of MMPs. We therefore investigated whether MMP activity was different in 2D than in 3D. Indeed, MMP activity was higher in non-spread cells in 2D than in non-spread cells in 3D, and its activity was dependent on NADPH oxidase activity since NADPH oxidase inhibitor DPI decreased MMP activity in 2D (Figure 18C). Inhibition of MMP activity with pharmacological inhibitors rescued cell death in 2D (Figure 18D), and 2D conditioned media induced cell death in 3D (Figure 18E). In addition, basement membrane was absent in 2D as shown by immune-staining for Laminin-5 on non-spread cell (Figure 18E). All together, these results suggest matrix dimensionality-dependent differential Rac signaling pathway activations.

Survival in the third dimension is supported by Arf6-dependent Rac1 and Pak1 activation.

Having shown the necessity of Rac1 and Pak1 activation in the laminin- β 4 integrin dependent survival phenotype, we still do not know how exactly Rac is being activated by β 4 integrin and how Rac activity is sustained in 3D. A number of studies have shown an activation of Rac1 downstream of the GTPase Arf6 activation in the case of actin polymerization and cell migration⁸⁵⁻⁸⁹. Arf6 is a member of the Arf (ADP-ribosylation factor) Ras-related GTPase family. Arf6 is the only ArfGTPase mainly localized at the plasma membrane and is involved in membrane trafficking and actin polymerization at the plasma membrane^{2,90,91}. We therefore tested Arf6 activation in non-spread cells in 2D and 3D. MCF10A cells had low levels of endogenous Arf6. To overcome this difficulty, we created MCF10A cells stably over-expressing HA-tagged WT Arf6 by lentiviral infection. When activated Arf6 was assayed in these cells in non-spread 2D and 3D conditions, the level of Arf6 was increased by a 2 fold in 3D compared to 2D (Figure 19A), suggesting a possible activation of Rac1 by Arf6. We showed a similar activation of endogenous Arf6 in HMT-3522 S1 with higher levels of endogenous Arf6 (Figure 19B). Rac-induced survival being dependent on signaling initiated by β 4 integrin binding to laminin, we tested Arf6 activation in MECs where the signaling by β 4 integrin was abolished by over-expression of the tailless mutant of β 4 integrin. Activation of Arf6 was decreased in these cells compared to control cells with intact β 4 integrin (Figure 19C), suggesting a β 4 integrin-dependent activation of Arf6. To verify a possible involvement of Arf6 in cell survival, we tested MECs over-expressing HA-tagged WT Arf6 or the HA-tagged fast-cycling mutant Arf6 T157A⁹². Both forms of Arf6 reverted cell death of non-spread MECs in 2D to comparable levels of non-spread cells in 3D (Figure 19D). Furthermore, over-expression of the HA tagged dominant-negative mutant Arf6 T27N induced cell death of non-spread MECs in 3D (Figure 19E), clearly linking Arf6 to the signaling pathway inducing cell survival in 3D. To show that Rac1 is indeed downstream and activated by Arf6 in MECs, we assayed cells over-expressing the fast-cycling HA-tagged Arf6T157A for activated Rac1. These cells had a 1.5 fold increase in active Rac compared to control cells (Figure 19F), linking activation of Rac to activation of Arf6. We also

confirmed that Pak1 activation was under control of Arf6 by assaying for phosphorylated Pak1 in non-spread 2D and 3D cells, and over-expressing WT Arf6, the constitutively active Arf6 Q67L mutant or the dominant negative mutant Arf6 T27N. In non-spread 2D conditions, WT Arf6 and Arf6 Q67L induced Pak1 phosphorylation to comparable or higher levels of non-spread cells in 3D (Figure 19G), and in 3D non-spread conditions Arf6 T27N inhibited Pak1 phosphorylation (Figure 19G). All together these results indicate that activation of Arf6 could contribute to survival of non-spread cells in 3D, downstream of β 4 integrin and upstream of Rac1 in the signaling cascade.

Arf6 activity is tightly regulated by GAPs (GTPase activating protein) and GEFs (Guanine nucleotide exchange factors). In order to identify GAPs and GEFs involved in survival of non-spread cells in 3D, we generated cell line where various GEFs or GAPs were knocked down by shRNAs. Knocking down an involved GAP should induce survival in 2D, while knocking down an involved GEF should induce cell death in 3D. By using this approach, we were able to identify the GAP ASAP1 and the GEF GEP100 as being potentially involved in survival of non-spread cells in 3D by controlling the Arf6 activity (Figure 20A & 20B). Interestingly, recent studies showed that the EGFR-GEP100-Arf6-ASAP1 pathway is involved in invasion and metastasis in breast cancer (reviewed in ⁹³). One could speculate that dimensionality somehow modifies EGFR activation or distribution at the plasma membrane leading to activation of Arf6 in 3D and survival. If that is the case, how is dimensionality affecting plasma membrane properties?

Survival in the third dimension can be linked to decrease membrane tension.

Because we could not merely account for the enhanced viability of MECs by elevated α 6 β 4 integrin signaling or Rac activity and to try to explain why Arf6 activity could be elevated in these non-spread 3D cultures of MECs we assayed for changes in cell shape, membrane remodeling and tension. Using the membrane dye FM 1-43, we observed changes in cell sphericity, cell becoming more spheric in 3D (Figure 21A). We also noted marked modifications in actin organization between 2D non-spread cells and 3D non-spread cells (Figure 21B). To determine whether the observed changes in cell shape and actin dynamics were reflected by an altered cellular rheology we used AFM. We noted that cells became substantially softer when they were ligated in 3D as compared to cell in 2D (Figure 21C). To further investigate if decreased cell tension could affect survival of non-spread cells, cells were treated with pharmacological inhibitors of myosin (blebbistatin) or of the myosin light chain kinase (MLCK) (ML-7) and we tested cell survival in 2D. Myosins, conjugated with actin filaments, are the major cytoskeletal proteins regulating cell tension. Cells in 2D became softer when treated with the inhibitors (Figure 21D) and surprisingly, myosin and MLCK inhibition, by decreasing cell tension, indeed induced survival of non-spread cells in 2D (Figure 21E).

Based upon these data our current working hypothesis is that ligating α 6 β 4 integrin in 3D alters cell shape to reduce cell tension and induce cytoskeletal and membrane remodeling, which in turn, modify the association of membrane factors that enhance Arf6 activity. Elevated Arf6 activity thereafter further promotes membrane and actin cytoskeletal remodeling and enhances the activity of pro survival signaling including Rac. By this mechanism we predict dimensionality can significantly modify cellular behavior. We believe that we might have identified a novel 3D regulatory mechanism which we intend to understand by exploring the link between Arf6, integrin β 4, cell cytoskeleton, cell survival and dimensionality.

Figure 15

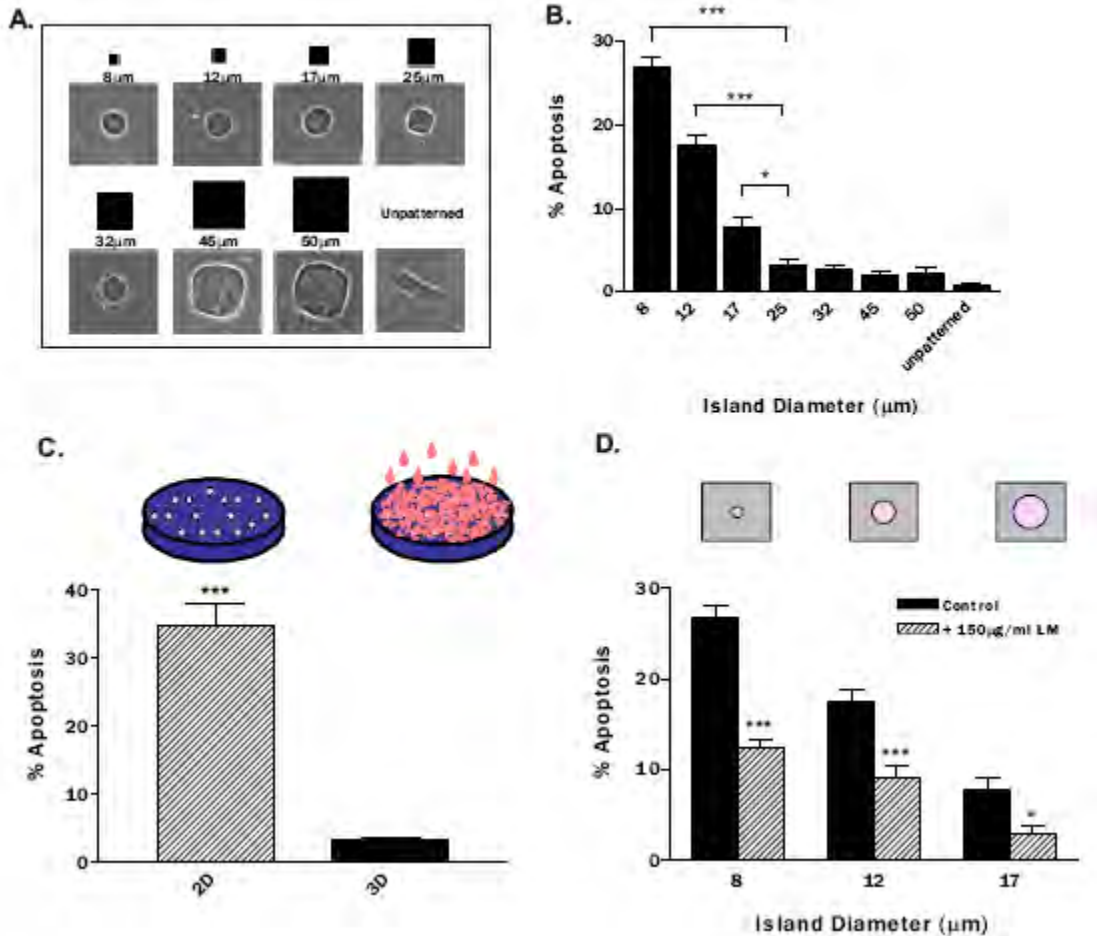


Figure 15. Matrix presentation in the 3rd Dimension promotes survival in the absence of cell spreading.

A. Spreading of MEC is enhanced when the size of 2D micropatterned substrate is increased. **B.** The rate of MEC survival increases as spreading is enhanced in 2D. **C.** Adding soluble laminin in the growth media which allows MECs to interact with matrix all around the cells, i.e. 3D, promoted MEC survival. **D.** 3D matrix presentation is essential for non-spread MEC survival on a stiff matrix.

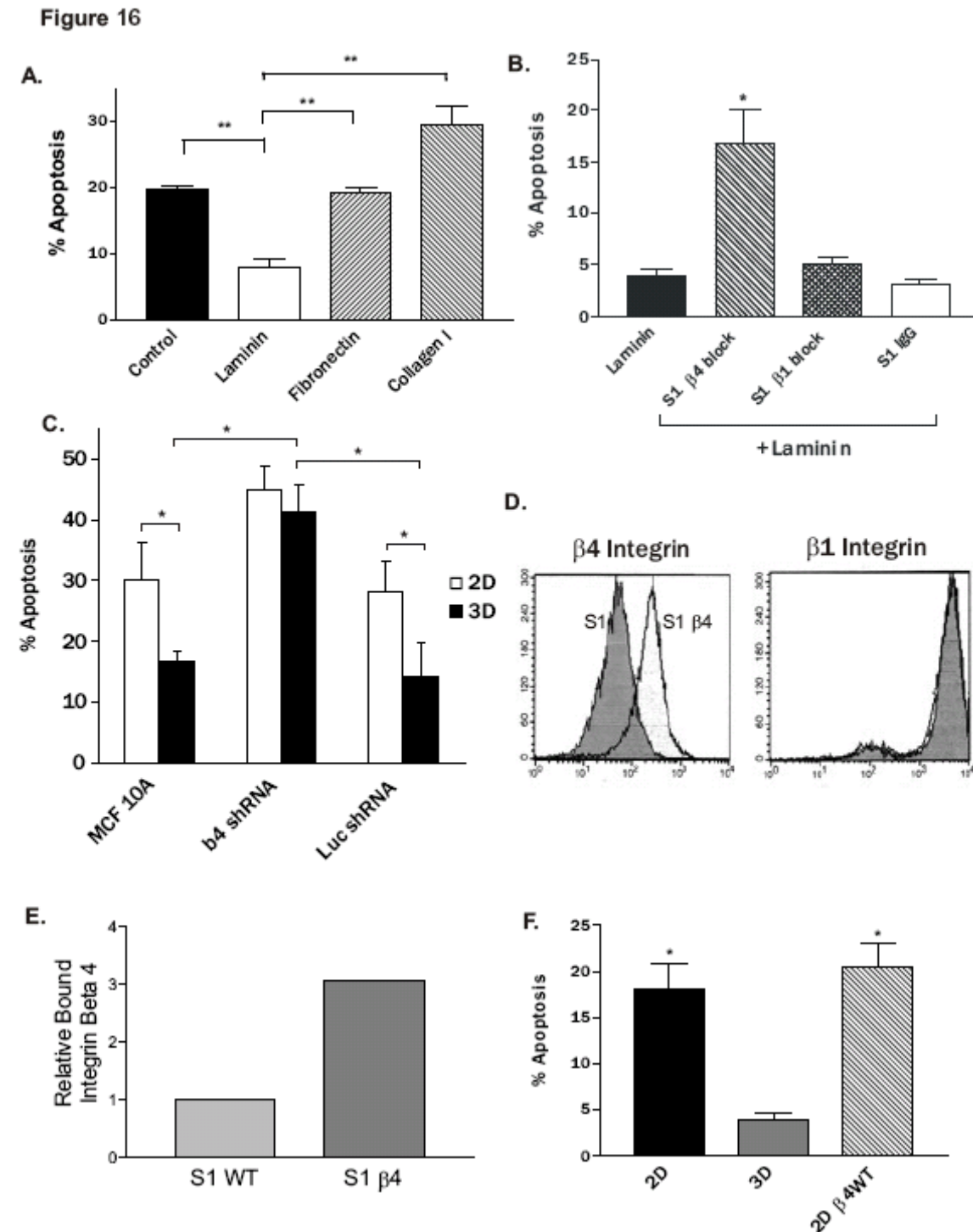


Figure 16: In the absence of cell spreading, laminin- $\alpha 6\beta 4$ integrin mediates survival in 3D. **A.** Specificity of the ligand Laminin-1 in cell shape regulated apoptosis. **B.** Laminin-1 ligation of integrin $\beta 4$ is necessary for the survival of MECs in 3D. **C.** $\beta 4$ expression is necessary for survival in 3D. **D.** Over-expressed integrin $\beta 4$ is present at the plasma membrane. **E.** MECs over-expressing integrin $\beta 4$ have more integrin-laminin bonds. **F.** Integrin $\beta 4$ over-expression fails to rescue spreading-independent survival in 2D.

Figure 17

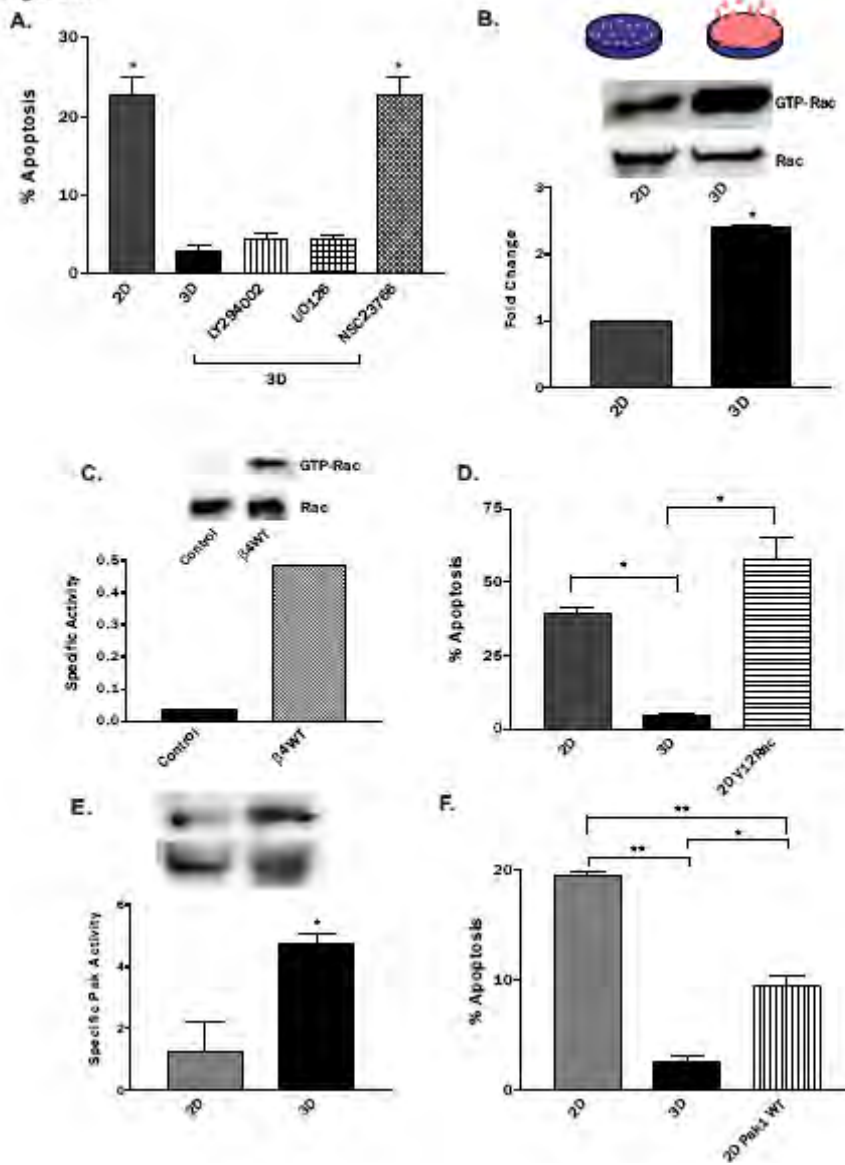


Figure 17. Laminin-ligated $\alpha 6\beta 4$ integrin activates Rac and Pak to mediate MEC survival in 3D and is necessary but not sufficient for MEC survival in 2D.

A. Rac1, but not ERK or PI3K, is necessary for survival in 3D. **B.** Rac activity is increased in MECs in 3D. **C.** Pak1 activity is increased when MECs are cultured in 3D. **D.** Constitutively active RacV12 over-expression fails to rescue survival of non-spread MECs in 2D. **E.** Pak1 over-expression partially mediates survival in 2D. **F.** Over-expression of Pak 1 WT partially rescues survival of non-spread MECs in 2D.

Figure 18

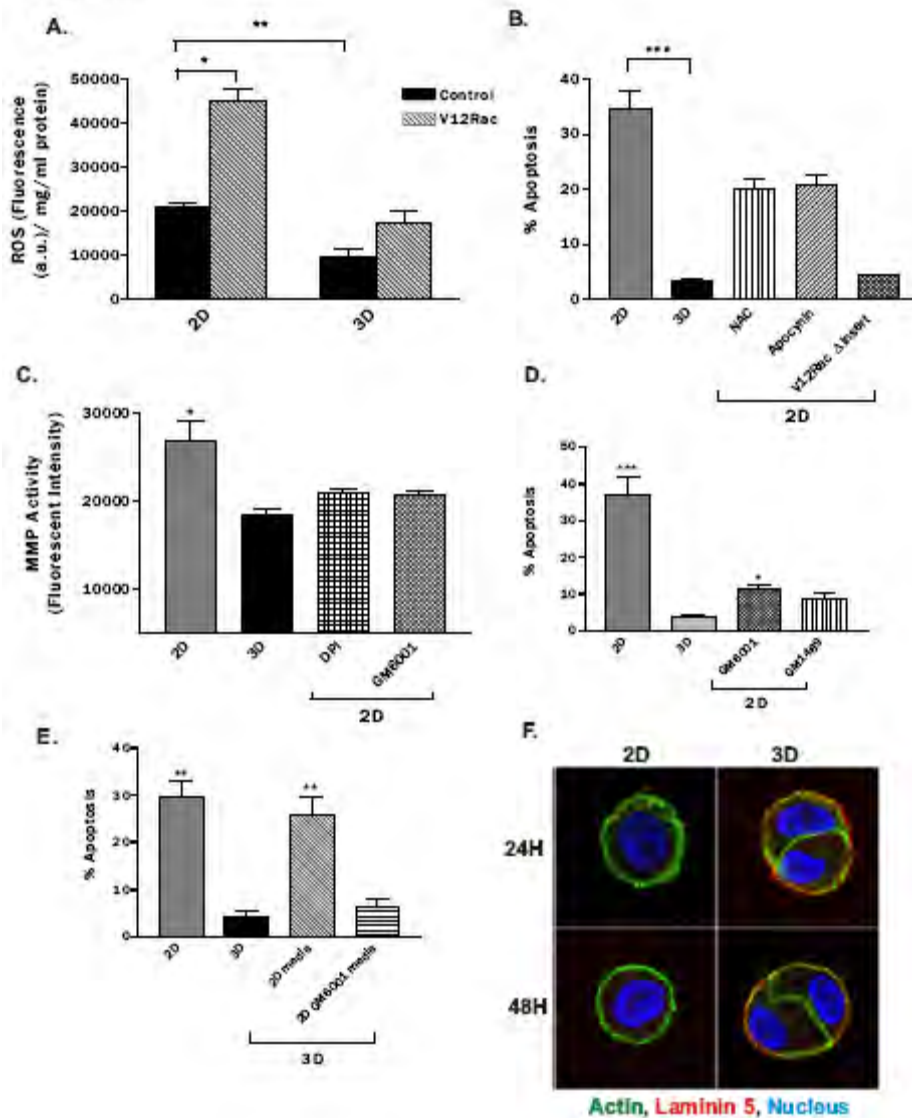


Figure 18: Matrix dimensionality regulates MEC survival by inhibiting MMP activity.

A. MEC produces less ROS in 3D. **B.** Decreasing ROS production induces MEC survival in 2D. **C.** MMP activity is decreased in 3D, and is dependent on NADPH oxidase activity. **D.** Inhibition of MMP activity through pharmacological agents permits the survival of non-spread MECs in 2D. **E.** Increased MMP activity in 3D permits MEC apoptosis. **F.** The basement membrane is absent in 2D.

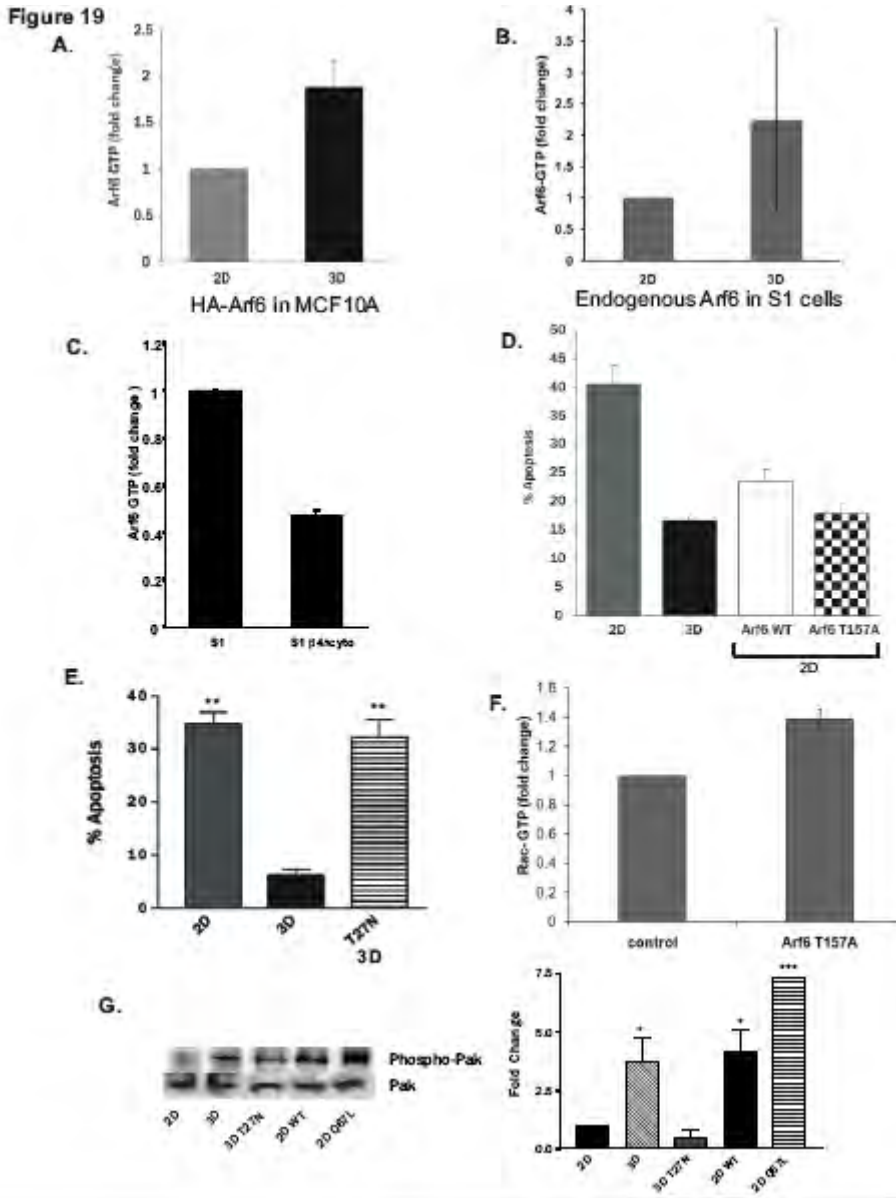


Figure 19: $\alpha 6\beta 4$ integrin-dependent Arf6 activation modulates survival of MECs in 3D by activation of Pak.

A. HA-Arf6-GTP is increased in 3D in MCF10A cells over-expressing HA-Arf6. **B.** Arf6-GTP is increased in 3D in S1 cells. **C.** Activation of Arf6 is dependent on signaling through $\beta 4$ integrin. **D.** Survival in 3D is compromised by dominant negative Arf6 T27N. **E.** Survival of MECs in 2D is promoted by Arf6 over-expression. **F.** Activation of Rac1 is downstream of activation of Arf6. **G.** Pak 1 activity is dependent on Arf6 activity.

Figure 20

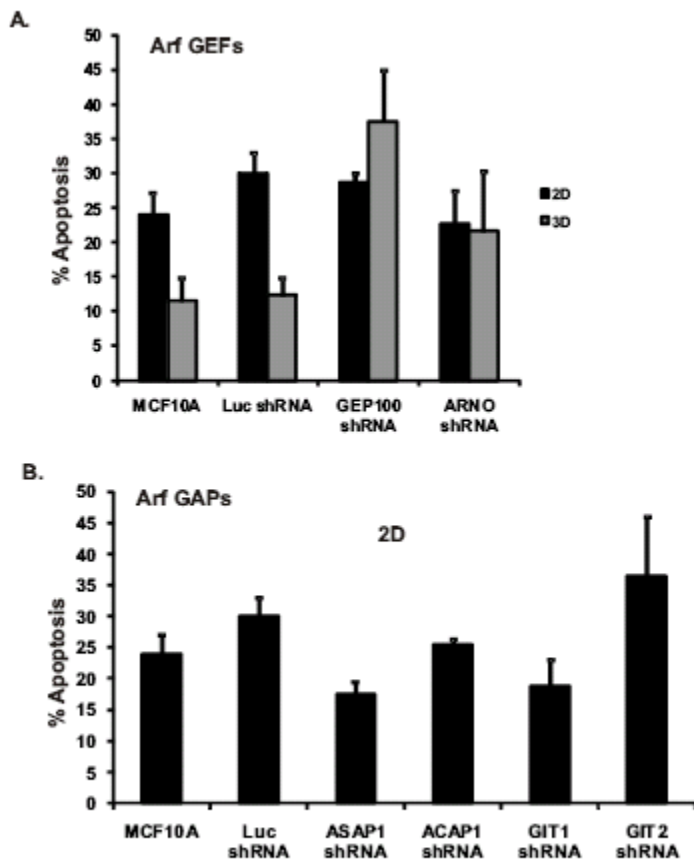


Figure 20: Potential Arf GAPs and Arf GEFs involved in cell death and survival.

A. The Arf GEFs GEP100 and ARNO seem to be necessary for survival in 3D. **B.** The Arf GAP ASAP1 seems to be involved in cell death in 2D.

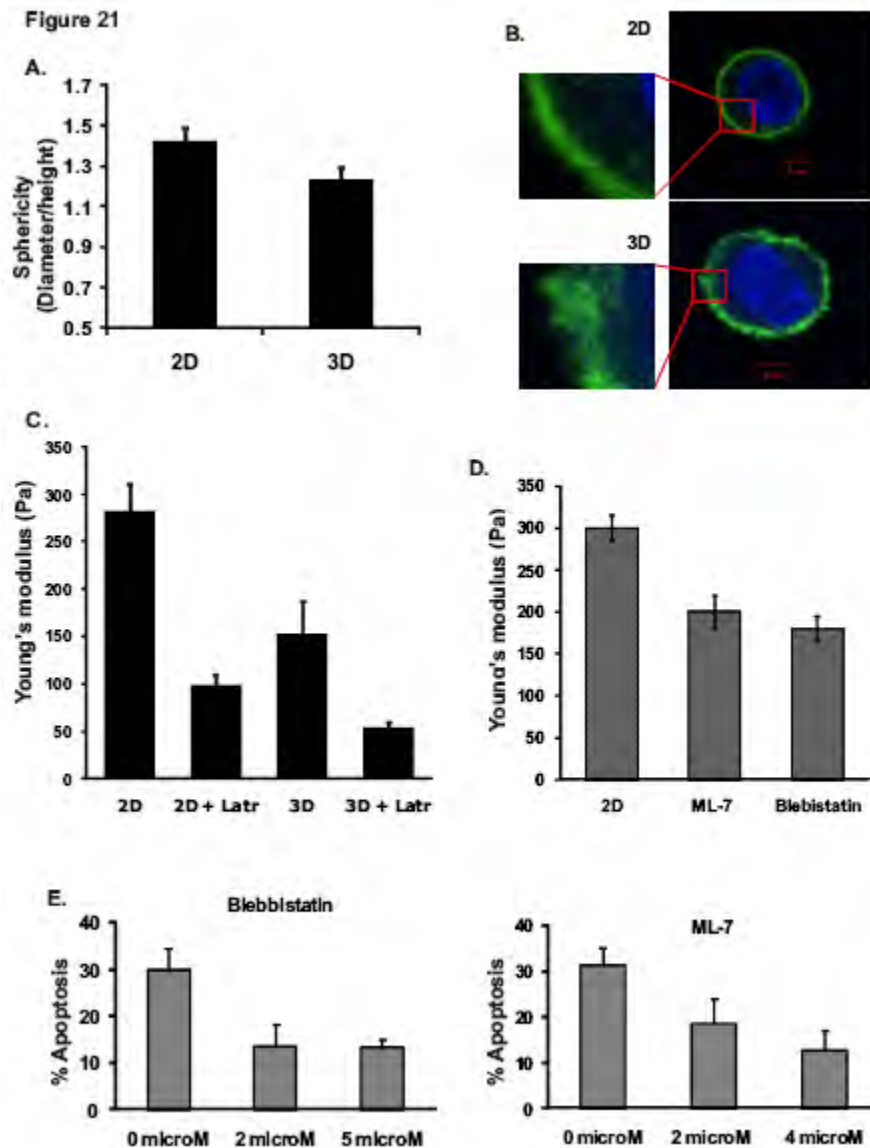


Figure 21: Cell shape and cell rheology is modulated by matrix dimensionality.

A. Non-spread MECs in 3D adopt a more spherical shape than non-spread MECs in 2D. **B.** Dimensionality modifies the actin cytoskeleton organization. **C.** Non-spread MECs ligated to ECM in 3D are softer than non-spread MECs ligated to ECM in 2D. **D.** Myosin contraction inhibitors decrease cell stiffness in 2D. **E.** Decreasing cell stiffness in 2D with myosin contraction inhibitors rescues cell death.

- j. **Finish writing and submit article** showing how matrix stiffness modulates chemotherapy response, immune receptor response and radiation responsiveness by altering stress response signaling through JNK and Rho. We anticipate that this work should be published in the next two years. (Months 6-18).

NOTE: This work was completed using the matrix conjugated polyacrylamide gels in which breast cells are overlaid with a basement membrane matrix. We hope to extend these studies in the next two years to include ECMs that can be readily remodeled and conditions in which mechanical force can be rigorously controlled. [A draft of this manuscript has been generated and is currently being revised. We hope to submit this revised article to either one of the PLOS journals or else to the Journal of Cell Science by the summer of 2011.](#)

PART B Continue to develop and characterize the biological behavior of nonmalignant and oncogenically/tumor suppressor modified breast cells in synthetic 3D model systems that recapitulate the biophysical and biochemical properties of primary and metastatic breast tumors.

- a. **Complete assessment of epithelial morphogenesis** behavior of nonmalignant and malignant breast cells in self assembling peptide polymer gels with calibrated stiffness. *(Months 8-18)* [This work has been completed using SAPs gels and has been accepted for publication in the Journal of Physical Biology.](#)

We could show that ECM stiffness modulates ECM tissue morphology and gene expression to elicit a tumor like phenotype at rigidities reaching 1000 Pascals and higher, similar to what we measured in human and mouse breast tumors.

- b. **Analyze the invasiveness** behavior of normal and MECs transformed with oncogenes and following knockdown of specific tumor suppressor genes in self-assembling peptide lattices for 3D studies with increasing stiffness with defined ECM (laminin) binding properties *(Months 8-20)* [These studies have yet to be initiated.](#)
- d. **Analyze the growth behavior** of normal and MECs transformed with oncogenes and following knockdown of specific tumor suppressor genes in self-assembling peptide lattices of increasing stiffness with defined ECM laminin binding properties. (Months 12-24) [These studies have yet to be initiated but we plan on conducting the work in this upcoming fiscal year.](#)
- e. **Analyze the survival behavior** of normal and MECs transformed with oncogenes and following knockdown of specific tumor suppressor genes in self-assembling peptide lattices of increasing stiffness with defined ECM laminin binding properties. *(Months 12-24)*. [These studies have yet to be initiated but we plan on conducting the work in this upcoming fiscal year.](#)
- f. **Analyze the apoptosis sensitivity** of normal and MECs transformed with oncogenes and following knockdown of specific tumor suppressor genes to chemotherapeutic agents (taxol, doxorubicin, etoposide), and immune receptor apoptotic agents (TRAIL, TNFalpha) and gamma radiation when embedded within self-assembling peptides lattices of increasing stiffness with defined ECM laminin binding properties. *(Months 16-24)*. [These studies have yet to be initiated but we plan on conducting the work in this upcoming fiscal year.](#)
- m. **Analyze the morphogenesis behavior** of normal and malignant MECs in HA gels of increasing stiffness. [These studies have not yet been initiated. We intend to begin these mid way through this upcoming year.](#)

- n. **Analyze the morphogenesis behavior** of normal and malignant MECs in HA gels with added rBM or laminin. (*Months 16-24*). *These studies have not yet been initiated. We intend to begin these mid way through this upcoming year.*
- o. **Analyze the growth behavior** of normal and malignant MECs in HA gels of increasing stiffness with added rBM or laminin. (*Months 12-36*). *These studies have not yet been initiated. We intend to begin these studies midway through this upcoming year.*
- p. **Analyze the survival behavior** of normal and malignant MECs in HA gels of increasing stiffness with added rBM or laminin. (*Months 12-24*). *These studies have not yet been initiated. We intend to begin these studies mid way through this upcoming year.*
- q. **Analyze the apoptosis sensitivity** of normal and malignant MECs to three commonly used chemotherapeutic agents (taxol, doxorubicin, etoposide), and two immune receptor apoptotic agents (trails, TNFalpha) and gamma radiation in HA gels with added rBM or laminin. (*Months 12-24*). *These studies have not yet been initiated. We intend to begin these studies mid way through this upcoming year.*
- r. **Analyze the invasive behavior** of nonmalignant, malignant and oncogenically primed MEC organoids in HA gels of increasing stiffness with added rBM or laminin with or without incorporated MMP cleavable conjugated collagen sequences. (*Months 18-24*). *These studies have not yet been initiated. We intend to begin these studies mid way through this upcoming year.*

Task 2: *Develop xenograft and transgenic mouse models to test whether ECM stiffness regulates apoptotic responsiveness of mammary epithelia in vivo.*

PART A. Xenograft studies to test whether ECM stiffness could regulate apoptotic responsiveness of a mammary epithelium in vivo. *These studies are being conducted in collaboration with Dr. Bernhard from the Radiation Biology Department at the University of Pennsylvania.*

- e. Based upon doses of established short-term and long-term re-growth assays **Weaver laboratory in collaboration with Werb laboratory** will then conduct xenograft assays of radiation sensitivity of tumorigenic MECs in vivo following their injection and establishment of viable, palpable tumors sub-cutaneously in nude mice based upon short-term viability effects as the end point. (*Months 6-36*). *Not yet initiated for the radiation treatment - However we have completed an analysis of chemotherapy response as related to NCoR2 status - a putative mechano force regulator of apoptosis resistance gene expression (see earlier comments and Tsai et al Nature Medicine, In Revision.*
- f. Based upon doses of established short term and long term re-growth assays **Weaver laboratory in collaboration with Werb laboratory** will conduct xenograft assays of radiation sensitivity of tumorigenic MECs in vivo following their injection and establishment of viable, palpable tumors sub-cutaneously in nude mice based upon long-term re-growth assays as an end point. (*Months 12-36*). *Not yet initiated*
- g. **Weaver laboratory will assess biocompatibility of PEG gels** injected sub-cutaneously into nude mice. (*Months 24-36*). *Not yet initiated*

- i. **Weaver laboratory in collaboration with Werb laboratory** will assess effect of radiation responsiveness of tumorigenic MECs embedded within soft versus stiff PEG gels and/or cross-linked collagen gels or collagen gels co injected with LOX expressing fibroblasts to induce collagen cross linking in vivo, injected sub-cutaneously into nude mice and assessed for short term viability as the end point. (*Months 24-36*). [Not yet initiated](#)
- j. **Weaver laboratory in collaboration with Werb laboratory** will assess effect of radiation responsiveness of tumorigenic MECs embedded within soft versus stiff self-assembling peptides and/or cross-linked collagen gels in vivo, injected sub-cutaneously into nude mice, and assessed for long term re-growth as the end point. (*Months 24-36*). [Not yet initiated](#)
- k. **Weaver laboratory in collaboration with Werb laboratory** will assess effect of radiation responsiveness of tumorigenic MECs embedded within soft versus stiff PEG gels and/or cross-linked collagen gels in vivo, injected sub-cutaneously into nude mice, and assessed for long term effects on tissue morphology as the end point. (*Months 24-36*). [Not yet initiated](#)
- l. **Weaver laboratory in collaboration with Werb laboratory** will assess effect of radiation responsiveness of tumorigenic MECs embedded within soft versus stiff PEG gels in vivo, injected sub-cutaneously into nude mice, and assessed for long term effects on gene expression markers as the end point. (*Months 24-36*). [Not yet initiated](#)
- m. **Weaver laboratory in collaboration with Werb laboratory** will assess effect of radiation responsiveness of tumorigenic MECs embedded within soft versus stiff PEG gels and/or cross-linked collagen gels in vivo, injected sub-cutaneously into nude mice, and assessed for long term effects on apoptosis resistance/stress response protein expression as the end point. (*Months 24-36*). [Not yet initiated](#)

PART B. Transgenic animal studies designed to test whether ECM stiffness could influence apoptosis regulation in vivo. These studies are being conducted in collaboration with Dr. Zena Werb.

- a. Validation of beta 1 integrin cluster mutant ES cell generation (*Months 0-4*) [Completed](#).

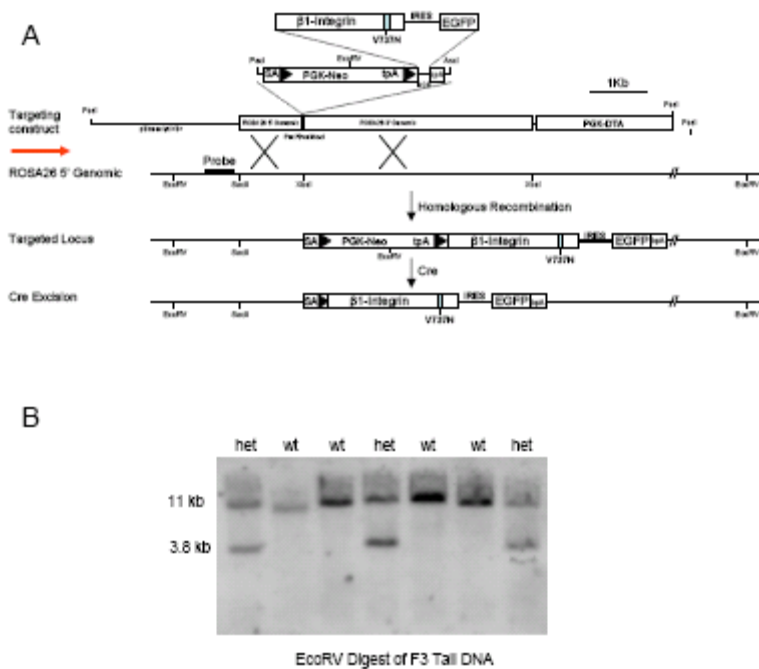
We created mice with conditional expression of a $\beta 1$ -Integrin Autoclustering Mutant by Knock-in into the Ubiquitously Expressed ROSA26 Locus. Figure 22A outlines the strategy we used to create conditional expression of the autoclustering $\beta 1$ integrin mutant in transgenic mice by gene targeting to the ubiquitously expressed ROSA26 locus. We successfully prepared the construct and were successful in targeting the gene to the ROSA26 locus in 129SV embryonic stem cells. Our transfection yield had a targeting efficiency of about 25% which is excellent and ensured success in obtaining transgenic mice expressing the target gene of interest. Accordingly, we chose several for follow up and injection into embryos.

- b. Generation of transgenic beta 1 integrin mouse model through the UCSF Cancer Center Sponsored cell center transgenic mouse resource. (*Months 4-12*) [Completed](#).

We found that several clones of transfected ES cells produced chimeric males following injection into C57BL/6 donor blastocysts. We then followed the animals and screened their progeny and were able to determine that at least 3 yielded germline transmission of the targeted allele (Figure 22B).

Figure 22. Generation of the "autoclustering" $\beta 1$ integrin mutant transgenic mouse.

A. Strategy for conditional expression of an "autoclustering" $\beta 1$ integrin mutant in a wild type $\beta 1$ integrin background by gene targeting into the ubiquitously expressed ROSA26 locus. A bicistronic mRNA coexpressing $\beta 1$ integrin with a V737N mutation in the transmembrane domain (that is predicted to increase the energy of interaction of the transmembrane domains of two closely apposed integrins) and EGFP via an internal ribosome entry site (IRES) was cloned downstream (relative to the direction of transcription from the ROSA26 locus; red arrow) of a floxed (black arrow heads) neomycin phosphotransferase expression cassette (PGK-neo tpa) in a ROSA 26 targeting construct and knocked into the wild type ROSA26 locus by gene targeting in 129SV embryonic stem cells. The presence of the neomycin expression cassette prevents expression of the bicistronic mutant $\beta 1$ integrin transgene by terminating the transcript at the polyadenylation signal tpa. Tissue specific expression of cre recombinase will excise the neomycin expression cassette (and tpa) juxtaposing a splice acceptor site (SA) upstream of the bicistronic mutant $\beta 1$ integrin transgene allowing its incorporation into a mature mRNA transcribed from the ROSA26 locus. B. Southern blot of genomic tail DNA from an F3 backcross of F2 129SVxFVB/n heterozygous transgenic male with a FVB/n female digested with EcoRV and probed with the indicated 5' probe showing heterozygotes (11kb wild type allele and 3.8kb targeted allele) and wild type littermates (11kb allele only) demonstrating predicted targeting and germline transmission of the targeted allele.



- c. Breeding and line generation of beta 1 integrin cluster mutant mouse model (*Months 12-24*) [In process.](#)

At present we are in the process of backcrossing transgenic mice carrying the allele into FVB/n mice. We are on our 5th backcross and already are at approximately 65-70% FVB background. We anticipate having viable mouse colonies to begin experimentation with by early summer 2011. To expedite our backcrossing we have begun to use speed congenics. Moreover, because many treatment studies are also conducted in the BalbC mouse background we will begin to backcross into this genetic background.

- d. Initial analysis of behavior of isolated mammospheres in 2D and 3D culture from beta 1 integrin cluster mutant transgenic mouse model (*Months 24-36*). [These manipulations have not been initiated.](#)

We have begun to assess the activity of the transgene in these mice through CRE-LOX infection of isolated fibroblasts and mammary epithelial cells. To this end we expect to conduct proof of principle experiments to determine whether elevated expression of a beta 1 integrin cluster mutant in the fibroblasts of mice would be sufficient to stiffen the tissue ECM and induce tissue fibrosis and eventually enhance tumor progression. These studies will require that the animals be backcrossed into at least 99% homogeneous background FVB or BalbC. Once we have completed our back crossing we will begin the long process of crossing our animals with inducible fibroblast specific lines including Tet regulatable FAP and FSP promoters as well as MMTV mammary epithelial specific expression so that we can examine effects on endogenous tissue behavior and tumorigenesis.

- e. Assessment of the effect of beta 1 integrin clustering on breast tissue behavior in vivo using xenograft manipulations and immortalized human mammary epithelial cells. (*Months 0-24*). [In our earlier reports we published our findings that enhancing beta 1 integrin clustering promoted tumor invasion in vitro and increased tumor size in vivo using immortalized cell lines including the MCF10AT cell line. This work was published in 2009 in Cell Journal Levental et al.](#)

We are now elaborating these studies to further experiments in vivo and in this next year will be exploiting the availability of MECs isolated from the transgenic model we generated as well as examining the intact mammary gland behavior when the transgene is induced.

- f. Characterization of the cross linking of mouse breast tissue before and during malignant transformation using biochemical analysis. (*Months 0-36*) [In Progress.](#)

We have made excellent progress towards setting up a comprehensive cross linking analysis method at our center at UCSF. Rather than using the traditional radioactive approach we have developed a new fluorescence method that has enhanced sensitivity. This is important since we will now be in a position to assay for changes in collagen cross-linking in small human biopsies. We present our data in this report to illustrate our competence with this method. In the next year we will begin in earnest to conduct cross-linking analysis on several banked mouse studies as well as on collected human breast tumor biopsies. We describe our progress to date in an earlier section of this report.

- g. Assessment of the status and effect of lysyl oxidase during breast tumorigenesis (*Months 0-18*) [Partially completed, additional studies in progress to extend the observations.](#)

In an earlier progress report 2010 (2009-2010) we reported the progress we made on studies we had conducted using the Her2/Neu mouse model and the initial very preliminary data we generated to explore effects on a more aggressive tumor model called the PyMT mouse. We have continued with

these studies and are pleased to report excellent progress towards defining the role of LOX on PyMT induced tumor initiation, progression and metastasis. We have additionally extended these results to include a very aggressive model with TGF beta receptor two knockdown. This PyMT crossed into the TGF beta receptor two knockdown recapitulates aggressive, triple negative human breast tumors. In the current report we present details of progress on the PyMT mouse studies and will report on our progress on the more aggressive model in next years report when we have made further progress. Please refer to earlier section in this report in which we discuss in detail our findings from these studies including several associated figures summarizing current findings.

- h. Assessment of the effect of increasing lysyl oxidase activity on breast transformation in vivo. (*Months 0-18*). [These results were reported as completed in an earlier report and were published in 2009 Levental et al Cell.](#)
- i. Assessment of the effect of decreasing lysyl oxidase activity on breast transformation in vivo using pharmacological inhibitors. (*Months 6-18*). [In last years report we discussed our findings on the Her2/Neu mouse model of breast cancer where we showed that LOX inhibition prevented tumor progression and reduced tumor incidence. The results were published in Cell Levental et al. 2009. We indicated that we were in the process of assessing the effect of LOX inhibition on PyMT induced tumor metastasis. These studies are still ongoing - and although we had anticipated that they would be completed by the end of this year - we have had to conduct several additional animal studies each of which takes 6-8 months. Therefore the work is still ongoing.](#)

Please see earlier section in which we discuss these studies in greater detail.

- j. Assessment of the effect of decreasing lysyl oxidase activity on breast transformation in vivo using antibody inhibition. (*Months 8-18*) [Partially completed and further studies are now in progress using additional mouse models.](#)

In last years report we summarized our findings in the Her2/Neu mouse model where we showed that inhibiting LOX activity using function blocking antibodies was a very potent inhibitor of tumor progression. Thus we have been anxious to continue with this work and extend these findings to additional breast tumor models to determine just how potent this effect could be and assess its suitability for clinical studies. However, one of the issues is obtaining sufficient quantities of antibody for experimental manipulation. To this end we have been collaborating with Giaccia's group at Stanford University to obtain access to the function blocking antibody his group developed. However, there have been quite a few delays that have prevented us from obtaining sufficient antibody to conduct our animal work. This has obviously delayed progress on these experiments. Accordingly to address this difficulty, we have offered to underwrite financially to generation of sufficient antibodies for our work. We have been assured that new antibody is forthcoming and so we should be in a position to conduct studies on our Metastasis models. Eventually we are considering alternate strategies such as siRNA mediated LOX knockdown. Towards that goal we have identified and conducted preliminary analysis on a putative siRNA for Lysyl oxidase. In addition, we have been generating a conditional LOX knockdown model - and while we successfully generated a targeting vector and were able to create ES knockout cells - and even mouse! There were problems with the mouse line that we generated and the animals were not fertile suggesting that somehow the insertion site corrupted the genome in these animals. Accordingly, this past year we re generated the ES cell lines. The first round of injections was negative which was most frustrating. However a second round of injections yielded multiple ES knockout clones. These have been carefully screened and validated using PCR before we move to generate a mouse. We are now validating these lines using southern analysis and once that has been accomplished we will be generating several mouse lines. Thus far things are advancing well and we are optimistic that we will have mouse

lines by mid summer. Our first goal will be to begin to rapidly backcross the mice as well as to validate the LOX knockdown in vivo and ensure that we have in fact created a true transgenic that transmits the genotype through the germ line. After that we will begin in earnest to conduct studies aimed at exploring the importance of LOX expression in a tissue specific AND cell line specific fashion. Something we have not been able to accomplish using either pharmacological OR LOX inhibitory antibody approaches.

- k. Assessment of the effect of circulating lysyl oxidase on breast tumor metastasis in vivo (*Months 12-36*). Partially completed. In our earlier report we summarized preliminary data which showed that inhibiting LOX using pharmacological inhibitors prevented lung metastasis in the PyMT mouse model.

This past year we have been able to confirm these results and are conducting additional studies to explore this phenotype further. In addition, we have initiated new studies to explore whether LOX inhibition will prevent lung metastasis in a very aggressive tumor type that recapitulates the tgfbeta receptor two mutant/knockdown phenotype of triple negative human breast cancer. Studies are now under way with the Moses group to assess the interplay between LOX mediated collagen cross linking and TGF beta and tumor metastasis. We are also interested in exploring molecular mechanisms. Please refer to earlier section of this report in which these studies have been discussed in more detail.

- l. Assessment of the biophysical properties of COLA mutant mice which fails to turn over collagen I due to a mutation in its MMP9 recognition site using shear rheology (*Months 24-36*). These studies have not been initiated.
- m. Assessment of the biophysical properties of the OS mouse which fails to assemble proper collagen bundles. (*Months 24-36*) These studies have not been initiated.
- n. Assessment of the effect of increasing collagen stiffness on breast tissue behavior and response to therapy ex vivo using collagen generated from the COLA mouse (*Months 24-36*) These studies have not been initiated.
- o. Assessment of the effect of decreasing collagen stiffness on breast tissue behavior and response to therapy ex vivo using collagen generated from the OS mouse. (*Months 24-36*). These studies have not been initiated.

Task 3: Build a computational model that can predict how changes in ECM compliance could influence integrin-dependent apoptosis responsiveness of mammary epithelia and query this model with clinical data.

Incorporate mechanical force values and assumptions into the basic adhesion model. These studies are to be conducted in collaboration with Dr. Hammer from the University of Pennsylvania Bioengineering Department.

- a. Amend basic cell adhesion model published in PLOS Computational - Paszek et al 2009 to incorporate force parameters. (*Months 28-36*) These studies are still in progress.
- b. Test mechano-adhesion model and compare theoretical values with experimental data obtained using cell culture model. (*Months 24-36*) These studies are close to completion and we anticipate in the next year we will be able to write and submit an article for publication.

- c. Adjust mechano-adhesion model to incorporate experimental data. (*Months 24-36*) Not yet initiated.

PART D. Initiate modeling studies using micro array data sets from the cell culture models.

- a. Isolate RNA from MECs within a 3D matrix with varying matrix compliances. (*Months 0-12*) Not yet initiated.
- b. Purify and prepare samples for micro array analysis. (*Months 0-12*) Not yet initiated.
- c. Generate micro array data sets from samples of MECs in 3D matrices of varying compliances. (*Months 12-18*) Not yet initiated.
- d. Conduct statistical analysis of micro array data sets generated from MECs in 3D matrices of varying compliances. (*Months 18-24*) Not yet initiated.
- e. Conduct bioinformatics analysis of micro array data sets generated from MECs in 3D matrices of varying compliances. (*Months 18-24*) Not yet initiated.
- f. Verify validity of micro array analysis by RT-PCR or real time PCR of 10 target genes. (*Months 24-36*) Not yet initiated.

PART E. Initiate pilot studies to analyze micro array data sets and clinical samples from neoadjuvant breast cancer clinical trial data using a simple model generated using gene data from culture systems. These studies are to be conducted in collaboration with Breast Surgeons Drs. Esserman and Hwang and Breast Pathologist Dr. Yunn Yi Chen from the University of California San Francisco.

- a. Select clinical samples to be examined in collaboration with Drs. Esserman and Hwang. (*Months 6-18*) We have been working closely with Drs Hwang and Esserman with consultation through the UCSF Cancer Center Pathology core and Alfred Au as well as Yunn Yi Chen to identify patient samples and collect these for analysis. In addition, last year we secured an IRB approval for a protocol which we have just gotten renewed for another year.

In the next year we will continue to acquire patient samples for this study.

- b. Obtain micro array data sets from clinical samples. (*Months 12-18*) In process. We have included some of these data analysis in an article that is now in revision for Nature Medicine.
- c. Conduct statistical analysis of clinical micro array data sets. (*Months 12-24*) In process.
- d. Conduct bioinformatics analysis of clinical micro array data sets. (*Months 12-36*). Not yet initiated.
- e. Test predictability of N-CoR2 gene signature in micro array data sets. (*Months 24-36*) Partially completed. We have completed initial analysis using publically available data sets and some of these data were included in the Tsai et al., Revised Nature Medicine article.

In this next year we intend to expand our analysis to include new publically available data sets as well as to access the data sets available through the UCSF SPORE program.

- f. Secure clinical biopsy specimens for experimental validation. (*Months 24-36*) These studies are partially completed. In the past year we have made encouraging progress towards securing these specimens and have assembled blocks for subsequent analysis.
- g. Target assessment of tractable biomarkers from the N-CoR2 signature using immunohistochemistry and/or in situ analysis. (*Months -30-36*). Not yet initiated.
- h. Begin to write IRB with Dr. Van Der Tier and Esserman so that we can incorporate the N-CoR2 gene therapy response signature into the I-SPY II study to determine if N-CoR2 gene signature can be used to predict therapeutic response to targeted therapies including some of the new generation kinase inhibitors as well as TRAIL Agonists and HDAC inhibitors. Completed and each year this task is completed through securing IRB renewals. Thus, the protocol has now been successfully renewed for another year.

REPORTABLE OUTCOMES

PUBLICATIONS

1. Lopez, J.I., Kang, I., You, W.K., MacDonald, D. and Weaver V.M. In Situ Force Mapping of Mammary Gland Transformation. J Integrative Biology, 2011, Resubmitted. **The final submitted article has been attached to the current report. NOTE: We refer to this in the text of this report as ATTACHMENT 1. Figures referred to are as per the figure number in the article.**
2. Miroshnikova, Y.A., Jorgens, D.M., Spirio, L., Auer, M., Sieminski, A.L., Weaver V.M. Engineering strategies to recapitulate epithelial morphogenesis within synthetic 3 dimensional matrix with tunable mechanical properties. J Physical Biology, 2011, In Press. **The uncorrected galley proofs have been attached to the current report. NOTE: We refer to this in the text of this report as ATTACHMENT 2. Figures referred to are as per the figure number in the article.**
3. Tsai K.K.C. Chatterjee, C., Su, J.J.M. Main, S., Werner, M.E., Jonathan N. Lakins, and Weaver V.M. N-CoR2 induces therapy resistance in tumors by repressing apoptosis amplification. Nature Medicine, In Revision. **The final article will be attached to next years report - attached to the current report is the version that was resubmitted and went out to the reviewers at Nature Medicine in late December 2010. NOTE: We refer to this in the text of this report as ATTACHMENT 3. Figures referred to are as per the figure number in the article.**
4. Gilbert, P., Mouw, J., Unger, M., Lakins, J.N., Gbegenon, M.K., Clemmer, V., Benezra, M., Feldman, M.D., Boudreau, N., Welm, A.L., Tsai, K.K.C., Weber, B., and Weaver, V.M. HoxA9 regulates BRCA1 expression to modulate mammary tissue growth and survival. J Clin Invest., 120:1535-50, 2010. PMID: 2860938. **The final published version has been attached to the current report. ATTACHMENT 4.**
5. Cohet, N., Stewart, K.M., Mudhasani, R, Asirvatham, A.J., Mallappa, C., Imbalzano, K.M., Weaver, V.M., Imbalzano, A.N., and Nickerson, J.A. SWI/SNFQ1 Chromatin Remodeling Enzyme ATPases Promote Cell Proliferation in Normal Mammary Epithelial Cells. J Cell Physiol. 223:667-78, 2010. PMID: 20333683. **The final published version has been attached to the current report. ATTACHMENT 5.**

6. Brown, X.Q., Bartolak-suki, E., Williams, C., Walker, M.L., Weaver, V.M., and Wong, J., Effect of substrate stiffness and PDGF on the behavior of vascular smooth muscle cells: implications for atherosclerosis, *J. Cell. Phys.* 225:115-22, 2010 PMID: 2920297. **The final published version has been attached to the current report. ATTACHMENT 6.**
7. Egeblad, M., Rasch, M.G., Weaver, V.M. Dynamic interplay between the collagen scaffold and tumor evolution. *Curr. Opin. Cell Biol.* 22:697-706, 2010 PMID: 2948601. **The final published version has been attached to the current report. ATTACHMENT 7.**
8. Frantz, C., Stewart, K.M., Weaver, V.M. The ECM at a Glance. *J Cell Sci.*, 123:4195-4200 2010 PMID: 2995612. **The final published version has been attached to the current report. ATTACHMENT 8.**
9. Yu, H., Mouw, J.K., Weaver, V.M. Forcing Form and Function: Biomechanical Regulation of Tumor Evolution. *Trends in Cell Biol.* 21:47-56 2011 PMID: 3014395. **The final published version has been attached to the current report. ATTACHMENT 9.**
10. Dvorak, H.F., Weaver, V.M., Tlsty, T.D. and Bergers, G. Tumor Microenvironment and Progression. *J Surgical Oncology* 2010, In Press. **The final published version has been attached to the current report. ATTACHMENT 10.**

ABSTRACTS ATTACHMENT 11.

1. Yu, H. and Weaver, V.M. Collagen remodeling and tissue mechanics at different mammary tumor development stages. AACR annual meeting, April 17th-21st 2010.
2. Lopez, J.I., DuFort, C., Yu, H., Kang, I., Acerbi I., Hwang, S., Au, A., and Weaver, V.M. Force Characterization of Tissue from Normal, Pre-invasive and Invasive Breast Cancer. BMES annual meeting, October 6th -9th 2010.
3. Lopez, J.I., Kang, I., You, W.K., MacDonald, D. and Weaver, V.M. *In Situ* Force Mapping of Breast Tissue Transformation. BMES annual meeting, October 6th -9th 2010.
4. Cassereau, L., Lopez, J.I., Weaver, V.M. The Interplay Between Three Dimensional Microenvironment and Breast Cancer Invasion. BMES annual meeting, October 6th -9th 2010.
5. Acerbi, I., Au, A., Lopez, J., DuFort, C., Hwang, H., Weaver, V.M. Cancer in Human Mammary Gland Shows Greatest Stiffness on Tumor Edge. ASCB annual meeting, Dec 11th-15th 2010.
6. Lopez, J.I., Miroshnikova, Y., Cassereau, L., Lakins, J., Weaver, V.M. $\alpha 5\beta 1$ Integrin-Fibronectin interactions mediate force response of cells to the microenvironment. ASCB annual meeting, Dec 11th-15th 2010.
7. Frantz, C., Friedland, J., Lakins, J., Lopez, J.I., Chernoff, J., Schwartz, M., Santy, L.C., Alcaraz, J., Chen, C., Boettiger, D., Weaver, V.M. Deconstructing the 3rd Dimension: How matrix dimensionality promotes survival. ASCB annual meeting, Dec 11th-15th 2010.
8. Cassereau, L., Lopez, J. I., Weaver, V. M. The Interplay Between Three Dimensional Microenvironment and Breast Cancer Invasion. ASCB annual meeting, Dec 11th-15th 2010.

9. Miroshnikova, Y.A., Jorgens, D.M., Auer, M., Spirio, L., Sieminski, A.L., Weaver V.M. Engineering strategies to recapitulate epithelial morphogenesis in synthetic 3 dimensional matrix with tunable mechanical properties. ASCB annual meeting, Dec 11th-15th 2010.

C. Oral Presentations Meetings Major Symposia and Mini Symposia

1. Weaver, V.M., Invited Symposium Speaker, "Forcing Transformation and Metastasis", First Annual NCI Physical Sciences - Oncology Network' Meeting, Washington, DC 4/07/2010
2. Weaver, V.M., .Invited Symposium Speaker, "Mechanics, Malignancy and Metastasis", Meet The Expert Sunrise Session, AACR 101st Annual Meeting 2010, Washington, D.C. 4/18/2010
3. Weaver, V.M., Invited Symposium Speaker, "Mechanics Meet Morphogenesis and Malignancy", Disease Microenvironment and Tumor Progression, 2nd EMBO Conference on Cellular Signaling and Molecular Medicine, Black Forest, Germany, 5/25/2010
4. Weaver, V.M., Invited Session Speaker, Gradients and Flow of Soluble Factors in the Tumor Microenvironment, "Mechanical Context and Tumor Progression", Workshop, NCI/TMEN Gradient Workshop, Bethesda, Maryland, 5/27/2010
5. Weaver, V.M., Invited Symposium Speaker, Metastasis and the Matrix, "The Force Journey of a Tumor Cell", Joint MRS-AACR Conference, Philadelphia, PA, 9/14/2010
6. Weaver, V.M., Invited Session Speaker, "The Force Dialogue of a Tumor Cell", UCSF/UCB Bioengineering Conference, UCSF/UCB Graduate Group in Bioengineering Fall 2010 Group Conference, UCSF/UCB , South Lake Tahoe, 9/24/2010
7. Weaver, V.M., Invited Symposium Speaker, "Sweet and Slimy Forces Regulate Integrin Adhesions", Conference on Cell Adhesion in Cancer, University of Missouri-Columbia, Columbia, MO, 10/18/2010
8. Weaver, V.M., Yaswen, P. and Werb Z. Invited Session Presenter, NIEHS/NCI Breast Cancer Meeting, Environmental Forces Regulate Breast Cancer, Susceptibility, New York, NY, 11/16/2010
9. Weaver, V.M., Invited Symposium Speaker, "The Interplay Between Force and Cancer", Asia Pacific Congress on Pancreas and Biliary Tract Cancer in Conjunction with the 14th Annual Meeting of the Taiwan Cooperative Oncology Group, 11/20/2010
10. Weaver, V.M., Invited Symposium Speaker, "Sweet and Slimy Forces Regulate Tumor Phenotype & Tissue Structure", 50th ASCB Annual Meeting, Philadelphia, PA, 12/11/2010
11. Weaver, V.M., Invited Symposium Speaker, "Force and Death Resistance: Implications for Tumor Therapy", Special Interest Subgroup on Epigenetics of Cancer, 50th ASCB Annual Meeting, Philadelphia, PA, 12/11/2010
12. Weaver, V.M. Invited Session Speaker, "Forcing Tumor Progression and Metastasis", "Session 5: Matrix, Stroma, and Metastatic Sites", NCI2011 Winter TMEN, Meeting, Bethesda, MD, 2/16/2011

W81XWH-05-1-330

Principal Investigator: Weaver, Valerie M. Ph.D.

13. Weaver, V.M., Invited Symposium Speaker, “Cell and Tissue Mechanics and Modeling – AFM and Rheology, Small to Tissue Scale Session”, The Force Journey of a Tumor Cell, Biophysical Society Meeting 2011, Baltimore, MD, 3/05/2011
14. Weaver, V.M., Invited Symposium Speaker, “Session 4: Tumor Cell and Stroma Therapeutics”, “Frontiers in Cancer Research and Therapy, "Forcing Tumor Progression and Metastasis”, Nobel Forum, Karolinska Institutet, Stockholm, Sweden, 3/10/2011
15. Weaver, V.M., Symposium Speaker, Session on Cell in Context. Sweet and Slimey Forces Regulate Tumor Progression, Max Planck Mechanobiology Conference, Dresden, Germany, 3/23/2011

D. Invited Institutional Presentations:

1. Weaver, V.M., “Forcing Tumor Progression and Metastasis”, Department of Bioengineering, Invited Seminar Speaker, University of Pittsburgh, Pittsburgh, PA., 4/22/2010
2. Weaver, V.M., The Force Journey of a Tumor, UCSD Department of Bioengineering, Invited Seminar Speaker, San Diego, CA, 4/30/2010
3. Weaver, V.M., Forcing Form and Function, Invited Retreat Speaker UCSF Helen Diller Family Comprehensive Cancer Center Retreat, Mill Valley, CA, 5/04/2010
4. Weaver, V.M., Force, Tissue Homeostasis and Malignancy, National Institute of Cancer Research Invited Institutional Speaker Visiting Scientist, National Health Research Institute, Taiwan, 11/24/2010.
5. Weaver, V.M., The force journey of a tumor, Cancer Biology & Genetics Research, Invited Seminar Speaker (CBG-RSS), Sloan Kettering Medical School, Department of Oncology New York, NY, 12/02/2010
6. Weaver, V.M., “The Force Journal of a Tumor Cell”, Florida International University, Department of Biological Sciences Invited Seminar Speaker, Miami, FL, 1/30/2011.
7. Weaver, V.M. “The Force Journey of a Tumor”, UCSD Department of Cell and Developmental Biology Invited Seminar Speaker, San Diego, CA, 2/07/2011.
8. Weaver, V.M., "Tissue Context and Treatment Resistance in Breast Tumors", Joint PSOC-ICBP Meeting, Invited Session Speaker, Berkeley, CA, 3/16/2011.
9. Weaver, V.M., "The Force Dialogue of a Tumor Cell", UCSF Special Conference on the Biophysics of Cancer, Mission Bay Campus, Helen Diller Comprehensive Cancer Center, San Francisco, CA, 3/18/2011.

F. Student Matriculation/Ph.D. Degrees

Ryan Giles, Masters Degree Bioinformatics UCSF 2011

F. Extramural Funding Acquired due to funding from the current award

1. P50 CA 58207 (van't Veer) 5/1/2010 – 4/30/2011 Effort as required

W81XWH-05-1-330**Principal Investigator:** Weaver, Valerie M. Ph.D.

NIH/NCI SPORE (Pilot Project PI)

\$23,000

Risk to Malignancy and Immune and Collagen Status

The major goals of this project are to assess functional links between immune infiltrate, collagen status and breast tumor risk and progression in primary fresh human breast specimens.

2. 1U01 ES019458-01 (Werb) 7/1/2010 – 6/30/2015 0.6 calendar
 NIH/NCI (Collaborator) \$95,000
 Environmental Effect on the Mammary Gland across the Lifespan

The major goal of this program is to determine the susceptible times in breast developments and how they are affected by environmental stressors.

3. R01 (Moses) 4/1/2011 – 3/31/2016 1.2 calendar
 NIH/NCI (Weaver: Co-PI) \$65,000
 TGF- β Suppression and Promotion of Mammary Carcinomas

The major goal of this project is to study the role of TGF beta on mammary tumor metastasis.

4. R01CA140663-01A2 (Parvin) 4/1/2011 – 3/31/2015 1.2 calendar
 NIH/NCI (Weaver: Co-PI) \$70,000
 High Content Representation and Association of 3D Cell Culture Models

The major goal of this study is to apply new quantitative strategies to clarify the molecular mechanisms whereby mechanical force could regulate malignant transformation.

Progress Summary and Conclusions

In this past fiscal year of year one of our no cost extension we successfully completed the work for, summarized findings and submitted studies for several peer reviewed publications dealing with the interplay between tissue tension - and in particular ECM stiffness and breast tumor progression and metastasis. Several additional manuscripts have been accepted and other articles directly relating to treatment resistance are in their second round of revision or are undergoing additional peer review. We have managed to use research findings generated through studies funded by this Scholar Award to obtain extramural NIH/NCI funding and have initiated several research collaborations with a focus on breast cancer and environmental risk factors as well as clinical translation (see above). Over the past year we have given over two dozen invited formal presentations at National and International Conferences and through invitations to research institutions and universities. We have also successfully assisted another student to complete their academic training with completion of a Masters degree in Bioinformatics from UCSF.

Experimentally we have continued to expand the scope of our analysis of the relevance of tissue tension on tumor progression through a series of studies to examine effects on tumor metastasis using several existing breast tumor models. These studies demonstrated that tissue tension primarily mediated through ECM remodeling and cross-linking significantly regulates not only primary tumor evolution but also breast tumor metastasis. Preliminary findings suggest that an altered ECM could promote tumor aggression by altering immune function and promoting tumor inflammation through modulation of chemokines and cytokines. Moreover, we found that reducing ECM tension also restores vascular perfusion of the tumor suggesting one potential mechanism whereby tissue tension promotes aggression could be by inducing tumor hypoxia. Studies in the upcoming year will focus on exploring these

mechanisms in more detail. In this regard, we have initiated collaborations with Dr. Harold Moses at Vanderbilt who has been studying how loss of TGF beta receptor two function in breast tumor epithelium promotes tumor aggression and metastasis through recruitment of myeloid progenitor cells. We found that myeloid progenitor cells express high levels of TGF beta. Because TGF beta directly regulates LOX expression we are in the process of exploring the functional importance of LOX mediated collagen cross linking and stiffness to this aggressive tumor type. Fortunately, we were able to secure NIH funding to partially fund this new work (see above).

We have made additional progress towards assessing the clinical relevance of ECM remodeling and stiffening. We have secured IRBs to explore the interplay between collagen remodeling, tumor inflammation and tumor progression and have begun to collect surgical discard tissue for mechanical analysis. Preliminary studies indicate that analogous to mouse cancer - human breast tumors are significantly stiffer than normal tissue. More exciting however is our observation that non progressive breast lesions, while stiffer than normal are not nearly as stiff as invasive breast lesions. In the next year we will be examining the status of the collagens in these tissues using an array of imaging as well and biochemical assays including a new cross-linking assay we set up recently in the laboratory. Thus, we have set up and validated a collagen cross-linking assay in our laboratory using HPLC which can now be used not only for our animal studies but also to assess the relevance of collagen cross-linking in human breast tumor risk to malignancy and tumor progression. It is our hope that this assay could assist with identifying high risk populations of women and stratify patients into groups with poor versus good prognosis.

To expedite our studies we have in addition, successfully generated a novel animal model in which beta 1 integrin is induced to cluster and assemble mature focal adhesions. Because studies using human cell lines indicated that clustering of beta 1 integrin promotes tumor progression and that ECM tension promotes tumorigenesis by inducing beta 1 integrin clustering and focal adhesion assembly we expect that this mutant will be a strong tumor promoter. The availability of this model will provide the breast cancer research community with an important new tool with which they can explore the interplay between tissue tension and integrin-dependent signaling in tumor progression and treatment responsiveness. In addition to this animal model we have also made excellent progress towards generating a second valuable LOX knockout model which should reduce ECM tension. This model will allow a careful examination of the importance of ECM stiffness in breast tumor progression and metastasis.

With respect to treatment responsiveness we have identified a novel molecular mechanism mediated through NCoR2 that induces treatment resistance in breast tumors by regulating IRF-1 dependent stress gene expression. The NCoR2 treatment resistance mechanism we identified and explored in our studies illustrates the importance of eliciting a field effect through gene amplification to efficiently treatment/eradicate breast tumors in situ. The clinical relevance and translation utility of an NCoR2 gene expression signature we generated is something we are now in the process of exploring in collaboration with the UCSF Breast Cancer Spore and with colleagues from the Huntsman Cancer Institute.

REFERENCES

- 1 Taylor, S. T., Hickman, J. A. & Dive, C. Epigenetic determinants of resistance to etoposide regulation of Bcl-X(L) and Bax by tumor microenvironmental factors. *J Natl Cancer Inst* **92**, 18-23 (2000).
- 2 Zahir, N. & Weaver, V. M. Death in the third dimension: apoptosis regulation and tissue architecture. *Current opinion in genetics & development* **14**, 71-80 (2004).
- 3 Unger, M. & Weaver, V. M. The tissue microenvironment as an epigenetic tumor modifier. *Methods in molecular biology (Clifton, N.J)* **223**, 315-347, (2003).
- 4 Truong, T., Sun, G., Doorly, M., Wang, J. Y. & Schwartz, M. A. Modulation of DNA damage-induced apoptosis by cell adhesion is independently mediated by p53 and c-Abl. *Proc Natl Acad Sci U S A* **100**, 10281-10286 (2003).
- 5 Lewis, J. M., Truong, T. N. & Schwartz, M. A. Integrins regulate the apoptotic response to DNA damage through modulation of p53. *Proc Natl Acad Sci U S A* **99**, 3627-3632 (2002).
- 6 White, D. E. *et al.* Targeted disruption of beta1-integrin in a transgenic mouse model of human breast cancer reveals an essential role in mammary tumor induction. *Cancer Cell* **6**, 159-170, (2004).
- 7 Weaver, V. M. *et al.* beta4 integrin-dependent formation of polarized three-dimensional architecture confers resistance to apoptosis in normal and malignant mammary epithelium. *Cancer Cell* **2**, 205-216. (2002).
- 8 Krouskop, T. A., Wheeler, T. M., Kallel, F., Garra, B. S. & Hall, T. Elastic moduli of breast and prostate tissues under compression. *Ultrason Imaging* **20**, 260-274. (1998).
- 9 Paszek, M. J. & Weaver, V. M. The tension mounts: mechanics meets morphogenesis and malignancy. *J Mammary Gland Biol Neoplasia* **9**, 325-342 (2004).
- 10 Paszek, M. J. *et al.* Tensional homeostasis and the malignant phenotype. *Cancer Cell* **8**, 241-254, (2005).
- 11 Grinnell, F. Fibroblast biology in three-dimensional collagen matrices. *Trends Cell Biol* **13**, 264-269. (2003).
- 12 Bershadsky, A. D., Balaban, N. Q. & Geiger, B. Adhesion-dependent cell mechanosensitivity. *Annu Rev Cell Dev Biol* **19**, 677-695 (2003).
- 13 Geiger, B., Bershadsky, A., Pankov, R. & Yamada, K. M. Transmembrane crosstalk between the extracellular matrix--cytoskeleton crosstalk. *Nat Rev Mol Cell Biol* **2**, 793-805 (2001).
- 14 Samani, A., Bishop, J., Luginbuhl, C. & Plewes, D. B. Measuring the elastic modulus of ex vivo small tissue samples. *Phys Med Biol* **48**, 2183-2198 (2003).
- 15 Butcher, D. T., Alliston, T. & Weaver, V. M. A tense situation: forcing tumour progression. *Nat Rev Cancer* **9**, 108-122, (2009).
- 16 Yu, H., Mouw, J. K. & Weaver, V. M. Forcing form and function: biomechanical regulation of tumor evolution. *Trends Cell Biol* **21**, 47-56, (2011).
- 17 Hansma, P. *et al.* The tissue diagnostic instrument. *Rev Sci Instrum* **80**, 054303, doi:10.1063/1.3127602 (2009).
- 18 Levental, K. R. *et al.* Matrix crosslinking forces tumor progression by enhancing integrin signaling. *Cell* **139**, 891-906, (2009).
- 19 Avery, N. C., Sims, T. J. & Bailey, A. J. quantitative determination of collagen cross-links. *Methods in molecular biology (Clifton, N.J)* **522**, 103-121 (2009).
- 20 Chen, J. D. & Evans, R. M. A transcriptional co-repressor that interacts with nuclear hormone receptors. *Nature* **377**, 454-457 (1995).
- 21 Horlein, A. J. *et al.* Ligand-independent repression by the thyroid hormone receptor mediated by a nuclear receptor co-repressor. *Nature* **377**, 397-404 (1995).

- 22 Li, J. *et al.* Both corepressor proteins SMRT and N-CoR exist in large protein complexes containing HDAC3. *Embo J* **19**, 4342-4350 (2000).
- 23 Tomita, A., Buchholz, D. R. & Shi, Y. B. Recruitment of N-CoR/SMRT-TBLR1 corepressor complex by unliganded thyroid hormone receptor for gene repression during frog development. *Mol Cell Biol* **24**, 3337-3346 (2004).
- 24 Yoon, H. G. *et al.* Purification and functional characterization of the human N-CoR complex: the roles of HDAC3, TBL1 and TBLR1. *Embo J* **22**, 1336-1346 (2003).
- 25 Zhang, J., Kalkum, M., Chait, B. T. & Roeder, R. G. The N-CoR-HDAC3 nuclear receptor corepressor complex inhibits the JNK pathway through the integral subunit GPS2. *Mol Cell* **9**, 611-623 (2002).
- 26 Espinosa, L., Santos, S., Ingles-Esteve, J., Munoz-Canoves, P. & Bigas, A. p65-NFkappaB synergizes with Notch to activate transcription by triggering cytoplasmic translocation of the nuclear receptor corepressor N-CoR. *J Cell Sci* **115**, 1295-1303 (2002).
- 27 Lee, S. K., Kim, J. H., Lee, Y. C., Cheong, J. & Lee, J. W. Silencing mediator of retinoic acid and thyroid hormone receptors, as a novel transcriptional corepressor molecule of activating protein-1, nuclear factor-kappaB, and serum response factor. *J Biol Chem* **275**, 12470-12474 (2000).
- 28 Luo, K. *et al.* The Ski oncoprotein interacts with the Smad proteins to repress TGFbeta signaling. *Genes Dev* **13**, 2196-2206 (1999).
- 29 Zhou, Y., Gross, W., Hong, S. H. & Privalsky, M. L. The SMRT corepressor is a target of phosphorylation by protein kinase CK2 (casein kinase II). *Mol Cell Biochem* **220**, 1-13 (2001).
- 30 Li, X. & McDonnell, D. P. The transcription factor B-Myb is maintained in an inhibited state in target cells through its interaction with the nuclear corepressors N-CoR and SMRT. *Mol Cell Biol* **22**, 3663-3673 (2002).
- 31 Melnick, A. *et al.* Critical residues within the BTB domain of PLZF and Bcl-6 modulate interaction with corepressors. *Mol Cell Biol* **22**, 1804-1818 (2002).
- 32 Asahara, H., Dutta, S., Kao, H. Y., Evans, R. M. & Montminy, M. Pbx-Hox heterodimers recruit coactivator-corepressor complexes in an isoform-specific manner. *Mol Cell Biol* **19**, 8219-8225 (1999).
- 33 Lutterbach, B. *et al.* ETO, a target of t(8;21) in acute leukemia, interacts with the N-CoR and mSin3 corepressors. *Mol Cell Biol* **18**, 7176-7184 (1998).
- 34 Bailey, P. *et al.* The nuclear receptor corepressor N-CoR regulates differentiation: N-CoR directly interacts with MyoD. *Mol Endocrinol* **13**, 1155-1168 (1999).
- 35 Guenther, M. G., Barak, O. & Lazar, M. A. The SMRT and N-CoR corepressors are activating cofactors for histone deacetylase 3. *Mol Cell Biol* **21**, 6091-6101 (2001).
- 36 Codina, A. *et al.* Structural insights into the interaction and activation of histone deacetylase 3 by nuclear receptor corepressors. *Proc Natl Acad Sci U S A* **102**, 6009-6014 (2005).
- 37 Huang, E. Y. *et al.* Nuclear receptor corepressors partner with class II histone deacetylases in a Sin3-independent repression pathway. *Genes Dev* **14**, 45-54 (2000).
- 38 Fischle, W. *et al.* Enzymatic activity associated with class II HDACs is dependent on a multiprotein complex containing HDAC3 and SMRT/N-CoR. *Mol Cell* **9**, 45-57 (2002).
- 39 Fischle, W. *et al.* Human HDAC7 histone deacetylase activity is associated with HDAC3 in vivo. *J Biol Chem* **276**, 35826-35835 (2001).
- 40 Dequiedt, F. *et al.* HDAC7, a thymus-specific class II histone deacetylase, regulates Nur77 transcription and TCR-mediated apoptosis. *Immunity* **18**, 687-698 (2003).
- 41 Khochbin, S., Verdel, A., Lemercier, C. & Seigneurin-Berny, D. Functional significance of histone deacetylase diversity. *Current opinion in genetics & development* **11**, 162-166 (2001).
- 42 McKinsey, T. A., Zhang, C. L. & Olson, E. N. MEF2: a calcium-dependent regulator of cell division, differentiation and death. *Trends Biochem Sci* **27**, 40-47 (2002).

- 43 Verdin, E., Dequiedt, F. & Kasler, H. G. Class II histone deacetylases: versatile regulators. *Trends Genet* **19**, 286-293 (2003).
- 44 Gregoire, S. *et al.* Histone deacetylase 3 interacts with and deacetylates myocyte enhancer factor 2. *Mol Cell Biol* **27**, 1280-1295 (2007).
- 45 Verdin, E., Dequiedt, F. & Kasler, H. HDAC7 regulates apoptosis in developing thymocytes. *Novartis Found Symp* **259**, 115-129; discussion 129-131, 163-119 (2004).
- 46 Marklund, U., Lightfoot, K. & Cantrell, D. Intracellular location and cell context-dependent function of protein kinase D. *Immunity* **19**, 491-501 (2003).
- 47 Parra, M., Kasler, H., McKinsey, T. A., Olson, E. N. & Verdin, E. Protein kinase D1 phosphorylates HDAC7 and induces its nuclear export after T-cell receptor activation. *J Biol Chem* **280**, 13762-13770 (2005).
- 48 Parra, M., Mahmoudi, T. & Verdin, E. Myosin phosphatase dephosphorylates HDAC7, controls its nucleocytoplasmic shuttling, and inhibits apoptosis in thymocytes. *Genes Dev* **21**, 638-643 (2007).
- 49 Baylin, S. B. & Ohm, J. E. Epigenetic gene silencing in cancer - a mechanism for early oncogenic pathway addiction? *Nat Rev Cancer* **6**, 107-116 (2006).
- 50 Esteller, M. Cancer epigenomics: DNA methylomes and histone-modification maps. *Nat Rev Genet* **8**, 286-298 (2007).
- 51 Lo, P. K. & Sukumar, S. Epigenomics and breast cancer. *Pharmacogenomics* **9**, 1879-1902 (2008).
- 52 Lin, R. J. *et al.* Role of the histone deacetylase complex in acute promyelocytic leukaemia. *Nature* **391**, 811-814 (1998).
- 53 Halkidou, K. *et al.* Upregulation and nuclear recruitment of HDAC1 in hormone refractory prostate cancer. *Prostate* **59**, 177-189 (2004).
- 54 Wilson, A. J. *et al.* Histone deacetylase 3 (HDAC3) and other class I HDACs regulate colon cell maturation and p21 expression and are deregulated in human colon cancer. *J Biol Chem* **281**, 13548-13558 (2006).
- 55 Zhang, X. *et al.* Histone deacetylase 3 (HDAC3) activity is regulated by interaction with protein serine/threonine phosphatase 4. *Genes Dev* **19**, 827-839 (2005).
- 56 Zhang, Z. *et al.* HDAC6 expression is correlated with better survival in breast cancer. *Clin Cancer Res* **10**, 6962-6968 (2004).
- 57 Witt, O., Deubzer, H. E., Milde, T. & Oehme, I. HDAC family: What are the cancer relevant targets? *Cancer Lett* (2008).
- 58 Atadja, P. W. HDAC inhibitors and cancer therapy. *Prog Drug Res* **67**, 175-195 (2011).
- 59 Dean, M. ABC transporters, drug resistance, and cancer stem cells. *J Mammary Gland Biol Neoplasia* **14**, 3-9 (2009).
- 60 Teicher, B. A. Acute and chronic in vivo therapeutic resistance. *Biochem Pharmacol* **77**, 1665-1673 (2009).
- 61 Nebbioso, A. *et al.* Selective class II HDAC inhibitors impair myogenesis by modulating the stability and activity of HDAC-MEF2 complexes. *EMBO Rep* **10**, 776-782 (2009).
- 62 Schwieger, M. *et al.* Homing and invasiveness of MLL/ENL leukemic cells is regulated by MEF2C. *Blood* **114**, 2476-2488, (2009).
- 63 Nagel, S. *et al.* MEF2C is activated by multiple mechanisms in a subset of T-acute lymphoblastic leukemia cell lines. *Leukemia* **22**, 600-607, (2008).
- 64 Potthoff, M. J. & Olson, E. N. MEF2: a central regulator of diverse developmental programs. *Development* **134**, 4131-4140 (2007).
- 65 Edmondson, D. G., Lyons, G. E., Martin, J. F. & Olson, E. N. Mef2 gene expression marks the cardiac and skeletal muscle lineages during mouse embryogenesis. *Development* **120**, 1251-1263 (1994).

- 66 Karamboulas, C. *et al.* Disruption of MEF2 activity in cardiomyoblasts inhibits cardiomyogenesis. *J Cell Sci* **119**, 4315-4321 (2006).
- 67 Molkentin, J. D., Black, B. L., Martin, J. F. & Olson, E. N. Cooperative activation of muscle gene expression by MEF2 and myogenic bHLH proteins. *Cell* **83**, 1125-1136 (1995).
- 68 Wang, D. Z., Valdez, M. R., McAnally, J., Richardson, J. & Olson, E. N. The Mef2c gene is a direct transcriptional target of myogenic bHLH and MEF2 proteins during skeletal muscle development. *Development* **128**, 4623-4633 (2001).
- 69 Mao, Z., Bonni, A., Xia, F., Nadal-Vicens, M. & Greenberg, M. E. Neuronal activity-dependent cell survival mediated by transcription factor MEF2. *Science* **286**, 785-790 (1999).
- 70 Mao, Z. & Wiedmann, M. Calcineurin enhances MEF2 DNA binding activity in calcium-dependent survival of cerebellar granule neurons. *J Biol Chem* **274**, 31102-31107 (1999).
- 71 Okamoto, S., Krainc, D., Sherman, K. & Lipton, S. A. Antiapoptotic role of the p38 mitogen-activated protein kinase-myocyte enhancer factor 2 transcription factor pathway during neuronal differentiation. *Proc Natl Acad Sci U S A* **97**, 7561-7566 (2000).
- 72 van de Vijver, M. J. *et al.* A gene-expression signature as a predictor of survival in breast cancer. *N Engl J Med* **347**, 1999-2009 (2002).
- 73 Johnstone, R. W., Ruefli, A. A. & Lowe, S. W. Apoptosis: a link between cancer genetics and chemotherapy. *Cell* **108**, 153-164 (2002).
- 74 Chen, C. S., Mrksich, M., Huang, S., Whitesides, G. M. & Ingber, D. E. Geometric control of cell life and death. *Science* **276**, 1425-1428. (1997).
- 75 Zahir, N. *et al.* Autocrine laminin-5 ligates alpha6beta4 integrin and activates RAC and NFkappaB to mediate anchorage-independent survival of mammary tumors. *J Cell Biol* **163**, 1397-1407 (2003).
- 76 Friedland, J. C. *et al.* alpha6beta4 integrin activates Rac-dependent p21-activated kinase 1 to drive NF-kappaB-dependent resistance to apoptosis in 3D mammary acini. *J Cell Sci* **120**, 3700-3712 (2007).
- 77 McBeath, R., Pirone, D. M., Nelson, C. M., Bhadriraju, K. & Chen, C. S. Cell Shape, Cytoskeletal Tension, and RhoA Regulate Stem Cell Lineage Commitment. *Developmental Cell* **6**, 483-495 (2004).
- 78 Kass, L., Erler, J. T., Dembo, M. & Weaver, V. M. Mammary epithelial cell: influence of extracellular matrix composition and organization during development and tumorigenesis. *Int J Biochem Cell Biol* **39**, 1987-1994 (2007).
- 79 Giancotti, F. G. Targeting integrin beta4 for cancer and anti-angiogenic therapy. *Trends Pharmacol Sci* **28**, 506-511, (2007).
- 80 Mercurio, A. M., Rabinovitz, I. & Shaw, L. M. The alpha 6 beta 4 integrin and epithelial cell migration. *Curr Opin Cell Biol* **13**, 541-545. (2001).
- 81 Dans, M. *et al.* Tyrosine phosphorylation of the beta 4 integrin cytoplasmic domain mediates Shc signaling to extracellular signal-regulated kinase and antagonizes formation of hemidesmosomes. *J Biol Chem* **276**, 1494-1502. (2001).
- 82 Van Aelst, L. & D'Souza-Schorey, C. Rho GTPases and signaling networks. *Genes Dev* **11**, 2295-2322 (1997).
- 83 Arias-Romero, L. E. & Chernoff, J. A tale of two Paks. *Biol Cell* **100**, 97-108, doi:BC20070109 [pii] 10.1042/BC20070109 (2008).
- 84 Wu, W. S. The signaling mechanism of ROS in tumor progression. *Cancer Metastasis Rev* **25**, 695-705, doi:10.1007/s10555-006-9037-8 (2006).
- 85 Santy, L. C. & Casanova, J. E. Activation of ARF6 by ARNO stimulates epithelial cell migration through downstream activation of both Rac1 and phospholipase D. *J Cell Biol* **154**, 599-610, (2001).
- 86 Szulc, J., Wiznerowicz, M., Sauvain, M. O., Trono, D. & Aebischer, P. A versatile tool for conditional gene expression and knockdown. *Nat Methods* **3**, 109-116 (2006).

- 87 Krugmann, S., Andrews, S., Stephens, L. & Hawkins, P. T. ARAP3 is essential for formation of lamellipodia after growth factor stimulation. *J Cell Sci* **119**, 425-432, (2006).
- 88 Koo, D. H. *et al.* Pinpointing phosphotyrosine-dependent interactions downstream of the collagen receptor DDR1. *FEBS Lett* **580**, 15-22 (2006).
- 89 Nola, S. *et al.* Scrib regulates PAK activity during the cell migration process. *Hum Mol Genet* **17**, 3552-3565, (2008).
- 90 D'Souza-Schorey, C. & Chavrier, P. ARF proteins: roles in membrane traffic and beyond. *Nat Rev Mol Cell Biol* **7**, 347-358, (2006).
- 91 Myers, K. R. & Casanova, J. E. Regulation of actin cytoskeleton dynamics by Arf-family GTPases. *Trends Cell Biol* **18**, 184-192, (2008).
- 92 Santy, L. C. Characterization of a fast cycling ADP-ribosylation factor 6 mutant. *J Biol Chem* **277**, 40185-40188, (2002).
- 93 Sabe, H. *et al.* The EGFR-GEP100-Arf6-AMAP1 signaling pathway specific to breast cancer invasion and metastasis. *Traffic* **10**, 982-993, (2009).

In Situ Force Mapping of Breast Tissue Transformation.

Jose I. Lopez¹, Inkyung Kang^{1,2} and Valerie Weaver^{1,3,4}

¹Department of Surgery and Center for Bioengineering and Tissue Regeneration, University of California at San Francisco, San Francisco, CA 94143

² Benaroya Research Institute at Virginia Mason, Seattle, WA 98101

³Departments of Anatomy and Bioengineering and Therapeutic Sciences, Eli and Edythe Broad Center of Regeneration Medicine and Stem Cell Research and Helen Diller Family Comprehensive Cancer Center, University of California, San Francisco, San Francisco, CA 94143.

⁴Address Correspondence to:

Valerie M. Weaver

University of California, San Francisco

Center for Bioengineering and Tissue Regeneration

Department of Surgery

513 Parnassus Ave, S1364-0456

San Francisco, CA 94143

Email: Valerie.Weaver@ucsfmedctr.org

Telephone: (415) 476-3826

Fax: (415) 476-3985

Introduction

It has long been understood that the development of malignancy resulting from tumor progression is contingent on the tumor epithelium acquiring characteristics that enable migration away from the site of origin and invasion of distant tissues. To become malignant, tumor epithelial cells must first limit their interactions with neighboring cells, compromise and penetrate the extracellular matrix that sequesters them at their site of origin, and gain the ability to efficiently migrate through tissues in order to access potential sites of dissemination such as lymphatics or vasculature^{1,2}. The acquisition of migratory and invasive characteristics by tumor cells is reliant upon both intrinsic genetic changes within the tumor epithelium, as well as a number of extrinsic biochemical and biomechanical changes that accumulate within tumor tissues as they progress towards malignancy^{3,4}. Historically, cancer research has focused on understanding the genetic and biochemical regulation of tumor progression while the biomechanical influences of tumor progression have only recently been studied in depth as technologies develop that enable researchers to closely and accurately examine the mechanical characteristics of the tumor epithelium and its microenvironment. Clear evidence has emerged indicating that mechanical forces arising from the increased volume of epithelial cells as they grow, contractile forces exerted by the tumor epithelial cells, and the desmoplastic response, are closely associated with tumor progression. In fact, it is becoming apparent that biomechanical cues are integrated with biochemical and genetic cues at every step of tumor progression from initiation through malignancy.

While numerous studies have come to the clear conclusion that biomechanical forces within the extracellular environment of the tumor epithelium widely affect tumor progression and malignancy at the cellular level, the methods used to examine the effect of biomechanics during tumor progression *in vivo* have been limited to low-resolution force measurements such as sonal elastography, as well as confined and unconfined compression testing. Nonetheless, acquisition of high-resolution force measurements of the *in vivo* tumor microenvironment is necessary to clearly identify the makeup and structural features of the tumor microenvironment that biomechanically influence tumor progression. Methods for acquiring high-resolutions force measurements with tools such as the atomic force microscope (AFM) are very attractive since measurements can be obtained while samples remain unfixed and hydrated at physiologic temperatures and in physiologically relevant buffers. In fact, AFM has been successfully utilized to obtain elastic measurements of soft tissues such as articular chondrocytes and cartilage from dissected tissues. Damage to tissues resulting from sharp AFM indentors, the strong adhesiveness between indentors and soft adipose tissues, precise optical positioning of indentors at the microscale and uneven tissue surfaces have all limited the use of AFM force measurements in the mammary gland. In this paper we describe a novel approach for obtaining a reliable young's modulus measurement from soft mammary tissues that relies on the rapid cryopreservation of the tissue in a manner that preserves the mechanical properties of the tissue. Using cryopreservation we are then able to section the tissue to obtain a proper geometry to increase the reliability of our young's modulus measurements, as well as improving our optical abilities in such a way that mechanical force mapping can be married to biochemical visualization methods such as immunofluorescence,

immunohistochemistry, or two-photon second generation harmonics generation microscopy.

Results

***In Situ* biomechanical measurements of mammary gland transformation.**

A variety of techniques such as unconfined compression, ultrasound and MRI elastography, have been used to measure the mechanical properties of mammary gland transformation (Ref). However, while the determination of the mechanical properties of the mammary gland using these techniques have clearly associated an altered biomechanical landscape with mammary epithelial transformation and progression, the relatively low resolution mapping used by these techniques have not yet clarified the nature of biomechanical transformation at a molecular level.

To examine how the biomechanical environment is altered during tumor progression at high resolution, we use AFM as it permits the acquisition of accurate and reproducible elasticity measurements with high spacial precision, even as tissue is immersed in a physiologically appropriate solution. Rhodamin (Rh) labeled lectin was perfused into the vasculature prior to the sacrifice of 8-12 week old FVB/MMTV-PyV mT/ACTB-EGFP female mice. Normal mammary gland and mammary gland tumors were excised and sub-dissected to measure 1 cm. in diameter and 2-5 mm. thick and adhered onto positively charged microscope slides. Processing of tissues in this manner allows for adequate visualization of the gross morphology of the *ex-vivo* tissue when placed under phase contrast or fluorescence lighting on an inverted microscope while also allowing the

correct placement of the AFM tip for indentation. Adipose cells resident in the mammary gland are clearly visualized under phase lighting yet remain optically clear to fluorescence allowing visualization of the tumor epithelium and of the tissue vasculature by CFP fluorescence and Rh-Lectin fluorescence imaging (Figure 1A). The fluorescently labeled mammary tumor allows the precise positioning of the AFM cantilever to either the mammary gland tumor or the surrounding tissue including the vasculature. Force mapping indentation experiments were carried out in the regions indicated (Figure 1A, Box). 9 indentations were collected for each region in a raster fashion to generate force maps (Figure 1A, graph). All indentations were carried out using pyramidal indentors ($k=0.06\text{N/m}$) that were coupled with a $5\mu\text{m}$ borosilicate sphere to minimize damage to the tissue, while also collecting measurements at the micro-scale.

AFM indenter positioning with high precision over the tumor epithelium, the vasculature or the surrounding tissue, allows for spatially precise examination of the mechanical properties of distinct regions in the mammary gland tumor associated with transformation. The mammary gland duct undergoes increased stiffening as it progresses from a normal duct, to hyperplasia and finally a tumor (Figure 1B), consistent with previously published measurements^{4,5}. However, measurements obtained by AFM indentation builds on previous work as indenter positioning can be placed to distinguish the tumor epithelium from the surrounding tissue. Improved positioning allows measurements of distinct regions within the tumor such as the invasive front of the tumor, or non-invasive areas (Fig 1B). Measurements taken in these regions show large biomechanical differences. The invasive fronts of the tumor measure approximately 4 times stiffer than non-invasive tumor fronts. This strongly suggests a role for the

biomechanical properties of the surrounding stroma in promoting the invasiveness of the mammary epithelium.

In the process of this study we discovered that although reliable elastic modulus measurements can be obtained from fresh mammary gland tissues numerous limitations and difficulties with this technique remain. Dissection of the tissue with surgical tools and shaping into the proper geometry to prepare for AFM indentation leads to the creation of tissue surfaces that, on occasion, restrict access of the AFM indenter and complicate the optical positioning of the AFM indenters. Sharp AFM indentors are not ideal for the acquisition of force measurements as these easily damage soft tissue. Instead, large spherical indenters should be used to acquire measurements at a greater scale and with less damage to the delicate mammary tissue. However, the natural adiposity of the mammary gland leads to strong adhesiveness between the large spherical indenters and the tissue making the acquisition of measurements a highly time consuming task that cannot not be performed in a routine manner. Additionally, the acquisition of measurements is limited a short time after dissection to maintain tissue freshness and preclude tissue degradation in an effort to maintain accurate and physiologically significant mechanical measurements. Thus, we found it necessary to improve our technique to maximize efficiency while also improving the reliability and repeatability of the technique.

Vitrification of mammary gland tissue does not alter mechanical properties.

To address the limitations of AFM when taking mechanical measurements on fresh tissues, we found it necessary to section the excised mammary gland tissues. Sectioning of tissue

sections creates a surface that is thin enough to provide optical clarity, and uniformly level to maximize access of the AFM indenter while minimizing adhesive forces between the spherical indenter and the tissue. The flat geometry of sectioned tissues improves the power of the Hertz equation to model the stiffness of a flat substrate when using a spherical indenter. Given the extremely pliable and adhesive nature of the mammary gland, attempts at sectioning freshly dissected mammary tissue on a conventional microtome or a vibratome were unsuccessful as the blades failed to cut into the tissue uniformly and often glide over the surface of the tissue causing significant damage. This holds true even when tissue is embedded in various kinds of molds to stabilize the tissue. To section the mammary gland tissue with conventional microtomes or vibratomes, it is necessary to either fix the tissues or chemically treat them, thus potentially compromising their biomechanical integrity.

Cryosectioning is commonly used during histologic examination to section mammary gland tissues, preserving the specimen biochemically intact to enable immunostaining of difficult antigens. However, it remained unclear whether freezing in the absence of fixatives preserves the biomechanical properties of the mammary gland. Damage to tissue resulting from freezing occurs due to rapid changes in osmolarity as well as the formation of ice crystals. Pure water exists in 3 distinct solid states; hexagonal crystals, cubic crystals or in a vitreous, amorphous form^{5,6}. Crystalline ice expands and physically damages tissues and may compromise the mechanical properties of the tissue. However, ice in the vitreous form remains amorphous, in a glass like state that does not expand upon solidification making it a highly desirable state of ice for the freezing and preservation of biological specimens. The solid state that water acquires depends not

temperature, but rather the rate at which the water is frozen. Slow freezing water promotes the formation of crystalline solid states of water, while high rates of freezing will confine water to its amorphous, vitreous form. Importantly for the preservation of biological specimens, water in the vitreous form can restructure into crystalline forms if deep freezing is not maintained. Amorphous ice can restructure into cubic crystals at temperatures above -121°C and into hexagonal crystals at temperatures above -80°C . Fortunately, the restructuring of water from one solid state to another is a slow conversion that depends largely on temperature gradients and the purity of the water.

To examine if rapidly freezing mammary gland tissue preserves the biomechanical properties of the specimens, we excised mammary glands from 12-14 week old MMTV- PyV mt/FVB mice as described above. The tissues were sub-dissected as described above and placed on a custom-made chamber. The tissues were indented as described above taking note of the placement of the AFM indenter on the tissues. Tissues were then either frozen slowly by progressively moving the custom-chamber through isopropanol chilled to -20°C and -80°C prior to immersing the tissue in liquid nitrogen, or tissues were flash-frozen in place by rapid immersion into liquid-nitrogen. The tissues were then thawed slowly by progressively moving the chamber in the reverse order to when frozen, or rapidly thawed by immersing the tissue in relatively large quantities of PBS at room temperature.

Tissues which had been slowly frozen and then slowly thawed showed large changes in their physical appearance that reflect damage inflicted by the expansion and crystallization of water (Figure 2A). Adipose cells appeared lysed, the volume of the tissue decreased, the optical clarity of the tissue was increased and the borders of the tissue were

less defined. Importantly, the measured young's modulus of the tissue decreased an average of 60% after slow-freeze and slow-thaw. On the other hand, tissue that was rapidly frozen and rapidly thawed maintained its morphology intact (Fig 2B). The small size of the dissected tissues and the large volume of liquid-nitrogen used relative to the size of the dissected tissues, minimize the formation of thermal gradients within the tissues that leads to the formation of crystals in the interior of the tissue. The cells in the tissue did not lyse, the optical density of pre and post frozen tissues were similar and the tissue maintained a similar shape and borders. Most importantly, indentation showed no significant changes in elastic mechanical properties of the tissue. Rapid-freezing/rapid-thawing of the tissue led to just an average 6% change in the Young's elastic modulus, while rapid-freezing/slow-thawing and slow-freezing/slow-thawing led to a 52% and 64% change in the Young's elastic modulus. Furthermore, the young's elastic modulus did not change regardless of the initial stiffness of the tissue. Biomechanical properties of the mammary gland were preserved on both stiff and soft tissues as long as the freezing and thawing rate of the cryopreservation occurred rapidly.

Given the high resolution of AFM indentation, even when using a 5 μ m indenter, and the heterogeneous nature of mammary gland tissues, we wanted to repeat the above experiment without moving the tissue on the stage to ensure that the pre-freeze and post-freeze indentations occurred in precisely the same geographic location on the tissue. To do this we mounted fresh tissue onto the custom-made chamber and indented the tissue in 5 locations as described above across a region containing fibrous tissue as well as adipose cells, making note of the precise geographic location of the indenter in software and then lifting the AFM head away from the tissue. Without moving the chamber or the tissue on

the stage, the tissue was immersed in liquid nitrogen while still on the AFM stage for 1min., the liquid nitrogen was then removed and rapidly perfused with large quantities of room temperature PBS to achieve a rapid freeze and a rapid thaw. The AFM head was then replaced in its original location and indentations then repeated at the same location on the tissue. Rapid freezing and thawing in this manner maintained tissue position on the stage and ensured that the AFM indenter could be placed precisely as it had been prior to freezing. Some differences could be observed in the optical clarity of the tissue, presumably due to the fact that liquid nitrogen immersion while tissues remain on the stage do not allow liquid nitrogen ready access to the base of the tissue (Figure 3b). This creates a temperature gradient within the tissue that can lead ice crystallization at the base of the tissue. In contrast, the surface of the tissue shows intact structures including adipose cells while the tissue maintained its shape and overall morphology. Most importantly, however, the elastic modulus of the surface of the tissue remained largely unchanged (Figure 3A). Indentations across the 5 different points showed variable elastic modulus ranging from 20-70kPa. Trends in the variation across these 5 points were maintained after rapid-freezing and rapid-thawing the tissue. The absolute values of the measurements also remained relatively constant varying only an average of 7% overall. These results indicate a potential for vitrification in preserving the mechanical properties of mammary gland tissue. However, it is clear that vitrification must occur in a uniform manner that is largely dependent on ready access of the liquid nitrogen to the tissue to prevent the formation of thermal gradients.

***In Situ* high resolution force mapping of mammary gland tissues.**

The biomechanical preservation of tissues by vitrification in liquid nitrogen facilitates sectioning of the tissue in a geometry that optimizes AFM indentation while improving optical clarity to ensure precise positioning of the indenter on regions of interest (Figure 4A). The flat geometry of sectioned tissue also minimizes the adhesive interactions between the tissue and the indenter material to increase the rate of indentation acquisition across the tissue. High-resolution force maps can be obtained with high geographic accuracy on the tissue, and in a very rapid manner. In fact, multiple force maps are easily generated from a single tissue section, representing multiple different microenvironments present within the tissue.

By positioning the tip at the interface between the tumor epithelium and the stroma, force maps are generated that demonstrate distinct biomechanical properties of the extracellular matrix across tumor types or between different areas of a single tumor. As the mammary epithelium progresses from normal, to pre-malignant and finally malignant tumors, a progressive increase in the young's elastic modulus of the ECM surrounding the tumor epithelium is mapped (Figure 4A). The young's elastic modulus of the ECM surrounding the ductal epithelium increases from an average of 1.1 kPa in the normal duct, to 1.3 in pre-malignant ducts and 1.5 kPa in malignant ducts. The Young's elastic modulus of adipose or epithelial cells remain unchanged, however. While cells are visible by phase contrast lighting, or when fluorescently tagged with Hoechst 3332 to label the nuclei, the mechanical integrity of these cells is compromised when cryo-sectioned. As a result,

measurements obtained from these compartments do not necessarily reflect the cortical stiffness of the cells.

AFM force mapping can be coupled to techniques traditionally used to visualize biomolecules using immunofluorescent or histochemical staining techniques to identify the molecular nature of biomechanical features that have been shown to affect tumor progression. Collagen crosslinking has been recently shown to alter the biomechanical properties of the microenvironment surrounding the mammary epithelium leading to biochemical changes in the epithelium such as enhanced PI3 kinase activity, promotion of focal adhesions and increased integrin clustering⁴. Force mapping of cryosectioned mammary gland tissue was coupled to histological examination of collagens by picosirius red to visualize how changes in the collagen content of tissues relates to its biomechanical properties. It is clear that as the epithelium progresses from hyperplasia, to ductal carcinoma in situ and finally to invasive carcinoma, drastic changes in collagen content surrounding the tumor are associated with progression. Normal epithelium and pre-malignant tumors are surrounded by a high degree of thick collagen fibers as indicated by red picosirius red staining (Figure 4A, top and middle row). On the other hand, invasive tumors are surrounded by increased amounts of thinner collagen bundles as indicated by the yellow color of the picosirius red staining (Figure 4A, bottom row).

Discussion

Sonal and MRI elastography, and physical palpations leave no doubt that the pathogenesis of metastatic breast cancer is clearly influenced by the biomechanical

microenvironment of the tumor epithelial cells and can be used as a prognostic to detect disease progression. While the influence of biomechanics on tumor epithelial cell behavior has been successfully studied *in vitro*, studies capable of examining the underlying physical changes leading altered biomechanical microenvironment with high resolution *in situ* have been limited by the available technology. In this paper we present a method of cryopreserving tissues *in situ* that allows the collection of accurate physical measurements of mammary tissue with AFM while also allowing subsequent biochemical examination.

The formation of damaging ice crystals and osmotic gradients during freezing is contingent on the rate of freezing. Rapid freezing and rapid thawing can preclude the formation of damaging ice crystals and osmotic gradients. In this study we demonstrate, that by utilizing these principles both the biochemical and biomechanical nature of the tissue can be preserved when tissues are rapidly frozen and then rapidly thawed. In fact, sectioning of tissues that have been cryo-preserved improves the biomechanical accuracy of AFM measurements as the geometry necessary for Hertz modeling of a spherical indenter interacting with a flat substrate is optimized. The optical clarity of thin tissue sectioning enables precise geographical positioning of the AFM indentors in a manner that allows subsequent histochemical examination of the very same location within the tissue. We present an example of sequential biomechanical and biochemical examination utilizing the Wnt mouse model of breast cancer. The ECM surrounding the ducts of these mice were force mapped and then stained for picosissius red so that a direct correlation can be made between collagen content and the nature of collagen fibers as well as their mechanical properties.

Despite the improvement in examining the nature and properties of the ECM that cryopreservation and AFM provide, this technique does not provide reliable information regarding the mechanics of the tumor epithelium. Sectioning of cryogenically preserved tissues results in lethal damage to cells that prevents the direct acquisition of mechanical measurements of cells. Thus, this technique is limited to querying the non-cellular tissue elements for their mechanical properties. Additionally, the use of spherical indentors to preclude tissue damage and adhesion that occurs with sharp indentors significantly increases the cost of this technique and require fitting AFM force curves to the Hertz model to derive the Young's elastic modulus, a labor and time intensive effort. Future improvements in Hertz model analysis and the fabrication of AFM spherical indentors can potentially alleviate this concern and improve the throughput of this type of assay.

Methods such as these open up the field of biological mechanics to a new line of inquiry that can ask questions regarding the biomechanical properties of pathological tissues and relate the physical properties of tissues to their biochemical makeup. This will allow new insight by indentifying the cell types and molecules are directly responsible for altered microenvironments such as those seen during the desmoplastic response, or whether epithelial cell metastasis follows cues other than chemotactic cues that can influence their malignancy. Additionally, a new metric for metastatic disease diagnosis may also emerge if it is found that a distinct biomechanical signature correlates with malignancy that may augment current histologic and biochemical diagnosis.

1. Chambers, A.F., Groom, A.C. & MacDonald, I.C. Dissemination and growth of cancer cells in metastatic sites. *Nat. Rev. Cancer* **2**, 563-572 (2002).
2. Wiseman, B.S. & Werb, Z. Stromal effects on mammary gland development and breast cancer. *Science* **296**, 1046-1049 (2002).
3. Butcher, D.T., Alliston, T. & Weaver, V.M. A tense situation: forcing tumour progression. *Nat Rev Cancer* **9**, 108-122 (2009).
4. Levental, K.R. et al. Matrix crosslinking forces tumor progression by enhancing integrin signaling. *Cell* **139**, 891-906 (2009).
5. Paszek, M.J. et al. Tensional homeostasis and the malignant phenotype. *Cancer Cell* **8**, 241-254 (2005).
6. Blackman, M. & Lisgarten, N.D. The Cubic and Other Structural Forms of Ice at Low Temperature and Pressure. *Proceedings of the Royal Society of London. Series A, Mathematical and Physical Sciences* **239**, 93-107 (1957).
7. Pegg, D.E. Principles of cryopreservation. *Methods Mol. Biol* **368**, 39-57 (2007).

Figure Legends:

Figure 1:

Biomechanical characterization of tumor progression. Excised mammary gland tumors are directly visualized by GFP fluorescence and the vasculature is visualized by perfused RH-Lectin fluorescence to precisely position the AFM indenter to force map the noted areas (A). Force map analysis of mammary tumor progression from normal epithelium to invasive tumor shows a corresponding progression in the biomechanical properties of the tumor and the surrounding stroma (B). Scale bar represent 100 μ m.

Figure 2:

Vitrification by rapid cryopreservation maintains biomechanical properties of mammary gland tissue. Cryopreservation of tissue by slow rate freezing causes extensive damage to the tissue while compromising the biomechanical properties of the tissue (A, top row). Rapid cryopreservation of tissue allows vitrification which does not damage tissue while preserving the biomechanical properties of the tissue in tact (A, bottom row). Quantification of the young's elastic modulus of tissue subjected to distinct cryopreservation techniques that that rapid-freeze/rapid-thaw does not lead to changes in the biomechanical properties while rapid-freeze/slow-thaw or slow-freeze/slow-thaw do significantly alter the young's elastic modulus of the tissue (B). Scale bar represent 100 μ m. Error bars represent standard error of the mean. *P<0.05, **P>0.05.

Figure 3:

In situ vitrification and indentation do not alter mechanical properties of tissues. Tissues pre-freeze (B, left) or post-freeze (B, right) were indented in a custom chamber without moving the tissue from the AFM stage to ensure no changes in indentation locations. Young's modulus obtained from these tissues indicates that vitrification preserves biomechanical properties across a wide range of stiffness (A). Scale bar represent 100 μ m.

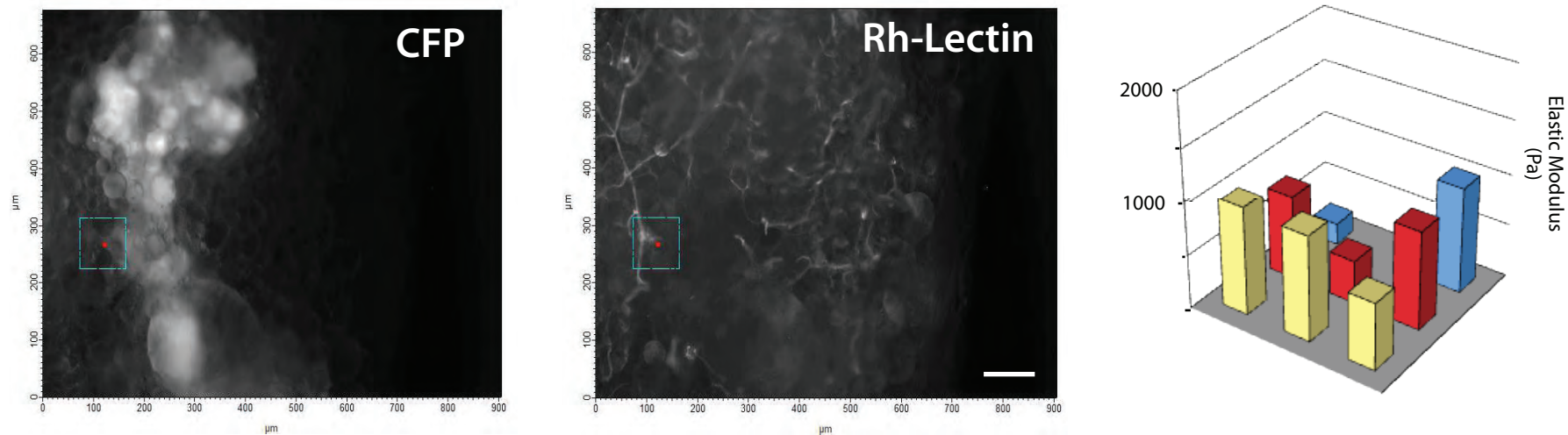
Figure 4:

In situ force mapping of cryosectioned mammary glands can be coupled to traditional histopathological techniques. Cryosectioning of tissues improves visual clarity and geometry of the tissue sample (A). Coupling of AFM with light microscopy enables precise placement of the AFM indenter and force mapping of multiple regions in the tissue (A, forced mapped region). Scale bar represent 100 μ m. Error bars represent standard error of the mean. *P<0.05, **P>0.05.

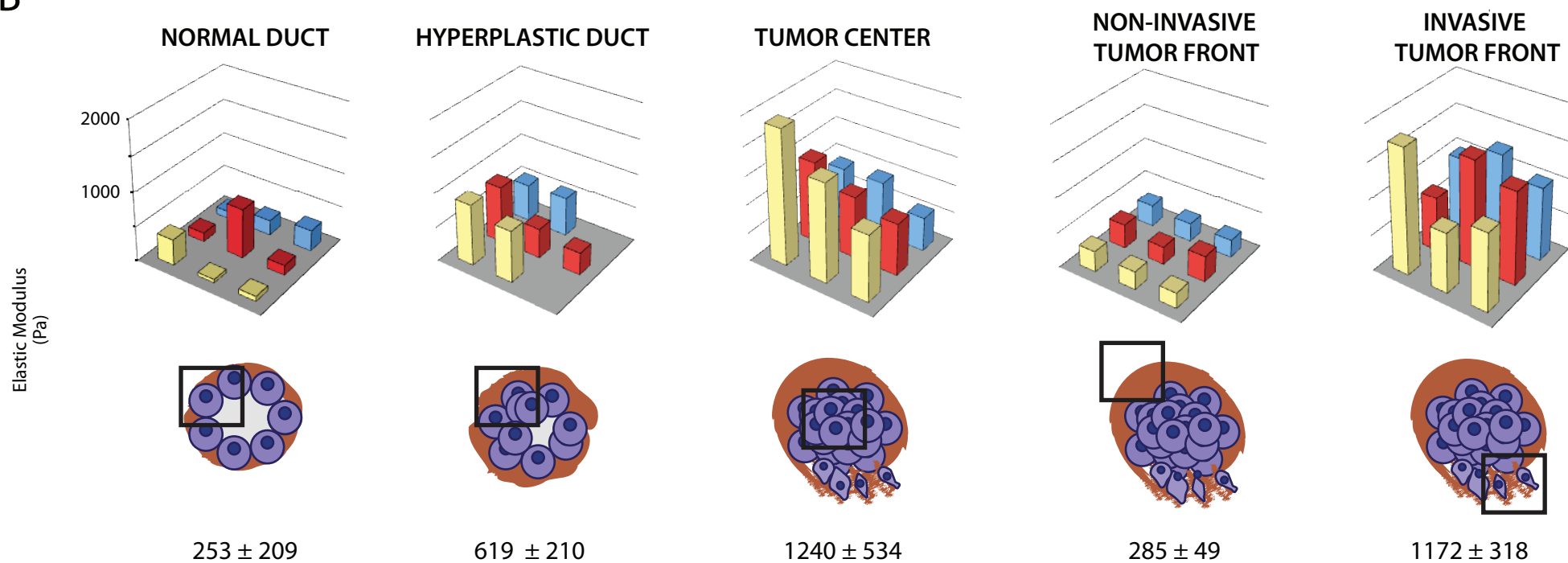
Statistics

Statistical analysis was performed with GraphPad Prism with a paired student's t-test or two-way ANOVA.

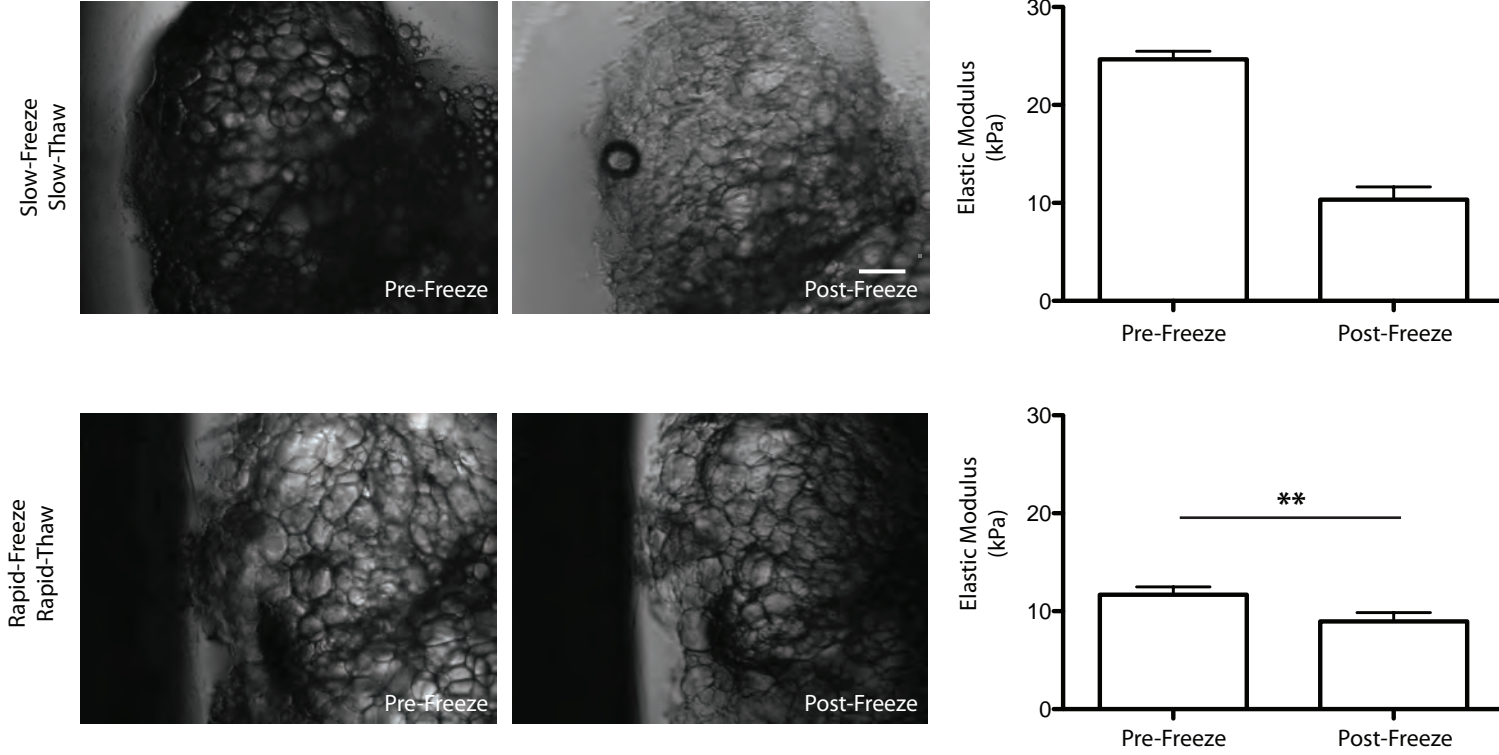
A



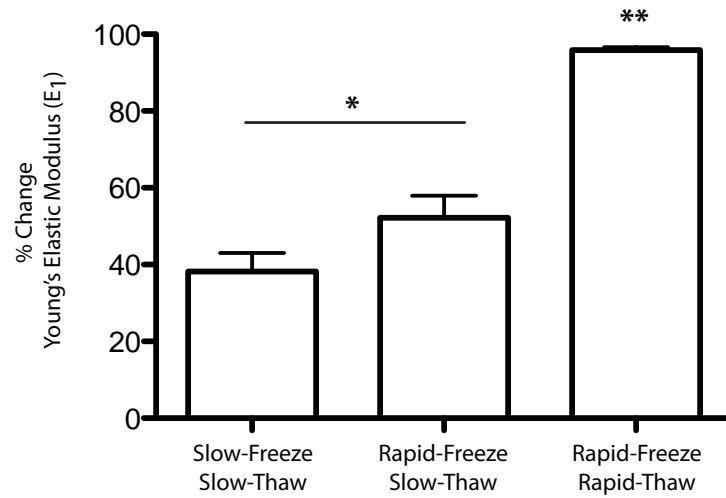
B



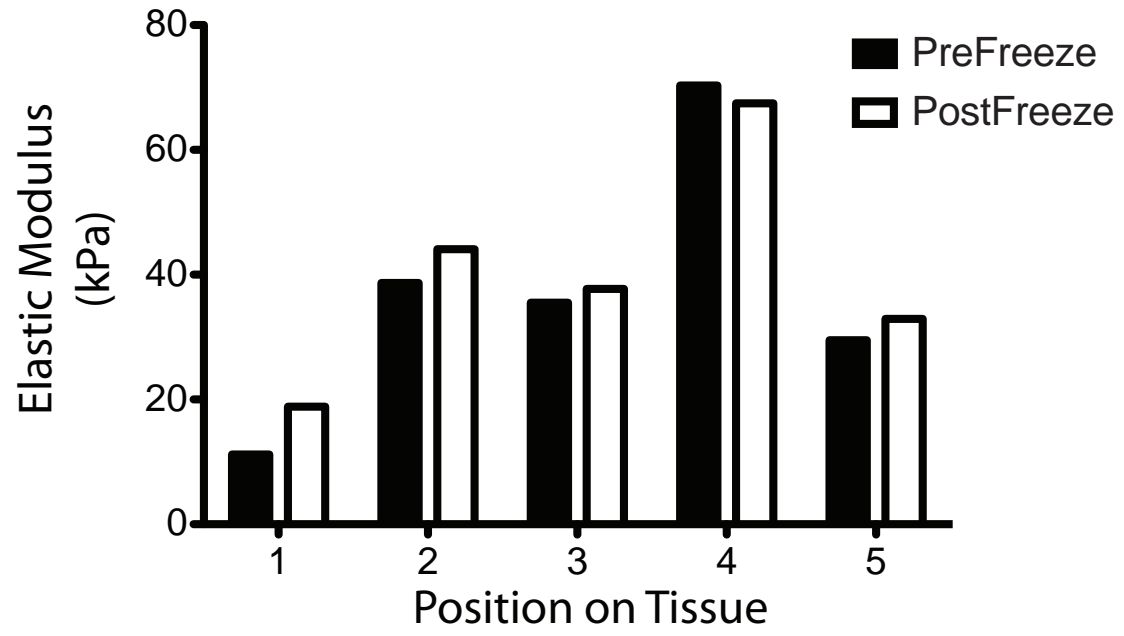
A



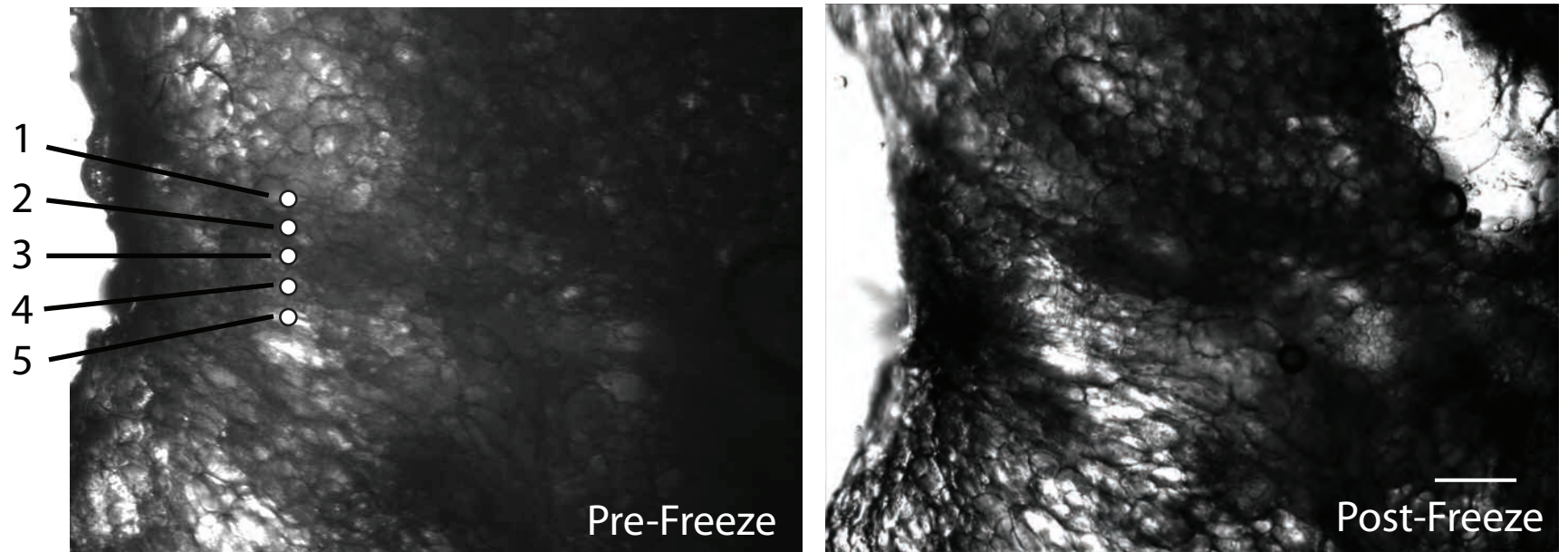
B



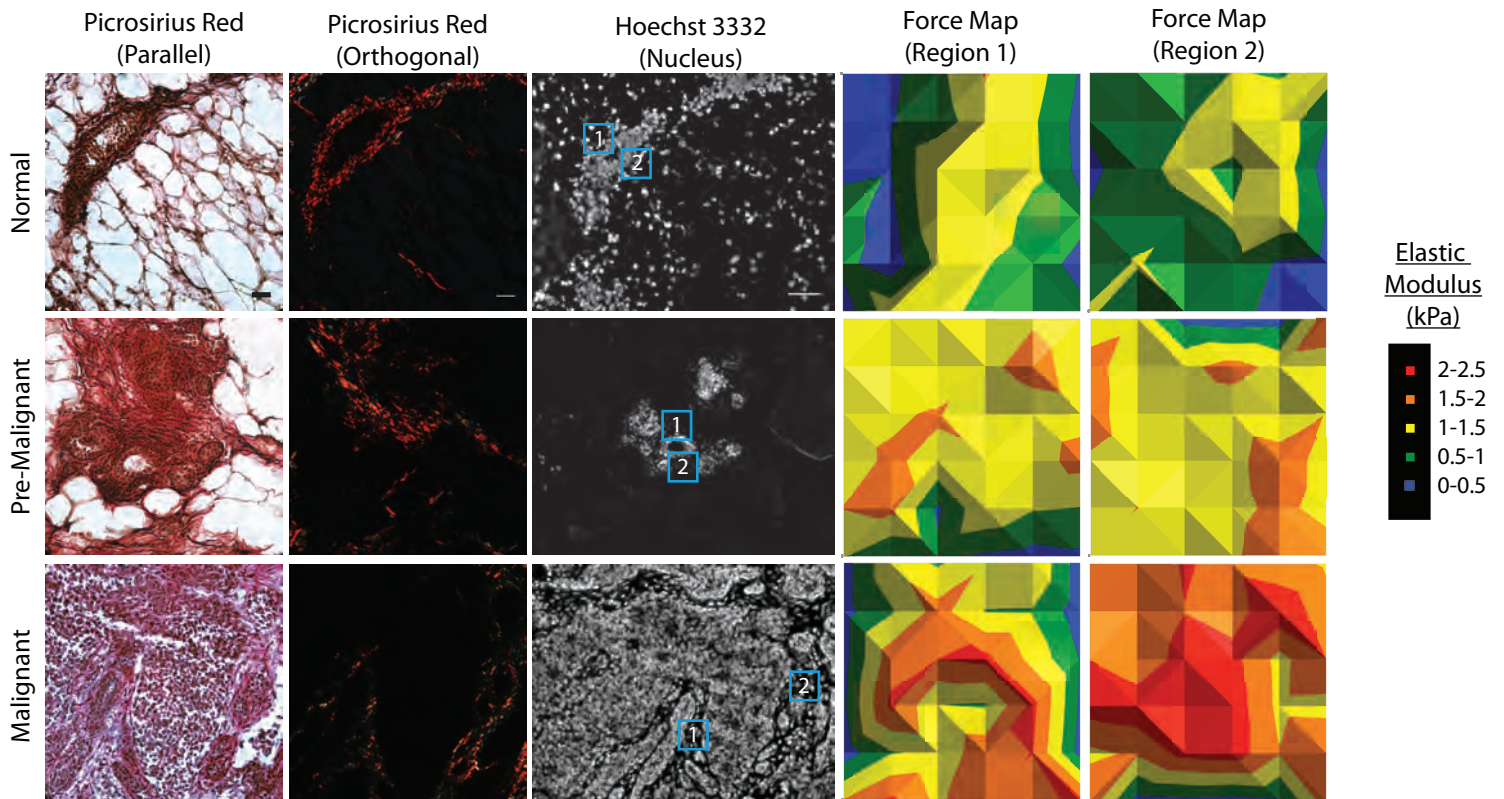
A



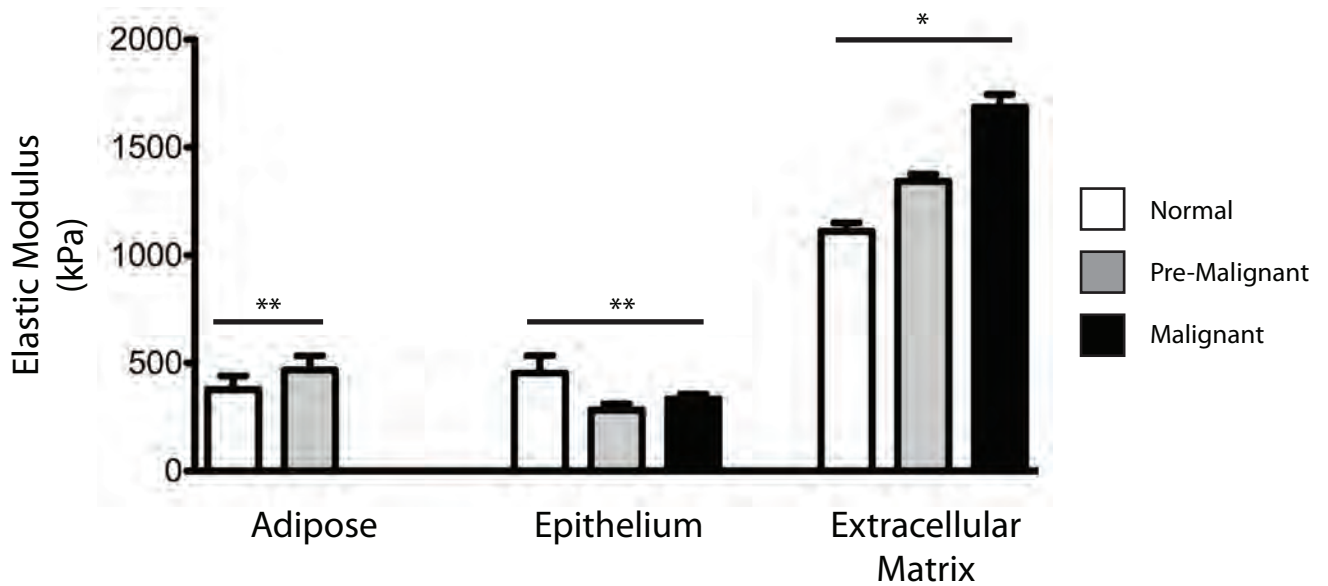
B



A



B



Engineering strategies to recapitulate epithelial morphogenesis within synthetic three-dimensional extracellular matrix with tunable mechanical properties

Y A Miroshnikova^{1,2}, D M Jorgens³, L Spirio⁴, M Auer³,
A L Sieminski-Sarang¹ and V M Weaver^{2,5,6}

¹ Olin College of Engineering, Needham, MA 02492, USA

² Department of Surgery, Center for Bioengineering and Tissue Regeneration, University of California, San Francisco, San Francisco, CA 94143, USA

³ Lawrence Berkeley National Laboratory, UC Berkeley, Berkeley, CA 94720, USA

⁴ PuraMatrix/3DM Inc., Cambridge, MA 02142, USA

⁵ Departments of Anatomy and Bioengineering and Therapeutic Sciences, Eli and Edythe Broad Center of Regeneration Medicine and Stem Cell Research and Helen Diller Family Comprehensive Cancer Center, University of California San Francisco, San Francisco, CA 94143, USA

E-mail: Valerie.weaver@ucsfmedctr.org

Received 26 October 2010

Accepted for publication 4 March 2011

Published DD MMM 2011

Online at stacks.iop.org/PhysBio/8/000000

Abstract

The mechanical properties (e.g. stiffness) of the extracellular matrix (ECM) influence cell fate and tissue morphogenesis and contribute to disease progression. Nevertheless, our understanding of the mechanisms by which ECM rigidity modulates cell behavior and fate remains rudimentary. To address this issue, a number of two and three-dimensional (3D) hydrogel systems have been used to explore the effects of the mechanical properties of the ECM on cell behavior. Unfortunately, many of these systems have limited application because fiber architecture, adhesiveness and/or pore size often change in parallel when gel elasticity is varied. Here we describe the use of ECM-adsorbed, synthetic, self-assembling peptide (SAP) gels that are able to recapitulate normal epithelial acini morphogenesis and gene expression in a 3D context. By exploiting the range of viscoelasticity attainable with these SAP gels, and their ability to recreate native-like ECM fibril topology with minimal variability in ligand density and pore size, we were able to reconstitute normal versus tumor-like phenotype and gene expression patterns in nonmalignant mammary epithelial cells. Accordingly, this SAP hydrogel system presents the first tunable system capable of independently assessing the interplay between ECM stiffness and multi-cellular epithelial phenotype in a 3D context.

Introduction

Cells *in vivo* are constantly exposed to an array of biophysical forces such as hydrostatic pressure, shear stress, compression loading and tensional forces. Cells rely on these physical cues to maintain homeostasis and adapt to them by altering cell signaling and gene expression and by remodeling their

local microenvironment [1, 2]. From an organismal point of view, extracellular matrix (ECM) compliance directs the development of tissues [1, 3] and influences the onset of many pathological conditions, including cardiovascular disease [4], arthritis [5] and neural degenerative diseases [6, 7]. The ECM also progressively stiffens in tumors and recent work suggests this phenotype has functional significance because increasing ECM rigidity promotes malignant transformation, while

⁶ Author to whom any correspondence should be addressed.

inhibiting ECM stiffening reduces tumor incidence [8–10]. Accordingly, clarifying the role by which ECM compliance influences diverse cellular and tissue level functions is central to understanding the molecular basis for development and organ homeostasis. Nevertheless, the molecular mechanisms whereby ECM compliance regulates cellular behavior and tissue phenotype remain poorly understood.

One frequently employed simplified model system used to study the effect of ECM stiffness on cell behavior is protein-conjugated polyacrylamide gels (PA gels) [11–15]. These nearly elastic 2D gels permit the systematic and predictable modulation of ECM compliance by changing cross-linker concentration while maintaining ligand density and growth factor milieu constant. PA gels have proved quite useful in exploring fundamental links between ECM stiffness and cell behavior, and when used in conjunction with a matrix overlay assay, they have illustrated a role for ECM tension in epithelial morphogenesis [3, 6, 10, 16–20]. These PA gels have also been used to identify molecular mechanisms by which ECM stiffness modulates cell phenotype including highlighting how ECM compliance can regulate cell behavior by influencing integrin adhesions and growth factor receptor signaling [10, 21–24]. Indeed, studies using PA gels have proved instrumental in illustrating how physical cues from the ECM are sensed and propagated and how ECM tension can alter membrane receptor function and nuclear morphology to modify gene expression [25–27]. Yet, most cells exist within the context of a three-dimensional (3D) tissue and it is now recognized that dimensionality per se is a profound regulator of cell and tissue phenotype [28–36]. In this regard, PA gels represent a pseudo 3D rigidity assay system because only the basal domain of the cell remains in contact with, and therefore responds to, the elasticity of the protein-laminated PA gel. Moreover, while animal studies have yielded important insight regarding the interplay between ECM topology, and rigidity within a 3D context [10, 35, 37, 38] *in vivo* tissues are inherently complex and hence do not lend themselves as readily to rigorous mechanistic manipulations and quantitative analysis. Accordingly, tractable *in vitro* systems are needed with which to study the molecular basis by which ECM stiffness influences cellular fate in the context of a 3D ECM.

A variety of natural matrices, such as Matrigel (rBM), collagen I (col I), and fibrin gels have been exploited with varying degrees of success to explore the effect of ECM stiffness and topology *in vitro* on cellular behavior and fate in a 3D context [39–43]. Using these hydrogel systems gel stiffness has been routinely modulated by altering the concentration or composition of the gel constituents or by varying cross-link density. Such approaches as these however, simultaneously alter gel pore size, fiber architecture, and/or the number or availability of adhesion sites [44, 45]. Further, these natural ECM systems frequently display inconsistencies and batch-to-batch variation. By contrast, synthetic biomaterials promise greater control of mechanical and adhesive properties. In this regard, a variety of approaches have been undertaken to design 3D scaffolds that combine biological functionality and the architecture of natural ECM materials with the robust controllability of synthetic materials.

These scaffolds include agarose-stiffened collagen I gels [46], polyethylene glycol (PEG) gels with tethered adhesion and degradation sites [47–50], as well as a variety of systems with dynamic biophysical and biochemical properties [51, 52]. Unfortunately however, many of these gel systems lack the appropriate ECM-like fiber architecture and display limited pore size with increased ECM stiffness.

Self-assembling peptides (SAPs) are a family of 8–32 amino acid peptides that, when exposed to physiological salt solutions, self-assemble into fibrils [53, 54]. SAPs are chemically defined and biologically compatible biomaterials that mimic the architectural features observed in some natural matrices such as type I collagen gels [55]. Moreover, SAP family members support cell adhesion and can direct the differentiated behavior of neural stem cells [56], osteoblasts [57], hepatocytes [58, 59] and endothelial cells [55]. Motivated by these results we decided to explore the applicability of PuraMatrix, one type of commercially available SAP, to study the interplay between ECM stiffness and mammary epithelial cell (MEC) morphogenesis in 3D. We determined that laminin-adsorbed (ligation of laminin receptors promotes MEC tissue polarity and differentiation) PuraMatrix SAPs not only support MEC acinar morphogenesis but that stiff SAPs promote an invasive epithelial tumor-like phenotype and do so without significantly changing pore size or gel architecture. Accordingly, we contend that these studies represent the first demonstration of a tractable, well-defined hydrogel system that is able to recapitulate the biochemical and micro architectural features of the native normal tissue ECM so that the interplay between ECM compliance and multi-cellular tissue behavior can be studied in a 3D ‘tissue-like’ context.

Methods

Chemicals and antibodies

We used commercial EHS matrix (Matrigel™; Collaborative Research) for the rBM assays, telopeptide intact type I rat tail collagen (1%; Sigma) for the collagen type I hydrogels and aqueous RAD16-I (1%; AcN-(RADA)4-CNH2; BD PuraMatrix, Becton Dickinson) for the SAP gels. Primary antibodies used in these studies included: mouse monoclonal anti-human cleaved caspases-3 (clone E83–77; Epitomics), E cadherin (clone 36; BD Transduction Laboratories), β 4 integrin (clone 3E1; Chemicon) and Ki-67 (clone 7B11; Invitrogen); rat monoclonal anti-human β 1 integrin (clone AIB2), and rabbit polyclonal anti-human fibronectin I (Millipore) and β -catenin (Sigma). Secondary antibodies used were: Alexa Fluor 488- and 555- and 633-conjugated anti-mouse, anti-rat and anti-rabbit IgGs (molecular probes). Additional reagents included TRITC-conjugated Phalloidin (molecular probes), diaminophenylindole (DAPI; Sigma), laminin (L2020, Sigma), and fetal bovine serum (Invitrogen).

Cell culture

Human nonmalignant MEC MCF10 As were propagated as monolayers on tissue culture plastic and assembled into 3D colonies in either rBM or collagen/rBM gels, as described [8, 60].

Cell death stimulation and analysis

MECs grown in rBM for 10–12 days (3D multi-cellular spheroid) were assayed for endogenous cell death via apoptosis through immuno-detection of activated caspase 3 or using a modified Live/Dead assay (Invitrogen). Percent death was quantified as the number of cells stained positive for activated caspase 3 or scored positive for death divided by the total number of cells, as described [34, 61]. The minimum number of cells scored was 200–300 per experimental condition. Cells were visualized using a fluorescence microscope (Nikon Inverted Eclipse TE300 microscope).

Immunofluorescence analysis

Cells were either triton extracted (0.1% Triton X-100; 5 min) and then fixed or directly fixed using paraformaldehyde (4%; Electron Microscopy Sciences). Specimens were thereafter incubated with primary antibody, followed by either Alexa Fluor 488 or 568-conjugated secondary antibody. Nuclei were counterstained with DAPI or Hoechst 33342. Cells were visualized using a Zeiss Laser Scanning Confocal microscope attached to a Nikon Diaphot 200 microscope. Images were recorded at 600 \times magnification.

Three-dimensional culture within self-assembling peptides

To assay for growth within a 3D SAP gel, trypsinized MECs (0.05%; trypsin/EDTA; Invitrogen) were washed and resuspended in sterile 20% sucrose containing either laminin (100 $\mu\text{g ml}^{-1}$; Sigma L2020) or rBM (Matrigel; 2 mg ml^{-1} protein; Becton Dickinson). The cell suspension (2 \times final desired cell concentration) was then combined 1:1 with a 2 \times solution of SAP (from 1% w/v sonicated peptide stock) to attain a final cell concentration of 1×10^5 cells ml^{-1} . A cellular–ECM mixture of 200 μl was thereafter aliquoted into inserts (PICM-012-50, Millipore) and gelation was induced by exposure to cell culture medium (DMEM F-12, 10% FBS, pH 7.4; Invitrogen). After 1 h, the gelation medium was decanted and replaced with MEC growth medium. Cultures were typically fed every other day and maintained for 18 days.

Scanning electron microscopy

Cell-free collagen and SAP gels were fixed in Jonson's reagent (24 h; 4C; Electron Microscopy Sciences) and cut into 4–5 smaller gels prior to further processing and staining to increase the number of exposed surfaces. After fixation samples were rinsed (3 \times ; 10 min; RT; 0.1 M sodium cacodylate buffer, pH 7.2; Tousimis), stained with 1% osmium tetroxide (1 h; RT), and rinsed with 0.1 M sodium cacodylate buffer (3 \times ; 5 min; RT). Samples were then subjected to ascending alcohol dehydration, followed by critical point drying procedure with an AutoSamdri 815 CPD critical point dryer (Tousimis). Samples were then transferred onto carbon-taped SEM stubs, sputter coated (Tousimis) with gold palladium and imaged with a Hitachi S-500 scanning electron microscope operated at 30 kV (resolution 3–5 nm).

Rheometry

Cell-free SAPs, and collagen/rBM gels of varying concentration were gelled in cylindrical molds (~ 7.5 mm ID), attached to 10% FBS/PBS-wetted parchment paper, polymerized under physiological conditions (48 h; 37C), released from molds, and transferred to a rheometer with an 8 mm plate (AR 2000ex, TA Instruments) [55]. The shear modulus (G_0) was recorded at a constant frequency of 1 rad s^{-1} for all samples; TA Instruments software accompanying the rheometer was used to fit all data and extract shear moduli from raw data ($n = 5$ gels for all conditions).

Extracellular matrix fibril quantification and data analysis

Projected fiber diameter and pore size were measured from the SEM images (five representative 60 000 \times images/each concentration of collagen and SAP) using ImageJ. Projected pore size was quantified via averaging two diagonals of every pore with clear edges on the SEM images. The projected fiber diameter was quantified by averaging measurements of at least 100 fibers/SEM image. A colony area was traced and analyzed in ImageJ ($n = 50$ acini/condition).

Statistical analysis

Statistical significance was assessed by performing 1/2-tailed student *t*-tests. *P*-values of less than 0.05 were considered to be significant as indicated by a * symbol in text and graphs, unless otherwise specified.

Quantitative PCR

RNA was isolated using phenol–chloroform extraction and total RNA for each sample was reverse transcribed using random primers (Amersham Biosciences). 18S rRNA primers run in parallel were used as controls. Quantitative PCR reactions (10 μl) were conducted using a LightCycler (Roche Diagnostics) with a LightCycler Fast Start DNA Master SYBR Mix (Roche) and a 1 pmol primer mixture.

Results

Increasing collagen concentration and rigidity stimulate epithelial growth and survival and compromise tissue morphogenesis and integrity

Primary and immortalized MECs have been used to study the role of the ECM and its receptors in tissue morphogenesis and differentiation. When incorporated into a 3D rBM (Matrigel) human and murine MECs assemble into growth-arrested, polarized multi-cellular structures that resemble terminal ductal lobular units of the *in vivo* mammary gland [31, 39]. MECs will also assemble into nonpolarized 3D organoids when grown within type I collagen gels and can be induced to polarize if either purified laminin or rBM (2 mg ml^{-1}) is added [62].

The viscoelasticity of collagen I gels is proportional to their concentration. As such collagen gels provide an attractive

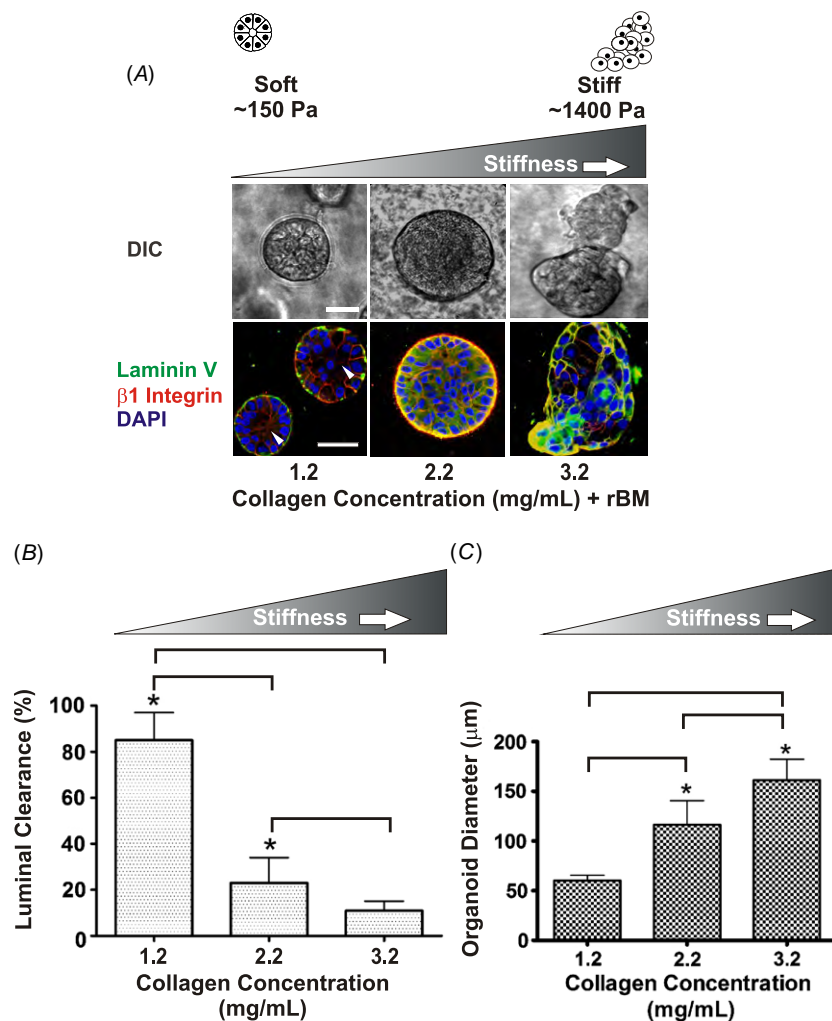


Figure 1. Increasing collagen concentration and rigidity stimulate epithelial growth and survival and compromise tissue morphogenesis and integrity. (A) (Top) phase contrast images of multi-cellular MEC colonies embedded within type 1 collagen gels of increasing concentration (1.2–3.2 mg ml⁻¹) and stiffness (150–1400 Pa) for 12 days. Bar equals 30 μm . (Bottom) laser confocal immunofluorescence images of multi-cellular MEC colonies as above, stained for $\beta 1$ integrin (red), laminin V (green), and nuclei (DAPI; blue). Bar equals 40 μm . (B) Bar graphs showing quantification of luminal clearance measured in colonies shown in A. (C) Bar graph showing average colony diameter of colonies shown in A. *indicates $p \leq 0.001$. Values shown in (B) and (C) represent mean \pm SEM of multiple measurements from at least three independent experiments.

system with which to study the effect of modulating ECM stiffness in a 3D context on tissue behavior. Accordingly, to study the effect of modulating ECM rigidity on epithelial behavior we generated type I collagen gels ranging from 1.2 to 3.2 mg ml⁻¹ incorporating rBM (Col/rBM cultures; 2 mg ml⁻¹) as a polarity cue. We showed previously that these concentrations of collagen achieve gel stiffness that recapitulates the viscoelasticity typically found in a normal, pre-malignant and early invasive tumorigenic human and mouse breast [8, 10, 63]. We then assayed for the effect of varying ECM stiffness in a 3D context on the growth and survival and morphogenesis of the nonmalignant human MEC line MCF10A, an immortalized human MEC line that undergoes multi-cellular epithelial morphogenesis in response to compliant 3D rBM cues [10].

Similar to what we and others observed previously, although the nonmalignant MECs incorporated into highly compliant Col/rBM gel (156 Pa \pm 42 Pa) grew rapidly for

the first 6 days, by day 10 they assembled growth-arrested acini as indicated by colonies with persistent diameters of $60.2 \pm 5.4 \mu\text{m}$ (figure 1(A); DIC image; figure 1(C)). After 10 days of culture mammary acini in the compliant gels (1.2 mg ml⁻¹) also showed evidence of cleared lumens (see arrow figure 1(A) DIC, top and immunofluorescence, bottom) and achieved apical–basal polarity as demonstrated by basal deposition of laminin and apical–basal localization of $\beta 1$ integrin (figure 1(A); lower left-hand panel). By contrast, even moderate stiffening (2.2 mg ml⁻¹) of the Col/rBM (457 ± 67.3 Pa) significantly increased colony size suggestive of elevated cell proliferation ($116.5 \pm 24.2 \mu\text{m}$; figure 1(A) DIC top middle panel, figure 1(C)). Yet, when gel stiffness approached that quantified in the stroma surrounding a pre-malignant breast epithelium [10], luminal clearing was compromised, indicative of enhanced cell survival (figure 1(B)). Furthermore, a collagen stiffness approaching 800–1000 Pa, similar to that measured in the ECM surrounding

early invasive breast lesions, significantly disrupted apical–basal polarity, as revealed by the diffuse localization of laminin V and relocalization of $\beta 1$ integrin along the basal domain of the colony (figure 1, bottom middle panel). Intriguingly, not only did MECs embedded within Col/rBM gels with ECM stiffness approaching that measured in breast tumors (1411 ± 350.3 Pa) grew quite large (161.3 ± 21.1 μm ; figure 1(C)) and formed highly disorganized, nonpolar colonies that lacked lumens (figure 1(A); lower panel right and figure 1(B)) but these colonies also showed a propensity to form membrane protrusions that projected into the surrounding ECM, consistent with the notion that ECM stiffness promotes a tumor-like phenotype. Importantly however, despite these provocative findings, none of the nonmalignant MECs from the mammary colonies assembled within the rigid rBM/collagen I gels invaded into the gels (figure 1(A) DIC top right).

Thus far, our findings were consistent with the notion that ECM stiffness compromises epithelial morphogenesis and tissue integrity and induces a ‘tumor-like’ phenotype even in nontransformed epithelial cells. Nevertheless, we noted that the interpretation of data obtained with these gels was complicated by the fact that collagen ligand available to bind to cell surface receptors including integrins and discoidin receptors also significantly increased when the gel concentration was increased to stiffen the ECM. Moreover, SEM analysis revealed that the projected pore size and fiber thickness also changed dramatically as the concentration of the collagen gel was progressively increased (figure 2(A)). Because ligand binding and pore size can significantly modify cell invasion, these findings indicate that studies aimed at assessing the interplay between ECM stiffness and cell invasion may be compromised using this approach. Furthermore, matrix topology per se can significantly modulate cellular phenotype further complicating the interpretation of experiments conducted using this gel system [46, 64–67]. Thus, these results emphasize that it is still not clear if ECM stiffness per se can induce invasion of nontransformed epithelial tissues. Indeed, the data imply that although collagen gels offer an attractive model system with which to rapidly assess the effect of modulating ECM stiffness on cellular behavior in a 3D context, several confounding variables seriously compromise any ability to rigorously isolate and interpret the effect of matrix stiffness per se on cellular behavior using this hydrogel model.

Self-assembling peptides (SAP): flexible, protein-absorbing, synthetic matrix that mimics collagen architecture

A number of materials are readily available whose elasticity can be dynamically modulated by maintaining ligand binding constant. Materials such as hyaluronic acid, poly(ethylene) glycol, and polyglycolic acid can be modified to provide rigorously controlled biochemical cues [46, 68–74]. Unfortunately, the architecture of these materials is strikingly different from that of natural ECMs such as type I collagen, thereby compromising their utility as natural ECM substrates. By contrast, SAP hydrogels are biocompatible synthetic

substrates that not only mimic the micro-architecture of natural collagen gels (figure 2(C)) but lend themselves to chemical modification. SAPs are composed of 16 repeating amino acid residues (alternating hydrophilic and hydrophobic chains) that self-assemble to form nanofibers under physiological salt conditions due to hydrophobic (between alanines) and ionic bonding (between arginine and aspartic acid residues) between the amino acids [55]. Although SAPs can be mechanically tethered with ligand [59, 75], these peptides are also protein adsorbing [76]. Thus, although they do not contain integrin-binding sites, and cannot therefore mediate ligand-dependent ECM receptor signaling, they can be readily conjugated, tethered or adsorbed with quantifiable concentrations of ligand via direct peptide conjugation or through ECM protein adsorption. Moreover, by varying the concentration of the SAP, the stiffness of the gel can be modulated over a physiologically appropriate range to achieve a viscoelasticity similar to soft tissues such as a healthy breast on the one hand and a cancerous breast on the other hand [8, 77–79].

To explore the utility of SAPs as biocompatible materials for exploring the effect of ECM stiffness on epithelial morphogenesis and homeostasis, we characterized the physical topology and mechanical properties of one of these commercially available SAP gels, PuraMatrix, over the range of viscoelasticity deemed useful for the study of normal and transformed epithelial behavior. We found that varying SAP concentration from 1.2 to 3.2 mg ml^{-1} generated a Young’s modulus that ranged from 120 to 1200 Pa, analogous to what we were able to achieve by varying collagen concentration from 1.2 to 3.2 mg ml^{-1} (figures 2(B) and (D)). Importantly, SEM analysis revealed that unlike collagen I gels, the micro-architecture of SAP gels did not substantially change within this stiffness range and gel concentration. Indeed, we noted that pore size only varied by approximately 10% and fibril topology remained within the range of 45–75 nm even when gel contraction was varied from 1.2 to 3.2 mg ml^{-1} (figures 2(E) and (F)). By contrast the pore size of the collagen gels varied by over 30% and fibril topology ranged from 50 to 170 μm when collagen concentration was modified across this same range (figures 2(E) and (F)). Curiously, although we detected no statistically significant differences in the overall fiber organization and matrix topology as a function of SAPs gel concentration and stiffness, we did quantify a modest, but consistent increase in peptide mass per volume (data not shown). The fact that the observed difference was only a 10% increase in the fraction of soluble peptide at the highest gel concentration indicates that the elevated gel stiffness likely reflects a subtle increase in either the fiber diameter, length, or absolute number. In this respect, we determined that the projected pore size and overall fiber mesh did not change drastically, suggesting that SAP gel stiffness was more than likely due to an increase in fiber diameter and/or enhanced fiber density. Indeed, there was a positive but-insignificant trend between SAP stiffness and decreased projected pore size and increased fiber thickness. The fact that we could not accurately document changes in these variables is more than likely due to the resolution limitation of our detection method

Q1

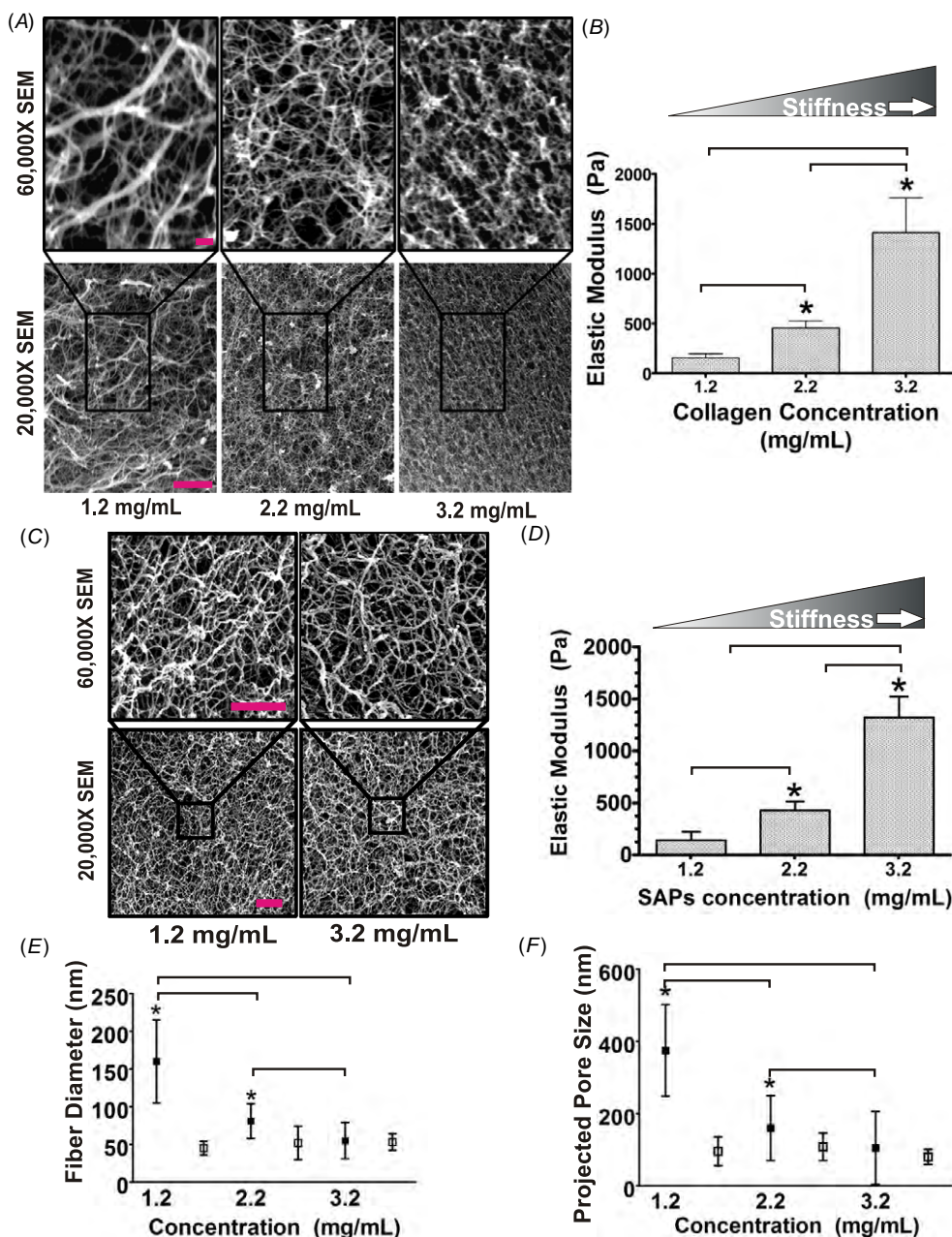


Figure 2. Self-assembling peptides (SAP): flexible, protein-absorbing, synthetic matrix that mimic collagen architecture. (A) SEM microscopy images of collagen gels taken at high (top) and low (bottom) magnification illustrating the structural changes induced in collagen morphology, topology and pore size when collagen concentration is increased. Bar equals 5 μm. (B) Bar graph quantifying Young's modulus of collagen gels of varying concentration as measured by shear rheology. (C) SEM microscopy images of SAP gels taken at high (top) and low (bottom) magnification illustrating minimal structural changes in gel fiber morphology, topology and pore size when gel concentration is increased. Bar equals 200 nm. SEM resolution is 3–5 nm (according to the manufacturer). (D) Bar graphs quantifying SAP gel stiffness as a function of gel concentration as measured by shear rheology. (E) Graphical depiction of fiber diameter quantified as a function of collagen (filled boxes) and SAP (open boxes) gel concentration. (F) Graphical depiction of pore size measured as projected pore size in collagen (filled boxes) and SAP (open boxes) gels as a function of gel concentration. *indicates $p \leq 0.001$. Values shown in B and (D) and (F) represent mean \pm SEM of multiple measurements from at least three independent experiments.

which is unable to detect such subtle nano-scale differences in fiber diameter and pore size variability. Consistently, the stiffness of a fibrous material can be largely attributed to the sum of the bending moments of all the fibers. Second moment of inertia is a shape property that can be used to predict deflections and stresses in the beams/fibers, which would be representative of its bulk stiffness. Assuming a

circular cross-section of the fibers, the moment of inertia, I_o , would be proportional to the radius raised to the fourth power ($I_o = \pi r^2/4$), such that incredibly small changes in the radius would be reflected by an increased capacity to dramatically alter the bendability or stiffness of the material. In these studies we observed an approximate six-fold increase in gel stiffness between the soft and the stiff SAP gels which can easily be

accounted for by a mere 2 nm change in fiber thickness. As such, the theoretical differences between soft and stiff SAP gels are well beyond the 3–5 nm resolution capacity of SEM imaging. Moreover and importantly, despite the fact that it is obvious that SAP morphology must vary to some degree as a function of gel concentration/stiffness, the magnitude of such a modest nanometer-scale variation would exert a negligible effect on cellular functions, such as migration and invasion, because cells operate on a length scale of 10–50 μm . Instead, variations in pore and fiber diameter within tens to hundreds of nanometers, which is comparable to what we quantified for collagen gels of increasing concentration/stiffness, are likely to significantly alter cellular invasion and migration. These findings suggest that SAP gels could provide a viable alternative ECM for studying the effect of ECM rigidity on epithelial invasive phenotype in a 3D context.

SAP gels support epithelial morphogenesis and direct apical–basal tissue polarity

To explore the utility of SAP gels as a tractable matrix system for studying the interplay between ECM stiffness and epithelial cell behavior in 3D, we grew MECs within un-conjugated, compliant, SAP gels in the absence of adsorbed ECM protein. We noted that MECs embedded within SAP gels survived and grew to assemble epithelial colonies. However, colony size was non-uniform and immuno-fluorescence analysis revealed that the colonies lacked polarity (data not shown). We therefore supplemented the SAP gels with laminin (100 $\mu\text{g ml}^{-1}$) or rBM (2 mg ml^{-1} ; 10%) and assayed for effects on MEC growth, survival and multi-cellular morphogenesis. Analogous to MECs embedded within rBM or a mixture of collagen I and rBM, MECs embedded within the laminin- or rBM-supplemented SAP gels proliferated rapidly for the first 5–6 days after which they growth-arrested, as revealed by loss of Ki-67 immuno-staining and the maintenance of a stable colony diameter, and initiated tissue morphogenesis, as indicated by elevated numbers of cells in the center of the colonies positive for activated caspase 3 (figures 3(B), 4(C) and (D)). Consistently, MEC colonies generated in the laminin-supplemented SAP gels assembled acini with cleared lumens that had similar diameters to those generated in rBM and collagen I/rBM gels (figures 3(A) and (C), quantified in 3B). Moreover, acini generated in the laminin-supplemented SAP gels achieved apical–basal polarity, as revealed by basally localized $\beta 4$ integrin (figure 3(D), left panel, see arrow), basal–lateral $\beta 1$ integrin, and cell–cell localized β -catenin (figure 3(D), middle and right panels, see arrows). These phenotypes are analogous to those observed in rBM or in 1.2 mg ml^{-1} collagen I gels supplemented with laminin or rBM (figure 1(A)). Moreover, and importantly, similar to what we and others have routinely observed using rBM gels, SAP gels were able to support stable acini development as revealed by uniform colony differentiation and repression of genes that compromise acini stability and differentiation, such as fibronectin (figure 3(D), right panel; figures 4(E) and (F)). These findings indicate that compliant SAP gels, when supplemented with the appropriate biochemical ECM cues,

can support normal MEC growth and viability and direct multi-cellular tissue morphogenesis.

Modulating SAP stiffness perturbs epithelial morphogenesis, disrupts apical–basal tissue polarity, and induces pro-tumor gene expression

We next asked whether increasing SAPs gel stiffness could perturb MEC morphogenesis and tissue integrity to induce a tumor-like phenotype. MECs were embedded within 1.2–3.2 mg ml^{-1} SAP gels at concentrations that generated mechanical properties (Young's modulus) that recapitulated what we previously measured for normal and early stage breast tumor tissue, respectively [10] (figure 2(D)). Similar to MECs within rBM gels, MEC colonies embedded within highly compliant laminin-supplemented SAPs assembled growth-arrested acini that showed negligible Ki-67 staining by day 10 of culture (figures 4(C) and (D)). Mammary acini within soft SAPs also consistently cleared their lumens, likely through induction of apoptosis in the cells lacking contact with the protein-adsorbed SAP gels, as revealed by elevated number of cells within the day 10–12 colony lumens with activated caspase 3 staining (figure 4(B)). By contrast, MEC colonies embedded within rigid SAP gels continued to proliferate, as revealed by elevated Ki-67 staining throughout the colony (figure 4(D)), showed negligible death of the cells within the center of the colony, as revealed by reduced activated caspase 3 positive cells in the center of the colonies (figure 4(C)), and consequently failed to clear their lumens (figures 4(A) and (B)). The colonies assembled within the rigid SAPs also lacked apical–basal polarity, as revealed by highly diffuse β -catenin and $\beta 1$ integrin (figure 4(E)). Intriguingly, we noted that the MECs embedded within the stiff SAPs matrix also showed severely compromised colony integrity, as revealed by gross disorganization of the colony and individual MECs disseminating away from the colony and invading into the surrounding matrix (figure 4(E)). These findings imply that matrix stiffness 'per se' may in fact promote cell invasion given the appropriate matrix context and cell state. In this regard, by way of a plausible mechanism, we noted that SAP stiffness induced the expression of two genes implicated in tumor progression and invasion, fibronectin 1 and EGFR (figure 4(F)), and additionally enhanced fibronectin 1 deposition by the MECs embedded within the gel (figures 4(E) and (F)).

Discussion

We exploited the unique properties of one SAP gel (PuraMatrix) to study the interplay between ECM stiffness and multi-cellular epithelial morphogenesis and transformation. SAP gels provide a versatile model system with tunable mechanical properties and a native-like ECM fibril morphology. We were able to show that 3D laminin- or rBM- adsorbed compliant SAP gels are able to recapitulate MEC morphogenesis and that a stiff SAPs gel disrupts tissue architecture, compromises tissue polarity and induces fibronectin and EGFR expression to promote an invasive,

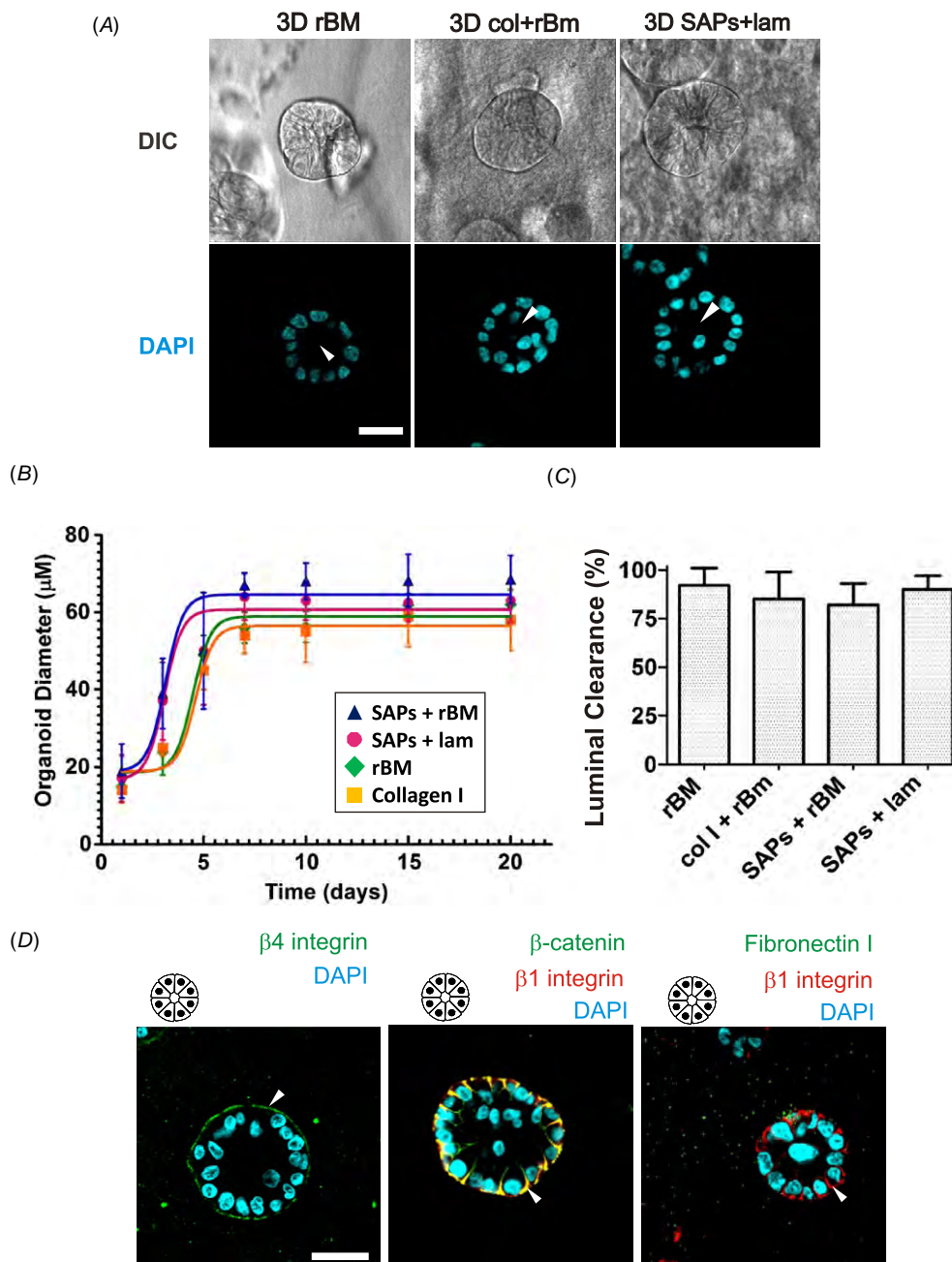


Figure 3. SAP gels support epithelial morphogenesis and direct apical–basal tissue polarity. (A) (Top) phase contrast images of representative multi-cellular MEC acini following growth within reconstituted basement membrane (rBM, Matrigel), type I collagen gels mixed with 10% rBM, or SAPs containing $100 \mu\text{g ml}^{-1}$ laminin for 20 days. (Bottom) laser confocal immunofluorescence images of cryosections ($10 \mu\text{m}$) of multi-cellular MEC colonies stained with DAPI to reveal nuclei (blue) showing presence of cleared lumens in acini generated in all gel conditions as described above. Bar equals $25 \mu\text{m}$. (B) Line graphs showing growth curves for mammary colonies grown within rBM (green diamond), type I collagen gels mixed with 10% rBM (orange box) and SAPs supplemented either with laminin (red circle) or rBM (blue triangle). (C) Bar graphs showing quantification of cleared lumens in mammary acini grown in rBM, type I collagen gels mixed with 10% rBM and SAPs supplemented either with laminin or rBM (differences in the diameters were not statistically significant). (D) Laser confocal immunofluorescence images of cryosections ($10 \mu\text{m}$) of multi-cellular acini generated in SAPs supplemented with laminin stained with (left image) $\beta 4$ integrin (green), (middle image) β -catenin (green) and $\beta 1$ integrin (red) and (right image) fibronectin (green) and $\beta 1$ integrin. All colonies were counter stained with DAPI (blue) to reveal nuclei. Bar equals $30 \mu\text{m}$. Values shown in (B) and (C) represent mean \pm SEM of multiple measurements from at least three independent experiments.

tumor-like phenotype without substantially altering ECM topology, pore size and ligand density. Thus, we maintain that this matrix is a defined and tractable system that could be used to definitively study the effect of ECM tension on multi-cellular epithelial cell behavior in a 3D tissue-like

context. The availability of such a versatile system could have profound clinical implications by permitting the execution of experiments aimed at clarifying the biophysically driven changes in tissue phenotype and molecular signature associated with tumor progression. One could imagine using

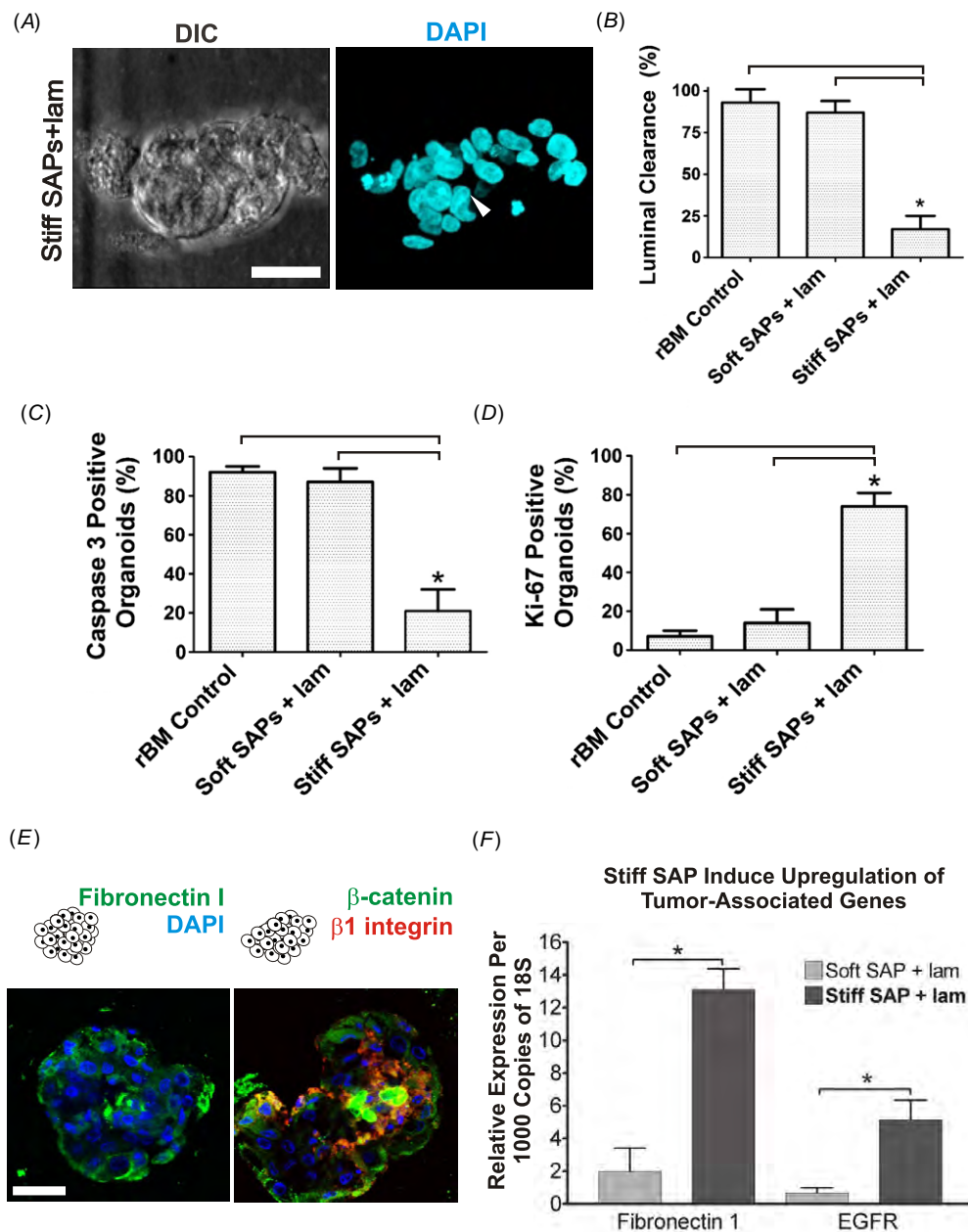


Figure 4. Modulating SAP stiffness perturbs epithelial morphogenesis, disrupts apical–basal tissue polarity, and alters gene expression. (A) (Left) phase contrast images of representative multi-cellular MEC acini following growth within rigid SAPs containing $100 \mu\text{g ml}^{-1}$ laminin for 20 days. (Right) laser confocal immunofluorescence image of a cryosection ($10 \mu\text{m}$) of a multi-cellular MEC colony, generated as described above, stained with DAPI to reveal nuclei (blue) showing absence of cleared lumen in colony generated in a rigid SAP. Note the arrow pointing to the cells migrating into the stiff SAP gel suggestive of invasive behavior. Bar equals $25 \mu\text{m}$. (B) Bar graphs showing quantification of cleared lumens in mammary acini grown in rBM as compared to MEC colonies assembled in the soft and stiff SAPs supplemented with laminin. Note the high percent of luminal clearance quantified in the acini assembled in either the rBM gels or the compliant SAP gels and a significant reduction of cleared lumens quantified in the colonies generated in the stiff SAP gels. (C) Bar graphs quantifying the number of caspase three positive lumens in colonies generated in rBM gels versus those assembled within compliant versus stiff SAP gels supplemented with laminin. Data indicate that SAP stiffness represses apoptosis in MECs. (D) Bar graphs quantifying the number of Ki67 positive colonies detected in rBM gels versus those assembled within compliant versus stiff SAP gels supplemented with laminin. Data show that SAP stiffness promotes MEC proliferation. (E) Laser confocal immunofluorescence showing representative image of cryosections ($10 \mu\text{m}$) of a multi-cellular MEC colony generated in a stiff SAP supplemented with laminin that was stained with (left) fibronectin (green) and (right) β -catenin (green) and $\beta 1$ integrin (red) and counter stained with DAPI (blue) to reveal nuclei. Bar equals $30 \mu\text{m}$. (F) Bar graphs showing the relative expression (by quantitative PCR) of fibronectin 1 and EGFR in acini isolated from soft and stiff laminin-supplemented SAP gels. Values shown in (B) and (D) and (F) represent mean \pm SEM of multiple measurements from at least three independent experiments.

this system for high throughput drug screening to identify novel therapeutics that would provide improved, personalized cancer therapeutics designed to not only target tumor cells but also to treat their phenotypic response to modifications in their surrounding ECM.

Unlike natural gels which exhibit striking changes in architecture, decreased pore size and altered ligand density as matrix stiffness is increased, SAP gels offer a tractable system with which to vary ECM stiffness over a dynamic range without significantly affecting any of these variables. In this regard, while other synthetic systems, including HA gels and PEG gels, have been adapted to study the effect of ECM rigidity on cell and tissue behavior these substrates fail to recapitulate the topology of natural matrices, cannot be remodeled without conjugation of collagenase digestible peptides, and often limit invasion due to minute pore size features (unpublished findings). Two major approaches for engineering *in vitro* systems with tunable mechanical properties have been the conjugation of cell-compatible adhesion peptides into synthetic matrices [48, 80–82] or the application of biophysically modified natural matrices (e.g. varying collagen gel concentration and/or cross-linking). Synthetic matrices allow for a robust control of ligand density as a function of stiffness; however, they typically fail to recapitulate the appropriate topological cues programmed in the networks of natural materials. On the other hand, natural materials not only offer physiologically relevant architectures, but also introduce an array of confounding biophysical cues when concentration is varied or cross-linking status is changed (as means to vary stiffness). This includes profound effects on ligand density, fiber diameter, pore size and overall micro-architecture. These complicating variables are not insignificant in that cells are able to sense and respond to matrix topology and presentation [83–87]. For instance, tumors show elevated contractility and enhanced crosstalk with stromal fibroblasts in response to changes in matrix topology and this perturbed dialogue promotes tension-dependent remodeling and linearization of collagen fibers that promote an invasive tumor matrix that can foster metastasis [88, 89]. Thus, due to a myriad of limitations endemic to current *in vitro* systems, the issue as to whether or not ECM compliance per se can modulate tissue morphology and transformation (as well as the identification of molecular mechanisms that drive these phenomena) remains unresolved. In this regard, the SAP system described here has a multitude of positive features that might overcome many of these limitations, and while mechanical fragility remains one challenge when manipulating these gels, their net benefit at present far outweighs this minor experimental difficulty.

Prior studies using 3D collagen gels with increasing concentration and/or elevated collagen cross-links (and hence stiffness) indicate that ECM stiffness perturbs multi-cellular epithelial morphogenesis but fails to induce invasion unless combined with elevated growth factor or oncogenic signaling [3, 10]. Such findings imply that ECM stiffness collaborates with oncogenes to drive tumor progression and argue that stiffness is a tumor promoter rather than initiator. We noted that elevating SAP stiffness was sufficient to drive

epithelial invasion suggesting stiffness alone could promote cell invasion. One plausible explanation for why prior studies failed to demonstrate invasion causality through ECM stiffness is that stiffened collagen gels (mediated through elevated protein concentration or cross-linking) simultaneously decrease pore size and limit growth factor diffusion, thereby complicating data interpretation because these variables would themselves impede and delay migration. Indeed, prior studies suggest that stiffer collagen or fibrin gels can in fact reduce the rate of cell migration and that migration within such gels relies critically on MMP-dependent matrix remodeling to permit tumor cell invasion [90–92]. Yet, ECM stiffness promotes invadopodia [92–94] and modulates integrin adhesion dynamics [23, 64, 95, 96]. Furthermore, ECM rigidity enhances cell contractility to enhance cell motility and promotes invasion through ECM reorganization and alignment, suggesting ECM stiffness should promote and not impede invasion. These findings indicate that ECM stiffness could be both a tumor promoter and initiator, a possibility that now needs to be rigorously addressed. In this regard, SAP gels could prove instrumental in addressing this intriguing possibility.

In conclusion, tumor progression is associated with loss of tissue organization and disassembly of multi-cellular tissue structures. We observed that compliant laminin-supplemented SAP gels are able to support MEC acini morphogenesis and that a stiff SAPs gel perturbs tissue polarity, destabilizes cell–cell adhesions and increases the expression of tumor promoting genes including fibronectin and the EGF receptor. These findings are consistent with the notion that ECM rigidity per se, in conjunction with appropriate architecture, could promote tumor progression through destabilization of tissue architecture, a findings that we now stand prepared to investigate using the SAP system of epithelial morphogenesis.

Acknowledgments

We thank C Frantz and J Lakins for technical assistance. This work was supported by an NCI U54CA143836-01 grant to J Liphardt and VMW, and 5R01CA138818-02 to VMW, a Department of Defense Breast Cancer Research Era of Hope Scholar award W81XWH-05-1-330 to VMW and a National Science Foundation (GRFP) Fellowship to YAM.

References

- [1] Ingber D E 2006 Mechanical control of tissue morphogenesis during embryological development *Int. J. Dev. Biol.* **50** 255–66
- [2] Yu H, Mouw J K and Weaver V M 2010 Forcing form and function: biomechanical regulation of tumor evolution *Trends Cell Biol.*
- [3] Engler A J *et al* 2006 Matrix elasticity directs stem cell lineage specification *Cell* **126** 677–89
- [4] Engler A J *et al* 2008 Embryonic cardiomyocytes beat best on a matrix with heart-like elasticity: scar-like rigidity inhibits beating *J. Cell Sci.* **121** 3794–802
- [5] Klocke R *et al* 2003 Arterial stiffness and central blood pressure, as determined by pulse wave analysis, in rheumatoid arthritis *Ann. Rheum. Dis.* **62** 414–8

Q3

Q4

Q5

- [6] Flanagan L A *et al* 2002 Neurite branching on deformable substrates *Neuroreport* **13** 2411–5
- [7] Flanagan L A, Ju Y E and Janmey P A 2000 Growth and branching of neuronal processes on deformable substrates *Mol. Biol. Cell* **11** 458
- [8] Levental K R *et al* 2009 Matrix crosslinking forces tumor progression by enhancing integrin signaling *Cell* at press
- [9] Paszek M J and Weaver V M 2004 The tension mounts: mechanics meets morphogenesis and malignancy *J. Mammary Gland Biol. Neoplasia* **9** 325–42
- [10] Paszek M J *et al* 2005 Tensional homeostasis and the malignant phenotype *Cancer Cell* **8** 241–54
- [11] Pelham R J Jr and Wang Y 1997 Cell locomotion and focal adhesions are regulated by substrate flexibility *Proc. Natl Acad. Sci. USA* **94** 13661–5
- [12] Yeung T *et al* 2005 Effects of substrate stiffness on cell morphology, cytoskeletal structure, and adhesion *Cell Motil. Cytoskeleton* **60** 24–34
- [13] Wong J Y *et al* 2003 Directed movement of vascular smooth muscle cells on gradient-compliant hydrogels *Langmuir* **19** 1908–13
- [14] Gaudet C *et al* 2003 Influence of type I collagen surface density on fibroblast spreading, motility, and contractility *Biophys. J.* **85** 3329–35
- [15] Heidemann S R and Wirtz D 2004 Towards a regional approach to cell mechanics *Trends Cell Biol.* **14** 160–6
- [16] Discher D E, Janmey P and Wang Y L 2005 Tissue cells feel and respond to the stiffness of their substrate *Science* **310** 1139–43
- [17] Engler A J *et al* 2004 Myotubes differentiate optimally on substrates with tissue-like stiffness: pathological implications for soft or stiff microenvironments *J. Cell Biol.* **166** 877–87
- [18] Reinhart-King C A, Dembo M and Hammer D A 2008 Cell–cell mechanical communication through compliant substrates *Biophys. J.* **95** 6044–51
- [19] Califano J P and Reinhart-King C A 2009 The effects of substrate elasticity on endothelial cell network formation and traction force generation *Conf. Proc. IEEE Eng. Med. Biol. Soc.* **2009** 3343–5
- [20] Khatiwala C B *et al* 2009 ECM compliance regulates osteogenesis by influencing MAPK signaling downstream of RhoA and ROCK *J. Bone Miner. Res.* **24** 886–98
- [21] Gardel M L *et al* 2008 Traction stress in focal adhesions correlates biphasically with actin retrograde flow speed *J. Cell Biol.* **183** 999–1005
- [22] Pasapera A M *et al* 2010 Myosin II activity regulates vinculin recruitment to focal adhesions through FAK-mediated paxillin phosphorylation *J. Cell Biol.* **188** 877–90
- [23] Gardel M L *et al* 2010 Mechanical integration of actin and adhesion dynamics in cell migration *Annu. Rev. Cell Dev. Biol.* **26** 315–33
- [24] Lee J S *et al* 2006 Ballistic intracellular nanorheology reveals ROCK-hard cytoplasmic stiffening response to fluid flow *J. Cell Sci.* **119** 1760–8
- [25] Khatau S B *et al* 2009 A perinuclear actin cap regulates nuclear shape *Proc. Natl Acad. Sci. USA* **106** 19017–22
- [26] Lee J S *et al* 2007 Nuclear lamin A/C deficiency induces defects in cell mechanics, polarization, and migration *Biophys. J.* **93** 2542–52
- [27] Spencer V A, Xu R and Bissell M J 2010 Gene expression in the third dimension: the ECM-nucleus connection *J. Mammary Gland Biol. Neoplasia* **15** 65–71
- [28] Boudreau N, Werb Z and Bissell M J 1996 Suppression of apoptosis by basement membrane requires three-dimensional tissue organization and withdrawal from the cell cycle *Proc. Natl Acad. Sci. USA* **93** 3509–13
- [29] Wang F *et al* 2002 Phenotypic reversion or death of cancer cells by altering signaling pathways in three-dimensional contexts *J. Natl Cancer Inst.* **94** 1494–503
- [30] Weaver V M *et al* 1997 Reversion of the malignant phenotype of human breast cells in three-dimensional culture and *in vivo* by integrin blocking antibodies *J. Cell Biol.* **137** 231–45
- [31] Weaver V M *et al* 1996 The importance of the microenvironment in breast cancer progression: recapitulation of mammary tumorigenesis using a unique human mammary epithelial cell model and a three-dimensional culture assay *Biochem. Cell Biol.* **74** 833–51
- [32] Pedersen J A and Swartz M A 2005 Mechanobiology in the third dimension *Ann. Biomed. Eng.* **33** 1469–90
- [33] Pampaloni F, Reynaud E G and Stelzer E H 2007 The third dimension bridges the gap between cell culture and live tissue *Nat. Rev. Mol. Cell Biol.* **8** 839–45
- [34] Weaver V M *et al* 2002 Beta4 integrin-dependent formation of polarized three-dimensional architecture confers resistance to apoptosis in normal and malignant mammary epithelium *Cancer Cell* **2** 205–16
- [35] Zahir N and Weaver V M 2004 Death in the third dimension: apoptosis regulation and tissue architecture *Curr. Opin. Genet. Dev.* **14** 71–80
- [36] Jacks T and Weinberg R A 2002 Taking the study of cancer cell survival to a new dimension *Cell* **111** 923–5
- [37] Tse J R and Engler A J 2011 Stiffness gradients mimicking *in vivo* tissue variation regulate mesenchymal stem cell fate *PLoS One* **6** e15978
- [38] Provenzano P P *et al* 2008 Collagen density promotes mammary tumor initiation and progression *BMC Med.* **6** 11
- [39] Barcellos-Hoff M H *et al* 1989 Functional differentiation and alveolar morphogenesis of primary mammary cultures on reconstituted basement membrane *Development* **105** 223–35
- [40] Foster C S *et al* 1983 Human mammary gland morphogenesis *in vitro*: the growth and differentiation of normal breast epithelium in collagen gel cultures defined by electron microscopy, monoclonal antibodies, and autoradiography *Dev. Biol.* **96** 197–216
- [41] Richards J *et al* 1983 Response of end bud cells from immature rat mammary gland to hormones when cultured in collagen gel *Exp. Cell Res.* **147** 95–109
- [42] Emerman J T, Burwen S J and Pitelka D R 1979 Substrate properties influencing ultrastructural differentiation of mammary epithelial cells in culture *Tissue Cell* **11** 109–19
- [43] Chalupowicz D G *et al* 1995 Fibrin II induces endothelial cell capillary tube formation *J. Cell Biol.* **130** 207–15
- [44] Ghajar C M *et al* 2008 The effect of matrix density on the regulation of 3D capillary morphogenesis *Biophys. J.* **94** 1930–41
- [45] Roeder B A *et al* 2002 Tensile mechanical properties of three-dimensional type I collagen extracellular matrices with varied microstructure *J. Biomech. Eng.* **124** 214–22
- [46] Ulrich T A *et al* 2010 Probing cellular mechanobiology in three-dimensional culture with collagen–agarose matrices *Biomaterials* **31** 1875–84
- [47] Lutolf M P *et al* 2003 Synthetic matrix metalloproteinase-sensitive hydrogels for the conduction of tissue regeneration: engineering cell-invasion characteristics *Proc. Natl Acad. Sci. USA* **100** 5413–8
- [48] Seliktar D *et al* 2004 MMP-2 sensitive, VEGF-bearing bioactive hydrogels for promotion of vascular healing *J. Biomed. Mater. Res. A* **68** 704–16
- [49] Schmedlen R H, Masters K S and West J L 2002 Photocrosslinkable polyvinyl alcohol hydrogels that can be modified with cell adhesion peptides for use in tissue engineering *Biomaterials* **23** 4325–32

- [50] Mann B K and West J L 2002 Cell adhesion peptides alter smooth muscle cell adhesion, proliferation, migration, and matrix protein synthesis on modified surfaces and in polymer scaffolds *J. Biomed. Mater. Res.* **60** 86–93
- [51] Kloxin A M *et al* 2009 Photodegradable hydrogels for dynamic tuning of physical and chemical properties *Science* **324** 59–63
- [52] DeForest C A, Polizzotti B D and Anseth K S 2009 Sequential click reactions for synthesizing and patterning three-dimensional cell microenvironments *Nat. Mater.* **8** 659–64
- [53] Caplan M R *et al* 2002 Control of self-assembling oligopeptide matrix formation through systematic variation of amino acid sequence *Biomaterials* **23** 219–27
- [54] Zhang S *et al* 1995 Self-complementary oligopeptide matrices support mammalian cell attachment *Biomaterials* **16** 1385–93
- [55] Sieminski A L *et al* 2007 The stiffness of three-dimensional ionic self-assembling peptide gels affects the extent of capillary-like network formation *Cell Biochem. Biophys.* **49** 73–83
- [56] Gelain F *et al* 2006 Designer self-assembling peptide nanofiber scaffolds for adult mouse neural stem cell 3-dimensional cultures *PLoS One* **1** e119
- [57] Horii A *et al* 2007 Biological designer self-assembling peptide nanofiber scaffolds significantly enhance osteoblast proliferation, differentiation and 3D migration *PLoS One* **2** e190
- [58] Wang S *et al* 2008 Three-dimensional primary hepatocyte culture in synthetic self-assembling peptide hydrogel *Tissue Eng.*
- [59] Genove E *et al* 2009 Functionalized self-assembling peptide hydrogel enhance maintenance of hepatocyte activity *in vitro* *J. Cell Mol. Med.* **13** 3387–97
- [60] Johnson K R, Leight J L and Weaver V M 2007 Demystifying the effects of a three-dimensional microenvironment in tissue morphogenesis *Methods Cell Biol.* **83** 547–83
- [61] Zahir N *et al* 2003 Autocrine laminin-5 ligates alpha6beta4 integrin and activates RAC and NFkappaB to mediate anchorage-independent survival of mammary tumors *J. Cell Biol.* **163** 1397–407
- [62] Gudjonsson T *et al* 2002 Normal and tumor-derived myoepithelial cells differ in their ability to interact with luminal breast epithelial cells for polarity and basement membrane deposition *J. Cell Sci.* **115** 39–50
- Q6 [63] Lopez *et al* 2010 in revision
- [64] Fischer R S *et al* 2009 Local cortical tension by myosin II guides 3D endothelial cell branching *Curr. Biol.* **19** 260–5
- [65] Zaman M H, Matsudaira P and Lauffenburger D A 2007 Understanding effects of matrix protease and matrix organization on directional persistence and translational speed in three-dimensional cell migration *Ann. Biomed. Eng.* **35** 91–100
- [66] Kim H D *et al* 2008 Epidermal growth factor-induced enhancement of glioblastoma cell migration in 3D arises from an intrinsic increase in speed but an extrinsic matrix- and proteolysis-dependent increase in persistence *Mol. Biol. Cell* **19** 4249–59
- [67] Provenzano P P *et al* 2008 Contact guidance mediated three-dimensional cell migration is regulated by Rho/ROCK-dependent matrix reorganization *Biophys. J.* **95** 5374–84
- [68] Cima L G *et al* 1991 Hepatocyte culture on biodegradable polymeric substrates *Biotechnol. Bioeng.* **38** 145–58
- [69] Cima L G *et al* 1991 Tissue engineering by cell transplantation using degradable polymer substrates *J. Biomech. Eng.* **113** 143–51
- [70] Domansky K *et al* 2010 Perfused multiwell plate for 3D liver tissue engineering *Lab Chip* **10** 51–8
- [71] Burdick J A and Anseth K S 2002 Photoencapsulation of osteoblasts in injectable RGD-modified PEG hydrogels for bone tissue engineering *Biomaterials* **23** 4315–23
- [72] Hoque M E *et al* 2005 Fabrication using a rapid prototyping system and *in vitro* characterization of PEG-PCL-PLA scaffolds for tissue engineering *J. Biomater. Sci. Polym. Ed.* **16** 1595–610
- [73] Brigham M D *et al* 2009 Mechanically robust and bioadhesive collagen and photocrosslinkable hyaluronic acid semi-interpenetrating networks *Tissue Eng. A* **15** 1645–53
- [74] Chung C *et al* 2009 The influence of degradation characteristics of hyaluronic acid hydrogels on *in vitro* neocartilage formation by mesenchymal stem cells *Biomaterials* **30** 4287–96
- [75] Genove E *et al* 2005 The effect of functionalized self-assembling peptide scaffolds on human aortic endothelial cell function *Biomaterials* **26** 3341–51
- [76] Sieminski A L *et al* 2008 Primary sequence of ionic self-assembling peptide gels affects endothelial cell adhesion and capillary morphogenesis *J. Biomed. Mater. Res. A* **87** 494–504
- [77] Paszek M J *et al* 2005 Tensional homeostasis and the malignant phenotype *Cancer Cell* **8** 241–54
- [78] Beil M *et al* 2003 Sphingosylphosphorylcholine regulates keratin network architecture and visco-elastic properties of human cancer cells *Nat. Cell Biol.* **5** 803–11
- [79] Colpaert C *et al* 2001 The presence of a fibrotic focus is an independent predictor of early metastasis in lymph node-negative breast cancer patients *Am. J. Surg. Pathol.* **25** 1557–8
- [80] Peyton S R *et al* 2006 The use of poly(ethylene glycol) hydrogels to investigate the impact of ECM chemistry and mechanics on smooth muscle cells *Biomaterials* **27** 4881–93
- [81] Peyton S R *et al* 2008 The effects of matrix stiffness and RhoA on the phenotypic plasticity of smooth muscle cells in a 3D biosynthetic hydrogel system *Biomaterials* **29** 2597–607
- [82] Patterson J and Hubbell J A 2010 Enhanced proteolytic degradation of molecularly engineered PEG hydrogels in response to MMP-1 and MMP-2 *Biomaterials* **31** 7836–45
- [83] Ayala P, Lopez J I and Desai T A 2010 Microtopographical cues in 3D attenuate fibrotic phenotype and extracellular matrix deposition: implications for tissue regeneration *Tissue Eng. A* **16** 2519–27
- [84] Collins J M *et al* 2010 Three-dimensional culture with stiff microstructures increases proliferation and slows osteogenic differentiation of human mesenchymal stem cells *Small* **6** 355–60
- [85] Bernards D A and Desai T A 2010 Nanotemplating of biodegradable polymer membranes for constant-rate drug delivery *Adv. Mater.* **22** 2358–62
- [86] Choquet D, Felsenfeld D P and Sheetz M P 1997 Extracellular matrix rigidity causes strengthening of integrin-cytoskeleton linkages *Cell* **88** 39–48
- [87] Chen C S *et al* 1997 Geometric control of cell life and death *Science* **276** 1425–8
- [88] Provenzano P P *et al* 2006 Collagen reorganization at the tumor–stromal interface facilitates local invasion *BMC Med.* **4** 38
- [89] Rhee S and Grinnell F 2007 Fibroblast mechanics in 3D collagen matrices *Adv. Drug Deliv. Rev.* **59** 1299–305
- [90] Harley B A *et al* 2008 Microarchitecture of three-dimensional scaffolds influences cell migration behavior via junction interactions *Biophys. J.* **95** 4013–24
- [91] Zaman M H *et al* 2005 Computational model for cell migration in three-dimensional matrices *Biophys. J.* **89** 1389–97
- [92] Zaman M H *et al* 2006 Migration of tumor cells in 3D matrices is governed by matrix stiffness along with cell-matrix adhesion and proteolysis *Proc. Natl Acad. Sci. USA* **103** 10889–94

- [93] Butcher D T, Alliston T and Weaver V M 2009 A tense situation: forcing tumour progression *Nat. Rev. Cancer* **9** 108–22
- [94] Albiges-Rizo C *et al* 2009 Actin machinery and mechanosensitivity in invadopodia, podosomes and focal adhesions *J. Cell Sci.* **122** 3037–49
- [95] Stricker J, Falzone T and Gardel M L 2010 Mechanics of the F-actin cytoskeleton *J. Biomech.* **43** 9–14
- [96] Borghi N *et al* 2010 Regulation of cell motile behavior by crosstalk between cadherin- and integrin-mediated adhesions *Proc. Natl Acad. Sci. USA* **107** 13324–9

QUERIES

Page 5

Q1

Author: Please check whether the edit made in the sentence ‘Importantly, SEM analysis revealed that unlike . . .’ retains your intended sense.

Page 9

Q2

Author: Please check whether the change in figure label from (*D*) to (*E*) in caption to figure 4 is okay as set.

Page 10

Q3

Author: Please check the details for any journal references that do not have a blue link as they may contain some incorrect information. Pale purple links are used for references to arXiv e-prints.

Q4

Author: Please provide volume number and page range in references [2] and [58].

Page 11

Q5

Author: Please provide volume number and page range in reference [8] if possible.

Page 12

Q6

Author: Please update reference [63] if possible.

N-CoR2 induces therapy-resistance in tumors by repressing apoptosis amplification

Kelvin K.-C. Tsai^{1,2,3,4}, Chandrima Chatterjee², Jimmy J.-M. Su⁴, I. Saira Mian⁵, Michael E.

Werner¹, Jonathan N. Lakins¹ and Valerie M. Weaver^{1,2,6}

¹Department of Surgery and Center for Bioengineering and Tissue Regeneration, University of California, San Francisco, San Francisco, CA 94143

²Department of Pathology and Institute for Medicine and Engineering, University of Pennsylvania, Philadelphia, PA 19104

³Graduate Institute of Clinical Medicine, Taipei Medical University School of Medicine, Taipei, 11031, Taiwan

⁴National Institute of Cancer Research, National Health Research Institutes, Tainan, 70456, Taiwan

⁵Life Sciences Division, Lawrence Berkeley National Laboratory, Berkeley, CA 94720

⁶Departments of Anatomy and Bioengineering and Therapeutic Sciences, Eli and Edythe Broad Center of Regeneration Medicine and Stem Cell Research and Helen Diller Family Comprehensive Cancer Center, University of California San Francisco, San Francisco, CA 94143

⁶To whom correspondence should be addressed:

Valerie M. Weaver, University of California, San Francisco

513 Parnassus Avenue, 565 Health Sciences East

San Francisco, CA 94143-0456

Email: Valerie.weaver@ucsfmedctr.org

Telephone: 415-476-3973

Fax: 415-476-3985

ABSTRACT

Death resistance in tumors contributes to therapeutic failure. We identified nuclear receptor co-repressor 2 (N-CoR2) modulation of IRF-1-dependent gene transcription as a mechanism whereby breast tissues resist chemotherapy, immune receptor and radiation-induced death. Multi-variant analysis showed that high N-CoR2 correlates with percent relapse-free and overall reduced breast cancer patient survival. Moreover, an N-CoR2-associated gene signature identified primary breast tumors predisposed to chemotherapy resistance and poor therapeutic outcome. Consistently, molecular studies *in vitro* and *in vivo* demonstrated that the N-CoR2/HDAC3 complex confers death resistance in breast tissues by restricting the CBP-IRF-1-dependent transcription of a network of pro-apoptotic genes. Thus, by exploiting a three-dimensional tissue-based assay we identified a novel transcriptional reprogramming mechanism up-regulated in aggressive, recurrent breast tumors that induces pleiotropic treatment resistance and associates with patient mortality.

INTRODUCTION

The development of drug resistance by tumor cells significantly limits the efficacy of anti-neoplastic treatment and is the major cause of patient mortality¹. Despite significant advances in understanding how apoptosis is executed at the cellular level² and clarifying the molecular basis of cell death resistance *in vitro*³ we still know relatively little about the pathogenesis of treatment resistance in cancerous tissues *in vivo*^{4,5}.

Therapeutic failure of human cancers could arise from environmental pressures that favor the growth and survival of a genetically-modified tumor cell population^{6,7}. Treatment resistance might also derive from the inherent survival advantages intrinsic to pre-existing “stem-like” or “pluripotent” cells within the tumor^{8,9,10}. Furthermore, treatment response varies between cancer cells located within the primary tumor tissue versus those at different metastatic sites, indicating tissue context and the tissue stroma also influence the treatment response of a tumor^{1,11,12,13-15}. In this regard, the extracellular stroma modulates tissue architecture, and tissue polarity and dimensionality significantly modulate the survival and apoptosis responsiveness of three-dimensional (3D) spheroids in culture and xenografted tumors *in vivo*¹⁶. How tissue architecture modulates cell survival and treatment resistance and the clinical relevance of these findings remains unclear.

Cells within 3D spheroids are more resistant to apoptotic stimuli than cells grown as a two dimensional (2D) monolayer^{16,17}. Multi-cellular "spheroid" resistance has been attributed

to reduced drug penetration, altered cell proliferation and tissue hypoxia^{17,18}. Yet, mammary epithelial cells (MECs) incorporated into 3D polarized, normoxic spheroids exhibit significant apoptosis resistance to diverse exogenous death stimuli, regardless of proliferation status and despite excellent drug penetration^{5,16}. This finding suggests additional factors associated with tissue architecture influence cell survival.

Tissue development is associated with epigenetic modulation of gene expression¹⁹. Morphogenesis of MECs in 3D reconstituted basement membrane (rBM) is likewise associated with striking changes in nuclear architecture and chromatin structure and altered patterns of histone acetylation and DNA methylation^{20,21}. Consistent with the notion that epithelial morphogenesis is linked to epigenetic reprogramming, spheroid (acini) morphogenesis correlates with global modulation of gene expression^{22,23}, and treatment of acini with HDAC or methylation inhibitors disrupts MEC differentiation, modifies gene expression and perturbs tissue architecture^{20,24}. These findings suggest functional links exist between tissue organization, epigenetic reprogramming and cell survival. Consistently, HDAC inhibitors can induce apoptosis in multidrug-resistant (MDR) tumor cells and HDAC inhibitors can sensitize cancer cells to chemotherapeutic agents and ionizing radiation (IR)²⁵⁻²⁷. As a consequence, HDAC inhibitors have been developed to treat cancers and are being tested in clinical trials as potential anti-tumor agents²⁸⁻³⁰. Here we asked whether the apoptosis resistance phenotype exhibited by breast spheroids could be attributed to epigenetic

reprogramming of gene expression, and how. We reasoned that treatment resistant tumors might exploit a similar mechanism to evade treatment so that identifying the molecular mechanism underlying this phenotype would provide novel insight towards solving the intractable clinical problem of treatment resistance in tumor tissues.

RESULTS

Treatment resistance in multi-cellular spheroids is linked to chromatin remodeling

We observed that nonmalignant S-1 HMT-3522 (S-1) MECs within rBM (3D) assemble acini with marked chromatin hypoacetylation indicated by reduced acetylated H3 and H4 and hypermethylation, as shown by high trimethyl (Me3)-H3K27 and Me3-H3K9 (**Fig 1a**). Chromatin remodeling was accompanied by increased levels of the methylation regulatory protein methyl-CpG-binding protein 2 (MeCP2) and heterochromatin protein 1 (HP1; **Fig 1a**) and a global modulation of gene expression (not shown). The acini also displayed a dose-dependent apoptosis resistance to the death receptor ligand TNF-related apoptosis inducing ligand (TRAIL), the chemotherapeutic agent paclitaxel and to IR exposure when compared to rBM-ligated MECs grown in 2D (**Fig 1b**)¹⁶. Critically, the acini were significantly sensitized to all death stimuli following pre-treatment with the HDAC inhibitor trichostatin A (100 nM; 12 hrs; TSA) (**Fig. 1b**) or the DNA methyltransferase inhibitor 5-Aza-2'-deoxycytidine (**Supplementary Fig. 1a**). These observations suggest that tissue morphogenesis, gene transcription and death resistance are coordinately regulated through an epigenetic mechanism.

N-CoR2 mediates treatment resistance in mammary acini

To identify candidate epigenetic regulators linked to tissue morphogenesis we interrogated

expression arrays for genes differentially-expressed between rBM-ligated MECs plated as 2D versus MECs within acini (3D; not shown). We focused on genes encoding nuclear proteins implicated in epigenetics. Nuclear receptor co-repressor 2 (N-CoR2; *NCOR2*) was identified as a gene significantly and consistently up-regulated at the mRNA and protein level in the S-1s in 3D as compared to 2D (**Fig. 1c,d**).

N-CoR2 and its paralog N-CoR are transcriptional co-repressors that mediate transcriptional repression through specific histone hypoacetylation^{31,32} by recruiting nuclear cofactors and activating HDACs^{33,34}. We observed that a component of the N-CoR2 protein complex, G protein pathway suppressor 2 (*GPS2*), was also up-regulated in the death-resistant acini, whereas HDAC1, another cellular deacetylase effector that binds to N-CoR2, and N-CoR1 (*NCOR1*), a paralog of N-CoR2, were not^{31,32,34}.

To explore the functional significance of N-CoR2 we stably knocked down endogenous N-CoR2 using retrovirus-based RNA interference and assayed for effects on treatment response (**Fig. 1e**). Stable knockdown of N-CoR2 did not modify growth or acinar morphogenesis nor did it compromise survival whether the S-1s were grown in 2D or 3D (**Fig. 1e**; **Supplementary Fig. 1b**). However, loss of N-CoR2 substantially increased the death responsiveness of acini to TRAIL-, paclitaxel-, doxorubicin- and IR-induced death, so that apoptosis levels were equivalent to that exhibited by either S-1s grown in 2D or 3D acini that had been treated with TSA (**Fig. 1f**). These results suggest that N-CoR2 contributes to the

death resistance phenotype of mammary acini.

N-CoR2 promotes treatment resistance in breast tumors

Because tumors often exploit developmental pathways to survive, and N-CoR2 regulates T cell development³⁵, we surveyed a cohort of 38 breast cancer specimens for N-CoR2 status.

We found that greater than 50 percent of breast tumor tissues (72.5%) expressed high N-CoR2 ($\geq 2+$) and that a large proportion showed robust nuclear staining (**Fig 2a**).

Multivariate analysis demonstrated that N-CoR2 expression associates significantly with the likelihood of breast cancer disease relapse and mortality, independent of standard clinico-pathological variables (CPV) and molecular subtype (see **Supplementary Table 1 and Fig. 2b** online). Moreover, in a large cohort of 295 breast cancer patients³⁶, those tumors that expressed higher levels of N-CoR2 had a significantly greater probability of post-therapeutic disease relapse and mortality (see **Supplementary Fig. 2a** online). We noted that N-CoR2 expression significantly associated with clinical outcome in patients who had received adjuvant chemotherapy (CT; **Fig. 2b**) implying N-CoR2 contributes to poor prognosis by attenuating the sensitivity of breast tumors to CT-induced regression.

To clarify links between N-CoR2 and tumor treatment, we retro-virally elevated N-CoR2 in two malignant, triple-negative breast tumor cell lines, HMT-3522 T4-2 (an early transformed progeny of S-1 cells¹⁶ and MDA-MB-231 MECs (metastatic breast cancer cells),

using a full-length, GFP-tagged N-CoR2 (**Fig. 2c**; top). Nuclear expression of GFP N-CoR2 (**Fig. 2c**; bottom) had minimal effects on cell proliferation and tissue architecture (data not shown) and rendered the tumor cells highly resistant to apoptosis following stimulation with TRAIL and paclitaxel (**Fig. 2d**). N-CoR2 also enhanced clonogenic survival, as illustrated by the rapid colony re-growth in rBM observed following acute exposure of breast cancer cells to IR (**Fig. 2f**). Both breast cancer cell lines expressing high N-CoR2 showed significantly enhanced death resistance whether they were plated in 2D or within 3D rBM as single cells or multi-cellular spheroid structures indicating N-CoR2 mediates death resistance through an intrinsic mechanism (**Fig. 2d,e**).

To explore the *in vivo* relevance of N-CoR2, MDA-MB-231 MECs retro-virally expressing a firefly luciferase together with empty vector or N-CoR2 were ortho-topically implanted into the mammary fat pads of immuno-deficient NOD-SCID mice. The injected mice were then assayed over a 6 week time frame for tumor growth using bioluminescence imaging (BLI) and cellular proliferation (Ki67) and viability (activated caspase 3) were monitored using immunohistochemistry in excised tissues. N-CoR2-expressing tumor cells showed similar proliferation rates to those formed by vector controls cells and formed lesions of a similar size 5-6 weeks after tumor cell implantation (**Fig. 2i** and see **Supplementary Fig. 2c** online). To determine whether N-CoR2 could modify the treatment responsiveness of these breast lesions, two weeks following tumor cell transplantation (when tumor size was

similar), weekly administration of a clinically relevant dose of paclitaxel (20 mg/kg) was initiated, and tumor growth was monitored using BLI. Paclitaxel treatment of the control tumors resulted in a 50% reduction of tumor bulk whereas the MDA-MB-231-N-CoR2 tumor xenografts remained refractory to the paclitaxel treatment. Thus, 4 weeks after treatment the N-CoR2 tumors were approximately double the size of the paclitaxel treated vector control tumors (**Fig. 2i**), and dissected tumors showed significantly reduced numbers of caspase positive cells (**Fig. 2h** and see **Supplementary Fig. 2c** online). Furthermore, compared with mice harboring vector control tumors, animals with N-CoR2-expressing tumors exhibited significantly reduced survival ($P < 0.001$) so that none of these animals survived 3 months beyond paclitaxel treatment (**Fig. 2j**). These findings identify N-CoR2 as an intrinsic and clinically relevant breast tumor treatment modifier in culture and *in vivo*.

N-CoR2 collaborates with HDAC3 to mediate treatment resistance in tumor cells

We next asked whether N-CoR2 regulated death responsiveness in breast cancer cells by modulating HDAC-driven chromatin remodeling. In line with this possibility, treatment with either the HDAC inhibitor suberoylanilide hydroxamic acid (SAHA) or TSA significantly increased the sensitivity of N-CoR2 expressing tumor spheroids to TRAIL (**Fig. 3a**) and chemotherapy-induced death (not shown). T4-2 cells expressing high N-CoR2 were also markedly sensitized to death stimuli and exhibited apoptosis levels comparable to tumor cells

with low N-CoR2 when HDAC3 was stably down-regulated using retroviral-mediated RNAi (**Fig. 3b**). Consistently, T4-2 cells expressing a mutant N-CoR K449A, which binds HDAC3 and inhibits its deacetylase activity, were remarkably sensitive to death stimuli (**Fig. 3c,d**)³². In fact, the apoptotic levels achieved by K449A expression greatly exceeded the amount of death induced in the T4-2 vector controls, consistent with the competitive inhibitory function of this mutant N-CoR2 on HDAC3 activity (**Fig. 3e**). These data indicate that the nuclear deacetylase activity of HDAC3 is critical for N-CoR2-mediated death resistance in breast tumor cells.

N-CoR2/HDAC3 transcriptional activity predicts treatment refractoriness in human breast cancers

We next addressed the clinical significance of N-CoR2. Analysis of the M.D. Anderson Cancer Center (MDACC) neoadjuvant chemotherapy (NACT) trial microarray data set, representing a cohort of 130 breast cancer patients with pathologically-defined treatment responsiveness who had received preoperative combination CT with paclitaxel and fluorouracil-doxorubicin-cyclophosphamide (T/FAC)³⁷ showed that tumors with higher N-CoR2 expression had a 2.2-fold increased odds ratio of NACT response failure when compared to tumors with lower N-CoR2 (**Fig. 4a** and see **Supplementary Table 2** online). We also noted that the link between elevated N-CoR2 and treatment refractoriness in cancer

patients was not CT regimen-specific, because we observed a similar association in breast cancer patients who had received other NACT chemotherapies including docetaxel³⁸ and epirubicin versus cyclophosphamide³⁹(**Fig. 4a**).

N-CoR2 is subject to complex post-transcriptional regulation and interacts with a multitude of cofactors that influence its nuclear localization and function^{40,41}. To address this issue we used a polygenic approach to monitor its transcriptional regulatory activity. We profiled the gene expression of vector control versus N-CoR2-expressing T4-2 rBM mammary spheroids (**Fig. 4b**) by compiling a list of 304 genes (represented by 350 Affymetrix probe sets) whose expression was significantly altered by N-CoR2 (**Fig. 4b,c**). We identified a list of 107 genes from these N-CoR2-associated genes (represented by 116 Affymetrix probe sets, designated as “*NCOR2-116*”) whose baseline expression variability correlated with the treatment response of the 130 breast tumors in the patients represented within the MDACC data set ($P < 0.05$ by Student’s *t* test). An unsupervised hierarchical clustering algorithm segregated these 107 genes into a distinct biphasic pattern of gene expression such that the 130 tumors segregated into highly chemo-responsive versus non-responsive groups (**Fig. 4d**). To verify associations between our experimentally-derived gene expression data set and clinical responsiveness of patients from the MDACC study we used Pearson’s correlation coefficient to develop a similarity score (S_{NCOR2}) (**Fig. 4e**). Tumors with a high S_{NCOR2} (*i.e.* that showed the greatest gene expression similarity to N-CoR2

expressing T4-2 spheroids) had a 10.7-fold increased odds ratio of NACT response failure (see **Supplementary Table 2** online). Moreover, compared with standard CPV of breast cancers such as age, tumor size, grade, LN, ER and HER2 status, the S_{NCOR2} score measure was the strongest (odds ratio 8.9) and most significant ($P < 0.001$) independent predictor of reduced NACT response (**Fig. 4f**). Application of the unsupervised, hierarchical clustering algorithm to the 110 breast tumors in the NKI data set of patients who had received adjuvant CT additionally showed a strong association between the N-CoR2-associated gene signature (“*NCOR2-63*”, which corresponds to the genes in *NCOR2-116*) and reduced time to relapse and percent survival (**Fig. 4g,h**). These findings imply that N-CoR2-associated polygenic transcriptional activity contributes to the intrinsic treatment responsiveness of human breast tumors in both the neoadjuvant and adjuvant settings. Accordingly, N-CoR2 transcriptional activity has potential significance as a predictor of patient outcome.

Functional gene annotation and clustering analysis showed that genes encoding secreted proteins and those involved in inflammatory response, migration, adhesion, differentiation and proliferation were enriched in the 304 N-CoR2-associated gene set (see **Supplementary Fig. 3** online). Nevertheless, genes directly regulating cell death execution and responsiveness or MDR were surprisingly under-represented, suggesting N-CoR2 must mediate cellular death resistance behavior through additional mechanisms.

Because N-CoR2 regulates the expression of inflammatory genes including NF- κ B,

AP-1, and ETS-dependent genes^{41,42}, and the efficiency of tumor treatment in patients relies upon transcriptional up-regulation of pro-apoptotic pathways that participate in death amplification and bystander-mediated cell death⁴³⁻⁴⁵, we asked whether N-CoR2 rendered tumor cells treatment resistant by preventing apoptosis amplification. We acutely treated N-CoR2 and vector control T4-2 spheroids with TRAIL (4 hours), a gene up-regulated in response to CT and radiation treatment⁴³, in the presence of caspase inhibitors to prevent apoptosis execution. A *Differential Response Index (DRI)* was then used to identify 1328 genes (represented by 1620 Affymetrix probe sets; designated as “*NCOR2-1620*”) whose induced or repressed differential expression depended upon N-CoR2. Most of these genes in *NCOR2-1620* were less inducible in the tumor spheroids with the higher N-CoR2 (**Fig. 4b**) and Venn analysis revealed that only 166 (12.5 %) of these 1328 genes overlapped with the N-CoR2-associated gene expression profile found in cells in the absence of exogenous stress stimuli (**Fig. 4c**). Functional gene clustering and promoter analysis of the *NCOR2-1620* gene data set demonstrated that following TRAIL treatment N-CoR2 profoundly repressed the expression of genes involved in organelle organization and biogenesis, acetylation and programmed cell death (PCD) including those implicated in bystander-mediated cell killing (**Fig. 5a** and data not shown). These data are consistent with the idea that N-CoR2 actively represses PCD and tempers amplification of cell killing following treatment^{41,42}.

N-CoR2 attenuates death induction by repressing the transcription of a signature of programmed cell death genes that regulate cell death amplification

To explore the molecular pathways by which N-CoR2 confers resistance to death stimuli in breast tumor cells, we focused on a list of 64 programmed cell death genes (PCD genes; GO:0012501; represented by 75 Affymetrix probe sets; **Fig. 5b**), derived from the *NCOR2-1620* gene set. Analysis showed that the majority of these PCD-related genes were less inducible following TRAIL or chemotherapy exposure when N-CoR2 expression was elevated (52 genes; see **Supplementary Table 3** online). Furthermore, several anti-apoptotic proteins, including *TRAF1*, *MYBL2*, *BIRC5* and *BCL2L1*, were more inducible by TRAIL exposure and chemotherapy treatment in the tumor cells expressing high N-CoR2 (**Fig. 5b,e**). Promoter analysis revealed that the 5' promoter region of many of these PCD-related genes contained the consensus binding site for pro-inflammatory transcription factors (TFs) such as interferon regulatory factor-1 (IRF-1), signal transducer and activator of transcription-1 (STAT-1), the forkhead box (FOX) protein forkhead-related activator 2 (FOXF-2) and the ETS domain protein ELK-4 (**Fig. 5c**). Although FOX and ETS family proteins, including FOXP-1 and TEL, interact with N-CoR2 in other cell types, and Fox proteins regulate cancer pathology^{42,46}, the most prevalent TF binding site identified in these PCD-related gene promoters was IRF-1 ($n = 28$; 50% of the genes analyzed; **Fig. 5b** (yellow bars) and see **Supplementary Table 4** online). Moreover, the IRF-1 regulated genes were by far the most

significantly repressed by N-CoR2 following TRAIL treatment (**Fig. 5c**), and IRF-1 is an important regulator of PCD⁴⁷. Based upon these observations we chose IRF-1 for additional analysis.

We verified that N-CoR2 consistently and significantly repressed TRAIL-dependent up-regulation of several IRF-1-regulated genes including *TNFSF10* and *STAT1* in both T4-2 and MDA-MB-231 breast tumor cells (**Fig. 5e** and data not shown). N-CoR2 also reduced the ability of the chemotherapeutic agents paclitaxel and doxorubicin from inducing the same PCD genes including *IRF1* and *TNFSF10* (**Fig. 5d**). Consistent with its ability to augment death, we identified Janus kinase-1 (*JAK1*), a kinase that regulates the interferon (INF) signaling, as another gene whose transcription was severely reduced in response to death stimuli when N-CoR2 levels were elevated (**Fig. 5e**). We thereafter implicated IRF-1 transcriptional repression as a key mechanism by which N-CoR2-mediates death resistance in tumor cells by demonstrating that several pro-apoptotic IRF-1-regulated enzymes, including caspases 1, 7 and 8, were also transcriptionally-repressed following TRAIL treatment in tumor cells expressing elevated N-CoR2 (**Fig. 5b,e**)^{48,49}.

We directly implicated IRF-1 transcriptional regulation in N-CoR2-mediated death resistance by demonstrating that N-CoR2 co-precipitated with IRF-1 in tumor cells ectopically-expressing GFP-labeled N-CoR2 (**Fig. 6a** (left)) and also interacted with the endogenous N-CoR2 expressed in the nonmalignant S-1 MECs (**Fig. 6a** (right)). Moreover,

while TRAIL treatment of breast tumor cells significantly increased the activity of an IRF-1 luciferase reporter containing the IRF regulatory factor element (IRF-E), ectopic expression of N-CoR2 significantly inhibited TRAIL-stimulated IRF transcriptional activity (**Fig. 6b** (left))⁴⁸. Indeed, IRF-1 luciferase activity assays demonstrated that N-CoR2 directly attenuates IRF-1-dependent transcription (**Fig. 6b** (right)). Importantly, chromatin immuno-precipitation (ChIP) assays showed that N-CoR2 and HDAC3 were directly recruited to the IRF-E consensus sequences in the promoter region of *TNFSF10* (**Fig. 6c** and see **Supplementary Fig. 4** online). Furthermore, ectopic expression of N-CoR2 induced significant histone hypoacetylation of the *TNFSF10* promoter and substantially attenuated interactions between IRF-1 and its coactivator CREB binding protein (CBP) indicative of dramatic effects on chromatin remodeling (**Fig. 6c,d**)⁵⁰. These findings suggest that N-CoR2 represses the transcriptional activity of IRF-1 by preventing co-activator recruitment and inducing HDAC3-dependent histone deacetylation (**Fig. 6g**).

The functional relevance of a link between IRF-N-CoR2 and HDAC3 and apoptosis resistance was illustrated by demonstrating that N-CoR2 was able to inhibit IRF-1-mediated cell death⁴⁷. Thus, whereas HEK293 cells transiently transfected with IRF-1 died rapidly by engaging pro-death apoptotic signaling, those cells simultaneously expressing exogenous N-CoR2 were significantly protected (**Fig. 6e**). Because the ChIP studies indicated that the cooperative recruitment of N-CoR2/HDAC3 and IRF to the *TNFSF10* promoter was

associated with local histone hypoacetylation (**Fig. 6c**), we asked whether chromatin remodeling and HDAC activity was critical to this death-resistance phenotype. Consistent with its repressor function N-CoR2 failed to inhibit expression of PCD genes in the absence of HDAC3 activity, as revealed by the strong TRAIL-stimulated induction of PCD genes in tumor cells expressing the functionally-deficient N-CoR2 (K449A) (**Fig. 5e**). These studies showed that HDAC3/N-CoR2 attenuates death induction in tumor cells by repressing the transcriptional amplification of a cassette of PCD genes critical for efficient cell killing. Indeed, many of the PCD genes are secreted and themselves induce apoptosis through the extrinsic pathway suggesting N-CoR2 restricts cell death in tumor cells not only by repressing cell death amplification but also likely by restricting bystander-mediated cell killing.

HDAC3/N-CoR2-mediates treatment resistance by tempering TRAIL-dependent bystander-mediated cell death amplification

The efficiency of tumor treatment relies on the concomitant transcriptional up-regulation of pro-apoptotic/pro-inflammatory cytokines such as TNF α and the TRAIL ligand, that following their secretion feedback through autocrine and paracrine signaling to amplify tumor cell killing by engaging cell death receptors^{51,52}. Consistent with this paradigm, amongst the N-CoR2-IRF-regulated PCD genes we observed that *TNFSF10* (TRAIL) was

repressed the most (*i.e.*, the lowest *DRI*) in response to death stimuli (**Fig. 5b**). Based on this result and the finding that transcriptional up-regulation and secretion of TRAIL induced cell death in leukemia cells following HDAC-inhibitor treatment⁵³, we reasoned that HDAC3/NCoR2 could repress death in breast cancer cells by blunting *TNFSF10* (TRAIL) transcription. Indeed, we could show that retroviral-mediated RNAi down-regulation of endogenous *TNFSF10* (TRAIL) significantly attenuated cell death induction in T4-2 breast cancer cells by approximately 50% (**Fig 6f**). These results underscore the importance of cell death amplification for efficient therapeutic responsiveness of tumors. They also identify a clinically-relevant "epigenetic" repressor mechanism that cripples this critical death amplification circuit to drive treatment resistance in tumors.

DISCUSSION

By exploiting a simple 3D MEC organoid model we defined a novel treatment resistance mechanism, mediated by the NCoR2 repressor complex, that is frequently up-regulated in recurrent, aggressive breast cancers and that predicts patient mortality. We found that breast tumor cells that express high levels of a functional N-CoR2/HDAC3 complex resist a plethora of pro-apoptotic stimuli (chemotherapies, immune receptor activators, gamma irradiation) and demonstrate enhanced clonogenic survival because this complex “epigenetically-inhibits cell death amplification” (**Fig. 6g**). Our findings indicate that this intrinsic N-CoR2-mediated death-resistance mechanism pre-exists within cells in the primary tumor, and that the phenotype is not confined to one breast cancer subtype. Our observations imply that this cell-death inhibitory phenotype manifests its effects following exposure to stress, at which time the complex confers profound resistance by coordinately modulating the levels of multiple components of the extrinsic and intrinsic cell death pathways. The data accord with the notion that apoptosis amplification, as exemplified by bystander-induced cell death, is a conserved, critical mechanism whereby the efficiency of tumor cell killing is increased in patients undergoing CT and radiation-treatment^{44,45}. The results are consistent with literature reporting that reduced expression or mutations in components of either the extrinsic or intrinsic cell death pathway account for some of the blunted therapy responsiveness observed in cultured cancer cells, in experimental tumors *in vivo* and in

cancer patients³. By extrapolation, the NCoR2-mediated survival mechanism builds upon the single hit mutation/selection/survival paradigm to define a novel mechanism whereby the activity of a few key chromatin remodeling proteins can dynamically modulate the level of multiple cell death regulatory molecules to significantly potentiate the treatment survival of a cell. As such, this PCD resistance mechanism could explain the quick evolution of MDR that arises in some cancers by incorporating the concept that chromatin remodeling can rapidly drive treatment resistance to a broad spectrum of reagents by epigenetically regulating intrinsic and extrinsic cell death signaling^{3,19,25-30}. Accordingly, this novel “epigenetic” mechanism may account for the enhanced mortality rates associated with many treatment-resistant, primary and metastatic human breast tumors. Indeed, our findings explain the observation that N-CoR2 is an independent predictor of poor outcome in breast cancer patients⁵⁴ and why high N-CoR2 associates significantly with some aggressive, therapy-resistant glioblastomas and ovarian carcinomas (data not shown). These results suggest that N-CoR2-mediated PCD gene regulation could be a fundamental mechanism by which many cancers evade therapy.

We identified NCoR2 as a death response regulator in MECs; findings that accord with work showing that N-CoR2 contributes to breast tumor recovery from IR by modulating the DNA-dependent protein kinase complex⁵⁵. Our studies expand this phenotype to show that N-CoR2 regulates the expression of a myriad of cell death signaling molecules (**Fig. 5c**).

While N-CoR2 was originally described as a repressor of non-ligated nuclear receptors³³, it is now appreciated that it facilitates gene silencing of a variety of non-receptor transcriptional factors⁵⁶. Consistently, we showed that the NCoR2/HDAC3 repressor complex augments the apoptotic responsiveness of cancer cells by actively competing with CBP to modulate the gene transcription of a network of IRF-1-regulated extrinsic and intrinsic cell death pathway molecules (**Fig. 6d**). In this respect our findings that *TNFSF10* (TRAIL) is tightly (and directly) regulated by the IRF-1/N-CoR2/HDAC3 complex echoes the idea that HDAC inhibitors efficiently enhance the killing of leukemia cells because they permit the re-expression of *TNFSF10* (TRAIL) to enhance bystander-mediated tumor kill⁵³. Our data bolster the argument that tumor exploit molecules directing developmental programs to their advantage because the N-CoR2/HDAC3/HDAC7 complex regulates survival in lymphocytes during positive and negative T cell selection and in endothelial cells during vascular remodeling^{35,57}. Indeed, several PCD genes that enhance cell survival during development, such as c-FLIP, the BCL2 family proteins and the inhibitor of apoptosis protein (IAP) family proteins, are frequently up-regulated in human cancers and are associated with tumor aggression, apoptosis resistance and poor patient prognosis³. Not only do our findings concur with these data, but they place the N-CoR2 complex upstream of and in control of many of these PCD regulatory molecules, implying that the complex can act as a master regulator of cell death. Indeed, because we showed that N-CoR2 expression and the N-CoR2-associated

gene expression signature is strongly linked to the therapeutic outcome of a primary breast tumor this implies that the MDR phenotype is acquired at an early stage of tumor development and is consequently epigenetically pre-determined prior to therapy. Accordingly, our N-CoR2 gene signature could be used to predict the sensitivity of a tumor to therapeutic agents including HDAC inhibitors or agents that target epigenetic pathways.

Genetic and epigenetic alterations contribute to tumor heterogeneity and influence the treatment response of cancer cells¹. While gene therapy could restore levels of tumor suppressors such as p53 that would enhance treatment response, pharmacological agents that inhibit the activity of HDACs and DNA methyltransferases are more clinically tractable²⁸. We identified high NCoR2 levels in aggressive, treatment resistant cancers and showed that it confers apoptosis resistance by inhibiting the stress-induced expression of a cassette of PCD genes (**Fig. 5b**) by remodeling chromatin through cooperative interactions with HDAC3 that modulate the expression of IRF-1, FOXF-2, STAT-1, and ELK-4-dependent gene transcription (**Fig. 5c**). Thereby, N-CoR2 joins the arsenal of chromatin remodeling proteins that promote tumor aggression. Yet, our findings also provide the first example by which MDR in malignant tissues can be driven through multi-gene expression alterations coordinated by a developmentally-conserved epigenetic mechanism. Thus, while a single gene-mediated resistance mechanism, mediated for instance via the methylation-dependent silencing of individual genes involved in DNA repair and apoptosis, such as *APAF1* and

*hMLH1*⁵⁸ is the prevailing dogma, our data suggest that the MDR phenotype is poly-genically and multi-factorially related. It therefore follows that other epigenetic regulators that modulate PCD during development might also be exploited by tumors to promote the MDR phenotype.

METHODS

Chemicals and antibodies. Antibodies and reagents used are in **Supplementary Methods**.

Cell culture. Human mammary HMT-3522 S-1, T4-2, MDA-MB-231 and HEK293 cells were propagated and manipulated as previously described^{16,59}.

Cell death stimulation and analysis. MECs either in 2D or 3D were treated with death stimuli and assayed for apoptosis 12-48 hrs after treatment, as described¹⁶. IR experiments employed a calibrated Mark I Cesium 137 irradiator (JL Shepherd & Associates). Clonogenic survival was assayed in single cells in rBM following exposure to IR (9 Gy) and outgrowth was monitored by weekly measurement of colony size followed by viability assay after 1 month.

Immunofluorescence and tissue microarray analysis. Cells and tissues were immunostained using protocols previously described^{16,60}. TMA of human breast cancers was obtained from US Biomax, Inc., code BR804. The nuclear and cytoplasmic staining patterns of N-CoR2 were quantified using the histological score (H-score; **Supplementary Methods**).

Chromatin immunoprecipitation (ChIP) and reporter assays. ChIP assays were

performed as per manufacturer's directions (Upstate) (**Supplementary Methods**). Reporter assays were conducted in transiently transfected HEK293 cells and employed the IRF-1 luciferase reporter vector pTL-Luc-IRF1 (Panomics)^{48,59}.

Gene manipulations. Stable retroviral-mediated knockdown of N-CoR2, HDAC3 and TRAIL was achieved using previously described oligonucleotide sequences³¹. Murine *NCOR2* cDNA was sub-cloned into pLZRS-MFG-*tet*-EGFP. Mutant N-CoR2 (K449A) was generated using the QuickChange Site-Directed Mutagenesis kit (Stratagene). Stable populations of MECs expressing EGFP-tagged retroviral constructs were FACS sorted or antibiotic selected and re-infected with high titer MFG virus expressing the tetracycline-controlled transcriptional transactivator.

Orthotopic breast tumorigenesis models and bioluminescence imaging (BLI).

pSFP-GFP-FFLuc (gift from R.J. Brentjens, Memorial Sloan Kettering Cancer Center), was transduced into MDA-MB-231-N-CoR2 cells. Cells (2×10^6 cells in 100 μ l 1:1 mixture rBM:HBSS) were inoculated into the mammary fat pads of 8-week-old female NOD/SCID mice (National Laboratory Animal Center, Taiwan). Once tumors had formed the mice were given intraperitoneal injections of paclitaxel (20 mg/kg) or vehicle every week for 6 consecutive weeks. Bioluminescence of the tumor mass was assessed by using the IVIS

Imaging System (Xenogen) weekly prior to treatment (**Supplementary Methods**).

HDAC activity assay. Nuclear protein extracts prepared from HEK 293 cells expressing myc-tagged N-CoR2, N-CoR2 (K449A) or a control EGFP construct were immunoprecipitated using mouse anti-myc antibody, and HDAC activity was determined in normalized aliquots using the Fluor de LysTM Assay System (Biomol).

Gene expression profiling and quantitative RT-PCR analysis. Total RNA from 3-4 independent organotypic culture experiments (Day 12-14 3D rBM culture, +/- N-CoR2, +/- 4 hours TRAIL treatment; 1 µg/mL; 4 hours + caspase inhibitors) was extracted (RNeasy Mini Kit; Qiagen), labeled, and cRNA was prepared, fragmented and hybridized to U133A 2.0 GeneChips containing 22,283 probes, as recommended (GeneChipTM protocol, Affymetrix, Inc.; **Supplementary Methods**). The gene expression data have been deposited in NCBI Gene Expression Omnibus (GEO, <http://www.ncbi.nlm.nih.gov/geo/>) and are accessible through GEO Series accession number GSE8346. For RT-PCR analysis, cDNA synthesized using MMLV reverse transcriptase (Promega) was used as template for PCR amplification using the LightCycler System (Roche). Oligonucleotide primers were designed according to Primer Bank (<http://pga.mgh.harvard.edu/primerbank/index.html>).

Bioinformatics analysis. The criteria for gene selection are in Supplementary Methods.

Differences in gene expression between N-CoR2 and TRAIL-treatment status and control was measured using the equation “ $\log_2(NT/N) - \log_2(VT/V)$ ”, which is designated as a *differential response index (DRI)*.

Gene ontology (GO)-based functional classification of the identified genes was performed systematically by DAVID (<http://david.abcc.ncifcrf.gov/>). TRANSFEC (<http://www.gene-regulation.com/pub/databases.html>) and oPOSSUM (<http://www.cisreg.ca/cgi-bin/oPOSSUM/oopossum>) were used to search for enriched TF binding sites in the promoter regions of different sets of genes identified from transcript profiling. Results were further processed and displayed using HotGene (<http://www.hotgene.net/>) (Hotgene Informatics). Tumor transcriptome data sets used for therapeutic outcome and survival analysis were reported previously and obtained from respective sources (Supplementary Methods).

Unsupervised clustering and construction of S_{NCOR2} . Average linkage clustering on the medium-centered gene expression values in the *NCOR2-116* gene set used the Cluster and TreeView software (<http://rana.lbl.gov/eisen>). The degree of resemblance between the expression profiles of the N-CoR2-associated genes in breast tumors and those in T4-2 spheroids with high (N-CoR2) versus low N-CoR2 (Vector) was assessed using Pearson’s

correlation coefficient, which yielded r_{NCOR2} and r_{vector} , respectively. Tumors with greater r_{NCOR2} than r_{vector} were viewed as exhibiting elevated N-CoR2-dependent transcription and the value of S_{NCOR2} was used to represent the difference between r_{NCOR2} and r_{vector} , $S_{NCOR2} = r_{NCOR2} - r_{vector}$ (**Supplementary Methods**).

Statistical analysis. We used the InStat software (Graphpad) and the SPSS 10.0 software (SPSS) for statistical analysis. Unless otherwise stated, two-tailed Student *t*-test was used for simple significance testing. Survival curves were generated using the method of Kaplan and Meier. The curves were plotted and compared using the log-rank test using the GraphPad Prism 5.02 software (GraphPad Software). Statistical significance was considered $P < 0.05$.

ACKNOWLEDGMENTS

We thank M. Lazar (University of Pennsylvania) for the monoclonal anti-N-CoR2-producing hybridoma cell line, G.M. Wahl (Salk Institute) for the pCLNR-H2BG vector, J. Park (Sungkyunkwan University) for the pcDNA3-IRF-1 vector, and R.J. Brentjens (Memorial Sloan Kettering Cancer Center) for the pSFP-GFP-FFLuc vector. We acknowledge L. Pusztai (M.D. Anderson Cancer Center) for clinical information on the MDACC data set; R. Kronenwett (Siemens Healthcare Diagnostics Products GmbH) for the breast cancer microarray data sets, and M.T. Lee (Kun Shan University) for expert assistance with

bioinformatics analysis. This work was supported by NIH grants R01-CA078731, U54CA143836 and CA138818-01A1 and DOD grant W81XWH-05-1-330 to V.M. Weaver and Taipei Medical University grant TMU96-AE1-B02 to K.K. Tsai.

AUTHOR CONTRIBUTIONS

V.M.W. conceived the concept and designed and directed the death studies and gene signature work. C.C., J.L. and K.K.T. executed the in vitro and in vivo death studies and gene array work. K.K.T. designed and with J.J.S. executed the promoter analysis studies. M.E.W. characterized the N-CoR2 mutant and I.S.M. analyzed the microarray data and directed the bioinformatics analysis. V.M.W. and K.K.T. co-wrote the manuscript.

REFERENCES

1. Szakacs, G., Paterson, J.K., Ludwig, J.A., Booth-Genthe, C. & Gottesman, M.M. Targeting multidrug resistance in cancer. *Nat Rev Drug Discov* **5**, 219-234 (2006).
2. Degtrev, A. & Yuan, J. Expansion and evolution of cell death programmes. *Nat Rev Mol Cell Biol* **9**, 378-390 (2008).
3. Igney, F.H. & Krammer, P.H. Death and anti-death: tumour resistance to apoptosis. *Nat Rev Cancer* **2**, 277-288 (2002).
4. Schmitt, C.A. & Lowe, S.W. Apoptosis and chemoresistance in transgenic cancer models. *J Mol Med* **80**, 137-146 (2002).
5. Zahir, N. & Weaver, V.M. Death in the third dimension: apoptosis regulation and tissue architecture. *Curr Opin Genet Dev* **14**, 71-80 (2004).
6. Creighton, C.J., *et al.* Residual breast cancers after conventional therapy display mesenchymal as well as tumor-initiating features. *Proc Natl Acad Sci U S A* **106**, 13820-13825 (2009).
7. Rankin, E.B. & Giaccia, A.J. The role of hypoxia-inducible factors in tumorigenesis. *Cell Death Differ* **15**, 678-685 (2008).
8. Dean, M., Fojo, T. & Bates, S. Tumour stem cells and drug resistance. *Nat Rev Cancer* **5**, 275-284 (2005).
9. Bao, S., *et al.* Glioma stem cells promote radioresistance by preferential activation of the DNA damage response. *Nature* **444**, 756-760 (2006).
10. Mohrin, M., *et al.* Hematopoietic stem cell quiescence promotes error-prone DNA repair and mutagenesis. *Cell Stem Cell* **7**, 174-185 (2010).
11. Gu, B., Espana, L., Mendez, O., Torregrosa, A. & Sierra, A. Organ-selective chemoresistance in metastasis from human breast cancer cells: inhibition of apoptosis, genetic variability and microenvironment at the metastatic focus. *Carcinogenesis* **25**, 2293-2301 (2004).
12. Sethi, T., *et al.* Extracellular matrix proteins protect small cell lung cancer cells against apoptosis: a mechanism for small cell lung cancer growth and drug resistance in vivo. *Nat Med* **5**, 662-668 (1999).
13. Hazlehurst, L.A., Landowski, T.H. & Dalton, W.S. Role of the tumor microenvironment in mediating de novo resistance to drugs and physiological mediators of cell death. *Oncogene* **22**, 7396-7402 (2003).
14. Olive, K.P., *et al.* Inhibition of Hedgehog signaling enhances delivery of chemotherapy in a mouse model of pancreatic cancer. *Science* **324**, 1457-1461 (2009).
15. DeNardo, D.G., Andreu, P. & Coussens, L.M. Interactions between lymphocytes and myeloid cells regulate pro- versus anti-tumor immunity. *Cancer Metastasis Rev* **29**, 309-316 (2010).

16. Weaver, V.M., *et al.* beta4 integrin-dependent formation of polarized three-dimensional architecture confers resistance to apoptosis in normal and malignant mammary epithelium. *Cancer Cell* **2**, 205-216 (2002).
17. Desoize, B. & Jardillier, J. Multicellular resistance: a paradigm for clinical resistance? *Crit Rev Oncol Hematol* **36**, 193-207 (2000).
18. Hamilton, G. Multicellular spheroids as an in vitro tumor model. *Cancer Lett* **131**, 29-34 (1998).
19. Feinberg, A.P. Phenotypic plasticity and the epigenetics of human disease. *Nature* **447**, 433-440 (2007).
20. Lelievre, S.A., *et al.* Tissue phenotype depends on reciprocal interactions between the extracellular matrix and the structural organization of the nucleus. *Proc Natl Acad Sci U S A* **95**, 14711-14716 (1998).
21. Le Beyec, J., *et al.* Cell shape regulates global histone acetylation in human mammary epithelial cells. *Exp Cell Res* **313**, 3066-3075 (2007).
22. Fournier, M.V., *et al.* Gene expression signature in organized and growth-arrested mammary acini predicts good outcome in breast cancer. *Cancer Res* **66**, 7095-7102 (2006).
23. Kenny, P.A., *et al.* The morphologies of breast cancer cell lines in three-dimensional assays correlate with their profiles of gene expression. *Mol Oncol* **1**, 84-96 (2007).
24. Plachot, C. & Lelievre, S.A. DNA methylation control of tissue polarity and cellular differentiation in the mammary epithelium. *Exp Cell Res* **298**, 122-132 (2004).
25. Jones, P.A. & Baylin, S.B. The epigenomics of cancer. *Cell* **128**, 683-692 (2007).
26. Camphausen, K., Scott, T., Sproull, M. & Tofilon, P.J. Enhancement of xenograft tumor radiosensitivity by the histone deacetylase inhibitor MS-275 and correlation with histone hyperacetylation. *Clinical Cancer Research* **10**, 6066-6071 (2004).
27. Singh, T.R., Shankar, S. & Srivastava, R.K. HDAC inhibitors enhance the apoptosis-inducing potential of TRAIL in breast carcinoma. *Oncogene* **24**, 4609-4623 (2005).
28. Kelly, W.K. & Marks, P.A. Drug insight: Histone deacetylase inhibitors--development of the new targeted anticancer agent suberoylanilide hydroxamic acid. *Nat Clin Pract Oncol* **2**, 150-157 (2005).
29. Minucci, S. & Pelicci, P.G. Histone deacetylase inhibitors and the promise of epigenetic (and more) treatments for cancer. *Nat Rev Cancer* **6**, 38-51 (2006).
30. Lane, A.A. & Chabner, B.A. Histone deacetylase inhibitors in cancer therapy. *J Clin Oncol* **27**, 5459-5468 (2009).
31. Ishizuka, T. & Lazar, M.A. The N-CoR/histone deacetylase 3 complex is required for repression by thyroid hormone receptor. *Mol Cell Biol* **23**, 5122-5131 (2003).
32. Codina, A., *et al.* Structural insights into the interaction and activation of histone

- deacetylase 3 by nuclear receptor corepressors. *Proc Natl Acad Sci U S A* **102**, 6009-6014 (2005).
33. Chen, J.D. & Evans, R.M. A transcriptional co-repressor that interacts with nuclear hormone receptors. *Nature* **377**, 454-457 (1995).
 34. Privalsky, M.L. The role of corepressors in transcriptional regulation by nuclear hormone receptors. *Annu Rev Physiol* **66**, 315-360 (2004).
 35. Verdin, E., Dequiedt, F. & Kasler, H.G. Class II histone deacetylases: versatile regulators. *Trends Genet* **19**, 286-293 (2003).
 36. van de Vijver, M.J., *et al.* A gene-expression signature as a predictor of survival in breast cancer. *N Engl J Med* **347**, 1999-2009 (2002).
 37. Hess, K.R., *et al.* Pharmacogenomic predictor of sensitivity to preoperative chemotherapy with paclitaxel and fluorouracil, doxorubicin, and cyclophosphamide in breast cancer. *J Clin Oncol* **24**, 4236-4244 (2006).
 38. Chang, J.C., *et al.* Gene expression profiling for the prediction of therapeutic response to docetaxel in patients with breast cancer. *Lancet* **362**, 362-369 (2003).
 39. Modlich, O., Prisack, H.B., Munnes, M., Audretsch, W. & Bojar, H. Predictors of primary breast cancers responsiveness to preoperative epirubicin/cyclophosphamide-based chemotherapy: translation of microarray data into clinically useful predictive signatures. *J Transl Med* **3**, 32 (2005).
 40. Hong, S.H. & Privalsky, M.L. The SMRT corepressor is regulated by a MEK-1 kinase pathway: inhibition of corepressor function is associated with SMRT phosphorylation and nuclear export. *Mol Cell Biol* **20**, 6612-6625 (2000).
 41. Hoberg, J.E., Yeung, F. & Mayo, M.W. SMRT derepression by the IkappaB kinase alpha: a prerequisite to NF-kappaB transcription and survival. *Mol Cell* **16**, 245-255 (2004).
 42. Ghisletti, S., *et al.* Cooperative NCoR/SMRT interactions establish a corepressor-based strategy for integration of inflammatory and anti-inflammatory signaling pathways. *Genes Dev* **23**, 681-693 (2009).
 43. Keane, M.M., Ettenberg, S.A., Nau, M.M., Russell, E.K. & Lipkowitz, S. Chemotherapy augments TRAIL-induced apoptosis in breast cell lines. *Cancer Res* **59**, 734-741 (1999).
 44. Kagawa, S., *et al.* Antitumor activity and bystander effects of the tumor necrosis factor-related apoptosis-inducing ligand (TRAIL) gene. *Cancer Res* **61**, 3330-3338 (2001).
 45. Chhipa, R.R. & Bhat, M.K. Bystander killing of breast cancer MCF-7 cells by MDA-MB-231 cells exposed to 5-fluorouracil is mediated via Fas. *J Cell Biochem* **101**, 68-79 (2007).
 46. Myatt, S.S. & Lam, E.W. The emerging roles of forkhead box (Fox) proteins in cancer.

- Nat Rev Cancer* **7**, 847-859 (2007).
47. Stang, M.T., *et al.* Interferon regulatory factor-1-induced apoptosis mediated by a ligand-independent fas-associated death domain pathway in breast cancer cells. *Oncogene* **26**, 6420-6430 (2007).
 48. Clarke, N., Jimenez-Lara, A.M., Voltz, E. & Gronemeyer, H. Tumor suppressor IRF-1 mediates retinoid and interferon anticancer signaling to death ligand TRAIL. *EMBO J* **23**, 3051-3060 (2004).
 49. Kim, P.K., *et al.* IRF-1 expression induces apoptosis and inhibits tumor growth in mouse mammary cancer cells in vitro and in vivo. *Oncogene* **23**, 1125-1135 (2004).
 50. Merika, M., Williams, A.J., Chen, G., Collins, T. & Thanos, D. Recruitment of CBP/p300 by the IFN beta enhanceosome is required for synergistic activation of transcription. *Mol Cell* **1**, 277-287 (1998).
 51. Spalding, A.C., *et al.* TRAIL and inhibitors of apoptosis are opposing determinants for NF-kappaB-dependent, genotoxin-induced apoptosis of cancer cells. *Oncogene* **21**, 260-271 (2002).
 52. Walczak, H., *et al.* Tumoricidal activity of tumor necrosis factor-related apoptosis-inducing ligand in vivo. *Nat Med* **5**, 157-163 (1999).
 53. Nebbioso, A., *et al.* Tumor-selective action of HDAC inhibitors involves TRAIL induction in acute myeloid leukemia cells. *Nat Med* **11**, 77-84 (2005).
 54. Green, A.R., *et al.* The prognostic significance of steroid receptor co-regulators in breast cancer: co-repressor NCOR2/SMRT is an independent indicator of poor outcome. *Breast Cancer Res Treat* **110**, 427-437 (2008).
 55. Yu, J., *et al.* The corepressor silencing mediator for retinoid and thyroid hormone receptor facilitates cellular recovery from DNA double-strand breaks. *Cancer Res* **66**, 9316-9322 (2006).
 56. Lee, S.K., Kim, J.H., Lee, Y.C., Cheong, J. & Lee, J.W. Silencing mediator of retinoic acid and thyroid hormone receptors, as a novel transcriptional corepressor molecule of activating protein-1, nuclear factor-kappaB, and serum response factor. *J Biol Chem* **275**, 12470-12474 (2000).
 57. Chang, S., *et al.* Histone deacetylase 7 maintains vascular integrity by repressing matrix metalloproteinase 10. *Cell* **126**, 321-334 (2006).
 58. Gifford, G., Paul, J., Vasey, P.A., Kaye, S.B. & Brown, R. The acquisition of hMLH1 methylation in plasma DNA after chemotherapy predicts poor survival for ovarian cancer patients. *Clin Cancer Res* **10**, 4420-4426 (2004).
 59. Gilbert, P.M., *et al.* HOXA9 regulates BRCA1 expression to modulate human breast tumor phenotype. *J Clin Invest* **120**, 1535-1550 (2010).
 60. Levental, K.R., *et al.* Matrix crosslinking forces tumor progression by enhancing integrin signaling. *Cell* **139**, 891-906 (2009).

LEGENDS

Figure 1. N-CoR2 is necessary for treatment-resistance in 3D mammary tissues. (a) Left, representative immunoblot images showing total nuclear acetylated (Ac)-histone H4 (Ac-H4); acetylated-histone H3 (Ac-H3); trimethyl (Me3)-H3K27 (Me3-H3K27); MeCP2; Me3-H3K9; HP1 and H2B in HMT-3522 S1 nonmalignant HMT-3522 mammary epithelial cells (S1 MECs) grown as two dimensional monolayers on rBM (2D) or as three dimensional acini in rBM (3D). Right, confocal images of S-1 MECs grown in 2D versus 3D stained for acetylated-histone H4K5 (Ac-H4K5); acetylated-histone H3K9 (Ac-H3-K9); Me3-H3K9; Me3-H3K27 and HP1 (red). Scale bar, 20 μ m. (b) Line graphs showing percent cell death in response to increasing dose of TRAIL, paclitaxel and ionizing irradiation (IR) in S-1 MECs grown in 2D versus 3D, with and without prior TSA (100 nM) treatment. (c) Bar graphs of relative mRNA levels of chromatin remodeling molecules in S-1 MECs grown in 2D versus 3D. (d) Left, representative immunoblots of N-CoR2, GPS2 and histone 2B (H2B) in S1 MECs grown in 2D versus 3D. Right, quantification of immunoblots shown at left. (e) Top, immunoblots showing total cellular protein level following shRNA-mediated knockdown of N-CoR2 in S1 MECs. Bottom, confocal images of S1 MEC rBM acini with and without shRNA-mediated knockdown of N-CoR2 treated with and without TRAIL (0.5 μ g/ml; 24 h) and stained for α 6 integrin (red; indicated by arrows), cleaved caspase 3 (green; see arrow in lower right hand image) and DAPI (nuclei; blue). Scale bar, 20 μ m. (f) Line graphs showing

percent cell death in S1 MECs grown in 2D versus 3D, with and without shRNA-mediated knockdown of N-CoR2 in response to increasing dose of TRAIL, paclitaxel, doxorubicin and IR. Error bars represent mean \pm s.e.m. ($n = 3-6$) for **b**, **c**, **d**, and **f**. ****** $P < 0.01$; ******* $P < 0.001$.

Figure 2. N-CoR2 mediates treatment resistance in human breast cancers and in

mammary tumors in culture and *in vivo*. (a) Left, representative immunohistochemistry

images of breast tumors showing intense (3+; *top*) or low staining (1+; *bottom*) for nuclear

N-CoR2. Scale bars, 100 μ m. Right, bar graphs quantifying N-CoR2 nuclear (open bars) and

cytoplasmic staining level (solid bars) in cancerous human breast tissues (38 specimens). (b)

Line graphs showing Kaplan-Meier survival analysis of the NKI data set following

illustrating patient survival disparities with (left) and without (right) systemic CT based upon

partitioning into quartiles by N-CoR2 status. P values were calculated using the log-rank test.

(c) Top, representative immunoblots showing N-CoR2 levels in HMT-3522 T4-2 (T4-2) and

MDA-MB-231 breast cancer cells expressing GFP or GFP-tagged N-CoR2. Bottom,

representative immunofluorescence images of T4-2 (*upper*) and MDA-MB-231 (*lower*) cells

expressing GFP or GFP-tagged N-CoR2. Scale bars, 25 μ m. (d) Line graphs showing percent

death of T4-2 cells expressing N-CoR2 or empty vector when grown as a monolayer on rBM

(2D; *right*) or as single cells (*middle*) or multicellular spheroids embedded within rBM (3D;

left) following exposure to increasing dose of TRAIL (*upper graphs*) or paclitaxel (*lower*

graphs). (e) Line graphs showing percent death of MDA-MB-231 cells expressing N-CoR2 or vector grown in 2D following exposure to increasing dose of TRAIL. (f) Line graph showing rate of T4-2 colony re-growth following exposure to IR. (g) Bioluminescence images (BLI) of NOD-SCID mammary fat pads inoculated with MDA-MB-231 cells expressing SFG-GFP-FFLuc and either N-CoR2 or empty vector 4 weeks following treatment with paclitaxel (10 mg/kg; weekly) or vehicle. (h) Left, immunohistochemistry of activated caspase-3 levels in the MDA-MB-231 tumor cell epithelium with (bottom) and without (top) ectopic overexpression of N-CoR2 after four weeks of growth and two rounds of paclitaxel treatment in the mammary glands of NOD-SCID mice. Scale bars, 100 μ m. Right, bar graph quantifying images shown at left. (i) Tumor bulk quantified as BLI normalized photon counts as a function of time in mice described in g. Arrows indicate the time of paclitaxel treatment. (j) Percent survival as a function of time following paclitaxel treatment of mice inoculated with MDA-MB-231 cells expressing N-CoR2 or empty vector. Error bars represent mean \pm s.e.m. ($n = 3-6$) for d, e, f, h, and i. $**P < 0.01$; $***P < 0.001$.

Figure 3. N-CoR2-mediated treatment resistance in MECs is HDAC3-dependent. (a) Bar graphs showing percent death induced in response to TRAIL (0.5 μ g/ml) in HMT-3522 T4-2 breast cancer cells (T4-2 cell) expressing either empty vector or N-CoR2 with or without prior treatment (24 hours) with SAHA (1-5 μ M) or TSA (0.5-1.0 μ M). (b) Left, representative

immunoblots of HDAC3 and β -tubulin in T4 cells before and after shRNA-mediated knockdown of HDAC3. Right, line graphs showing percent cell death in response to increasing dose of TRAIL in T4-2 cells expressing either empty vector or N-CoR2 either with or without shRNA-mediated knockdown of HDAC3. (c) Representative immunoblots of myc, HDAC3 and lamin B1 in total nuclear lysate (bottom) or myc-immunoprecipitated nuclear lysate (top) from HEK 293 cells expressing myc-tagged N-CoR2, N-CoR2 (K449A) or empty vector. (d) Bar graphs showing relative HDAC activity before and after TSA treatment in myc-immunoprecipitated nuclear lysates from the HEK 293 cells described in c. (e) Line graphs showing percent cell death in response to increasing dose of TRAIL in T4 cells expressing empty vector, wild-type N-CoR2 or N-CoR2 (K449A). Error bars represent mean \pm s.e.m. ($n = 3-6$) in **a**, **b**, **d**, and **e**. * $P < 0.05$; ** $P < 0.01$; *** $P < 0.001$.

Figure 4. N-CoR2-regulated gene expression predicts NACT and CT responsiveness in breast cancer patients. (a) Box plots showing N-CoR2 transcript levels of responding (R) and nonresponding (NR) breast cancer patients receiving NACT with T/FAC ($n = 130$)³⁷, docetaxel ($n = 24$)³⁸ or EC ($n = 82$)³⁹. (b) Upper, schemata depicting experimental protocol used to construct basal and TRAIL-stimulated N-CoR2 transcript profile. Lower, percent repressed and induced N-CoR2 regulated steady-state and TRAIL-regulated genes. (c) Venn diagram showing steady-state and TRAIL-regulated genes differentially modulated by

N-CoR2 in T4-2 breast cancer cells grown as 3D rBM spheroids. **(d)** Hierarchical clustering of the 130 breast tumors in the MDACC data set using the 107-gene N-CoR2-regulated gene set. The relative level of gene expression is depicted either as a high (red) or low (green) colorgram. A dendrogram shown at the top segregates the tumors into two subgroups with tumors from the Rs or NRs denoted. **(e)** Schematic representation of the derivation of S_{NCOR2} . The tumors in the MDACC data set have been sorted in descending order according to S_{NCOR2} and then classified into two NACT response groups with optimal accuracy (solid line). **(f)** Multivariate analysis illustrating the likelihood of patient failure to respond to NACT. Tumors were segregated into subcategories according to clinic-pathological variables and S_{NCOR2} with optimal classification accuracy as shown in **e**. CI denotes 95% confidence interval. **(g)** Hierarchical clustering of the 110 breast tumors in the NKI data set who had received adjuvant CT time using the 63-gene N-CoR2-associated gene set applying a colorgram scheme as described above in **d**. **(h)** Line graphs showing Kaplan-Meier analysis of percent relapse free (*left*) and percent survival (*right*) of the patients represented by the NKI data set illustrating patient relapse and survival rates based upon cluster A versus B gene expression similarity as shown in **g**. P values were calculated using the log-rank test.

Figure 5. N-CoR2 coordinately modulates the expression of key programmed cell death regulators. **(a)** Enriched functional gene categories (EFGC) and their predicted associations

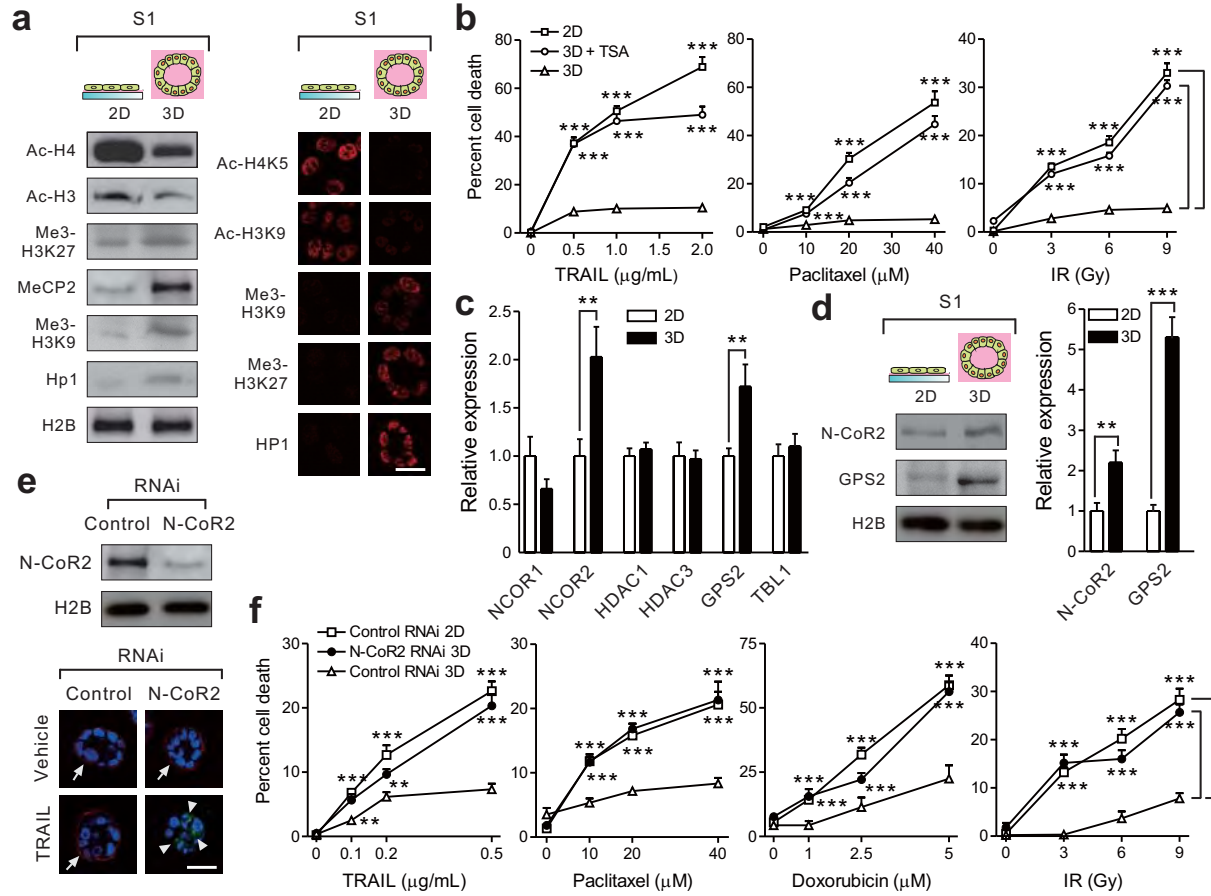
in the *NCOR2-1620* gene set. Each EFGC was segregated according to gene ontology biological process (GO-BP) and Swissprot Keywords (SPK) and are depicted as squares with the cross sectional area and the intensity of the red color margin representing the number and the average fold gene change of the genes included each category. **(b)** Expression patterns of the 64 PCD genes (75 probe sets) ranked according to *DRI*. The fold change in mean transcript level (on a \log_2 scale) have been plotted to illustrate their differential response to TRAIL. Those genes with IRF-1 consensus sites in their promoter are highlighted in yellow. **(c)** The transcription factor (TF)-target gene association network indicating 5 of the top ranked N-CoR2-modulated PCD genes. TFs with binding sites enriched in the PCD promoters are illustrated as squares with the cross sectional area representing the number of regulated target genes and red delineating increased and green depicting decreased *DRI* following TRAIL treatment. **(d)** Transcript levels of *IRF1* (*top*) and *TNFSF10* (*lower*) in T4-2 cells expressing empty vector or N-CoR2 as a function of time following TRAIL (0.5 $\mu\text{g/ml}$; not shown), paclitaxel (500 nM) or doxorubicin (1 μM) treatment. **(e)** Fold change in mRNA of selected PCD genes following TRAIL treatment normalized to vehicle control in T4-2 cells expressing empty vector, wild type N-CoR2 or mutant N-CoR2 (K449A). Error bars represent mean \pm s.e.m. ($n = 3-6$) in **d** and **e**. * $P < 0.05$; ** $P < 0.01$; *** $P < 0.001$.

Figure 6. N-CoR2 suppresses IRF-1-dependent transcription to restrict

bystander-mediated cell death amplification. (a) Left, representative immunoblots of (bottom) total cellular GFP-tagged N-CoR2, and IRF-1, HDAC3 and H2B and (top) IRF-1, HDAC3 and IgG co-immunoprecipitated with exogenously expressed, GFP-tagged N-CoR2 in T4-2 breast cancer cells. Right, total cellular (bottom) N-CoR2, IRF-1, HDAC3 and H2B and (top) IRF-1, HDAC3 and IgG co-immunoprecipitated with endogenous N-CoR2 in S-1 nonmalignant MECs with shRNA-mediated knockdown of N-CoR2 or control shRNA. (b) Left, bar graphs showing transcriptional activity of IRF-1 (pTL-Luc-IRF1) as measured by luciferase activity in HEK293 cells with and without N-CoR2 expression (+/- doxycycline) before and after TRAIL treatment. Right, bar graphs quantifying IRF-1 promoter activity (as in b) with and without co-expressed N-CoR2, before and after ectopic IRF-1 expression (pcDNA3-IRF-1). (c) Representative ChIP assay data showing results of N-CoR2 association with the TRAIL promoter in T4-2 tumor cells using anti-GFP, HDAC3, Ac-H3, and mouse IgG antibodies. (d) Representative immunoblots of total (bottom) cellular CBP, IRF-1 and H2B and (top) IRF-1 and IgG co-immunoprecipitated with CBP before (left) and after (right) N-CoR2 expression in T4-2 breast cancer cells. (e) Bar graphs showing percent death in HEK293 cells expressing IRF-1 with and without DOX-induced N-CoR2. (f) Left, bar graphs showing level of RNAi-mediated knockdown of TRAIL in T4-2 cells. Right, bar graphs showing percent TRAIL-induced cell death (0.5 µg/ml) induced in T4-2 control cells compared to T4-2 cells in which TRAIL was knocked down or rendered non-inducible

through ectopic expression of N-CoR2. Error bars represent mean \pm s.e.m. ($n = 3-6$) in **b**, **e**, and **f**. $P < 0.05$; $**P < 0.01$; $***P < 0.001$. (**g**) A cartoon depicting a model by which N-CoR2 induces treatment resistance in breast cells. In the absence of N-CoR2, IRF-1 interacts readily with CBP to facilitate chromatin remodeling and favor promoter accessibility which permits cells to up-regulate a plethora of pro-death IRF-1-regulated genes in response to an exogenous cell death cue. One of the more prominent of these genes is TRAIL, which via a positive feed back bystander-mediated effect engages the extrinsic cell death machinery to significantly enhance cell killing. In the presence of N-CoR2 this transcriptional amplification mechanism is severely inhibited. Thus, when the N-CoR2 complex is active CBP-IRF-1 interactions are outcompeted and IRF-1-mediated transcription is repressed so that the induction of stress-induced genes such as TRAIL is severely inhibited following exposure to death stimuli. The net result is that cells expressing an activated N-CoR2 repressor complex exhibits a greatly blunted response to cell death induction and bystander mediated death amplification is critically curtailed. While this mechanism protects normal cells from death it can impede the efficiency of tumor treatment.

Fig. 1



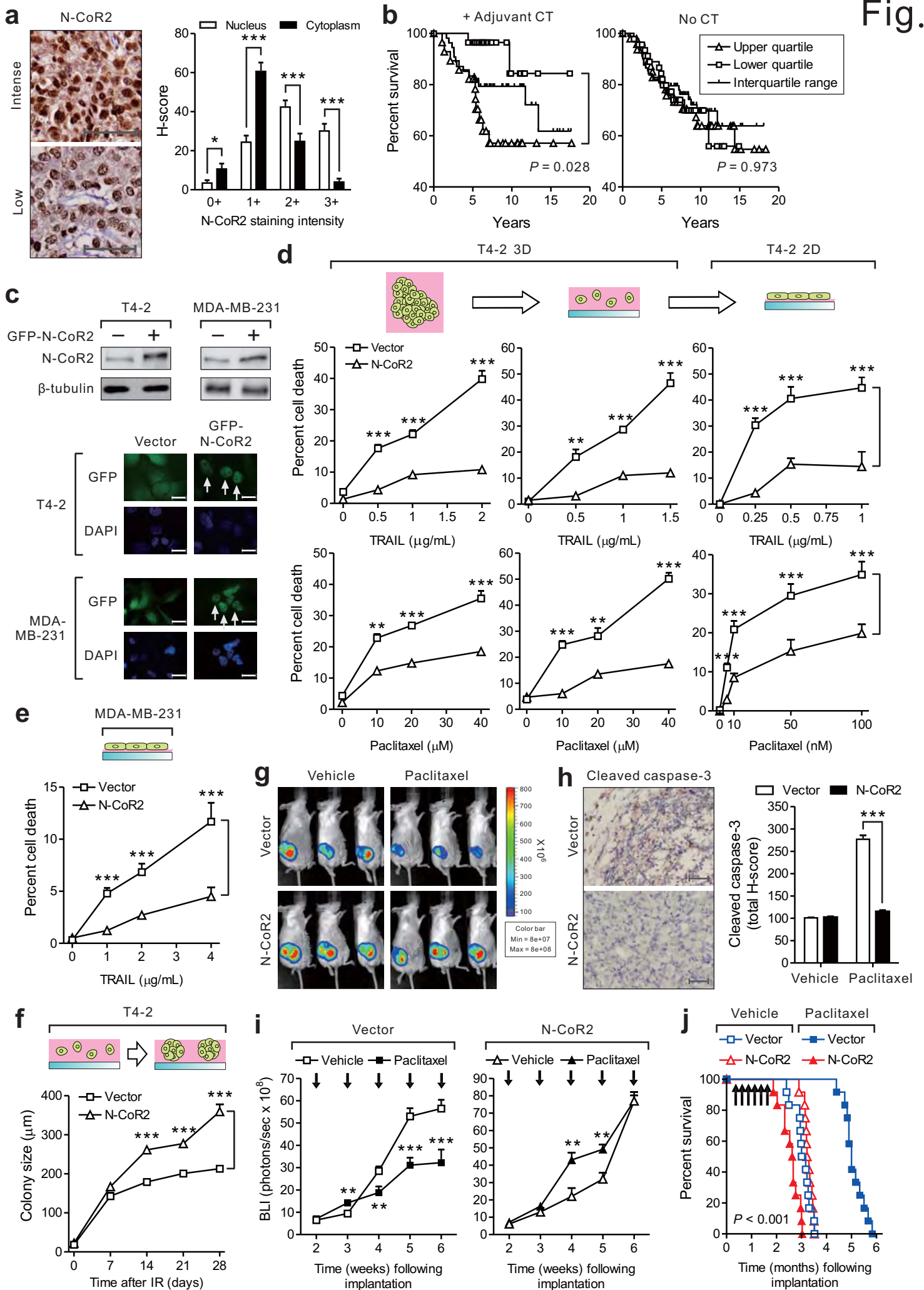


Fig. 3

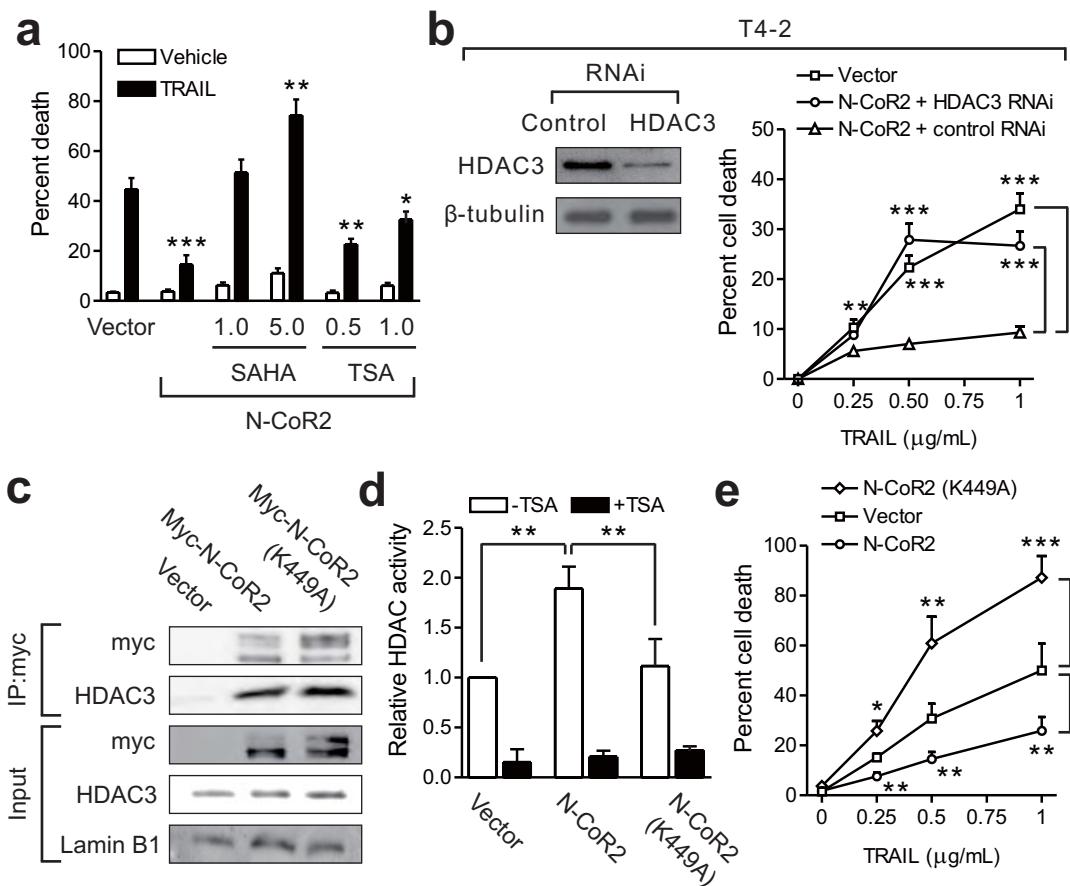


Fig. 4

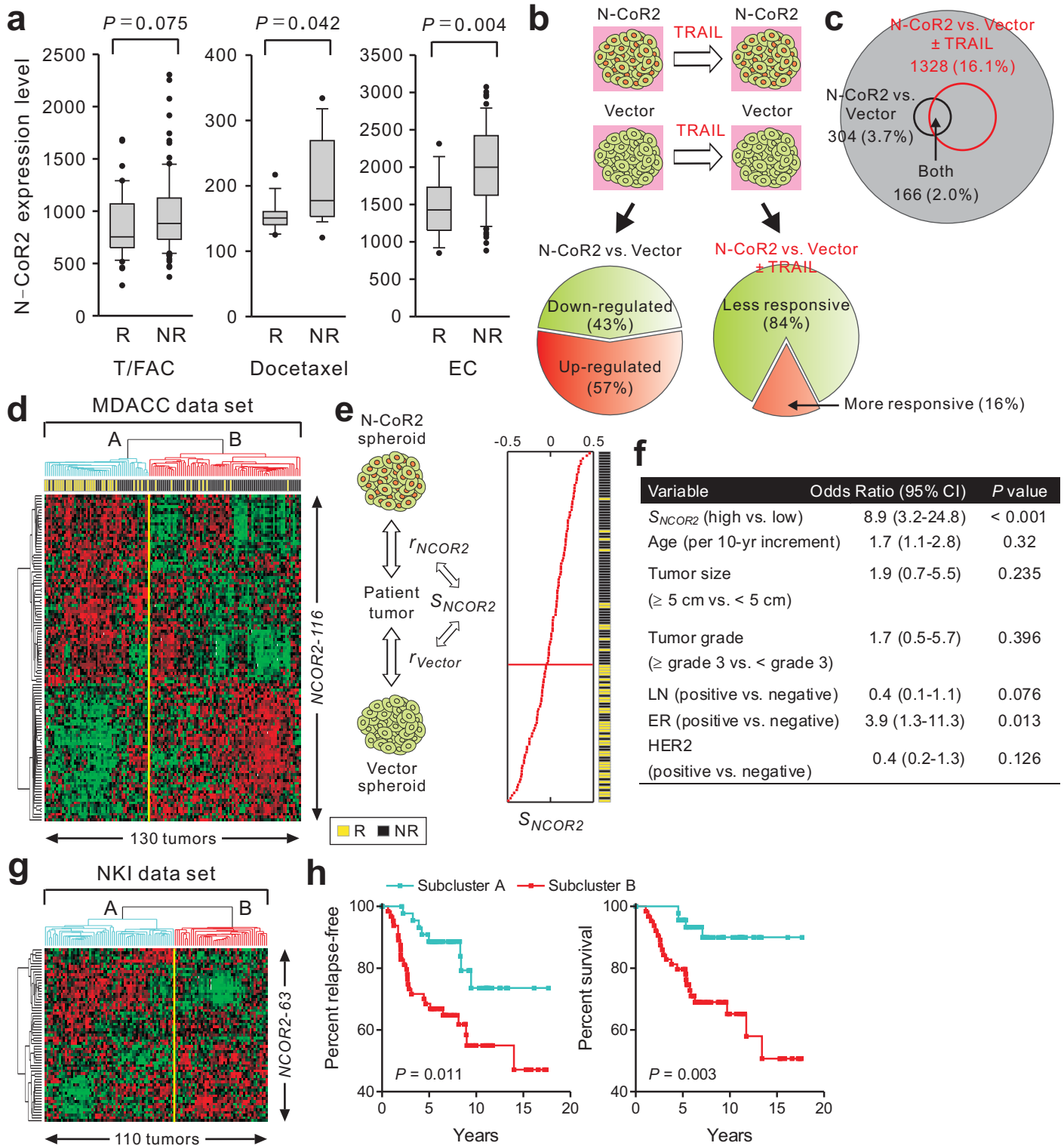


Fig. 5

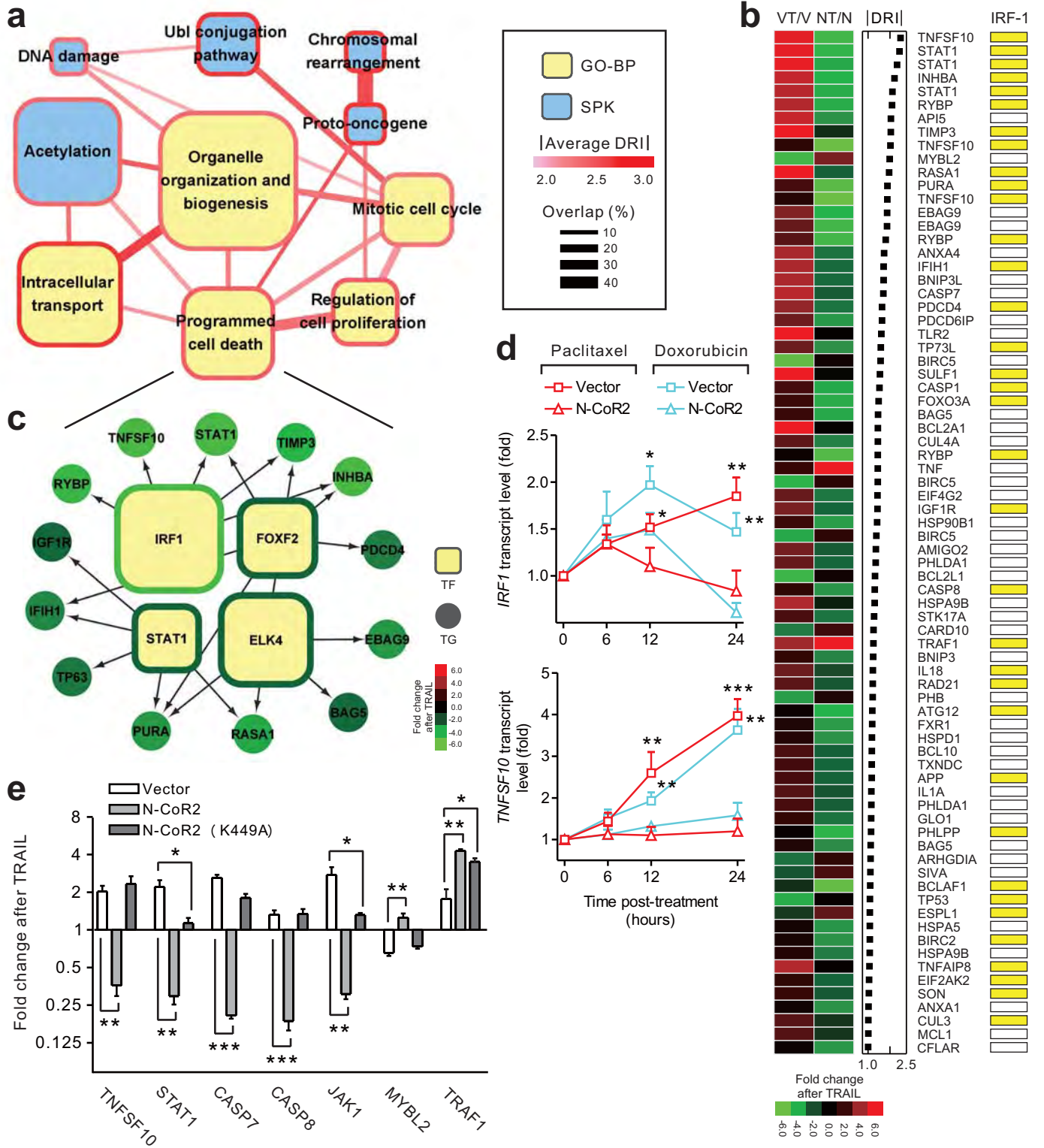
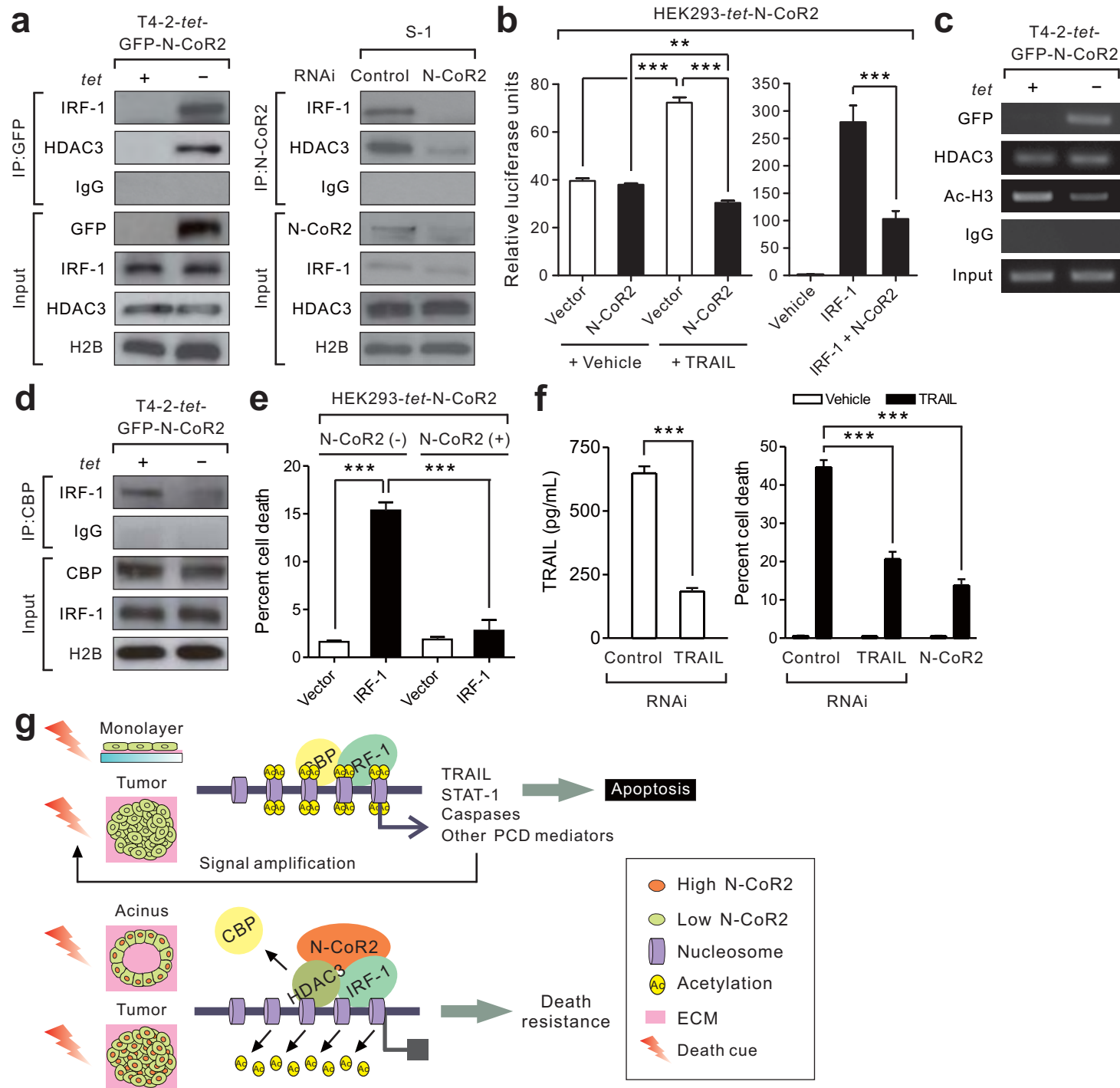


Fig. 6



Tsai et al.

Supplementary Information

N-CoR2 induces therapy-resistance in tumors by repressing apoptosis amplification

Kelvin K.-C. Tsai, Chandrima Chatterjee, Jimmy J.-M. Su, I. Saira Mian, Michael E. Werner,
Jonathan N. Lakins, and Valerie M. Weaver

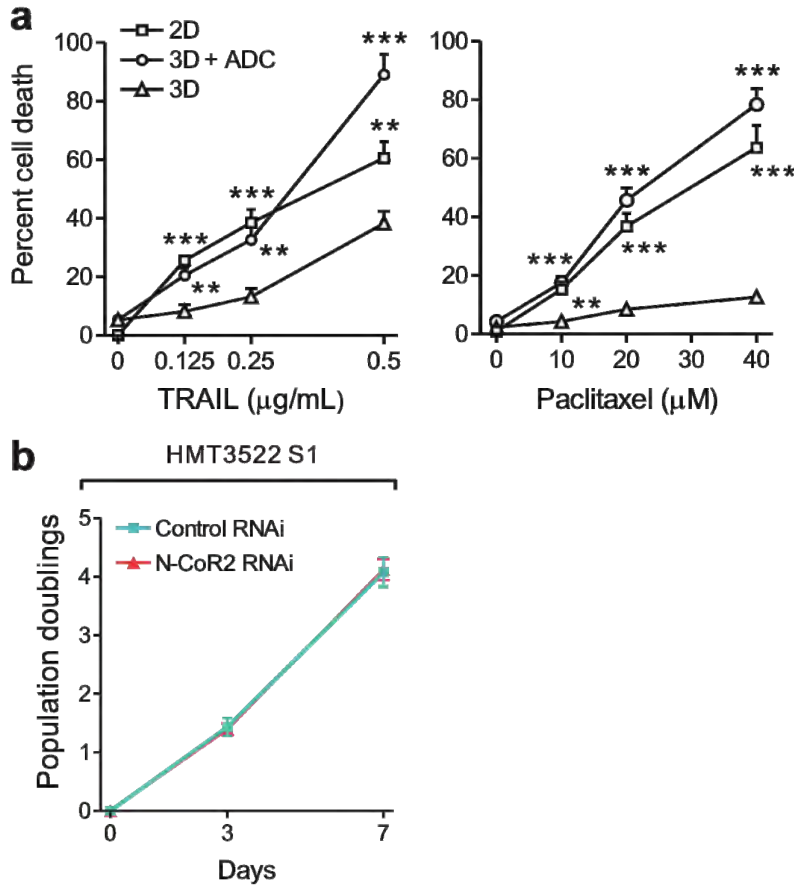
Contents:

Supplementary Figures 1-4

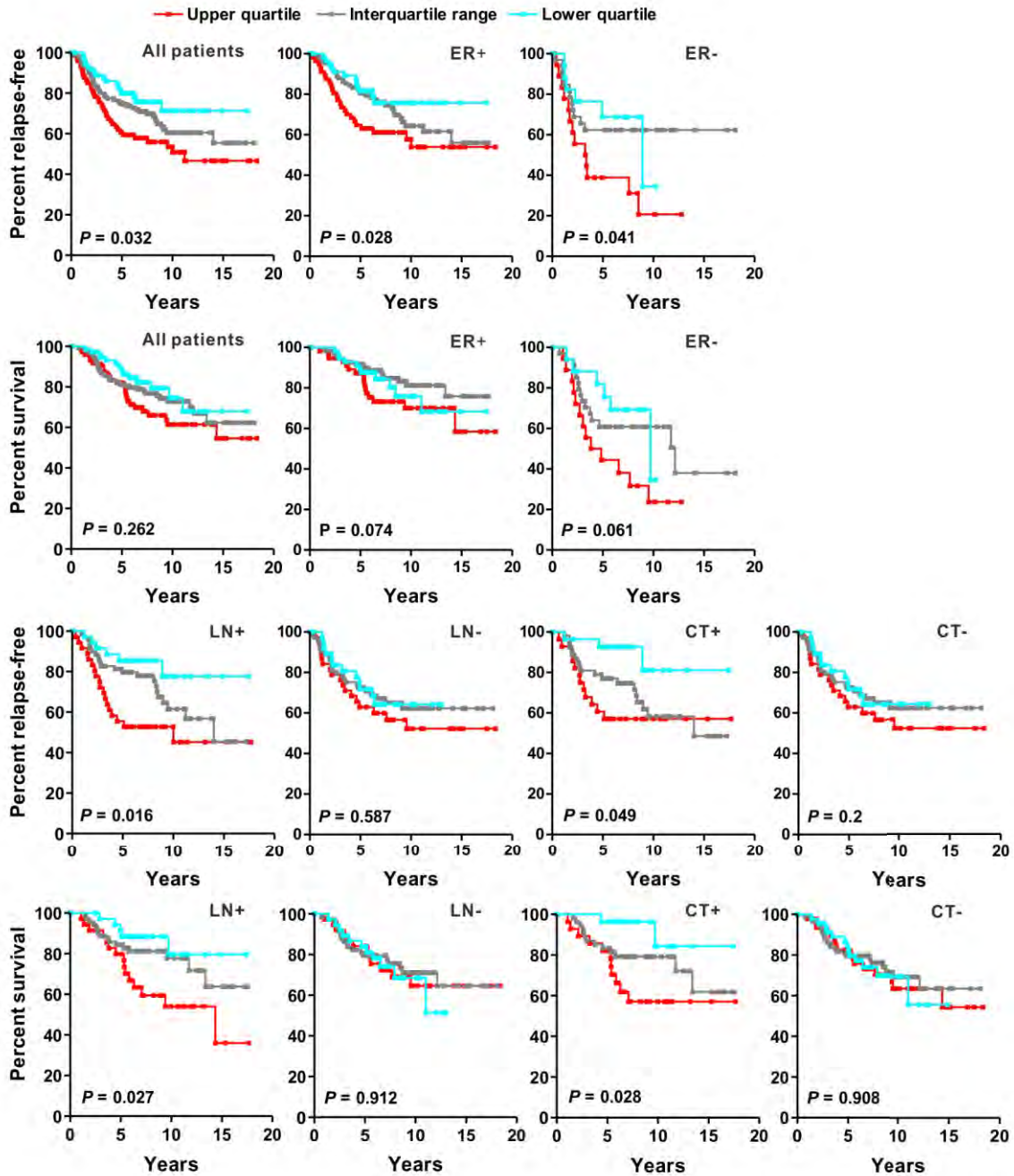
Supplementary Tables 1-4

Supplementary Methods

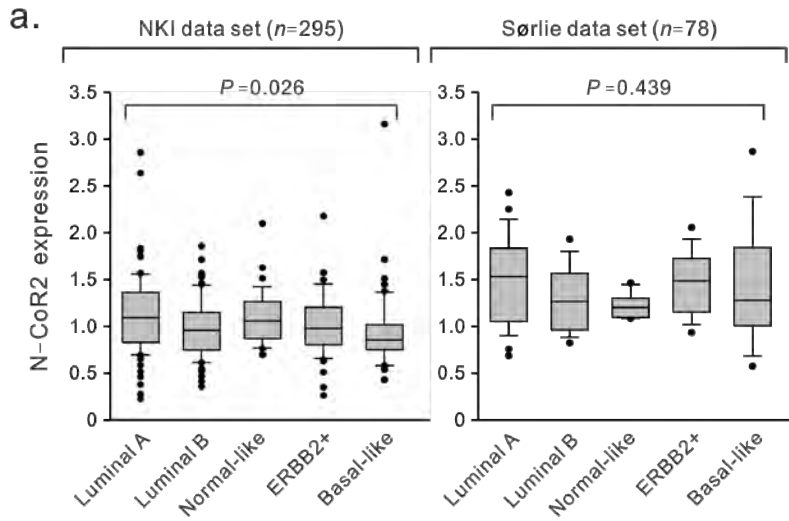
Supplementary References



Supplementary Figure 1. (a) The DNA methyltransferase inhibitor 5-Aza-2'-deoxycytidine (ADC) sensitizes S1 rBM acini to an array of death stimuli. Left, line graphs showing percent cell death in response to increasing concentration of TRAIL ligand (*left*) or the chemotherapy agent paclitaxel (*right*) in S1 MECs grown as a 2D monolayer or within rBM acini that had been pre-treated (12 hours) with either ADC (0.5 μM) or vehicle. (b) N-CoR2 does not affect growth of the nonmalignant HMT-3522 S-1 MECs. Line graphs showing the rate of grow of HMT-3522 S1 nonmalignant MECs stably expressing either N-CoR2 shRNA or control shRNA. Cells were seeded on culture plastics and cell number was determined at indicated time points. Population doubling was calculated as $\ln(\text{cell number at day } n / \text{cell number at day } 0) / \ln 2$. Error bars represent mean \pm s.e.m. ($n = 3$) for **a** and **b**. ** $P < 0.01$; *** $P < 0.001$.



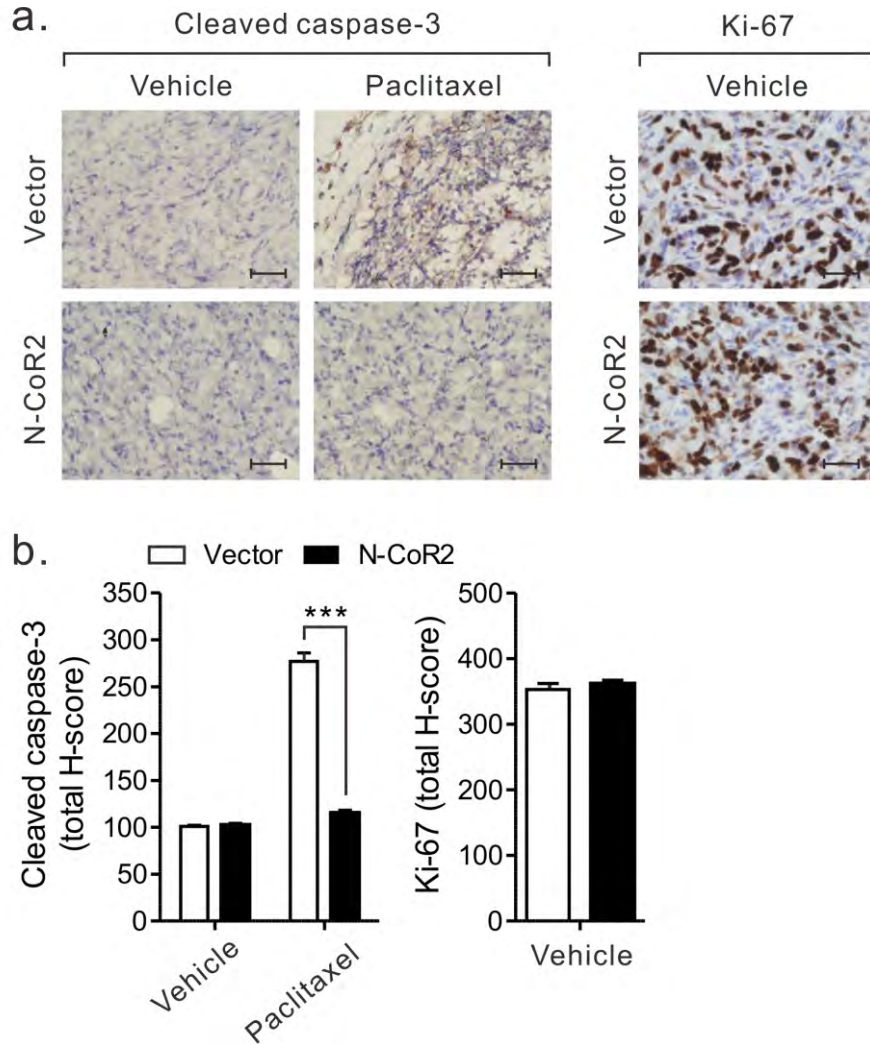
Supplementary Figure 2a. Kaplan-Meier analysis of the probability that a patient from the 295 breast cancer patients from the NKI data set will remain relapse-free or survive following therapy¹. Line graphs showing patient data stratified according to lymph node (LN) and estrogen receptor (ER) status, and whether or not they received adjuvant chemotherapy (CT). For assessment data were combined irrespective of breast cancer molecular subtype². In each group, the patients were grouped into quartiles according to the level of N-CoR2 expression. The log-rank test was used to calculate the P value.



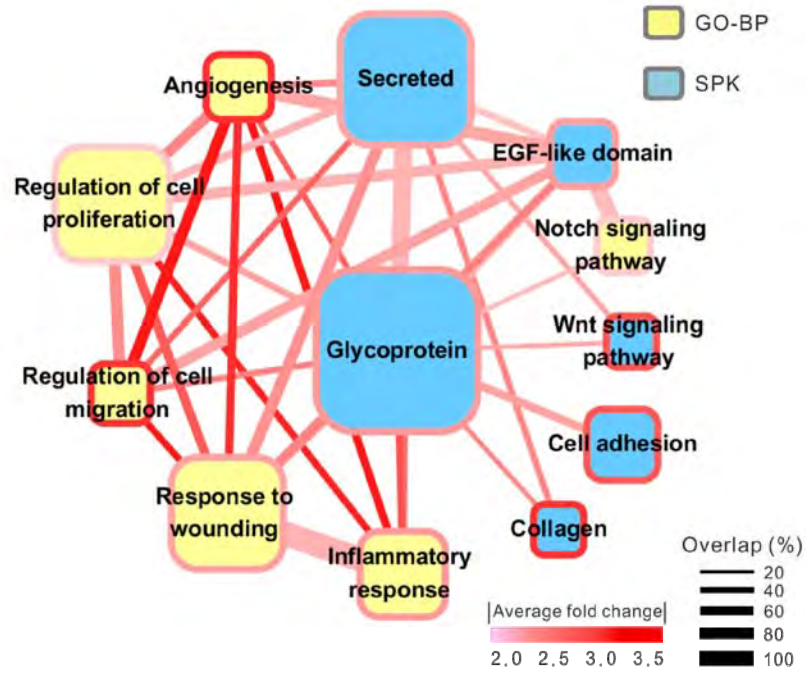
b.

Variable	Relapse		Death	
	Hazard Ratio (95% CI)	P Value	Hazard Ratio (95% CI)	P Value
N-CoR2 expression	3.6 (1.8-7.4)	< 0.001	4.7 (2.2-10.2)	< 0.001
Molecular subtype		0.118		0.005
Normal-like and luminal B vs. luminal A	1.8 (0.6-5.0)	0.267	2.4 (0.6-9.6)	0.208
Basal & ERBB2+ vs. luminal A	2.9 (1.0-8.3)	0.047	6.9 (1.8-26.3)	0.005

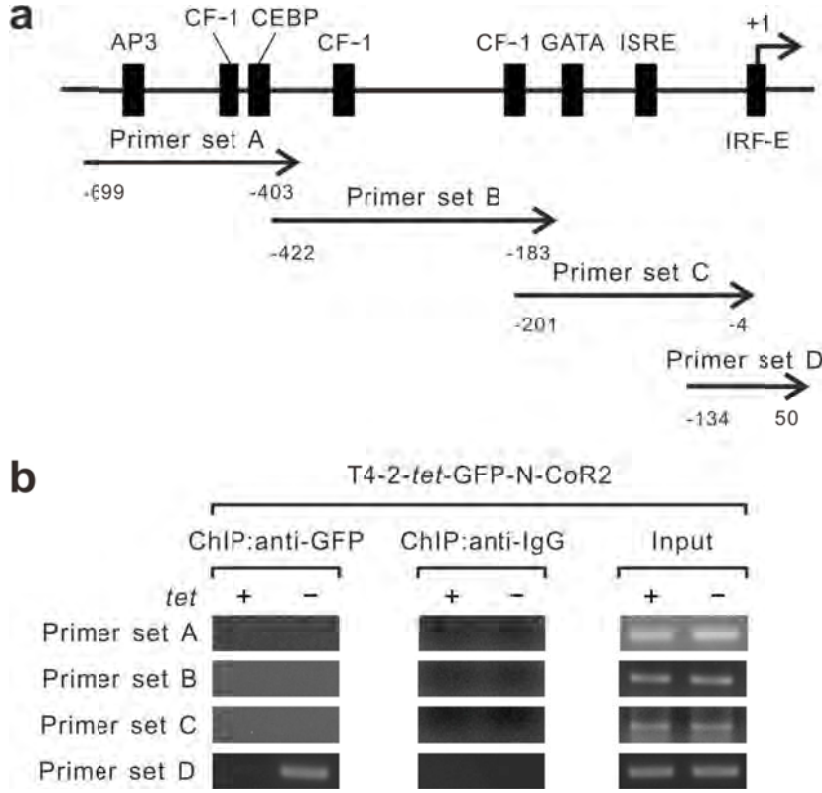
Supplementary Figure 2b. N-CoR2 expression and its prognostic value in breast cancer is independent of molecular subtype. (a.) Box plot graphical depiction of the level of N-CoR2 transcript in breast cancers of different molecular subtypes² using the NKI¹ or Sørлие² data sets. The data contain all outliers. The P values were determined using ANOVA. Notably, NCOR2 transcript levels were not elevated even within the poor prognostic ERBB2+ or basal-like breast cancer subtype relative to levels found in the other breast cancer subtypes. (b.) Table showing multivariate analysis of the 110 breast cancer patients who received adjuvant CT in the NKI data set for distant metastasis-free and overall survival according to *NCOR2* and breast cancer molecular subtype. Breast cancer molecular subtype is based on nearest centroid classification as described by Sørлие *et al.*². *NCOR2* transcript expression was modeled as a continuous variable. CI denotes confidence interval. Data illustrate that *NCOR2* expression is the most significant prognostic predictor ($P < 0.001$) even when the different molecular subtypes of breast cancer are included in the model.



Supplementary Figure 2c. Breast tumors with ectopic N-CoR2 expression retain viability and demonstrate apoptosis resistance *in vivo* following interval treatment of mice with paclitaxel. (a.) Left, representative images of tissues stained for cleaved (activated) caspase-3 from the xenografted tumors of MDA-MB-231 cells expressing N-CoR2 (*bottom*) or vector (*top*) following interval treatment with paclitaxel or vehicle. Right, representative images of tissues stained for Ki-67 from the xenografted tumors of MDA-MB-231 cells expressing N-CoR2 (*bottom*) or vector (*top*). Scale bars, 100 μ m. (b.) Bar graphs quantifying the images shown in (a.) using the H-score. Data are mean \pm s.e.m. ($n = 3$ mice per group). *** $P < 0.001$.



Supplementary Figure 3. Functional clustering of the 304 N-CoR2-associated genes. Shown is a cartoon of the enriched functional gene categories (EFGC) associated with N-CoR2 in T4-2 multicellular spheroids. The EFGC according to gene ontology biological processes (GO-BP, yellow) and Swissprot Keywords (SPK, blue) are depicted as squares with the cross sectional area and the intensity of the red color margin representing the number and the average fold change (absolute value), respectively, of the genes included in that specific category. The width of the lines represent the number of shared genes between the two connected EFGC.



Supplementary Figure 4. Approach used to map the N-CoR2 binding site within the *TNFSF10* promoter. **(a)** Cartoon showing the 5' flanking sequence of TRAIL gene with the putative and known *cis*-acting elements plotted according to previous reports³⁻⁵. The regions amplified by the different primer sets in the ChIP-PCR are shown below the promoter cartoon. Nucleotide numbering is referenced to the transcription start site (+1). **(b)** Representative images showing ChIP achieved using antibodies against GFP and normal IgG for the different *TNFSF10* promoter regions within T4-2 tumor cells ectopically expressing tetracycline (*tet*) regulated, GFP-tagged N-CoR2 with (*tet*-) and without (*tet*+) induction of N-CoR2 expression.

Supplementary table 1 Multivariate analysis for distant metastasis-free and overall survival according to N-CoR2 and N-CoR2 complex and CPV in breast cancer patients who received adjuvant CT

Variable	Relapse		Death	
	Hazard Ratio (95% CI)	<i>P</i> Value	Hazard Ratio (95% CI)	<i>P</i> Value
<i>NCOR1</i>	0.191 (0.02-1.86)	0.154	0.347 (0.026-4.591)	0.422
<i>NCOR2</i>	5.589 (2.36-13.235)	<0.001	9.327 (2.975-29.237)	<0.001
<i>HDAC1</i>	0.743 (0.173-3.188)	0.689	0.303 (0.042-2.174)	0.235
<i>HDAC3</i>	1.667 (0.327-8.495)	0.538	9.235 (1.446-58.963)	0.019
<i>GPS2</i>	0.766 (0.131-4.471)	0.767	1.621 (0.165-15.904)	0.678
<i>TBL1</i>	1.442 (0.422-4.929)	0.56	2.189 (0.488-9.829)	0.306
Age (per 10-yr increment)	0.663 (0.322-1.364)	0.264	0.562 (0.237-1.331)	0.19
Tumor size (per cm)	1.518 (1.011-2.279)	0.044	1.798 (1.085-2.979)	0.023
Tumor grade		0.576		0.281
Grade 2 vs. grade 1	1.223 (0.375-3.986)	0.739	2.327 (0.407-13.308)	0.342
Grade 3 vs. grade 1	1.839 (0.538-6.287)	0.331	3.974 (0.7-22.564)	0.119
Positive LN status vs. negative status	0.59 (0.119-2.923)	0.518	0.371 (0.062-2.211)	0.276
Positive ER status vs. negative status	0.265 (0.069-1.028)	0.055	0.077 (0.014-0.415)	0.003
Hormonal treatment vs. no treatment	0.48 (0.124-1.854)	0.287	0.143 (0.013-1.52)	0.107
Mastectomy vs. breast-conserving therapy	0.83 (0.374-1.845)	0.648	0.964 (0.377-2.464)	0.94
Molecular subtype		0.719		0.383
Normal-like & luminal B vs. luminal A	1.398 (0.41-4.764)	0.592	3.504 (0.538-22.814)	0.19

Basal & ERBB2+ vs. luminal A	0.897 (0.208-3.87)	0.885	1.791 (0.261-12.302)	0.554
---------------------------------	-----------------------	-------	-------------------------	-------

The analysis included the 110 breast cancer patients who had received adjuvant systemic CT in the NKI data set. Molecular subtypes of breast cancers are based on nearest centroid classification as used by Sorlie *et al.* *NCOR1*, *NCOR2*, *HDAC1*, *HDAC3*, *GPS2* and *TBL1* transcript expression, and age and tumor size were modeled as continuous variables. CI denotes confidence interval.

Supplementary table 2 Odds ratio for NACT non-responsiveness stratified according to N-CoR2 or *NCOR2-116* level

Predictor	Group	NR (%)	R (%)	OR (95% CI)	<i>P</i> value
N-CoR2	High	50 (76.9)	15 (23.1)	2.2 (1.0-5.1)	0.029
	Low	39 (60)	26 (40)	1	
	Subgroup B	67 (87.0)	10 (13.0)	9.4 (3.7-24.6)	<0.001
<i>NCOR2-116</i>	Subgroup A	22 (41.5)	31 (58.5)	1	
	High S_{NCOR2}	69 (87.3)	10 (12.7)	10.7 (4.2-28.2)	<0.001
	Low S_{NCOR2}	20 (39.2)	31 (60.8)	1	

The analysis included the 130 patients with breast cancers who received NACT from the MDACC data set. The tumors were segregated into subgroups according to the expression level of N-CoR2, unsupervised hierarchical clustering based on *NCOR2-116* (**Fig. 4d**) or S_{NCOR2} determined based on *NCOR2-116* (**Fig. 4e**). NR, non-responder; R, responder; OR, odds ratio; CI, 95% confidence interval. *P* values were calculated with use of Fisher's exact test.

Tsai et al

Supplementary table 3 The identity of the 64 PCD genes (represented by 75 Affymetrix probe sets) listed in **Fig. 5b** and their predicted role in PCD. The genes are ranked descendingly according to their respective value of *DRI*. Data in the last column indicate whether the expression of the gene is more TRAIL-inducible in either T4-2-vector control colonies (*V*) or T4-2 colonies expressing N-CoR2 (*N*).

Affymetrix probe set ID	Gene symbol	RefSeq Transcript ID	Description	Role in PCD	<i>DRI</i> (absolute value)	More induced by TRAIL
214329_x_at	<i>TNFSF10</i>	NM_003810	Tumor necrosis factor (ligand) superfamily, member 10	Apoptosis	2.48	<i>V</i>
200887_s_at	<i>STAT1</i>	NM_007315 NM_139266	Signal transducer and activator of transcription 1	Apoptosis	2.43	<i>V</i>
210511_s_at	<i>INHBA</i>	NM_002192	Inhibin, beta A	Apoptosis	2.21	<i>V</i>
209969_s_at	<i>STAT1</i>	NM_007315 NM_139266	Signal transducer and activator of transcription 1	Apoptosis	2.11	<i>V</i>
201845_s_at	<i>RYBP</i>	NM_012234	RING1 and YY1 binding protein	Apoptosis	2.09	<i>V</i>
201687_s_at	<i>API5</i>	NM_006595	Apoptosis inhibitor 5	Anti-apoptosis	2.04	<i>V</i>
201150_s_at	<i>TIMP3</i>	NM_000362	TIMP metalloproteinase inhibitor 3	Apoptosis	2.04	<i>V</i>
202688_at	<i>TNFSF10</i>	NM_003810	Tumor necrosis factor (ligand) superfamily, member 10	Apoptosis	2.02	<i>V</i>
201710_at	<i>MYBL2</i>	NM_002466	v-myb myeloblastosis viral oncogene homolog (avian)-like 2	Anti-apoptosis	1.99	<i>N</i>

Tsai et al

202677_at	<i>RASA1</i>	NM_002890 NM_022650	RAS p21 protein activator 1	Regulation of apoptosis	1.96	<i>V</i>
204020_at	<i>PURA</i>	NM_005859	Purine-rich element binding protein A	Apoptosis	1.89	<i>V</i>
202687_s_at	<i>TNFSF10</i>	NM_003810	Tumor necrosis factor (ligand) superfamily, member 10	Apoptosis	1.88	<i>V</i>
204274_at	<i>EBAG9</i>	NM_004215 NM_198120	Estrogen receptor binding site associated, antigen, 9	Apoptosis	1.87	<i>V</i>
204278_s_at	<i>EBAG9</i>	NM_004215 NM_198120	Estrogen receptor binding site associated, antigen, 9	Apoptosis	1.87	<i>V</i>
201844_s_at	<i>RYBP</i>	NM_012234	RING1 and YY1 binding protein	Apoptosis	1.81	<i>V</i>
201302_at	<i>ANXA4</i>	NM_001153	Annexin A4	Anti-apoptosis	1.73	<i>V</i>
219209_at	<i>IFIH1</i>	NM_022168	Interferon induced with helicase C domain 1	Regulation of apoptosis	1.71	<i>V</i>
221478_at	<i>BNIP3L</i>	NM_004331	BCL2/adenovirus E1B 19kDa interacting protein 3-like	Apoptosis	1.71	<i>V</i>

Tsai et al

207181_s_at	<i>CASP7</i>	NM_001227 NM_033338 NM_033339 NM_033340	Caspase 7	Apoptosis	1.7	<i>V</i>
212593_s_at	<i>PDCD4</i>	NM_014456 NM_145341	Programmed cell death 4	Apoptosis	1.64	<i>V</i>
217746_s_at	<i>PDCD6IP</i>	NM_013374	Programmed cell death 6 interacting protein	Apoptosis	1.64	<i>V</i>
204924_at	<i>TLR2</i>	NM_003264	Toll-like receptor 2	Apoptosis	1.61	<i>V</i>
209863_s_at	<i>TP73L</i>	NM_003722	Tumor protein p73-like	Apoptosis	1.58	<i>V</i>
202094_at	<i>BIRC5</i>	NM_001012270 NM_001012271 NM_001168	Baculoviral IAP repeat-containing 5 (survivin)	Anti-apoptosis	1.57	<i>N</i>
212354_at	<i>SULF1</i>	NM_015170	Sulfatase 1	Apoptosis	1.54	<i>V</i>

Tsai et al

211368_s_at	<i>CASP1</i>	NM_001223 NM_033292 NM_033293 NM_033294 NM_033295	Caspase 1, apoptosis-related cysteine peptidase (interleukin 1, beta, convertase)	Apoptosis	1.52	<i>V</i>
204131_s_at	<i>FOXO3A</i>	NM_001455 NM_201559	Forkhead box O3A	Apoptosis	1.48	<i>V</i>
202985_s_at	<i>BAG5</i>	NM_001015048 NM_001015049 NM_004873	BCL2-associated athanogene 5	Apoptosis	1.46	<i>V</i>
205681_at	<i>BCL2A1</i>	NM_004049	BCL2-related protein A1	Anti-apoptosis/ regulation of apoptosis	1.45	<i>V</i>
201424_s_at	<i>CUL4A</i>	NM_001008895 NM_003589	Cullin 4A	Apoptosis	1.45	<i>V</i>
201846_s_at	<i>RYBP</i>	NM_012234	RING1 and YY1 binding protein	Apoptosis	1.45	<i>V</i>
207113_s_at	<i>TNF</i>	NM_000594	Tumor necrosis factor	Apoptosis/anti- apoptosis	1.44	<i>N</i>

Tsai et al

210334_x_at	<i>BIRC5</i>	NM_001012270 NM_001012271 NM_001168	Baculoviral IAP repeat-containing 5 (survivin)	Anti-apoptosis	1.44	<i>N</i>
200004_at	<i>EIF4G2</i>	NM_001418	Eukaryotic translation initiation factor 4 gamma, 2	Cell death	1.43	<i>V</i>
203628_at	<i>IGF1R</i>	NM_000875	Insulin-like growth factor 1 receptor	Anti-apoptosis	1.43	<i>V</i>
200599_s_at	<i>HSP90B1</i>	NM_003299	Heat shock protein 90kDa beta (Grp94), member 1	Anti-apoptosis	1.42	<i>V</i>
202095_s_at	<i>BIRC5</i>	NM_001012270 NM_001012271 NM_001168	Baculoviral IAP repeat-containing 5 (survivin)	Anti-apoptosis	1.38	<i>N</i>
222108_at	<i>AMIGO2</i>	NM_181847	Adhesion molecule with Ig-like domain 2	Regulation of apoptosis	1.36	<i>V</i>
217999_s_at	<i>PHLDA1</i>	NM_007350	Pleckstrin homology-like domain, family A, member 1	Apoptosis	1.35	<i>V</i>
215037_s_at	<i>BCL2L1</i>	NM_001191 NM_138578	Bcl2-like 1 (Bcl-xL)	Anti-apoptosis	1.32	<i>N</i>

Tsai et al

213373_s_at	<i>CASP8</i>	NM_001228 NM_033355 NM_033356 NM_033358	Caspase 8, apoptosis-related cysteine peptidase	Apoptosis	1.31	<i>V</i>
200690_at	<i>HSPA9B</i>	NM_004134	Heat shock 70kDa protein 9B (mortalin-2)	Anti-apoptosis	1.3	<i>V</i>
202693_s_at	<i>STK17A</i>	NM_004760	Serine/threonine kinase 17a	Apoptosis	1.28	<i>V</i>
210025_s_at	<i>CARD10</i>	NM_014550	Caspase recruitment domain family, member 10	Regulation of apoptosis	1.25	<i>N</i>
205599_at	<i>TRAF1</i>	NM_005658	TNF receptor-associated factor 1	Anti-apoptosis	1.25	<i>N</i>
201849_at	<i>BNIP3</i>	NM_004052	BCL2/adenovirus E1B 19kDa interacting protein 3	Apoptosis	1.24	<i>V</i>
206295_at	<i>IL18</i>	NM_001562	Interleukin 18	Apoptosis	1.22	<i>V</i>
200608_s_at	<i>RAD21</i>	NM_006265	RAD21 homolog	Apoptosis	1.22	<i>V</i>
200658_s_at	<i>PHB</i>	NM_002634	Prohibitin	Regulation of apoptosis	1.21	<i>N</i>
213026_at	<i>ATG12</i>	NM_004707	ATG12 autophagy related 12 homolog	Autophagy	1.2	<i>V</i>

Tsai et al

201637_s_at	<i>FXR1</i>	NM_001013438 NM_001013439 NM_005087	Fragile X mental retardation, autosomal homolog 1	Apoptosis	1.19	<i>V</i>
200807_s_at	<i>HSPD1</i>	NM_002156 NM_199440	Heat shock 60kDa protein 1	Regulation of apoptosis	1.18	<i>V</i>
205263_at	<i>BCL10</i>	NM_003921	B-cell CLL/lymphoma 10	Apoptosis	1.18	<i>V</i>
209476_at	<i>TXNDC</i>	NM_030755	Thioredoxin domain containing	Anti-apoptosis	1.17	<i>V</i>
200602_at	<i>APP</i>	NM_000484 NM_201413 NM_201414	Amyloid beta (A4) precursor protein	Apoptosis	1.17	<i>V</i>
210118_s_at	<i>IL1A</i>	NM_000575	Interleukin 1, alpha	Apoptosis	1.15	<i>V</i>
217997_at	<i>PHLDA1</i>	NM_007350	Pleckstrin homology-like domain, family A, member 1	Apoptosis	1.15	<i>V</i>
200681_at	<i>GLO1</i>	NM_006708	Glyoxalase I	Anti-apoptosis	1.15	<i>V</i>
212719_at	<i>PHLPP</i>	NM_194449	PH domain and leucine rich repeat protein phosphatase	Apoptosis	1.14	<i>V</i>

Tsai et al

202984_s_at	<i>BAG5</i>	NM_001015048 NM_001015049 NM_004873	BCL2-associated athanogene 5	Apoptosis	1.12	<i>V</i>
201167_x_at	<i>ARHGDI1</i>	NM_004309	Rho GDP dissociation inhibitor (GDI) alpha	Anti-apoptosis	1.12	<i>N</i>
203489_at	<i>SIVA</i>	NM_006427 NM_021709	CD27-binding (Siva) protein	Regulation of apoptosis	1.11	<i>N</i>
201084_s_at	<i>BCLAF1</i>	NM_014739	BCL2-associated transcription factor 1	Apoptosis	1.1	<i>None</i>
211300_s_at	<i>TP53</i>	NM_000546	Tumor protein p53	Apoptosis	1.09	<i>None</i>
38158_at	<i>ESPL1</i>	NM_012291	Extra spindle poles like 1	Apoptosis	1.09	<i>N</i>
211936_at	<i>HSPA5</i>	NM_005347	Heat shock 70kDa protein 5	Anti-apoptosis	1.08	<i>V</i>
202076_at	<i>BIRC2</i>	NM_001166	Baculoviral IAP repeat-containing 2	Anti-apoptosis	1.08	<i>V</i>
200691_s_at	<i>HSPA9B</i>	NM_004134	Heat shock 70kDa protein 9B	Anti-apoptosis	1.08	<i>V</i>
210260_s_at	<i>TNFAIP8</i>	NM_014350	Tumor necrosis factor, alpha-induced protein 8	Regulation of apoptosis	1.07	<i>V</i>
204211_x_at	<i>EIF2AK2</i>	NM_002759	Eukaryotic translation initiation factor 2-alpha kinase 2	Apoptosis	1.05	<i>V</i>

Tsai et al

214988_s_at	<i>SON</i>	NM_003103 NM_032195 NM_058183 NM_138925 NM_138926 NM_138927	SON DNA binding protein	Anti-apoptosis	1.04	<i>V</i>
201012_at	<i>ANXA1</i>	NM_000700	Annexin A1	Anti-apoptosis	1.02	<i>V</i>
201371_s_at	<i>CUL3</i>	NM_003590	Cullin 3	Apoptosis	1.01	<i>V</i>
200797_s_at	<i>MCL1</i>	NM_021960 NM_182763	Myeloid cell leukemia sequence 1	Regulation of apoptosis	1.01	<i>V</i>
211316_x_at	<i>CFLAR</i>	NM_003879	CASP8 and FADD-like apoptosis regulator	Regulation of apoptosis	1.01	<i>V</i>

Supplementary table 4 Genes that contain conserved IRF1 and STAT1 binding sites in the N-CoR2-associated PCD genes listed in **Fig. 5b**

Gene symbol	Entrez gene ID	RefSeq Transcript ID	Description	Binding sites ¹
<i>TNFSF10</i>	8743	NM_003810	tumor necrosis factor superfamily, member 10	IRF1 ²
<i>STAT1</i>	6772	NM_007315 NM_139266	signal transducer and activator of transcription 1	IRF1 ³
<i>INHBA</i>	3624	NM_002192	inhibin, beta A	IRF1
<i>RYBP</i>	23429	NM_012234	RING1 and YY1 binding protein	IRF1
<i>TIMP3</i>	7078	NM_000362	TIMP metallopeptidase inhibitor 3	IRF1
<i>RASA1</i>	5921	NM_002890 NM_022650	RAS p21 protein activator 1	IRF1, STAT1
<i>PURA</i>	5813	NM_005859	purine-rich element binding protein A	IRF1, STAT1
<i>IFIH1</i>	64135	NM_022168	interferon induced with helicase C domain 1	IRF1, STAT1
<i>PDCD4</i>	27250	NM_014456 NM_145341	programmed cell death 4	IRF1
<i>TP73L</i>	8626	NM_003722	tumor protein p73-like	IRF1, STAT1
<i>SULF1</i>	23213	NM_015170	sulfatase 1	IRF1

<i>CASP1</i>	834	NM_001223	caspase 1, apoptosis-related	IRF1 ⁴
		NM_033292	cysteine peptidase	
		NM_033293	(interleukin 1, beta,	
		NM_033294	convertase)	
		NM_033295		
<i>FOXO3A</i>	2309	NM_001455	forkhead box O3A	IRF1
		NM_201559		
<i>IGF1R</i>	3480	NM_000875	insulin-like growth factor 1 receptor	IRF1, STAT1
<i>CASP8</i>	841	NM_001228	caspase 8, apoptosis-related	IRF1 ^{5,6}
		NM_033355	cysteine peptidase	
		NM_033356		
		NM_033358		
<i>CARD10</i>	29775	NM_014550	caspase recruitment domain family, member 10	STAT1
<i>TRAF1</i>	7185	NM_005658	TNF receptor-associated factor 1	IRF1
<i>IL18</i>	3606	NM_001562	interleukin 18	IRF1
<i>RAD21</i>	5885	NM_006265	RAD21 homolog	IRF1
<i>ATG12</i>	9140	NM_004707	ATG12 autophagy related 12 homolog	IRF1
<i>APP</i>	351	NM_000484	amyloid beta (A4) precursor	IRF1, STAT1
		NM_201413	protein	
		NM_201414		
<i>PHLPP</i>	23239	NM_194449	PH domain and leucine rich repeat protein phosphatase	IRF1, STAT1

Tsai et al.

<i>BCLAF1</i>	9774	NM_014739	BCL2-associated transcription factor 1	IRF1
<i>TP53</i>	7157	NM_000546	tumor protein p53	STAT1
<i>ESPL1</i>	9700	NM_012291	extra spindle poles like 1	IRF1, STAT1
<i>BIRC2</i>	329	NM_001166	baculoviral IAP repeat-containing 2	IRF1
<i>TNFAIP8</i>	25816	NM_014350	tumor necrosis factor, alpha-induced protein 8	IRF1, STAT1
<i>EIF2AK2</i>	5610	NM_002759	eukaryotic translation initiation factor 2-alpha kinase 2	IRF1, STAT1
<i>SON</i>	6651	NM_003103 NM_032195 NM_058183 NM_138925 NM_138926 NM_138927	SON DNA binding protein	IRF1
<i>CUL3</i>	8452	NM_003590	cullin 3	IRF1

¹Conserved IRF1 and STAT1 binding sites detected by oPOSSUM. A total of 54 genes from the original 64 PCD genes were analyzed, amongst which 24 contain conserved IRF1 binding sites and 12 have conserved STAT1 binding sites identified at their promoter regions.

²Clarke, N., Jimenez-Lara, A. M., Voltz, E. & Gronemeyer, H. Tumor suppressor IRF-1 mediates retinoid and interferon anticancer signaling to death ligand TRAIL. *EMBO J.* **23**, 3051-3060 (2004).

³Wong, L. H. *et al.* Isolation and characterization of a human STAT1 gene regulatory element. *J. Biol. Chem.* **277**, 19408-19417 (2002).

⁴Iwase, S. *et al.* Defective binding of IRFs to the initiator element of interleukin-1 β -converting enzyme (ICE) promoter in an interferon-resistant Daudi subline. *FEBS Lett.* **450**, 263-267 (1999).

Tsai et al.

⁵Ruiz-Ruiz, C., de Almodóvar, C. R., Rodríguez, A., Ortiz-Ferrón, G., Redondo, J. M. & López-Rivas, A. The up-regulation of human caspases-8 by interferon- γ in breast tumor cells requires the induction and action of the transcription factor interferon regulatory factor-1. *J. Biol. Chem.* **279**, 19712-19720 (2004).

⁶Casciano, I. *et al.* Expression of the caspases-8 gene in neuroblastoma cells is regulated through an essential interferon-sensitive response element (ISRE). *Cell Death Differ.* **11**, 131-134 (2004).

SUPPLEMENTARY METHODS

CHEMICALS AND ANTIBODIES

The caspase-3, 6 and 8 inhibitors DEVD-CHO and Ac-IETD-CHO (Biomol) were used at 1 μ M in DMSO. The histone deacetylase inhibitor trichostatin A (Upstate) was used at 100-500 nM in DMSO and suberoylanilide hydroxamic acid (SAHA) was at 1-5 μ M in DMSO (Merck Research Laboratories). The methylase inhibitor, 5-Aza-2'-deoxycytidine (ADC; Sigma-Aldrich) was used at 0.5 μ M and dissolved in DMSO. The chemotherapy agent paclitaxel (Sigma-Aldrich) was used at 10-40 μ M in ddH₂O and doxorubicin (Calbiochem) was at 5 mM in PBS. For immunoblotting and/or immunostaining experiments, we used rabbit polyclonals: anti-acetyl-histone H4, and anti-trimethyl-histone H3 (Lys9) (Millipore), anti-MeCP2 (Affinity BioReagents), anti-cleaved caspases-3 (Cell Signaling), anti-IRF-1 (H-205), anti-histone-H2B (FL-126), anti-HDAC3 (H-99), and anti-mouse-SMRTe (H-300; Santa Cruz) as well as anti-lamin B1 (Abcam). We also used the rat monoclonals (mAbs) anti- α 6 integrin (NKI-GoH3), rabbit mAb anti-acetyl (Lys27)-histone H3 (D2W; Millipore), anti-acetyl (Lys5)-histone H4 (EP1000Y), anti-caspase-3 (active) (E83-77) and anti-acetyl (Lys9)-histone H3 (Y28) (Epitomics), and anti-HP1 α (C7F11) and anti-trimethyl-histone H3 (Lys 27) (C36B11, Cell Signaling) as well as the mouse mAbs anti-GPS2 (3C4; Abnova), anti- β -tubulin (5H1; BD Transduction Laboratories), and anti-Ki-67 (7B11, Invitrogen). For IP and ChIP experiments, we used mouse mAb anti-GFP (7.1 & 13.1, Roche Applied Science), rabbit polyclonal anti-SMRTe (Millipore) and anti-CBP (A-22; Santa Cruz). The hybridoma cell line producing the monoclonal anti-N-CoR2 (gift from M. A. Lazar, University of Pennsylvania) was described previously⁶.

CELL CULTURE AND DEATH ASSAYS

Tsai et al.

Cell culture

The HMT-3522 nonmalignant S-1 and tumorigenic T4-2 MECs lines were propagated as monolayers on tissue culture plastic or culture dishes coated with a layer of 1:100 Matrigel diluted in PBS in chemically defined medium as previously described⁷. MECs were embedded and grown for 12 days to form 3D structures within rBM (Matrigel, BD Biosciences). MDA-MB-231 and HEK293 cells were grown as monolayers on tissue culture plastic in DMEM supplemented with 10% fetal bovine serum and antibiotics.

Induction and analysis of cell death

Cell death was initiated either by treatment with recombinant, purified human TRAIL peptide (Biomol) or various chemotherapeutic agents or by inducing DNA damage by exposure to gamma irradiation using a Mark I Cesium 137 irradiator (JL Shepherd & Associates). Cell death was determined by quantifying percent active caspase 3 by indirect immunofluorescence (Cell Signaling) or counting the nuclei of dead cells using the CYTOX-orange or CYTOX-blue dyes (Invitrogen) and normalizing dead cells to total cell number estimated by counterstaining nuclei with the cell permeable dye Hoechst 33342 (Invitrogen)⁸. In select experiments, cells constitutively expressing human nuclear histone H2B-GFP or H2B-mRFP fusion protein were used to estimate the number of cells present in the 3D organoids. Clonogenic survival was assessed in 3D rBM cultures by monitoring spheroid outgrowth and measuring the size of colonies formed by single seeded cells exposed to IR as a function of time (9 Gy; four weeks incubation).

GENE EXPRESSION MANIPULATIONS

N-CoR2 or HDAC3 knockdown was achieved by retroviral-mediated RNAi using

Tsai et al.

oligonucleotide sequences previously described⁹. The oligonucleotides specifying the small hairpin RNAs (shRNAs) were sub-cloned from pSilencer-H1 into pLZRS-MFG-CMV-Neo-U6, a recombinant self-inactivating retroviral vector constructed from the backbone of an MFG provirus that directs the expression of shRNA under the control of the U6 promoter^{10,11}. Stable knockdown of TRAIL was achieved by the pRetroSuper-puro system (OligoEngine) using oligonucleotide sequences previously described¹². The retroviral construct used for inducible expression of HA- and EGFP-epitope tagged N-CoR2 was prepared by subcloning murine *NCOR2* cDNA (e isoform, NCBI RefSeq #NM_011424) from pCMX-FLAG-NCOR2 (gift from M. A. Lazar, University of Pennsylvania)¹³ into pBluescriptII KS+ (Stratagene) to facilitate the addition of the N-terminal HA-epitope tag, which was then recloned into a modified hybrid Epstein-Barr virus/retroviral vector pLZRS-MFG-*tet*-EGFP that contains a tetracycline regulated promoter that allows stable multicopy episomal replication in the retroviral packaging lines^{14,15} to generate the final expression construct pLZRS-MFG-*tet*-HA-EGFP-NCOR2. The mutant N-CoR2 (K449A) was constructed using the QuickChange Site-Directed Mutagenesis kit (Stratagene) using pMFG-*tet*-HA-EGFP-NCOR2 as template. The retroviral vector encoding the human histone H2B-GFP, pCLNR-H2BG (gift from G. M. Wahl, Salk Institute), has been described previously¹⁶. The retroviral expression construct for the histone H2B-monomeric red fluorescence protein (mRFP) fusion protein was generated by fusing the genes encoding mRFP and human histone H2B by PCR amplification and subcloning from pcDNA3.1-mRFP (Addgene) and pCLNR-H2BG into the pMXs-IRES-blasticidin retroviral vector (Cell Biolabs). Amphotropic retrovirus was produced in modified 293 cells or in Phoenix amphi cells (G. Nolan, Stanford University) with packaging vectors pCgp and pVSVG to boost viral titer. Cells were spin infected with retrovirus carrying wild-type or mutant N-CoR2, followed by infection with a high titer MFG virus expressing the tetracycline-controlled transcriptional transactivator

Tsai et al.

produced in the packaging cell line 293GPG as described¹⁷. To obtain a polyclonal population of cells in which the majority of cells can competently induce N-CoR2 or mutant N-CoR2 expression cells were expanded in the presence of tetracycline (1 μ g/mL) and wild type or mutant N-CoR2 expression was induced by withdrawal of tetracycline (2-4 days), followed by FAC sorting for GFP positive cells. Sorted cells were thereafter expanded in the presence of tetracycline. The tetracycline-regulated expression of N-CoR2 or its mutant was thereafter activated 2-3 days prior to cell manipulation to maintain high transgene expression in the population. Cells expressing the various shRNA constructs were generated using a similar protocol. Level of gene expression and/or knockdown was verified by real-time PCR (RT-PCR) and confirmed through immunoblot analysis. The IRF-1 expression vector, pcDNA3-IRF-1, was a kind gift from J. Park, Sungkyunkwan University, Seoul, Korea¹⁸. Transient transfection experiments were performed using Lipofectamine 2000 (Invitrogen).

ANIMAL EXPERIMENTS AND IMMUNOHISTOCHEMISTRY STUDIES

Xenograft breast tumorigenesis models and paclitaxel treatment

The retroviral vector encoding GFP or GFP-tagged N-CoR2 and firefly luciferase, pSFP-GFP-FFLuc (gift from R.J. Brentjens, Memorial Sloan Kettering Cancer Center)¹⁹ were transduced into MDA-MB-231 cells and the GFP-positive cells were sorted by FACS. Cells (2×10^6 cells in 100 μ l 1:1 mixture of Matrigel and HBSS) were inoculated into the mammary fat pads of 8-week-old female NOD/SCID mice (National Laboratory Animal Center, Taiwan). Ten days post inoculation when tumor bulk was similar between the two groups (similar bioluminescence imaging (BLI) intensity and palpable tumors), mice were given intraperitoneal injections of paclitaxel (20 mg/kg) or vehicle (15% ethanol in 0.9% NaCl) every week for six consecutive weeks. Tumor mass was assessed by BLI weekly before each treatment. The

Tsai et al.

antitumor effect of paclitaxel was evaluated using the T/C value (%), where T is the relative tumor bulk of the treated group and C the relative tumor bulk of the control group²⁰. The relative tumor bulk was determined by calculating the ratio of the bioluminescence signal intensity of the tumor at a given time and that of the initial tumor size (*i.e.* at time of treatment initiation). The protocols for animal care and experiments were approved by the Institutional Animal Care and Use Committee (IACUC) of National Health Research Institutes, Taiwan.

Immunohistochemistry of human specimens.

TMA of breast cancer was obtained from US Biomax, Inc., code BR804. TMA sections were deparaffinized, hydrated, immersed in citrate buffer at pH 6.0 for epitope retrieval in a microwave. Endogenous peroxidase activity was quenched in 3% hydrogen peroxidase for 15 minutes, and slides were then incubated with 10% normal horse serum to block nonspecific immunoreactivity. The indicated antibody was subsequently applied and detected by using the DAKO EnVision kit (DAKO). For negative controls, the primary antibody was replaced by the citrate buffer. All the immunohistochemical and TMA staining were evaluated by the same pathologist and the nuclear and cytoplasmic staining patterns of N-CoR2 were quantified using the histological score (H-score)²¹.

Bioluminescence imaging (BLI)

BLI was performed by using the IVIS Imaging System (Xenogen). Mice were anesthetized with 2% isoflurane and injected intraperitoneally with 150 mg/kg D-luciferin (Xenogen) 6 min before image acquisition. Tumor bulk was determined by measuring the photon flux from a region of interest drawn around the bioluminescence signal using Live Imaging Software (Xenogen) according to the manufacturer's recommendations.

RNA AND PROTEIN BIOCHEMISTRY EXPERIMENTS

RNA extraction and quantitative RT-PCR analysis

Total RNA was extracted by a modified TRI reagent procedure as described²² and purified using the RNeasy Mini Kit (Qiagen) and total RNA (1.0 µg) was used as a template for cDNA synthesis using MMLV reverse transcriptase (Promega). cDNA (100 ng) was used as template for PCR amplification using the LightCycler FastStart DNA MASTER^{PLUS} SYBR Green I Kit and the LightCycler System (Roche) according to the manufacturer's instructions. Oligonucleotide primers were designed using LightCycler Probe Design Software 2.0 (Roche) or Primer Bank (<http://pga.mgh.harvard.edu/primerbank/index.html>) and the sequences are available upon request. Transcript expression was quantified by normalizing the gene of interest copy number (per µL) to absolute levels of an endogenous, stably expressed reference gene, ribosomal protein L13a (*RPL13A*)²³.

Immunoblot Analysis

For immunoblot protein analysis Laemmli lysate containing protease and phosphatase inhibitors was prepared from cells grown as monolayer or from colonies isolated from 3D rBM using ice-cold PBS/EDTA as previously described^{24,25}. Total and soluble TRAIL protein levels (pg/mL) were determined using the human TRAIL ELISA Kit (Biomol) standardized to total cell protein extract (mg/mL), according to the supplier's instructions.

HDAC activity assay

HEK 293 cells were retrovirally infected with retroviral constructs inducibly expressing myc tagged N-CoR2, N-CoR2 (K449A) or a control EGFP construct

Tsai et al.

(pLZRS-MFG-*tet*-myc(4)-EGFP-N-CoR2, pLZRS-MFG-*tet*-myc(4)-EGFP-N-CoR2 (K449A) or pLZRS-MFG-*tet*-myc(4)-EGFP). Myc tagged protein expression was induced through doxycycline treatment (1 μ g/mL; 16 hours) and nuclear protein extracts were prepared as described previously²⁶. Briefly, cells were scraped and collected in PBS on ice. Cells were swollen in a hypotonic buffer (10 mM HEPES pH 7.9, 1.5 mM MgCl₂, 10 mM KCl, 1 mM EGTA, 0.5 mM DTT, 0.2 mM PMSF, 0.1% NP40) and homogenized on ice. Nuclei were separated via centrifugation and treated with high salt buffer (20 mM HEPES, 1.5 mM MgCl₂, 1.2 M KCl, 0.2 mM EDTA, 1 mM EGTA, 0.5 mM DTT, 0.2 mM PMSF, 0.1% NP40) and 600 μ g of nuclear extract was pre incubated with 50 μ L of equilibrated in diluent buffer (15 mM HEPES pH 7.9, 1 mM MgCl₂, 0.2 mM EDTA, 150 mM KCl, 20% glycerol, 0.5 mM DTT, 0.2 mM PMSF) protein G agarose beads (Invitrogen) for 1 hour at 4°C. Nuclear lysate was transferred and incubated (4°C; 3 hours) with 50 μ L of equilibrated protein G agarose beads (Invitrogen) and 5 μ g of purified hybridoma mouse anti-myc antibody. Beads were washed three times with wash buffer (diluent buffer with 0.5 M KCl) and once with diluent. Washed conjugated beads were used in the Fluor de Lys Assay System (Biomol) per kit instructions to determine HDAC activity associated with the immunoprecipitation. Fluorescence was determined using a Spectra Max M5 fluorimetric plate reader (Molecular Devices).

Chromatin immunoprecipitation (ChIP) and reporter assays

ChIP experiments were carried out using primers specific for the different segments of the TRAIL promoter, as described previously^{5,27}. The primers used in **Supplementary Fig. 4b** included: primer set A: 5'-TGTGATGGGGTTAATATTTTGGGA and 5'-GCTACTGTGAGGGTGGGAAG; primer set B: 5'-CTTCCCACCTCACAGTAGC and 5'-CACTCACCTCAAGCCCATTTCTC; primer set C: 5'- AATGGGCTTGAGGTGAGTGCAGAT

Tsai et al.

and 5'- ATGAGTTGTTTTCTGGGTTCTGT; primer set D:
5'-AGTTTCCCTCCTTTCCAACG and 5'-CACTGAAGCCCTTCCTTCTCT. The putative *cis*-acting elements and upstream regulatory regions on the 5' flanking sequence of the TRAIL gene have been reported previously³⁻⁵. For each ChIP assay, the samples were immunoprecipitated using 5 g/ml of the selected antibody or equivalent concentrations of normal rabbit IgG. Approximately 2-5 µl of ChIP-enriched chromatin was subjected to a standard ChIP-PCR and the enrichment of specific genomic regions was assessed relative to either control IgG or the control cells. Each ChIP experiment was repeated at least in triplicate. The IRF-1 luciferase reporter vector pTL-Luc-IRF1 was purchased from Panomics. Reporter assays were conducted in HEK293 cells by transient transfection, as previously described⁵.

MICROARRAY EXPERIMENTS

Total RNA for microarray analysis of genes differentially expressed between MECs grown as 2D monolayers and those grown as 3D acini was extracted from triplicate samples and from 3 independent culture preparations using the modified TRI reagent procedure²² and RNA was purified using an RNeasy Mini Kit (Qiagen). For transcript profiling of N-CoR2 regulated genes, transformed T4-2 MECs expressing vector ("V") or wild type N-CoR2 ("N") and those treated with TRAIL (1 µg/mL; 4 hours; "VT" versus "NT") or vehicle, total RNA was extracted in duplicate from the 6 day MEC cultures of each of the 4 experimental groups. To prevent apoptosis induction MEC cultures were pretreated with initiator and executioner caspase inhibitors at least 2 hours before stimulation and inhibition was maintained throughout the duration of TRAIL treatment (*i.e.* 4 hours).

Gene expression analysis was performed on an Affymetrix Human Genome U133A 2.0

Tsai et al.

GeneChip platform containing 22,283 probes according to the manufacturer's protocol (Affymetrix). Biotinylated cRNA was produced from total RNA (20 g) from each sample. After hybridization, washing and staining, arrays were scanned using a confocal scanner (Affymetrix). The hybridization intensity data was processed using the GeneChip Operating software (Affymetrix). Affymetrix .cel files (probe intensity files) were processed with ArrayAssist Lite (v3.4, Stratagene). The files were imported and processed with the GC-RMA algorithm to yield probe set intensities and additionally, Affymetrix Preset, Absent, Marginal flags were computed. These values were exported in .chp files, which were subsequently imported into the Partek Genomics Suite software (v6.2, Partek). The genes were filtered based on the Affymetrix P/A/M flags to retain only those genes that were present in at least 2 of the 16 samples. From the 22,283 probe sets, 12,656 (representing 8,255 genes) were included for further analysis. The gene expression data have been deposited in NCBI's Gene Expression Omnibus (GEO, <http://www.ncbi.nlm.nih.gov/geo/>) and are accessible through GEO Series accession number GSE8346.

BIOINFORMATICS AND STATISTICAL ANALYSIS

Bioinformatics and statistical analysis

To select genes that were differentially induced or repressed in response to N-CoR2 and following exposure to TRAIL, the GC-RMA expression values of all the 16 transcriptomes were log₂ transformed and a two way ANOVA was calculated, yielding 3 *P* values for each gene. These included one that reflects whether or not the gene's expression is significantly different before and after N-CoR2 expression, with and without TRAIL treatment, and whether differential expression of the gene in response to TRAIL depends upon the presence or absence of N-CoR. Additional pair wise contrasts were performed for each of the 4 paired conditions,

Tsai et al.

yielding both P values and fold changes between the mean expression values of the different conditions. The difference between TRAIL-induced changes in the level of gene expression between T4-2-N-CoR2 cells and T4-2-vector cells was measured by using the equation “ $\log_2(NT/N) - \log_2(VT/V)$ ”, which was designated as a *differential response index (DRI)*. A filtering criterion ($P < 0.05$ by two-way ANOVA, $DRI \geq 1.0$ or ≤ -1.0) was used to select genes that were differentially responsive to TRAIL compared between T4-2-N-CoR2 and the vector control cells.

The differentially expressed genes in the 304-gene N-CoR2-associated gene set (represented by 350 Affymetrix probe sets) or those in the *NCOR-1620* gene set were functionally annotated using a comprehensive functional annotation bioinformatics microarray analysis tool DAVID (<http://david.abcc.ncifcrf.gov/>) and the results were further processed and displayed using an interactive gene set analysis interface HotGene (<http://www.hotgene.net/>) (HotGene Informatics). Briefly, the genes were uploaded to DAVID and a ranked list of functional annotations was executed and generated by the system. Functional annotations were then selected according to Gene Ontology Biological Processes (GO-BP) and SwissProt Keywords (SPK) with P -value less than 0.05. For GO-BP annotations, the level five from the root of the Gene Ontology Tree was retained as a default setting while the level of the Gene Ontology annotations was adjusted dynamically. The GO Redundancy Filter (GORF) function was additionally applied in the HotGene Annotation Relation Enrichment Analysis (AREA) interface to the resultant GO-BP annotations by tracing back the Gene Ontology Tree and verifying whether the two functional terms shared the same root among the Gene Ontology annotation tree. If the two terms shared the same terms and the genes shared by the two functional annotations are greater than 80%, these two functional annotations were considered redundant and were therefore removed. After removing redundant GO-BP terms using GORF, the top five or six functional annotations of each

Tsai et al.

category were selected and genes shared by any two of the selected annotations were identified which enabled the construction of a network provided the best informative distribution and association amongst the most enriched functional annotations. In the HotGene AREA interface as shown in **Fig. 5a** and **Supplementary Fig. 3**, the selected functional categories according to GO-BP and SKP are represented by blue and yellow square nodes, respectively. The size of the nodes indicates the number of genes within the corresponding functional categories and the border color of each functional category node represents the average fold changes (absolute values) amongst the genes residing in each of the corresponding functional categories. The line segments connecting any two nodes indicates the extent to which the same genes are shared by the two functional categories with the thickness and the color of the line segments representing the percentage of shared genes and the average fold changes (absolute values) of the shared genes, respectively.

The enriched transcriptional factor binding sites in the promoter regions of genes in the N-CoR2-associated gene sets were searched using oPOSSUM (<http://www.cisreg.ca/cgi-bin/oPOSSUM/opossum>). Over-represented binding sites were determined by Z-score and the one-tailed Fisher exact probability test. The oPOSSUM algorithm identified several transcription factors that interact with and are modulated by N-CoR2, including the homeobox factor Pbx, the ETS family protein ELK-1, the activating protein-1 (AP-1) member c-FOS, serum response factor (SRF), the nuclear factor- κ B (NF κ B) family members p65, p50, and c-Rel, in the N-CoR2 regulated gene list²⁸⁻³².

To analyze the transcriptional regulation amongst the 64 PCD genes identified from the *NCOR2-1620* gene set (**Fig. 4c**), the enriched transcription factors (TFs) from these PCD genes

Tsai et al.

was interrogated using TRANSFEC (<http://www.gene-regulation.com/pub/databases.html>) and oPOSSUM and the association between the enriched TFs and their target genes (TGs) was displayed using HotGene (<http://www.hotgene.net/>) (HotGene Informatics). Briefly, the enriched TFs were sorted by their Fisher scores and the top enriched transcription factors and their respective TGs were selected. In the HotGene TFTG Association Network interface as shown in **Fig. 5c**, the square nodes represent the enriched TFs and the circle nodes indicate the TGs of the corresponding TFs with the association between TFs and TGs indicated by grey arrows. For each TF the top 5 TGs that showed the highest fold changes in gene expression following treatment with TRAIL are displayed. Similar to the HotGene AREA interface the size of the TF square node indicates the number of TGs and the border color of each square node represents the average fold change in gene expression in the corresponding TGs following TRAIL treatment.

Data mining of the gene expression profiles of tumors and clinical cancer specimens

The tumor transcriptome data and associated clinicopathological variables (CPVs) and tumor molecular subtypes of the 295 breast cancer patients in the Netherlands Cancer Institute (NKI) data set has been reported previously and was downloaded from the publically accessible website (<http://www.rii.com/publications/2002/nejm.html>)¹. We searched the probe hybridization ratio of N-CoR2 (*NCOR2*) and HDAC3 (*HDAC3*) and chose the probe set that displayed the highest hybridization intensity for *NCOR2* (*IMAGE:80772*) to complete our analysis. The patients were stratified according to their local lymph node (LN) or estrogen receptor (ER) status, whether or not they received adjuvant chemotherapy (CT) as well as the molecular subtype of the breast cancer. The patients were further grouped into quartiles based on the relative (untransformed) expression levels of *NCOR2* or *HDAC3* present in the respective data sets. The probability of remaining relapse-free or showing reduced overall rate of survival was computed using the

Tsai et al.

method of Kaplan and Meier. The curves were plotted and compared using the log-rank test with the software packages SPSS 10.0 (SPSS) and GraphPad Prism 5.02 (GraphPad Software). The log-rank test was used to calculate the *P* values.

Multivariate analyses with Cox's proportional-hazards regression were performed on the expression level of *NCOR2* and/or *HDAC3* and the CPVs and molecular subtypes of breast cancer as provided in the NKI data set. Statistical analyses were performed using SPSS 10.0 (SPSS).

Gene expression profiles of the pretreatment breast cancer tissues from the 133 breast cancer patients who received neoadjuvant combination chemotherapy (NACT) with paclitaxel and fluorouracil-doxorubicin-cyclophosphamide (T/FAC) (L. Pusztai, University of Texas M.D. Anderson Cancer Center (MDACC), Houston, TX) were downloaded from the website (<http://bioinformatics.mdanderson.org/pubdata.html>)³³. For the expression levels of *NCOR2*, the Affymetrix probe set *207760_s_at* that displayed the highest hybridization intensity was used for the analysis. We considered those patients who did not have residual cancer cells in the breast by pathological examination following NACT as demonstrating a clinically beneficial response (*i.e.*, “responders”) and those in which residual cancer cells were identified in the breast as “non-responders”. Three patients without available information on the post-treatment breast pathological data from the original data set were excluded, which left a total of 130 cases for the final analysis.

The transcript levels of *NCOR2* in the pretreated breast cancer tissues of 24 breast cancer patients who received NACT with docetaxel were downloaded from NCBI's Gene Expression

Tsai et al.

Omnibus (accession number GSE6434)³⁴. The two Affymetrix probe sets (*31709_at* and *39359_s_at*) that represent *NCOR2* displayed similar expression patterns across the samples and one of these (*31709_at*) was depicted in **Fig. 4a**.

Gene expression profiles of the pretreated breast cancer tissues from the 82 breast cancer patients who received NACT with epirubicin and cyclophosphamide were provided by Siemens Healthcare Diagnostics Products GmbH³⁵. The Affymetrix probe set *207760_s_at* that displayed the highest hybridization intensity for *NCOR2* was used for the analysis. We considered the patients with pathologically defined complete absence of invasive carcinoma in the breast following NACT as “responders” and those who displayed only partial response or no response as “nonresponders” of NACT.

Hierarchical clustering analysis and construction of S_{NCOR2}

The 304 N-CoR2-associated genes, as represented by 350 Affymetrix probe sets, were identified from the microarray experiments as described above, based upon whether their level of expression (on a \log_2 base) was significantly different as determined (fold change ≥ 2 and a cutoff P -value < 0.05 by Student's t test) between tumors expressing exogenous N-CoR2 or vector. The expression levels of the 304 genes between the responders and nonresponders in the MDACC data set using the Student's t test was then used to identify a list of 116 Affymetrix probe sets representing 107 genes ($P < 0.05$; designated as “*NCOR2-116*”). These genes were then median-centered and average linkage clustering (ALC) was conducted using the Cluster and TreeView software³⁶ and the 130 breast tumors in the MDACC data set were segregated into two predominant classes based on the first bifurcation in the dendrogram (**Fig. 4d**).

Tsai et al.

To test whether the 107 N-CoR2-associated genes could robustly segregate breast tumors according to their chemotherapy responsiveness the NKI data set was interrogated. A list of 63 genes, designated as “*NCOR2-63*”, that correspond to the 107 N-CoR2-associated genes was identified. Using the method of Kaplan and Meier the same analytical procedure was used to segregate the 110 breast tumors from the patients who received adjuvant chemotherapy into two major response subgroups (**Fig. 4g**) and to assess the probability of these patients remaining relapse-free or showing changes in the rate of their overall survival (**Fig. 4h**).

To determine whether the N-CoR2-associated gene expression profile derived from the T4-2 3D organoid culture experiments reflected a similar functional behavior in human breast tumors the average expression levels (on a \log_2 scale) of the gene probes in *NCOR2-116* in T4-2-N-CoR2 cells, the vector control cells and the 130 breast tumors in the MDACC data set were normalized and median-centered. The degree of resemblance between the expression profiles of the gene probes in *NCOR2-116* in the 130 breast tumors and those represented in the T4-2 N-CoR2 cells and vector control cells were measured using Pearson’s correlation coefficient to yield r_{NCOR2} and r_{vector} , respectively. Tumors with greater r_{NCOR2} than r_{vector} were considered as exhibiting a higher transcriptional activity that was associated with N-CoR2 and a “NCOR2-related transcription similarity score” or “ S_{NCOR2} ” was used to represent the difference between r_{NCOR2} and r_{vector} ,

$$S_{NCOR2} = r_{NCOR2} - r_{vector} \quad (\text{Equation 1})$$

Supplementary references

1. van de Vijver, M.J., *et al.* A gene-expression signature as a predictor of survival in breast cancer. *N Engl J Med* **347**, 1999-2009 (2002).
2. Sorlie, T., *et al.* Gene expression patterns of breast carcinomas distinguish tumor subclasses with clinical implications. *Proc Natl Acad Sci U S A* **98**, 10869-10874 (2001).
3. Gong, B. & Almasan, A. Genomic organization and transcriptional regulation of human Apo2/TRAIL gene. *Biochem Biophys Res Commun* **278**, 747-752 (2000).
4. Tanaka, N., Kawakami, T. & Taniguchi, T. Recognition DNA sequences of interferon regulatory factor 1 (IRF-1) and IRF-2, regulators of cell growth and the interferon system. *Mol Cell Biol* **13**, 4531-4538 (1993).
5. Clarke, N., Jimenez-Lara, A.M., Voltz, E. & Gronemeyer, H. Tumor suppressor IRF-1 mediates retinoid and interferon anticancer signaling to death ligand TRAIL. *EMBO J* **23**, 3051-3060 (2004).
6. Guenther, M.G., *et al.* A core SMRT corepressor complex containing HDAC3 and TBL1, a WD40-repeat protein linked to deafness. *Genes Dev* **14**, 1048-1057 (2000).
7. Weaver, V.M., *et al.* Reversion of the malignant phenotype of human breast cells in three-dimensional culture and in vivo by integrin blocking antibodies. *J Cell Biol* **137**, 231-245 (1997).
8. Zahir, N., *et al.* Autocrine laminin-5 ligates alpha6beta4 integrin and activates RAC and NFkappaB to mediate anchorage-independent survival of mammary tumors. *J Cell Biol* **163**, 1397-1407 (2003).
9. Ishizuka, T. & Lazar, M.A. The N-CoR/histone deacetylase 3 complex is required for repression by thyroid hormone receptor. *Mol Cell Biol* **23**, 5122-5131 (2003).
10. Danos, O. & Mulligan, R.C. Safe and efficient generation of recombinant retroviruses with amphotropic and ecotropic host ranges. *Proc Natl Acad Sci U S A* **85**, 6460-6464 (1988).
11. Dranoff, G., *et al.* Vaccination with irradiated tumor cells engineered to secrete murine granulocyte-macrophage colony-stimulating factor stimulates potent, specific, and long-lasting anti-tumor immunity. *Proc Natl Acad Sci U S A* **90**, 3539-3543 (1993).
12. Nebbioso, A., *et al.* Tumor-selective action of HDAC inhibitors involves TRAIL induction in acute myeloid leukemia cells. *Nat Med* **11**, 77-84 (2005).
13. Park, E.J., *et al.* SMRTe, a silencing mediator for retinoid and thyroid hormone receptors-extended isoform that is more related to the nuclear receptor corepressor. *Proc Natl Acad Sci U S A* **96**, 3519-3524 (1999).
14. Kinsella, T.M. & Nolan, G.P. Episomal vectors rapidly and stably produce high-titer

- recombinant retrovirus. *Hum Gene Ther* **7**, 1405-1413 (1996).
15. Gossen, M. & Bujard, H. Tight control of gene expression in mammalian cells by tetracycline-responsive promoters. *Proc Natl Acad Sci U S A* **89**, 5547-5551 (1992).
 16. Kanda, T., Sullivan, K.F. & Wahl, G.M. Histone-GFP fusion protein enables sensitive analysis of chromosome dynamics in living mammalian cells. *Curr Biol* **8**, 377-385 (1998).
 17. Ory, D.S., Neugeboren, B.A. & Mulligan, R.C. A stable human-derived packaging cell line for production of high titer retrovirus/vesicular stomatitis virus G pseudotypes. *Proc Natl Acad Sci U S A* **93**, 11400-11406 (1996).
 18. Park, J., *et al.* Elevated level of SUMOylated IRF-1 in tumor cells interferes with IRF-1-mediated apoptosis. *Proc Natl Acad Sci U S A* **104**, 17028-17033 (2007).
 19. Brentjens, R.J., *et al.* Genetically targeted T cells eradicate systemic acute lymphoblastic leukemia xenografts. *Clin Cancer Res* **13**, 5426-5435 (2007).
 20. Kubota, T., *et al.* Antitumor activity of paclitaxel against human breast carcinoma xenografts serially transplanted into nude mice. *J Surg Oncol* **64**, 115-121 (1997).
 21. Budwit-Novotny, D.A., *et al.* Immunohistochemical analyses of estrogen receptor in endometrial adenocarcinoma using a monoclonal antibody. *Cancer Res* **46**, 5419-5425 (1986).
 22. Chomczynski, P. & Mackey, K. Short technical reports. Modification of the TRI reagent procedure for isolation of RNA from polysaccharide- and proteoglycan-rich sources. *Biotechniques* **19**, 942-945 (1995).
 23. Mogal, A. & Abdulkadir, S.A. Effects of Histone Deacetylase Inhibitor (HDACi); Trichostatin-A (TSA) on the expression of housekeeping genes. *Mol Cell Probes* **20**, 81-86 (2006).
 24. Plachot, C. & Lelievre, S.A. DNA methylation control of tissue polarity and cellular differentiation in the mammary epithelium. *Exp Cell Res* **298**, 122-132 (2004).
 25. Johnson, K.R., Leight, J.L. & Weaver, V.M. Demystifying the effects of a three-dimensional microenvironment in tissue morphogenesis. *Methods Cell Biol* **83**, 547-583 (2007).
 26. Dignam, J.D., Lebovitz, R.M. & Roeder, R.G. Accurate transcription initiation by RNA polymerase II in a soluble extract from isolated mammalian nuclei. *Nucleic Acids Res* **11**, 1475-1489 (1983).
 27. Yu, J., *et al.* Integrative genomics analysis reveals silencing of beta-adrenergic signaling by polycomb in prostate cancer. *Cancer Cell* **12**, 419-431 (2007).
 28. Asahara, H., Dutta, S., Kao, H.Y., Evans, R.M. & Montminy, M. Pbx-Hox heterodimers recruit coactivator-corepressor complexes in an isoform-specific manner. *Mol Cell Biol*

- 19**, 8219-8225 (1999).
29. Ghisletti, S., *et al.* Cooperative NCoR/SMRT interactions establish a corepressor-based strategy for integration of inflammatory and anti-inflammatory signaling pathways. *Genes Dev* **23**, 681-693 (2009).
 30. Lee, S.K., Kim, J.H., Lee, Y.C., Cheong, J. & Lee, J.W. Silencing mediator of retinoic acid and thyroid hormone receptors, as a novel transcriptional corepressor molecule of activating protein-1, nuclear factor-kappaB, and serum response factor. *J Biol Chem* **275**, 12470-12474 (2000).
 31. Heinzel, T., *et al.* A complex containing N-CoR, mSin3 and histone deacetylase mediates transcriptional repression. *Nature* **387**, 43-48 (1997).
 32. Hoberg, J.E., Yeung, F. & Mayo, M.W. SMRT derepression by the IkappaB kinase alpha: a prerequisite to NF-kappaB transcription and survival. *Mol Cell* **16**, 245-255 (2004).
 33. Hess, K.R., *et al.* Pharmacogenomic predictor of sensitivity to preoperative chemotherapy with paclitaxel and fluorouracil, doxorubicin, and cyclophosphamide in breast cancer. *J Clin Oncol* **24**, 4236-4244 (2006).
 34. Chang, J.C., *et al.* Gene expression profiling for the prediction of therapeutic response to docetaxel in patients with breast cancer. *Lancet* **362**, 362-369 (2003).
 35. Modlich, O., Prisack, H.B., Munnes, M., Audretsch, W. & Bojar, H. Predictors of primary breast cancers responsiveness to preoperative epirubicin/cyclophosphamide-based chemotherapy: translation of microarray data into clinically useful predictive signatures. *J Transl Med* **3**, 32 (2005).
 36. Eisen, M.B., Spellman, P.T., Brown, P.O. & Botstein, D. Cluster analysis and display of genome-wide expression patterns. *Proc Natl Acad Sci U S A* **95**, 14863-14868 (1998).



HOXA9 regulates BRCA1 expression to modulate human breast tumor phenotype

Penney M. Gilbert,^{1,2} Janna K. Mouw,³ Meredith A. Unger,⁴ Johnathon N. Lakins,³ Mawuse K. Gbegnon,^{1,2} Virginia B. Clemmer,⁵ Miriam Benezra,⁶ Jonathan D. Licht,⁷ Nancy J. Boudreau,³ Kelvin K.C. Tsai,⁸ Alana L. Welm,⁹ Michael D. Feldman,² Barbara L. Weber,⁴ and Valerie M. Weaver^{1,2,3,10}

¹Institute for Medicine and Engineering, and ²Department of Pathology, University of Pennsylvania, Philadelphia, Pennsylvania, USA. ³Center for Bioengineering and Tissue Regeneration and Department of Surgery, UCSF, San Francisco, California, USA. ⁴Abramson Family Cancer Research Institute, University of Pennsylvania, Philadelphia, Pennsylvania, USA. ⁵St. Francis Hospital, Wilmington, Delaware, USA. ⁶Mount Sinai School of Medicine, New York, New York, USA. ⁷Department of Medicine, Northwestern University Feinberg School of Medicine, Chicago, Illinois, USA. ⁸Graduate Institute of Clinical Research, Taipei Medical University, Taipei, Taiwan. ⁹Department of Oncological Sciences, Huntsman Cancer Institute, University of Utah, Salt Lake City, Utah, USA. ¹⁰Department of Anatomy and Department of Bioengineering and Therapeutic Sciences, Eli and Edythe Broad Center of Regeneration Medicine and Stem Cell Research, and UCSF Helen Diller Comprehensive Cancer Center, UCSF, San Francisco, California, USA.

Breast cancer 1, early onset (BRCA1) expression is often reduced in sporadic breast tumors, even in the absence of BRCA1 genetic modifications, but the molecular basis for this is unknown. In this study, we identified homeobox A9 (HOXA9) as a gene frequently downregulated in human breast cancers and tumor cell lines and noted that reduced HOXA9 transcript levels associated with tumor aggression, metastasis, and patient mortality. Experiments revealed that loss of HOXA9 promoted mammary epithelial cell growth and survival and perturbed tissue morphogenesis. Restoring HOXA9 expression repressed growth and survival and inhibited the malignant phenotype of breast cancer cells in culture and in a xenograft mouse model. Molecular studies showed that HOXA9 restricted breast tumor behavior by directly modulating the expression of BRCA1. Indeed, ectopic expression of wild-type BRCA1 phenocopied the tumor suppressor function of HOXA9, and reducing BRCA1 levels or function inhibited the antitumor activity of HOXA9. Consistently, HOXA9 expression correlated with BRCA1 in clinical specimens and with tumor aggression in patients lacking estrogen receptor/progesterone receptor expression in their breast tissue. These findings indicate that HOXA9 restricts breast tumor aggression by modulating expression of the tumor suppressor gene BRCA1, which we believe provides an explanation for the loss of BRCA1 expression in sporadic breast tumors in the absence of BRCA1 genetic modifications.

Introduction

Developmental regulators that specify tissue morphogenesis are often functionally subverted in adult tissues to promote cancer (1, 2). In particular, the homeobox (HOX) gene family of morphogenic regulators is critical for the establishment of embryonic patterning during embryogenesis and for the maintenance of tissue differentiation in the adult organism (3). HOX genes are transcription factors that regulate the expression of multiple genes that influence cell growth and viability and that mediate stromal-epithelial interactions to drive tissue-specific differentiation (2). HOX expression is frequently perturbed in tumors (3), in which they can act as oncogenes by promoting cell growth and invasion (4, 5) or as tumor suppressors (TSs), because they can alter cell survival and morphogenesis (6–9). HOX genes are especially important in the mammary gland, which undergoes repeated rounds of developmental cycles in the adult organism (10, 11). In the breast, HOX genes have been implicated in the control of embryonic development, branching morphogenesis, and hormonally controlled differentiation (10, 12), and HOX genes are frequently lost or overexpressed in breast tumors (12). Nevertheless, the molecular mechanisms whereby HOX genes regulate mammary development and might modulate breast cancer remain poorly defined.

Women with hereditary mutations in BRCA1 are predisposed to develop breast and ovarian cancers (13). BRCA1 maintains genome integrity through its ubiquitin ligase activity (14) and regulates transcription to modulate the cellular stress response (15, 16). BRCA1 has an established role as a regulator of mammary epithelial cell (MEC) growth, survival, morphogenesis, and transformation (17–20). Moreover, loss of BRCA1 expression and/or function is associated with increased breast tumor aggression, enhanced cancer metastasis, and a poor clinical prognosis (21). There is also a clinical association between familial BRCA1 tumors and an aggressive, triple-negative, basal-like breast cancer phenotype (22). Interestingly, many sporadic breast cancers show decreased BRCA1 expression and display a “BRCA1-like” phenotype, despite the absence of genetic deletions, methylation, or haploinsufficiency (23, 24). The molecular mechanisms leading to reduced BRCA1 expression and/or function in this group of aggressive, sporadic breast cancers remain unclear (20, 25). Studies designed to elucidate molecular modifiers of BRCA1 have identified negative regulators, which in some cases are overexpressed during breast tumorigenesis (26–29, 30, 31). Conversely, the identification of transcription factors that positively and directly regulate BRCA1 expression and whose expression might be concurrently lost during malignant transformation has proven elusive.

BRCA1 expression and MEC proliferation are functionally linked, suggesting BRCA1 could regulate mammary gland development and homeostasis and inhibit tumorigenesis by restricting MEC growth (32–34). BRCA1 also modulates mammary gland

Authorship note: Penney M. Gilbert and Janna K. Mouw contributed equally to this work.

Conflict of interest: The authors have declared that no conflict of interest exists.

Citation for this article: *J Clin Invest* doi:10.1172/JCI39534.

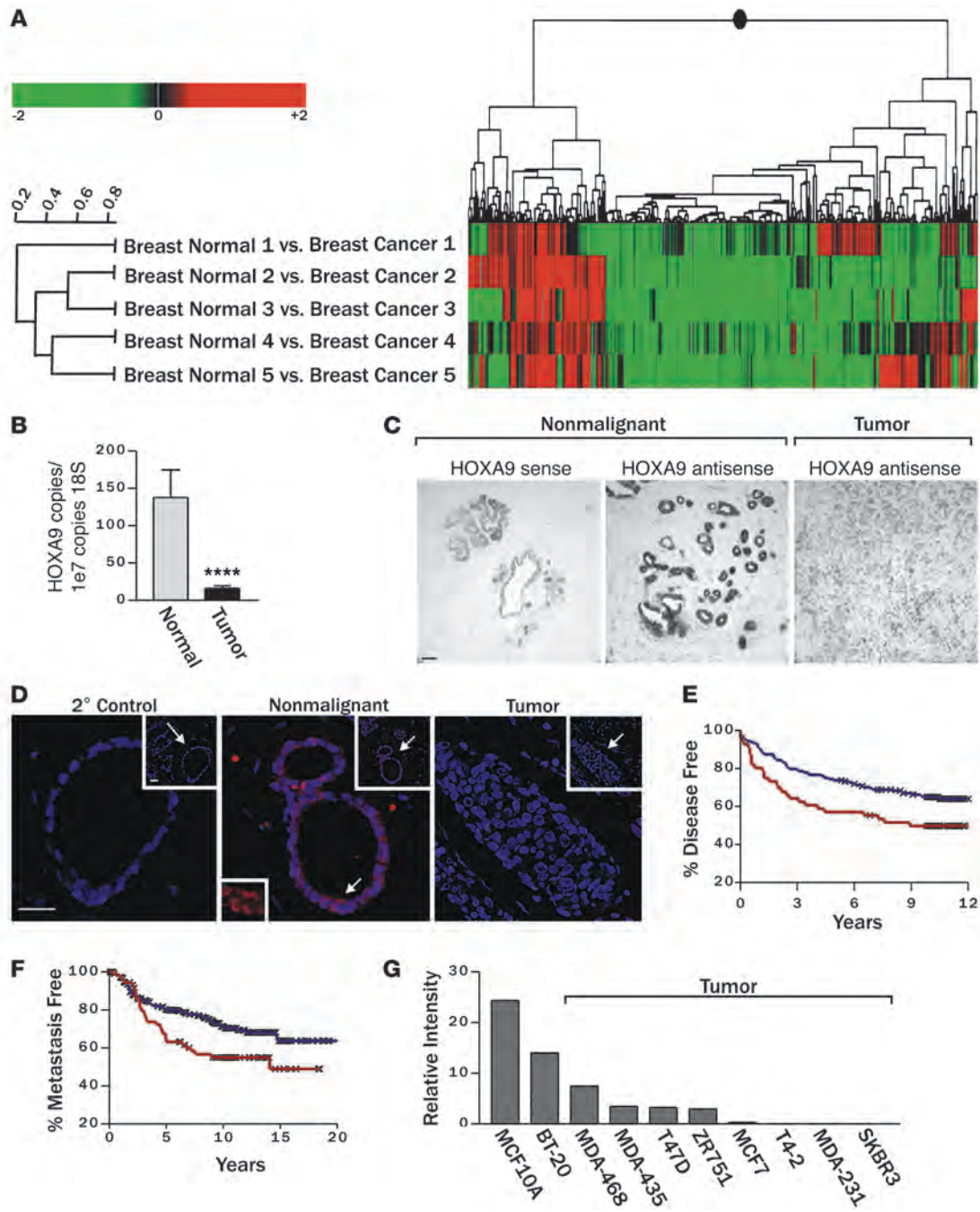


Figure 1

Breast malignancy is associated with reduced HOXA9 expression. **(A)** Cluster diagram of Affymetrix microarray data using Rosetta Resolver to compare gene expression profiles of matched normal mammary tissue and adjacent primary breast cancers, revealing significantly lower *HOXA9* transcript levels in 4 out of 5 expression sets analyzed ($P \leq 0.01$). **(B)** Levels of *HOXA9* mRNA (by quantitative RT-PCR) in primary human mammary tumors ($n = 47$) compared with normal breast tissue ($n = 16$). **** $P = 0.00035$. **(C)** In situ hybridization using a *HOXA9* probe on nonmalignant ($n = 4$) or malignant ($n = 6$) mammary epithelial tissue. Scale bar: 100 μm . **(D)** Immunofluorescent staining for *HOXA9* (red) and nuclei (blue) demonstrates robust cytoplasmic and nuclear localized *HOXA9* protein in the epithelium of nonmalignant human breast tissue and reduced levels in breast tumors. Top right insets (original magnification, $\times 20$) show a broader view of the breast tissue, with arrows indicating regions blown up in the main images. The arrow in the center main image corresponds with the bottom left inset, which shows a view of *HOXA9* staining (original magnification, $\times 30$). Scale bar: 50 μm . The 2° control shows no nonspecific staining. **(E)** Breast cancer patients whose tumors expressed the lowest *HOXA9* level (lowest expression quartile; red line) experienced significantly reduced disease-free survival compared with all other patients in the study (blue line). An “X” is used to denote each censored sample. $P = 0.00035$. **(F)** Patients with the lowest *HOXA9* levels in their tumors (lowest expression quartile; red line) also had significantly increased metastasis as a first event when compared with all other patients (blue line). An “X” is used to denote each censored sample. $P = 0.02$. **(G)** Bar graph demonstrating relative *HOXA9* gene expression levels in nonmalignant and malignant MEC lines.

**Table 1**Multivariate analysis for relapse-free and overall survival, comparing *HOXA9* transcript expression and clinical characteristics in breast cancer patients

Variable	Death		Relapse	
	Hazard ratio (95% CI)	P value	Hazard ratio (95% CI)	P value
ER positive				
HOXA9	1.185 (0.91–1.541)	0.208	1.227 (1.045–1.439)	0.012
Age (per 10-yr increment)	0.615 (0.341–1.109)	0.106	0.527 (0.331–0.842)	0.007
Tumor size (per cm)	1.174 (0.832–1.658)	0.361	1.177 (0.896–1.546)	0.242
Tumor grade				
Grade 2 vs. grade 1	3.38 (1.123–10.172)	0.03	2.185 (1.075–4.445)	0.031
Grade 3 vs. grade 1	6.215 (2.063–18.718)	0.001	3.254 (1.559–6.792)	0.002
Positive vs. negative LN status	2.366 (0.995–5.628)	0.051	2.061 (1.011–4.201)	0.046
Chemotherapy vs. no chemotherapy	0.341 (0.137–0.844)	0.02	0.385 (0.185–0.802)	0.011
Hormonal treatment vs. no treatment	0.753 (0.239–2.373)	0.628	0.662 (0.265–1.656)	0.378
Mastectomy vs. breast-conserving therapy	1.283 (0.678–2.428)	0.444	1.377 (0.821–2.312)	0.225
Molecular subtype				
Normal-like and luminal B vs. luminal A	1.734 (0.804–3.74)	0.161	1.516 (0.843–2.726)	0.165
Basal and ERBB2+ vs. luminal A	2.309 (0.883–6.043)	0.088	1.608 (0.754–3.432)	0.219
ER negative				
HOXA9	0.394 (0.181–0.857)	0.019	0.433 (0.187–1.002)	0.05
Age (per 10-yr increment)	0.59 (0.338–1.027)	0.062	0.552 (0.314–0.973)	0.04
Tumor size (per cm)	1.58 (1.037–2.409)	0.033	1.49 (0.958–2.319)	0.077
Tumor grade (poorly vs. well differentiated)	0.923 (0.365–2.331)	0.865	1.053 (0.382–2.902)	0.921
Positive vs. negative LN status	0.64 (0.209–1.954)	0.433	0.566 (0.196–1.631)	0.291
Chemotherapy vs. no chemotherapy	1.596 (0.513–4.962)	0.419	1.53 (0.54–4.335)	0.423
Hormonal treatment vs. no treatment	0.423 (0.083–2.154)	0.3	0.436 (0.089–2.149)	0.308
Mastectomy vs. breast-conserving therapy	2.1 (0.926–4.759)	0.076	2.187 (0.925–5.171)	0.075

The analysis included the 226 ER-positive and the 69 ER-negative breast cancer patients in the Netherlands Cancer Institute data set. *HOXA9* transcript expression, age, and tumor size were modeled as continuous variables. The molecular subtypes of breast cancer are not included in the model for the ER-negative cancers, as none of the tumors is categorized as the luminal A subtype, plus there is no event of death or relapse for tumors categorized as the normal-like or luminal B subtype. Statistically significant *P* values are shown in bold.

differentiation, and *BRCA1* expression is repressed following reconstituted basement membrane-induced (rBM-induced) acinar morphogenesis (19, 33–36). *BRCA1* expression increases during embryonic mammary gland development and spikes prior to acquisition of acini polarity and pregnancy-associated lactation, consistent with the idea that *BRCA1* expression is functionally linked to breast tissue differentiation (27, 32, 37, 38). If true, *BRCA1* could restrict MEC growth and survival and regulate genome integrity by cooperating with molecules such as homeobox genes, which regulate tissue differentiation.

We identified *HOXA9*, a homeobox gene previously implicated in breast tissue differentiation (39), as a gene whose levels were reduced in breast tumors and whose reexpression promoted breast tumor morphogenesis. Although, paradoxically, *HOXA9* has been characterized as a leukemic oncogene (4) and angiogenesis promoter (40), *HOXA9* also plays an important role in skeletal (41), urogenital tract (42), kidney (43), and mammary gland development (39), and *HOXA9* expression can be regulated by microRNAs that have been implicated in tissue differentiation (44). We found that *HOXA9* promotes breast tumor cell differentiation and inhibits cancer progression by directly regulating expression of the TS gene *BRCA1*. Because *HOXA9* is frequently methylated in breast tumors, the findings offer an alternate explanation for why *BRCA1*

expression is frequently lost in sporadic human breast tumors, even in the absence of genetic modification (45). They further suggest that homeobox genes could regulate tissue development and restrict tumorigenesis by modulating TS genes.

Results

Breast malignancy is associated with reduced HOXA9 expression. Expression profiling is a useful tool to identify gene expression signatures associated with patient prognosis (46, 47), treatment responsiveness (48–50), and risk of tumor metastasis (46, 51–53). However, because sporadic mammary tumors likely arise through input from multiple cooperating yet poorly penetrating genetic, epigenetic, and microenvironmental factors, gene profiling has proven more challenging when applied to identify breast TSs (54, 55). Therefore, to increase the probability of identifying a low abundance breast TS gene using this approach, we selected 5 paired sets of tumor tissue with similar phenotype. Our objective was to discover genes that have lost expression in the tumor tissues when compared with their patient-matched “normal” tissue. Because of the compelling link between developmental regulators and tumor aggression, we focused on identifying misexpressed developmental regulators (1, 56, 57). Moreover, given the paucity of information on basal-like tumors and their recognized aggressive nature

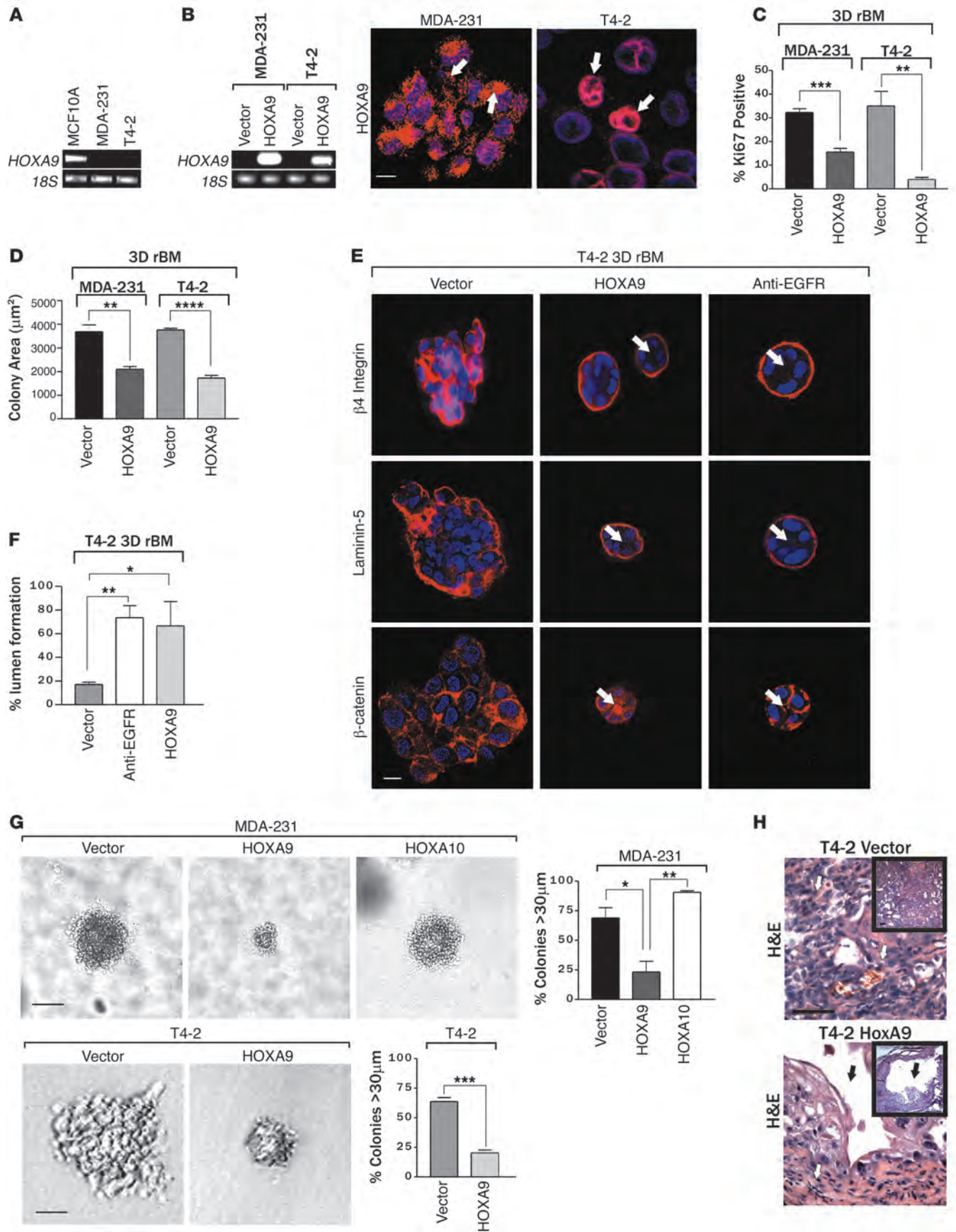


**Figure 2**

HOXA9 modulates the growth and survival of breast cancer cells. (A) Semiquantitative PCR gel, indicating *HOXA9* mRNA levels expressed in human nonmalignant (MCF10A), metastatic (MDA-231), and transfected (T4-2) MECs. *18S* rRNA was used as a control. (B) Semiquantitative PCR gel showing transgenic *HOXA9* mRNA levels in MDA-231 and T4-2 cell lines. Immunofluorescence images of nuclei (blue) and FLAG-tagged HOXA9 (red) in MDA-231 and T4-2 cells. Arrows indicate localization of Flag-tagged HOXA9-positive cells. Scale bar: 10 μ m. (C) Proliferation in MDA 231 and T4-2 cells following HOXA9 reexpression. $**P = 0.0025$, $***P = 0.0003$. (D) Cross-sectional area of MDA-231 and T4-2 breast tumor colonies in rBM expressing either the vector or HOXA9 transgene. $****P = 0.0001$, $**P = 0.0068$. (E) Immunofluorescence images of β_4 integrin (red), Laminin-5 (red), β -catenin (red), and nuclei (blue) in T4-2 colonies expressing the vector or HOXA9 or phenotypically reverted acini (anti-EGFR) by inhibiting EGFR activity using tyrphostin. Arrows indicate cleared lumen. Scale bar: 10 μ m. (F) Lumens observed in rBM-generated T4-2 colonies expressing the vector, HOXA9, or anti-EGFR phenotypically reverted acini. $*P = 0.0188$, $**P = 0.0076$. (G) The percentage of tumor colonies greater than 30 μ m in diameter, and phase contrast images of tumor colonies embedded within soft agar. Scale bar: 50 μ m (top panel); 20 μ m (bottom panel). $*P = 0.0221$, $**P = 0.018$, $***P = 0.0005$. (H) High- and low-magnification phase images of H&E-stained tissue sections of control tumor (T4-2 vector) and HOXA9 reexpressing tumor (T4-2 HOXA9) xenografts. Vascolarized regions of T4-2 control tumors are indicated with white arrows, and cystic regions of T4-2 HOXA9 reexpressing tumors are indicated with black arrows. Original magnification, $\times 40$; $\times 10$ (insets). Scale bar: 100 μ m.

in younger patients, we chose samples from individuals whose ages ranged from 44 to 54 years and whose tumors were at least 1.5 cm in diameter (Supplemental Table 1; supplemental material available online with this article; doi:10.1172/JCI39534DS1), estrogen receptor/progesterone receptor (ER/PR) negative, and of uniformly high nuclear and histological grade.

Analysis of gene expression, using Rosetta Resolver 2D agglomerative clustering, showed significant differential expression, when comparing normal adjacent and invasive tumor tissue and identified 40 transcripts whose expression was elevated in the tumors and 115 transcripts with reduced gene expression ($P \leq 0.01$; Figure 1A and Supplemental Table 2). Among the genes with reduced expression were 2 developmental HOX genes: *HOXA4* (mean 3.1-fold reduction) and *HOXA9* (mean 4.4-fold reduction). Findings from the *hoxa9-hoxb9-hoxd9* triple knockout mouse suggest that HoxA9 regulates mammary gland differentiation (39), leukemia studies implicate HoxA9 in oncogenesis (4), and in a small cohort of breast cancer patient samples HoxA9 was silenced via methylation (45); therefore, we selected HoxA9 for further study.

Quantitative RT-PCR verified that *HOXA9* mRNA levels were significantly reduced in the normal compared with tumor-matched clinical samples (M.A. Unger, unpublished observations) and that HOXA9 levels were significantly reduced (~75%) in an expanded clinical cohort of ER/PR-positive and -negative, invasive, primary ductal breast carcinomas ($n = 47$), when compared with levels of transcript expressed in normal human breast ($n = 16$; Figure 1B and Supplemental Figure 1). In situ and immunohistochemical analysis confirmed that *HOXA9* mRNA and HOXA9 protein were expressed in the normal breast epithelium and that levels were greatly reduced in mammary tumors (Figure 1, C and D). To explore the clinical relationship between HOXA9 levels and breast cancer clinical histopathology, we used

the OncoPrint Cancer Profiling Database (<http://www.onco-print.org>) to survey a large number of breast cancers from multiple independent studies. We found that low levels of HOXA9 expression correlate with features of aggressive disease, such as large- or high-grade tumors, late-stage disease, lymph node involvement, and distant metastasis (Supplemental Table 3). This approach not only validated our original observation that HOXA9 levels were reduced in breast cancers when compared with normal breast tissue, but they also indicated that reduced HOXA9 levels more significantly associate with tumor aggression in ER/PR-negative tumors.

To follow-up on this intriguing observation, we next analyzed publicly available gene expression data sets to look for potential associations between HOXA9 and breast cancer patient clinical outcome. First, we assessed the relationship between *HOXA9* mRNA levels and relapse-free survival in 2 patient data sets that included a cohort of 227 patients, with available clinical follow-up information, and a second independent set of data from 295 patients (47, 58). We found that those patients whose tumors expressed the lowest *HOXA9* levels (lowest quartile) experienced a significantly reduced relapse-free survival, regardless of ER/PR status ($P = 0.025$; Figure 1E). To determine whether low HOXA9 levels could predict distant metastasis, we also assessed the data sets from patients with early-stage breast cancer, all of whom had no evidence of distant metastasis at the time of tumor collection, for a relationship between tumor aggression and HOXA9 levels (47). Upon examination, we noted that the group of patients whose primary tumors expressed *HOXA9* in the lowest quartile developed significantly more distant metastasis as a first adverse event, when compared with all other patients in the study ($P = 0.02$; Figure 1F). A multivariate Cox proportional-hazards analysis revealed that HOXA9 significantly predicts death or disease relapse, independent of standard clinicopathological variables of breast cancers in ER-negative tumors (Table 1). In contrast, the correlation between HOXA9 expression levels and clinical outcomes was less prominent in ER-positive tumors (Table 1). These data show that HOXA9 is significantly downregulated in breast cancer and that its loss correlates with increased disease aggression.

HOXA9 modulates the growth and survival of breast cancer cells. To explore the functional relevance of HOXA9 loss to breast cancer, we examined the effect of HOXA9 reexpression on tumor cell growth, survival, and tissue differentiation. We observed that *HOXA9* mRNA was abundant in the MCF10A nonmalignant human MEC line (Figure 1G and Figure 2A), reduced in the noninvasive, ER-positive breast cancer cell lines T47-D and MCF-7 (Figure 1G), and virtually nondetectable in the ER-negative, basal-like breast cancer cell lines MDA-MB-231 (MDA-231) and HMT-3522 T4-2 (T4-2) (Figure 1G and Figure 2A) (59). We then created multiple pooled clonal populations of MDA-231 and T4-2 breast cancer cells expressing either HA- or FLAG-tagged wild-type HOXA9. Transgene expression was confirmed at the mRNA and protein

Table 2

Physical attributes of excised breast tumor cell xenografts

Xenograft description	Cell mass (mg)	Lesion	Cystic
T4-2 vector	186 \pm 46.7 ^A	10/10 ^A	0/10
T4-2 HOXA9	82 \pm 32.3	2/10	2/10

^A $P < 0.05$.

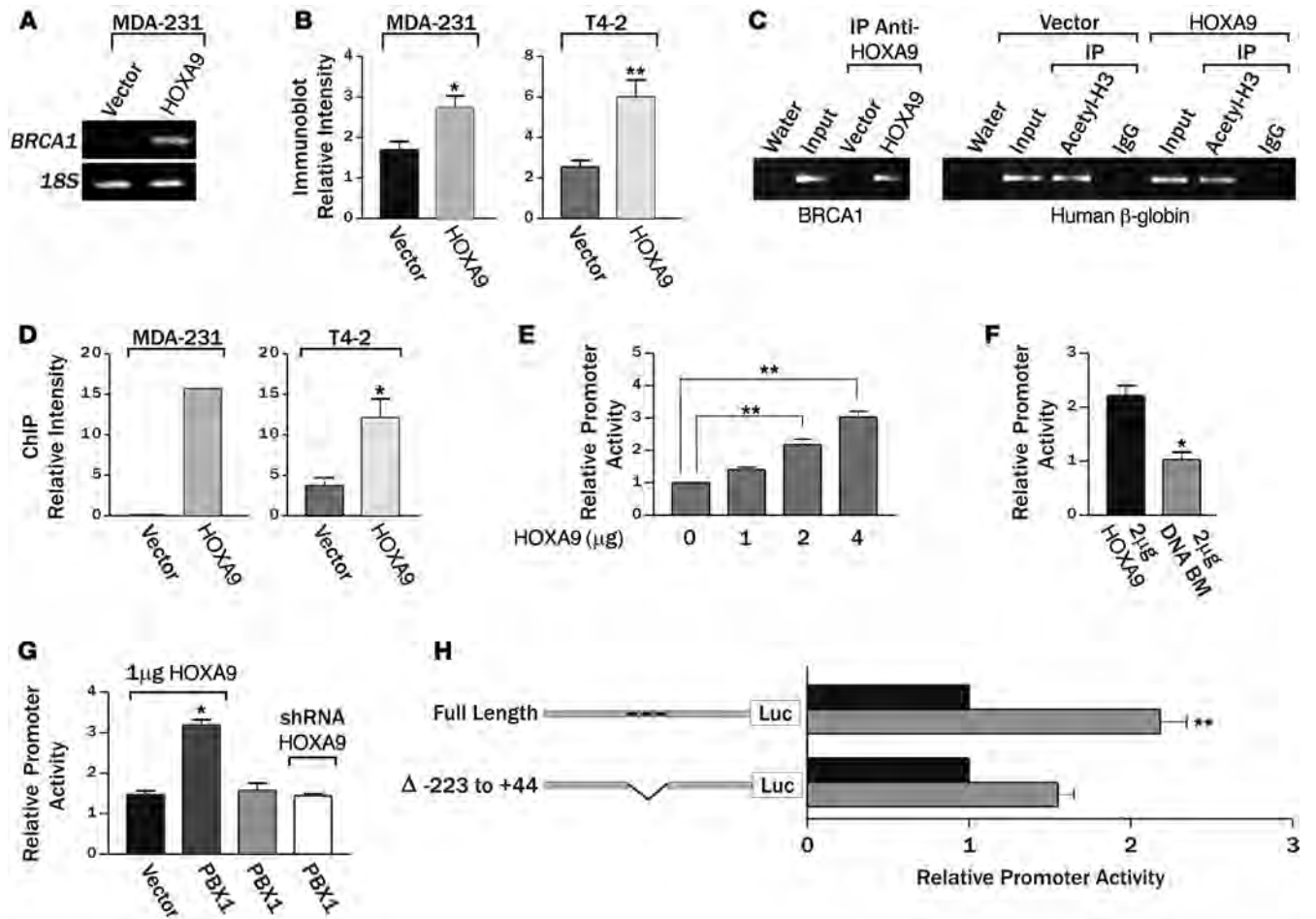


Figure 3 HOXA9 regulates BRCA1 expression. (A) Semiquantitative PCR gel, indicating increased *BRCA1* expression with the reexpression of HOXA9 in MDA-231 cells. (B) Bar graph quantifying immunoblot data from multiple experiments, showing increased BRCA1 protein in MDA-231 or T4-2 breast tumor cells reexpressing HOXA9. **P* = 0.0457, ***P* = 0.0028. (C) Representative gel of ChIP studies in breast cancer cells, revealing coprecipitation of HOXA9 with the BRCA1 promoter and acetylated acetyl-H3-histone with the β-globin promoter. (D) Bar graphs quantifying ChIP experiments in MDA-231 (*n* = 2) and T4-2 cells (**P* = 0.0178; *n* = 4). (E) Luciferase reporter analysis, showing a dose-dependent increase in BRCA1 promoter activity in response to addition of wild-type HOXA9. ***P* = 0.001. (F) Luciferase reporter analysis, displaying loss of BRCA1 promoter activity upon addition of HOXA9 containing an N255T (DNA BM) mutation in the conserved DNA binding domain. **P* = 0.03 (G) Luciferase reporter analysis, indicating enhanced HOXA9-mediated BRCA1 promoter activity upon addition of PBX1 cofactor (2 μg), compared with Pbx1 alone or Pbx1 cotransfected with a shRNA reducing HOXA9 expression. **P* = 0.0259. (H) Luciferase reporter analysis, showing a diminished responsiveness of a BRCA1 promoter construct containing a deletion in residues -223 to +44, which contains 3 putative Hox binding sites (gray bar). Data are normalized to matched vector control (black bars). Negative numbers refer to basepairs upstream of the BRCA1 transcription start site. ***P* = 0.02.

level (Figure 2B and Supplemental Figure 2), and the expressed protein was found to localize in both the nucleus and cytoplasm of the infected cells (Figure 2B; see white arrows), in a manner similar to endogenous HOXA9 protein expression (Figure 1, C and D). For easy visualization and manipulation, the HOXA9 transgene was expressed bi-cistronically with EGFP under the control of a tetracycline-repressible promoter (Supplemental Figure 3).

Although HOXA9 reexpression had only a marginal effect on breast tumor cell growth when the cells were propagated on tissue culture plastic (Supplemental Figure 4), we noted that upon embedment within rBM, both MDA-231 and T4-2 breast cancer cells reexpressing HOXA9 grew much slower than their respective vector-only controls, as quantified by significantly reduced Ki-67 levels (Figure 2C), and both cell lines had a decreased colony size

at day 10 (Figure 2D). In fact, reexpression of HOXA9 reverted the malignant phenotype of both of the tumor cell lines toward that of a smaller, more uniform, less invasive, and more cohesive non-malignant colony, similar to that reported previously when epidermal growth factor receptor signaling was inhibited in these cell lines (Figure 2E; see white arrows) (60, 61). HOXA9 reexpression had a particularly pronounced effect on the tissue morphology of the T4-2 rBM colonies, such that the HOXA9-reexpressing tumor colonies reassembled adherens junctions, as indicated by a relocalization of β-catenin to sites of cell-cell interaction, and acquired apical-basal polarity, as revealed by basal relocalization of (α6)β4 integrin and deposition of an endogenous laminin-5 BM around the periphery of the acini (Figure 2E and Supplemental Figure 5). We also noted that HOXA9 reexpression exerted a substantial



effect on cell viability, as revealed by the appearance of lumens within the acini (Figure 2, E and F). Soft agar assays confirmed that HOXA9 but not HOXA10 reexpression, another member of the HOXA cluster (2), influenced tumor cell survival, as shown by a significant inhibition of anchorage-independent growth and survival in both the HMT-3522 T4-2 and MDA-MB-231 tumor cells (Figure 2G, Supplemental Figure 6, and Supplemental Figure 7).

To address the functional relevance of our cell culture observations to breast cancer *in vivo*, we conducted xenograft studies using BalbC *nu/nu* mice. T4-2 breast cancer cells reexpressing HOXA9 (to levels comparable to that detected in the nonmalignant HMT-3522 S-1 MECs; data not shown) failed to grow and survive when injected into the rear flanks of the BalbC *nu/nu* mice (Figure 2H and Table 2). Thus, while vector control T4-2 MECs grew continuously and rapidly to form large, highly angiogenic tumors that were densely populated with actively dividing cancer cells (10 out of 10 lesions), the lesions formed by the T4-2 MECs expressing HOXA9 either completely regressed within 56 days (8 out of 10 lesions) or were highly cystic, avascular, and fibrotic (2 out of 10 lesions) (Figure 2H and Table 2). These data in conjunction with our *in vitro* data suggest that HOXA9 restricts tumorigenic behavior of breast cancer cells by inhibiting cell growth, survival, and invasion and by promoting tissue morphogenesis.

HOXA9 directly regulates BRCA1 expression. Hox genes are transcriptional regulators that exert their effect on cell and tissue phenotype indirectly by modulating gene expression (2). To identify putative HOXA9 targets critical for breast tumor suppression, we defined the global transcriptional profile of MDA-231 breast cancer cells before and after tetracycline-dependent HOXA9 expression (Supplemental Table 4). Among the genes upregulated after HOXA9 reexpression, we observed that the level of the breast cancer susceptibility gene *BRCA1* was dramatically increased and confirmed this by semiquantitative RT-PCR (Figure 3A). Because *BRCA1* is a TS gene that regulates MEC growth, survival, and invasion and can modulate rBM morphogenesis, we next explored the functional relationship between HOXA9 and *BRCA1* regulation (19, 32–34, 38, 62). Immunoblot analysis demonstrated that HOXA9 reexpression consistently elevated *BRCA1* protein levels in MDA-231 and T4-2 breast cancer cells (Figure 3B). These results suggested that HOXA9 could repress breast tumor behavior by regulating expression of the TS gene *BRCA1*.

BRCA1 can be induced by multiple stimuli that might each be independently regulated by HOXA9 (27). While a number of negative regulators of *BRCA1* transcription have been reported, identification of factors that directly upregulate *BRCA1* expression has proven elusive (26–31). Because HOXA9 is a transcription factor, we reasoned there was a strong probability HOXA9 was regulating *BRCA1* levels by directly inducing *BRCA1* gene expression. Computer-assisted analysis confirmed that there were indeed several putative HOX consensus binding sites in the *BRCA1* promoter. To definitively test whether HOXA9 could directly modulate *BRCA1* expression, we conducted *BRCA1* promoter ChIP studies using HA-tagged, exogenously expressed HOXA9 as the bait. Whereas acetyl H3 histone easily and repeatedly coprecipitated the β -globin promoter from both vector control- and HOXA9-expressing cell lines, we could only amplify *BRCA1* promoter product above background from the breast tumor cells reexpressing the exogenous HA-tagged HOXA9 (Figure 3, C and D). Reporter assays, using regions of the *BRCA1* 5' promoter region containing HOXA9 consensus binding sites, confirmed basal luciferase activity could be significantly enhanced after cotransfection with

increasing amounts of a wild-type HOXA9 but not with a HOXA9 expression plasmid containing an N255T mutation (DNA BM) in the conserved DNA binding domain (Figure 3, E and F) (63). Furthermore, HOXA9-dependent *BRCA1* reporter induction could be significantly enhanced by addition of the HOX gene cofactor PBX1 (Figure 3G) (64). In contrast, no increase in reporter activity could be induced by PBX1 alone, PBX1 cotransfected with an shRNA knocking down HOXA9 expression, or HOXA9 cotransfection with *BRCA1* luciferase promoter constructs lacking residues –223 to +44, wherein reside putative HOXA9 consensus binding sites (Genbank U37574; Figure 3, G and H). Interestingly, site-directed mutagenesis of individual HOXA9 consensus binding sites did not significantly compromise *BRCA1* promoter activity, suggesting cooperative release of tandem HOX consensus binding sites might be necessary to ablate HOXA9-dependent control of *BRCA1* gene expression (Supplemental Figure 8). These observations are consistent with previous reports of promoter site cooperation and redundancy in other HOX-regulated genes (65–67). The findings indicate that DNA binding of HOXA9 directly regulates *BRCA1* expression in breast cells.

HOXA9 regulates nonmalignant MEC growth by modulating BRCA1 expression. We identified 2 independent shRNA lentiviral clones that could substantially reduce HOXA9 protein (P.M. Gilbert, unpublished observations) and *HOXA9* mRNA levels in nonmalignant MCF-10A MECs (Supplemental Figure 9) to implicate HOXA9 as a TS. Loss of HOXA9 expression disrupted rBM morphogenesis, as revealed by the formation of larger invasive colonies (Figure 4B), as indicated by lack of β -catenin at sites of cell-cell adherens junctions (Figure 4A, top), loss of basally polarized ($\alpha 6$) $\beta 4$ integrin (Figure 4A, middle), and a discontinuous endogenous laminin-5 basement membrane (Figure 4A, bottom). In addition, MCF-10A MECs with reduced HOXA9 levels exhibited an enhanced survival phenotype, as evidenced by a failure of these structures to clear their lumens (Figure 4A, see arrows; quantified in Figure 4C), and robust anchorage-independent growth and survival (Figure 4, E and F). Consistent with the notion that HOXA9 mediates these TS effects on MEC behavior by regulating *BRCA1* levels, the nonmalignant MECs in which HOXA9 had been knocked down using shRNA showed a greatly blunted induction of *BRCA1* transcription in response to an exogenous stress of 5 Gray irradiation (Figure 4D) (68).

To determine whether reducing *BRCA1* in nontransformed MECs could similarly promote malignant behavior in these MECs, we identified 2 shRNA clones and demonstrated efficient knock down of *BRCA1* protein levels (P.M. Gilbert, unpublished observations). Consistent with prior data implicating *BRCA1* in breast differentiation (19, 32–34, 38), reducing *BRCA1* in the MCF-10A MECs increased cell proliferation in response to rBM cues (inferred by elevated colony size; Figure 4, G and H), enhanced their survival as revealed by luminal filling in the rBM colonies (Figure 4G, see arrow; quantified in Figure 4I), and disrupted tissue morphogenesis (evidenced by loss of cell-cell localized β -catenin; Figure 4G). Likewise, compromising *BRCA1* function in the MCF-10A cells by expressing the *BRCA1* Δ exon11b mutant (Supplemental Figure 10) promoted MEC growth and survival in a 3D rBM and perturbed tissue morphogenesis (Figure 4, J–L). These observations illustrate the importance of HOXA9 and *BRCA1* expression to MEC growth and survival and rBM-induced tissue morphogenesis.

HOXA9 regulates BRCA1 to repress the malignant behavior of MECs. We next manipulated the expression and function of *BRCA1* and HOXA9 in breast cancer cells and assayed for effects on tumor

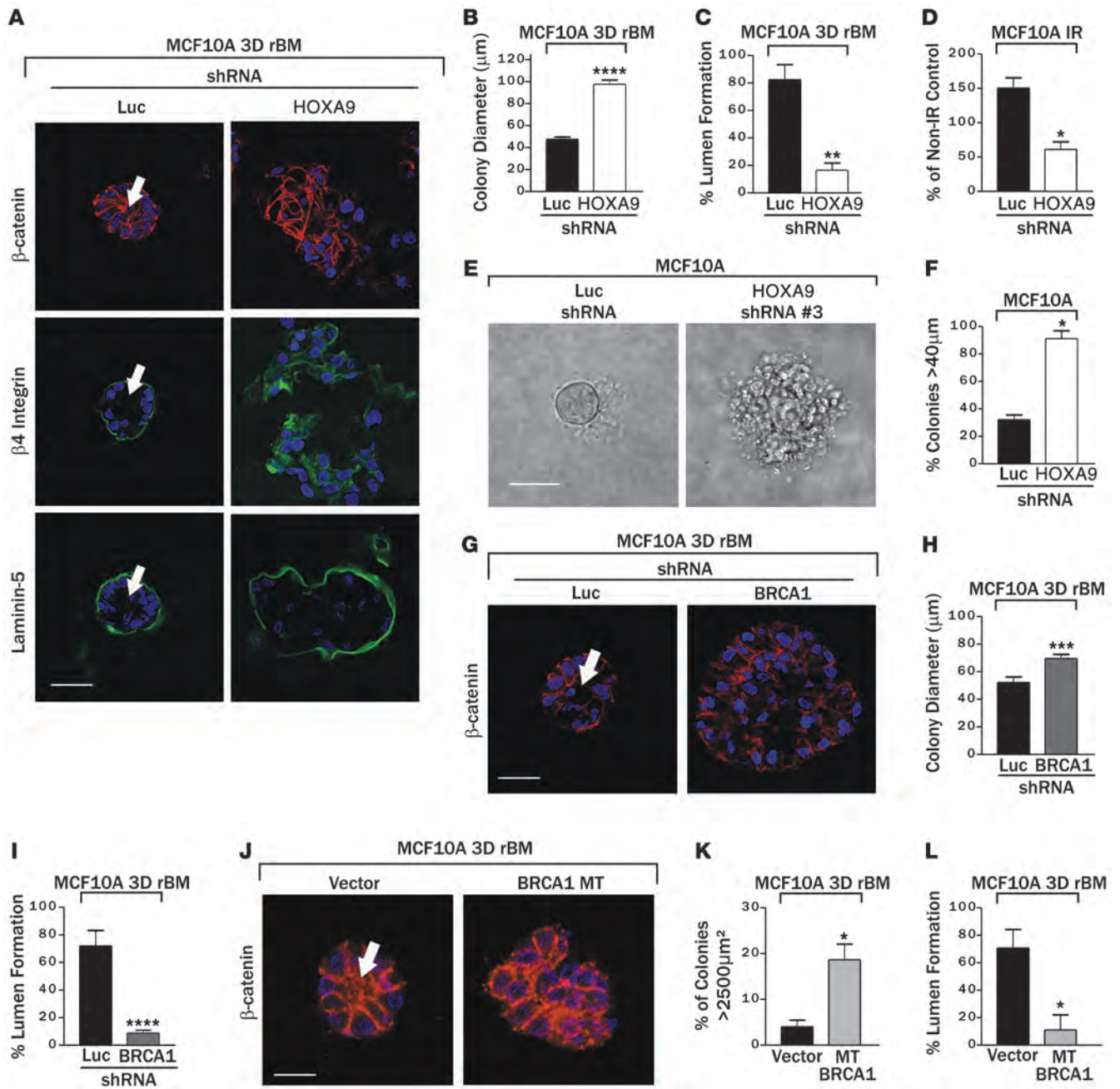
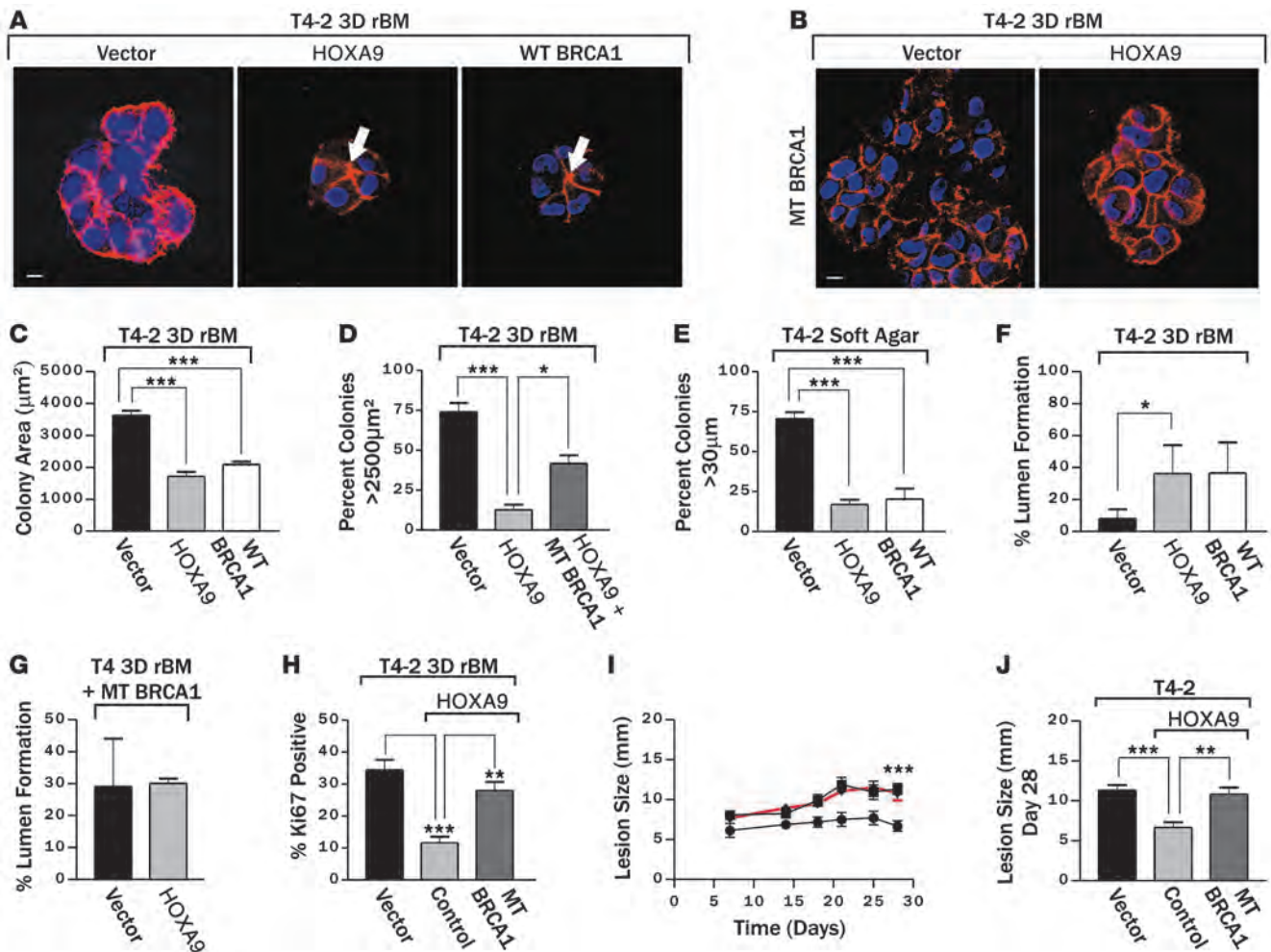


Figure 4

HOXA9 regulates nonmalignant MEC growth by modulating BRCA1 expression. (A) Immunofluorescence images of β -catenin (red), β 4 integrin (green), Laminin-5 (green), and nuclei (blue) in MCF-10A colonies expressing either luciferase control shRNA or shRNA-HOXA9 clone 3. Arrows indicate cleared lumen. Scale bar: 50 μ m. (B) Colony size of MCF-10A cells cultured within a rBM and expressing reduced HOXA9 levels. **** P = 0.0001. (C) Lumens observed in MCF-10A colonies expressing luciferase control shRNA as compared with those with shRNA-mediated HOXA9 knockdown. ** P = 0.010. (D) The response (BRCA1 protein levels) of MCF-10A cells expressing reduced HOXA9 levels to 5 Gray irradiation compared with nonirradiated samples. * P < 0.001. (E and F) Phase images of tumor colonies embedded within soft agar (E) and the percentage of colonies greater than 40 μ m in diameter (F). Scale bar: 50 μ m. * P = 0.001. (G) Immunofluorescence images of β -catenin (red) and nuclei (blue) in MCF-10A colonies, expressing either luciferase control shRNA or shRNA-BRCA1 clone 5. The arrow indicates cleared lumen. Scale bar: 50 μ m. (H) Colony size of MCF-10A cells cultured within a rBM and expressing reduced BRCA1 levels. *** P = 0.0024. (I) Quantification of lumens observed in MCF-10A colonies expressing luciferase control shRNA as compared with those with shRNA-mediated BRCA1 knockdown. **** P = 0.0003. (J) Immunofluorescence images of β -catenin (red) and nuclei (blue) in MCF-10A colonies expressing vector or mutant BRCA1 (BRCA1 MT). The arrow indicates cleared lumen. Scale bar: 10 μ m. (K) Quantification of cross-sectional area of MCF-10A colonies in cells cultured within a rBM and coexpressing mutant BRCA1. * P = 0.05. (L) Quantification of lumens observed in MCF-10A colonies expressing vector control as compared with those expressing a mutant BRCA1. * P = 0.05.

**Figure 5**

HOXA9 regulates BRCA1 to repress the malignant behavior of MECs. (A) Immunofluorescence images of β -catenin (red) and nuclei (blue) in T4-2 colonies reexpressing HOXA9 or BRCA1. Arrows indicate cleared lumens. Scale bar: 10 μm . (B) Immunofluorescence images of β -catenin (red) and nuclei (blue) in T4-2 colonies reexpressing HOXA9 alone or with a mutant BRCA1. Scale bar: 10 μm . (C) Quantification of colony size of T4-2 cells reexpressing HOXA9 or BRCA1. $***P = 0.001$. (D) Quantification of cross-sectional area of T4-2 colonies formed by cells reexpressing HOXA9 alone or with a mutant BRCA1. $*P = 0.05$, $***P = 0.001$. (E) Quantification of anchorage-independent growth and survival in T4-2 cells reexpressing either HOXA9 or BRCA1. $***P = 0.001$. (F) Quantification of the percentage of T4-2 colonies that formed lumens following the reexpression of HOXA9 or BRCA1. $*P = 0.0263$. (G) Quantification of lumen formation in rBM T4-2 colonies with reexpressed HOXA9, when BRCA1 function has been compromised through coexpression of a mutant BRCA1. (H) Quantification of proliferation in T4-2 cells following HOXA9 reexpression with a mutant BRCA1. $**P = 0.0025$, $***P = 0.0003$. (I) The time course of the progressive increase in xenograft size (5–30 days). Reexpression of HOXA9 in T4-2 tumor cells significantly reduced the rate of lesion expansion (filled circles) compared with the T4-2 vector controls (filled squares), which could be restored to that of T4-2 breast tumor cells if coexpressed with a mutant BRCA1 (filled triangles with red line). $***P = 0.001$. (J) Lesion size (28 days) in each experimental group. $**P = 0.01$, $***P = 0.001$.

cell behavior in culture and in vivo. Consistent with a functional link between HOXA9 and BRCA1, increasing the levels of wild-type BRCA1 in breast tumor cells significantly reduced their rBM-dependent growth and normalized their survival behavior, such that they assembled colonies with cleared lumens (Figure 5A, see arrows; quantified in Figure 5F) that were similar in size and morphology to those formed by tumor cells reexpressing HOXA9 (compare in Figure 5, A, C, and F). In addition, rBM-dependent tumor colonies expressing higher wild-type BRCA1 were no longer invasive and had cell-cell localized β -catenin (Figure 5A), indicating that, analogous to HOXA9, BRCA1 also reverted the

malignant phenotype of breast cells toward a normal polarized, growth-arrested acini structure (see Figure 2). Consistent with its TS function, ectopic expression of wild-type BRCA1 reduced the anchorage-independent growth and survival of breast cancer cells (Figure 5E). These data show how BRCA1 can phenocopy the TS effects of HOXA9 and can repress the growth, survival, and invasive behavior of breast tumor cells in rBM.

We compromised BRCA1 function in the T4-2 tumor cells reexpressing HOXA9 through coexpression of the Δ exon 11b BRCA1 mutant and then assayed for effects on rBM growth, survival, and colony morphology to explore the functional relationship between

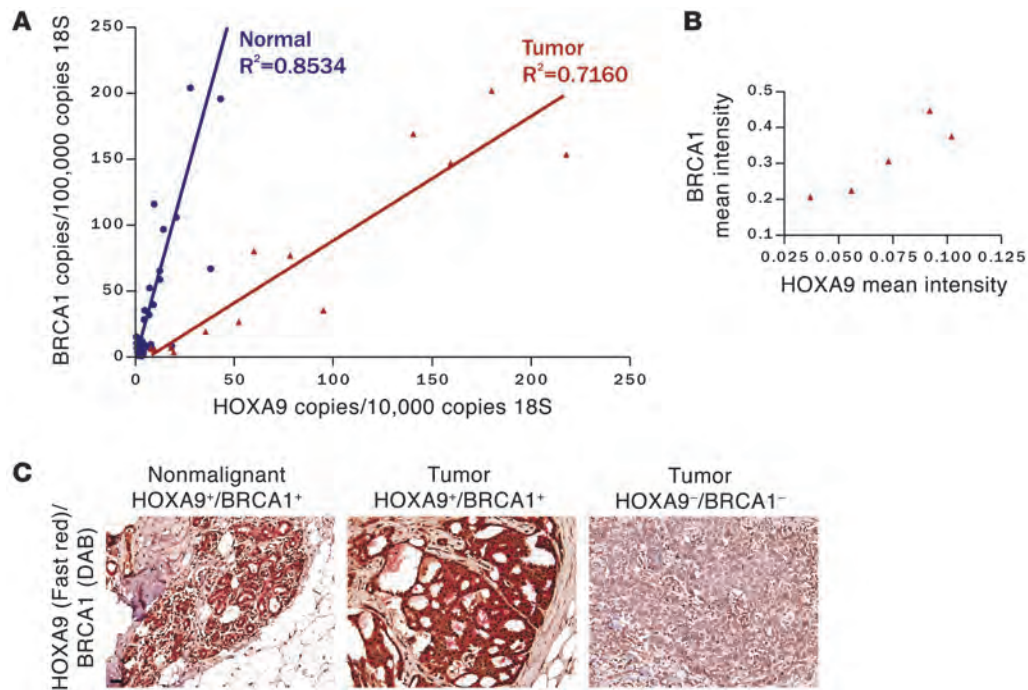


Figure 6

Clinical correlation between HOXA9 and BRCA1 expression. **(A)** Line graph illustrating that significant correlations exist between *HOXA9* and *BRCA1* mRNA levels expressed in a cohort of normal (shown in blue; $P \leq 0.0001$; $r^2 = 0.8534$) and tumorigenic (shown in red; $P \leq 0.0001$; $r^2 = 0.7160$) human breast tissue specimens ($n = 53$). **(B)** Graph illustrating the relationship between HOXA9 and BRCA1 protein levels in human ER⁻/PR⁻/ErbB2⁻ breast samples. **(C)** Immunohistochemistry showing colocalized expression of HOXA9 and BRCA1 protein in the epithelium of normal human breast tissue and HOXA9⁺/BRCA1⁺ tumor samples, as compared with HOXA9⁻/BRCA1⁻ tumor samples. (HOXA9 was “stained” with Fast Red, and BRCA1 was “stained” with DAB). Scale bar: 100 μ m.

HOXA9 and BRCA1 expression and MEC phenotype. Disrupting BRCA1 function antagonized the ability of HOXA9 to repress the malignant behavior of the T4-2 tumor cells (Figure 5B). Thus, tumor cells simultaneously expressing HOXA9 and the Δ exon 11b BRCA1 mutant failed to phenotypically revert when grown within rBM and instead formed continuously growing, invasive, and nonpolarized colonies that lacked cell-cell localized β -catenin and cleared lumens (Figure 5, B, D, G, and H). These studies demonstrated that the ability of HOXA9 to repress the malignant behavior of MECs is functionally dependent upon BRCA1.

To address the *in vivo* relevance of a functional link between HOXA9 and BRCA1, we conducted xenograft studies using BalbC *nu/nu* mice injected with human breast cancer cells, with and without HOXA9 and a functional BRCA1, and assayed tumor growth (as indicated by lesion size). Reexpression of HOXA9 in T4-2 breast cancer cells significantly reduced lesion growth rate as compared with T4-2 vector controls (Figure 5, I and J). In contrast, the HOXA9 expressing T4-2 MECs in which BRCA1 function was simultaneously compromised, through coexpression of the Δ exon11b BRCA1 mutant, grew robustly and had growth rates that were comparable to that observed in the vector control T4-2 MECs. T4-2 HOXA9 tumor cells in which BRCA1 function was compromised developed lesions that were, on average, comparable in size and morphology to those formed by the wild-type tumors (28 days; Figure 5, I and J). These data demonstrate that HOXA9 restricts the growth and survival of human breast cancer cells by regulating BRCA1 expression both in culture and *in vivo*.

Clinical correlation between HOXA9 and BRCA1 expression. To address the clinical relevance of a functional link between HOXA9 and BRCA1, we examined mRNA and protein expression and colocalization of HOXA9 and BRCA1 in cohorts of clinically diverse (ER/PR-positive and -negative) human breast cancers and normal tissue ($n = 56$). Quantitative RT-PCR data showed that HOXA9 correlates significantly with BRCA1 in normal ($r^2 = 0.8534$; Figure 6A, blue line) and transformed breast tissue (ER/PR positive and negative; $r^2 = 0.7160$; Figure 6A, red line). Quantitative immunohistochemistry of a panel of 12 triple-negative breast tumors revealed a strong positive association between nuclear HOXA9 and BRCA1 (Figure 6B and Table 3). We also noted that the epithelium of the normal breast coexpressed appreciable levels of cytoplasmic and nuclear HOXA9 and BRCA1 protein (Figure 6C, left), as did the more differentiated, triple-negative breast tumor tissues (Figure 6C, middle). In contrast, less differentiated triple-negative tumors showed complete loss of both proteins (Figure 6C, right). Interestingly, we observed that a loss in HOXA9 expression was associated with a greater reduction in *BRCA1* mRNA in the breast tumor samples as compared with normal tissue (Figure 6A, compare normal to tumor). These clinical findings, together with our experimental data, are consistent with the notion that HOXA9 modulates BRCA1 expression by cooperating with multiple negative and positive regulatory factors, differentially expressed in human breast tumors, whose expression correlates with loss of ER/PR expression and tumor aggression (20, 27).



Discussion

To identify developmental regulators misexpressed during malignant transformation of the breast, we used global expression profiling of microdissected breast tumors and their adjacent normal tissue. We identified the homeobox gene *HOXA9*, previously implicated in mammary development (12, 39), as a gene whose levels were significantly downregulated. We confirmed the microarray observation using RT-PCR, in situ hybridization, and immunohistochemistry and showed that *HOXA9* was highly expressed in the luminal epithelium of the normal breast and that its expression was frequently decreased in a high proportion of invasive human breast tumors and breast cancer cell lines (Figure 1, B and G). Bioinformatics analysis confirmed these findings and also indicated that *HOXA9* loss significantly correlated with features of aggressive disease in ER/PR-negative breast tumors, including large- and high-grade tumors, late-stage disease, lymph node involvement, distant metastasis, and reduced patient survival (Figure 1, E and F, Table 1, and Supplemental Table 3). Using 2 ER/PR/ErBB2-negative, basal-like breast cancer cell lines, we then showed that reexpressing *HOXA9* (but not another member of the *HOXA* cluster, *HOXA10*) inhibited tumor cell growth and survival and promoted acini morphogenesis in culture and restricted tumorigenesis in vivo. Furthermore, we showed that reducing levels of *HOXA9* in nonmalignant MECs enhanced growth and survival and perturbed acini morphogenesis (Figures 2 and 4). Although investigators have previously reported that *HOXA9* is methylated and that its expression is reduced in breast, lung, and ovarian cancers (45, 69, 70), this is the first study to our knowledge to assess the clinical relationship of *HOXA9* loss to solid tumors, to analyze the functional relevance of *HOXA9* to the malignant behavior of MECs in culture, in vivo and in clinical specimens, and to identify a molecular mechanism for these effects. In this respect, we found that *HOXA9* restricts the aggressive and malignant behavior of MECs by directly modulating *BRCA1*, implying that *HOXA9* reduces risk to malignancy and controls tumor aggressiveness by controlling levels of an established mammary gland TS gene. These findings are consistent with the notion that developmental regulators, such as the *HOX* family of transcription factors, influence adult tissue homeostasis by regulating the expression and/or activity of key TS genes that regulate cell growth and survival and morphogenesis (12).

Homeobox genes regulate embryonic development and tissue patterning, and their expression is frequently perturbed and often aberrantly increased in tumors (2, 3, 12, 71). Until recently, the prevailing dogma has been that inappropriate expression of homeobox genes promotes tumor progression. Consistently, the homeobox genes that are highly expressed during early embryogenesis, that promote cell proliferation and survival, and that induce migration are those that are most often over expressed in transformed cells and tissues (6, 8, 72, 73). These are the homeobox genes that have been implicated in altered growth receptor signaling, deregulated cell cycle control, and the elevated growth and apoptosis resistance of cancer cells and that appear to regulate tumor invasion and metastasis and promote angiogenesis (40, 72, 74–76). For instance, the homeobox gene *Six1* is highly expressed during early mammary gland development, where it drives epithelial cell proliferation by modulating levels of the cell cycle gene cyclin A1 (77). Although *Six1* levels are downregulated and barely detectable in the differentiated adult mammary gland, *Six1* is frequently overexpressed in aggressive breast tumors, in which it pro-

Table 3

Relationship between *HOXA9* and *BRCA1* nuclear protein levels in human ER-/PR-/ErBB2- breast samples

Case no.	Nuclear <i>HOXA9</i>	Nuclear <i>BRCA1</i>
4309	+	+++
9667	+	++
6073	+	+
11947	+	+
462	++	–
6697	+	–
8147	–	++
8715	–	+
8954	–	+
6912	–	+
9533	–	–
2440	–	–

Expression is relative between samples. –, no detectable expression; +, low expression; ++, moderate expression; +++, high expression.

motes cell growth and survival, enhances genomic instability, and promotes tumor metastasis (78). Similarly, enforced expression of the early embryonic homeobox gene *Msx1*, which is also often elevated in tumors, promotes the proliferation of undifferentiated stem cells, blocks the terminal differentiation of myoblasts, and downregulates expression of the myogenic differentiation factor *MyoD1* to induce their malignant transformation (79–81).

It is now appreciated that homeobox genes of the ANT-C/BX-C type that control rostral-caudal patterning during embryogenesis and are abundantly expressed in differentiated tissues can repress malignancy and may function as “tumor modulators” (9, 71, 82–84). Data that support this concept exist, although, unfortunately, many findings linking homeobox gene loss with tumorigenesis are largely circumstantial (45, 69, 70, 79). At present, few methodical studies exist that clarify molecular mechanisms whereby reduced homeobox levels could restrict tumor progression and/or metastasis (9, 84). In this article, we present evidence that one of the posteriorly expressed homeobox genes, *HOXA9*, is necessary for normal MEC growth and survival and acini morphogenesis, a finding that is consistent with a previous article implicating *HOXA9* in mammary gland differentiation in the mouse (Figures 2 and 4) (39). Our findings clarify these earlier observations and indicate that *HOXA9* inhibits cell growth and survival and promotes morphogenesis in normal and transformed MECs by directly regulating expression of the TS gene *BRCA1* (Figures 3 and 5). Our observations are consistent with and extend prior studies showing that *PITX1*, which is frequently downregulated in prostate, bladder, and colon cancers (6), could function as a TS by inhibiting oncogenic Ras signaling and indicating that *HOXA5*, which is lost in greater than 60% of mammary tumors and breast cancer cell lines, may restrict breast cancer by regulating levels of the TS p53 to alter inappropriate MEC survival (8, 73). Distinct from these reports, we could show that *HOXA9* not only modulates *BRCA1* levels but also directly binds to and regulates *BRCA1* transcription and that *HOXA9*-dependent *BRCA1* induction is markedly enhanced during tissue remodeling and following exposure of breast cells to an exogenous stress, consistent with a role for *BRCA1* in cell cycle regulation and the DNA damage response (85, 86). Intriguingly, *HoxC8* was shown to bind directly to and regulate the mammalian



homolog of lethal giant larvae TS gene; however, to date no functional data exist to clarify the relevance of this relationship (7). In the present studies, we not only showed that HOXA9 directly regulates BRCA1 transcription, but we demonstrated that HOXA9-dependent BRCA1 expression is critical for the growth, survival, and morphogenesis activity of HOXA9 in culture and for its TS-like activity in vivo (Figures 4 and 5). We also provided additional evidence that this relationship has clinical relevance (Figures 5 and 6). Indeed, our findings argue that loss of HOXA9 is a critical determinant of tumor aggression, especially in ER/PR-negative breast tumors, which likely harbor additional modifications that negatively modulate BRCA1 levels. Our findings emphasize the importance of examining the role of homeobox family members as critical regulators of normal tissue differentiation and homeostasis and illustrate the potential permissive role of HOXA9 loss in tumor progression and aggressiveness and as a potential regulator of treatment responsiveness.

In contrast to our observation that HOXA9 restricts the growth, survival, and malignant behavior of breast epithelial cells, it is well known that HOXA9 plays an essential role in normal myeloid lineage development, because it promotes expansion of the stem cell pool and inhibits differentiation (87). Consistently, increased expression or activation of HOXA9 in myeloid stem cells is causally linked to acute myeloid leukemia (88), and enforced expression of HOXA9 in myeloid cells, due to chromosome translocation or overexpression of its regulator MLL, drives transformation (4). Furthermore, elevated HOXA9 expression induces angiogenesis by regulating growth, migration, and invasion of endothelial cells (40). Interestingly, neither myeloid cells nor human endothelial cells ectopically overexpressing HOXA9 upregulate *BRCA1* transcript levels, thereby offering one likely explanation for the strikingly different phenotypic consequences of HOXA9 expression between MECs versus lymphocytes and endothelial cells (P.M. Gilbert, unpublished observations) (89, 90). This observation is consistent with previous studies indicating that homeobox target genes are cell and tissue specific. The data are also in accord with results showing that the expression profile and gene targets of each HOX factor depend upon the complement of cofactors present in each cell and the extracellular microenvironment the cell resides within (91). Thus, while HOXA5 can induce p53 expression in MECs, sustained HOXA5 failed to modulate p53 in endothelial cells and instead induced Thrombospondin-2 (8, 92). Such findings serve to illustrate the urgency of conducting comparative functional studies of homeobox gene regulation in different tissues and stress the relevance of tissue context as a key regulator of cellular behavior. The work also underscores the importance of considering tissue-specific gene regulation in order to understand cancer pathogenesis as well as to identify tissue-specific treatments.

BRCA1 is either lost or mutated in many cases of familial breast cancer (27, 93, 94). Nevertheless, BRCA1 expression is also frequently reduced in sporadic breast cancers, and gene methylation and silencing only account for a subset of these sporadic tumors (27, 93). This means that other parameters and factors that are altered during breast carcinogenesis likely exist to regulate tissue-specific levels of BRCA1 (20, 27). Indeed, the BRCA1 promoter is a highly complex, bidirectional transcriptional unit, with multiple binding motifs, and it is subject to dynamic interactions between its promoter and terminator regions. Its activity can be modulated by multiple generic and tissue-specific factors, including 53BP1,

E2F proteins, and GABP- α/β , and conditions, including stress, hypoxia, growth factors, and estrogens (95, 96). However, despite these findings, very few factors have been shown to bind to and directly modulate BRCA1 expression and, of these, most have been negative regulators. Furthermore, there is a paucity of evidence to link these BRCA1 regulators to defined BRCA1-dependent phenotypes. Metastasis-associated tumor antigen 1 (MTA1) has been implicated in the transcriptional repression of BRCA1 and in abnormal centrosome number and chromosomal instability (30), and E2F4 and the pocket proteins p130/p107 bind the BRCA1 promoter and repress its basal transcription, thereby regulating cell growth (97). In these studies, we demonstrate that HOXA9 directly and positively modulates BRCA1 transcription, thereby restricting the abnormal growth, survival, and stress response of breast cancer cells and nonmalignant MECs in culture and in vivo. This relationship has clinical relevance because loss of HOXA9 significantly predicts tumor aggression in ER/PR-negative cancers. In this respect, HOXA9 correlated significantly with *BRCA1* mRNA and BRCA1 protein levels in breast tissues, in which we observed that reduced HOXA9 expression was associated with a more profound reduction of BRCA1 in tumor cells and that loss of HOXA9 and BRCA1 was strongly associated with a less differentiated phenotype in triple-negative breast tumors. Because basal-like tumors also frequently express “BRCA1 repressors,” these results argue that HOXA9 likely cooperates with other intrinsic or acquired factors to modulate BRCA1 expression in breast cancers. The fact that expression profiling did not reveal reduced *BRCA1* transcripts in the 4 primary tumors with reduced HOXA9 expression is not surprising (Supplemental Table 2). In general, expression levels of *BRCA1* are below the detection sensitivity of Affymetrix arrays, and thus transcript level changes would not normally be noted. Instead, BRCA1 expression is tightly linked to cell cycling and the presence of damaged DNA (98), and we observed a robust induction of BRCA1 in response to HOXA9 most predominantly during tissue remodeling (J.K. Mouw, unpublished observations) or after exposure to an exogenous stress (Figure 4D). Thus, because the HOXA9 promoter is frequently methylated and HOXA9 levels are often reduced in invasive breast tumors, and we showed that HOXA9 is often lost in breast tumors, our data offer an attractive explanation for why BRCA1 expression could be so frequently lost in sporadic human breast tumors, even in the absence of genetic aberrations, promoter methylation, or haploinsufficiency.

Intriguingly, not only did we find that HOXA9-dependent BRCA1 expression restricts tumor progression by inhibiting MEC growth and survival, but we also observed that elevated HOXA9 and BRCA1 levels restored cell-cell adhesions and normalized acini morphogenesis (Figures 2 and 5). These findings are consistent with previous reports that showed that loss of BRCA1 compromises the ability of nonmalignant MCF10A MECs to undergo morphogenesis into polarized acinar structures in a 3D rBM assay (19, 35, 36) and are consistent with data indicating that BRCA1 is critical for lumen formation in primary murine MECs (38). Indeed, during mammary gland remodeling, BRCA1 levels peak prior to tight junction assembly and tissue-specific differentiation, and they decline to barely detectable levels during lactation (27, 37, 38). Consistently, recent studies in which BRCA1 was overexpressed in the epithelium of the murine breast showed that there was a moderate increase in lobular alveolar differentiation in the mammary gland, consistent with accelerated development, and these mice also showed resistance to mutagen-induced mammary neoplasia. In contrast, age-matched



mice expressing a mutated BRCA1 morphologically resembled animals at mid-pregnancy, consistent with increased proliferation and secondary branching, and these mice showed enhanced DMBA-induced transformation (99). Our findings raise the intriguing possibility that some HOX genes, particularly those expressed late during development and those that are expressed in differentiated tissues such as HOXA9, might regulate growth, survival, and invasion to modulate body plan patterning during development, by regulating levels of TSs that control these orchestrated processes. In this respect, HOXA9 plays an important role in skeletal (41), urogenital tract (42), kidney (43), and mammary gland development (39), and HOXA9 expression can be regulated by microRNAs that have been implicated in tissue differentiation (44).

Methods

Substrates, antibodies, and pharmacological reagents. The materials used were as follows: Commercial EHS matrix (Matrigel; Collaborative Research) for the rBM assays; Vitrogen (Vitrogen 100, Inamed Biomaterials; bovine skin collagen I), 3 mg/ml, for coating culture dishes; and Collagen AC-5, 0.5% (ICN Biomedical Inc.) for morphogenesis assays. Primary antibodies used were as follows: actin, clone AC-40 (Sigma-Aldrich); BRCA1, clone Ab-1 (Oncogene); β -Catenin, clone 14 (BD Biosciences – Transduction Laboratories); β_4 integrin, clone 3E1 (Invitrogen); FLAG, clone M2 (Sigma-Aldrich); HA.11, clone 16B12 (Covance Research Products); HA, clone Y-11 (Santa Cruz Biotechnologies Inc.); acetyl H3 histone, rabbit polyclonal (Upstate); Ki-67 clone 35 (BD Biosciences – Transduction Laboratories); HOXA9 (N-20), goat polyclonal (Santa Cruz Biotechnologies Inc.); HOXA9, rabbit polyclonal (a gift from T. Nakamura, Japanese Foundation for Cancer Research, Tokyo, Japan); HOXA10 rabbit polyclonal (Abcam); and laminin 5 (a gift from M.P. Marinkovich, Stanford University School of Medicine, Stanford, California, USA) (100). Secondary antibodies used were Alexa Fluor 488- and 555-conjugated polyclonal anti-rabbit and anti-mouse IgGs (Molecular Probes) and HRP-conjugated polyclonal rabbit and anti-mouse IgGs (Amersham Pharmacia). Pharmaceutical reagents included Tyrphostin AG 1478 (100 μ M; DMSO) (Calbiochem); *p*-Nitrophenyl phosphate disodium salt hexahydrate (Fisher Scientific); and D-Luciferin, potassium salt (Biotium).

cDNA, lentiviral and retroviral, and shRNA constructs and vectors. Please refer to the Supplemental Methods section for a detailed description of constructs used.

Cell culture. The HMT-3522 S-1 and T4-2 MECs were grown and manipulated in 2D and 3D, and the T4-2s were phenotypically reverted exactly as described previously (60, 101). MDA-MB-231, MCF-7, and MCF10A cells were cultured according to manufacturer's recommendations (ATCC) and grown in 3D as described previously (102). BT-20, MDA-MB-468, MDA-MB-435, T47D, ZR751, and SK-BR-3 cells were cultured according to manufacturer's recommendations (ATCC).

Retroviral and lentiviral infections. Amphitrophic retrovirus was produced (103), and retroviral supernatant was harvested and used directly to spin infected cells, followed by antibiotic-induced selection with puromycin (0.5 μ g/ml media) or neomycin (100 μ g/ml) 72 hours after infection (104). Lentiviral particles were produced, harvested, and used to infect target cells as previously described (105).

Soft agar assay. Anchorage-independent growth was assessed using a soft agar assay (60). In brief, 25,000 cells in 1.5 ml 0.35% agarose containing 1X growth media were overlaid with 1.5 ml 0.5% agarose containing 1X growth media, and colonies larger than 30 μ m in diameter were scored positive after 14 days.

In vivo studies. All experiments were performed in accordance with the guidelines of Laboratory Animal Research at the University of Pennsylvania. Four-week-old BalbC *nu/nu* mice were subcutaneously injected in the rear flanks (5×10^6 cells/injection, together with Matrigel), and palpable lesions were

detected, measured, and monitored biweekly for 56 days (Instant read-out digital calipers; Electron Microscopy Sciences). At experiment termination, mice were sacrificed, and lesions were dissected, measured, macroscopically analyzed, fixed in 4% paraformaldehyde, and paraffin embedded, and H&E sections were evaluated for histopathological evidence of tumor phenotype.

Immunofluorescence. Immunofluorescence analysis of cells grown in 2D, 3D, and paraffin-embedded tissues was performed as previously described (101, 102).

Proliferation. Cell proliferation was measured by calculating the percentage of Ki-67-labeled nuclei and quantified as previously described (106).

Immunoblotting. Equal amounts of cell protein lysate (Laemmli; BCA; Pierce) were separated on reducing SDS-PAGE gels, transferred to nitrocellulose or PVDF membrane, and probed with primary antibody. Bands were visualized and quantified using a Fujifilm Gel Documentation system, in conjunction with HRP-conjugated secondary antibodies and ECL-Plus (Amersham Pharmacia). For the irradiation response of MCF-10A cells, cells were irradiated (5 Gray) and lysed 24 hours later.

ChIP. ChIP assays were performed according to the manufacturer's directions (Upstate). In brief, proteins were cross-linked to chromatin (formaldehyde; 1%), cells were lysed, and the chromatin was sheared (sonication; Misonix Ultrasonic). HA-tagged HOXA9/DNA fragments were immunoprecipitated (overnight; at 4°C) using polyclonal anti-HA (clone Y-11) or polyclonal anti-HOXA9, with polyclonal anti-acetyl H3 histone serving as a positive control and isotype-matched IgG serving as a negative control. Protein/DNA complexes were captured (Protein A agarose beads), washed (6–10 times), and eluted from beads, and cross-links were reversed (NaCl and phenol/chloroform extraction). DNA was ethanol precipitated and used directly for PCR reactions. To amplify a human BRCA1 promoter fragment from anti-HOXA9 ChIP experiments we used the following primers: forward, 5'-GATGGGACCTTGTGGAAGAA-3', and reverse, 5'-ACGACCAAACCAACCAAT-3'. To amplify the human β -globin gene (107) from anti-acetyl H3 histone ChIP experiments we used the following primers: forward, 5'-ATCTTCTCCACAGCTCCT-3', and reverse, 5'-TTTGCAGCCTCACCTTCTTT-3'. Bar graph data is normalized to an IgG control ChIP.

BRCA1 reporter assay. Luciferase *BRCA1* gene reporter assays were conducted in 293 cells by transient transfection and normalizing transfection efficiency, by quantifying SEAP expression using a MRX microplate reader (Dyex Technologies) 36 hours after transfection, as previously described (108). Forty-eight hours after transfection, cells were lysed (25 mM glycylglycine, 2 mM EGTA, pH 8.0, 1% Triton X-100, 1 mM DTT, pH 7.8), aliquots of lysate were diluted (1:5) in assay buffer (25 mM glycylglycine, 2 mM EGTA, pH 8.0, 10 mM MgSO₄, 2.2 mM ATP, 0.275 mM Acetyl CoA, 1 mM DTT, pH 7.8), transferred to a Microfluor plate (Thomas Scientific), and mixed with equal quantity of luciferin buffer (25 mM glycylglycine, 2 mM EGTA, pH 8.0, 10 mM MgSO₄, 1 mM DTT, 0.55 mM luciferin, pH 7.8). Light emission from the reaction was detected using a Microtiter plate luminometer (Dyex Technologies) in conjunction with Revelation software. Experiments were quantified as the fold change over appropriate control conditions.

Morphometric analysis. Colony size and morphology in 3D rBM was assessed at indicated times, essentially as previously described (101, 102). Briefly, cell-cell integrity within a 3D MEC acinus was considered intact when β -catenin staining was localized and continuous around the periphery of all cells. A 3D MEC acinus was considered properly polarized when β_4 integrin and laminin were expressed continuously and exclusively around the basal surface of the acinar structure.

Expression profiling. Please see the Supplemental Methods section for a detailed description of the expression profiling.

Semiquantitative PCR. Purified total RNA (2.0 μ g) was reverse transcribed, using random primers (Amersham Biosciences), and resultant samples were serially diluted 1:10, 1:100, and 1:1,000 for subsequent PCR reactions.



An initial PCR was performed to amplify the 18S rRNA subunit, together with a standard curve to determine cDNA copy number for each sample. Primer sequences were as follows: 18S rRNA, forward, 5'-CGGCTACCA-CATCCAAGGAA-3', and 18S rRNA, reverse, 5'-GCTGGAATTACCGCG-GCT-3'. Corrected cDNA concentrations were calculated and a second PCR reaction was performed in which equal amounts of cDNA were added to primers specific for HOXA9. The primer sequences used to amplify HOXA9 cDNA were 5'-GCTTGTGGTTCTCCTCCAGT-3' and 5'-CCAGGGTCTG-GTGTTTTGTA-3'. These primers cross the exon 1–2 boundary and thus should not amplify contaminating genomic DNA. The primer sequences used to amplify BRCA1 cDNA were 5'-GGAACCTAACCAACGGAGCA-3' and 5'-TAGGTTTCTGCTGTGCTCGA-3'. The primer sequences used to amplify HOXA10 cDNA were 5'-TATCCCACAACAATGTCATGCTC-3' and 5'-GTCGCCTGGAGATTCATCAGGA-3'.

Quantitative real-time PCR. Total RNA was reverse transcribed using random primers (Amersham Biosciences), and 18S rRNA primers were used to control for cDNA concentration in a separate PCR reaction for each sample (see above for sequences). Primers used to amplify HOXA9 exon 2, using the LightCycler apparatus (Roche Diagnostics), are listed above. LightCycler Fast Start DNA Master SYBR Green Mix (Roche) was added to each PCR reaction along with cDNA and 1 pmol primer in a total volume of 10 µl. The primers and conditions used to amplify the BRCA1 cDNA junction between exon 12 and 13 were previously described (109).

In situ hybridization. Sense and antisense riboprobes against HOXA9 were generated as previously described (83). Digoxigenin-labeled probes were prepared using T7 or SP6 RNA polymerase (Roche). Paraffin-embedded human breast tissue was hybridized with 800 ng/ml of probe as previously described (83). Six normal and four invasive ductal carcinoma human breast samples were examined.

Immunohistochemistry. Formalin-fixed, paraffin-embedded human breast tissue sections, lacking any patient-identifying information, were obtained with IRB approval from the University of Pennsylvania and the Huntsman Cancer Institute Tissue Resource and Acquisition Core Facility with patient consent. Sections were deparaffinized and rehydrated through 3 concentrations of alcohol and incubated in 3% H₂O₂ for 15 minutes to block endogenous peroxidase. Antigen retrieval was carried out in 0.1 M citrate buffer, pH 6.0, at 95 °C for 20 minutes, followed by 20 minutes at room temperature. Nonspecific binding was blocked using PBS containing 1% BSA and 5% goat serum for 30 minutes. Sections were probed with anti-HOXA9 (1:200) and anti-BRCA1 antibodies. Biotinylated secondary

antibody and ABC reagent were used as directed (Vector Laboratories). Fast red (HOXA9) and DAB (BRCA1) were used as chromogens (Vector Laboratories). Sections were counterstained with Mayer's hematoxylin (Sigma-Aldrich). Please refer to the supplemental method section for information regarding multispectral image acquisition and analysis. Six normal and four invasive ductal carcinoma samples were examined.

Bioinformatics analysis. Please refer to the Supplemental Methods section for a detailed description of the bioinformatics analysis.

Statistics. We used InStat software (Graphpad) to conduct the statistical analysis of our data. Unless otherwise stated, 2-tailed Student *t*-tests were used for simple significance testing, and 2-tailed Pearson tests were used for correlation analysis (mean ± SEM of 3–5 independent experiments). *P* values of less than 0.05 were considered to be significant. Unless otherwise noted, *n* = 3.

Acknowledgments

We thank P. Marinkovich for the BM165 mAb, H. Blau for the Hermes-HRS-puro-IRES-EGFP construct, C. Largman for the PRC-CMV-HOXA9 construct, F. Rauscher for the HA-tagged wild-type and Δexon11b BRCA1 constructs, and L.A. Chodosh for the pGL2-BRCA1 luciferase construct. This work was supported by NIH grants R01-CA078731 and U54CA143836; DOD grants DAMD17-01-1-0368, DAMD17-03-1-0396, and W81XWH-05-1-330; DOE grant A107165; CIRM grant RS1-00449 (to V.M. Weaver); Komen grant DISS0402407 (to P.M. Gilbert); DOD grant BC062562 (to J.K. Mouw); and by the Huntsman Cancer Foundation/Huntsman Cancer Institute (to A.L. Welm).

Received for publication April 13, 2009, and accepted in revised form February 8, 2010.

Address correspondence to: Valerie M. Weaver, UCSF, Center for Bioengineering and Tissue Regeneration, Department of Surgery, 513 Parnassus Avenue, S1364C-0456, San Francisco, California 94143, USA. Phone: 415.476.3826; Fax: 415.476.3985; E-mail: Valerie.Weaver@ucsfmedctr.org.

Penney M. Gilbert's present address is: Baxter Laboratories in Stem Cell Biology, Department of Microbiology and Immunology, Institute for Stem Cell Biology and Regenerative Medicine, Stanford University School of Medicine, Stanford, California, USA.

- Chen H, Sukumar S. HOX genes: emerging stars in cancer. *Cancer Biol Ther.* 2003;2(5):524–525.
- Grier DG, Thompson A, Kwasniewska A, McGonigle GJ, Halliday HL, Lappin TR. The pathophysiology of HOX genes and their role in cancer. *J Pathol.* 2005;205(2):154–171.
- Samuel S, Naora H. Homeobox gene expression in cancer: insights from developmental regulation and deregulation. *Eur J Cancer.* 2005;41(16):2428–2437.
- Nakamura T, et al. Fusion of the nucleoporin gene NUP98 to HOXA9 by the chromosome translocation t(7;11)(p15;p15) in human myeloid leukaemia. *Nat Genet.* 1996;12(2):154–158.
- Ford HL, Kabling EN, Bump EA, Mutter GL, Pardee AB. Abrogation of the G2 cell cycle checkpoint associated with overexpression of HSIX1: a possible mechanism of breast carcinogenesis. *Proc Natl Acad Sci U S A.* 1998;95(21):12608–12613.
- Kolfschoten IG, et al. A genetic screen identifies PITX1 as a suppressor of RAS activity and tumorigenicity. *Cell.* 2005;121(6):849–858.
- Tomotsune D, Shoji H, Wakamatsu Y, Kondoh H, Takahashi N. A mouse homologue of the Drosophila tumour-suppressor gene *l(2)gl* controlled by Hox-C8 in vivo. *Nature.* 1993;365(6441):69–72.
- Raman V, et al. Compromised HOXA5 function can limit p53 expression in human breast tumours. *Nature.* 2000;405(6789):974–978.
- Carrio M, Arderiu G, Myers C, Boudreau NJ. Homeobox D10 induces phenotypic reversion of breast tumor cells in a three-dimensional culture model. *Cancer Res.* 2005;65(16):7177–7185.
- Lewis MT. Homeobox genes in mammary gland development and neoplasia. *Breast Cancer Res.* 2000;2(3):158–169.
- Duverger O, Morasso MI. Role of homeobox genes in the patterning, specification, and differentiation of ectodermal appendages in mammals. *J Cell Physiol.* 2008;216(2):337–346.
- Chen H, Sukumar S. Role of homeobox genes in normal mammary gland development and breast tumorigenesis. *J Mammary Gland Biol Neoplasia.* 2003;8(2):159–175.
- Friedman LS, et al. Confirmation of BRCA1 by analysis of germline mutations linked to breast and ovarian cancer in ten families. *Nat Genet.* 1994;8(4):399–404.
- Starita LM, Horwitz AA, Keogh MC, Ishioka C, Parvin JD, Chiba N. BRCA1/BARD1 ubiquitinate phosphorylated RNA polymerase II. *J Biol Chem.* 2005;280(26):24498–24505.
- Fan W, et al. BRCA1 regulates GADD45 through its interactions with the OCT-1 and CAAT motifs. *J Biol Chem.* 2002;277(10):8061–8067.
- Aprelikova O, Pace AJ, Fang B, Koller BH, Liu ET. BRCA1 is a selective co-activator of 14-3-3 sigma gene transcription in mouse embryonic stem cells. *J Biol Chem.* 2001;276(28):25647–25650.
- Rosen EM, Fan S, Pestell RG, Goldberg ID. BRCA1 gene in breast cancer. *J Cell Physiol.* 2003;196(1):19–41.
- Burga LN, et al. Altered proliferation and differentiation properties of primary mammary epithelial cells from BRCA1 mutation carriers. *Cancer Res.* 2009;69(4):1273–1278.
- Furuta S, Jiang X, Gu B, Cheng E, Chen PL, Lee WH. Depletion of BRCA1 impairs differentiation but enhances proliferation of mammary epithelial cells. *Proc Natl Acad Sci U S A.* 2005;102(26):9176–9181.
- Thompson ME, Jensen RA, Obermiller PS, Page DL, Holt JT. Decreased expression of BRCA1 accelerates growth and is often present during sporadic breast cancer progression. *Nat Genet.* 1995;9(4):444–450.
- Honrado E, Benitez J, Palacios J. The molecular



- pathology of hereditary breast cancer: genetic testing and therapeutic implications. *Mod Pathol*. 2005;18(10):1305–1320.
22. Sorlie T, et al. Repeated observation of breast tumor subtypes in independent gene expression data sets. *Proc Natl Acad Sci U S A*. 2003;100(14):8418–8423.
23. Turner N, Tutt A, Ashworth A. Hallmarks of 'BRCAness' in sporadic cancers. *Nat Rev Cancer*. 2004;4(10):814–819.
24. Wei M, et al. BRCA1 promoter methylation in sporadic breast cancer is associated with reduced BRCA1 copy number and chromosome 17 aneuploidy. *Cancer Res*. 2005;65(23):10692–10699.
25. Futreal PA, et al. BRCA1 mutations in primary breast and ovarian carcinomas. *Science*. 1994;266(5182):120–122.
26. Baldassarre G, et al. Negative regulation of BRCA1 gene expression by HMGA1 proteins accounts for the reduced BRCA1 protein levels in sporadic breast carcinoma. *Mol Cell Biol*. 2003;23(7):2225–2238.
27. Mueller CR, Roskelley CD. Regulation of BRCA1 expression and its relationship to sporadic breast cancer. *Breast Cancer Res*. 2003;5(1):45–52.
28. Antonova L, Mueller CR. Hydrocortisone down-regulates the tumor suppressor gene BRCA1 in mammary cells: a possible molecular link between stress and breast cancer. *Genes Chromosomes Cancer*. 2008;47(4):341–352.
29. Beger C, et al. Identification of Id4 as a regulator of BRCA1 expression by using a ribozyme-library-based inverse genomics approach. *Proc Natl Acad Sci U S A*. 2001;98(1):130–135.
30. Molli PR, Singh RR, Lee SW, Kumar R. MTA1-mediated transcriptional repression of BRCA1 tumor suppressor gene. *Oncogene*. 2008;27(14):1971–1980.
31. Thakur S, et al. Regulation of BRCA1 transcription by specific single-stranded DNA binding factors. *Mol Cell Biol*. 2003;23(11):3774–3787.
32. Marquis ST, et al. The developmental pattern of Brca1 expression implies a role in differentiation of the breast and other tissues. *Nat Genet*. 1995;11(1):17–26.
33. Xu X, et al. Conditional mutation of Brca1 in mammary epithelial cells results in blunted ductal morphogenesis and tumour formation. *Nat Genet*. 1999;22(1):37–43.
34. Kubista M, Rosner M, Kubista E, Bernaschek G, Hengstschlager M. Brca1 regulates in vitro differentiation of mammary epithelial cells. *Oncogene*. 2002;21(31):4747–4756.
35. O'Connell FC, Martin F. Laminin-rich extracellular matrix association with mammary epithelial cells suppresses Brca1 expression. *Cell Death Differ*. 2000;7(4):360–367.
36. Miralem T, Avraham HK. Extracellular matrix enhances heregulin-dependent BRCA1 phosphorylation and suppresses BRCA1 expression through its C terminus. *Mol Cell Biol*. 2003;23(2):579–593.
37. Magdinier F, Dalla Venezia N, Lenoir GM, Frappart L, Dante R. BRCA1 expression during prenatal development of the human mammary gland. *Oncogene*. 1999;18(27):4039–4043.
38. Murtagh J, McArdle E, Gilligan E, Thornton L, Furlong F, Martin F. Organization of mammary epithelial cells into 3D acinar structures requires glucocorticoid and JNK signaling. *J Cell Biol*. 2004;166(1):133–143.
39. Chen F, Capecchi MR. Paralogous mouse Hox genes, Hoxa9, Hoxb9, and Hoxd9, function together to control development of the mammary gland in response to pregnancy. *Proc Natl Acad Sci U S A*. 1999;96(2):541–546.
40. Bruhl T, Urbich C, Aicher D, Acker-Palmer A, Zeiger AM, Dimmeler S. Homeobox A9 transcriptionally regulates the EphB4 receptor to modulate endothelial cell migration and tube formation. *Circ Res*. 2004;94(6):743–751.
41. Chen F, Capecchi MR. Targeted mutations in hoxa-9 and hoxb-9 reveal synergistic interactions. *Dev Biol*. 1997;181(2):186–196.
42. Taylor HS, Vanden Heuvel GB, Igarashi P. A conserved Hox axis in the mouse and human female reproductive system: late establishment and persistent adult expression of the Hoxa cluster genes. *Biol Reprod*. 1997;57(6):1338–1345.
43. Dintilhac A, Bihan R, Guerrier D, Deschamps S, Pellerin I. A conserved non-homeodomain Hoxa9 isoform interacting with CBP is co-expressed with the 'typical' Hoxa9 protein during embryogenesis. *Gene Expr Patterns*. 2004;4(2):215–222.
44. Shen WF, Hu YL, Uttarwar L, Passegue E, Largman C. MicroRNA-126 regulates HOXA9 by binding to the homeobox. *Mol Cell Biol*. 2008;28(14):4609–4619.
45. Reynolds PA, et al. Tumor suppressor p16INK4A regulates polycomb-mediated DNA hypermethylation in human mammary epithelial cells. *J Biol Chem*. 2006;281(34):24790–24802.
46. van't Veer LJ, et al. Gene expression profiling predicts clinical outcome of breast cancer. *Nature*. 2002;415(6871):530–536.
47. van de Vijver MJ, et al. A gene-expression signature as a predictor of survival in breast cancer. *N Engl J Med*. 2002;347(25):1999–2009.
48. Sotiriou C, et al. Gene expression profiles derived from fine needle aspiration correlate with response to systemic chemotherapy in breast cancer. *Breast Cancer Res*. 2002;4(3):R3.
49. Perou CM, et al. Molecular portraits of human breast tumours. *Nature*. 2000;406(6797):747–752.
50. Petty RD, et al. Tumor transcriptome reveals the predictive and prognostic impact of lysosomal protease inhibitors in non-small-cell lung cancer. *J Clin Oncol*. 2006;24(11):1729–1744.
51. Livasy CA, et al. Phenotypic evaluation of the basal-like subtype of invasive breast carcinoma. *Mod Pathol*. 2006;19(2):264–271.
52. Ramaswamy S, Ross KN, Lander ES, Golub TR. A molecular signature of metastasis in primary solid tumors. *Nat Genet*. 2003;33(1):49–54.
53. Weigelt B, Glas AM, Wessels LF, Witteveen AT, Peterse JL, van't Veer LJ. Gene expression profiles of primary breast tumors maintained in distant metastases. *Proc Natl Acad Sci U S A*. 2003;100(26):15901–15905.
54. Kurose K, Hoshaw-Woodard S, Adeyinka A, Lemeshow S, Watson PH, Eng C. Genetic model of multi-step breast carcinogenesis involving the epithelium and stroma: clues to tumour-microenvironment interactions. *Hum Mol Genet*. 2001;10(18):1907–1913.
55. Comings DE, Gade-Andavolu R, Cone LA, Muhleman D, MacMurray JP. A multigene test for the risk of sporadic breast carcinoma. *Cancer*. 2003;97(9):2160–2170.
56. Mani SA, et al. Mesenchyme Forkhead 1 (FOXC2) plays a key role in metastasis and is associated with aggressive basal-like breast cancers. *Proc Natl Acad Sci U S A*. 2007;104(24):10069–10074.
57. Mani SA, et al. The epithelial-mesenchymal transition generates cells with properties of stem cells. *Cell*. 2008;133(4):704–715.
58. Ivshina AV, et al. Genetic reclassification of histologic grade delineates new clinical subtypes of breast cancer. *Cancer Res*. 2006;66(21):10292–10301.
59. Kenny PA, et al. The morphologies of breast cancer cell lines in three-dimensional assays correlate with their profiles of gene expression. *Mol Oncol*. 2007;1(1):84–96.
60. Wang F, et al. Reciprocal interactions between beta1-integrin and epidermal growth factor receptor in three-dimensional basement membrane breast cultures: a different perspective in epithelial biology. *Proc Natl Acad Sci U S A*. 1998;95(25):14821–14826.
61. Wang F, et al. Phenotypic reversion or death of cancer cells by altering signaling pathways in three-dimensional contexts. *J Natl Cancer Inst*. 2002;94(19):1494–1503.
62. Rajan JV, Wang M, Marquis ST, Chodosh LA. Brca2 is coordinately regulated with Brca1 during proliferation and differentiation in mammary epithelial cells. *Proc Natl Acad Sci U S A*. 1996;93(23):13078–13083.
63. Thakur S, Croce CM. Positive regulation of the BRCA1 promoter. *J Biol Chem*. 1999;274(13):8837–8843.
64. Moens CB, Selleri L. Hox cofactors in vertebrate development. *Dev Biol*. 2006;291(2):193–206.
65. Maconochie M, Nonchev S, Morrison A, Krumlauf R. Paralogous Hox genes: function and regulation. *Annu Rev Genet*. 1996;30:529–556.
66. Chang CP, Brocchieri L, Shen WF, Largman C, Cleary ML. Pbx modulation of Hox homeodomain amino-terminal arms establishes different DNA-binding specificities across the Hox locus. *Mol Cell Biol*. 1996;16(4):1734–1745.
67. Beachy PA, Varkey J, Young KE, von Kessler DP, Sun BI, Ekker SC. Cooperative binding of an Ultrabithorax homeodomain protein to nearby and distant DNA sites. *Mol Cell Biol*. 1993;13(11):6941–6956.
68. Xu B, Kim S, Kastan MB. Involvement of Brca1 in S-phase and G(2)-phase checkpoints after ionizing irradiation. *Mol Cell Biol*. 2001;21(10):3445–3450.
69. Choi JS, et al. Comparative genomic hybridization array analysis and real-time PCR reveals genomic copy number alteration for lung adenocarcinomas. *Lung*. 2006;184(6):355–362.
70. Wu Q, et al. DNA methylation profiling of ovarian carcinomas and their in vitro models identifies HOXA9, HOXB5, SCGB3A1, and CRABP1 as novel targets. *Mol Cancer*. 2007;6:45.
71. Abate-Shen C. Deregulated homeobox gene expression in cancer: cause or consequence? *Nat Rev Cancer*. 2002;2(10):777–785.
72. Hartwell KA, Muir B, Reinhardt F, Carpenter AE, Sgroi DC, Weinberg RA. The Spemann organizer gene, Goosecoid, promotes tumor metastasis. *Proc Natl Acad Sci U S A*. 2006;103(50):18969–18974.
73. Stasinopoulos IA, Mironchik Y, Raman A, Wildes F, Winnard P Jr, Raman V. HOXA5-twist interaction alters p53 homeostasis in breast cancer cells. *J Biol Chem*. 2005;280(3):2294–2299.
74. Boudreau N, Andrews C, Srebrow A, Ravanpay A, Cheresch DA. Induction of the angiogenic phenotype by Hox D3. *J Cell Biol*. 1997;139(1):257–264.
75. Myers C, Charboneau A, Boudreau N. Homeobox B3 promotes capillary morphogenesis and angiogenesis. *J Cell Biol*. 2000;148(2):343–351.
76. Boudreau NJ, Varner JA. The homeobox transcription factor Hox D3 promotes integrin alpha5beta1 expression and function during angiogenesis. *J Biol Chem*. 2004;279(6):4862–4868.
77. Coletta RD, et al. The Six1 homeoprotein stimulates tumorigenesis by reactivation of cyclin A1. *Proc Natl Acad Sci U S A*. 2004;101(17):6478–6483.
78. Coletta RD, Christensen KL, Micalizzi DS, Jedlicka P, Varella-Garcia M, Ford HL. Six1 overexpression in mammary cells induces genomic instability and is sufficient for malignant transformation. *Cancer Res*. 2008;68(7):2204–2213.
79. Ruhin-Poncet B, et al. Msx and dlx homeogene expression in epithelial odontogenic tumors. *J Histochem Cytochem*. 2009;57(1):69–78.
80. Lee H, Habas R, Abate-Shen C. MSX1 cooperates with histone H1b for inhibition of transcription and myogenesis. *Science*. 2004;304(5677):1675–1678.
81. Song K, Wang Y, Sassoon D. Expression of Hox-7.1 in myoblasts inhibits terminal differentiation and induces cell transformation. *Nature*. 1992;360(6403):477–481.
82. Ma L, Teruya-Feldstein J, Weinberg RA. Tumour invasion and metastasis initiated by microRNA-10b in breast cancer. *Nature*. 2007;449(7163):682–688.
83. Myers C, Charboneau A, Cheung I, Hanks D, Boudreau N. Sustained expression of homeobox D10 inhibits angiogenesis. *Am J Pathol*. 2002;161(6):2099–2109.
84. Abate-Shen C, et al. Nkx3.1; Pten mutant mice



- develop invasive prostate adenocarcinoma and lymph node metastases. *Cancer Res.* 2003; 63(14):3886-3890.
85. Mullan PB, Quinn JE, Harkin DP. The role of BRCA1 in transcriptional regulation and cell cycle control. *Oncogene.* 2006;25(43):5854-5863.
86. Yoshida K, Miki Y. Role of BRCA1 and BRCA2 as regulators of DNA repair, transcription, and cell cycle in response to DNA damage. *Cancer Sci.* 2004;95(11):866-871.
87. Thorsteinsdottir U, et al. Overexpression of the myeloid leukemia-associated Hoxa9 gene in bone marrow cells induces stem cell expansion. *Blood.* 2002;99(1):121-129.
88. Look AT. Oncogenic transcription factors in the human acute leukemias. *Science.* 1997; 278(5340):1059-1064.
89. Dorsam ST, et al. The transcriptome of the leukemogenic homeoprotein HOXA9 in human hematopoietic cells. *Blood.* 2004;103(5):1676-1684.
90. Ferrell CM, et al. Activation of stem-cell specific genes by HOXA9 and HOXA10 homeodomain proteins in CD34+ human cord blood cells. *Stem Cells.* 2005;23(5):644-655.
91. Boudreau N, Bissell MJ. Extracellular matrix signaling: integration of form and function in normal and malignant cells. *Curr Opin Cell Biol.* 1998; 10(5):640-646.
92. Rhoads K, Arderiu G, Charboneau A, Hansen SL, Hoffman W, Boudreau N. A role for Hox A5 in regulating angiogenesis and vascular patterning. *Lymphat Res Biol.* 2005;3(4):240-252.
93. Turner NC, et al. BRCA1 dysfunction in sporadic basal-like breast cancer. *Oncogene.* 2007; 26(14):2126-2132.
94. Margolin S, Lindblom A. Familial breast cancer, underlying genes, and clinical implications: a review. *Crit Rev Oncog.* 2006;12(1-2):75-113.
95. Tan-Wong SM, French JD, Proudfoot NJ, Brown MA. Dynamic interactions between the promoter and terminator regions of the mammalian BRCA1 gene. *Proc Natl Acad Sci U S A.* 2008;105(13):5160-5165.
96. MacDonald G, Stramwasser M, Mueller CR. Characterization of a negative transcriptional element in the BRCA1 promoter. *Breast Cancer Res.* 2007;9(4):R49.
97. Bindra RS, Glazer PM. Basal repression of BRCA1 by multiple E2Fs and pocket proteins at adjacent E2F sites. *Cancer Biol Ther.* 2006;5(10):1400-1407.
98. Venkitaraman AR. Cancer susceptibility and the functions of BRCA1 and BRCA2. *Cell.* 2002; 108(2):171-182.
99. Hoshino A, et al. Effects of BRCA1 transgene expression on murine mammary gland development and mutagen-induced mammary neoplasia. *Int J Biol Sci.* 2007;3(5):281-291.
100. Russell AJ, et al. Alpha 6 beta 4 integrin regulates keratinocyte chemotaxis through differential GTPase activation and antagonism of alpha 3 beta 1 integrin. *J Cell Sci.* 2003;116(Pt 17):3543-3556.
101. Weaver VM, et al. Reversion of the malignant phenotype of human breast cells in three-dimensional culture and in vivo by integrin blocking antibodies. *J Cell Biol.* 1997;137(1):231-245.
102. Paszek MJ, et al. Tensional homeostasis and the malignant phenotype. *Cancer Cell.* 2005;8(3):241-254.
103. Kinsella TM, Nolan GP. Episomal vectors rapidly and stably produce high-titer recombinant retrovirus. *Hum Gene Ther.* 1996;7(12):1405-1413.
104. Zahir N, et al. Autocrine laminin-5 ligates alpha-6beta4 integrin and activates RAC and NFkappaB to mediate anchorage-independent survival of mammary tumors. *J Cell Biol.* 2003;163(6):1397-1407.
105. Zufferey R, et al. Self-inactivating lentivirus vector for safe and efficient in vivo gene delivery. *J Virol.* 1998;72(12):9873-9880.
106. Weaver VM, et al. beta4 integrin-dependent formation of polarized three-dimensional architecture confers resistance to apoptosis in normal and malignant mammary epithelium. *Cancer Cell.* 2002; 2(3):205-216.
107. Nikiforov MA, et al. TRRAP-dependent and TRRAP-independent transcriptional activation by Myc family oncoproteins. *Mol Cell Biol.* 2002; 22(14):5054-5063.
108. Sogaard TM, Jakobsen CG, Justesen J. A sensitive assay of translational fidelity (readthrough and termination) in eukaryotic cells. *Biochemistry (Mosc).* 1999;64(12):1408-1417.
109. Kroupis C, Stathopoulou A, Zygalki E, Ferekidou L, Talieri M, Lianidou ES. Development and applications of a real-time quantitative RT-PCR method (QRT-PCR) for BRCA1 mRNA. *Clin Biochem.* 2005;38(1):50-57.

SWI/SNF Chromatin Remodeling Enzyme ATPases Promote Cell Proliferation in Normal Mammary Epithelial Cells

NATHALIE COHET,¹ KATHLEEN M. STEWART,² RAJINI MUDHASANI,¹ ANANTHI J. ASIRVATHAM,¹ CHANDRASHEKARA MALLAPPA,¹ KAREN M. IMBALZANO,¹ VALERIE M. WEAVER,² ANTHONY N. IMBALZANO,^{1*} AND JEFFREY A. NICKERSON^{1*}

¹Department of Cell Biology, University of Massachusetts Medical School, Worcester, Massachusetts

²Department of Surgery, Center for Bioengineering and Tissue Regeneration, University of California at San Francisco, San Francisco, California

The ATPase subunits of the SWI/SNF chromatin remodeling enzymes, Brahma (BRM) and Brahma-related gene 1 (BRG1), can induce cell cycle arrest in BRM and BRG1 deficient tumor cell lines, and mice heterozygous for Brg1 are pre-disposed to breast tumors, implicating loss of BRG1 as a mechanism for unregulated cell proliferation. To test the hypothesis that loss of BRG1 can contribute to breast cancer, we utilized RNA interference to reduce the amounts of BRM or BRG1 protein in the nonmalignant mammary epithelial cell line, MCF-10A. When grown in reconstituted basement membrane (rBM), these cells develop into acini that resemble the lobes of normal breast tissue. Contrary to expectations, knockdown of either BRM or BRG1 resulted in an inhibition of cell proliferation in monolayer cultures. This inhibition was strikingly enhanced in three-dimensional rBM culture, although some BRM-depleted cells were later able to resume proliferation. Cells did not arrest in any specific stage of the cell cycle; instead, the cell cycle length increased by approximately 50%. Thus, SWI/SNF ATPases promote cell cycle progression in nonmalignant mammary epithelial cells.

J. Cell. Physiol. 223: 667–678, 2010. © 2010 Wiley-Liss, Inc.

The mammalian SWI/SNF complexes are a family of chromatin-remodeling enzymes that regulate gene expression by disrupting histone–DNA contacts in an ATP-dependent manner (Imbalzano et al., 1994; Kwon et al., 1994). The complexes are evolutionarily conserved in eukaryotes and contain either Brahma (BRM) or Brahma-related gene 1 (BRG1) as the central ATPase subunit (Khavari et al., 1993; Muchardt and Yaniv, 1993; Wang et al., 1996). SWI/SNF enzyme complexes include other proteins known as BRG1 and BRM-associated factors (BAFs) that can modulate the activity of the ATPase subunits and might provide gene-specific recruitment (Wang et al., 1996). The BRM and BRG1 proteins are highly similar, with a sequence identity of 74% in humans, and they display similar enzymatic properties (Khavari et al., 1993; Muchardt and Yaniv, 1993; Chiba et al., 1994; Phelan et al., 1999; Sif et al., 2001). Both are involved in developmental processes in plants, invertebrates, and vertebrates (reviewed in de la Serna et al., 2006; Kwon and Wagner, 2007). Despite these similarities, the two alternative ATPase subunits can serve different functions in the regulation of differentiation, transcriptional control, and other important cell processes (Reyes et al., 1998; Bultman et al., 2000; Kadam and Emerson, 2003).

BRG1 and BRM are important for cell cycle arrest. Reintroduction of BRG1 or BRM into deficient tumor cell lines induces cell cycle arrest and a “flat cell” phenotype by a mechanism requiring RB family members (Dunaief et al., 1994; Strober et al., 1996; Trouche et al., 1997; Zhang et al., 2000; Strobeck et al., 2000b). RB and BRM (or BRG1) cooperate to repress E2F1-mediated activation (Trouche et al., 1997; Wang et al., 2002) and repress levels of CDK2, cyclin A, and cyclin E (Strobeck et al., 2000a,b; Coisy et al., 2004; Roberts and Orkin, 2004). BRM can compensate for BRG1 loss in RB signaling pathways, suggesting a redundancy between the two factors in

this mechanism of cell cycle control (Reisman et al., 2002; Strobeck et al., 2002).

Approximately 10% of mice heterozygous for Brg1 develop tumors, mostly mammary carcinomas (Bultman et al., 2008). This study and earlier work (Bultman et al., 2000) firmly established BRG1 as a tumor suppressor in vivo. Although Brm deficient mice do not present with tumors, depending on the strain background, they can be physically larger, with an increased tissue and organ size because of increased proliferation (Reyes et al., 1998). In addition, immortalized fibroblasts derived from Brm-deficient mouse embryos have a delayed and shorter S-phase, and a prolonged mitosis (Coisy-Quivy et al., 2006). Together, these previous studies indicate that BRG1 and BRM are negative regulators of cell cycle progression in culture and are likely to decrease proliferation in vivo. A logical prediction from this literature would be that the loss of BRG1 or BRM should lead to the loss of growth control, to hyperplasia, and to cancer progression.

Additional Supporting Information may be found in the online version of this article.

Contract grant sponsor: National Cancer Institute;
Contract grant number: PO1 CA82834.

*Correspondence to: Anthony N. Imbalzano and Jeffrey A. Nickerson, Department of Cell Biology, University of Massachusetts Medical School, Lake Avenue North, Worcester, MA 01655. E-mail: anthony.imbalzano@umassmed.edu; jeffrey.nickerson@umassmed.edu

Received 14 December 2009; Accepted 16 December 2009

Published online in Wiley InterScience
(www.interscience.wiley.com.), 23 March 2010.
DOI: 10.1002/jcp.22072

The MCF-10A line immortalized spontaneously in culture from primary cells taken from a patient with fibrocystic disease (Soule et al., 1990). The MCF-10A line has a stable, near-diploid karyotype (Soule et al., 1990; Yoon et al., 2002), but has lost the p16 locus (Yaswen and Stampfer, 2002; Debnath et al., 2003). The cells express wild type p53 (Merlo et al., 1995; Debnath et al., 2003). MCF-10A cells cultured in three-dimensional reconstituted basement membrane (rBM) culture develop important features of normal breast tissue by a program of proliferation, cell cycle arrest, apical—basolateral polarization, and apoptosis to create a luminal space (Debnath et al., 2002, 2003; Underwood et al., 2006). In addition, cell nuclei of mammary epithelial cells forming acini in three-dimensional rBM culture recapitulate the architecture of mammary epithelial cells in tissue (Lelievre et al., 1998).

To address the function of the SWI/SNF ATPases in normal mammary epithelial cells, we generated MCF-10A cells with inducible knockdowns of either BRG1 or BRM. The depletion of either ATPase subunit decreased the rate of cell proliferation without inducing a complete cell growth arrest in monolayer culture. The decrease in proliferation was amplified in three-dimensional rBM culture. Further analysis demonstrated that the length of the cell cycle increased after depletion of either SWI/SNF ATPase, indicating a role for BRG1 and BRM as positive regulators of cell cycle progression.

Materials and Methods

Cell culture

MCF-10A cells from the Karmanos Cancer Institute (Detroit, MI) were maintained in monolayer as described (Debnath et al., 2003).

Doxycycline-inducible BRG1 and BRM knockdowns

Generation of vectors. Lentiviral vectors were from the D. Trono lab (www.tronolab.unige.ch) and obtained from Addgene, Cambridge, MA: pLV-tTRKRAB-Red encoding the TetR-KRAB regulator, pLVTHM, for cloning the shRNA, the packaging vector pCMV-dR8.91 and the Envelope vector pMD2.G. The shRNA sequences for BRG1 and BRM were from previously designed siRNAs (Rosson et al., 2005). Annealed oligonucleotides were cloned in the pSUPER.retro.puro vector then inserted between the EcoRI/ClaI sites of pLVTHM to express the shRNA under the control of the HI promoter. The first forward sequence was 5'-GATCCCCGTGCGACATGTCTGCGCTG TTCAAGACACAGCGCAGACATGTCGCACTTTTTGGAAA-3' where the underlined sequence is specific for the BRG1 ATPase domain. The second forward sequence was 5'-GATCCCCGTCTGAAGATCGTGCTGCTTTCAAGAGAAG-CAGCACGATCTTCAGACTTTTTGGAAA-3' where the underlined sequence is specific for the BRM ATPase domain. The control scrambled (SCRAM) forward sequence was 5'-ATCCCCAGTTACTAGACGCGATCGTTCAAGAGACGATCGCGTCTAGTAACT-GTTTTTA-3'.

For the double BRG1 and BRM knockdown, a new shBRM lentivector was engineered with Gateway[®] Technology (Invitrogen, Carlsbad, CA). The cassette tetO-HI-shBRM was removed from the pLVTHM and cloned in the Entry vector pENTR1A-no ccdB (a gift of Eric Campeau) used to transfer the shBRM expression cassette into a lentiviral destination vector. We used the promoter-less lentiviral destination vector pLenti 2X Puro DEST, clone #w16.1 (E. Campeau), which contains elements that allow packaging of the construct and a puromycin resistance marker for selection of stably transduced cells (Campeau et al., 2009). The LR Recombination Reaction was performed by using the Gateway LR clonase[™] II enzyme Mix (Invitrogen).

Lentivirus production. 5×10^6 293T cells were seeded in a 10 cm dish and transfected the following day with the Lipofectamine[®] 2000 reagent (Invitrogen). Viral supernatants were collected and 0.45 μ m filtered at 48 and 72 h post-transfection, then stored at -80°C .

Transduction of MCF-10A cells. MCF-10A cells at 75% confluence were incubated for 16 h with lentivirus (LV) diluted in growth media containing 8 μ g/ml polybrene. The next day the viruses

were removed, the cells were rinsed twice with PBS, and fresh media were added. Cells were passed twice before FACS sorting. To induce shRNA-GFP expression, Doxycycline was used at 0.01–0.5 μ g/ml.

Cell sorting

To obtain a population of cells expressing the shRNA and GFP under doxycycline control, the cells were FACS-sorted twice. The first sort was of uninduced cells and selected dsRED-positive cells that constitutively expressed the tTR-KRAB protein coupled to the dsRed marker (constitutive expression). The second sort was performed 2 days after doxycycline induction and selected both dsRED- and GFP-positive cells that expressed both shRNA and GFP after doxycycline induction. Cells were FACS selected prior to every experiment.

Western blot analysis

Whole cell extracts were prepared from MCF-10A cells in monolayer culture after trypsinization and two washes with 5 ml of cold $1 \times$ PBS. Then, cells were lysed in 100 μ l Laemmli lysis buffer (1% SDS, 0.04 M Tris—HCl pH 6.8, 6% glycerol, 0.003% bromophenol blue, 0.015 M β -mercaptoethanol) for every 10^6 cells, boiled for 5 min, and stored at -80°C . Proteins were separated on 7.5% SDS—PAGE, transferred to a nitrocellulose membranes, and detected with primary antibodies and ECL detection (Amersham/GE Healthcare Bio-Sciences, Piscataway, NJ). The antibodies used were: BRG1 (dilution 1:1000, anti-serum; de La Serna et al., 2000), BRM (dilution 1:1000, Abcam, Cambridge, MA, ab15597), PI3Kinase p85, H-SH2 domain (dilution 1:1000, Upstate/Millipore, Billerica, MA, cat. no. 06-496), GFP (dilution 1:1000, Roche, Indianapolis, IN, cat. no. 1814460), p21 Waf1/Cip1 (I2D1) Rabbit mAb (dilution 1:1000, Cell Signaling, Beverly, MA, 2947S), p53 (dilution 1:1000, Cell Signaling, 9282), phospho-p53 (Ser15) (dilution 1:1000, Cell Signaling, 9284S), phospho-p53 (Ser46) (dilution 1:1000, Cell Signaling, 2521S), phospho-p53 (Ser20) (dilution 1:1000, Cell Signaling, 9287S), cyclin A (BF683) mouse mAb (dilution 1:1000, Cell Signaling, 4656), mTOR (dilution 1:1000, Millipore, Billerica, MA, 04-385), phospho-mTOR (Ser 2448) (dilution 1:1000, Millipore, 09-213), p70 S6 kinase (S6K) (dilution 1:1000, Millipore, 06-926).

Proliferation assays

Direct cell counting. Cells were grown for 2 days in the presence (pre-induction) or absence of doxycycline (0.05 or 0.1 μ g/ml) prior to seeding in a 12-well plate (4,000 cells/well) with or without doxycycline. Cells were counted daily after trypsin treatment using either a hemacytometer or a ZI Coulter counter.

DNA quantification using the Cyquant cell proliferation kit (Invitrogen). Cells were seeded in a 96-well plate at different densities in triplicate. One plate was prepared per day for the time course. Cell growth was stopped by removing the medium and freezing the plate immediately with storage at -80°C . The kit uses a proprietary green fluorescent dye, Cyquant[®] GR dye, which exhibits strong fluorescence enhancement when bound to DNA. Fluorescence was measured using a fluorescence microplate reader. A reference standard curve (with cell numbers from 50 to 50,000 cells) was used to convert fluorescence values into cell numbers.

Immunofluorescent staining of monolayer cultures

Monolayer cultures were prepared following the methods of Wagner et al. (2003). Before mounting coverslips with Prolong Gold (Invitrogen), cells were stained with DAPI (2 μ g/ml) and DRAQ5 (Alexis, Alexis/Enzo Life Sciences, Plymouth Meeting, PA, 1:5,000) DNA dyes in PBS for 5 min at room temperature then washed once with PBS.

Phospho-histone H3 (serine 10) antibody was from Upstate Millipore. All the secondary antibodies (Alexa Fluor[®] 488 or 568 conjugated) were from Molecular Probes/Invitrogen, Carlsbad, CA. For the observation of expressed fluorescent proteins, cells on coverslips were washed in PBS and directly fixed in 4%

paraformaldehyde in CSK for 50 min, rinsed in TBS—0.05% Tween-20, and stained with DAPI and DRAQ5.

BrdU incorporation assay

Cell cycle length of non-synchronized MCF-10A cells was measured by labeling cells with bromodeoxyuridine (BrdU). 2×10^5 cells were plated on a coverslip in each well of a 6-well dish. At time 0, BrdU was added to the culture medium to a final concentration of 20 μ M. At each time point (1, 5, 10, and 15 h of BrdU incorporation) cells were washed twice with cold DPBS, permeabilized with 0.5% Triton X-100 in CSK buffer for 3 min, and fixed with 4% formaldehyde in CSK buffer for 20 min. All steps were performed on ice. Then cells were washed thrice with PBS-0.5% Tween 20 for 10 min each at room temperature. DNA was denatured by 2 N HCl for 30 min at 37°C, followed by two washes with PBS. All antibodies were diluted in TBS-1. Coverslips were incubated with anti-BrdU (clone BU-33, Sigma-Aldrich, St. Louis, MO, 1:400) for 1 h at 37°C or overnight at 4°C. The second antibody was goat anti-mouse IgG1 coupled to Alexa Fluor 568 (Invitrogen, 1:2,000). After each antibody incubation, cells were rinsed thrice in PBS containing 0.05% Tween 20 for 10 min each at room temperature. Before mounting coverslips with Prolong Gold (Invitrogen), cells were stained with DAPI (2 μ g/ml) and DRAQ5 (Alexis, 1:5,000) diluted in PBS for 5 min at room temperature followed by a last wash with PBS. Images of 10 fields were taken at low magnification and BrdU-positive cells were counted in each field with ImageJ. A linear regression was applied to extrapolate the time needed for 100% to incorporate BrdU. This time is the cell cycle length.

mRNA analysis

RNA was isolated from MCF-10A monolayer culture using Trizol (Invitrogen) and reverse transcribed. The cDNA was amplified using the Qiagen HotStarTaq Master Mix kit (Qiagen, Hilden, Germany, #203445) containing 0.1 μ g of specific primers and SYBR green. RT-PCR and real-time PCR were performed using procedures previously described (Ohkawa et al., 2006). Primers for measuring GAS5 RNA levels were CAG TGT GGC TCT GGA TAG CA (forward) and TTA AGC TGG TCC AGG CAA GT (reverse).

Three-dimensional culture of MCF-10A cells on reconstituted basement membrane

MCF-10A cells were cultured in either Reduced Growth Factor Matrigel without phenol red (lot#11346, BD Biosciences, San Jose, CA) or Non-Reduced Growth Factor Matrigel with phenol red (lot#22704, BD Biosciences) following the procedures of Debnath et al. (2003). Briefly, for overlay cultures, cells were prepared for three-dimensional rBM culture by growing to 20–30% confluency in monolayer and seeding in a single cell suspension on 100 μ l of matrigel in a 35 mm well at 7,000–15,000 cells/well or on 40 μ l matrigel in a 8-well chamber slide at 5,000 cells/well. Cells in rBM were grown in assay media (Debnath et al., 2003) containing 2% horse serum, 5 ng/ml EGF, and 2% Matrigel. All cultures were incubated at 37°C in a 5% CO₂ humidified incubator for up to 20 days. Media was replaced every 2–4 days. Morphology was observed every 2 days via phase contrast microscopy. Acinar size was determined from phase contrast micrographs. Two diameters were measured per acinus with ImageJ software. The minimum number of measured acini per sample was 15.

Cell counting in rBM culture

Three-dimensional cultures were incubated for 30–40 min in a 37°C incubator with 0.25% trypsin—EDTA. As soon as the Matrigel was dissolved, the acinar cell suspension was centrifuged 5 min at 1,000 rpm, the supernatant was discarded and the pellet was resuspended with 0.05% trypsin—EDTA then put back in the dish for incubation at 37°C. When a single cell suspension was

observed, trypsin activity was stopped with resuspension media (DMEM/F12 containing 20% horse serum and antibiotics) and cells were counted by trypan blue exclusion in a hemocytometer, or without trypan blue with an automatic cell counter.

Results

Inducible knockdown of SWI/SNF ATPase subunits in MCF-10A human mammary epithelial cells

We engineered the conditional expression of a short hairpin (sh) sequence targeting BRG1 (Rosson et al., 2005) in the human breast epithelial cell line, MCF-10A (Soule et al., 1990). A doxycycline-inducible LV (Wiznerowicz and Trono, 2003) stably introduced the shRNA gene into MCF-10A cells. Two lentiviral constructs were used. The first expressed the tTR-KRAB transactivator and dsRed (LV-tetR-KRAB-dsRed), whereas the second expressed the shRNA and GFP under tTR-KRAB transcriptional repression (LV-shBRG1i-GFP). We used two different strategies of lentiviral infection without noting any significant difference in outcome. In some experiments, cells were modified in one step by a double infection with both LVs. In other experiments, cells were engineered by sequential infection, first with LV-tetR-KRAB-dsRed and, after sorting for dsRed fluorescence, with LV-shBRG1i-GFP. Pools of cells were FACS sorted for dsRed fluorescence and doxycycline-induced GFP fluorescence, without a requirement for cloning or drug selection (Fig. S1).

This inducible knockdown system was used both in monolayer culture and in three-dimensional culture in rBM. As expected, cultures maintained in the absence of doxycycline constitutively expressed dsRED, which marks cells also expressing the TetR-KRAB repressor (Fig. 1). This repressor prevents expression of the GFP marker and the shRNA, which are both encoded by the second virus. Addition of doxycycline-induced expression of both GFP and the shRNA. Because of the molecular and functional similarity between BRG1 and the other SWI-SNF ATPase subunit, BRM, we also generated MCF-10A cells with an inducible BRM knockdown using the same lentiviral vector system. The control vector conditionally expressed a scrambled sequence shRNA.

We evaluated the efficiency of the BRG1 and BRM knockdown by Western blotting (Fig. 2). Protein lysates were obtained from cells expressing the BRG1 shRNA (BRG1i), the BRM shRNA (BRMi), or the scrambled sequence control shRNA (SCRAM), with or without induction with 0.01 μ g/ml doxycycline in monolayer culture for 3 days. As shown in Figure 2 upper, the protein level of BRG1 was efficiently knocked down in BRG1i cells (compare lanes 4 and 5), but was not decreased in the BRMi cells (compare lanes 6 and 7). Similarly, BRM levels (Fig. 2 lower) were not decreased in BRG1i cells but were greatly reduced in BRMi cells, demonstrating the specificity of each shRNA. GFP expression was monitored as an additional marker of doxycycline induction. Protein levels were measured by quantification of Western blot signals. The knockdown of BRG1 protein in BRG1i cells was determined to be 75%, whereas the knockdown of BRM was 90% in BRMi cells, with minor variations between experiments. Optimizing this inducible system, we determined that 48 h were needed to get maximal protein decrease (Fig. S2) at an optimal concentration of doxycycline of between 0.01 and 0.05 μ g/ml (Fig. S3). We also noticed a small but consistent increase in the amount of BRM protein in the BRG1i cell line (Fig. 2 lower, compare lanes 4 and 5) and a similar small but reproducible increase in the amount of BRG1 in BRMi cells (Fig. 2 upper, compare lanes 6 and 7). These observations suggest a compensation effect in protein levels of the two SWI/SNF ATPase subunits BRG1 and BRM.

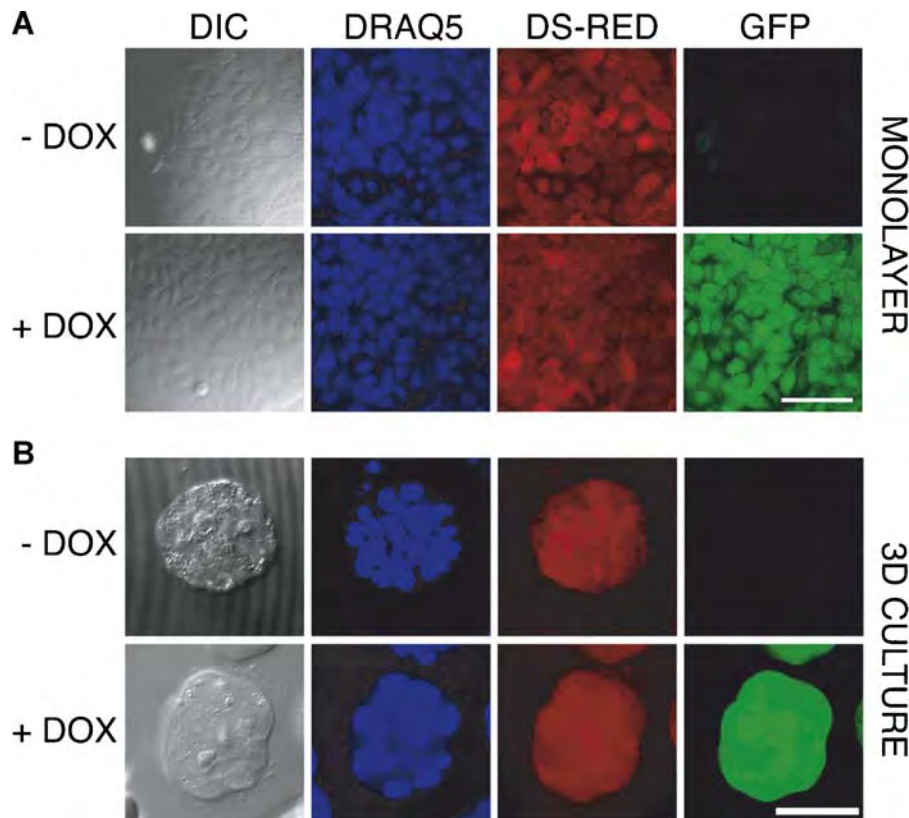


Fig. 1. Doxycycline-inducible shRNA expression in MCF-10A cells. In this system, dsRED and the TET-KRAB regulator are constitutively expressed from the same vector whereas GFP fluorescence is expressed only after doxycycline induction of the shRNA targeting BRG1. Cells were sorted after 2 days of doxycycline induction (0.1 $\mu\text{g}/\text{ml}$). Then, after 5 days of culture without doxycycline, cells were seeded on coverslips and induced or not with 0.05 $\mu\text{g}/\text{ml}$ doxycycline for 3 days before fixing with formaldehyde and staining nuclei with DRAQ5. Confocal image stacks, shown here for the MCF-10A-SCRAM control cell line, were collected for both monolayer (panel 1A, scale bar = 100 μm) and 3D culture (panel 1B, scale bar = 50 μm). The micrographs of the acinus (panel B) were maximum intensity projections. Confocal settings were held constant so that linear quantitative comparisons could be made between samples with and without doxycycline induction.

One concern with siRNA technology is the capacity of dsRNA to trigger a non-specific interferon response in some cellular systems (Bridge et al., 2003; Diebold et al., 2003; Sledz et al., 2003). The inclusion of the scrambled sequence SCRAM controls in every experiment controlled for these effects, but to further validate the system, we directly measured the level of mRNAs coding for the interferon response genes IFITM1, MX1, and OAS1. The results showed that the interferon response was not activated by any of the shRNAs in this experimental system (data not shown).

BRG1 or BRM knockdown impedes the early proliferation stage of MCF-10A acinus formation

Normal MCF-10A mammary epithelial cells, when cultured in three-dimensional rBM culture, reproduce important features of normal breast tissue in a well-characterized temporal and spatial program (Petersen et al., 1992; Weaver et al., 1995, 1997, 2002; Debnath et al., 2002, 2003). An initial stage of proliferation produces loosely connected groups of cells and is followed by cell cycle arrest. Acini form from these groups of cells by basal deposition of a basement membrane and luminal clearance of cells not apposing the basement membrane. Malignant changes in cells alter this program of development in rBM culture with the formation of structures having an altered morphology, loss of cell cycle arrest, and basement membrane-independent cell survival (Imbalzano et al., 2009).

To determine whether the depletion of BRG1 caused these malignant alterations in acinar development, we cultured wild type MCF-10A human mammary epithelial cells, BRG1i cells expressing the doxycycline-inducible shRNA targeting BRG1, and control SCRAM cells in three-dimensional rBM culture. These cells were pre-induced with doxycycline 2 days before being plated on a layer of rBM with an overlay of 2% rBM in culture medium and were maintained in culture for 18 days (Debnath et al., 2003). Twenty-four hours after establishing these overlay cultures, the cells from all three cell lines (wild-type MCF-10A, BRG1i, and SCRAM) had attached to the rBM. After 2 days, all the cell lines formed spherical masses of cells. The diameter of these structures was measured. As shown in Figure 3A,B,D,E from 4 days of culture, the size of the multicellular structures of BRG1i cells expressing the shBRG1 after doxycycline induction were smaller than the structures formed from non-induced BRG1i cells or from controls (SCRAM and wild type MCF-10A). This size difference increased with time in culture (Fig. 3D,E). Dead cells were rare as determined by dye-exclusion. Cell counting, performed after digestion of the extracellular matrix and dissociation of the cell masses, revealed a dramatic decrease in proliferation (Fig. 3C).

BRMi cells with a doxycycline-inducible knockdown of BRM and control SCRAM cells were grown in three-dimensional rBM culture, with conditions matched to the BRG1 knockdown experiments. As illustrated in Figure 4A, the BRMi cells expressing the shBRM with doxycycline produced smaller

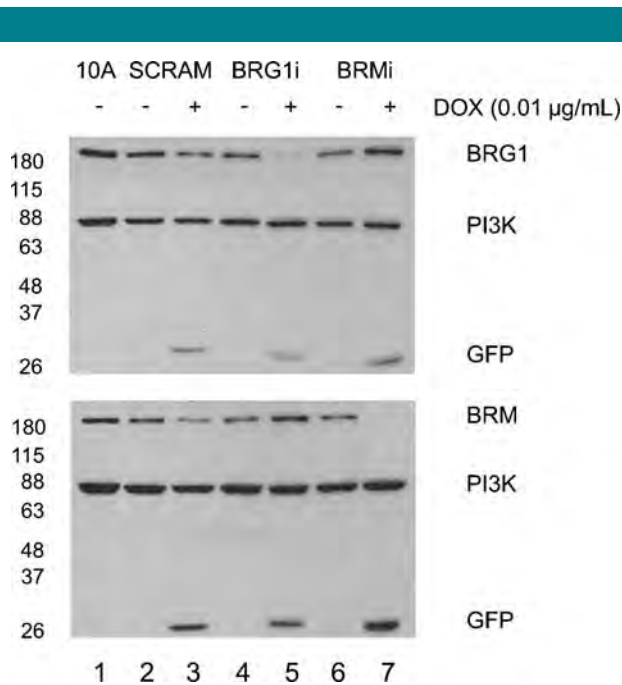


Fig. 2. Doxycycline-inducible knockdown of BRG1 and BRM in MCF-10A cells. Total protein was extracted from cells treated or not for 3 days with 0.01 $\mu\text{g/ml}$ doxycycline. BRG1 (upper gel), BRM (lower gel) and GFP protein expression were examined by Western blotting. The protein of 0.5×10^5 cells per lane was separated by SDS-PAGE (7.5%) and probed with the indicated antibodies. PI3 kinase was the loading control. The migration of protein standards, listed by molecular mass in kilodaltons, is shown to the left of each gel.

multicellular masses than the uninduced BRMi without doxycycline and the SCRAM control cells (data not shown). These changes were clear from day 4 in culture. The median diameter (Fig. 4B) and the size distribution (Fig. 4C) of the multicellular structures were determined. In the early proliferation stage of differentiation (day 0 to day 8), the MCF-10A cells expressing the shBRM (+doxycycline) recapitulated the striking decrease in proliferation observed previously with the BRG1 knockdown MCF-10A cells. An analysis of size distributions (Fig. 4C, compare fraction of acini with a diameter $<40 \mu\text{m}$) showed a larger fraction of small multicellular structures after BRM knockdown than was observed in the controls from day 4 to day 11. However, unlike BRG1i cells, the difference in size between BRMi cells induced to deplete BRM and uninduced cells decreased with time in culture (see Fig. 4A after day 8). A subset of cells escaped from the growth defect and formed multicellular structures that were larger than normal acini. Subsequent work has established that these escaping structures have developed a tumor like phenotype via altered integrin expression (V. M. Weaver, manuscript in preparation).

BRG1 and BRM knockdown decreases proliferation in monolayer culture

To ascertain whether growth in three-dimensional rBM culture was required for this unexpected decrease in proliferation after BRM or BRG1 depletion, we grew the same cell lines with or without doxycycline induction in monolayer culture. After 2 days of pre-induction, we seeded the different cell lines at the same density in 12-well dishes. Each day from day 2 to day 6, cells were trypsinized and counted. A 50% decrease in cell number was observed four or five days after seeding

(Fig. 5A), roughly matching the 4-day delay observed in three-dimensional culture (see Figs. 3 and 4).

To more precisely quantify the proliferation decrease after BRG1 or BRM knockdown, we used a second method that was more robust and sensitive than simple cell counting, eliminated the need for trypsinization, and allowed larger numbers of replicates of each sample. This method measured the density of adherent cells using a dye that fluoresces strongly when bound to cellular nucleic acids, and confirmed the previous results obtained from cell counting. There was a 50% proliferation decrease by day 5 after BRG1 or BRM knockdown (Fig. 5B).

To eliminate the possibility that BRG1 knockdown was only causing the detachment of cells, we manually counted the unattached cells suspended in the culture medium during the 5 days of the proliferation assay. Viability was measured by trypan blue exclusion. There was no increase in the number of detached live or dead cells after knockdown. We also examined whether cellular senescence might explain the reduced proliferation. β -Galactosidase staining marks senescent cells (Dimri et al., 1995) and we observed no increase in β -galactosidase-positive cells after knockdown. We also stained the cell cultures with toluidine blue to observe cell morphology and detect structural changes characteristic of senescent or apoptotic cells. No changes were observed that were characteristic of senescence or programmed cell death.

A decrease of proliferation without complete arrest might be due to an abnormal stimulation of cell contact inhibition. A delay of 4 days for a proliferation decrease to become significant might be explained by this hypothesis. Induction of contact inhibition depends on cell density and might need some time after cell seeding to develop (Nelson and Chen, 2003; Liu et al., 2006; Gray et al., 2008). To determine whether contact inhibition was involved in the decrease of cell proliferation after BRG1 or BRM knockdown, we plated the cell lines on glass coverslips in 6-well plates. After 5 days of doxycycline induction, we immunostained the cells with an antibody that specifically recognizes the mitosis-specific serine 10 phosphorylation of histone H3 (Fig. 6A) (Ajiro et al., 1983; Ajiro and Nishimoto, 1985; Shibata et al., 1990; Goto et al., 1999; Wei et al., 1999; Li et al., 2005; Eberlin et al., 2008). The fraction of cells in mitosis and the location of those mitotic cells within the epithelial colonies were measured (Fig. 6). The overall percentage of cells in mitosis was low, as would be expected after 5 days in culture, but the number of mitotic cells after BRG1 or BRM knock down was reduced ($P < 0.05$) relative to the uninduced control (Fig. 6B). This confirmed the growth inhibition caused by BRG1 or BRM depletion using a third method, and showed that the decrease in proliferation was not caused by a mitotic arrest.

The localization of mitotic cells was scored according to whether they were inside the colony, crowded by other cells, or whether they were at the edge of the colony. As seen in Figure 6A—C, mitotic cells were preferentially located at the edges of colonies. Quantification (Fig. 6C) was consistent with previous studies reporting contact inhibition in MCF-10A cells (Liu et al., 2006). The percent of mitotic cells inside the colonies was about 20% and this was not significantly changed by knockdown of either BRG1 or BRM (Fig. 6B). Taken together these data are inconsistent with the hypothesis that a decrease in cell proliferation after BRG1 or BRM knockdown was caused by the hyper-activation of cell contact inhibition.

Reduction of BRG1 or BRM levels lengthens the cell cycle

FACS sorting of propidium iodide- and DAPI-stained cells showed no significant changes in the fraction of cells in each phase of the cell cycle after reduction of BRG1 or BRM levels. To measure the length of the cell cycle, we performed a time

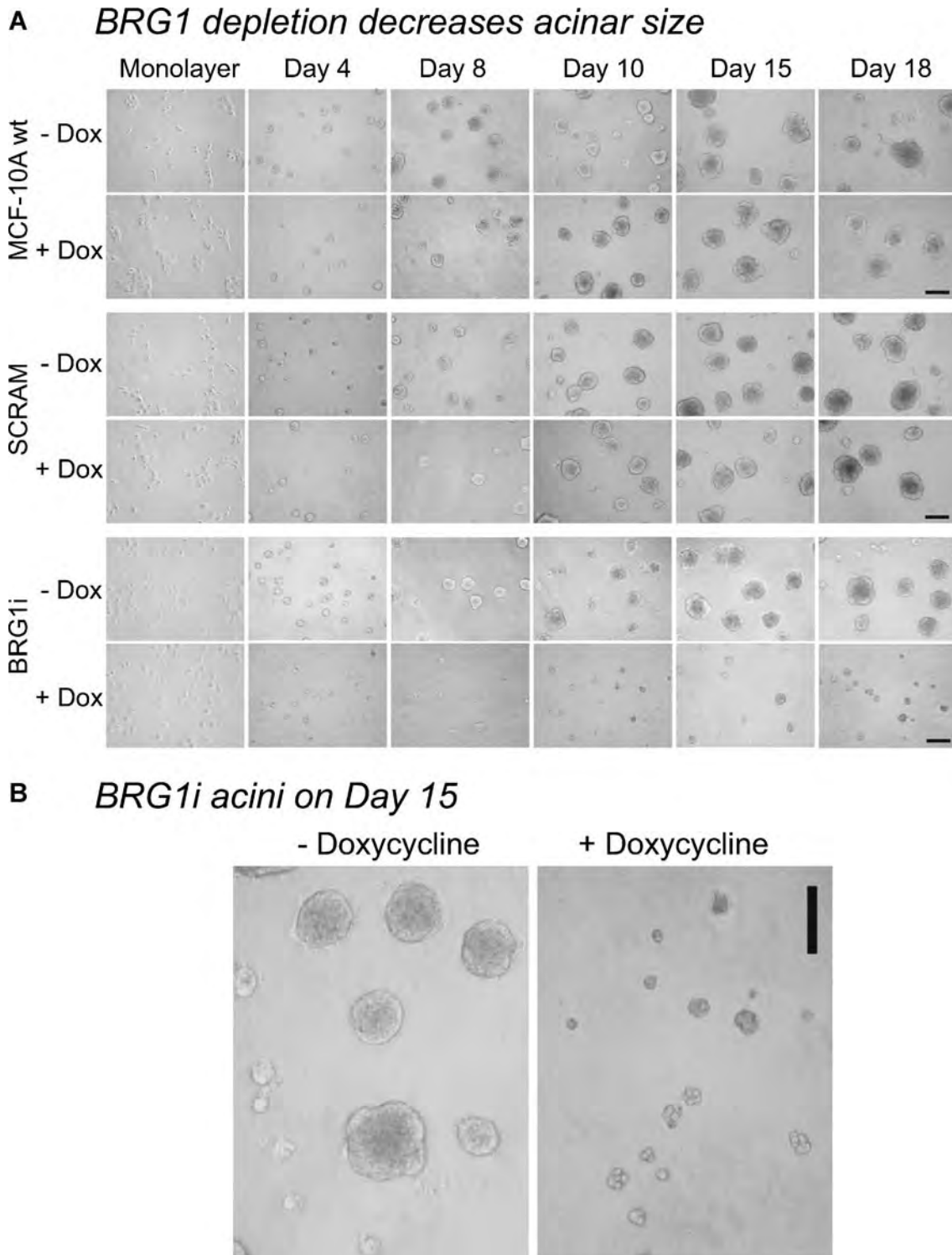


Fig. 3. Decreased proliferation after *BRG1* knockdown in rBM culture. **A:** MCF-10A cells were seeded with or without doxycycline in Matrigel. The micrograph for day 0 shows the initial monolayer culture. Every 2 days, media with or without doxycycline were replaced and phase contrast micrographs were taken. Decreased proliferation was observed from day 4 in MCF-10A cells expressing the shRNA targeting *BRG1* (+doxycycline). Size bar: 150 μm . **B:** Representative micrographs of MCF-10A *BRG1i* acini grown in the presence or absence of doxycycline for 15 days. These pictures were among those used to make the measurements of acinar diameter presented in part D. Size bar: 150 μm . **C:** The three-dimensional Matrigel cultures were trypsinized to obtain a single cell suspension at different times after seeding (days 4 and 9). Then, cells were counted both using a hemacytometer with trypan blue to detect dead cells, and with an automatic cell counter. The asterisk indicates that no increase of trypan blue positive dead cells was detected in the *BRG1i* cells grown with doxycycline. **D:** Median acinar diameter during differentiation. For each cell sample, the median acinus size was calculated ($n \geq 10$ acini with 2 measurements of diameter for each acinus). Statistical analysis was by a Student's *t*-test. The comparisons had a high degree of statistical significance (** $P \leq 0.01$). **E:** Size distribution of acini. The percentage of acini with a diameter smaller than 22 μm , contained in the interval 22–65 μm , 65–110 μm , or greater than 110 μm were calculated.

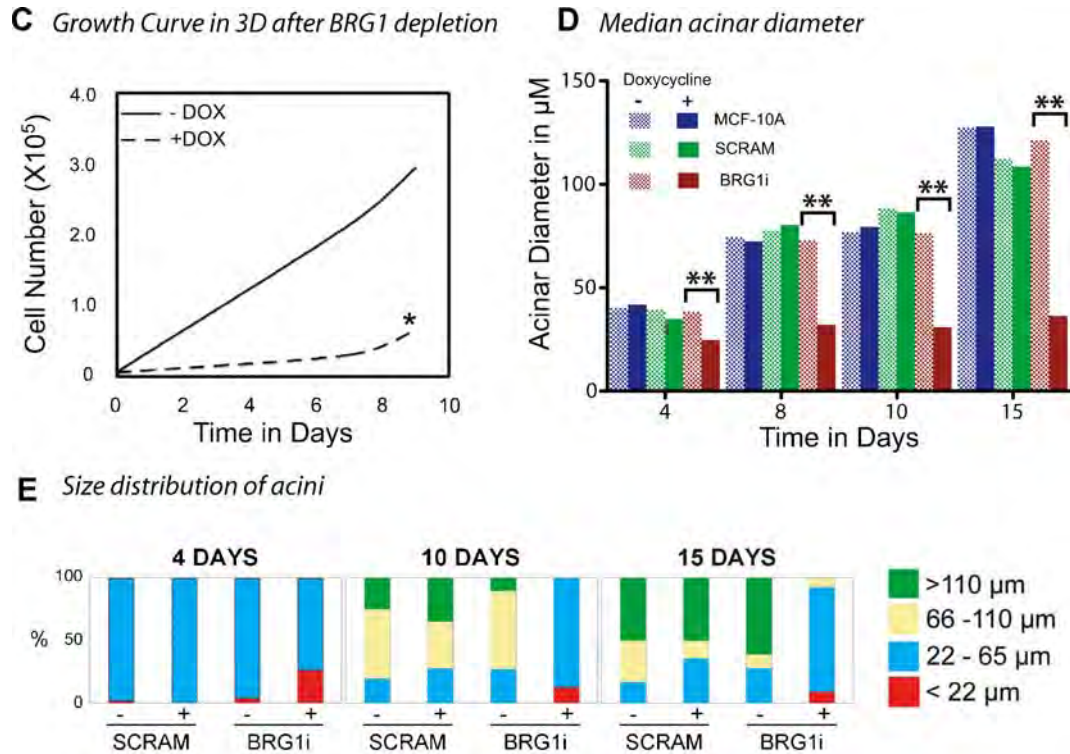


Fig. 3. (Continued)

course experiment after pulse labeling cells with BrdU (Fig. 7). BrdU is only incorporated into DNA during S-phase, so we were able to measure the cell cycle length of each cell line by counting the fraction of BrdU positive cells at different times after pulse labeling. Using a linear regression method, we extrapolated the results to 100% incorporation, which corresponded to the time needed for one complete cell cycle (Fig. 7A). The normal cell cycle length of wild-type MCF-10A cells, control SCRAM cells, and uninduced BRG1 and BRM knockdown cells (no doxycycline) was 18–22 hours (Fig. 7A, B). The induced BRG1 and BRM knockdown cells exhibited a longer cell cycle of 31–32 hours. We concluded that an extra 10–14 hours were needed to complete one cell cycle for MCF-10A cells depleted for either BRG1 or BRM and, consequently, that BRG1 and BRM regulate cell cycle length.

A BRG1-BRM double knockdown is lethal

The reciprocal increase of BRM protein level in BRG1 knockdown MCF-10A cells and an increase in BRG1 levels in BRM knockdown cells (Fig. 2) implicates a compensatory mechanism for these two ATPase subunits. This suggests that a more severe phenotype might result from knocking down both BRM and BRG1. To evaluate this, we created a double knockdown in MCF-10A cells. MCF-10A cells with a doxycycline-inducible knockdown of BRG1 were infected with a LV expressing both shRNA targeting BRM and a puromycin resistance gene. After adding doxycycline and puromycin to the media, most of these cells died and the remaining drug-resistant cells did not show the expected decrease in BRM protein. Presumably, the drug treatment conditions selected for cells that escaped BRM knockdown. As a control, MCF-10A cells expressing only the TetR-KRAB regulator were infected under the same conditions. After selection and doxycycline induction, there

was minimal cell death and these cells showed the expected BRM knockdown (data not shown).

Upregulation of GAS5 in cells depleted for BRM

To address the mechanisms reducing proliferation rates in MCF10-A cells with reduced BRG1 or BRM, a number of cell cycle regulators were examined. Most of these were not altered after BRG1 or BRM knockdown.

One difference observed was in the levels of GAS5 in BRM, but not BRG1, deficient cells. GAS5 is an alternatively spliced, long non-coding RNA with several snoRNAs in its introns (Coccia et al., 1992; Muller et al., 1998; Smith and Steitz, 1998; Raho et al., 2000). Overexpression of specific GAS5 transcripts can induce cell cycle arrest in some cell lines and sensitize cells to apoptotic signals (Mourtada-Maarabouni et al., 2008, 2009). GAS5 was reported to be down-regulated in breast cancer-derived cell lines (Mourtada-Maarabouni et al., 2009). Q-PCR using primers for regions of GAS5 common to all splice variants showed that GAS5 levels were up-regulated in BRM depleted MCF-10A cells, but not BRG1 depleted cells (Fig. 8). Pathways converging on GAS5 are not yet known, but our data establish a correlation between the overexpression of a noncoding RNA that can negatively regulate cell cycle progression and the decreased proliferation of MCF-10A cells after BRM reduction.

Cyclin A has been implicated in cell cycle control by BRG1 during RB-mediated cell cycle arrest (Strobeck et al., 2000b; Zhang et al., 2000) and is a direct target of BRM in some cells (Coisy et al., 2004). We observed no differences in the expression level of cyclin A in either BRG1 or BRM deficient MCF10-A cells (Fig. S4A). The mTOR pathway can also affect cell cycle progression via control of translation (Ma and Blenis, 2009). Western blot analysis of mTOR, phospho-mTOR, and

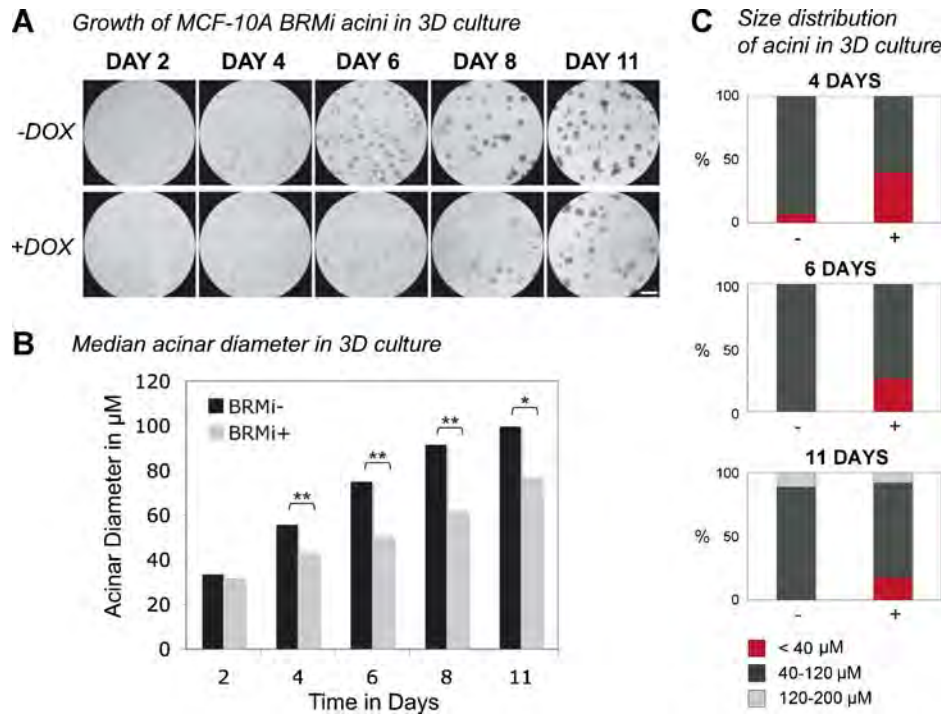


Fig. 4. MCF-10A cells induced to knock down BRM formed acini with a more variable median size in rBM culture. **A:** MCF-10A cells with an inducible BRM knockdown or control scrambled shRNA were seeded in Matrigel overlay culture. Cultures were fed every 2 days with medium containing 0.05 μM doxycycline or medium without doxycycline. Every 2 days phase contrast micrographs were taken of the live cultures. Smaller acini were observed from day 4 in the MCF-10A cells expressing the shRNA targeting BRMi (+doxycycline). No differences in size were observed in MCF-10A cells expressing scrambled shRNA in the presence or absence of doxycycline (data not shown). Size bar: 250 μm . Most acini were smaller after the induced knockdown of BRM, but a few acini were able to escape this decrease in proliferation. **B:** For each cell line and condition, the median acinar diameter was calculated from micrographs including the one in part A. Two measurements of diameter were averaged for each acinus and more than 24 acini were measured for each sample and time point. Statistical analysis was by a Student's *t*-test. The comparisons marked with one asterisk were significant ($P < 0.05$) and those marked with two asterisks (**) were highly significant ($P \leq 0.01$). **C:** The size distribution of acini in 3D culture is shown for the data of parts A and B. The percent of acini with a diameter inferior to 40 μm , contained in the interval 40–120 μm , and contained in the interval 120–200 μm were calculated.

the mTOR downstream target, p70 S6K, showed no changes due to BRG1 or BRM depletion (Fig. S4B).

A recent report indicated that BRG1 depletion activated p53 in several tumor cell lines (Naidu et al., 2009). We examined total p53 and serine-15 phosphorylated p53 protein levels in BRG1- and BRM-depleted MCF10-A cells by Western blot, but observed no increase (Fig. S4C) as might be expected if the p53 pathway were activated.

Discussion

BRG1 and BRM depletion reduces proliferation in MCF-10A mammary epithelial cells

We knocked down BRG1 and BRM in MCF-10A cells, an immortalized but largely normal mammary epithelial cell line (Soule et al., 1990; Yoon et al., 2002). Grown in three-dimensional rBM culture, MCF-10A cells form acini that resemble structures in normal breast tissue (Debnath et al., 2002). Contrary to expectations, we did not observe an increased rate of proliferation in either monolayer or three-dimensional rBM culture. rBM cultures of breast tumor-derived cells (Weaver et al., 1997) or of malignant cells engineered from MCF-10A cells (Miller et al., 1993; Dawson et al., 1996; Strickland et al., 2000; Santner et al., 2001) form larger, disorganized structures without proliferation arrest or lumen formation (Imbalzano et al., 2009). BRG1 depleted MCF-10A cells did not have a tumor-like phenotype. Instead,

the cells grew more slowly in monolayer culture and, in rBM culture, they failed to expand or form acini. MCF-10A cells with reduced BRM levels also proliferated more slowly on average in both monolayer and for the first 6 days in three-dimensional rBM culture.

Multiple methods confirmed the decrease in proliferation of both BRG1 and BRM knockdown MCF-10A cells. In monolayer culture, cells having reduced levels of BRG1 or BRM did not arrest in any specific phase of the cell cycle. BrdU incorporation kinetics definitively showed that cells having reduced levels of BRG1 or BRM simply took longer to traverse the cell cycle. The conclusions that can be reached from these studies are that BRG1 and BRM act as positive regulators of cell cycle progression and BRG1 is required for acinus formation in three-dimensional rBM culture.

MCF-10A cells expressing shRNA targeting either BRG1 or BRM showed nearly identical decreases in proliferation and increases in cell cycle length in monolayer culture. However, the cells remained proliferative, which suggests that either protein is sufficient to support some proliferation. The proteins are similar structurally and, while some functions are unique to one or the other ATPase (Kadam and Emerson, 2003), there are also circumstances where the one ATPase can compensate for the absence of the other (Reyes et al., 1998; Strobeck et al., 2002). Given that cells died when we attempted to knock down both BRG1 and BRM, and that in the absence of one protein the levels of the other increased (Fig. 2), we propose that either BRG1 or BRM is necessary to promote cell proliferation and

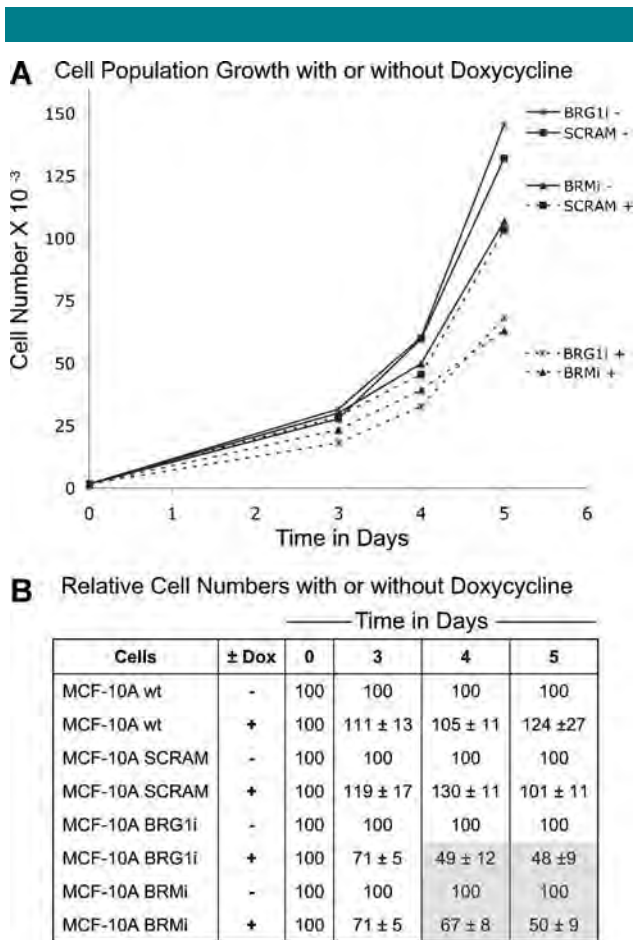


Fig. 5. The knockdown of BRG1 slowed proliferation in MCF-10A cells grown in monolayer culture. **A:** Growth curves for MCF-10A cells after BRG1 or BRM shRNA knockdown, or expressing a scrambled sequence shRNA (SCRAM). Cells were pre-incubated for 2 days with 0.05 μ g/ml doxycycline (+) before being seeded in a 12-well dish at 1,500 cells per well at day 0. Control cells (-) were not treated with doxycycline and did not express the shRNA. Cells were trypsinized and then counted each day from day 2 to day 5. **B:** Cell proliferation was measured every day by quantifying DNA (Cyquant kit) in parallel with the cell counting of part A. The decrease of proliferation was quantified by calculating the ratio (%) of the cell number with doxycycline to the cell number of the matched doxycycline-free control.

that the cells undergo some form of compensation to increase the levels of the remaining protein when the other is knocked down.

Recently, two reports have established a BRG1 requirement for cell proliferation. These reports differ from the present study in the cell types examined, which suggests that the function of BRG1, and likely BRM, is cell context dependent. In several tumor cell lines with wild type p53, the depletion of BRG1, but not the depletion of BRM, led to activation of p53 and cell senescence (Naidu et al., 2009). In contrast, our results are in a non-tumorigenic cell and do not implicate the p53 pathway. A second study using adult fibroblasts from mice that are deficient for Brm and/or Brg1 showed that the absence of Brg1, but not the absence of Brm, decreased genome integrity, leading to aberrant mitoses and decreased proliferative capacity (Bourgo et al., 2009). In contrast, our results implicate both BRG1 and BRM in promoting cell proliferation.

Efforts to address the mechanisms responsible for decreased proliferation showed that neither the p53 nor the mTOR

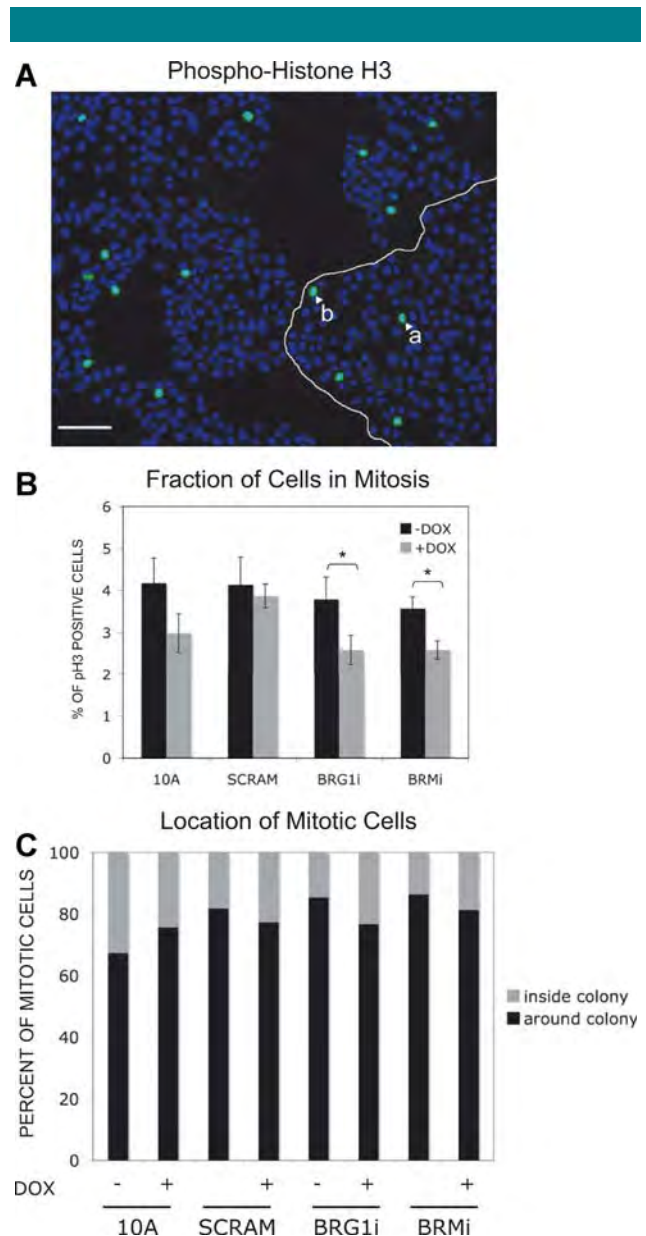


Fig. 6. The knockdown of BRG1 or of BRM reduced the percentage of cells MCF-10A cells in monolayer culture that were in mitosis.

A: In this micrograph, nuclei are stained blue with DAPI and mitotic cells are identified by immunostaining for serine 10 phosphorylated Histone H3 (green) Size bar: 100 μ m. The number of mitotic cells was determined, along with their position in the colonies. For example, on this picture, the white arrows show one peripheral (b) and one internal mitotic (a) cell. **B:** This histogram compares the percentage of mitotic cells at all positions within colonies after 7 days in the presence or absence of doxycycline. The asterisk indicates a difference that had statistical significance ($P \leq 0.05$). **C:** The position of mitotic cells in MCF-10A monolayer colonies was scored from micrographs including that of part A. The compiled data quantify the percentage of mitotic cells at the periphery of the colony and the percentage at interior positions. For each cell sample, $n \geq 2,000$ cells.

pathways were altered in BRG1 or BRM knockdown MCF-10A cells. We did find that BRM, but not BRG1, deficient cells contained elevated levels of the large non-coding RNA, GAS5. GAS5 is an inhibitor of cell cycle progression, but is also reported to sensitize cells to apoptotic signaling (Mourtada-Maarabouni et al., 2009). We observed no apoptosis after BRM knockdown. The correlation between cell cycle length and

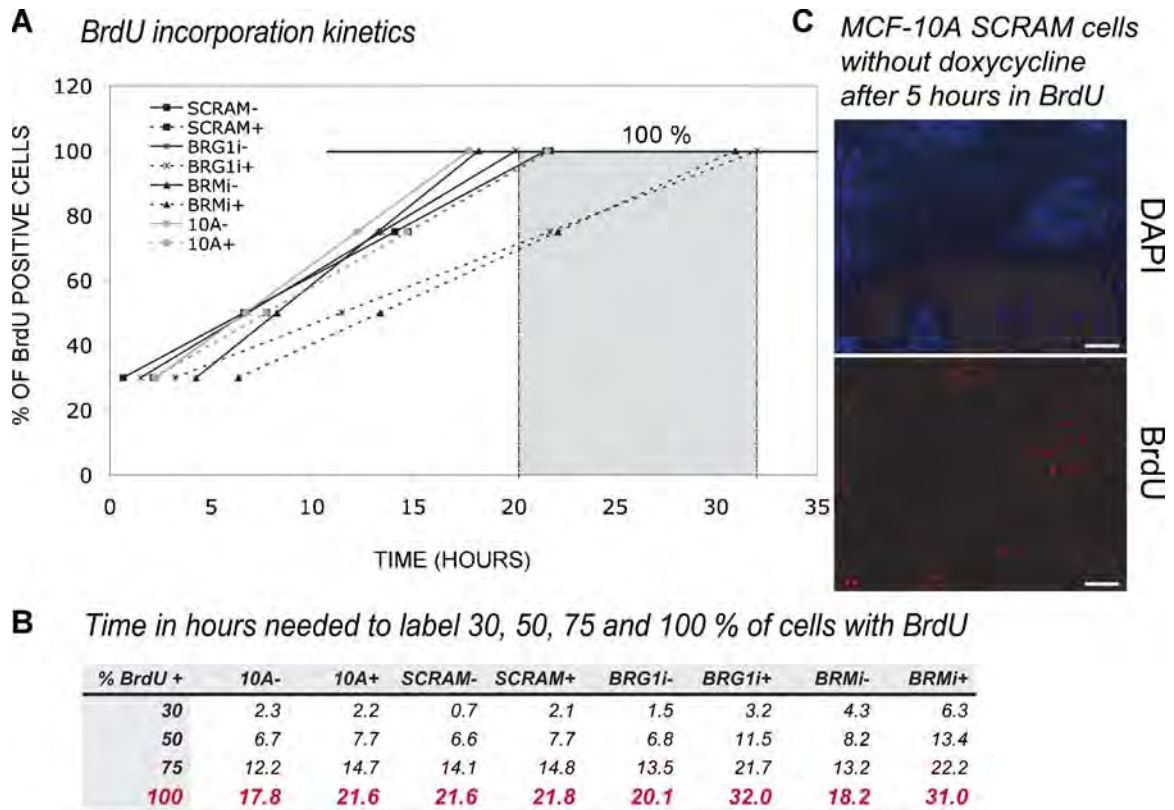


Fig. 7. The knockdown of *BRG1* or of *BRM* increased the length of the cell cycle as determined by pulse labeling with BrdU. **A:** Cell cycle length was measured from a time course of BrdU incorporation. The graph plots the percent of BrdU positive cells as a function of time in hours. A linear extrapolation to the time when 100% of cells were BrdU-positive cells calculated the mean length of a single cell cycle. **B:** Calculated according to the linear regression method, the time in hours needed for 30%, 50%, 75% and 100% of cells to become BrdU-positive. **C:** A representative micrograph from which the measurements of parts **A** and **B** were made shows MCF-10A cells with the SCRAM control shRNA in absence of doxycycline after 5 hours in BrdU. The number of BrdU positive cells (lower) and the number of total cells (upper, DAPI fluorescence) were counted. Seven fields were analyzed for each group in each of two independent experiments.

elevated *GAS5* RNA was observed only for *BRM*-deficient MCF-10A cells, despite the similar decrease in cell proliferation rate observed after *BRG1* knockdown. The mechanisms by which *BRG1* and *BRM* alter cell cycle progression may be different.

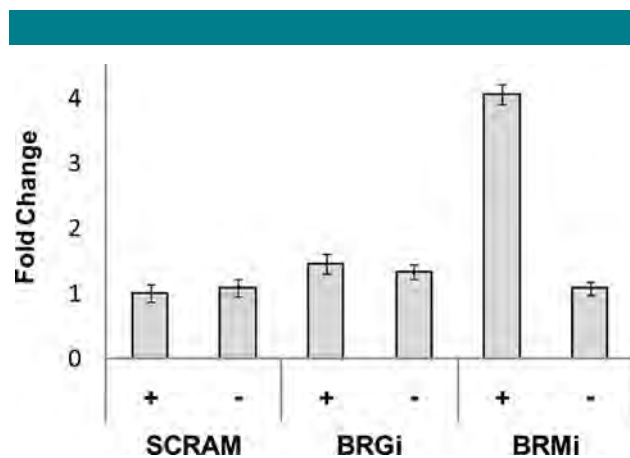


Fig. 8. Overexpression of *GAS5* RNA in *BRM*, but not *BRG1*, deficient cells. Real-time PCR analysis of *GAS5* RNA levels in each cell line. The data represent the mean plus or minus a standard deviation for three independent experiments.

BRG1 in breast cancer progression

There are numerous links between *BRG1*, *BRM*, and cancer. While *Brg1* null mice are embryonic lethal, heterozygous *Brg1* mice have an increased susceptibility to epithelial tumors of the breast (Bultman et al., 2000, 2008). Tissue-specific knockout of one *Brg1* allele in the lung potentiates tumor formation in an induced carcinogenesis model (Glaros et al., 2008). In contrast, *Brm* null mice are viable and do not have increased tumor rates, a result attributed to compensation for *Brm* loss by elevated levels of *Brg1* (Reyes et al., 1998). In addition, the knockout of *Brm* does not cause additional tumors in *Brg1*^{+/-} mice (Bultman et al., 2008). Despite the lack of tumor formation in *Brm* null mice, the levels and localization of *BRM* have prognostic value in staging human lung tumors (Reisman et al., 2003; Fukuoka et al., 2004).

Our results strongly suggest that, at least in normal mammary epithelial cells, reduction of *BRG1* or *BRM* protein levels does not cause a loss of proliferation control leading to accelerated growth. These are different results than those obtained in prior studies using tumor cells, where loss of *BRG1/BRM* accelerates proliferation. This transformation-specific difference might be due to additional genetic lesions accumulating in cancer cells prior to loss of *BRG1* or *BRM* function.

In conclusion, both *BRG1* and *BRM* are positive regulators of normal mammary cell cycle progression. Despite previous studies indicating that loss of one *Brg1* allele predisposes mice

to breast tumors, significant reduction of BRG1 levels in normal but immortalized human mammary epithelial cells does not promote properties associated with tumor or transformed cells. This suggests that reduction of BRG1 levels is not sufficient for mammary epithelial cell transformation. BRG1 is required for acinus formation in three-dimensional rBM culture, a model system that recapitulates many aspects of normal breast tissue development. These results are consistent with previous observations that functional SWI/SNF ATPases are necessary for the development and differentiation of many tissue types (reviewed in de la Serna et al., 2006). We propose that SWI/SNF ATPases, and BRG1 in particular, contribute to normal cell growth and differentiation, whereas the contribution of BRG1 deficiency to oncogenesis requires additional genetic changes.

Acknowledgments

This work was funded by the National Cancer Institute (PO1 CA82834). We thank Eric Campeau (UMass Medical School) for contributing LV vectors, including the pLenti 2X Puro DEST vector of his design, and for his advice and support. Timothy Pasek provided valuable technical assistance. Samisubbu Naidu and Elliott Androphy provided helpful discussion and antibodies, and Jean Underwood generously provided microscopy support. We acknowledge additional support from DOD grants DAMD17-01-1-0368 and W81XWH-05-1-330 to VMW. Core facilities were subsidized by Diabetes Endocrinology Research Center grant P30 DK32520.

Literature Cited

- Ajiro K, Nishimoto T. 1985. Specific site of histone H3 phosphorylation related to the maintenance of premature chromosome condensation. Evidence for catalytically induced interchange of the subunits. *J Biol Chem* 260:15379–15381.
- Ajiro K, Nishimoto T, Takahashi T. 1983. Histone H1 and H3 phosphorylation during premature chromosome condensation in a temperature-sensitive mutant (tsBN2) of baby hamster kidney cells. *J Biol Chem* 258:4534–4538.
- Bourgo RJ, Siddiqui H, Fox S, Solomon D, Sansam CG, Yaniv M, Muchardt C, Metzger D, Chambon P, Roberts CW, Knudsen ES. 2009. SWI/SNF-Deficiency Results in aberrant chromatin organization, mitotic failure, and diminished proliferative capacity. *Mol Biol Cell* 20:3192–3199.
- Bridge AJ, Pebernard S, Ducraux A, Nicoulaz AL, Iggo R. 2003. Induction of an interferon response by RNAi vectors in mammalian cells. *Nat Genet* 34:263–264.
- Bultman S, Gebuhr T, Yee D, La Mantia C, Nicholson J, Gilliam A, Randazzo F, Metzger D, Chambon P, Crabtree G, Magnuson T. 2000. A Brg1 null mutation in the mouse reveals functional differences among mammalian SWI/SNF complexes. *Mol Cell* 6:1287–1295.
- Bultman SJ, Herschkowitz JI, Godfrey V, Gebuhr TC, Yaniv M, Perou CM, Magnuson T. 2008. Characterization of mammary tumors from Brg1 heterozygous mice. *Oncogene* 27:460–468.
- Campeau E, Ruhl VE, Rodier F, Smith CL, Rahmberg BL, Fuss JO, Campisi J, Yaswen P, Cooper PK, Kaufman PD. 2009. A versatile viral system for expression and depletion of proteins in mammalian cells. *PLoS ONE* 4:e6529.
- Chiba H, Muramatsu M, Nomoto A, Kato H. 1994. Two human homologues of *Saccharomyces cerevisiae* SWI2/SNF2 and *Drosophila* brahma are transcriptional coactivators cooperating with the estrogen receptor and the retinoic acid receptor. *Nucleic Acids Res* 22:1815–1820.
- Coccia EM, Cicala C, Charlesworth A, Ciccarelli C, Rossi GB, Philipson L, Sorrentino V. 1992. Regulation and expression of a growth arrest-specific gene (gas5) during growth, differentiation, and development. *Mol Cell Biol* 12:3514–3521.
- Coisy M, Roure V, Ribot M, Philips A, Muchardt C, Blanchard JM, Dantoni JC. 2004. Cyclin A repression in quiescent cells is associated with chromatin remodeling of its promoter and requires Brahma/SNF2alpha. *Mol Cell* 15:43–56.
- Coisy-Quivy M, Disson O, Roure V, Muchardt C, Blanchard JM, Dantoni JC. 2006. Role for Brm in cell growth control. *Cancer Res* 66:5069–5076.
- Dawson PJ, Wolman SR, Tait L, Heppner GH, Miller FR. 1996. MCF10AT: a model for the evolution of cancer from proliferative breast disease. *Am J Pathol* 148:313–319.
- de la Serna IL, Carlson KA, Hill DA, Guidi CJ, Stephenson RO, Sif S, Kingston RE, Imbalzano AN. 2000. Mammalian SWI—SNF complexes contribute to activation of the hsp70 gene. *Mol Cell Biol* 20:2839–2851.
- de la Serna IL, Ohkawa Y, Imbalzano AN. 2006. Chromatin remodeling in mammalian differentiation: lessons from ATP-dependent remodelers. *Nat Rev Genet* 7:461–473.
- Debnath J, Mills KR, Collins NL, Reginato MJ, Muthuswamy SK, Brugge JS. 2002. The role of apoptosis in creating and maintaining luminal space within normal and oncogene-expressing mammary acini. *Cell* 111:29–40.
- Debnath J, Muthuswamy SK, Brugge JS. 2003. Morphogenesis and oncogenesis of MCF-10A mammary epithelial acini grown in three-dimensional basement membrane cultures. *Methods* 30:256–268.
- Diebold SS, Montoya M, Unger H, Alexopoulou L, Roy P, Haswell LE, Al-Shamkhani A, Flavell R, Borrows P, Reis e Sousa C. 2003. Viral infection non-plasmacytoid dendritic cells into high interferon producers. *Nature* 424:324–328.
- Dimri GP, Lee X, Basile G, Acosta M, Scott G, Roskelley C, Medrano EE, Linskens M, Rubelj I, Pereira-Smith O, et al. 1995. A biomarker that identifies senescent human cells in culture and in aging skin in vivo. *Proc Natl Acad Sci USA* 92:9363–9367.
- Dunaief JL, Strober BE, Guha S, Khavari PA, Alin K, Luban J, Begemann M, Crabtree GR, Goff SP. 1994. The retinoblastoma protein and BRG1 form a complex and cooperate to induce cell cycle arrest. *Cell* 79:119–130.
- Eberlin A, Grauffel C, Oulad-Abdelghani M, Robert F, Torres-Padilla ME, Lambrot R, Spohner D, Ponce-Perez L, Wurtz JM, Stote RH, Kimmins S, Schultz P, Dejaegere A, Tora L. 2008. Histone H3 tails containing dimethylated lysine and adjacent phosphorylated serine modifications adopt a specific conformation during mitosis and meiosis. *Mol Cell Biol* 28:1739–1754.
- Farrants AK. 2008. Chromatin remodelling and actin organisation. *FEBS Lett* 582:2041–2050.
- Fukuoka J, Fujii T, Shih JH, Dracheva T, Meerzaman D, Player A, Hong K, Settnek S, Gupta A, Buetow K, Hewitt S, Travis WD, Jen J. 2004. Chromatin remodeling factors and BRM/BRG1 expression as prognostic indicators in non-small cell lung cancer. *Clin Cancer Res* 10:4314–4324.
- Glaros S, Cirrincione GM, Palanca A, Metzger D, Reisman D. 2008. Targeted knockout of BRG1 potentiates lung cancer development. *Cancer Res* 68:3689–3696.
- Goto H, Tomono Y, Ajiro K, Kosako H, Fujita M, Sakurai M, Okawa K, Iwamatsu A, Okigaki T, Takahashi T, Inagaki M. 1999. Identification of a novel phosphorylation site on histone H3 coupled with mitotic chromosome condensation. *J Biol Chem* 274:25543–25549.
- Gray DS, Liu WF, Shen CJ, Bhadriraju K, Nelson CM, Chen CS. 2008. Engineering amount of cell-cell contact demonstrates biphasic proliferative regulation through RhoA and the actin cytoskeleton. *Exp Cell Res* 314:2846–2854.
- Imbalzano AN, Kwon H, Green MR, Kingston RE. 1994. Facilitated binding of TATA-binding protein to nucleosomal DNA. *Nature* 370:481–485.
- Imbalzano KM, Tatarikova I, Imbalzano AN, Nickerson JA. 2009. Increasingly transformed MCF-10A cells have a progressively tumor-like phenotype in three-dimensional basement membrane culture. *Cancer Cell Int* 9:7.
- Kadam S, Emerson BM. 2003. Transcriptional specificity of human SWI/SNF BRG1 and BRM chromatin remodeling complexes. *Mol Cell* 11:377–389.
- Khavari PA, Peterson CL, Tamkun JW, Crabtree GR. 1993. BRG1 contains a conserved domain of the SWI2/SNF2 family necessary for normal mitotic growth and transcription. *Nature* 366:170–174.
- Kwon CS, Wagner D. 2007. Unwinding chromatin for development and growth: a few genes at a time. *Trends Genet* 23:403–412.
- Kwon H, Imbalzano AN, Khavari PA, Kingston RE, Green MR. 1994. Nucleosome disruption and enhancement of activator binding by a human SWI/SNF complex. *Nature* 370:477–481.
- Lelievre SA, Weaver VM, Nickerson JA, Larabell CA, Bhaumik A, Petersen OW, Bissell MJ. 1998. Tissue phenotype depends on reciprocal interactions between the extracellular matrix and the structural organization of the nucleus. *Proc Natl Acad Sci USA* 95:1471–1476.
- Li DW, Yang Q, Chen JT, Zhou H, Liu RM, Huang XT. 2005. Dynamic distribution of Ser-10 phosphorylated histone H3 in cytoplasm of MCF-7 and CHO cells during mitosis. *Cell Res* 15:120–126.
- Liu WF, Nelson CM, Pirone DM, Chen CS. 2006. E-cadherin engagement stimulates proliferation via Rac1. *J Cell Biol* 173:431–441.
- Ma XM, Blenis J. 2009. Molecular mechanisms of mTOR-mediated translational control. *Nat Rev Mol Cell Biol* 10:307–318.
- Merlo GR, Basolo F, Fiore L, Duboc L, Hynes NE. 1995. p53-dependent and p53-independent activation of apoptosis in mammary epithelial cells reveals a survival function of EGF and insulin. *J Cell Biol* 128:1185–1196.
- Miller FR, Soule HD, Tait L, Pauley RJ, Wolman SR, Dawson PJ, Heppner GH. 1993. Xenograft model of progressive human proliferative breast disease. *J Natl Cancer Inst* 85:1725–1732.
- Mourtaada-Maarabouni M, Hedge VL, Kirkham L, Farzaneh F, Williams GT. 2008. Growth arrest in human T-cells is controlled by the non-coding RNA growth-arrest-specific transcript 5 (GASS). *J Cell Sci* 121:939–946.
- Mourtaada-Maarabouni M, Pickard MR, Hedge VL, Farzaneh F, Williams GT. 2009. GASS, a non-protein-coding RNA, controls apoptosis and is downregulated in breast cancer. *Oncogene* 28:195–208.
- Muchardt C, Yaniv M. 1993. A human homologue of *Saccharomyces cerevisiae* SNF2/SWI2 and *Drosophila* brm genes potentiates transcriptional activation by the glucocorticoid receptor. *EMBO J* 12:4279–4290.
- Muller AJ, Chatterjee S, Teresky A, Levine AJ. 1998. The gas5 gene is disrupted by a frameshift mutation within its longest open reading frame in several inbred mouse strains and maps to murine chromosome 1. *Mamm Genome* 9:773–774.
- Naidu SR, Love IM, Imbalzano AN, Grossman SR, Androphy EJ. 2009. The SWI/SNF chromatin remodeling subunit BRG1 is a critical regulator of p53 necessary for proliferation of malignant cells. *Oncogene* 28:2492–2501.
- Nelson CM, Chen CS. 2003. VE-cadherin simultaneously stimulates and inhibits cell proliferation by altering cytoskeletal structure and tension. *J Cell Sci* 116:3571–3581.
- Ohkawa Y, Marfella CG, Imbalzano AN. 2006. Skeletal muscle specification by myogenin and Mef2D via the SWI/SNF ATPase Brg1. *EMBO J* 25:490–501.
- Petersen OW, Ronnov-Jessen L, Howlett AR, Bissell MJ. 1992. Interaction with basement membrane serves to rapidly distinguish growth and differentiation pattern of normal and malignant human breast epithelial cells. *Proc Natl Acad Sci USA* 89:9064–9068.
- Phelan ML, Sif S, Narlikar GJ, Kingston RE. 1999. Reconstitution of a core chromatin remodeling complex from SWI/SNF subunits. *Mol Cell* 3:247–253.
- Raho G, Barone V, Rossi D, Philipson L, Sorrentino V. 2000. The gas 5 gene shows four alternative splicing patterns without coding for a protein. *Gene* 256:13–17.
- Reisman DN, Strobeck MW, Betz BL, Sciarrotta J, Funkhouser W Jr, Murchardt C, Yaniv M, Sherman LS, Knudsen ES, Weissman BE. 2002. Concomitant down-regulation of BRM and BRG1 in human tumor cell lines: differential effects on RB-mediated growth arrest vs CD44 expression. *Oncogene* 21:1196–1207.
- Reisman DN, Sciarrotta J, Wang W, Funkhouser WK, Weissman BE. 2003. Loss of BRG1/BRM in human lung cancer cell lines and primary lung cancers: correlation with poor prognosis. *Cancer Res* 63:560–566.
- Reyes JC, Barra J, Muchardt C, Camus A, Babinet C, Yaniv M. 1998. Altered control of cellular proliferation in the absence of mammalian brahma (SNF2alpha). *EMBO J* 17:6979–6991.
- Roberts CW, Orkin SH. 2004. The SWI/SNF complex—Chromatin and cancer. *Nat Rev Cancer* 4:133–142.
- Rosson GB, Bartlett C, Reed W, Weissman BE. 2005. BRG1 loss in MiaPaCa2 cells induces an altered cellular morphology and disruption in the organization of the actin cytoskeleton. *J Cell Physiol* 205:286–294.
- Santner SJ, Dawson PJ, Tait L, Soule HD, Eliason J, Mohamed AN, Wolman SR, Heppner GH, Miller FR. 2001. Malignant MCF10CA1 cell lines derived from premalignant human breast epithelial MCF10AT cells. *Breast Cancer Res Treat* 65:101–110.

- Shibata K, Inagaki M, Ajiro K. 1990. Mitosis-specific histone H3 phosphorylation in vitro in nucleosome structures. *Eur J Biochem* 192:87–93.
- Sif S, Saurin AJ, Imbalzano AN, Kingston RE. 2001. Purification and characterization of mSin3A-containing Brg1 and hBrm chromatin remodeling complexes. *Genes Dev* 15:603–618.
- Sledz CA, Holko M, de Veer MJ, Silverman RH, Williams BR. 2003. Activation of the interferon system by short-interfering RNAs. *Nat Cell Biol* 5:834–839.
- Smith CM, Steitz JA. 1998. Classification of gas5 as a multi-small-nucleolar-RNA (snoRNA) host gene and a member of the 5'-terminal oligopyrimidine gene family reveals common features of snoRNA host genes. *Mol Cell Biol* 18:6897–6909.
- Soule HD, Maloney TM, Wolman SR, Peterson VWD Jr, Brenz R, McGrath CM, Russo J, Pauley RJ, Jones RF, Brooks SC. 1990. Isolation and characterization of a spontaneously immortalized human breast epithelial cell line, MCF-10. *Cancer Res* 50:6075–6086.
- Strickland LB, Dawson PJ, Santner SJ, Miller FR. 2000. Progression of premalignant MCF10AT generates heterogeneous malignant variants with characteristic histologic types and immunohistochemical markers. *Breast Cancer Res Treat* 64:235–240.
- Strobeck MW, Fribourg AF, Puga A, Knudsen ES. 2000a. Restoration of retinoblastoma mediated signaling to Cdk2 results in cell cycle arrest. *Oncogene* 19:1857–1867.
- Strobeck MW, Knudsen KE, Fribourg AF, DeCristofaro MF, Weissman BE, Imbalzano AN, Knudsen ES. 2000b. BRG-1 is required for RB-mediated cell cycle arrest. *Proc Natl Acad Sci USA* 97:7748–7753.
- Strobeck MW, Reisman DN, Gunawardena RW, Betz BL, Angus SP, Knudsen KE, Kowalik TF, Weissman BE, Knudsen ES. 2002. Compensation of BRG-1 function by Brm: Insight into the role of the core SWI-SNF subunits in retinoblastoma tumor suppressor signaling. *J Biol Chem* 277:4782–4789.
- Strober BE, Dunaief JL, Guha S, Goff SP. 1996. Functional interactions between the hBRM/hBRG1 transcriptional activators and the pRB family of proteins. *Mol Cell Biol* 16:1576–1583.
- Trouche D, Le Chalony C, Muchardt C, Yaniv M, Kouzarides T. 1997. RB and hbrm cooperate to repress the activation functions of E2F1. *Proc Natl Acad Sci USA* 94:11268–11273.
- Underwood JM, Imbalzano KM, Weaver VM, Fischer AH, Imbalzano AN, Nickerson JA. 2006. The ultrastructure of MCF-10A acini. *J Cell Physiol* 208:141–148.
- Wagner S, Chiosea S, Nickerson JA. 2003. The spatial targeting and nuclear matrix binding domains of SRm160. *Proc Natl Acad Sci USA* 100:3269–3274.
- Wang W, Xue Y, Zhou S, Kuo A, Cairns BR, Crabtree GR. 1996. Diversity and specialization of mammalian SWI/SNF complexes. *Genes Dev* 10:2117–2130.
- Wang S, Fusaro G, Padmanabhan J, Chellappan SP. 2002. Prohibitin co-localizes with Rb in the nucleus and recruits N-CoR and HDAC1 for transcriptional repression. *Oncogene* 21:8388–8396.
- Weaver VM, Howlett AR, Langton-Webster B, Petersen OW, Bissell MJ. 1995. The development of a functionally relevant cell culture model of progressive human breast cancer. *Semin Cancer Biol* 6:175–184.
- Weaver VM, Petersen OW, Wang F, Larabell CA, Briand P, Damsky C, Bissell MJ. 1997. Reversion of the malignant phenotype of human breast cells in three-dimensional culture and in vivo by integrin blocking antibodies. *J Cell Biol* 137:231–245.
- Weaver VM, Lelievre S, Lakins JN, Chrenek MA, Jones JC, Giancotti F, Werb Z, Bissell MJ. 2002. beta4 integrin-dependent formation of polarized three-dimensional architecture confers resistance to apoptosis in normal and malignant mammary epithelium. *Cancer Cell* 2:205–216.
- Wei Y, Yu L, Bowen J, Gorovsky MA, Allis CD. 1999. Phosphorylation of histone H3 is required for proper chromosome condensation and segregation. *Cell* 97:99–109.
- Wiznerowicz M, Trono D. 2003. Conditional suppression of cellular genes: lentivirus vector-mediated drug-inducible RNA interference. *J Virol* 77:8957–8961.
- Yaswen P, Stampfer MR. 2002. Molecular changes accompanying senescence and immortalization of cultured human mammary epithelial cells. *Int J Biochem Cell Biol* 34:1382–1394.
- Yoon DS, Wersto RP, Zhou W, Chrest FJ, Garrett ES, Kwon TK, Gabrielson E. 2002. Variable levels of chromosomal instability and mitotic spindle checkpoint defects in breast cancer. *Am J Pathol* 161:391–397.
- Zhang HS, Gavin M, Dahiya A, Postigo AA, Ma D, Luo RX, Harbour JW, Dean DC. 2000. Exit from G1 and S phase of the cell cycle is regulated by repressor complexes containing HDAC-Rb-hSWI/SNF and Rb-hSWI/SNF. *Cell* 101:79–89.

Effect of Substrate Stiffness and PDGF on the Behavior of Vascular Smooth Muscle Cells: Implications for Atherosclerosis

XIN Q. BROWN,¹ ERZSEBET BARTOLAK-SUKI,^{1,2} CORIN WILLIAMS,¹ MATHEW L. WALKER,¹ VALERIE M. WEAVER,³ AND JOYCE Y. WONG^{1*}

¹Department of Biomedical Engineering, Boston University, Boston, Massachusetts

²CelluTraf Scientific, Boston, Massachusetts

³Department of Surgery and Anatomy, University of California, San Francisco, California

Vascular disease, such as atherosclerosis, is accompanied by changes in the mechanical properties of the vessel wall. Although altered mechanics is thought to contribute to disease progression, the molecular mechanisms whereby vessel wall stiffening could promote vascular occlusive disease remain unclear. It is well known that platelet-derived growth factor (PDGF) is a major stimulus for the abnormal migration and proliferation of vascular smooth muscle cells (VSMCs) and contributes critically to vascular disease. Here we used engineered substrates with tunable mechanical properties to explore the effect of tissue stiffness on PDGF signaling in VSMCs as a potential mechanism whereby vessel wall stiffening could promote vascular disease. We found that substrate stiffness significantly enhanced PDGFR activity and VSMC proliferation. After ligand binding, PDGFR followed distinct routes of activation in cells cultured on stiff versus soft substrates, as demonstrated by differences in its intensity and duration of activation, sensitivity to cholesterol extracting agent, and plasma membrane localization. Our results suggest that stiffening of the vessel wall could actively promote pathogenesis of vascular disease by enhancing PDGFR signaling to drive VSMC growth and survival.

J. Cell. Physiol. 225: 115–122, 2010. © 2010 Wiley-Liss, Inc.

Uncontrolled proliferation and migration of vascular smooth muscle cells (VSMCs) coupled with increased deposition of extracellular matrix (ECM) are major causes of intimal thickening during the development of vascular occlusive disease (Nikkari et al., 1994; Thyberg et al., 1997; Thyberg, 1998; Imanaka-Yoshida et al., 2001). Moreover, cellular and molecular compositional changes in the vessel wall modulate the mechanical properties of the vessel (Glagov, 1990; Lee et al., 1991; Matsumoto et al., 2002; Jacot et al., 2004). For example, the elastic modulus of a normal vessel is around 30 kPa, but for a diseased vessel with increased VSMC number and collagen content, the modulus is in the range of 80 kPa (Matsumoto et al., 2002).

Substrate stiffness influences adhesion, proliferation, and differentiation in a variety of cell types (Pelham and Wang, 1997; Wang et al., 2000; Paszek and Weaver, 2004; Engler et al., 2004b; Paszek et al., 2005; Friedland et al., 2009). Specifically, we and others have found that VSMC migration and proliferation increase with substrate stiffness (Wong et al., 2003; Engler et al., 2004a; Brown et al., 2005; Peyton and Putnam, 2005; McDaniel et al., 2007; Isenberg et al., 2009). Such findings suggest that VSMC behavior could be modified due to increased vessel stiffness during the development of vascular disease.

Cells sense the mechanical properties of their substrate through integrins (Wang et al., 2001; Ingber, 2003b; Katsumi et al., 2004; Paszek et al., 2005). Changes in substrate stiffness can potentially influence cellular responses to growth factors through cross-talk between integrin and growth factor receptor (GFR) signaling pathways. As reviewed in an article by Lee and Juliano, common downstream signaling molecules such as Ras, Rho, FAK, and PI3K integrate simultaneous inputs from integrins and GFRs to generate a single mitogenic output (Miranti and Brugge, 2002; Lee and Juliano, 2004).

Integrin and GFR cross-talk often occurs in lipid rafts. Lipid rafts are cholesterol-rich, organized lipid membrane

microdomains. They play a central role in the signal transduction of cell surface receptors because many essential downstream signaling molecules are targeted to the rafts from the cytosol through post-translational modification (Simons and Toomre, 2000; Simons and Ehehalt, 2002; Resh, 2004). By bringing the cell surface receptors and their downstream effectors into close proximity to each other, these organized lipid membrane microdomains increase the efficiency of these signaling processes. It has been demonstrated by many groups that disruption of lipid rafts by sequestering cholesterol significantly decreases the activities of the cell surface receptors (Stehr et al., 2003; Decker and French-Constant, 2004; Makoto et al., 2004; Arcaro et al., 2007).

Platelet-derived growth factor (PDGF) plays a major role in VSMC migration and proliferation during the development of vascular occlusive disease (reviewed in Raines, 2004). Although PDGF mRNA has been detected in both healthy and diseased vessels (Barrett and Benditt, 1988), VSMC migration and proliferation has only been found to occur in diseased vessels. Despite the fact that increased vessel stiffness is characteristic of vascular disease, little is known about the influence of

Contract grant sponsor: NIH;
Contract grant number: R01 HL072900.
Contract grant sponsor: DOD;
Contract grant number: W81XWH-05-1-0330.

*Correspondence to: Joyce Y. Wong, Department of Biomedical Engineering, Boston University, Boston, MA 02215.
E-mail: jywong@bu.edu

Received 23 November 2009; Accepted 5 April 2010

Published online in Wiley InterScience
(www.interscience.wiley.com.), 21 May 2010.
DOI: 10.1002/jcp.22202

substrate stiffness on the stimulatory effect of PDGF. We hypothesize that substrate stiffness modulates VSMC response to PDGF. In this study, we used a defined model system that mimicked the stiffness of healthy and diseased vessels to investigate the effects of substrate stiffness on VSMC response to PDGF and its underlying mechanisms.

Materials and Methods

Substrate preparation

Our engineered model system was comprised of polyacrylamide (PAAm) gels with RGD peptides incorporated into the bulk of the gel. Acryloyl-PEG-GRGDSP was synthesized according to the method first described by Hubbell's group (Jackman et al., 1999; Stegemann et al., 2007). Briefly, equal molar of acryloyl-PEG-*N*-hydroxysuccinimide ester (Nektar Therapeutics, San Carlos, CA) and GRGDSP peptide (American Peptide, Sunnyvale, CA) were incubated in sodium bicarbonate buffer (pH 8.5) at room temperature for 2 h. Unreacted peptide and sodium bicarbonate were removed by dialysis in dl water. PAAm substrates were prepared as described previously (Leach et al., 2007). Briefly, prior to making the gel solution, 25 mm round cover slips were activated. Cover slips were passed through a Bunsen burner flame, treated sequentially with 0.1 M NaOH and 3-aminopropyltrimethoxy silane (Sigma, St. Louis, MO), washed with distilled water, and then incubated with 0.5% glutaraldehyde (Polysciences, Warrington, PA) for 30 min at room temperature. A typical acrylamide/bis-acrylamide mixture contained 10% acrylamide (Bio-Rad, Hercules, CA), 0.03–0.3% bis-acrylamide (Bio-Rad), 0.05 M HEPES, 0.15% TEMED (Sigma), 0.05% ammonium persulfate (Sigma), and 10 μ M acryloyl-PEG-GRGDSP. The stiffness of the PAAm substrate was modulated by changing the bis-acrylamide concentration. A 30 μ l drop of the gel solution was cast between an activated and non-activated cover slip and allowed to polymerize at room temperature. The non-activated cover slip was then removed, and the substrates were incubated in 2 M glycine overnight to quench the residual unreacted acryloyl-PEG-*N*-hydroxysuccinimide ester in the gel. All gels were washed thoroughly with PBS before each experiment.

Substrate characterization

The stiffness of the substrates was determined by a microindentation method (Jacot et al., 2006). Briefly, a 100 μ m diameter glass bead attached to a glass fiber was used as indenter tip. Images were captured as the tip was lowered into the substrate. Indenter tip displacement and deflection were measured from the images, and the elastic modulus of the substrate was calculated from the unloading portion of the indenter tip force versus displacement curve.

The rate of acryloyl-PEG-GRGDSP incorporation into the substrate was determined using I-125-labeled peptide. Briefly, 10 μ Ci I-125-labeled YRGDS (5 μ Ci/ μ g, Phoenix Pharmaceuticals, Belmont, CA) was mixed with 1 mg GRGDSP and acryloyl-PEG-*N*-hydroxysuccinimide ester to generate I-125-labeled ligand. The resulting product was then used to cast gels with different stiffness values, and the radioactivity of the substrates was measured with a gamma-counter. The amount of ligand per square micron of each substrate throughout the thickness of the gel was calculated assuming that I-125-labeled YRGDS and unlabeled GRGDSP had the same incorporation rate.

The surface ligand density was determined by ELISA using biotin-labeled peptide (GRGDSPY-biotin, American Peptide). Briefly, biotin-labeled GRGDSPY was mixed with GRGDSP at a 1:100 molar ratio to generate a mixture of biotinylated and non-biotinylated ligand, which were then used to cast substrates. After blocking with 2% BSA and 0.1% Tween-20, the substrates were incubated first with monoclonal rabbit anti-biotin antibody (Abcam, Inc., Cambridge, MA) at 1:5,000 dilution and then with

HRP-labeled anti-rabbit antibody at 1:10,000 dilution (Jackson ImmunoResearch Labs, West Grove, PA). Soluble TMB substrate (Thermo Fischer, Rockford, IL) was used for colorimetric measurements (OD450) to determine the surface ligand density.

Cell culture and manipulations

Primary bovine VSMCs (AG08504, Coriell Cell Repositories, Camden, NJ) were maintained in Dulbecco's Modified Eagle Medium (DMEM) supplemented with 10% bovine calf serum, 200 mM L-glutamine, and penicillin–streptomycin in a 5% CO₂ humidified incubator. All cell culture reagents were from Invitrogen (San Diego, CA). Cells with passage number between 10 and 15 were used for the experiments.

For projected cell area analysis, VSMCs were serum starved for 2 days before being seeded onto the substrates in serum-free media at a density of 10⁴ cells/cm². After 4 h of attachment, non-adherent cells were removed and phase contrast images were captured at 10 random positions of each substrate. Projected cell area was analyzed using ImageJ software (National Institute of Health). The areas of at least 100 cells were determined for each substrate.

For cell growth studies, VSMCs cultured on soft and stiff substrates were serum starved for 24 h before stimulation with 0.5% serum with or without 10 ng/ml PDGF-BB (R&D Systems, Minneapolis, MN). The number of cells at the day of stimulation (day 0) and 3 days after stimulation (day 3) was analyzed using the acid phosphatase assay. The rate of cell growth was calculated by dividing the number of cells on day 3 by the number of cells on day 0.

For analysis of PDGFR activation, VSMCs were serum starved for 24 h. Just before PDGF-BB stimulation, VSMCs were treated with or without 10 mM methyl- β -cyclodextrin (MBCD, Sigma) for 1 h. After PDGF-BB stimulation, cells were lysed in a buffer containing 20 mM Tris, pH 7.4, 150 mM NaCl, 1% Triton 100, 5 mM EDTA, 5 mM EGTA, 1 mM PMSF, 1 μ g/ml leupeptin, 1 μ g/ml aprotinin, and 0.2 mM Na₃VO₄.

Western blot

Cell lysates with equal amounts of total protein were separated on denaturing SDS–polyacrylamide gels and transferred onto polyvinylidene fluoride membranes (Millipore, Bedford, MA). Phosphorylated PDGFR was detected with PY20 (BD Transduction Laboratories, San Diego, CA), and total PDGFR was detected with PDGFR- β anti-serum (a generous gift from Dr. Kazlauskas at the Schepens Eye Research Institute). The blots were analyzed with ImageJ software, and the level of PDGFR phosphorylation was normalized to total PDGFR. Fold PDGFR activation in PDGF-BB-treated samples was calculated against untreated samples.

Immunocytochemistry and fluorescent microscopy

Adherent VSMCs were fixed with 3% phosphate-buffered formalin for 20 min and permeabilized with 0.5% TritonX-100. F-actin was stained with Rhodamine-labeled Phalloidin (Invitrogen, Inc., Carlsbad, CA), and cell nuclei were stained with Hoechst 33342 (Invitrogen, Inc., Carlsbad, CA). To visualize PDGFR activation and lipid microdomains, samples were subjected to MBCD and/or PDGF treatment as described above. After fixing and permeabilization, non-specific binding was first blocked with 2.5% goat serum (Vector Laboratories, Burlingame, CA) for 1 h. The first primary antibody incubation was with rabbit polyclonal phospho-PDGFR β (Abcam, Inc.) at a dilution of 1:50 for 1 h, followed by a second incubation with FITC-conjugated goat anti-rabbit antibody (Vector Laboratories) for 1 h. Samples were then washed 3 \times 15 min with PBS and blocked with 2.5% horse serum (Vector Laboratories) for 1 h. The second primary antibody incubation was with mouse monoclonal Flotillin-1 (BD Transduction Laboratories, Franklin Lakes, NJ) at a dilution of 1:250 for 1 h, followed by an incubation with Texas Red-conjugated horse anti-mouse antibody

(Vector Laboratories) for 1 h, followed by a 3×15 min PBS wash. Both secondary antibodies were used at the manufacturer's suggested concentrations. All incubations and washes were at room temperature. Fluorescent images were captured with confocal microscopy (Olympus FV1000).

Statistical analysis

Statistics were performed using Student's *t*-test assuming equal variances for paired comparisons and ANOVA for more than two groups of data.

Results

Characterization of polyacrylamide substrates

We prepared a series of PAAm substrates with 10% acrylamide with varying bis-acrylamide concentrations (0.03–0.3%). As measured by microindentation, when the bis-acrylamide concentration was increased from 0.03% to 0.3%, the elastic modulus increased linearly from 19 to 84 kPa (Fig. 1A). These values are in the range of stiffness that has been reported for normal and atherosclerotic vessels (Matsumoto et al., 2002); thus, we were able to tune the mechanical properties of our model substrates to mimic the stiffness of healthy and diseased vessels simply by varying the bis-acrylamide concentration.

Changes in ligand density influence cell adhesion, migration, and proliferation (Rowley and Mooney, 2002; Gaudet et al., 2003; Rajagopalan et al., 2004; Engler et al., 2004a). To ensure that substrate stiffness was the only variable in our model system, we used I-125-labeled YRGDS to calculate the rate of peptide incorporation. When the elastic modulus increased from 19 to 84 kPa, we found no statistical differences in the peptide concentration in the bulk of the gel ($5,846 \pm 452$ molecule/ μm^2 , $P = 0.37$, Fig. 1B). We also compared the amount of peptide on the gel surface available for cell binding using biotinylated GRGDSPY peptide and anti-biotin antibody. When the input peptide concentration in the initial gel mix was increased from 0.04 to 40 μM , the peptide surface concentration increased linearly at first, which then reached a maximum at 4 μM input peptide concentration for the 84 kPa gels and 10 μM for the 31 kPa gels (Fig. 1C). We did not detect any statistical differences in the surface peptide density between 31 kPa gels and 84 kPa gels at peptide input concentrations above 0.04 μM . In order to ensure maximum and equal surface ligand concentration on our substrates, we used a peptide input of 10 μM throughout our study.

Increase in substrate stiffness leads to increased cytoskeletal organization and VSMC proliferation

Using our model system, we first investigated whether changes in mechanical properties of substrates mimicking vessel stiffness would affect VSMC survival and proliferation. For anchorage-dependent cells, cell adhesion regulates cell survival and proliferation. Successful cell adhesion is indicated by an increase in projected cell area and the formation of stress fibers. From short-term (4 h) adhesion studies, we found that projected cell area and the formation of stress fibers increased significantly with increased substrate stiffness (Fig. 2A,B). The projected cell area on the 84 kPa substrates was 1.8-fold larger than on the 31 kPa substrates ($P < 0.01$), which in turn was 1.6-fold larger than on the 19 kPa substrates ($P < 0.01$) (Fig. 2A). On 19 kPa substrates, F-actin was diffuse and concentrated around the nucleus. In contrast, on 84 kPa substrates, stress fibers were fully formed in the cell body (Fig. 2B).

VSMCs did not adhere well on the 19 kPa substrate and did not survive overnight culture. We therefore concentrated our study on the 31 kPa substrate, which mimicked the stiffness of a healthy vessel, and the 84 kPa substrate, which mimicked the

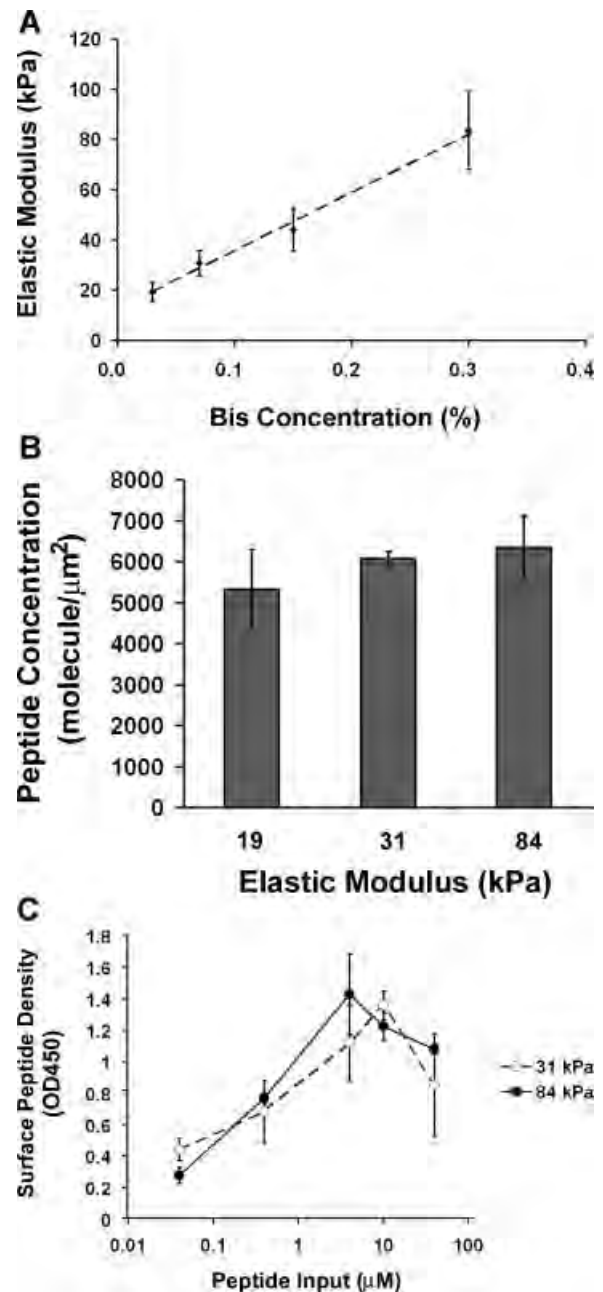


Fig. 1. Substrate characterization. A: Substrate stiffness increases with bis-acrylamide concentration ($n = 10$). B: Ligand concentration in the bulk of the substrate remains the same as substrate stiffness increases ($n = 3$). C: Surface ligand densities are dependent on input peptide concentration but not substrate stiffness ($n = 3$). All error bars represent standard deviation.

stiffness of a diseased vessel. After 3 days of serum stimulation, there was no statistically significant change in the number of VSMCs on 31 kPa substrates; the number of VSMCs on 84 kPa substrates, however, was almost threefold the original number before the start of stimulation (Fig. 2C). After 3 days of combined serum and PDGF-BB stimulation, the number of VSMCs on 31 kPa substrates was only 1.6-fold of the original number, while the number of VSMCs on 84 kPa substrates reached 4.5-fold the original number (Fig. 2C). These results

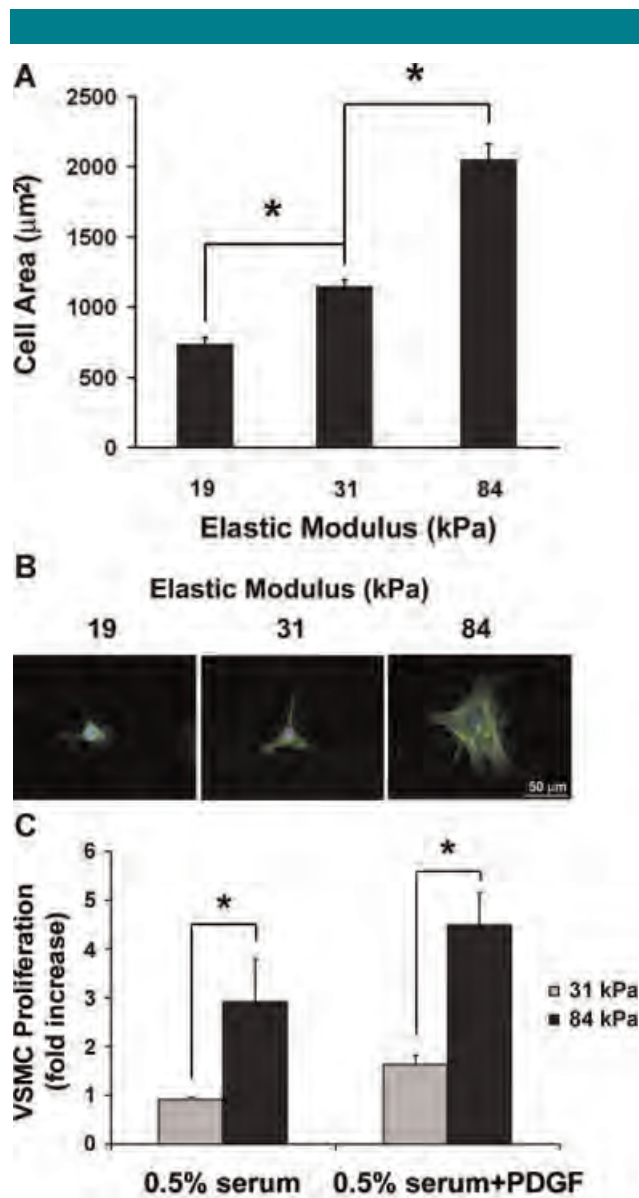


Fig. 2. Substrate stiffness regulates cytoskeletal organization and VSMC proliferation. **A:** VSMC projected cell area increases with substrate stiffness ($n > 100$). Error bars represent SEM ($*P < 0.01$). **B:** Fluorescent images of VSMC show more defined stress fibers as substrate stiffness increases. F-actin (green) was stained with Rhodamine-labeled Phalloidin and cell nuclei (blue) were stained with Hoechst 33342. **C:** The rate of VSMC proliferation is higher on stiff substrates ($n = 3$). Error bars represent standard deviation ($*P < 0.01$). [Color figure can be viewed in the online issue, which is available at www.interscience.wiley.com.]

indicate that substrate stiffness promotes VSMC survival and proliferation under both serum and PDGF stimulation.

Substrate stiffness enhances the stimulating effect of PDGF-BB

In light of our observed changes in vessel stiffness during the progression of vascular disease, an important question to address is the role of mechanical stiffness in VSMC response to PDGF. We already observed an increase in the rate of VSMC proliferation with increased substrate stiffness when cells were cultured in the presence of both serum and PDGF-BB. To

eliminate the possible activation of PDGFR by serum, we exposed serum-starved VSMCs to PDGF-BB and investigated the level of PDGFR activation on 31 and 84 kPa substrates. Using PY20, a general antibody that recognizes phosphorylated tyrosine, we identified three phosphorylated proteins in VSMC lysates at 190, 125, and 90 kDa (Fig. 3A). Because 190 and 125 kDa are the molecular weights (MW) for PDGFR and FAK, respectively (Heldin et al., 1983), it is likely that the 190 kDa protein corresponds to phosphorylated PDGFR, and the 125 kDa protein corresponds to phosphorylated FAK. In addition, we detected proteins at the same MW positions using PDGFR- β antiserum and monoclonal anti-FAK antibody (Fig. 3A, data not shown).

After normalizing to total PDGFR protein level, we calculated changes in the level of phosphorylated PDGFR in cells exposed to PDGF-BB compared to cells that were not exposed to PDGF-BB (fold activation). We found after the 10 ng/ml PDGF-BB stimulation, fold activation of PDGFR in cells on 31 kPa substrates remained low throughout a 30 min time course (Fig. 3A,B). On 84 kPa substrates however, fold activation of PDGFR was twice as much as on 31 kPa substrates during the first 15 min and decreased rapidly to the same level as on 31 kPa substrates at 30 min. This indicates that substrate stiffness affects the intensity and dynamics of PDGFR activation in VSMCs.

We further investigated the effect of substrate stiffness on PDGFR activation in VSMCs by exposing VSMCs to increasing amounts of PDGF-BB (5, 10, and 20 ng/ml) for 10 min. Fold activation of PDGFR increased in a dose-dependent manner in VSMCs on both 31 and 84 kPa substrates (Fig. 3C,D). However, levels of PDGFR activation were significantly higher in VSMCs on 84 kPa substrates than on 31 kPa substrates, and VSMCs responded more significantly to increasing amounts of PDGF-BB on 84 kPa substrates. When PDGF concentration increased fourfold from 5 to 20 ng/ml, the level of PDGFR activation increased sixfold on 84 kPa substrates versus twofold on 31 kPa substrates. The time course experiment and dose-response experiment together demonstrate that substrate stiffness enhances the stimulating effect of PDGF in VSMCs. In addition, we also observed a decrease in total PDGFR protein level in cells on 84 kPa substrates exposed to high concentrations of PDGF (20 ng/ml), but not in cells on 31 kPa substrates, indicating a difference in the regulation of PDGFR in cells on soft versus stiff substrates.

Substrate stiffness modulates VSMC response to PDGF through organized membrane domains

We wanted to dissect out the possibility that substrate stiffness modulates PDGFR signaling in organized membrane microdomain lipid rafts. In order to address this, we treated VSMCs with MBCD—an agent that extracts cholesterol from the cells and disrupts lipid rafts. In MBCD-treated cells, the level of PDGFR activation was significantly reduced on 84 kPa substrates, suggesting lipid rafts are involved in PDGFR activation (Fig. 4A,B). On 31 kPa substrates, however, the level of PDGFR activation in PDGF-stimulated cells increased slightly after MBCD treatment, suggesting a lipid raft-independent mechanism of PDGFR activation.

We also examined the phosphorylation of PDGFR in VSMCs using confocal microscopy. We observed positive staining for phosphorylated PDGFR β (Fig. 4C, red) and lipid raft marker flotillin-1 (Fig. 4C, green) in cells on both 31 and 84 kPa substrates. The staining pattern for phospho-PDGFR β and flotillin-1 appeared diffuse in cells before PDGF stimulation on both substrates (Fig. 4C, left parts). After PDGF stimulation, phospho-PDGFR β and flotillin-1 were rearranged to a punctate state on the 84 kPa substrate (Fig. 4C, center bottom part), whereas on the 31 kPa substrate, the staining remained diffuse

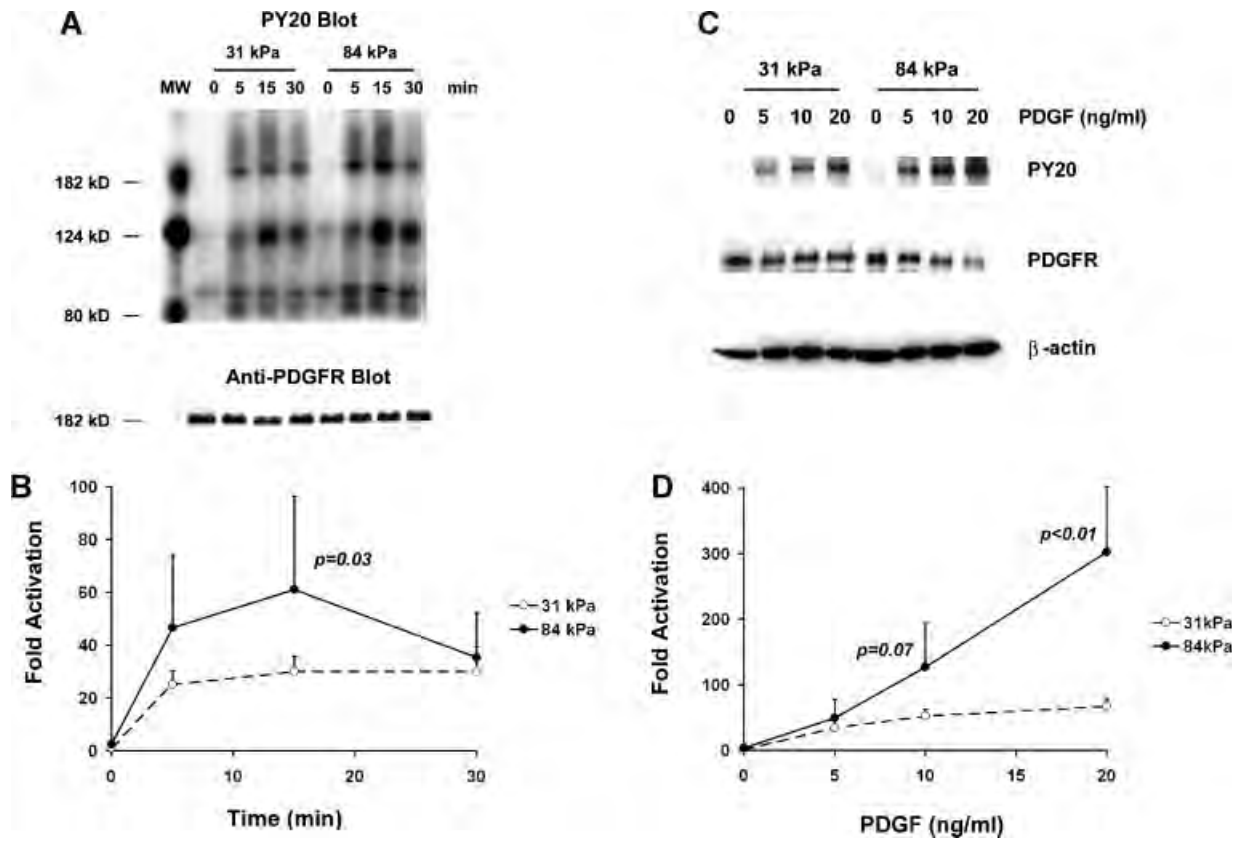


Fig. 3. Substrate stiffness enhances the stimulating effect of PDGF in VSMCs. **A:** Representative Western blots of VSMCs stimulated with 10 ng/ml PDGF over a 30-min time course. **B:** VSMCs on stiff substrates show higher levels of PDGFR phosphorylation during the first 30 min of PDGF stimulation ($n = 3$). **C:** Representative Western blots of VSMCs stimulated with increasing concentrations of PDGF for 10 min. **D:** VSMCs on stiff substrates show higher levels of PDGFR phosphorylation over a range of PDGF concentrations ($n = 3$). Error bars represent standard deviation.

(Fig. 4C, center top part). In PDGF-stimulated cells, MBCD eliminated phosphorylation of PDGFR β in VSMCs on the 84 kPa substrate (Fig. 4C, bottom right part). In contrast, MBCD had no effect on the phosphorylation of PDGFR β in VSMCs on the 31 kPa substrate (Fig. 4C, top right part). These data further suggest that ligand-dependent PDGFR activation on the 84 kPa substrate is lipid raft dependent, whereas PDGFR signaling on the 31 kPa substrate is independent of these membrane domains.

Discussion

Using a model system that represents the stiffness of a healthy vessel (31 kPa) and a diseased vessel (84 kPa), here we showed that substrate stiffness enhances the stimulating effect of PDGF on VSMCs. VSMCs on stiff (84 kPa) substrates had significantly higher growth in response to PDGF compared to VSMCs on soft (31 kPa) substrates. On the stiff substrate, PDGFR activation by PDGF was strong and appeared to be dependent on cholesterol rich lipid rafts. However, on the soft substrate, PDGFR phosphorylation was weak and appeared to be independent of lipid rafts.

In addition to the different dependencies on lipid rafts during PDGFR activation, we also observed other differences in the regulation of PDGFR signaling in VSMCs when substrate stiffness is changed. After PDGF stimulation, the high level of PDGFR activation on stiff substrates (84 kPa) was transient (Fig. 3A,B), whereas the low level of PDGFR activation on soft

substrates remained steady in the time frame we examined. When treated with increasing concentrations of PDGF, total PDGFR protein decreased in VSMCs on stiff substrates (84 kPa, Fig. 3C), indicating PDGFR internalization and degradation through ligand-bound PDGFR, which could also explain the transient nature of PDGFR activation on stiff substrates. In contrast, on soft substrates (31 kPa) total PDGFR protein did not decrease in the concentration range used in this study. Despite decreased total PDGFR protein levels, the level of phosphorylated PDGFR increased with PDGF concentration on stiff substrates. As a matter of fact, after normalization to PDGFR protein level, the level of PDGFR phosphorylation increased significantly more on stiff substrates compared to soft substrates with increasing PDGF concentrations (Fig. 3D). This suggests an increased sensitivity to PDGF when VSMCs are on stiffer substrates.

Cells sense matrix stiffness through integrins (Wang et al., 2001; Ingber, 2003b; Katsumi et al., 2004; Paszek et al., 2005; Friedland et al., 2009). Paszek et al. (2005) showed increased stroma stiffness during breast cancer development leads to integrin clustering, enhanced ERK and ROCK activation. A recent article by Friedland et al. (2009) showed that an increase in substrate stiffness switches the conformation of $\alpha 5\beta 1$ integrins from a relaxed state to a tensioned state, which strengthens the association between integrins and fibronectin and leads to higher level of FAK phosphorylation at Y397 position. We observed increased projected cell area and stress fiber formation in VSMCs on stiff substrates, indicating

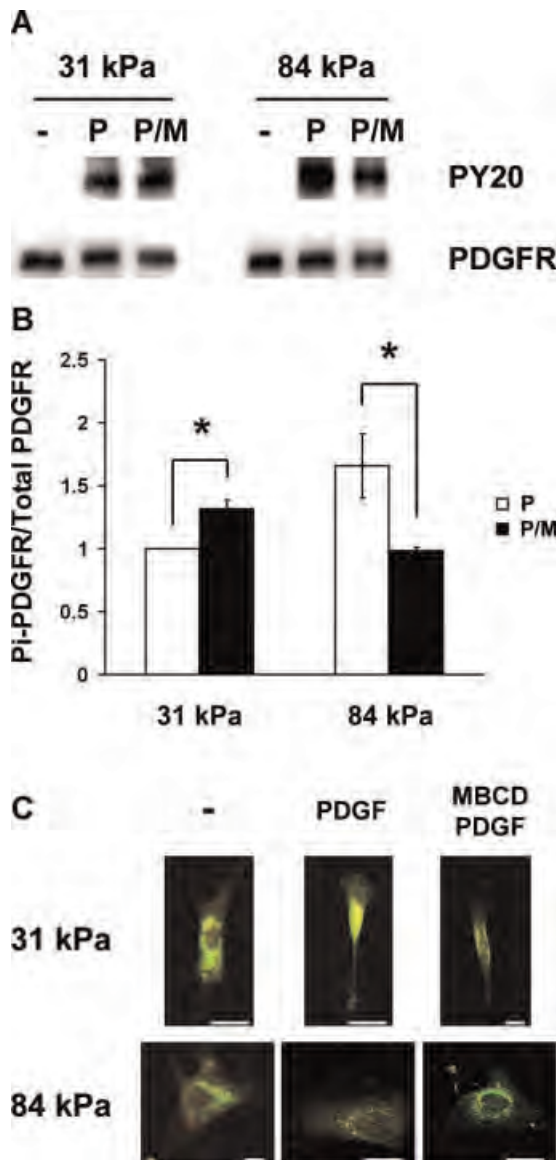


Fig. 4. Lipid rafts are involved in PDGFR activation in VSMCs on stiff substrates. **A:** Representative Western blots of MBCD-treated and PDGF-stimulated VSMCs. **B:** PDGFR phosphorylation is diminished by MBCD treatment on stiff substrates only ($n = 3$). Error bars represent standard deviation ($*P < 0.01$). **C:** Double-label fluorescence immunocytochemistry for flotillin-1 (green) and phospho-PDGFR β (red) as a function of substrate stiffness in the presence or absence of MBCD and/or PDGF. Scale bars represent 10 μm .

enhanced integrin signaling (Fig. 2A,B). Our preliminary data also showed increased FAK and ERK phosphorylation in VSMCs on stiff substrates (data not shown). Further investigation is required to elucidate the specific mechanism of integrin activation in our model system, that is, determining whether activation is achieved through integrin clustering and/or via changes in integrin conformation. We note that these two proposed mechanisms are not mutually exclusive.

Increase in substrate stiffness enhances integrin activation, whereas integrin engagement and activation is essential for the formation and stabilization of organized lipid membrane microdomains (Pankov et al., 2005; Gaus et al., 2006; Echarri

et al., 2007). In addition, the expression levels of lipid raft associated molecules were found to be up-regulated when VSMCs were cultured on stiff tissue culture plastic when compared with a soft spherical culture (Monastyrskaya et al., 2003). Mitsuda et al. (2002) and Stehr et al. (2003) observed that, although phosphorylation of PDGFR upon PDGF binding might be independent of the localization of the receptor, PDGFR signals more efficiently when localized in lipid rafts. We observed that on stiff (84 kPa) substrates, phosphorylated PDGFR molecules aggregate into punctate domains in PDGF-stimulated VSMCs (Fig. 4C, bottom parts), and the level of PDGFR phosphorylation on stiff substrates is high but significantly diminished after disruption of lipid rafts by using a cholesterol extracting agent (Fig. 4A,B). On soft (31 kPa) substrates however, the localization of phosphorylated PDGFR is dispersed (Fig. 4C, top parts), and the level of PDGFR phosphorylation is low but not further reduced by the cholesterol extracting agent (Fig. 4A,B). In fact, we observed a slight increase in the phosphorylation of PDGFR (Fig. 4B), which is possibly due to ligand-independent activation of PDGFR by cholesterol extracting agents (Liu et al., 2007). Our data highlight the fact that PDGFR activation is regulated differently when substrate stiffness is changed. On the stiff substrate, PDGFR activation appears to be lipid raft dependent, as depleting cholesterol decreases the level of PDGFR phosphorylation. In contrast, on the soft substrate, PDGFR activation seems to be lipid raft independent, as depleting cholesterol increases the level of PDGFR phosphorylation in a ligand-independent manner.

Based on previous reports and our own observations, we propose the following mechanism (Fig. 5): when cells are attached to a stiff substrate, there is enough force to induce high levels of integrin activation (clustering or conformational changes) and the formation of organized membrane domain lipid rafts. PDGFR and its downstream effectors are recruited to these membrane microdomains, and PDGF-induced signaling follows the similar pathway that we observe on tissue culture plastic surfaces. When cells are attached to a soft substrate, there is not enough integrin activation to stabilize lipid rafts. As a consequence, PDGF signaling follows a lipid raft-independent pathway.

Changes in ECM stiffness occurs during many physiological and pathological conditions (Belousov et al., 1997; Ingber, 2003a; Czirok et al., 2004; Paszek and Weaver, 2004). Using a model system that mimics normal and diseased vessel stiffness, we found that VSMCs respond differently to a growth factor (i.e., PDGF) and a pharmacological agent (i.e., MBCD) when substrate stiffness is changed (Figs. 3 and 4). The fact that VSMCs on substrates with the stiffness of a normal vessel (31 kPa) respond to PDGF stimulation with lipid raft-independent and low-level PDGFR activation suggests that the softer, healthy vessel keeps VSMCs in a quiescent state even in the presence of a growth factor. However, that VSMCs on substrates with the stiffness of a diseased vessel (84 kPa) respond to PDGF stimulation with lipid raft-dependent and high-level PDGFR activation indicates that the stiffer, diseased vessel promotes the stimulation of VSMCs by the growth factor. Increased sensitivity of VSMC to PDGF with increased vessel stiffness may result in a positive feedback loop that leads to further VSMC migration and proliferation, and thus, further progression of vascular disease. Although we do not have direct evidence to show whether survival and proliferation signals are relatively insensitive to perturbations in PDGF level in the healthy vessel wall in vivo, other in vitro findings suggest that substrate biochemical composition in a healthy vessel renders VSMC relatively insensitive to PDGF stimulation. For example, when VSMCs are cultured on laminin, FAK is not phosphorylated and PDGF does not stimulate VSMC proliferation; in contrast, on fibronectin, FAK is

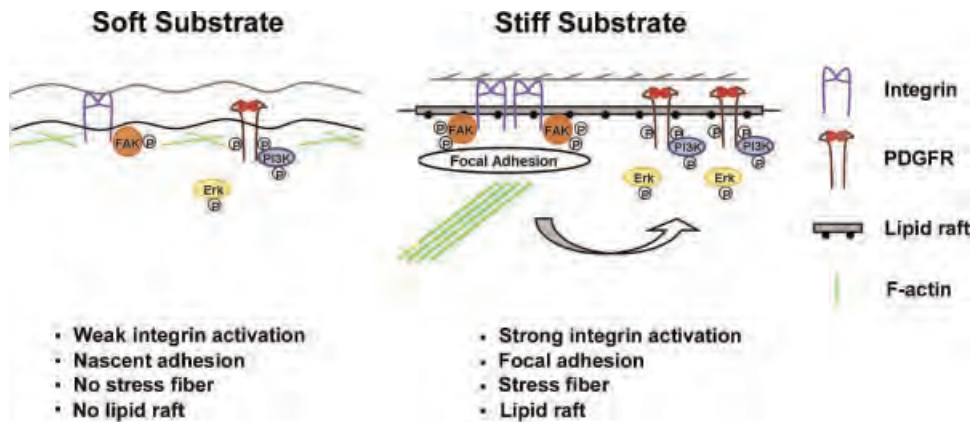


Fig. 5. A proposed model for the regulation of PDGFR signaling by substrate stiffness. When cells are attached to a soft substrate, there is not enough force to induce high level of integrin activation, and there is little organized membrane domain lipid rafts. As a consequence, PDGFR activation is independent of lipid rafts and weak. When cells are attached to a stiff substrate, there is enough force to induce high level of integrin activation and formation of lipid rafts. PDGFR and its downstream effectors are recruited to these membrane domains, and PDGFR activation is strong. [Color figure can be viewed in the online issue, which is available at www.interscience.wiley.com.]

phosphorylated and PDGF does stimulate VSMC proliferation (Morla and Mogford, 2000). As we know, in the healthy vessel, the basement membrane is intact and laminin is the major component of the ECM underlining VSMCs; however, in a diseased vessel, the basement membrane is damaged and fibronectin is the major component of the ECM underlining VSMCs (Thyberg et al., 1997; Newby and Zaltsman, 2000). Morla and Mogford's finding together with our data presented here indicate that changes in the properties of the ECM (mechanical or biochemical) during the development of vascular occlusive disease can potentially increase the sensitivity of VSMCs to PDGF stimulation. Regardless of the initial insult that causes the onset of vascular occlusive disease, vessel stiffness increases during the development of the disease. Hence, stiffness changes can play a major role in supporting the progressive nature of the disease by enhancing PDGF signaling. Here, we offer a possible mechanism for the progression of vascular occlusive disease that should be taken under consideration when developing therapeutic interventions.

Acknowledgments

We thank Dr. Matthew Nugent at Boston University School of Medicine for helpful discussions. We also thank Dr. Andrius Kazlauskas at the Schepens Eye Research Institute for the generous gift of PDGFR- β anti-serum. We also acknowledge contribution to the discussion of an anonymous reviewer. This work is supported by NIH R01 HL072900 grant awarded to J.Y. Wong and DOD W81XWH-05-1-0330 grant awarded to V.M. Weaver.

Literature Cited

Arcaro A, Aubert M, Espinosa del Hierro ME, Khanzada UK, Angelidou S, Tetley TD, Bittermann AG, Frame MC, Seckl MJ. 2007. Critical role for lipid raft-associated Src kinases in activation of PI3K-Akt signalling. *Cell Signal* 19:1081.

Barrett TB, Benditt EP. 1988. Platelet-derived growth factor gene expression in human atherosclerotic plaques and normal artery wall. *Proc Natl Acad Sci USA* 85:2810-2814.

Belousov LV, Kazakova NI, Luchinskaia NN, Novoselov VV. 1997. Studies in developmental cytomechanics. *Int J Dev Biol* 41:793-799.

Brown XQ, Ookawa K, Wong JY. 2005. Evaluation of polydimethylsiloxane scaffolds with physiologically-relevant elastic moduli: Interplay of substrate mechanics and surface chemistry effects on vascular smooth muscle cell response. *Biomaterials* 26:3123-3129.

Czirok A, Rongish BJ, Little CD. 2004. Extracellular matrix dynamics during vertebrate axis formation. *Dev Biol* 268:111-122.

Decker L, French-Constant C. 2004. Lipid rafts and integrin activation regulate oligodendrocyte survival. *J Neurosci* 24: 3816-3825.

Echarri A, Muriel O, Del Pozo MA. 2007. Intracellular trafficking of raft/caveolae domains: Insights from integrin signaling. *Semin Cell Dev Biol* 18:627-637.

Engler A, Bacakova L, Newman C, Hategan A, Griffin M, Discher D. 2004a. Substrate compliance versus ligand density in cell on gel responses. *Biophys J* 86:617-628.

Engler AJ, Griffin MA, Sen S, Bonnemann CG, Sweeney HL, Discher DE. 2004b. Myotubes differentiate optimally on substrates with tissue-like stiffness: Pathological implications for soft or stiff microenvironments. *J Cell Biol* 166:877-887.

Friedland JC, Lee MH, Boettiger D. 2009. Mechanically activated integrin switch controls $\alpha 5 \beta 1$ function. *Science* 323:642-644.

Gaudet C, Marganski WA, Kim S, Brown CT, Gunther V, Dembo M, Wong JY. 2003. Influence of type I collagen surface density on fibroblast spreading, motility, and contractility. *Biophys J* 85:3329-3335.

Gaus K, Le Lay S, Balasubramanian N, Schwartz MA. 2006. Integrin-mediated adhesion regulates membrane order. *J Cell Biol* 174:725-734.

Glagov S, Newman WP, III, Schaffer SA. 1990. Pathology of the human atherosclerotic plaque. Berlin, Heidelberg, New York: Springer.

Heidin CH, Ek B, Ronnstrand L. 1983. Characterization of the receptor for platelet-derived growth factor on human fibroblasts. Demonstration of an intimate relationship with a 185,000-Dalton substrate for the platelet-derived growth factor-stimulated kinase. *J Biol Chem* 258:10054-10061.

Imanaka-Yoshida K, Matsuura R, Isaka N, Nakano T, Sakakura T, Yoshida T. 2001. Serial extracellular matrix changes in neointimal lesions of human coronary artery after percutaneous transluminal coronary angioplasty: Clinical significance of early tenascin-C expression. *Virchows Arch* 439:185-190.

Ingber DE. 2003a. Mechanobiology and diseases of mechanotransduction. *Ann Med* 35:564-577.

Ingber DE. 2003b. Mechanosensation through integrins: Cells act locally but think globally. *Proc Natl Acad Sci* 100:1472-1474.

Iseberg BC, DiMilla PA, Walker M, Kim S, Wong JY. 2009. Vascular smooth muscle cell durotaxis depends on substrate stiffness gradient strength. *Biophys J* 97: 1313-1322.

Jackman RJ, Duffy DC, Cherniavskaya O, Whitesides GM. 1999. Using elastomeric membranes as dry resists and for dry lift-off. *Langmuir* 15:2973-2984.

Jacot JG, Abdullah I, Belkin M, Gerhard-Herman M, Gaccione P, Polak JF, Donaldson MC, Whittemore AD, Conte MS. 2004. Early adaptation of human lower extremity vein grafts: Wall stiffness changes accompany geometric remodeling. *J Vasc Res* 39:547-555.

Jacot JG, Dianis S, Schnall J, Wong JY. 2006. A simple microindentation technique for mapping the microscale compliance of soft hydrated materials and tissues. *J Biomed Mater Res A* 79:485-494.

Katsumi A, Orr AW, Tzima E, Schwartz MA. 2004. Integrins in mechanotransduction. *J Biol Chem* 279:12001-12004.

Leach JB, Brown XQ, Jacot JG, DiMilla PA, Wong JY. 2007. Neurite outgrowth and branching of PC12 cells on very soft substrates sharply decreases below a threshold of substrate rigidity. *J Neural Eng* 4:26-34.

Lee JW, Juliano R. 2004. Mitogenic signal transduction by integrin- and growth factor receptor-mediated pathways. *Mol Cells* 17:188-202.

Lee RT, Grodzinsky AJ, Frank EH, Kamm RD, Schoen FJ. 1991. Structure-dependent dynamic mechanical behavior of fibrous caps from human atherosclerotic plaques. *Circulation* 83:1764-1770.

Liu YT, Song L, Templeton DM. 2007. Heparin suppresses lipid raft-mediated signaling and ligand-independent EGF receptor activation. *J Cell Physiol* 211:205-212.

Makoto Y, Kazuo N, Tetsuya T. 2004. Roles of lipid rafts in integrin-dependent adhesion and gp130 signalling pathway in mouse embryonic neural precursor cells. *Genes Cells* 9:801-809.

Matsumoto T, Abe H, Ohashi T, Kato Y, Sato M. 2002. Local elastic modulus of atherosclerotic lesions of rabbit thoracic aortas measured by pipette aspiration method. *Physiol Meas* 23:635-648.

McDaniel DP, Shaw GA, Elliott JT, Bhadriraju K, Meuse C, Chung KH, Plant AL. 2007. The stiffness of collagen fibrils influences vascular smooth muscle cell phenotype. *Biophys J* 92:1759-1769.

- Miranti CK, Brugge JS. 2002. Sensing the environment: A historical perspective on integrin signal transduction. *Nat Cell Biol* 4:E83.
- Mitsuda T, Furukawa K, Fukumoto S, Miyazaki H, Urano T, Furukawa K. 2002. Overexpression of ganglioside GM1 results in the dispersion of platelet-derived growth factor receptor from glycolipid-enriched microdomains and in the suppression of cell growth signals. *J Biol Chem* 277:11239–11246.
- Monastyrskaya K, Babiychuk EB, Schittny JC, Rescher U, Gerke V, Mannherz HG, Draeger A. 2003. The expression levels of three raft-associated molecules in cultivated vascular cells are dependent on culture conditions. *Cell Mol Life Sci* 60:2702–2709.
- Morla AO, Mogford JE. 2000. Control of smooth muscle cell proliferation and phenotype by integrin signaling through focal adhesion kinase. *Biochem Biophys Res Commun* 272:298–302.
- Newby AC, Zaltsman AB. 2000. Molecular mechanisms in intimal hyperplasia. *J Pathol* 190:300–309.
- Nikkari ST, Jarvelainen HT, Wight TN, Ferguson M, Clowes AW. 1994. Smooth muscle cell expression of extracellular matrix genes after arterial injury. *Am J Pathol* 144:1348–1356.
- Pankov R, Markovska T, Hazarosova R, Antonov P, Ivanova L, Momchilova A. 2005. Cholesterol distribution in plasma membranes of beta1 integrin-expressing and beta1 integrin-deficient fibroblasts. *Arch Biochem Biophys* 442:160–168.
- Paszek MJ, Weaver VM. 2004. The tension mounts: Mechanics meets morphogenesis and malignancy. *J Mammary Gland Biol Neoplasia* 9:325–342.
- Paszek MJ, Zahir N, Johnson KR, Lakins JN, Rozenberg GI, Gefen A, Reinhart-King CA, Margulies SS, Dembo M, Boettiger D, Hammer DA, Weaver VM. 2005. Tensional homeostasis and the malignant phenotype. *Cancer Cell* 8:241–254.
- Pelham RJ, Wang YL. 1997. Cell locomotion and focal adhesions are regulated by substrate flexibility. *Proc Natl Acad Sci USA* 94:13661–13665.
- Peyton SR, Putnam AJ. 2005. Extracellular matrix rigidity governs smooth muscle cell motility in a biphasic fashion. *J Cell Physiol* 204:198–209.
- Raines EW. 2004. PDGF and cardiovascular disease. *Cytokine Growth Factor Rev* 15:237–254.
- Rajagopalan P, Marganski WA, Brown XQ, Wong JY. 2004. Direct comparison of the spread area, contractility, and migration of balb/c 3T3 fibroblasts adhered to fibronectin- and RGD-modified substrata. *Biophys J* 87:2818–2827.
- Resh MD. 2004. Membrane targeting of lipid modified signal transduction proteins. *Subcell Biochem* 37:217–232.
- Rowley JA, Mooney DJ. 2002. Alginate type and RGD density control myoblast phenotype. *J Biomed Mater Res* 60:217–223.
- Simons K, Ehehalt R. 2002. Cholesterol, lipid rafts, and disease. *J Clin Invest* 110:597–603.
- Simons K, Toomre D. 2000. Lipid rafts and signal transduction. *Nat Rev Mol Cell Biol* 1:31–39.
- Stegemann JP, Kaszuba SN, Row SL. 2007. Advances in vascular tissue engineering using protein-based biomaterials. *Tissue Eng* 13:2601–2613.
- Stehr M, Adam RM, Khoury J, Zhuang L, Solomon KR, Peters CA, Freeman MR. 2003. Platelet derived growth factor-BB is a potent mitogen for rat ureteral and human bladder smooth muscle cells: Dependence on lipid rafts for cell signaling. *J Urol* 169:1165–1170.
- Thyberg J. 1998. Phenotypic modulation of smooth muscle cells during formation of neointimal thickenings following vascular injury. *Histol Histopathol* 13:871–891.
- Thyberg J, Blomgren K, Roy J, Tran PK, Hedin U. 1997. Phenotypic modulation of smooth muscle cells after arterial injury is associated with changes in the distribution of laminin and fibronectin. *J Histochem Cytochem* 45: 837–846.
- Wang HB, Dembo M, Wang YL. 2000. Substrate flexibility regulates growth and apoptosis of normal but not transformed cells. *Am J Physiol Cell Physiol* 279:C1345–C1350.
- Wang HB, Dembo M, Hanks SK, Wang Y. 2001. Focal adhesion kinase is involved in mechanosensing during fibroblast migration. *Proc Natl Acad Sci USA* 98:11295–11300.
- Wong JY, Velasco A, Rajagopalan P, Pham Q. 2003. Directed movement of vascular smooth muscle cells on gradient-compliant hydrogels. *Langmuir* 19:1908–1913.

Dynamic interplay between the collagen scaffold and tumor evolution

Mikala Egeblad¹, Morten G Rasch^{1,2} and Valerie M Weaver^{3,4,5}

The extracellular matrix (ECM) is a key regulator of cell and tissue function. Traditionally, the ECM has been thought of primarily as a physical scaffold that binds cells and tissues together. However, the ECM also elicits biochemical and biophysical signaling. Controlled proteolysis and remodeling of the ECM network regulate tissue tension, generate pathways for migration, and release ECM protein fragments to direct normal developmental processes such as branching morphogenesis. Collagens are major components of the ECM of which basement membrane type IV and interstitial matrix type I are the most prevalent. Here we discuss how abnormal expression, proteolysis and structure of these collagens influence cellular functions to elicit multiple effects on tumors, including proliferation, initiation, invasion, metastasis, and therapy response.

Addresses

¹ Cold Spring Harbor Laboratory, 1 Bungtown Road, Cold Spring Harbor, NY 11724, USA

² The Finsen Laboratory, Rigshospitalet, 2200 Copenhagen, Denmark

³ Center for Bioengineering and Tissue Regeneration, Department of Surgery, University of California at San Francisco, San Francisco, CA 94143, USA

⁴ Department of Anatomy, University of California at San Francisco, San Francisco, CA 94143, USA

⁵ Department of Bioengineering and Therapeutic Sciences, Eli and Edythe Broad Center of Regeneration Medicine and Stem Cell Research and Helen Diller Family Comprehensive Cancer Center, University of California at San Francisco, San Francisco, CA 94143, USA

Corresponding author: Egeblad, Mikala (egeblad@cshl.edu)

Current Opinion in Cell Biology 2010, 22:697–706

This review comes from a themed issue on Cell-to-cell contact and extracellular matrix Edited by Peter Friedl and Jennifer Zallen

Available online 6th September 2010

0955-0674/\$ – see front matter

© 2010 Elsevier Ltd. All rights reserved.

DOI [10.1016/j.ceb.2010.08.015](https://doi.org/10.1016/j.ceb.2010.08.015)

Introduction

Many of the processes that regulate tissue and organ development are hijacked in cancer [1]. For example, the epithelial migration and invasion occurring in mammary carcinomas are morphologically and molecularly similar to epithelial branching morphogenesis in mammary gland development [2,3]. However, while epithelial

invasion is stringently regulated in development, solid tumors display deregulated and persistent invasion. In both instances, the extracellular matrix (ECM) provides a physical scaffold for cell adhesion and migration, it influences tissue tension and it signals to cells through ECM receptors. Proteolysis of the ECM regulates cellular migration by modifying the structure of the ECM scaffold and by releasing ECM fragments with biological functions. ECM proteolysis is therefore tightly controlled in normal tissues but typically deregulated in tumors.

Collagens are major constituents of the ECM, representing as much as 30% of total mammalian protein mass ([4], see Box 1). Type I collagen is the main structural protein in the interstitial ECM [5]. Type IV collagen is a key component of the basement membrane (BM), which is found at the basal surface of epithelial and endothelial cells and is essential for tissue polarity [6]. Epithelial invasion in both branching morphogenesis and cancer requires that the cells must interact with these collagens. The BM is breached as both normal and transformed epithelial cells invade into the interstitial tissue. It is also compromised at the site of the vasculature by metastasizing cancer cells [7*].

The desmoplastic response in cancer

Fibrosis is an accumulation of ECM proteins, including type I collagen [8]. Organ fibrosis and cancer are associated, although the association may simply reflect collagen accumulation due to increased activity of inflammatory and tumorigenic factors such as TGF- β [9]. Nevertheless, many malignancies are associated with a strong fibrotic reaction, termed ‘desmoplasia’, which is characterized by an accumulation of fibrillar collagen types I and III and increased degradation of type IV collagen [10–12]. Such fibrotic foci correlate with adverse prognosis in mammary carcinomas [13]. Desmoplasia has also been observed at metastatic sites where it may facilitate the successful establishment of metastases [14,15]. Indeed, increased expression of type I collagen and many of its modifying enzymes is frequently observed in the gene expression signatures associated with increased risk of metastasis [16*,17*].

Architectural changes of fibrillar collagen in cancer

The architecture of the collagen scaffolds in tumors is severely altered. Tumor-associated collagens are often linearized and crosslinked reflecting elevated deposition

Box 1 Collagen structure

At least 46 distinct collagen polypeptide α -chains have been identified in vertebrates and they can be assembled into 28 different collagens [103*].

Collagens are categorized according to their structural properties in the ECM. These include the classic fibrillar and network forming types, the FACITs (fibril-associated collagens with interrupted triple helices), the MACITs (membrane-associated collagens with interrupted triple helices), and the MULTIPLEXINs (multiple triple-helix domains and interruptions) [103*].

Collagens are composed of three polypeptide α -chains, which can be either homotrimers or heterotrimers. In the endoplasmic reticulum, the α -chains are packed into a tight triple-helical structure forming the collagenous domain [5].

The tight packing of the collagen triple-helix is facilitated by repeated Glycine-X-Y motifs in the collagenous domain of the collagen molecules (4-hydroxyproline is often found in the Y position) [5].

The α -chains also contain non-collagenous domains, which are proteolytically removed in the fibrillar collagens (e.g. types I, II, III). For other collagens, non-collagenous domains are important for supramolecular network formation, which for example is mediated by the C-terminal non-collagenous (NC1) domain of type IV collagen.

Collagens are matured by posttranslational modifications including proteolytic processing of the N-terminus and C-terminus for the fibrillar types (e.g. type I collagen), hydroxylation of peptidyl prolyl and lysyl residues, sulfilimine linking (type IV collagen), glycosylation of hydroxylysine residues by galactose and glucose, and enzymatic (lysyl-oxidase (LOX)-mediated) and non-enzymatic (glycation-mediated) covalent crosslinking [4,33,104*].

The non-collagenous domains can upon proteolytic removal exert new functions. Such collagen-derived proteolytic fragments include endostatin (from type XVIII collagen), restin (from type XV collagen) and tumstatin (from type IV collagen) that have anti-angiogenic and tumor growth inhibitory functions [4,105].

and significant posttranslational modification ([18,19**] and Figure 1). This physical restructuring of interstitial collagen progressively stiffens the ECM which thereafter elicits diverse effects on cellular differentiation, gene expression, proliferation, survival and migration [20,21**,22,23**]. These cellular effects can in turn significantly modify tumor progression and influence treatment response.

The linearization of interstitial collagen in invasive tumors is, at least in part, due to an increased number of covalent crosslinks between collagen molecules [19**]. Collagen crosslinking is predominantly catalyzed by enzymes such as lysyl oxidase (LOX). During the early stages of breast carcinogenesis, LOX is synthesized by stromal cells, likely in response to TGF- β . In late stage tumors, LOX is induced also in the carcinoma cells in response to hypoxia [24,25]. In a mouse model of ErbB2-induced breast carcinoma, treatment with LOX inhibitors, before tumors form, decreases ECM crosslinking and prevents tissue stiffening ([19**], and Figure 1b). This in turn inhibits focal adhesion maturation and decreases growth factor receptor signaling and concomitantly

reduces tumor incidence and size and delays tumor progression. The cancer-cell-secreted LOX enzymes in late stage cancer may also promote metastasis by regulating the behavior of the cancer cells and modifying the ECM of the metastatic niche [26**,27]. Consistently, increased expression of LOX and its related family members correlate clinically with tumor progression and elevated metastatic risk [27,28].

Fibronectin binds collagen and regulates collagen fibril organization [29]. Stretching of fibronectin stimulates its fibrillogenesis by revealing cryptic binding sites within the unfolded molecules, leading in turn to increased fibronectin rigidity [30]. Increased rigidity greatly increases binding forces between fibronectin and its receptor $\alpha 5 \beta 1$ integrin [31]. The size, density and rigidity of fibronectin fibrils *in vivo* therefore influence the function of the collagen fibrils, and vice versa. This dynamic and reciprocal relationship between collagens and fibronectin likely plays a role in tumor progression. Indeed, fibronectin deposition has been implicated as an early step in metastasis [15].

SPARC (secreted protein acidic and rich in cysteine) is a glycoprotein that participates in ECM organization and binds to types I and IV collagen [32*]. In a murine model of pancreatic cancer, SPARC deficiency reduces expression levels of types I, III and IV collagen and decreases collagen fibrillogenesis [32*]. Nevertheless, these animals show elevated metastasis, possibly due to an abnormal vascular BM that facilitates intravasation and extravasation of the cancer cells.

Sugars such as glucose and ribose induce covalent bonds with lysine residues in collagen fibrils to introduce non-enzymatic and random crosslinking, and these glycation adducts in turn form intermolecular covalent links [33]. Consistently, Diabetes Mellitus patients with uncontrolled glucose metabolism have increased numbers of glucose adducts on long-lived proteins like collagen [34]. These patients also have an elevated risk of developing tumors [35], suggesting that collagen glycation and the resulting ECM stiffening could be possible risk factors.

Collagen fibers as highways for migration

The collagen fibers surrounding the normal epithelial structures in soft tissues such as the mammary gland and lung are typically curly and anisotropic. However, following tumor initiation many of the fibers progressively thicken and linearize ([18,19**], and Figure 1a). This linearization is most notable adjacent to the tumor vasculature and in areas with cancer cell invasion [18,19**,36]. Linearized fibers are stiffer than curly ones and the resulting increased ECM stiffness can substantially potentiate growth-factor-dependent cell migration [19**,37]. These abnormal collagen fibers could promote metastasis by fostering cell migration into the interstitial

matrix and toward the vasculature. Indeed, intravital imaging shows that cancer cells and leukocytes migrate rapidly in collagen-rich regions on the collagen fibers [36,38,39]. Cancer cells might exploit these remodeled 'linear' collagen fibers as invasion 'highways' analogous to the preferential migration of glioma cancer cells along the matrix associated with blood vessels and rigid myelin sheath bundles [40] (Figure 2). The mechanisms whereby matrix rigidity could enhance cancer cell migration likely involve activation of collagen receptors, including integrins [41] and discoidin domain receptor (DDR) 1 [42] (see Box 2 for more on collagen receptors), and modulation of growth factor receptor signaling. Interestingly, an unusual form of type I collagen, a homotrimer of the $\alpha 1$ chains (in contrast to the normal $\alpha 1/\alpha 1/\alpha 2$ heterotrimer, see Figure 1a), enhances carcinoma cell migration *in vitro* [43]. Moreover, the homotrimers are secreted solely by carcinoma cells and are resistant to cleavage by matrix metalloproteinases (MMPs) [43].

Proteolysis of collagen – effects on cancer beyond path generation

Although cells migrate along collagen fibers, collagen in tissues also represents a physical barrier against invasion [44]. Thus, collagen degradation by proteases, including cathepsins and MMPs, and uptake of the degraded collagen is important for cancer cell invasion [10,45,46]. For many cells, proteolysis of types I and IV collagen is essential for migration through the ECM [7,45,47–49]. Proteolysis of the ECM generates pathways for cells to migrate through [50,51,52,53]. In addition, proteolysis of types I and IV collagen can also reveal RGD sequences in the molecules that activate $\alpha \nu$ integrins [54,55].

Cleavage of type I collagen by MMP-1, MMP-8, MMP-13 and MMP-14 (MT1-MMP) results in the generation of characteristic fragments that are 3/4 and 1/4 of the length of the native molecule ([56,57], Figure 1a). These fragments may act as antagonists of full-length collagen because they bind but fail to activate $\alpha 2\beta 1$ integrin [58]. However, the fragments might also promote cellular migration and survival by activating $\alpha \nu \beta 3$ integrin [59–62].

DDR signaling is also affected by collagen proteolysis. Intact type I collagen can inhibit cancer cell proliferation via DDR2 activation, but this growth restriction is released by MMP-mediated proteolysis [63]. This fits well with the overlap between a DDR2 binding site and the MMP-14 cleavage site in type I collagen [64,65].

Collagen proteolysis is also a critical step in angiogenesis [66,67]. However, non-collagenous (NC) domains of collagens (see Box 1) released by proteolysis can also inhibit tumor angiogenesis. For example, endostatin, a C-terminal fragment of type XVIII collagen, inhibits endothelial cell migration and thus tumor angiogenesis [4]. Several other inhibitors of angiogenesis are generated by the

Box 2 Collagen receptors — not just anchoring poles

Collagen signals are mediated to cells via a variety of receptors, including integrins, discoidin domain receptors (DDRs), leukocyte-associated Ig-like receptors (LAIRs), mannose receptor family members and glycoprotein VI (reviewed in [91]).

Integrins are composed of α and β sub-units. Native collagens are recognized by four integrins: $\alpha 1\beta 1$, $\alpha 2\beta 1$, $\alpha 10\beta 1$ and $\alpha 11\beta 1$. Integrin $\alpha 1\beta 1$ binds both types I and IV collagens whereas $\alpha 2\beta 1$ only binds type I collagen [91].

DDRs are tyrosine kinase receptors activated by collagen [106]. Both DDR1 and DDR2 are activated by intact fibrillar collagens, including type I. DDR1, but not DDR2, also is activated by type IV collagen [106].

LAIRs bind collagens at Glycine-Proline-Hydroxyproline repeats [107]. They are expressed on most immune cells and the interaction between LAIR-1 and collagen inhibits immune cell activation (reviewed in [83]).

Several members of the mannose receptor family bind collagen, including the mannose receptor and uPARAP/endo180 [91]. The main function of these receptors appears to be to internalize collagen for intracellular degradation.

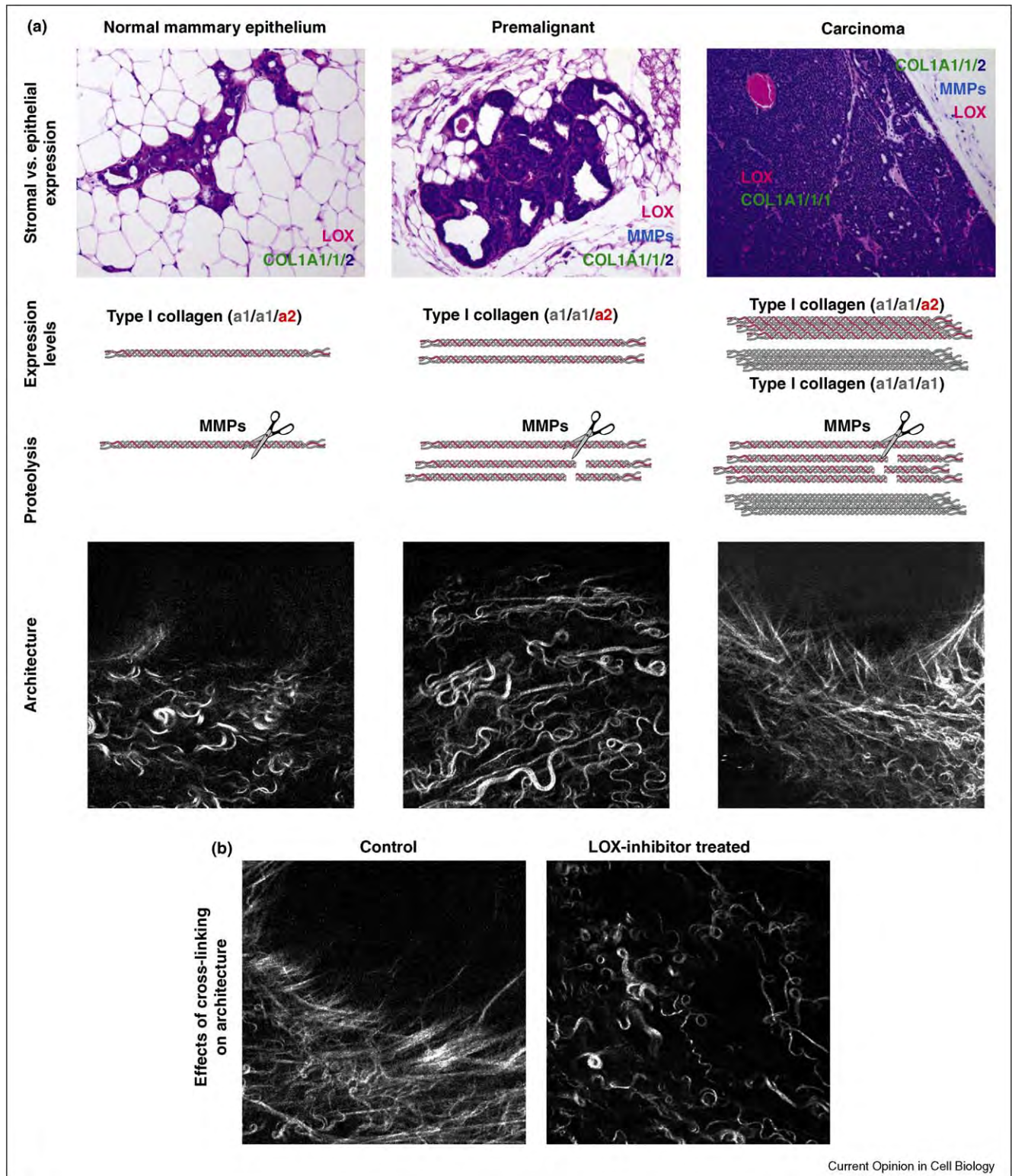
proteolysis of type IV collagen [6], including tumstatin, a fragment of the type IV $\alpha 3$ chain generated by MMP-9 [68]. The type IV collagen-derived anti-angiogenic fragments affect endothelial cellular functions by modulating $\alpha \nu \beta 3$ and $\alpha \nu \beta 5$ integrin signaling [68,69]. The ability of these fragments to inhibit angiogenesis suggests that they act as antagonists of $\alpha \nu \beta 3$ and $\alpha \nu \beta 5$ integrins, because these integrins are normally activated on endothelial cells by matrix components surrounding actively remodeling blood vessels (e.g. vitronectin, fibrinogen, and fibronectin).

Collagen as a regulator of response to therapy

Resistance to cancer therapy can be caused by cancer cell intrinsic mechanisms, such as overexpression of anti-apoptotic genes, but factors in the tumor microenvironment can also regulate therapy response [1].

Types I and IV collagen can induce chemoresistance by directly interacting with integrins on cancer cells [70,71]. The level and structural organization of collagen can also indirectly influence therapeutic efficacy by regulating drug delivery. In many tumors, drug delivery is impaired by an increased interstitial fluid pressure. The increased interstitial fluid pressure is due in part to a leaky vasculature and sparse or nonfunctional lymphatics [72]. However, increased ECM stiffness and a dense collagen interstitial fiber network can also influence interstitial fluid pressure. For example, deficiency in fibromodulin, which binds to collagen to stabilize the fibrils [73], decreases collagen fibril size in tumors and reduces interstitial fluid pressure [74]. Consistently, collagenase treatment of tumors decreases interstitial fluid pressure and enhances drug delivery [75,76]. A dense collagen network can also directly impede the diffusion of large molecular weight drugs to compromise treatment efficiency [77,78]. Finally, drug delivery

Figure 1



Changes in the type I collagen scaffold with tumor progression. **(a)** Relative levels of stromal versus epithelial expression of type I collagen, the collagen crosslinking enzyme lysyl oxidase (LOX) and the collagenolytic matrix metalloproteinases (MMPs) during tumor progression. In early stage tumors, LOX is highly expressed by stromal cells, and in late stage tumors, its expression also increases in carcinoma cells. In late stage tumors, the carcinoma cells begin to express an increased ratio of the $\alpha 1$ -chain to $\alpha 2$ -chain of type I collagen. The net result is an increase in both the normal type I collagen $\alpha 1, \alpha 1, \alpha 2$ -heterotrimer and in an MMP-resistant type I collagen $\alpha 1, \alpha 1, \alpha 1$ -homotrimer. The carcinoma-associated changes in collagen and

can also be inhibited by binding and sequestering of drugs to components in the ECM, including collagens [79].

Improved drug responses have been achieved when the collagen content in tumors has been reduced. This can for example be accomplished by vaccinating mice against fibroblast-activating protein, a proteinase expressed by carcinoma-associated fibroblasts. As a result, the carcinoma-associated fibroblasts are killed, leading to a reduction in the amount of type I collagen in the tumors and improved drug delivery and efficacy of chemotherapy [80[•]]. An increased delivery and efficacy of chemotherapy is also achieved by the depletion of tumor-associated fibrotic stroma through inhibition of Hedgehog signaling in a mouse model of pancreatic ductal adenocarcinoma [81[•]].

Interactions between collagen and the tumor immune infiltrate

A variety of immune cells are present in tumors and many of these accumulate and migrate within regions of dense fibrillar collagen [36,38,82]. How might the dense fibrillar collagen influence the function of immune cells? ECM stiffness promotes integrin-mediated adhesion assembly [21^{••}], which could influence, for example, T cell activation. Another possibility is via collagen-mediated activation of leukocyte-associated Ig-like receptors (LAIRs). LAIRs are highly expressed on most immune cells and can through their ITIMs (immunoreceptor tyrosine-based inhibition motifs) inhibit immune cell activation (reviewed in [83]). Although it is not clear whether LAIRs and integrins cooperate, activation of LAIRs is a plausible mechanism whereby high levels of deposited tumor collagen could lead to inhibition of an anti-tumor immune response.

Collagen can regulate leukocyte infiltration into tumors. Activation of the collagen receptor DDR1 is necessary for macrophage infiltration into atherosclerotic plaques [84]. Consistently, type I collagen and collagen fragments are chemotactic for monocytes (macrophage precursors) and neutrophils ([85,86[•]] and references therein).

Collagen may regulate the balance between tumor-inhibiting and tumor-promoting effects of immune cells. For example, culturing macrophages on type I collagen reduces their cytotoxicity against cancer cells [87], suggesting that this inhibits the polarization of the macrophages to the tumoricidal M1-like type. The possibility that the collagen scaffold can regulate macrophage polarization is further supported by the increase in pro-tumorigenic, M2-like macrophages observed in tumors of *Sparc*^{-/-} mice with an abnormal collagen scaffold [32[•]].

Collagen influences the immune cell infiltrate, but immune cells also influence collagen architecture. Macrophages regulate mammary epithelial invasion during normal development [88]. This may in part be through their ability to initiate the remodeling and reorganization of the collagen fibers surrounding the developing epithelium [89], probably achieved through secretion of a repertoire of soluble factors such as MMPs. Macrophages can also take up collagen for intracellular degradation via binding to the glycoprotein Mfge8 [90], the mannose receptor, and uPARAP/endo180 [91[•]].

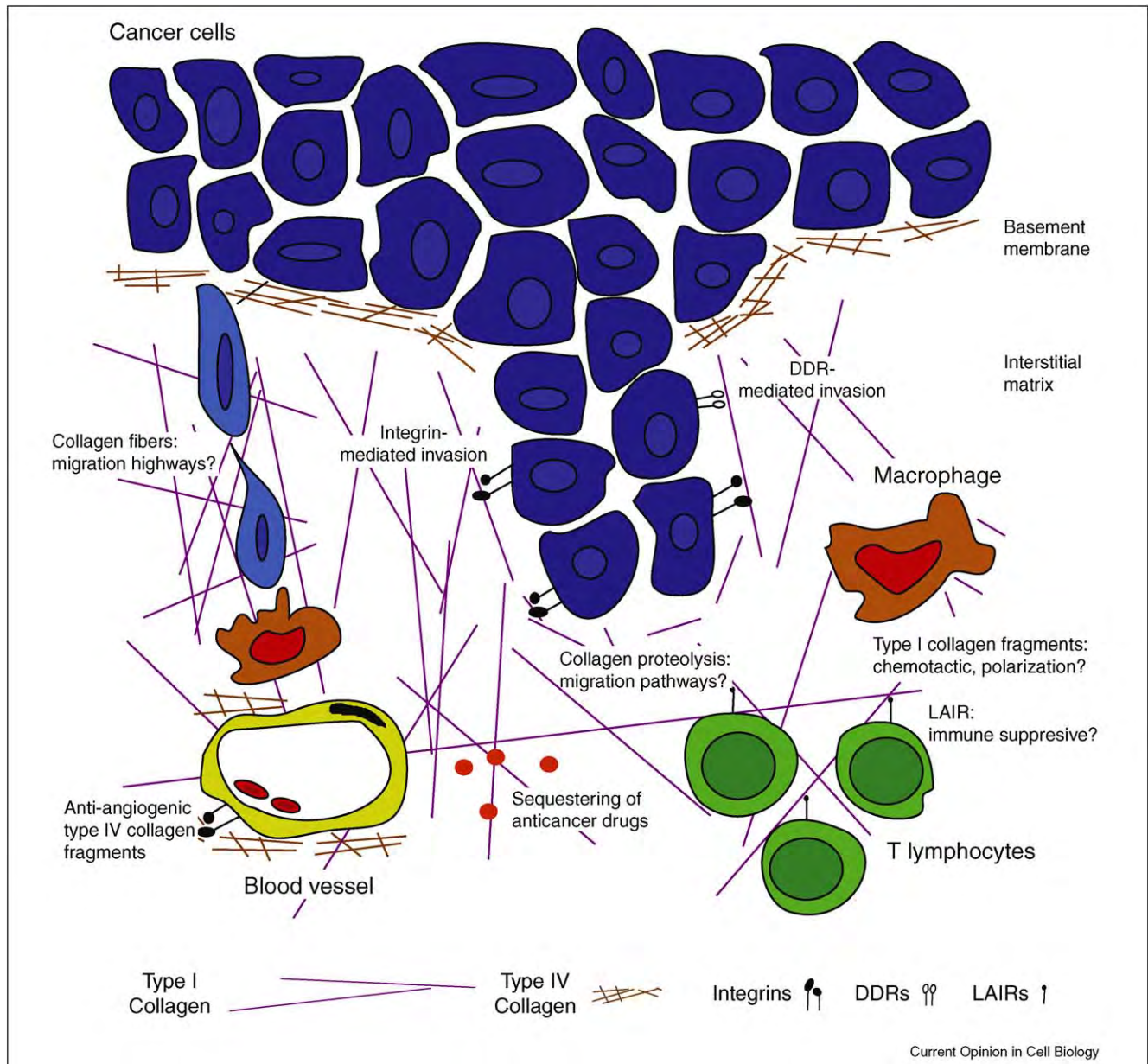
Collagen and regulation of differentiation

Matrix stiffness can determine stem cell lineage specification and direct mesenchymal stem cell differentiation into bone, neurons or muscle cells [92]. During bone development, inhibition of MMP-mediated cleavage of type I collagen leads to osteopenia, a loose bone structure, rather than increased bone formation [93], suggesting that an abnormal collagen scaffold modifies the balance between bone-forming osteoblasts and bone-resorbing osteoclasts. Indeed, the collagenolytic activity of MMP-14 regulates the differentiation of mesenchymal stem cells into bone-producing osteoblasts in three-dimensional (3D) collagen matrices [47]. By analogy, the modified levels, fibril organization and proteolysis of collagens in tumors could influence the differentiation state of cancer cells. Interestingly, type I collagen and Matrigel (which contains BM constituents such as laminin-111 and type IV collagen) increase engraftment of cancer cells in mice [94–96]. So how does collagen influence tumor engraftment? One potential clue is that the percentage of cancer cells that express stem cell markers increases when the cells are exposed to type I collagen [97]. Furthermore, breast cancer cells with stem cell-like characteristics express increased levels of types I, IV and XVIII collagen, suggesting that an ECM autocrine circuit might promote tumor evolution [98].

Integrins are strong contenders for linking collagen and cancer cell differentiation [41]. Integrin $\alpha\beta3$ is a marker of luminal progenitor cells in the mammary epithelium and $\beta3$ integrin (also known as CD61) is also a marker of a cancer stem cell-like population [99,100]. Integrin $\alpha\beta3$ is not activated by intact type I collagen, but by MMP-generated collagen fragments [59–62] and by stretched/denatured fibronectin, suggesting that collagen remodeling and stiffening could regulate stem cell differentiation by modulating the activity of this integrin. Indeed, collagen remodeling by MMP-14 regulates the differentiation of adipocytes from preadipocytes [23^{••}]. Whether these effects are due to a reduction in tissue rigidity or through generation of bioactive collagen fragments remains to be determined.

(Figure1 Legend Continued) collagen remodeling enzymes modify the architecture of the collagen scaffold such that early, thin and relaxed collagens (curly fibrils) progressively thicken and linearize coinciding with tumor progression and invasion. **(b)** Inhibition of collagen crosslinking through LOX-inhibition prevents collagen remodeling and maintains a normal collagen architecture. Photomicrographs are from [19^{••}] and reprinted with permission.

Figure 2



Cellular effects of the collagen scaffold in carcinomas. Types I and IV collagen influence multiple steps in tumor evolution. Type IV collagen is degraded as carcinomas break through the basement membrane to invade. It is breached again as cells intravasate en route to form metastases. Proteolysis of type IV collagen in vascular basement membranes results in generation of fragments with anti-angiogenic activity acting through integrins. Type I collagen fibers mediate invasion at several levels. Uncleaved fibers may act as 'highways' for cell migration, possibly facilitated by macrophages. Both integrin and discoidin domain receptor (DDR) mediated signaling can facilitate cell invasion. This type of invasion may also require the generation of pathways through the collagen scaffold by proteolysis. The immune reaction against tumors may be regulated by collagen: most immune cells express leukocyte-associated Ig-like receptors (LAIRs), which upon collagen binding inhibits immune cell activation. Macrophages may also be regulated by type I collagen fragments, which are chemotactic for macrophage precursors and possibly involved in regulation of their polarization.

The challenges ahead

The overall architecture of the ECM is affected by collagen concentration, posttranslational modification (e.g. crosslinking) and proteolysis. In cancer, all of these levels of collagen metabolism are deregulated, resulting in an abnormal ECM architecture. However,

to determine how this influences tumor evolution is challenging.

The study of the effects of collagen architecture on tumor evolution using *in vitro* assays has been informative, but a major concern is the ability to accurately replicate the

complicity of the ECM architecture found *in vivo*. There is therefore a strong need to study collagen structure/function *in vivo* and to develop tractable methods to manipulate biochemical composition, architectural features and mechanical properties of collagen while simultaneously monitoring cancer cell behavior. To address these concerns, second harmonic generation using two-photon microscopy has been used in live animals to monitor how epithelial and stromal cells interact with and initiate collagen remodeling to regulate its architecture [36,39,49,78,89,101^{••}]. In addition, recent work with Atomic Force Microscopy has yielded high resolution force 'heat' maps that demonstrate the existence of stiffness tracts that register with regions of collagen fiber enlargement and linearization (Lopez *et al.*, unpublished data).

Collagens are often used *in vitro* as barriers that cells must cross in invasion assays. Yet, it is clear that collagen has much more complex cellular effects than merely acting as an inert scaffolding protein and migration barrier. Indeed, such a simplistic view betrays the elegant reciprocal relationship between the ECM and cell behavior [102]. Our limited understanding of the effects of collagen in cancer is well illustrated by the findings described above: both increased [19^{••}] and decreased [32[•]] deposition of collagen can be associated with increased malignancy. These findings suggest that many of the effects of collagen are mediated by its architecture or by the dynamics of its remodeling rather than solely by protein level.

Analysis of human tumors has revealed an association between collagen expression or collagen modifying enzymes and poor prognosis [16[•],17[•],27,28,57], supporting the notion that collagen remodeling is highly relevant to human cancer progression. The challenge for ECM biologists is to deconstruct the collagen 'code', or in other words, to determine just how the structure of the collagen triple-helix translates into cellular effects to promote malignancy.

Acknowledgements

We thank Dr. Mark Sternlicht for his contribution to Figure 1. This work was supported by NIH grants U01CA141451 to ME and U54CA143836 and CA138818-01A1 to VMW and DOD grant W81XWH-05-1-0330 to VMW, as well as funding from the Breast Cancer Alliance, the Susan G Komen for the Cure, and Long Island 2 Day Walk to Fight Breast Cancer to ME. MGR was supported by Rigshospitalet, Augustinus fonden, Dagmar Marshalls fond, and the European Association for Cancer Research (EACR).

References and recommended reading

Papers of particular interest, published within the period of review, have been highlighted as:

- of special interest
 - of outstanding interest
1. Egeblad M, Nakasone E, Werb Z: **The tumor as an organ: complex tissues that interface with the entire organism.** *Dev Cell* 2010, **18**:884.
 2. Ewald AJ, Brenot A, Duong M, Chan BS, Werb Z: **Collective epithelial migration and cell rearrangements drive mammary branching morphogenesis.** *Dev Cell* 2008, **14**:570-581.
 3. Wiseman BS, Werb Z: **Stromal effects on mammary gland development and breast cancer.** *Science* 2002, **296**:1046-1049.
 4. Myllyharju J, Kivirikko KI: **Collagens, modifying enzymes and their mutations in humans, flies and worms.** *Trends Genet* 2004, **20**:33-43.
 5. Boot-Handford RP, Tuckwell DS: **Fibrillar collagen: the key to vertebrate evolution? A tale of molecular incest.** *Bioessays* 2003, **25**:142-151.
 6. Kalluri R: **Basement membranes: structure, assembly and role in tumour angiogenesis.** *Nat Rev Cancer* 2003, **3**:422-433.
 7. Rowe RG, Weiss SJ: **Breaching the basement membrane: who, when and how?** *Trends Cell Biol* 2008, **18**:560-574.
 - A comprehensive review on how different cell types cross the basement membrane during development and in cancer.
 8. Lopez-Novoa JM, Nieto MA: **Inflammation and EMT: an alliance towards organ fibrosis and cancer progression.** *EMBO Mol Med* 2009, **1**:303-314.
 9. Margadant C, Sonnenberg A: **Integrin-TGF-beta crosstalk in fibrosis, cancer and wound healing.** *EMBO Rep* 2010, **11**:97-105.
 10. Huijbers IJ, Iravani M, Popov S, Robertson D, Al-Sarraj S, Jones C, Isacke CM: **A role for fibrillar collagen deposition and the collagen internalization receptor endo180 in glioma invasion.** *PLoS One* 2010, **5**:e9808.
 11. Zhu GG, Risteli L, Makinen M, Risteli J, Kauppila A, Stenback F: **Immunohistochemical study of type I collagen and type I pN-collagen in benign and malignant ovarian neoplasms.** *Cancer* 1995, **75**:1010-1017.
 12. Kauppila S, Stenback F, Risteli J, Jukkola A, Risteli L: **Aberrant type I and type III collagen gene expression in human breast cancer in vivo.** *J Pathol* 1998, **186**:262-268.
 13. Hasebe T, Sasaki S, Imoto S, Mukai K, Yokose T, Ochiai A: **Prognostic significance of fibrotic focus in invasive ductal carcinoma of the breast: a prospective observational study.** *Mod Pathol* 2002, **15**:502-516.
 14. Erler JT, Weaver VM: **Three-dimensional context regulation of metastasis.** *Clin Exp Metastasis* 2009, **26**:35-49.
 15. Kaplan RN, Riba RD, Zacharoulis S, Bramley AH, Vincent L, Costa C, MacDonald DD, Jin DK, Shido K, Kerns SA *et al.*: **VEGFR1-positive haematopoietic bone marrow progenitors initiate the pre-metastatic niche.** *Nature* 2005, **438**:820-827.
 16. Tavazoie SF, Alarcon C, Oskarsson T, Padua D, Wang Q, Bos PD, Gerald WL, Massague J: **Endogenous human microRNAs that suppress breast cancer metastasis.** *Nature* 2008, **451**:147-152.
 - This paper documents an association between risk of metastasis and a gene expression signature that includes COL1A1.
 17. Ramaswamy S, Ross KN, Lander ES, Golub TR: **A molecular signature of metastasis in primary solid tumors.** *Nat Genet* 2003, **33**:49-54.
 - This paper documents an association between risk of metastasis and a gene expression signature that includes COL1A1 and COL1A2.
 18. Provenzano PP, Eliceiri KW, Campbell JM, Inman DR, White JG, Keely PJ: **Collagen reorganization at the tumor-stromal interface facilitates local invasion.** *BMC Med* 2006, **4**:38.
 19. Levental KR, Yu H, Kass L, Lakins JN, Egeblad M, Erler JT, Fong SF, Csiszar K, Giaccia A, Weninger W *et al.*: **Matrix crosslinking forces tumor progression by enhancing integrin signaling.** *Cell* 2009, **139**:891-906.
 - This paper demonstrates that collagen crosslinking during breast tumorigenesis stiffens the ECM to promote focal adhesions, enhancing PI3 kinase (PI3K) activity, and fostering invasion of an oncogene-initiated epithelium.
 20. Paszek MJ, Weaver VM: **The tension mounts: mechanics meets morphogenesis and malignancy.** *J Mammary Gland Biol Neoplasia* 2004, **9**:325-342.

21. Paszek MJ, Zahir N, Johnson KR, Lakins JN, Rozenberg GI, Gefen A, Reinhart-King CA, Margulies SS, Dembo M, Boettiger D *et al.*: **Tensional homeostasis and the malignant phenotype.** *Cancer Cell* 2005, **8**:241-254.
This paper demonstrated for the first time that tissue stiffness promotes malignant behavior by inducing Rho-dependent cell tension. Furthermore, by reducing cancer cell tension, the tumor behavior was normalized towards a non-invasive, non-proliferating tissue. The clustering of integrins induced by tissue stiffness or by myosin-induced contractility perturbs epithelial morphogenesis and induces a tumor-like behavior by disrupting adherens junctions, destabilizing tissue polarity, and enhancing growth.
22. Wozniak MA, Desai R, Solski PA, Der CJ, Keely PJ: **ROCK-generated contractility regulates breast epithelial cell differentiation in response to the physical properties of a three-dimensional collagen matrix.** *J Cell Biol* 2003, **163**:583-595.
23. Chun TH, Hotary KB, Sabeh F, Saltiel AR, Allen ED, Weiss SJ: **A pericellular collagenase directs the 3-dimensional development of white adipose tissue.** *Cell* 2006, **125**:577-591.
This paper shows that the differentiation of adipocytes requires MMP-14-mediated proteolysis that modulates pericellular collagen rigidity.
24. Peyrol S, Raccurt M, Gerard F, Gleyzal C, Grimaud JA, Sommer P: **Lysyl oxidase gene expression in the stromal reaction to in situ and invasive ductal breast carcinoma.** *Am J Pathol* 1997, **150**:497-507.
25. Santhanam AN, Baker AR, Hegamyer G, Kirschmann DA, Colburn NH: **Pdcd4 repression of lysyl oxidase inhibits hypoxia-induced breast cancer cell invasion.** *Oncogene* 2010, **29**:3921-3932.
26. Erler JT, Bennewith KL, Cox TR, Lang G, Bird D, Koong A, Le QT, Giaccia AJ: **Hypoxia-induced lysyl oxidase is a critical mediator of bone marrow cell recruitment to form the premetastatic niche.** *Cancer Cell* 2009, **15**:35-44.
This paper shows that lysyl oxidase is critical for defining metastatic sites through a mechanism that involves type IV collagen modification and recruitment of myeloid cells.
27. Erler JT, Bennewith KL, Nicolau M, Dornhofer N, Kong C, Le QT, Chi JT, Jeffrey SS, Giaccia AJ: **Lysyl oxidase is essential for hypoxia-induced metastasis.** *Nature* 2006, **440**:1222-1226.
28. Akiri G, Sabo E, Dafni H, Vadasz Z, Kartvelishvily Y, Gan N, Kessler O, Cohen T, Resnick M, Neeman M *et al.*: **Lysyl oxidase-related protein-1 promotes tumor fibrosis and tumor progression in vivo.** *Cancer Res* 2003, **63**:1657-1666.
29. Velling T, Risteli J, Wennerberg K, Mosher DF, Johansson S: **Polymerization of type I and III collagens is dependent on fibronectin and enhanced by integrins alpha 11beta 1 and alpha 2beta 1.** *J Biol Chem* 2002, **277**:37377-37381.
30. Klotzsch E, Smith ML, Kubow KE, Muntwyler S, Little WC, Beyeler F, Gourdon D, Nelson BJ, Vogel V: **Fibronectin forms the most extensible biological fibers displaying switchable force-exposed cryptic binding sites.** *Proc Natl Acad Sci U S A* 2009, **106**:18267-18272.
31. Friedland JC, Lee MH, Boettiger D: **Mechanically activated integrin switch controls alpha5beta1 function.** *Science* 2009, **323**:642-644.
32. Arnold SA, Rivera LB, Miller AF, Carbon JG, Dineen SP, Xie Y, Castrillon DH, Sage EH, Puolakkainen P, Bradshaw AD *et al.*: **Lack of host SPARC enhances vascular function and tumor spread in an orthotopic murine model of pancreatic carcinoma.** *Dis Model Mech* 2010, **3**:57-72.
This paper shows that organization of the collagen network by SPARC regulates metastasis and polarization of pro-tumorigenic, alternatively activated macrophages.
33. Furber JD: **Extracellular glycation crosslinks: prospects for removal.** *Rejuvenation Res* 2006, **9**:274-278.
34. Wolff SP, Jiang ZY, Hunt JV: **Protein glycation and oxidative stress in diabetes mellitus and ageing.** *Free Radic Biol Med* 1991, **10**:339-352.
35. Coughlin SS, Calle EE, Teras LR, Petrelli J, Thun MJ: **Diabetes mellitus as a predictor of cancer mortality in a large cohort of US adults.** *Am J Epidemiol* 2004, **159**:1160-1167.
36. Condeelis J, Segall JE: **Intravital imaging of cell movement in tumours.** *Nat Rev Cancer* 2003, **3**:921-930.
37. Zaman MH, Trapani LM, Sieminski AL, Mackellar D, Gong H, Kamm RD, Wells A, Lauffenburger DA, Matsudaira P: **Migration of tumor cells in 3D matrices is governed by matrix stiffness along with cell-matrix adhesion and proteolysis.** *Proc Natl Acad Sci U S A* 2006, **103**:10889-10894.
38. Wyckoff JB, Wang Y, Lin EY, Li JF, Goswami S, Stanley ER, Segall JE, Pollard JW, Condeelis J: **Direct visualization of macrophage-assisted tumor cell intravasation in mammary tumours.** *Cancer Res* 2007, **67**:2649-2656.
39. Wang W, Wyckoff JB, Frohlich VC, Oleynikov Y, Huttelmaier S, Zavadil J, Cermak L, Bottinger EP, Singer RH, White JG *et al.*: **Single cell behavior in metastatic primary mammary tumors correlated with gene expression patterns revealed by molecular profiling.** *Cancer Res* 2002, **62**:6278-6288.
40. Giese A, Kluwe L, Laube B, Meissner H, Berens ME, Westphal M: **Migration of human glioma cells on myelin.** *Neurosurgery* 1996, **38**:755-764.
41. Desgrosellier JS, Cheresch DA: **Integrins in cancer: biological implications and therapeutic opportunities.** *Nat Rev Cancer* 2010, **10**:9-22.
42. Vogel WF, Aszodi A, Alves F, Pawson T: **Discoidin domain receptor 1 tyrosine kinase has an essential role in mammary gland development.** *Mol Cell Biol* 2001, **21**:2906-2917.
43. Makareeva E, Han S, Vera JC, Sackett DL, Holmbeck K, Phillips CL, Visse R, Nagase H, Leikin S: **Carcinomas, contain a matrix metalloproteinase-resistant isoform of type I collagen exerting selective support to invasion.** *Cancer Res* 2010, **70**:4366-4374.
This paper demonstrates that the type I collagen $\alpha 1$ homotrimer, found in carcinomas, is resistant to matrix metalloproteinases and enhances proliferation and migration of invasive cancer cells. This suggests that invasive cancer cells use MMP-resistant type I collagen homotrimers for directed migration.
44. Liotta LA: **Tumor invasion and metastases — role of the extracellular matrix: Rhoads Memorial Award lecture.** *Cancer Res* 1986, **46**:1-7.
45. Sabeh F, Shimizu-Hirota R, Weiss SJ: **Protease-dependent versus -independent cancer cell invasion programs: three-dimensional amoeboid movement revisited.** *J Cell Biol* 2009, **185**:11-19.
This paper discusses the importance of proteolysis of the collagen network for cancer cell migration.
46. Curino AC, Engelholm LH, Yamada SS, Holmbeck K, Lund LR, Molinolo AA, Behrendt N, Nielsen BS, Bugge TH: **Intracellular collagen degradation mediated by uPARAP/Endo180 is a major pathway of extracellular matrix turnover during malignancy.** *J Cell Biol* 2005, **169**:977-985.
47. Lu C, Li XY, Hu Y, Rowe RG, Weiss SJ: **MT1-MMP controls human mesenchymal stem cell trafficking and differentiation.** *Blood* 2010, **115**:221-229.
48. Pilcher BK, Dumin JA, Sudbeck BD, Krane SM, Welgus HG, Parks WC: **The activity of collagenase-1 is required for keratinocyte migration on a type I collagen matrix.** *J Cell Biol* 1997, **137**:1445-1457.
49. Wolf K, Alexander S, Schacht V, Coussens LM, von Andrian UH, van Rheenen J, Deryugina E, Friedl P: **Collagen-based cell migration models in vitro and in vivo.** *Semin Cell Dev Biol* 2009, **20**:931-941.
50. Friedl P, Wolf K: **Plasticity of cell migration: a multiscale tuning model.** *J Cell Biol* 2010, **188**:11-19.
A comprehensive review on how ECM architecture regulates different types of cell migration.
51. Friedl P, Wolf K: **Tube travel: the role of proteases in individual and collective cancer cell invasion.** *Cancer Res* 2008, **68**:7247-7249.
52. Wolf K, Wu YI, Liu Y, Geiger J, Tam E, Overall C, Stack MS, Friedl P: **Multi-step pericellular proteolysis controls the**

- transition from individual to collective cancer cell invasion. *Nat Cell Biol* 2007, **9**:893-904.
This paper demonstrates the importance of pericellular fibrillar collagen remodeling as well as force generation for cellular migration.**
53. Sabeh F, Ota I, Holmbeck K, Birkedal-Hansen H, Soloway P, Balbin M, Lopez-Otin C, Shapiro S, Inada M, Krane S *et al.*: **Tumor cell traffic through the extracellular matrix is controlled by the membrane-anchored collagenase MT1-MMP.** *J Cell Biol* 2004, **167**:769-781.
 54. Davis GE: **Affinity of integrins for damaged extracellular matrix: alpha v beta 3 binds to denatured collagen type I through RGD sites.** *Biochem Biophys Res Commun* 1992, **182**:1025-1031.
 55. Xu J, Rodriguez D, Petitclerc E, Kim JJ, Hangai M, Moon YS, Davis GE, Brooks PC: **Proteolytic exposure of a cryptic site within collagen type IV is required for angiogenesis and tumor growth in vivo.** *J Cell Biol* 2001, **154**:1069-1079.
 56. Ohuchi E, Imai K, Fujii Y, Sato H, Seiki M, Okada Y: **Membrane type 1 matrix metalloproteinase digests interstitial collagens and other extracellular matrix macromolecules.** *J Biol Chem* 1997, **272**:2446-2451.
 57. Egeblad M, Werb Z: **New functions for the matrix metalloproteinases in cancer progression.** *Nat Rev Cancer* 2002, **2**:161-174.
 58. Messent AJ, Tuckwell DS, Knauper V, Humphries MJ, Murphy G, Gavrilovic J: **Effects of collagenase — cleavage of type I collagen on alpha2beta1 integrin-mediated cell adhesion.** *J Cell Sci* 1998, **111**(Pt 8):1127-1135.
 59. Stringa E, Knauper V, Murphy G, Gavrilovic J: **Collagen degradation and platelet-derived growth factor stimulate the migration of vascular smooth muscle cells.** *J Cell Sci* 2000, **113**(Pt 11):2055-2064.
 60. Montgomery AM, Reisfeld RA, Cheresch DA: **Integrin alpha v beta 3 rescues melanoma cells from apoptosis in three-dimensional dermal collagen.** *Proc Natl Acad Sci U S A* 1994, **91**:8856-8860.
 61. Fera E, O'Neil C, Lee W, Li S, Pickering JG: **Fibroblast growth factor-2 and remodeled type I collagen control membrane protrusion in human vascular smooth muscle cells: biphasic activation of Rac1.** *J Biol Chem* 2004, **279**:35573-35582.
 62. Petitclerc E, Stromblad S, von Schalscha TL, Mitjans F, Piulats J, Montgomery AM, Cheresch DA, Brooks PC: **Integrin alpha(v)beta3 promotes M21 melanoma growth in human skin by regulating tumor cell survival.** *Cancer Res* 1999, **59**:2724-2730.
 63. Wall SJ, Werner E, Werb Z, DeClerck YA: **Discoidin domain receptor 2 mediates tumor cell cycle arrest induced by fibrillar collagen.** *J Biol Chem* 2005, **280**:40187-40194.
 64. Konitsiotis AD, Raynal N, Bihan D, Hohenester E, Farndale RW, Leitinger B: **Characterization of high affinity binding motifs for the discoidin domain receptor DDR2 in collagen.** *J Biol Chem* 2008, **283**:6861-6868.
 65. Wu H, Byrne MH, Stacey A, Goldring MB, Birkhead JR, Jaenisch R, Krane SM: **Generation of collagenase-resistant collagen by site-directed mutagenesis of murine pro alpha 1(I) collagen gene.** *Proc Natl Acad Sci U S A* 1990, **87**:5888-5892.
 66. Seandel M, Noack-Kunmann K, Zhu D, Aimes RT, Quigley JP: **Growth factor-induced angiogenesis in vivo requires specific cleavage of fibrillar type I collagen.** *Blood* 2001, **97**:2323-2332.
 67. Chun TH, Sabeh F, Ota I, Murphy H, McDonagh KT, Holmbeck K, Birkedal-Hansen H, Allen ED, Weiss SJ: **MT1-MMP-dependent neovessel formation within the confines of the three-dimensional extracellular matrix.** *J Cell Biol* 2004, **167**:757-767.
 68. Hamano Y, Zeisberg M, Sugimoto H, Lively JC, Maeshima Y, Yang C, Hynes RO, Werb Z, Sudhakar A, Kalluri R: **Physiological levels of tumstatin, a fragment of collagen IV alpha3 chain, are generated by MMP-9 proteolysis and suppress angiogenesis via alphaV beta3 integrin.** *Cancer Cell* 2003, **3**:589-601.
 69. Cooke VG, Kalluri R: **Chapter 1. Molecular mechanism of type IV collagen-derived endogenous inhibitors of angiogenesis.** *Methods Enzymol* 2008, **444**:1-19.
 70. Armstrong T, Packham G, Murphy LB, Bateman AC, Conti JA, Fine DR, Johnson CD, Benyon RC, Iredale JP: **Type I collagen promotes the malignant phenotype of pancreatic ductal adenocarcinoma.** *Clin Cancer Res* 2004, **10**:7427-7437.
 71. Sethi T, Rintoul RC, Moore SM, MacKinnon AC, Salter D, Choo C, Chilvers ER, Dransfield I, Donnelly SC, Strieter R *et al.*: **Extracellular matrix proteins protect small cell lung cancer cells against apoptosis: a mechanism for small cell lung cancer growth and drug resistance in vivo.** *Nat Med* 1999, **5**:662-668.
This paper demonstrates that adhesion to ECM components, including type IV collagen, can suppress chemotherapy-induced apoptosis through activation of beta1 integrin.
 72. Heldin CH, Rubin K, Pietras K, Ostman A: **High interstitial fluid pressure — an obstacle in cancer therapy.** *Nat Rev Cancer* 2004, **4**:806-813.
 73. Svensson L, Aszodi A, Reinholt FP, Fassler R, Heinegard D, Oldberg A: **Fibromodulin-null mice have abnormal collagen fibrils, tissue organization, and altered lumican deposition in tendon.** *J Biol Chem* 1999, **274**:9636-9647.
 74. Oldberg A, Kalamajski S, Salnikov AV, Stuhr L, Morgelin M, Reed RK, Heldin NE, Rubin K: **Collagen-binding proteoglycan fibromodulin can determine stroma matrix structure and fluid balance in experimental carcinoma.** *Proc Natl Acad Sci U S A* 2007, **104**:13966-13971.
 75. Gade TP, Buchanan IM, Motley MW, Mazaheri Y, Spees WM, Koutcher JA: **Imaging intratumoral convection: pressure-dependent enhancement in chemotherapeutic delivery to solid tumors.** *Clin Cancer Res* 2009, **15**:247-255.
 76. McKee TD, Grandi P, Mok W, Alexandrakis G, Insin N, Zimmer JP, Bawendi MG, Boucher Y, Breakefield XO, Jain RK: **Degradation of fibrillar collagen in a human melanoma xenograft improves the efficacy of an oncolytic herpes simplex virus vector.** *Cancer Res* 2006, **66**:2509-2513.
 77. Netti PA, Berk DA, Swartz MA, Grodzinsky AJ, Jain RK: **Role of extracellular matrix assembly in interstitial transport in solid tumors.** *Cancer Res* 2000, **60**:2497-2503.
 78. Brown E, McKee T, diTomaso E, Pluen A, Seed B, Boucher Y, Jain RK: **Dynamic imaging of collagen and its modulation in tumors in vivo using second-harmonic generation.** *Nat Med* 2003, **9**:796-800.
 79. Minchinton AI, Tannock IF: **Drug penetration in solid tumours.** *Nat Rev Cancer* 2006, **6**:583-592.
 80. Loeffler M, Kruger JA, Niethammer AG, Reisfeld RA: **Targeting tumor-associated fibroblasts improves cancer chemotherapy by increasing intratumoral drug uptake.** *J Clin Invest* 2006, **116**:1955-1962.
This paper demonstrates that the killing of tumor-associated fibroblasts, by using a DNA vaccine targeting fibroblast activation protein, resulted in decreased type I collagen expression and significantly better uptake of and response to chemotherapeutic drugs.
 81. Olive KP, Jacobetz MA, Davidson CJ, Gopinathan A, McIntyre D, Honess D, Madhu B, Goldgraben MA, Caldwell ME, Allard D *et al.*: **Inhibition of Hedgehog signaling enhances delivery of chemotherapy in a mouse model of pancreatic cancer.** *Science* 2009, **324**:1457-1461.
This paper demonstrates that the delivery and efficacy of the chemotherapeutic drug gemcitabine is improved by coadministration of a drug that depletes tumor-associated stromal tissue by the inhibition of the Hedgehog signaling pathway in mice.
 82. Egeblad M, Ewald AJ, Askautrud HA, Truitt ML, Welm BE, Bainbridge E, Peeters G, Krummel MF, Werb Z: **Visualizing stromal cell dynamics in different tumor microenvironments by spinning disk confocal microscopy.** *Dis Model Mech* 2008, **1**:155-167.
 83. Meyaard L: **The inhibitory collagen receptor LAIR-1 (CD305).** *J Leukoc Biol* 2008, **83**:799-803.
 84. Franco C, Britto K, Wong E, Hou G, Zhu SN, Chen M, Cybulsky MI, Bendeck MP: **Discoidin domain receptor 1 on bone marrow-derived cells promotes macrophage accumulation during atherosclerosis.** *Circ Res* 2009, **105**:1141-1148.

85. Postlethwaite AE, Kang AH: **Collagen- and collagen peptide-induced chemotaxis of human blood monocytes.** *J Exp Med* 1976, **143**:1299-1307.
86. Weathington NM, van Houwelingen AH, Noerager BD, Jackson PL, Kraneveld AD, Galin FS, Folkerts G, Nijkamp FP, Blalock JE: **A novel peptide CXCR ligand derived from extracellular matrix degradation during airway inflammation.** *Nat Med* 2006, **12**:317-323.
- This paper demonstrates that a tripeptide (N-acetyl Pro-Gly-Pro) derived from the breakdown of collagen causes chemotaxis of neutrophils through CXC receptors.
87. Kaplan G: **In vitro differentiation of human monocytes. Monocytes cultured on glass are cytotoxic to tumor cells but monocytes cultured on collagen are not.** *J Exp Med* 1983, **157**:2061-2072.
88. Gouon-Evans V, Rothenberg ME, Pollard JW: **Postnatal mammary gland development requires macrophages and eosinophils.** *Development* 2000, **127**:2269-2282.
89. Ingman WV, Wyckoff J, Gouon-Evans V, Condeelis J, Pollard JW: **Macrophages promote collagen fibrillogenesis around terminal end buds of the developing mammary gland.** *Dev Dyn* 2006, **235**:3222-3229.
90. Atabai K, Jame S, Azhar N, Kuo A, Lam M, McKleroy W, Dehart G, Rahman S, Xia DD, Melton AC *et al.*: **Mfge8 diminishes the severity of tissue fibrosis in mice by binding and targeting collagen for uptake by macrophages.** *J Clin Invest* 2009, **119**:3713-3722.
91. Leitingner B, Hohenester E: **Mammalian collagen receptors.**
- *Matrix Biol* 2007, **26**:146-155.
- A comprehensive review on the structure and function of the different collagen receptors.
92. Engler AJ, Sen S, Sweeney HL, Discher DE: **Matrix elasticity directs stem cell lineage specification.** *Cell* 2006, **126**:677-689.
93. Egeblad M, Shen HC, Behonick DJ, Wilmes L, Eichten A, Korets LV, Kheradmand F, Werb Z, Coussens LM: **Type I collagen is a genetic modifier of matrix metalloproteinase 2 in murine skeletal development.** *Dev Dyn* 2007, **236**:1683-1693.
94. Del Buono R, Pignatelli M, Hall PA: **Control of differentiation in a rectal adenocarcinoma cell line: the role of diffusible and cell-associated factors.** *J Pathol* 1991, **164**:59-66.
95. Iwasaki H, Suda T: **Cancer stem cells and their niche.** *Cancer Sci* 2009, **100**:1166-1172.
96. Quintana E, Shackleton M, Sabel MS, Fullen DR, Johnson TM, Morrison SJ: **Efficient tumour formation by single human melanoma cells.** *Nature* 2008, **456**:593-598.
97. Kirkland SC: **Type I collagen inhibits differentiation and promotes a stem cell-like phenotype in human colorectal carcinoma cells.** *Br J Cancer* 2009, **101**:320-326.
98. Gupta PB, Onder TT, Jiang G, Tao K, Kuperwasser C, Weinberg RA, Lander ES: **Identification of selective inhibitors of cancer stem cells by high-throughput screening.** *Cell* 2009, **138**:645-659.
99. Asselin-Labat ML, Sutherland KD, Barker H, Thomas R, Shackleton M, Forrest NC, Hartley L, Robb L, Grosveld FG, van der Wees J *et al.*: **Gata-3 is an essential regulator of mammary-gland morphogenesis and luminal-cell differentiation.** *Nat Cell Biol* 2007, **9**:201-209.
100. Vaillant F, Asselin-Labat ML, Shackleton M, Forrest NC, Lindeman GJ, Visvader JE: **The mammary progenitor marker CD61/beta3 integrin identifies cancer stem cells in mouse models of mammary tumorigenesis.** *Cancer Res* 2008, **68**:7711-7717.
101. Perentes JY, McKee TD, Ley CD, Mathiew H, Dawson M, Padera TP, Munn LL, Jain RK, Boucher Y: **In vivo imaging of extracellular matrix remodeling by tumor-associated fibroblasts.** *Nat Methods* 2009, **6**:143-145.
- This paper describes the use of multiphoton laser scanning microscopy to determine the rate of remodeling of the collagen network by tumor-associated stromal cells in live mice.
102. Bissell MJ, Hall HG, Parry G: **How does the extracellular matrix direct gene expression?** *J Theor Biol* 1982, **99**:31-68.
103. Shoulders MD, Raines RT: **Collagen structure and stability.**
- *Annu Rev Biochem* 2009, **78**:929-958.
- A comprehensive review on the biochemistry of collagen.
104. Vanacore R, Ham AJ, Voehler M, Sanders CR, Conrads TP, Veenstra TD, Sharpless KB, Dawson PE, Hudson BG: **A sulfilimine bond identified in collagen IV.** *Science* 2009, **325**:1230-1234.
- This paper demonstrates that a sulfilimine bond is responsible for the covalent crosslinking of adjoining protomers of type IV collagen in the basement membrane.
105. Mundel TM, Kalluri R: **Type IV collagen-derived angiogenesis inhibitors.** *Microvasc Res* 2007, **74**:85-89.
106. Vogel WF, Abdulhussein R, Ford CE: **Sensing extracellular matrix: an update on discoidin domain receptor function.** *Cell Signal* 2006, **18**:1108-1116.
107. Lebbink RJ, de Ruiter T, Adelmeijer J, Brenkman AB, van Helvoort JM, Koch M, Farndale RW, Lisman T, Sonnenberg A, Lenting PJ *et al.*: **Collagens are functional, high affinity ligands for the inhibitory immune receptor LAIR-1.** *J Exp Med* 2006, **203**:1419-1425.

The extracellular matrix at a glance

Christian Frantz¹, Kathleen M. Stewart¹ and Valerie M. Weaver^{1,2,*}

¹Department of Surgery and Center for Bioengineering and Tissue Regeneration, University of California San Francisco, San Francisco, CA 94143, USA

²Department of Anatomy, Department of Bioengineering and Therapeutic Sciences, Eli and Edythe Broad Center of Regeneration Medicine and Stem Cell Research at UCSF, UCSF Helen Diller Comprehensive Cancer Center, University of California San Francisco, San Francisco, CA 94143, USA

*Author for correspondence (valerie.weaver@ucsfmedctr.org)

Journal of Cell Science 123, 4195-4200

© 2010. Published by The Company of Biologists Ltd

doi:10.1242/jcs.023820

Introduction

The extracellular matrix (ECM) is the non-cellular component present within all tissues and organs, and provides not only essential physical scaffolding for the cellular constituents but also initiates crucial biochemical and biomechanical cues that are required for tissue morphogenesis, differentiation and homeostasis. The importance of the ECM is vividly illustrated by the wide range of syndromes, which can be anything from minor to severe, that arise from genetic abnormalities in ECM proteins (Jarvelainen et al., 2009). Although, fundamentally, the ECM is composed of water, proteins and polysaccharides, each tissue has an ECM with a unique composition and topology that is generated during tissue development through a dynamic and reciprocal, biochemical and biophysical dialogue between the various cellular components (e.g. epithelial, fibroblast, adipocyte, endothelial elements) and the evolving cellular and protein microenvironment. Indeed, the physical, topological, and biochemical composition of the ECM is not only tissue-specific, but is also markedly heterogeneous. Cell adhesion to the ECM is mediated by ECM receptors, such as integrins, discoidin domain receptors and syndecans (Harburger and Calderwood, 2009; Humphries et al., 2006; Leitinger and Hohenester, 2007; Xian et al., 2010). Adhesion mediates cytoskeletal coupling to the ECM and is involved in cell migration through the ECM (Schmidt and Friedl, 2010). Moreover, the ECM is a highly dynamic structure that is constantly being remodeled, either enzymatically or non-enzymatically, and its molecular components are subjected to a myriad of post-translational modifications. Through these physical and biochemical characteristics the ECM generates the biochemical and mechanical properties of each organ, such as its tensile and compressive strength and elasticity, and also mediates protection by a buffering action that maintains extracellular homeostasis and water retention. In addition, the ECM directs essential morphological organization and physiological function by binding growth factors (GFs) and interacting with cell-surface receptors to elicit signal transduction and regulate gene transcription. The biochemical and biomechanical, protective and organizational properties of the ECM in a given tissue can vary tremendously from one tissue to another (e.g. lungs versus skin versus bone) and even within one tissue (e.g. renal cortex versus renal medulla), as well as from one physiological state to another (normal versus cancerous). In this Cell Science at a Glance article, we briefly describe the main molecular components of the ECM and then compare and



(See poster insert)

contrast the ECM within a normal simple epithelial tissue with that found within a pathologically modified tissue, as exemplified in aged tissue, wounded or fibrotic tissue and tumors. We particularly focus on the composition and architecture of the ECM and interactions with its cellular constituents, and describe in detail common post-translational modifications that evoke defined topological and viscoelasticity changes in the tissue. We thereafter discuss the functional consequences of ECM remodeling on cellular behaviors including altered GF sensitivity elicited by changes in ECM tension. Owing to space limitations and because the basement membrane (BM) is a unique ECM that has been reviewed in detail elsewhere (LeBleu et al., 2007), we focus here on the interstitial stroma of simple glandular epithelial tissues. We complete our review with a brief discussion of the application of natural and synthetic ECMs that can be used to either recapitulate the interstitial ECM in culture to study tissue behaviors or to deconstruct and analyze how specific ECM parameters (stiffness, fiber orientation, ligand presentation, dimensionality) provoke specific cellular behaviors.

Bits and pieces – molecular composition of the ECM

The ECM is composed of two main classes of macromolecules: proteoglycans (PGs) and fibrous proteins (see Boxes 1 and 2) (Jarvelainen et al., 2009; Schaefer and Schaefer, 2010). The main fibrous ECM proteins are collagens, elastins, fibronectins and laminins (see panel 1 of the poster) (Alberts et al., 2007). PGs fill the majority of the extracellular interstitial space within the tissue in the form of a hydrated gel (Box 1) (for details, see Jarvelainen et al., 2009). PGs have a wide variety of functions that reflect their unique buffering, hydration, binding and force-resistance properties. For example, in the kidney glomerular BM, perlecan has a role in glomerular filtration (Harvey and Miner, 2008; Morita et al., 2005). By contrast, in ductal epithelial tissues, decorin, biglycan and lumican associate with collagen fibers to generate a molecular structure within the ECM that is essential for mechanical buffering and hydration and that, by binding GFs, provides an easy, enzymatically accessible repository for these factors (Iozzo and Murdoch, 1996).

Collagen is the most abundant fibrous protein within the interstitial ECM and constitutes up to 30% of the total protein mass of a multicellular animal. Collagens, which constitute the main structural element of the ECM, provide tensile strength, regulate cell adhesion, support chemotaxis and migration, and direct tissue development (Rozario and DeSimone, 2010).

Box 1. Structure and function of proteoglycans

Proteoglycans (PGs) are composed of glycosaminoglycan (GAG) chains covalently linked to a specific protein core (with the exception of hyaluronic acid) (Iozzo and Murdoch, 1996; Schaefer and Schaefer, 2010). PGs have been classified according to their core proteins, localization and GAG composition. The three main families are: small leucine-rich proteoglycans (SLRPs), modular proteoglycans and cell-surface proteoglycans (Schaefer and Schaefer, 2010). The GAG chains on the protein core are unbranched polysaccharide chains composed of repeating disaccharide units [sulfated *N*-acetylglucosamine or *N*-acetylglucosamine- β 1,3-galactose- β 1] that can be divided further into sulfated (chondroitin sulfate, heparan sulfate and keratan sulfate) and non-sulfated (hyaluronic acid) GAGs (Schaefer and Schaefer, 2010). These molecules are extremely hydrophilic and, accordingly, adopt highly extended conformations that are essential for hydrogel formation and that enable matrices that are formed by these molecules to withstand high compressive forces. Many genetic diseases have been linked to mutations in PG genes (Jarvelainen et al., 2009; Schaefer and Iozzo, 2008). SLRPs have been involved in multiple signaling pathways including binding to and activation of epidermal growth factor receptor (EGFR), insulin-like growth factor 1 receptor (IGF1R) and low-density lipoprotein-receptor-related protein 1 (LRP1), regulation of inflammatory response reaction, binding to and activation of TGF β (Goldoni and Iozzo, 2008; Schaefer and Iozzo, 2008; Schaefer and Schaefer, 2010). Modular PGs can modulate cell adhesion, migration and proliferation (Schaefer and Schaefer, 2010). Basement membrane modular PGs (perlecan, agrin and collagen type XVIII) have a dual function as pro- and anti-angiogenic factors (Iozzo et al., 2009). Cell-surface PGs (syndecans and glypicans) can act as co-receptor facilitating ligand encounters with signaling receptors (Schaefer and Schaefer, 2010).

The bulk of interstitial collagen is transcribed and secreted by fibroblasts that either reside in the stroma or are recruited to it from neighboring tissues (De Wever et al., 2008). By exerting tension on the matrix, fibroblasts are able to organize collagen fibrils into sheets and cables and, thus, can dramatically influence the alignment of collagen fibers. Although within a given tissue, collagen fibers are generally a heterogeneous mix of different types, one type of collagen usually predominates.

Collagen associates with elastin, another major ECM fiber. Elastin fibers provide recoil to tissues that undergo repeated stretch. Importantly, elastin stretch is crucially limited by tight association with collagen fibrils (Wise and Weiss, 2009). Secreted tropoelastin (the precursor of elastin) molecules assemble into fibers and become highly crosslinked to one another via their lysine residues by members of the lysyl oxidase (LOX) enzyme family, which include LOX and LOXL (Lucero and Kagan, 2006). Elastin fibers are covered by glycoprotein microfibrils, mainly fibrillins, which are also essential for the integrity of the elastin fiber (Wise and Weiss, 2009).

A third fibrous protein, fibronectin (FN) is intimately involved in directing the organization of the interstitial ECM and, additionally, has a crucial role in mediating cell attachment and function. FN can be stretched several times over its resting length by cellular traction forces (Smith et al., 2007). Such force-dependent unfolding of FN exposes cryptic integrin-binding sites within the molecule that result in

pleiotropic changes in cellular behavior and implicate FN as an extracellular mechanoregulator (Smith et al., 2007). Indeed, 'tensed' FN modulates the catch bond 'force-activation' and adhesion assembly of α 5 β 1-integrin through exposure of its synergy site (Friedland et al., 2009). FN is also important for cell migration during development and has been implicated in cardiovascular disease and tumor metastasis (Rozario and DeSimone, 2010; Tsang et al., 2010). Like FN, other ECM proteins such as tenascin exert pleiotropic effects on cellular behavior, including the promotion of fibroblast migration during wound healing (Trebaut et al., 2007; Tucker and Chiquet-Ehrismann, 2009). Indeed, levels of tenascins C and W are elevated in the stroma of some transformed tissues where they can inhibit the interaction between syndecan4 and FN to promote tumor growth and metastasis (Tucker and Chiquet-Ehrismann, 2009).

The definition of normal – the ECM and tissue homeostasis

Normal glandular epithelial tissues are composed of a simple layer of epithelial cells that adopt apical–basal polarity, where the basal side contacts the BM and the apical side is opposite the fluid-filled lumen. In some glandular epithelium there is a basal or myoepithelial cell layer that separates the luminal epithelium from the interstitial ECM (Barsky and Karlin, 2005). Epithelial tissue homeostasis depends on the maintenance of tissue organization and a dynamic dialogue with

a surrounding stroma composed primarily of non-activated fibroblasts and adipocytes, and a steady-state population of transiting, non-stimulated leukocytes (Ronnov-Jessen et al., 1996). Thus, non-activated tissue fibroblasts secrete and organize type I and III collagens, elastin, fibronectin, tenascin and a repertoire of PGs (hyaluronic acid and decorin), which all maintain the structural and functional integrity of the interstitial ECM. Most glandular epithelial tissues including breast, saliva gland, lung, and prostate are in a state of tensional homeostasis so that their normal state is highly mechanically compliant (Paszek and Weaver, 2004). The ECM in a compliant tissue is composed of a relaxed meshwork of type I and III collagens and elastin that, together with FN, form a relaxed network of fibers that are surrounded by and embedded in a hydrogel of glycosaminoglycan-chain-containing PGs (Bosman and Stamenkovic, 2003). Consequently, the relaxed network of collagen and elastin fibers allow the healthy ECM to resist a wide range of tensile stresses. A functionally competent normal tissue can also easily resist compressive stresses because of the binding of the hydrated glycosaminoglycan (GAG) network to the fibrous ECM molecules (Scott, 2003). Thus, the tissue ECM is a highly dynamic entity that continuously undergoes regulated remodeling, whose precise orchestration is crucial to the maintenance of normal function (Egeblad et al., 2010; Kass et al., 2007). Tissue homeostasis is mediated by the coordinated secretion of fibroblast metalloproteinases (MMPs) (Mott and Werb, 2004); this is counterbalanced by tissue inhibitors of metalloproteinases (TIMPs) (Cruz-Munoz and Khokha, 2008) and the controlled activity of other enzymes, such as LOX, and also transglutaminases that crosslink and, consequently, stiffen the ECM (Lucero and Kagan, 2006). A plethora of GFs that are bound to the ECM direct these processes (Friedl, 2010; Hynes, 2009; Macri et al., 2007; Murakami et al., 2008; Oehrl and Panayotou, 2008). These ECM-bound GFs differentially modulate cell growth and migration and, when released, comprise part of a tightly controlled feedback circuit that is essential for normal tissue homeostasis (Hynes, 2009).

Stiffening up – the ECM and tissue aging

As a tissue ages the levels of junctional proteins such as cadherin, catenin or occludin decrease and this loss can compromise junctional integrity as revealed by the appearance of gaps between the epithelial cells (Akintola et al., 2008; Bolognia, 1995). Old tissue is also characterized by a thinning of the BM, probably

Box 2. Collagen and fibronectin synthesis

To date, 28 types of collagen have been identified in vertebrates (Gordon and Hahn, 2010). The majority of collagen molecules form a triple-stranded helix that subsequently can assemble into supramolecular complexes, such as fibrils and networks, depending on the type of collagen. Fibrous collagens form the backbone of the collagen fibril bundles within the interstitial tissue stroma, whereas network collagens are incorporated into the basal membrane (BM). Synthesis of collagen type I involves a number of enzymatic post-translational modifications (Gordon and Hahn, 2010; Myllyharju and Kivirikko, 2004), mainly the hydroxylation of proline and lysine residues, glycosylation of lysine and the cleavage of N- and C-terminal propeptides. Following their cleavage, collagen fibrils are strengthened by the covalent crosslinking between lysine residues of the constituent collagen molecules by lysyl oxidases (LOX) (Myllyharju and Kivirikko, 2004; Robins, 2007).

FN is secreted as a dimer joined by two C-terminal disulfide bonds and has several binding sites to other FN dimers, to collagen, to heparin and also to cell-surface integrin receptors (Pankov and Yamada, 2002). Cell-surface binding of the soluble FN dimer is essential for its assembly into longer fibrils. Moreover, cell contraction through the actomyosin cytoskeleton and the resulting integrin clustering promotes FN–fibril assembly by exposing cryptic binding sites, thus allowing them to bind one another (Leiss et al., 2008; Mao and Schwarzbauer, 2005; Vakonakis and Campbell, 2007).

because of elevated MMP-mediated degradation and reduced BM protein synthesis (Callaghan and Wilhelm, 2008). Moreover, the resident fibroblasts in aged tissues are growth-arrested and resistant to apoptotic cues, which is indicative of senescence (Campisi and d'Adda di Fagagna, 2007). Indeed, senescent fibroblasts typically express elevated levels of FN, MMPs, GFs, interleukins and cytokines, as well as high levels of the plasminogen activator inhibitor (PAI) (Coppe et al., 2010) and mitochondrial-related reactive oxygen species (ROS) (Untergasser et al., 2005) and, as a result, are frequently in a state of chronic inflammation. Indeed, the combination of chronic inflammation and elevated MMPs, PAI and ROS destroy the integrity of the elastin network and modify the collagen fiber network, whereas reduced levels of tissue-associated GAGs compromise the integrity of the BM (Callaghan and Wilhelm, 2008; Calleja-Agius et al., 2007; Nomura, 2006). Nevertheless, and somewhat paradoxically, in an aging tissue, collagen fibers are frequently – inappropriately – crosslinked through glycation, by byproducts of lipid oxidation and through exposure to UV light (Robins, 2007). The combination of elevated and inappropriate collagen crosslinking contributes to tissue stiffening so that an aged tissue is mechanically weaker and less elastic but also more rigid than a young tissue (Calleja-Agius et al., 2007; Robins, 2007). This aberrant mechanical state can severely compromise ECM organization, and modify epithelial organization and function, potentially promoting age-related diseases such as cancer (Coppe et al., 2010; Freund et al., 2010; Sprenger et al., 2008).

Tensional homeostasis and fibrosis

Acute injury activates the fibrogenic machinery and induces wound healing. One of the first

events that characterize a wound response is vascular damage and the formation of a fibrin clot, which stimulates monocyte infiltration to the damaged ECM. Upon binding to ECM-degradation products and cytokines, monocytes rapidly differentiate into macrophages (Clark, 2001). These activated macrophages, in turn, secrete and release multiple GFs, MMPs and cytokines that promote angiogenesis and stimulate fibroblast migration and proliferation (Schultz and Wysocki, 2009). Thereafter, recruited fibroblasts begin to synthesize and deposit large quantities of ECM proteins, including collagen type I and III, FN and hyaluronic acid. The elevated mechanical stress associated with this profound ECM deposition can induce the transdifferentiation of fibroblasts and other tissue-resident cells – i.e. epithelial-to-mesenchymal transition (EMT) of epithelial cells – or of circulating bone marrow-derived mesenchymal stem cells into myofibroblasts (Schultz and Wysocki, 2009; Velnar et al., 2009). Myofibroblasts, which have a high capacity to synthesize ECM components and are highly contractile, can promote the formation of large, rigid collagen bundles that, if crosslinked by LOX enzymes, mechanically strengthen and stiffen the tissue (Szauder et al., 2005). This wounded ‘stiffened’ microenvironment disrupts the BM that surrounds the epithelium and compromises tissue integrity with loss of apical–basal polarity and destabilized cell–cell adhesions. The remodeled ECM also promotes the directional migration of cells within the tissue towards the wound site (Schafer and Werner, 2008). In some instances, the release of transforming growth factor β (TGF- β) by tension and MMPs induces EMT of the resident epithelium (Schultz and Wysocki, 2009; Wipff et al., 2007; Xu et al., 2009). In a healthy tissue, once the wound has been repopulated, strict

feedback mechanisms are initiated that ensure restoration of tissue homeostasis and resolution of fibrosis (Schultz and Wasyocki, 2009; Velnar et al., 2009). Under extreme conditions, such as repeated injury or when normal feedback mechanisms are compromised, continuous ECM synthesis, deposition and remodeling ensue and myofibroblasts remain, in which TIMP production prevails over MMP synthesis. These aberrant conditions promote chronic vascular remodeling and enhanced ECM crosslinking that eventually leads to aberrant fibrosis and an inability of the tissue to heal properly. This aberrant wound healing scenario is characterized by the altered mechanical stability and reduced elasticity that is typical of scarred tissue (Kisseleva and Brenner, 2008). In extreme cases, a chronic wound can also promote a tumor phenotype (De Wever et al., 2008).

Tumors – a tough situation

Cancer is the loss of tissue organization and aberrant behavior of the cellular components. Cell transformation results from genetic mutations and epigenetic alterations. Yet, tumors have also been likened to wounds that fail to heal (Schafer and Werner, 2008). Thus, the tumor stroma exhibits some of the characteristics found in an unresolved wound (Bissell and Radisky, 2001). For example, tumors are characteristically stiffer than the surrounding normal tissue. The stiffening of tumors is induced by ECM deposition and remodeling by resident fibroblasts, and by increased contractility of the transformed epithelium (Butcher et al., 2009; Levental et al., 2009). Moreover, chemokines and GFs (De Wever et al., 2008) induce inflammation and modify the repertoire of infiltrating T lymphocytes (Tan and Coussens, 2007). Tissue inflammation potentiates stromal fibroblast activation and induces their trans-differentiation into myofibroblasts, thus exacerbating and promoting tissue desmoplasia (De Wever et al., 2008; Desmouliere et al., 2004). Myofibroblasts deposit copious quantities of ECM proteins, secrete GFs and exert strong contraction forces on the ECM (De Wever et al., 2008; Desmouliere et al., 2004). As a consequence, newly deposited and remodeled collagen and elastin fibers are reoriented and, thereafter, crosslinked by LOX and transglutaminase, thus generating larger, more-rigid fibrils that further stiffen the tissue ECM (Butcher et al., 2009; Erler and Weaver, 2009; Levental et al., 2009; Lucero and Kagan, 2006; Payne et al., 2007; Rodriguez et al., 2008). MMPs, which are secreted and activated by tumor cells and by myofibroblasts (De Wever et al., 2008; Kessenbrock et al., 2010), also remodel the BM surrounding the tumor and release and activate

ECM-embedded GFs (Bosman and Stamenkovic, 2003; Kessenbrock et al., 2010). The release of GFs, including vascular endothelial growth factor (VEGF), enhances vascular permeability and promotes new vessel growth, which generates interstitial tissue pressure. Thus, an amplifying circuitry between tumor-associated ECM stiffening, an ensuing reciprocal ECM resistance that is induced by resident tumor cells, and myoepithelial and cell-generated contractility act as a vicious, positive-feedback loop to potentiate tumor growth and survival. This induces angiogenesis and invasion and, eventually, fosters metastasis (Butcher et al., 2009; Erler and Weaver, 2009; Paszek and Weaver, 2004; Paszek et al., 2005).

Where do we go from here?

Challenges encountered with natural and synthetic ECMs

Considering the importance of the ECM to so many fundamental cellular processes, a myriad of tissue-culture models have been developed to study the interplay between its biochemical and biophysical properties, and to understand the molecular origins of cellular behaviors regulated by ECM ligation. With respect to assessing the fundamental nature of cell adhesion and its effects on cell behavior, the majority of cancer researchers have relied on coating tissue culture dishes (whether plastic or glass) with purified preparations or mixtures of ECM proteins in order to obtain 2D monolayers (Kuschel et al., 2006). To address the issue of ECM rigidity, functionalized polyacrylamide (PA) gels crosslinked with reconstituted basement membrane (rBM) – generated from Engelbreth-Holm-Swarm mouse carcinoma (commercially available as Matrigel™), collagen type I, FN or ECM peptides – has become the standard approach (Johnson et al., 2007; Pelham and Wang, 1997). Yet, none of these strategies faithfully recapitulates the behavior of cells within tissues, which demand not only a 3D format, but an ECM that can be readily remodeled. To address the aspect of 3D and ECM remodeling, researchers have used natural ECM and reconstituted ECM gels to recapitulate specific aspects of tissue-specific differentiation and architecture (see poster, panel 3). For instance, the rBM, which mimics some of the biochemical and biophysical properties of endogenous epithelial basement membranes, has been used frequently in 3D organotypic culture assays, for xenograft manipulations or tissue engineering, and to study tissue-specific morphogenesis (e.g. branching, acini formation) and differentiation (Kleinman and Martin, 2005; Kleinman et al., 1986). Unfortunately, BM preparations such as Matrigel™, although useful for studying normal

epithelial or endothelial behavior and to distinguish between the ‘normal’ and ‘malignant’ behavior of some tissues, has a complex and rudimentarily defined composition, and fails to reconstruct the physical state of the native interstitial ECM. Fibrin has also been used as natural biodegradable scaffold with reasonable success in vascular tissue engineering, but lacks the mechanical strength and durability of native interstitial ECM (Blomback and Bark, 2004; Shaikh et al., 2008). By contrast, type I collagen is reasonably useful and can be combined with rBM, purified laminin or FN to reconstitute some of the biological aspects of normal and diseased interstitial ECM (Friess, 1998; Gudjonsson et al., 2002). Moreover, collagen type I readily assembles into a mechanically tense network of fibrils that can be oriented, functionally modified, and enzymatically or chemically crosslinked and stiffened. Thus collagen I gels are useful substrates to assess the role of collagen and FN stiffness, and organization on the pathogenesis of tumor progression and invasion (Levental et al., 2009; Provenzano et al., 2009). Nevertheless, collagen gels are quite heterogeneous, and modifying their architecture changes their organization, pore size and ligand concentration, thereby complicating the interpretation of data generated from experiments conducted by using this natural scaffold (Johnson et al., 2007). To overcome this issue, tissue engineers and biomaterial specialists have generated denuded ECM scaffold from various tissues (Macchiaroni et al., 2008). These scaffolds, combined with colonies of seeded stem cells, can reconstitute normal tissues with reasonable fidelity (Lutolf et al., 2009). ECMs have also been isolated and extracted from various tissues, such as small intestine, skin (from cadavers), pancreas and breast (Rosso et al., 2005), and these ECMs have been used to engineer skin grafts (Badylak, 2007), enhance wound healing and to study tumor progression. One such example is given by porcine-derived small intestinal submucosa (SIS), which has proven clinical success for treating patients with hernias (Franklin et al., 2002) (reviewed in Badylak, 2007). Although these purified ECMs certainly have useful applications, their use is limited in scope owing to the need for well-defined microenvironments in tissue regeneration and stem cell transplantation in which animal byproducts and contaminants are limited. Moreover, to understand the molecular and biophysical mechanisms by which the ECM elicits diverse effects on cellular differentiation and morphogenesis it is crucial to use chemically and physically defined, modular ECMs that can be reliably reproduced. In this respect, synthetic

matrices have been developed that feature defined and tunable compositions, organization, mechanics and ECM remodeling capabilities. Indeed, in response to this need there has been literally an explosion of publications describing the generation and application of synthetic ECMs for tissue regeneration, and the reader is referred to some excellent reviews on these topics (Ayres et al., 2009; Dutta and Dutta, 2009; Lutolf and Hubbell, 2005; McCullen et al., 2009; Rosso et al., 2005; Zisch et al., 2003). One example is given by polyethylene glycol (PEG) hydrogels – frequently used biologically compatible synthetic matrices that support cell adhesion, viability and growth (Lutolf and Hubbell, 2005). Although these matrices can be covalently modified with ECM ligands and collagenase-degradable peptides and GFs (Ehrbar et al., 2007; Zisch et al., 2003), they do not mimic the organizational features of native collagen gels and all too often their pore sizes strongly impede cell migration. By contrast, peptide-based hydrogels, such as peptide-amphiphiles, assemble into secondary structures that recapitulate the collagen triple helix, and readily support stem cell growth and viability, and direct multicellular morphogenesis (Hauser and Zhang, 2010; Sieminski et al., 2008; Smith and Ma, 2004; Ulijn and Smith, 2008). These peptides-amphiphiles are amenable to modification by covalent binding of native proteins and MMP-degradable ECM peptides. Alternatively, poly(lactic-co-glycolic acid) (PLGA), a copolymer of glycolic acid and lactic acid (McCullen et al., 2009) that is inherently biodegradable as it is hydrolyzed into lactic acid and glycolic acid, has been developed and can be readily conjugated to various ECM ligands and peptides, or coated with collagen or chitosan to support cell adhesion, viability and growth. Indeed, one of the most exciting recent advances in the field has been the development of modular biocompatible ECMs, which contain ligand-binding cassettes and have tunable stiffness features that permit a precise patterning of cell adhesion in 2D and 3D formats (Serban and Prestwich, 2008). The realization that ECM organization is a crucial aspect of cellular behavior has led to the development of new methodologies and generated ECMs whose fiber size, orientation, stiffness, ligand-binding function and remodeling potential can be strictly controlled and monitored – including electrospun silk, and lactic-acid polymer (PLLA) and PLGA scaffolds (Zhang et al., 2009). Anisotropically nanofabricated substrates formed from scalable biocompatible PEG (Kim et al., 2010; Smith et al., 2009) are exciting new developments in the biomaterials field, whose only major impediment to their biological application appears to be a lack of

functional assessment in physiological culture assays and animal models. Although only time can tell whether this new generation of biomaterials will indeed prove useful, it is an appealing time to be an ECM biologist and our next challenge will be to embrace this smorgasbord of enticing new tools – which hopefully will at last allow us to decipher the language of the matrix.

This work was supported by the NIH grants U54CA143836 and CA138818-01A1 and the DOD grant W81XWH-05-1-0330 to V.M.W. Deposited in PMC for release after 12 months.

References

- Akintola, A. D., Crislip, Z. L., Catania, J. M., Chen, G., Zimmer, W. E., Burghardt, R. C. and Parrish, A. R. (2008). Promoter methylation is associated with the age-dependent loss of N-cadherin in the rat kidney. *Am. J. Physiol. Renal Physiol.* **294**, F170-F176.
- Alberts, B., Johnson, A., Lewis, J., Raff, M., Roberts, K. and Walter, P. (2007). *Molecular Biology of the Cell*. London: Garland Science.
- Ayres, C. E., Jha, B. S., Sell, S. A., Bowlin, G. L. and Simpson, D. G. (2009). Nanotechnology in the design of soft tissue scaffolds: innovations in structure and function. *Wiley Interdiscip. Rev. Nanomed. Nanobiotechnol.* **2**, 20-34.
- Badyrak, S. F. (2007). The extracellular matrix as a biologic scaffold material. *Biomaterials* **28**, 3587-3593.
- Barsky, S. H. and Karlin, N. J. (2005). Myoepithelial cells: autocrine and paracrine suppressors of breast cancer progression. *J. Mammary Gland Biol. Neoplasia* **10**, 249-260.
- Bissell, M. J. and Radisky, D. (2001). Putting tumours in context. *Nat. Rev. Cancer* **1**, 46-54.
- Blombäck, B. and Bark, N. (2004). Fibrinopeptides and fibrin gel structure. *Biophys. Chem.* **112**, 147-151.
- Bologna, J. L. (1995). Aging skin. *Am. J. Med.* **98**, 99S-103S.
- Bosman, F. T. and Stamenkovic, I. (2003). Functional structure and composition of the extracellular matrix. *J. Pathol.* **200**, 423-428.
- Butcher, D. T., Alliston, T. and Weaver, V. M. (2009). A tense situation: forcing tumour progression. *Nat. Rev. Cancer* **9**, 108-122.
- Callaghan, T. M. and Wilhelm, K. P. (2008). A review of ageing and an examination of clinical methods in the assessment of ageing skin. Part 2, Clinical perspectives and clinical methods in the evaluation of ageing skin. *Int. J. Cosmet. Sci.* **30**, 323-332.
- Calleja-Aguis, J., Muscat-Baron, Y. and Brinca, M. P. (2007). Skin ageing. *Menopause Int.* **13**, 60-64.
- Campisi, J. and d'Adda di Fagnana, F. (2007). Cellular senescence: when bad things happen to good cells. *Nat. Rev. Mol. Cell Biol.* **8**, 729-740.
- Clark, R. A. (2001). Fibrin and wound healing. *Ann. NY Acad. Sci.* **936**, 355-367.
- Coppe, J. P., Desprez, P. Y., Krtolica, A. and Campisi, J. (2010). The senescence-associated secretory phenotype: the dark side of tumor suppression. *Annu. Rev. Pathol.* **5**, 99-118.
- Cruz-Munoz, W. and Khokha, R. (2008). The role of tissue inhibitors of metalloproteinases in tumorigenesis and metastasis. *Crit. Rev. Clin. Lab. Sci.* **45**, 291-338.
- De Wever, O., Demetter, P., Mareel, M. and Bracke, M. (2008). Stromal myofibroblasts are drivers of invasive cancer growth. *Int. J. Cancer* **123**, 2229-2238.
- Desmouliere, A., Guyot, C. and Gabbiani, G. (2004). The stroma reaction myofibroblast: a key player in the control of tumor cell behavior. *Int. J. Dev. Biol.* **48**, 509-517.
- Dutta, R. C. and Dutta, A. K. (2009). Cell-interactive 3D-scaffold: advances and applications. *Biotechnol. Adv.* **27**, 334-339.
- Egeblad, M., Rasch, M. G. and Weaver, V. M. (2010). Dynamic interplay between the collagen scaffold and tumor evolution. *Curr. Opin. Cell Biol.* **22**, 697-706.
- Ehrbar, M., Rizzi, S. C., Schoenmakers, R. G., Miguel, B. S., Hubbell, J. A., Weber, F. E. and Lutolf, M. P.

- (2007). Biomolecular hydrogels formed and degraded via site-specific enzymatic reactions. *Biomacromolecules* **8**, 3000-3007.
- Erler, J. T. and Weaver, V. M. (2009). Three-dimensional context regulation of metastasis. *Clin. Exp. Metastasis* **26**, 35-49.
- Franklin, M. E., Jr, Gonzalez, J. J., Jr, Michaelson, R. P., Glass, J. L. and Chock, D. A. (2002). Preliminary experience with new bioactive prosthetic material for repair of hernias in infected fields. *Hernia* **6**, 171-174.
- Freund, A., Orjalo, A. V., Desprez, P. Y. and Campisi, J. (2010). Inflammatory networks during cellular senescence: causes and consequences. *Trends Mol. Med.* **16**, 238-246.
- Friedl, A. (2010). Proteoglycans: master modulators of paracrine fibroblast-carcinoma cell interactions. *Semin. Cell Dev. Biol.* **21**, 66-71.
- Friedland, J. C., Lee, M. H. and Boettiger, D. (2009). Mechanically activated integrin switch controls alpha5beta1 function. *Science* **323**, 642-644.
- Friess, W. (1998). Collagen-biomaterial for drug delivery. *Eur. J. Pharm. Biopharm.* **45**, 113-136.
- Goldoni, S. and Iozzo, R. V. (2008). Tumor microenvironment: modulation by decorin and related molecules harboring leucine-rich tandem motifs. *Int. J. Cancer* **123**, 2473-2479.
- Gordon, M. K. and Hahn, R. A. (2010). Collagens. *Cell Tissue Res.* **339**, 247-257.
- Gudjonsson, T., Ronnov-Jessen, L., Villadsen, R., Rank, F., Bissell, M. J. and Petersen, O. W. (2002). Normal and tumor-derived myoepithelial cells differ in their ability to interact with luminal breast epithelial cells for polarity and basement membrane deposition. *J. Cell Sci.* **115**, 39-50.
- Harburger, D. S. and Calderwood, D. A. (2009). Integrin signalling at a glance. *J. Cell Sci.* **122**, 159-163.
- Harvey, S. J. and Miner, J. H. (2008). Revisiting the glomerular charge barrier in the molecular era. *Curr. Opin. Nephrol. Hypertens.* **17**, 393-398.
- Hauser, C. A. and Zhang, S. (2010). Designer self-assembling peptide nanofiber biological materials. *Chem. Soc. Rev.* **39**, 2780-2790.
- Humphries, J. D., Byron, A. and Humphries, M. J. (2006). Integrin ligands at a glance. *J. Cell Sci.* **119**, 3901-3903.
- Hynes, R. O. (2009). The extracellular matrix: not just pretty fibrils. *Science* **326**, 1216-1219.
- Iozzo, R. V. and Murdoch, A. D. (1996). Proteoglycans of the extracellular environment: clues from the gene and protein side offer novel perspectives in molecular diversity and function. *FASEB J.* **10**, 598-614.
- Iozzo, R. V., Zoeller, J. J. and Nystrom, A. (2009). Basement membrane proteoglycans: modulators of Par Excellence of cancer growth and angiogenesis. *Mol. Cells* **27**, 503-513.
- Jarvelainen, H., Sainio, A., Koulu, M., Wight, T. N. and Penttinen, R. (2009). Extracellular matrix molecules: potential targets in pharmacotherapy. *Pharmacol. Rev.* **61**, 198-223.
- Johnson, K. R., Leight, J. L. and Weaver, V. M. (2007). Demystifying the effects of a three-dimensional microenvironment in tissue morphogenesis. *Methods Cell Biol.* **83**, 547-583.
- Kass, L., Erler, J. T., Dembo, M. and Weaver, V. M. (2007). Mammary epithelial cell: influence of extracellular matrix composition and organization during development and tumorigenesis. *Int. J. Biochem. Cell Biol.* **39**, 1987-1994.
- Kessenbrock, K., Plaks, V. and Werb, Z. (2010). Matrix metalloproteinases: regulators of the tumor microenvironment. *Cell* **141**, 52-67.
- Kim, D. H., Lipke, E. A., Kim, P., Cheong, R., Thompson, S., Delannoy, M., Suh, K. Y., Tung, L. and Levchenko, A. (2010). Nanoscale cues regulate the structure and function of macroscopic cardiac tissue constructs. *Proc. Natl. Acad. Sci. USA* **107**, 565-570.
- Kisseleva, T. and Brenner, D. A. (2008). Mechanisms of fibrogenesis. *Exp. Biol. Med. (Maywood)* **233**, 109-122.
- Kleinman, H. K. and Martin, G. R. (2005). Matrigel: basement membrane matrix with biological activity. *Semin. Cancer Biol.* **15**, 378-386.
- Kleinman, H. K., McGarvey, M. L., Hassell, J. R., Star, V. L., Cannon, F. B., Laurie, G. W. and Martin, G. R. (1986). Basement membrane complexes with biological activity. *Biochemistry* **25**, 312-318.

- Kuschel, C., Steuer, H., Maurer, A. N., Kanzok, B., Stoop, R. and Angres, B. (2006). Cell adhesion profiling using extracellular matrix protein microarrays. *Biotechniques* **40**, 523-531.
- LeBleu, V. S., Macdonald, B. and Kalluri, R. (2007). Structure and function of basement membranes. *Exp. Biol. Med. (Maywood)* **232**, 1121-1129.
- Leiss, M., Beckmann, K., Giros, A., Costell, M. and Fassler, R. (2008). The role of integrin binding sites in fibronectin matrix assembly in vivo. *Curr. Opin. Cell Biol.* **20**, 502-507.
- Leitinger, B. and Hohenester, E. (2007). Mammalian collagen receptors. *Matrix Biol.* **26**, 146-155.
- Levental, K. R., Yu, H., Kass, L., Lakins, J. N., Egeblad, M., Erler, J. T., Fong, S. F., Csiszar, K., Giaccia, A., Weninger, W. et al. (2009). Matrix crosslinking forces tumor progression by enhancing integrin signaling. *Cell* **139**, 891-906.
- Lucero, H. A. and Kagan, H. M. (2006). Lysyl oxidase: an oxidative enzyme and effector of cell function. *Cell. Mol. Life Sci.* **63**, 2304-2316.
- Lutolf, M. P. and Hubbell, J. A. (2005). Synthetic biomaterials as instructive extracellular microenvironments for morphogenesis in tissue engineering. *Nat. Biotechnol.* **23**, 47-55.
- Lutolf, M. P., Gilbert, P. M. and Blau, H. M. (2009). Designing materials to direct stem-cell fate. *Nature* **462**, 433-441.
- Macchiarini, P., Jungebluth, P., Go, T., Asnaghi, M. A., Rees, L. E., Cogan, T. A., Dodson, A., Martorell, J., Bellini, S., Parnigotto, P. P. et al. (2008). Clinical transplantation of a tissue-engineered airway. *Lancet* **372**, 2023-2030.
- Macri, L., Silverstein, D. and Clark, R. A. (2007). Growth factor binding to the pericellular matrix and its importance in tissue engineering. *Adv. Drug Deliv. Rev.* **59**, 1366-1381.
- Mao, Y. and Schwarzbauer, J. E. (2005). Fibronectin fibrillogenesis, a cell-mediated matrix assembly process. *Matrix Biol.* **24**, 389-399.
- McCullen, S. D., Ramaswamy, S., Clarke, L. I. and Gorga, R. E. (2009). Nanofibrous composites for tissue engineering applications. *Wiley Interdiscip. Rev. Nanomed. Nanobiotechnol.* **1**, 369-390.
- Morita, H., Yoshimura, A., Inui, K., Ideura, T., Watanabe, H., Wang, L., Soiminen, R. and Tryggvason, K. (2005). Heparan sulfate of perlecan is involved in glomerular filtration. *J. Am. Soc. Nephrol.* **16**, 1703-1710.
- Mott, J. D. and Werb, Z. (2004). Regulation of matrix biology by matrix metalloproteinases. *Curr. Opin. Cell Biol.* **16**, 558-564.
- Murakami, M., Elfenbein, A. and Simons, M. (2008). Non-canonical fibroblast growth factor signalling in angiogenesis. *Cardiovasc. Res.* **78**, 223-231.
- Myllyharju, J. and Kivirikko, K. I. (2004). Collagens, modifying enzymes and their mutations in humans, flies and worms. *Trends Genet.* **20**, 33-43.
- Nomura, Y. (2006). Structural change in decorin with skin aging. *Connect. Tissue Res.* **47**, 249-255.
- Oehrl, W. and Panayotou, G. (2008). Modulation of growth factor action by the extracellular matrix. *Connect. Tissue Res.* **49**, 145-148.
- Pankov, R. and Yamada, K. M. (2002). Fibronectin at a glance. *J. Cell Sci.* **115**, 3861-3863.
- Paszek, M. J. and Weaver, V. M. (2004). The tension mounts: mechanics meets morphogenesis and malignancy. *J. Mammary Gland Biol. Neoplasia* **9**, 325-342.
- Paszek, M. J., Zahir, N., Johnson, K. R., Lakins, J. N., Rozenberg, G. I., Gefen, A., Reinhart-King, C. A., Margulies, S. S., Dembo, M., Boettiger, D. et al. (2005). Tensional homeostasis and the malignant phenotype. *Cancer Cell* **8**, 241-254.
- Payne, S. L., Hendrix, M. J. and Kirschmann, D. A. (2007). Paradoxical roles for lysyl oxidases in cancer-a prospect. *J. Cell Biochem.* **101**, 1338-1354.
- Pelham, R. J., Jr and Wang, Y. (1997). Cell locomotion and focal adhesions are regulated by substrate flexibility. *Proc. Natl. Acad. Sci. USA* **94**, 13661-13665.
- Provenzano, P. P., Eliceiri, K. W. and Keely, P. J. (2009). Shining new light on 3D cell motility and the metastatic process. *Trends Cell. Biol.* **19**, 638-648.
- Robins, S. P. (2007). Biochemistry and functional significance of collagen cross-linking. *Biochem. Soc. Trans.* **35**, 849-852.
- Rodriguez, C., Rodriguez-Sinovas, A. and Martinez-Gonzalez, J. (2008). Lysyl oxidase as a potential therapeutic target. *Drug News Perspect.* **21**, 218-224.
- Ronnov-Jessen, L., Petersen, O. W. and Bissell, M. J. (1996). Cellular changes involved in conversion of normal to malignant breast: importance of the stromal reaction. *Physiol. Rev.* **76**, 69-125.
- Rosso, F., Marino, G., Giordano, A., Barbarisi, M., Parmeggiani, D. and Barbarisi, A. (2005). Smart materials as scaffolds for tissue engineering. *J. Cell Physiol.* **203**, 465-470.
- Rozario, T. and DeSimone, D. W. (2010). The extracellular matrix in development and morphogenesis: a dynamic view. *Dev. Biol.* **341**, 126-140.
- Schaefer, L. and Iozzo, R. V. (2008). Biological functions of the small leucine-rich proteoglycans: from genetics to signal transduction. *J. Biol. Chem.* **283**, 21305-21309.
- Schaefer, L. and Schaefer, R. M. (2010). Proteoglycans: from structural compounds to signaling molecules. *Cell Tissue Res.* **339**, 237-246.
- Schafer, M. and Werner, S. (2008). Cancer as an overhealing wound: an old hypothesis revisited. *Nat. Rev. Mol. Cell Biol.* **9**, 628-638.
- Schmidt, S. and Friedl, P. (2010). Interstitial cell migration: integrin-dependent and alternative adhesion mechanisms. *Cell Tissue Res.* **339**, 83-92.
- Schultz, G. S. and Wysocki, A. (2009). Interactions between extracellular matrix and growth factors in wound healing. *Wound Repair Regen.* **17**, 153-162.
- Scott, J. E. (2003). Elasticity in extracellular matrix 'shape modules' of tendon, cartilage, etc. A sliding proteoglycan-filament model. *J. Physiol.* **553**, 335-343.
- Serban, M. A. and Prestwich, G. D. (2008). Modular extracellular matrices: solutions for the puzzle. *Methods* **45**, 93-98.
- Shaikh, F. M., Callanan, A., Kavanagh, E. G., Burke, P. E., Grace, P. A. and McGloughlin, T. M. (2008). Fibrin: a natural biodegradable scaffold in vascular tissue engineering. *Cells Tissues Organs* **188**, 333-346.
- Sieminski, A. L., Semino, C. E., Gong, H. and Kamm, R. D. (2008). Primary sequence of ionic self-assembling peptide gels affects endothelial cell adhesion and capillary morphogenesis. *J. Biomed. Mater. Res. A* **87**, 494-504.
- Smith, I. O., Liu, X. H., Smith, L. A. and Ma, P. X. (2009). Nanostructured polymer scaffolds for tissue engineering and regenerative medicine. *Wiley Interdiscip. Rev. Nanomed. Nanobiotechnol.* **1**, 226-236.
- Smith, L. A. and Ma, P. X. (2004). Nano-fibrous scaffolds for tissue engineering. *Colloids Surf. B Biointerfaces* **39**, 125-131.
- Smith, M. L., Gourdon, D., Little, W. C., Kubow, K. E., Eguiluz, R. A., Luna-Morris, S. and Vogel, V. (2007). Force-induced unfolding of fibronectin in the extracellular matrix of living cells. *PLoS Biol.* **5**, e268.
- Sprenger, C. C., Plymate, S. R. and Reed, M. J. (2008). Extracellular influences on tumour angiogenesis in the aged host. *Br. J. Cancer* **98**, 250-255.
- Szauter, K. M., Cao, T., Boyd, C. D. and Csiszar, K. (2005). Lysyl oxidase in development, aging and pathologies of the skin. *Pathol. Biol.* **53**, 448-456.
- Tan, T. T. and Coussens, L. M. (2007). Humoral immunity, inflammation and cancer. *Curr. Opin. Immunol.* **19**, 209-216.
- Trebaul, A., Chan, E. K. and Midwood, K. S. (2007). Regulation of fibroblast migration by tenascin-C. *Biochem. Soc. Trans.* **35**, 695-697.
- Tsang, K. Y., Cheung, M. C., Chan, D. and Cheah, K. S. (2010). The developmental roles of the extracellular matrix: beyond structure to regulation. *Cell Tissue Res.* **339**, 93-110.
- Tucker, R. P. and Chiquet-Ehrismann, R. (2009). The regulation of tenascin expression by tissue microenvironments. *Biochim. Biophys. Acta* **1793**, 888-892.
- Ulijin, R. V. and Smith, A. M. (2008). Designing peptide based nanomaterials. *Chem. Soc. Rev.* **37**, 664-675.
- Untergasser, G., Madersbacher, S. and Berger, P. (2005). Benign prostatic hyperplasia: age-related tissue-remodeling. *Exp. Gerontol.* **40**, 121-128.
- Vakonakis, I. and Campbell, I. D. (2007). Extracellular matrix: from atomic resolution to ultrastructure. *Curr. Opin. Cell Biol.* **19**, 578-583.
- Velnar, T., Bailey, T. and Smrkolj, V. (2009). The wound healing process: an overview of the cellular and molecular mechanisms. *J. Int. Med. Res.* **37**, 1528-1542.
- Wipff, P. J., Rifkin, D. B., Meister, J. J. and Hinz, B. (2007). Myofibroblast contraction activates latent TGF-beta1 from the extracellular matrix. *J. Cell Biol.* **179**, 1311-1323.
- Wise, S. G. and Weiss, A. S. (2009). Tropoelastin. *Int. J. Biochem. Cell Biol.* **41**, 494-497.
- Xian, X., Gopal, S. and Couchman, J. R. (2010). Syndecans as receptors and organizers of the extracellular matrix. *Cell Tissue Res.* **339**, 31-46.
- Xu, J., Lamouille, S. and Derynck, R. (2009). TGF-beta-induced epithelial to mesenchymal transition. *Cell Res.* **19**, 156-172.
- Zhang, X., Reagan, M. R. and Kaplan, D. L. (2009). Electrospun silk biomaterial scaffolds for regenerative medicine. *Adv. Drug Deliv. Rev.* **61**, 988-1006.
- Zisch, A. H., Lutolf, M. P. and Hubbell, J. A. (2003). Biopolymeric delivery matrices for angiogenic growth factors. *Cardiovasc. Pathol.* **12**, 295-310.

Cell Science at a Glance on the Web
Electronic copies of the poster insert are available in the online version of this article at jcs.biologists.org. The JPEG images can be downloaded for printing or used as slides.

Forcing form and function: biomechanical regulation of tumor evolution

Hongmei Yu^{1,2}, Janna Kay Mouw^{1,2} and Valerie M. Weaver^{1,2,3}

¹ Department of Surgery, University of California at San Francisco, San Francisco, CA 94143, USA

² Center for Bioengineering and Tissue Regeneration, University of California at San Francisco, San Francisco, CA 94143, USA

³ Departments of Anatomy and Bioengineering and Therapeutic Sciences, Eli and Edythe Broad Center of Regenerative Medicine and Stem Cell Research, and Helen Diller Comprehensive Cancer Center, University of California-San Francisco, San Francisco, CA 94143, USA

Cancer cells exist in a constantly evolving tissue micro-environment of diverse cell types within a proteinaceous extracellular matrix. As tumors evolve, the physical forces within this complex microenvironment change, with pleiotropic effects on both cell- and tissue-level behaviors. Recent work suggests that these biomechanical factors direct tissue development and modulate tissue homeostasis, and, when altered, crucially influence tumor evolution. In this review, we discuss the biomechanical regulation of cell and tissue homeostasis from the molecular, cellular and tissue levels, including how modifications of this physical dialogue could contribute to cancer etiology. Because of the broad impact of biomechanical factors on cell and tissue functions, an understanding of tumor evolution from the biomechanical perspective should improve risk assessment, clinical diagnosis and the efficacy of cancer treatment.

Tumor evolution within a biomechanical context

Tumors are composed of a heterogeneous collection of cells surrounded by various soluble factors and an evolving extracellular matrix (ECM). In addition to the roles of genetic and biochemical events in tumor development, recent studies support the notion that biomechanical factors also crucially direct tissue development, sculpt tissue organization and maintain tissue homeostasis [1]. Central to this assumption is the concept that every tissue component (e.g. cells, proteins) is a biomaterial possessing unique mechanical properties that respond specifically to various physical forces. Mechanical inputs, such as tumor expansion leading to tissue compression and increased interstitial pressure, can increase both cell and tissue tension within the confined stroma, leading to the release, concentration and activation of various growth factors, ultimately assisting in tumor progression [2,3]. Additionally, within the tumor, oncogene-mediated alterations in cellular actomyosin contractility and Rho GTPase activity can compromise cell-cell junction integrity to destroy tissue polarity and promote cell invasion, whereas ECM remodeling and stiffening drive integrin clustering and actin remodeling to re-enforce focal adhesions. Taken together, these

alterations enhance intracellular growth factor receptor signaling within the increased extracellular pool of activated growth factors, drive tumor cell growth and survival, and confer tumor drug resistance [4–6].

In this review, the effects of cell and tissue level forces on tissue behavior are discussed, with recent studies on the role of mechanics in tumor development and evolution highlighted. Because the composition and organization of tumors is continuously evolving, the influence of cell and tissue architecture on the material properties and physical behavior at the molecular, cellular and tissue

Glossary

Tension: a load that acts in the direction perpendicular to a surface and tends to pull an object apart.

Compression: a load that acts in the direction perpendicular to a surface and tends to push an object.

Tensile strength: the maximum amount of tensile stress that a material can be subjected to before failure. (Unit: force per unit area.)

Stress: describes the internal resistance of a material to distortion by an external force (average force per unit area). There are three basic stresses: tensile, compression and shear stress. **Tensile and compression stress** are the stresses normal to the cross-sectional area of a body; **Shear stress** is the stress tangential to the cross-sectional area of a body. (Unit: forces per unit area.)

Strain: the ratio of the change in length to the original length of a material in the loading direction (dimensionless).

Stiffness: describes the elasticity of a material or the property of restoration to its original shape after deformation. The unit of stiffness is force per unit length, which can be determined by the slope of the load-displacement curve in the linear region of loading. (Unit: force per unit length.) **Compliance** is inversely related to stiffness.

Elasticity: describes the ability of the tissue to return to its original shape after a load is removed. Mathematically, elasticity is described by the **Modulus of elasticity**, which is defined as the ratio of stress to strain. For example, **Young's modulus (E)** describes the elasticity of a material subjected to tensile or compression loading; **Shear modulus (G)** describes the shear elasticity of a material subjected to shear loading. E and G can be related by: $E = 2G(1 + \gamma)$ where γ is the Poisson's ratio (ratio of lateral strain to axial strain in an axial-loaded material).

Viscoelasticity: is the property of materials that exhibit both elastic and viscous properties when undergoing deformation. Most biological materials are viscoelastic. The strain of **viscous** materials is time-dependent, whereas that of **elastic** materials is time-independent. A dynamic test of viscoelastic materials is often performed to determine the frequency-dependent **complex shear modulus**, which contains the **elastic storage modulus** and the **viscous loss modulus**.

Dynamic tests: refers to material tests with periodic deformation or frequency-dependent loading, such as the shear rheometric test. **Static tests** refer to those tests with gradually increasing force at a slow speed, such as the classic tensile test.

Corresponding author: Weaver, V.M. (valerie.weaver@ucsfmedctr.org).

levels are discussed. Finally, the clinical implications of current research on tumor mechanics, as well as future research directions, are discussed.

Tissue mechanics and mechano-transduction

Cells and tissues experience various physical forces that can be classified as externally applied or cell-generated. These physical forces can directly and indirectly affect many fundamental biological processes and, in turn, contribute to normal physiological and pathological phenomena. The direct impact of these forces on the cells and tissues subjected to these cues include displacement, deformation, and an alteration of tissue morphology and organization. For example, externally applied compression force can deform the ECM and decrease the interstitial space, which alters the transport and distribution of soluble factors within the ECM thereby modifying cell behavior [7]. Indirect effects of mechanical force on tissues include changes in levels and/or activity of various growth, differentiation and motility regulators, as well as ECM remodeling. The specificity of these force-induced effects can depend on the direction of the force (e.g. tension, compression and shear forces, see [Glossary](#)) as well as its magnitude and duration. For instance, transient tensile forces upregulate TGF- β 1 expression in smooth muscle cells whereas constant tensile forces upregulate both TGF- β 1 and collagen I expression [8]. Dynamic loading ([Glossary](#)) increases MMP-9 (matrix metalloproteinase-9) in fibroblasts whereas static loading upregulates MMP-2 [9]. Hydrostatic pressure decreases cell proliferation and increases hyaluronan production [10]. These findings demonstrate the specific interactions between cells and biochemical cues. It will be very important to investigate how different forces can induce different cellular responses, which often occur in a complex tumor macroenvironment.

Importantly, cells can actively generate forces through multiple mechanisms including Rho-dependent actin-myosin contraction and actin assembly, and transmit these forces through cell-cell and cell-ECM interactions. These cell-generated forces contribute to the branching morphogenesis of both embryonic lungs and cultured epithelial cell cysts, facilitate blood vessel 'sprouting' (angiogenesis), and influence convergent extension during embryonic development [11–13]. Accumulating data demonstrate that cell-generated forces play broad roles in regulating cell survival, growth, migration and differentiation, as well as cell-cell and cell-ECM communication and the

spatial organization of cells and tissues [14]. Externally applied and cell-generated forces do not operate independently within normal tissues and instead are typically balanced through multiple mechanisms. This orchestrated behavior helps to maintain cell and tissue structure and homeostasis. To facilitate our understanding of how externally applied and cell-generated forces are transmitted in both normal physiological and pathological conditions, the basic concepts of the common mechanical properties of cells and tissues are reviewed below.

Mechanical properties of tissues, cells and ECM

Tissues are composed of multiple cell types, various ECM proteins and other constituents, each with unique mechanical characteristics such as elasticity, plasticity, viscosity, tensile strength and stiffness ([Glossary](#)). These physical properties collectively define the material properties of the tissue and dictate how the tissue responds to mechanical cues and how it will sense and transmit force. Specifically, the elasticity and stiffness of cells and tissues have been implicated in cancer biology. Methods such as tissue level tensile, compression and shear testing, and cellular and subcellular level atomic force microscopy (AFM) have been employed to measure these properties. These techniques have yielded valuable information that demonstrates the unique mechanical properties of each cell type that are reflected in its function, cellular origin and microenvironment ([Table 1](#)). These parameters allow the monitoring of differentiation or activation status of cells, as well as a method of assessing the state of disease progression.

The viscoelasticity of a tissue is dictated by its ECM and individual cellular constituents. Differences in the elastic moduli of various cell types or cellular states are partly owing to structural variations in the cytoskeletal elements including filamentous actin, intermediate filaments and microtubules, and their organization [15]. In response to biochemical and biomechanical cues from their local environment (e.g. ECM and adjacent interacting cells), cells can tune their elastic moduli by altering their transmembrane receptors, intracellular cytoskeletal organization, actomyosin contraction and cytoskeletal tension, and remodel the local microenvironment to achieve mechanical equilibrium ([Figure 1](#)). This active adaptation to the rigidity of the environment also contributes to the elasticity of a cell [16,17]. Cellular elasticity and cell-generated forces are therefore closely related; the intracellular and extracellular mechano-responsive elements are linked by these dy-

Table 1. Elastic moduli of tissues and cells involved in cancer

		Normal or resting state	Pathological or activated state
Tissue	Breast [20,115,116]	0.4~2 kPa	4~12 kPa
	Lung [117]	10 kPa	25~35 kPa
	Brain [48]	0.26~0.49 kPa	7 kPa
	Bone [116,118,119]	2~14 G Pa	>689 MPa
	Liver [120,121]	0.3~0.6 kPa	1.6 ~20 kPa
	Cells	Epithelial cells [76,122]	~ 2 kPa
	Fibroblasts [78]	~ 0.4 kPa	~1 kPa
	Mesenchymal stem cells [123]	0.25~0.9 kPa	N/A
	Macrophages [79]	1.5 kPa	0.5 kPa
	Myeloid [124]	N/A	0.17~1.5 kPa (HL60 cells)
	T lymphocyte [124]	0.013~0.083 kPa (Jurkat cells)	N/A
	Neutrophils [124]	0.07~0.24 kPa	N/A

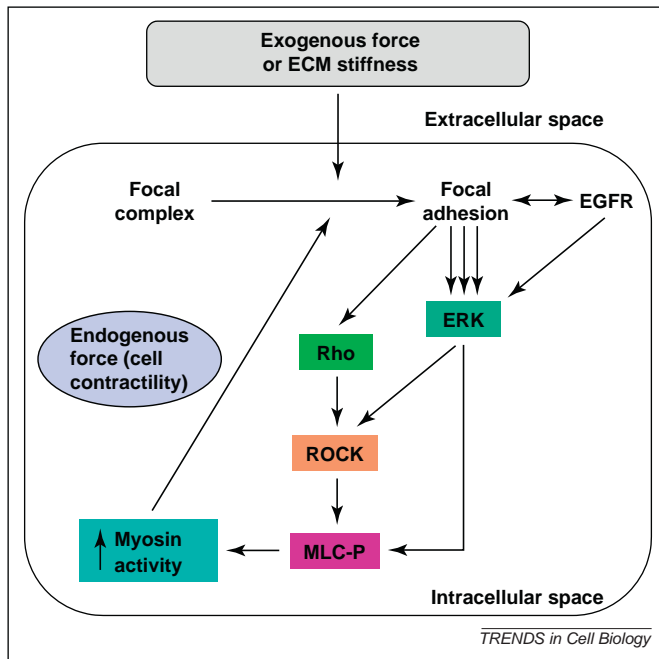


Figure 1. Dynamic and reciprocal conversation between matrix stiffness and cell tension. Non-malignant cells can respond to exogenous mechanical forces and matrix stiffness by enhancing focal complex maturation, resulting in Rho and ROCK activation, MLC phosphorylation and actomyosin contraction. Cell-generated forces from increased myosin contraction feed into focal adhesion maturation to adjust focal adhesion size and contract the ECM until the exogenous forces are balanced and the elastic modulus of cells are 'tuned' to reflect the ECM stiffness. This mechano-signaling circuit is crucial in the dynamic and reciprocal conversation between exogenous and cell-generated mechanical factors. (ROCK, Rho-associated kinase; MLC, myosin light chain.) (Adapted with permission from [20]).

dynamic and reciprocal conversations (Figure 1). Together, the extracellular and intracellular forces, the mechano-responsive elements, their mechanical properties and the crosstalk with intracellular signaling pathways maintain mechanical equilibrium and regulate diverse cellular behaviors such as adhesion, spreading, receptor signaling, gene expression and extracellular microenvironment remodeling [7]. This mechanical regulatory paradigm is essential for normal tissue structure and function, as demonstrated by the fact that tissue-specific cells often prefer mechanical microenvironments that closely mimic those of their native tissues such as the improved growth of CNS neurites in neurite and glial cell co-cultures and the morphogenesis of normal mammary epithelial cells on soft matrices [18–20].

Mechano-sensing and transduction

To respond to a mechanical stimulus, the cell must possess elements capable of responding to the applied force and translating this mechanical information into a biochemical signal. These cellular mechano-signaling pathways often overlap, feed into, and are themselves regulated by biochemical cascades. Several mechano-sensors that respond to different magnitudes and types of force have been identified, including highly specialized structures such as the mechano-sensory apparatus of the auditory hair bundle and the primary cilia in tubular epithelial cells [21,22]. Biochemical signaling can also be initiated by force-induced conformational changes and exposure of functional sites of signaling proteins (e.g. tension-induced conformation changes in fibronectin, intracellular talin

and membrane ion channels) (Figure 2a) [23–25]. Alternatively, intracellular signaling cascades can be activated by force-mediated alterations in membrane curvature, tension, and the distribution of membrane signaling molecules as seen with the transactivation of Ephrin receptors [26] and with integrin clustering [27] (Figure 2b). Cells can also sense force via cell–cell junctions deformed by mechanical forces, leading to a global remodeling of their cytoskeletal filaments (Figure 2c) [28,29]. Many of these mechano-sensitive mechanisms operate concurrently, overlapping and interacting with simultaneously occurring biochemical pathways. When these mechano-sensing and transduction events at cellular and subcellular level are coordinated at the multicellular and organ levels, they contribute to tissue and organ functions, such as wound closure and muscle contraction (Figure 2d,e).

Dynamic dialogue between biomechanical and biological signaling during tumor evolution

Normal tissue structure is disrupted during tumor initiation and progression. The microenvironment becomes both mechanically and biologically active, highlighted by continuous and progressive remodeling of the tumor mass and the stromal compartments. Within the tumor mass, the transformation of tumor cells is accompanied by increased cell division, reduced apoptosis, loss of tissue polarity, and alterations in the composition and organization of ECM components. Adjacent to the tumor mass, the tumor stroma assists tumor development via multiple stromal cells, ECM molecules, soluble factors and the circulatory systems (blood and lymphatic vessels). Tumor-associated stromal cells, including fibroblasts, myofibroblasts, endothelial cells, mesenchymal stem cells, inflammatory cells and immune cells are often recruited, locally differentiated or activated during different tumor development stages. These cells actively participate in ECM remodeling and tumor angiogenesis, providing growth factors and chemokines that promote tumor growth and metastasis [30,31]. The non-cellular components of the tumor stroma, such as collagens, fibronectin, tenascin and proteoglycans, can be abnormally expressed and remodeled, resulting in new biochemical and mechanical signals [32]. Soluble signals, produced by tumor or stromal cells, released from cleaved ECM molecules and delivered from the circulatory system, can re-distribute within this tumor stromal compartment and regulate cell functions and ECM composition during tumor progression [32].

Different from the well-maintained tissue homeostasis and mechanical equilibrium in normal physiological conditions, the loss of growth control and the disrupted tissue structure and organization during tumor evolution lead to unbalanced physical forces and altered material properties of each tumor component. Because the behavior, structure and organization of tumors are continuously changing as the cancer evolves, the mechanical state in a tumor also evolves as the tumor develops (Figure 3). In breast cancer, the mechanical characteristics in a hyperplasia, carcinoma *in situ*, invasive lesion and metastasis lesion can be very different. A dysplastic lesion typically involves the loss of normal cell polarization and organization, the changes in cell–cell contacts and cell–ECM interactions, which result

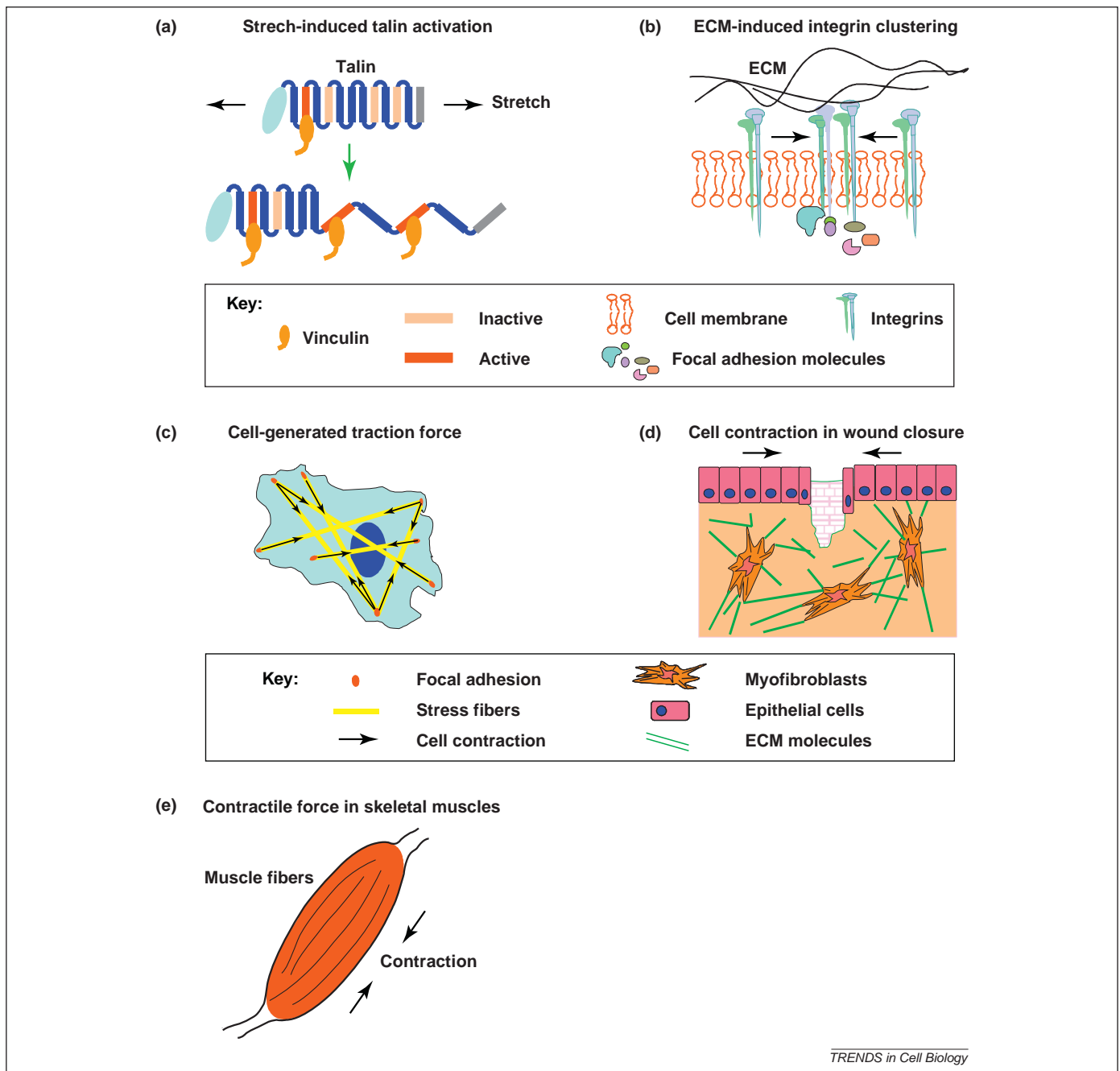


Figure 2. Examples of mechanical behaviors at different levels of biological systems. **(a)** At the single-molecule level, mechanical stretching of talin rods exposes the cryptic binding sites for vinculin, which then activates downstream biochemical signaling pathways important in cell signaling, adhesion, and migration. **(b)** At the multimolecule-level, increased matrix stiffness enhances integrin clustering, promotes large focal adhesions and activates downstream signaling cascades. **(c)** At the single-cell level, cells can generate traction forces via actin polymerization (e.g. stress fibers) and actomyosin contraction between focal adhesions. **(d)** At the tissue level, myofibroblasts differentiated from fibroblasts at wound sites exert contractile forces on the surrounding ECM and rearrange the ECM to close wounds. **(e)** At the organ level, a muscle that contains multiple muscle fibers surrounded by connective tissues and sheaths can contract synchronously, generating tension and muscle motion upon the reception of signals from motor neurons.

in altered cellular tension and mechano-sensing and transduction [33,34]. Increased matrix deposition, cell proliferation and altered cell tension in dysplastic lesions also result in the thickening and remodeling of the basement membrane (BM) architecture (Figure 3a) [35]. Carcinoma *in situ* is characterized by active cell growth and/or reduced cell death within an intact BM and interstitial ECM. This uncontrolled cell growth, and/or reduced cell death, confined by an intact BM leads to a restricted tumor volume expansion and corresponding reaction forces within the various BM and stromal components [36–38]. In turn, the resistance of the BM and ECM to the expanding tumor

mass leads to compression of the tumor mass [39]. Simultaneously, ECM remodeling, as a consequence of tumor compression and stromal reaction, results in altered mechanical properties of the ECM that can further increase cell-generated forces and cell tension (Figure 3b) [40]. In advanced carcinoma *in situ* lesions, intra-tumor pressure can be further elevated owing to hypoxia and necrosis. Tumor and stromal cells secrete soluble factors, facilitating matrix remodeling and angiogenesis [41]. Inefficient transport and dense ECM networks result in further increases in interstitial fluid pressure within the tumor [42]. Increased interstitial flow owing to blood vessel and BM

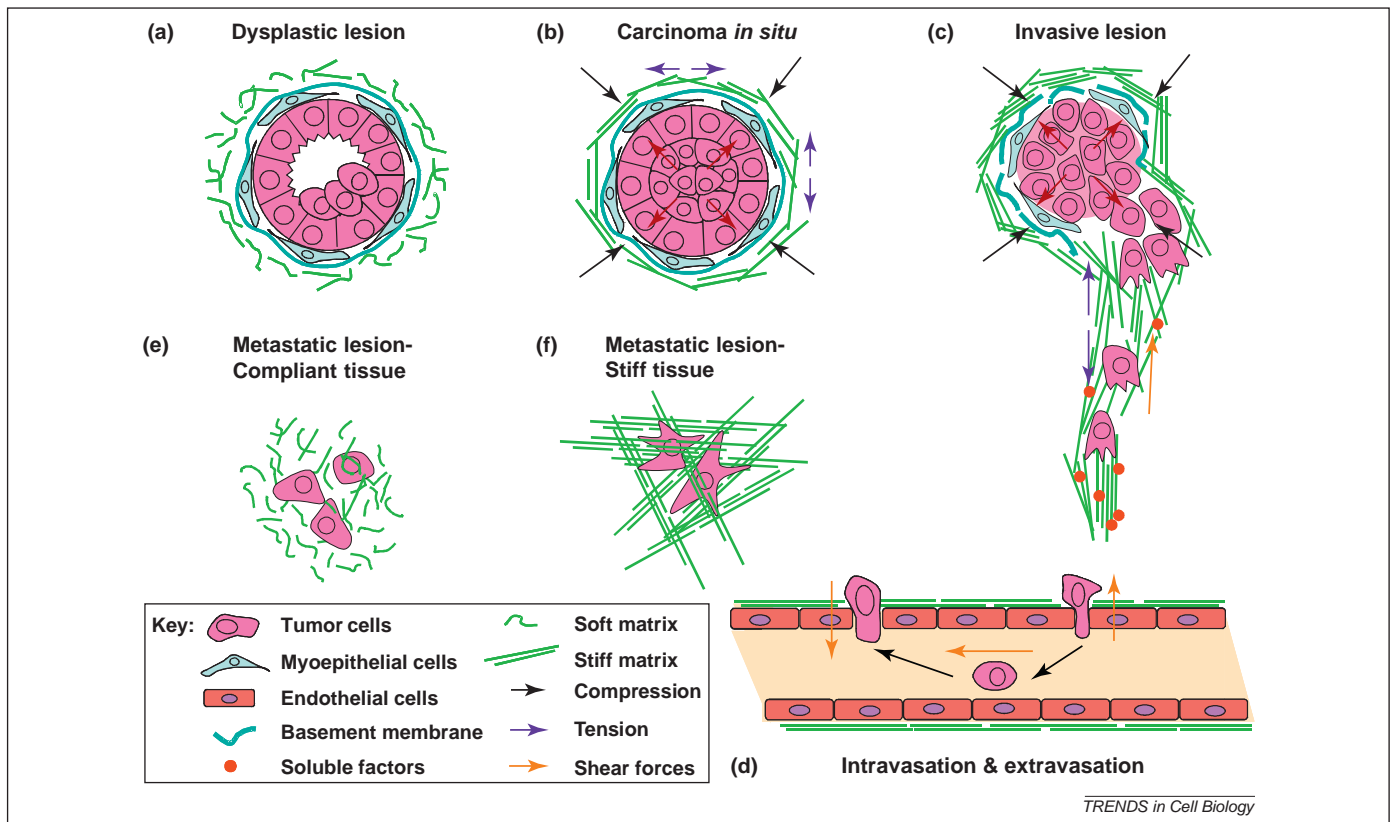


Figure 3. Tumor progression is associated with continuous alterations in tissue and cell mechanics. (a) In dysplastic lesions, cells gradually lose polarity and grow into the luminal space. The myoepithelial cell layer and the basement membrane (BM) remain intact and the surrounding ECM is compliant. (b) In carcinoma *in situ* lesions, cell polarity is lost and the lumen is filled by cells. This volume expansion and resistance from the BM and interstitial ECM lead to increased forces between tumor cells and the stromal matrix. Simultaneously, ECM components are abnormally deposited and remodeled, which results in increased ECM and tissue stiffness, and in turn, cell-generated tension. (c) In invasive lesions, tumor cells break down the BM and invade into the interstitial ECM. The reciprocal forces between tumor cells and the ECM continuously increase. Abnormal deposition and remodeling of ECM collagen further increase ECM and tissue stiffness. Tumor cells generate greater tension in response to this increased mechanical stimulation. As tumor cells invade through the BM and ECM, they experience a range of different forces from the dense ECM network. These external forces together with genetic and epigenetic events can change the contractility and viscoelasticity of tumor cells. (d) During intravasation and extravasation, tumor cells experience various forces including shear forces exerted by the ECM, blood flow and neighboring cells, which facilitate their transport and attachment to the endothelium. (e, f) Cancer cells often metastasize to different organs, which can have very different microenvironmental and mechanical properties [e.g. (e) soft tissue lung; (f) stiff tissue bone]. The mechanics of remote tissues and cancer cells could regulate cell dormancy, proliferation and differentiation in these organs.

permeability in the tumor microenvironment could promote TGF- β dependent myofibroblast differentiation [43]. In invasive tumors, cell–cell interactions further decrease and intracellular contractility increases, leading to the dissemination of tumor cells from the tumor mass and invasion through the BM and interstitial ECM. Invading cells are accompanied by non-transformed stromal cells (e.g. fibroblasts, macrophages) and migrate through a progressively stiffened ECM and biochemical gradients towards the circulatory system [44–47]. Various mechanical forces, such as interstitial compression and shear, interstitial fluidic pressure and ECM stiffness can crucially influence the rate and direction of tumor cell migration (Figure 3c) [48]. During intravasation, transportation (in the bloodstream or lymphatic flow) and extravasation, tumor cells are exposed to shear forces from adjacent cells and hydrodynamic flow. These shear forces assist tumor cell transport and facilitate interactions with leukocytes and endothelial cells to permit extravasation (Figure 3d) [49]. Cancer cells display organ-specific metastasis which can depend on the intrinsic genetics of the tumor cells, the affinity of tissues to host a metastatic lesion and the pattern of circulation within the tissue [50–52]. Additionally, different organs exhibit very different mechanical properties (e.g. lung is soft whereas bone is very stiff).

Because cells can selectively grow on and within specific substrates according to their mechanical properties, organ-specific mechanical properties could contribute to the preferential migration, attachment, survival and proliferation of cancer cells in specific organs (Figure 3e, f) (Table 1) [48,53–55].

Influence of the ECM and tumor cell biomechanics on tumor progression

ECM mechanics broadly impact cell transcription, cell cycle control, cell–cell interactions, cell differentiation and migration. The mechanical influences of the ECM in tumor progression directly depend on the ECM composition, structure and organization, as well as the mechanical dialogue with intracellular mechano-responsive elements and cell generated forces (Figure 1) [32,56,57]. Recent work demonstrates that breast tumor progression is often accompanied by increased deposition, crosslinking and de-regulated cleavage of type I collagen [58]. This collagen remodeling is largely owing to the increased expression and activity of various enzymes (lysyl oxidase, transglutaminase and MMPs) in the active tumor stroma [40,59–62]. Increased collagen crosslinking and resulting tissue stiffening intensify the biomechanical feedback in breast tissue and promote breast tumor progression [40]. Disrupting this

feedback by targeting the crosslinking of fibrillar collagen through inhibition of the enzyme lysyl oxidase can delay both malignant transformation and tumor progression (Figure 4) [40]. In addition, cell migration can be guided by the gradient of ECM stiffness ('durotaxis') [63,64], indicating such a gradient might serve as an important cue leading the directional migration of cancer cells in the interstitial ECM towards the intravasation sites. Other ECM proteins, such as fibronectin, tenascin, decorin, fibromodulin, lumican and osteopontin, are also involved in tumor development and modify the mechanical properties of the ECM; however, their roles in tumor mechanics and tumor development have yet to be clarified [32,65–67].

Growth factors bound by the ECM can be released and activated by mechanical perturbation. For example, mechanical stretch or contraction of the ECM can release ECM-bound TGF- β into the extracellular space, increasing the availability of active TGF- β [3,68]. TGF- β plays a key

role during tumor progression; it is a strong chemoattractant for both monocytes and macrophages, a stimulant for pro-angiogenic factors such as bFGF (basic fibroblast growth factor), MCP-1 (monocyte chemotactic protein-1), TNF- α (tumor necrosis factor α) and IL-1 β (interleukin-1 β), an activator of ECM remodeling enzymes, a potent activating and differentiating signal for stromal fibroblasts, and a key regulator of the modes of cancer cell motility [69,70]. Fibroblasts differentiated into myofibroblasts are able to generate stronger adhesions and greater cellular contractility, which, in turn, increase ECM tension, remodeling and deposition that potentiate the further release of TGF- β from the ECM [68]. Indeed, TGF- β signaling and myofibroblast differentiation associate with invasive human breast cancers, implying that the initiation of mechanical signaling by TGF- β could be very important in tumor development. Similarly, the expression and release of other factors, such as PDGF (platelet-derived growth factor), VEGF (vascular

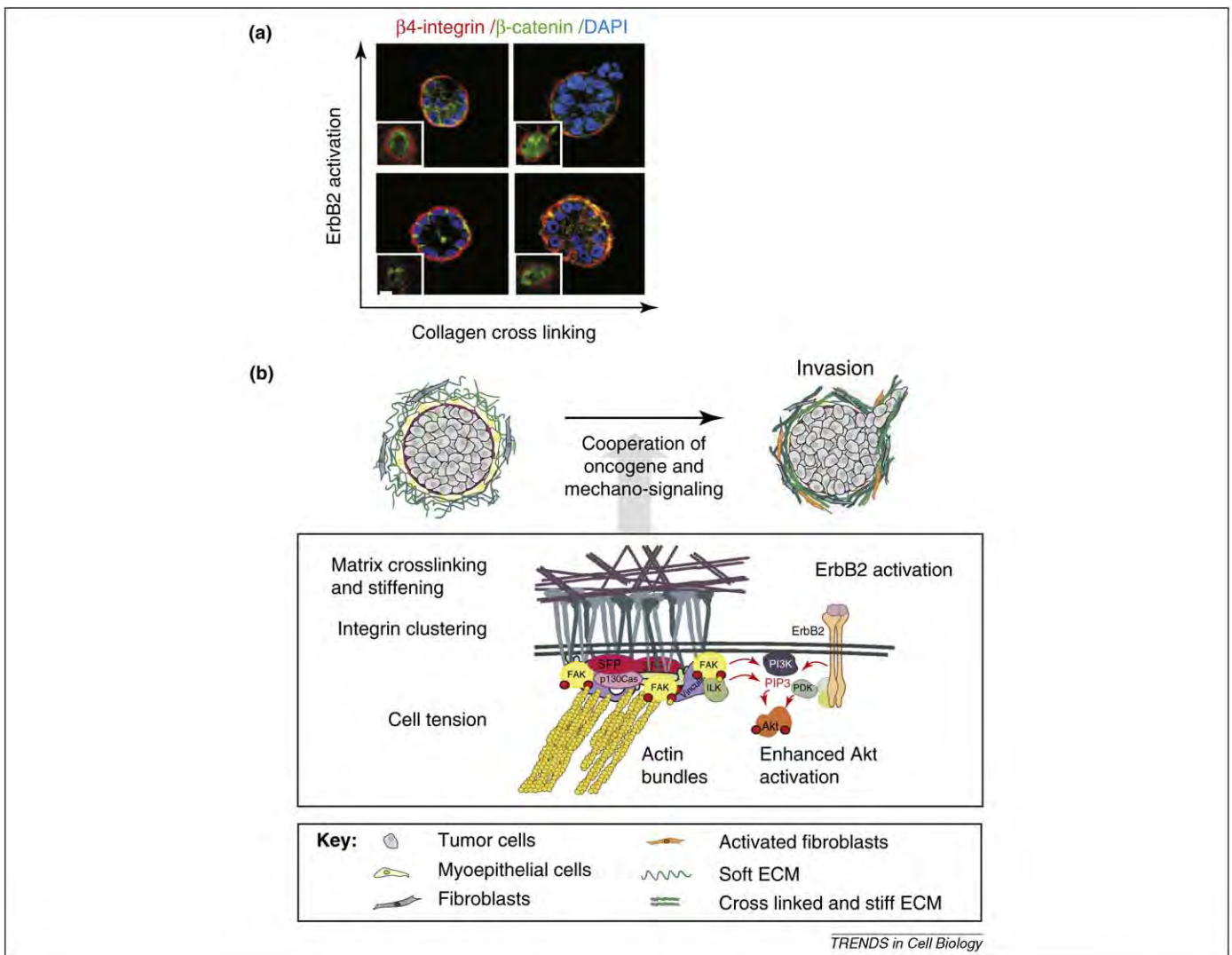


Figure 4. Increased collagen crosslinking and matrix stiffness modify the context of signaling and promote invasion of oncogene-transformed pre-malignant mammary cells. **(a)** MCF10A cells (non-malignant mammary epithelial cells) expressing either a drug-activated ErbB2/NGFR (NGFR, neural growth factor receptor) chimera or a tetracycline-inducible ErbB2 construct form polarized, growth-arrested colonies in soft collagen/rBM gels (bottom left). Stiffening the collagen gel (by adding ribose to crosslink the collagen) or activating ErbB2 signaling increases cell proliferation but fails to drive cell invasion (bottom right and top left). MCF10A colonies start invading into collagen gels only when the collagen gels are stiffened and ErbB2 signaling is activated. (top right) (Bar 20 μ m; β -catenin, green; β 4 integrin, red; DAPI, blue.) Second harmonic generation images show the collagen alignment and bundling around the colonies (insert). **(b)** Schematic presentation of the cooperation between matrix stiffening and ErbB2 signaling in driving the invasive phenotype. Increased collagen crosslinking stiffens the ECM, which drives integrin clustering and promotes focal adhesion assembly, thereby activating PI3K and potentiating ErbB2/PI3K/Akt signaling. (Adapted with permission from [40]).

endothelial growth factor) and bFGF, which are also involved in tumor cell growth, angiogenesis, cell invasion, and matrix deposition, can also be regulated by mechanical loading and mechanical properties of substrates [71–74].

Tumor cells exhibit very different mechanical properties than their normal counterparts (Table 1). Studies with isolated cancer cells suggest that they become increasingly compliant as they transform, such that highly metastatic tumor cells are less stiff than normal cells [75,76]. However, this point is still under contention because all of these measurements were conducted in culture and the apparent viscoelasticity of living cells *in situ* and in isolation can be very different. Indeed, the viscoelasticity of living cells can be substantially modified by many factors present in the context of a three-dimensional (3D) tissue including heterotypic cell–cell interactions, localized effects of the vasculature and the ECM. In this respect, isolated cancer cells are hypersensitive to substrate stiffness [20,54,77] and exhibit elevated actomyosin-generated contractility when compared with matched normal cells [20]. The increased cell contractility exhibited by tumor cells is mediated by increased activation of MLCK (myosin light chain kinase) and acto-myosin contraction through elevated Rho GTPase activity and EGFR signaling (Figure 1). Pharmacologically or genetically inhibiting these pathways is sufficient to reduce cell tension and normalize tumor tissue phenotype [20]. These results suggest that the intrinsic adhesion and cytoskeletal behavior of cancer cells that participate in their tension behavior contribute to their tumor phenotype. This means that enhanced mechano-responsiveness coupled with increased stiffening of the tissue ECM could contribute to the progressive and incremental stiffening of tumor cells *in situ* (Lopez *et al.*, unpublished). Conversely, inhibiting cell or ECM tension could inhibit tumor progression [40]. Notably, ECM stiffness varies dramatically within the same tumor and ECM organization is non-uniform, providing a provocative explanation for some of the variability noted in tumor cell behavior within a cancerous tissue *in vivo* (Table 1) [40] (Lopez *et al.*, unpublished). The discrepancy between *in situ* analysis and those studies using isolated tumor cells underscores the influences of the tissue microenvironment on cellular mechanical properties and the intrinsic differences of the mechanical properties between transformed and normal cells.

Importantly, the stromal cells associated with tumors also exhibit changes in their viscoelastic properties as tumors progress. Activated, highly contractile myofibroblasts, which frequently appear early during tumor progression, are stiffer than their non-malignant counterparts [78]. Additionally, activated tumor-associated macrophages are more compliant than resting macrophages [79] and tumor-derived endothelial cells exhibit enhanced mechano-sensing [80] (Table 1). These stromal cells, as well as infiltrating lymphocytes, monocytes and mesenchymal stem cells, frequently participate in the remodeling of interstitial collagen and produce a wide array of growth factors, cytokines and chemokines which help to establish the chemical and rigidity gradients for the growth, transformation and directional metastasis of tumor cells [46,63,81–84]. Indeed, intravital imaging has shown that cancer cells and leukocytes migrate rapidly in collagen-rich

regions [47,85] and that paracrine signaling between cancer cells and leukocytes facilitate the directional migration of cancer cells [82]. Considering the many genetic and epigenetic modifications that occur in tumor-associated stromal cells [86] and the functional diversity of these cells, it is clear that it will be important to study the mechano-sensitivity of the vast array of tumor-related cells and to understand how ECM remodeling, mechanical regulation and stromal cell activities contribute to tumor progression.

Tissue mechanics and oncogenic transformation

Tumor cells encounter various ECM environments and physical forces during tumor initiation, progression, and metastasis (Figure 3). Concurrently, tumor cells undergo malignant transformation, adopting a series of genetic and epigenetic changes, including genetic mutations and expression changes of different ECM adhesion receptors, cell adhesion receptors, growth factor receptors and intracellular signaling molecules. These changes modify the ability of tumor cells to sense and respond to external and internal forces, as well as to the mechanical properties of other cells and the ECM. One widely studied family of mechano-sensors is the cell surface integrin family [87]. Integrins can mediate the sensing of mechanical properties of the ECM by changing their avidity, conformation, clustering and recruitment, and transducing these signals downstream to focal adhesion kinase (FAK), which then leads to the stabilization of focal adhesions and the activation of downstream intracellular signaling cascades. Stiff ECM substrates increase integrin clustering, and induce focal adhesion formation and FAK activation, which intensifies the oncogene ErbB2-mediated PI3K (phosphoinositide 3-kinase) and ERK (extracellular signal-regulated kinase) signaling pathways and promotes tumor cell malignant transformation in both 3D culture and mouse models for breast cancer (Figure 4) [20,40]. Inhibiting Rho GTPase-induced contractility normalizes tumor cell behavior and the inhibition of ECM stiffening delays oncogene-induced tumor progression. Other studies have demonstrated that elevated Rho signaling via oncogene Ras-driven ERK activation or ErbB2-driven PI3K induce cytoskeletal contractility, cell growth, and destabilize tissue architecture [88]. These small GTPases and their effectors are key regulators of cytoskeleton dynamics, cell polarity and migration, and are often found over-expressed in different types of human tumors [89–93]. Thus, knocking out specific small GTPase effectors including Tiam (a Rac activation factor) and GEP100 (an Arf6 activation factor) in mice reduced tumor incidences and metastasis [94,95]. Taken together, these data suggest that the crosstalk between mechanical and oncogene signaling pathways is essential for oncogene-initiated tumor progression. Accordingly, targeting these abnormal mechanical stimuli and mechano-transduction pathways with pharmacological reagents could potentially be of benefit to clinical cancer therapies.

Conclusion and future directions

Tumors are composed of heterogeneous tumor cell populations. This heterogeneity originates from genetic instability and/or the differentiation spectrum of cancer stem cells

(CSCs), potentially leading to drug resistance in cancer therapies [96]. Therefore, an understanding of the properties and regulation of tumor heterogeneity might improve clinical cancer treatment. As discussed in this review, the tumor microenvironment is also heterogeneous and can induce a series of non-uniform biological and biomechanical modifications in tumor cells and the surrounding ECM. Particularly, the biomechanical changes in a tumor microenvironment caused by multiple variable factors including tumor growth and expansion, increased interstitial pressure, cell contraction and ECM deposition and remodeling can modify the biochemical and biomechanical properties of both the tumor stromal microenvironment and tumor cells. This biomechanically modified tumor microenvironment exerts a higher resistance to drug delivery and penetration [97], enhancing the survival of tumor cells owing to mechano-chemical coupling in the 3D context and rendering the cells further resistant to drug-induced cell death [98]. Drugs targeting certain oncogenes or signaling pathways might be less effective when these oncogenes and signaling pathways are connected to mechanical signaling at multiple levels (e.g. integrins, ERK, PI3K, Rho GTPase) (Figures 1 and 4).

Current work suggests CSCs contribute to drug resistance because of their special properties, including the ability to remain quiescent during tumor progression as well as their increased resistance to DNA damage and external environmental insults [99]. What remains unknown is whether the tumor microenvironment also regulates these special properties of CSCs. CSCs have similar properties as stem cells, such as self-renewal, lineage differentiation and residence within specific niches. Studies on embryonic and adult stem cells revealed that self-renewal and differentiation can be regulated by various mechanical cues [100], suggesting that CSCs could also be similarly regulated by tissue mechanics. Indeed, the frequency of cancer stem cells is very sensitive to different microenvironments [101]. CSCs express abundant adhesion molecules including integrins and CD44 [102–104] and require specialized niches composed of soluble factors (e.g. Wnt, Notch, hedgehog and TGF- β) [105–107], stromal cells [108,109], and tension-regulated ECM proteins (e.g. tenascin, fibronectin and laminin) for their self-renewal and differentiation [110,111]. Many of these niche components can modulate and be modulated by cell- and tissue-level tension to regulate cell growth, survival and migration [112–114]. Therefore, the properties of CSCs could be directly and indirectly regulated by the tumor microenvironment. If so, the drug resistance of CSCs might be potentially addressed by targeting the mechanical links in the CSC niches (ECM, stromal cells, and soluble signals). Clearly, elucidating the composition and structure of tumor microenvironment and their local and global mechanical influence on tumor phenotype and pathogenesis will be important for the understanding of cancer biology and for the treatment of multiple cancer types.

Both biochemical and biomechanical factors contribute crucial information to tumor development and evolution. Integral to this dialogue is the complex interplay between soluble factors, cell–cell and cell–ECM interactions and the mechanical environment, which cooperatively drive tumor

progression. Indeed, we and others have demonstrated that genetic and epigenetic changes in cells combine with alterations in matrix architecture and material properties, propelling tumor evolution. However, many questions linking biomechanics and tumor progression still require resolution. Traditional cell biology approaches might need supplementation with techniques from materials science, engineering and physics. It will be crucial to clarify the molecular basis of mechano-transduction in the development and progression of tumors to identify novel anticancer therapeutic targets.

Acknowledgments

We acknowledge Christian Frantz for contributing valuable figures and discussions. We apologize to the authors whose work is not cited owing to space limitation. This work was supported by DOD- W81XWH-05-1-0330, NCI-U54CA143836-01, NIH/NCI R01 CA138818-01A1 (to V.M.W.) and DOD BC062562 (to J.K.M.).

References

- 1 Paszek, M.J. and Weaver, V.M. (2004) The tension mounts: mechanics meets morphogenesis and malignancy. *J. Mammary Gland. Biol. Neoplasia* 9, 325–342
- 2 Yang, J.H. *et al.* (2000) Biomechanical regulation of human monocyte/macrophage molecular function. *Am. J. Pathol.* 156, 1797–1804
- 3 Wells, R.G. and Discher, D.E. (2008) Matrix elasticity, cytoskeletal tension, and TGF-beta: the insoluble and soluble meet. *Sci. Signal.* 1, pe13
- 4 Egeblad, M. *et al.* (2005) The fibroblastic coconspirator in cancer progression. *Cold Spring Harb. Symp. Quant. Biol.* 70, 383–388
- 5 Swartz, M.A. and Fleury, M.E. (2007) Interstitial flow and its effects in soft tissues. *Annu. Rev. Biomed. Eng.* 9, 229–256
- 6 Mantovani, A. *et al.* (2008) Cancer-related inflammation. *Nature* 454, 436–444
- 7 Butcher, D.T. *et al.* (2009) A tense situation: forcing tumour progression. *Nat. Rev. Cancer* 9, 108–122
- 8 Gutierrez, J.A. and Perr, H.A. (1999) Mechanical stretch modulates TGF-beta1 and alpha1(I) collagen expression in fetal human intestinal smooth muscle cells. *Am. J. Physiol.* 277, G1074–G1080
- 9 Prajapati, R.T. *et al.* (2000) Mechanical loading regulates protease production by fibroblasts in three-dimensional collagen substrates. *Wound Repair Regen.* 8, 226–237
- 10 Toda, S. *et al.* (2002) A new organotypic culture of thyroid tissue maintains three-dimensional follicles with C cells for a long term. *Biochem. Biophys. Res. Commun.* 294, 906–911
- 11 Moore, K.A. *et al.* (2002) Control of embryonic lung branching morphogenesis by the Rho activator, cytotoxic necrotizing factor 1. *J. Surg. Res.* 104, 95–100
- 12 Miao, H. *et al.* (2003) EphA kinase activation regulates HGF-induced epithelial branching morphogenesis. *J. Cell Biol.* 162, 1281–1292
- 13 Butler, L.C. *et al.* (2009) Cell shape changes indicate a role for extrinsic tensile forces in *Drosophila* germ-band extension. *Nat. Cell Biol.* 11, 859–864
- 14 Jaalouk, D.E. and Lammerding, J. (2009) Mechanotransduction gone awry. *Nat. Rev. Mol. Cell Biol.* 10, 63–73
- 15 Fletcher, D.A. and Mullins, R.D. (2010) Cell mechanics and the cytoskeleton. *Nature* 463, 485–492
- 16 Solon, J. *et al.* (2007) Fibroblast adaptation and stiffness matching to soft elastic substrates. *Biophys. J.* 93, 4453–4461
- 17 Wang, N. *et al.* (2002) Cell prestress. I. Stiffness and prestress are closely associated in adherent contractile cells. *Am. J. Physiol. Cell Physiol.* 282, C606–C616
- 18 Balgude, A.P. *et al.* (2001) Agarose gel stiffness determines rate of DRG neurite extension in 3D cultures. *Biomaterials* 22, 1077–1084
- 19 Georges, P.C. *et al.* (2006) Matrices with compliance comparable to that of brain tissue select neuronal over glial growth in mixed cortical cultures. *Biophys. J.* 90, 3012–3018
- 20 Paszek, M.J. *et al.* (2005) Tensional homeostasis and malignant phenotype. *Cancer Cell* 8, 241–254

- 21 Fettiplace, R. and Hackney, C.M. (2006) The sensory and motor roles of auditory hair cells. *Nat. Rev. Neurosci.* 7, 19–29
- 22 Praetorius, H.A. and Spring, K.R. (2005) A physiological view of the primary cilium. *Annu. Rev. Physiol.* 67, 515–529
- 23 Vogel, V. and Sheetz, M. (2006) Local force and geometry sensing regulate cell functions. *Nat. Rev. Mol. Cell Biol.* 7, 265–275
- 24 del Rio, A. *et al.* (2009) Stretching single talin rod molecules activates vinculin binding. *Science* 323, 638–641
- 25 Sbrana, F. *et al.* (2008) Role for stress fiber contraction in surface tension development and stretch-activated channel regulation in C2C12 myoblasts. *Am. J. Physiol. Cell Physiol.* 295, C160–C172
- 26 Salaita, K. *et al.* (2010) Restriction of receptor movement alters cellular response: physical force sensing by EphA2. *Science* 327, 1380–1385
- 27 Paszek, M.J. *et al.* (2009) Integrin clustering is driven by mechanical resistance from the glycocalyx and the substrate. *PLoS Comput. Biol.* 5, e1000604
- 28 Chu, Y.S. *et al.* (2004) Force measurements in E-cadherin-mediated cell doublets reveal rapid adhesion strengthened by actin cytoskeleton remodeling through Rac and Cdc42. *J. Cell Biol.* 167, 1183–1194
- 29 Gao, M. *et al.* (2006) Molecular mechanisms of cellular mechanics. *Phys. Chem. Chem. Phys.* 8, 3692–3706
- 30 DeNardo, D.G. *et al.* (2008) Immune cells as mediators of solid tumor metastasis. *Cancer Metastasis Rev.* 27, 11–18
- 31 Whiteside, T.L. (2006) The role of immune cells in the tumor microenvironment. *Cancer Treat. Res.* 130, 103–124
- 32 Hynes, R.O. (2009) The extracellular matrix: not just pretty fibrils. *Science* 326, 1216–1219
- 33 Borghi, N. and Nelson, J.W. (2009) Intercellular adhesion in morphogenesis: molecular and biophysical considerations. *Curr. Top. Dev. Biol.* 89, 1–32
- 34 Schwartz, M.A. and DeSimone, D.W. (2008) Cell adhesion receptors in mechanotransduction. *Curr. Opin. Cell Biol.* 20, 551–556
- 35 Ingber, D.E. (2008) Can cancer be reversed by engineering the tumor microenvironment? *Semin. Cancer Biol.* 18, 356–364
- 36 Helmlinger, G. *et al.* (1997) Solid stress inhibits the growth of multicellular tumor spheroids. *Nat. Biotechnol.* 15, 778–783
- 37 Padera, T.P. *et al.* (2004) Pathology: cancer cells compress intratumour vessels. *Nature* 427, 695
- 38 Volokh, K.Y. (2006) Stresses in growing soft tissues. *Acta Biomater.* 2, 493–504
- 39 Sarntinoranont, M. *et al.* (2003) Interstitial stress and fluid pressure within a growing tumor. *Ann. Biomed. Eng.* 31, 327–335
- 40 Levental, K.R. *et al.* (2009) Matrix crosslinking forces tumor progression by enhancing integrin signaling. *Cell* 139, 891–906
- 41 Tlsty, T.D. and Coussens, L.M. (2006) Tumor stroma and regulation of cancer development. *Annu. Rev. Pathol.* 1, 119–150
- 42 Heldin, C.H. *et al.* (2004) High interstitial fluid pressure – an obstacle in cancer therapy. *Nat. Rev. Cancer* 4, 806–813
- 43 Chee, P.N. *et al.* (2005) Interstitial fluid flow induces myofibroblast differentiation and collagen alignment in vitro. *J. Cell Sci.* 118, 4731–4739
- 44 Wyckoff, J.B. *et al.* (2000) A critical step in metastasis: in vivo analysis of intravasation at the primary tumor. *Cancer Res.* 60, 2504–2511
- 45 Wyckoff, J.B. *et al.* (2007) Direct visualization of macrophage-assisted tumor cell intravasation in mammary tumors. *Cancer Res.* 67, 2649–2656
- 46 Condeelis, J. and Pollard, J.W. (2006) Macrophages: obligate partners for tumor cell migration, invasion, and metastasis. *Cell* 124, 263–266
- 47 Lohela, M. and Werb, Z. (2010) Intravital imaging of stromal cell dynamics in tumors. *Curr. Opin. Genet. Dev.* 20, 72–78
- 48 Kumar, S. and Weaver, V.M. (2009) Mechanics, malignancy, and metastasis: the force journey of a tumor cell. *Cancer Metastasis Rev.* 28, 113–127
- 49 Liang, S. *et al.* (2008) Hydrodynamic shear rate regulates melanoma-leukocyte aggregation, melanoma adhesion to the endothelium, and subsequent extravasation. *Ann. Biomed. Eng.* 36, 661–671
- 50 Nguyen, D.X. *et al.* (2009) Metastasis: from dissemination to organ-specific colonization. *Nat. Rev. Cancer* 9, 274–284
- 51 Joyce, J.A. and Pollard, J.W. (2009) Microenvironmental regulation of metastasis. *Nat. Rev. Cancer* 9, 239–252
- 52 Erler, J.T. and Weaver, V.M. (2009) Three-dimensional context regulation of metastasis. *Clin. Exp. Metastasis* 26, 35–49
- 53 Kostic, A. *et al.* (2009) Differential matrix rigidity response in breast cancer cell lines correlates with the tissue tropism. *PLoS One* 4, e6361
- 54 Lam, W.A. *et al.* (2010) Extracellular matrix rigidity modulates neuroblastoma cell differentiation and N-myc expression. *Mol. Cancer* 9, 35
- 55 Pathi, S.P. *et al.* (2010) A novel 3-D mineralized tumor model to study breast cancer bone metastasis. *PLoS One* 5, e8849
- 56 Vakonakis, I. and Campbell, I.D. (2007) Extracellular matrix: from atomic resolution to ultrastructure. *Curr. Opin. Cell Biol.* 19, 578–583
- 57 Buehler, M.J. (2006) Nature designs tough collagen: explaining the nanostructure of collagen fibrils. *Proc. Natl. Acad. Sci. U. S. A.* 103, 12285–12290
- 58 Kass, L. *et al.* (2007) Mammary epithelial cell: influence of extracellular matrix composition and organization during development and tumorigenesis. *Int. J. Biochem. Cell Biol.* 39, 1987–1994
- 59 Provenzano, P.P. *et al.* (2006) Collagen reorganization at the tumor-stromal interface facilitates local invasion. *BMC Med.* 4, 38
- 60 Provenzano, P.P. *et al.* (2008) Collagen density promotes mammary tumor initiation and progression. *BMC Med.* 6, 11
- 61 Egeblad, M. and Werb, Z. (2002) New functions for the matrix metalloproteinases in cancer progression. *Nat. Rev. Cancer* 2, 161–174
- 62 Sabeh, F. *et al.* (2009) Secreted versus membrane-anchored collagenases: relative roles in fibroblast-dependent collagenolysis and invasion. *J. Biol. Chem.* 284, 23001–23011
- 63 Lo, C.M. *et al.* (2000) Cell movement is guided by the rigidity of the substrate. *Biophys. J.* 79, 144–152
- 64 Hadjipanayi, E. *et al.* (2009) Guiding cell migration in 3D: a collagen matrix with graded directional stiffness. *Cell Motil. Cytoskeleton* 66, 121–128
- 65 Arnold, S.A. *et al.* (2010) Lack of host SPARC enhances vascular function and tumor spread in an orthotopic murine model of pancreatic carcinoma. *Dis. Model Mech.* 3, 57–72
- 66 Klotzsch, E. *et al.* (2009) Fibronectin forms the most extensible biological fibers displaying switchable force-exposed cryptic binding sites. *Proc. Natl. Acad. Sci. U. S. A.* 106, 18267–18272
- 67 Oldberg, A. *et al.* (2007) Collagen-binding proteoglycan fibromodulin can determine stroma matrix structure and fluid balance in experimental carcinoma. *Proc. Natl. Acad. Sci. U. S. A.* 104, 13966–13971
- 68 Wipff, P.J. *et al.* (2007) Myofibroblast contraction activates latent TGF-beta1 from the extracellular matrix. *J. Cell Biol.* 179, 1311–1323
- 69 Bierie, B. and Moses, H.L. (2010) Transforming growth factor beta (TGF-beta) and inflammation in cancer. *Cytokine Growth Factor Rev.* 21, 49–59
- 70 Giampieri, S. *et al.* (2009) Localized and reversible TGFbeta signalling switches breast cancer cells from cohesive to single cell motility. *Nat. Cell Biol.* 11, 1287–1296
- 71 Yung, Y.C. *et al.* (2009) Cyclic tensile strain triggers a sequence of autocrine and paracrine signaling to regulate angiogenic sprouting in human vascular cells. *Proc. Natl. Acad. Sci. U. S. A.* 106, 15279–15284
- 72 Smith, J.D. *et al.* (2001) Cyclic stretch induces the expression of vascular endothelial growth factor in vascular smooth muscle cells. *Endothelium* 8, 41–48
- 73 Petrigliano, F.A. *et al.* (2007) The effects of local bFGF release and uniaxial strain on cellular adaptation and gene expression in a 3D environment: implications for ligament tissue engineering. *Tissue Eng.* 13, 2721–2731
- 74 Brown, X.Q. *et al.* (2010) Effect of substrate stiffness and PDGF on the behavior of vascular smooth muscle cells: implications for atherosclerosis. *J. Cell Physiol.* 225, 115–122
- 75 Suresh, S. (2007) Biomechanics and biophysics of cancer cells. *Acta Biomater.* 3, 413–438
- 76 Cross, S.E. *et al.* (2008) AFM-based analysis of human metastatic cancer cells. *Nanotechnology* 19, 384003
- 77 Baker, E.L. *et al.* (2009) Extracellular matrix stiffness and architecture govern intracellular rheology in cancer. *Biophys. J.* 97, 1013–1021
- 78 Park, S. *et al.* (2005) Cell motility and local viscoelasticity of fibroblasts. *Biophys. J.* 89, 4330–4342
- 79 Leporatti, S. *et al.* (2006) Elasticity and adhesion of resting and lipopolysaccharide-stimulated macrophages. *FEBS Lett.* 580, 450–454

- 80 Ghosh, K. *et al.* (2008) Tumor-derived endothelial cells exhibit aberrant Rho-mediated mechanosensing and abnormal angiogenesis in vitro. *Proc. Natl. Acad. Sci. U. S. A.* 105, 11305–11310
- 81 Karnoub, A.E. *et al.* (2007) Mesenchymal stem cells within tumour stroma promote breast cancer metastasis. *Nature* 449, 557–563
- 82 Patsialou, A. *et al.* (2009) Invasion of human breast cancer cells in vivo requires both paracrine and autocrine loops involving the colony-stimulating factor-1 receptor. *Cancer Res.* 69, 9498–9506
- 83 Isenberg, B.C. *et al.* (2009) Vascular smooth muscle cell durotaxis depends on substrate stiffness gradient strength. *Biophys J.* 97, 1313–1322
- 84 Gaggioli, C. *et al.* (2007) Fibroblast-led collective invasion of carcinoma cells with differing roles for RhoGTPases in leading and following cells. *Nat. Cell Biol.* 9, 1392–1400
- 85 Egeblad, M. *et al.* (2008) Visualizing stromal cell dynamics in different tumor microenvironments by spinning disk confocal microscopy. *Dis. Model Mech.* 1, 155–167
- 86 Hu, M. and Polyak, K. (2008) Molecular characterisation of the tumour microenvironment in breast cancer. *Eur. J. Cancer* 44, 2760–2765
- 87 Baker, E.L. and Zaman, M.H. (2010) The biomechanical integrin. *J. Biomech.* 43, 38–44
- 88 Zhong, C. *et al.* (1997) Rho-stimulated contractility contributes to the fibroblastic phenotype of Ras-transformed epithelial cells. *Mol. Biol. Cell* 8, 2329–2344
- 89 Fritz, G. *et al.* (1999) Rho GTPases are over-expressed in human tumors. *Int. J. Cancer* 81, 682–687
- 90 Bellizzi, A. *et al.* (2008) RhoA protein expression in primary breast cancers and matched lymphocytes is associated with progression of the disease. *Int. J. Mol. Med.* 22, 25–31
- 91 Bos, J.L. *et al.* (2007) GEFs and GAPs: critical elements in the control of small G proteins. *Cell* 129, 865–877
- 92 Engers, R. *et al.* (2000) Tiam1 mutations in human renal-cell carcinomas. *Int. J. Cancer* 88, 369–376
- 93 Sahai, E. and Marshall, C.J. (2002) RHO-GTPases and cancer. *Nat. Rev. Cancer* 2, 133–142
- 94 Morishige, M. *et al.* (2008) GEP100 links epidermal growth factor receptor signalling to Arf6 activation to induce breast cancer invasion. *Nat. Cell Biol.* 10, 85–92
- 95 Lambert, J.M. *et al.* (2002) Tiam1 mediates Ras activation of Rac by a PI(3)K-independent mechanism. *Nat. Cell Biol.* 4, 621–625
- 96 Gillet, J.P. and Gottesman, M.M. (2010) Mechanisms of multidrug resistance in cancer. *Methods Mol. Biol.* 596, 47–76
- 97 Minchinton, A.I. and Tannock, I.F. (2006) Drug penetration in solid tumours. *Nat. Rev. Cancer.* 6, 583–592
- 98 Zahir, N. and Weaver, V.M. (2004) Death in the third dimension: apoptosis regulation and tissue architecture. *Curr. Opin. Genet. Dev.* 14, 71–80
- 99 Baguley, B.C. (2010) Multidrug resistance in cancer. *Methods Mol. Biol.* 596, 1–14
- 100 Keung, A.J. *et al.* (2010) Presentation counts: microenvironmental regulation of stem cells by biophysical and material cues. *Annu. Rev. Cell Dev. Biol.* 26, 533–556
- 101 Quintana, E. *et al.* (2008) Efficient tumour formation by single human melanoma cells. *Nature* 456, 593–598
- 102 Lathia, J.D. *et al.* (2010) Integrin alpha 6 regulates glioblastoma stem cells. *Cell Stem Cell* 6, 421–432
- 103 Taddei, I. *et al.* (2008) Beta1 integrin deletion from the basal compartment of the mammary epithelium affects stem cells. *Nat. Cell Biol.* 10, 716–722
- 104 Kirkland, S.C. and Ying, H. (2008) Alpha2beta1 integrin regulates lineage commitment in multipotent human colorectal cancer cells. *J. Biol. Chem.* 283, 27612–27619
- 105 Kawaguchi-Ihara, N. *et al.* (2008) Promotion of the self-renewal capacity of human acute leukemia cells by Wnt3A. *Anticancer Res.* 28, 2701–2704
- 106 Reedijk, M. *et al.* (2008) Activation of Notch signaling in human colon adenocarcinoma. *Int. J. Oncol.* 33, 1223–1229
- 107 Michael, L.E. *et al.* (2008) Bmi1 is required for hedgehog pathway-driven medulloblastoma expansion. *Neoplasia* 10, 1343–1349
- 108 Colmone, A. *et al.* (2008) Leukemic cells create bone marrow niches that disrupt the behavior of normal hematopoietic progenitor cells. *Science* 322, 1861–1865
- 109 Gilbertson, R.J. and Rich, J.N. (2007) Making a tumour's bed: glioblastoma stem cells and the vascular niche. *Nat Rev Cancer.* 7, 733–736
- 110 Liu, J.M. *et al.* (2008) The postoperative brain tumour stem cell (BTSC) niche and cancer recurrence. *Adv Ther.* 25, 389–398
- 111 Sneddon, J.B. and Werb, Z. (2007) Location, location, location: the cancer stem cell niche. *Cell Stem Cell* 1, 607–611
- 112 Whitehead, J. *et al.* (2008) Mechanical factors activate beta-catenin-dependent oncogene expression in APC mouse colon. *HFSP J.* 2, 286–294
- 113 Desprat, N. *et al.* (2008) Tissue deformation modulates twist expression to determine anterior midgut differentiation in *Drosophila* embryos. *Dev. Cell* 15, 470–477
- 114 Lee, J.Y. *et al.* (2006) Wnt/Frizzled signaling controls *C. elegans* gastrulation by activating actomyosin contractility. *Curr. Biol.* 16, 1986–1997
- 115 Samani, A. (2003) Measuring the elastic modulus of ex vivo small tissue samples. *Phys. Med. Biol.* 48, 2183–2198
- 116 Gefen, A. and Dilmoney, B. (2007) Mechanics of the normal woman's breast. *Technol. Health Care* 15, 259–271
- 117 Ebihara, T. *et al.* (2000) Changes in extracellular matrix and tissue viscoelasticity in bleomycin-induced lung fibrosis. Temporal aspects. *Am. J. Respir. Crit. Care Med.* 162, 1569–1576
- 118 Zysset, P.K. *et al.* (1999) Elastic modulus and hardness of cortical and trabecular bone lamellae measured by nanoindentation in the human femur. *J. Biomech.* 32, 1005–1012
- 119 Odgaard, A. and Linde, F. (1991) The underestimation of Young's modulus in compressive testing of cancellous bone specimens. *J. Biomech.* 24, 691–698
- 120 Wells, R.G. (2008) The role of matrix stiffness in regulating cell behavior. *Hepatology* 47, 1394–1400
- 121 Yeh, W.C. *et al.* (2002) Elastic modulus measurements of human liver and correlation with pathology. *Ultrasound Med. Biol.* 28, 467–474
- 122 Guck, J. *et al.* (2005) Optical deformability as an inherent cell marker for testing malignant transformation and metastatic competence. *Biophys. J.* 88, 3689–3698
- 123 Tan, S.C. *et al.* (2008) Viscoelastic behaviour of human mesenchymal stem cells. *BMC Cell Biol.* 9, 40
- 124 Rosenbluth, M.J. *et al.* (2006) Force microscopy of nonadherent cells: a comparison of leukemia cell deformability. *Biophys. J.* 90, 2994–3003

REVIEW

Tumor Microenvironment and Progression

HAROLD F. DVORAK, MD,^{1*} VALERIE M. WEAVER, PhD,² THEA D. TLSTY, PhD,³ AND GABRIELE BERGERS, PhD⁴

¹Department of Pathology, Center for Vascular Biology Research, Beth Israel Deaconess Medical Center, Harvard Medical School, Boston, Massachusetts

²Department of Surgery & Anatomy, Center for Bioengineering and Tissue Regeneration, University of California, San Francisco, California

³Department of Pathology, University of California, San Francisco, California

⁴Department of Neurological Surgery and Anatomy, Helen Diller Family Cancer Research Building, University of California, San Francisco, California

Tumor blood vessels are heterogeneous, of at least six distinct types, are induced primarily by vascular endothelial growth factor-A (VEGF-A), and provide a potentially useful therapeutic target. Breast cancer is characterized by changes in the microenvironment that result in altered tensional homeostasis. Also, breast cancers arise as the result of epigenetic as well as genetic changes. Tumor blood vessel pericytes result, in part, from bone marrow precursor cells, and VEGF is a negative regulator of glioblastoma tumor cell invasion.

J. Surg. Oncol. © 2010 Wiley-Liss, Inc.

KEY WORDS: angiogenesis; mechano-biology; patterning

INTRODUCTION

Like normal tissues, tumors are composed of two discrete but interactive compartments, parenchyma and stroma [1]. In tumors, the tumor cells themselves are the parenchyma, whereas the stroma is composed of a mixture of non-malignant cells and connective tissue elements. Stromal elements include blood and lymphatic vessels, as well as fibroblasts and inflammatory cells. In addition, stroma includes a variety of extracellular macromolecules that serve to provide structural support; these include collagen, fibronectin, fibrin, various proteoglycans, and hyaluronan. The quantities of these different stromal cells and extracellular deposits differ widely in different tumors. For example, in desmoplastic tumors, stroma may account for >80% of the tumor mass, whereas in other tumors (e.g., many lymphomas) stroma may account for only a tiny fraction. Tumor malignancy does not correlate closely with the amount of stroma deposited; both highly and less malignant tumors can possess abundant or limited amounts of stroma. Nonetheless, all tumors require at least some stroma to meet their needs of nutrition, waste removal, and structure. Even “liquid tumors,” that is, leukemias, have stroma, the blood plasma in which they circulate. Though long neglected, it has become clear in recent years that stroma is essential for tumor maintenance and growth and has potential as a therapeutic target. As one example, anti-angiogenic agents have recently been found to impede tumor growth and prolong survival when used in adjuvant mode, thus proving in principle that attacking stroma can be a useful approach to therapy [2,3]. Going forward, it is likely that other approaches will be used to target tumor stroma. Therefore, it was appropriate to begin the 3rd International Symposium on Cancer Metastasis and the Lympho-vascular System with a session on the tumor microenvironment. Four speakers addressed various aspects of tumor stroma, as follows.

TUMOR BLOOD VESSELS: THE WHAT, THE HOW, AND THE WHY (Harold F. Dvorak)

The tumor vasculature is an important component of the tumor microenvironment [1,4]. The current view of tumor angiogenesis can be

summarized as follows: tumors must induce the formation of new blood vessels if they are to grow beyond minimal size; they do so by secreting growth factors, particularly vascular permeability factor/vascular endothelial growth factor-A (VEGF-A); the resulting tumor blood vessels are highly abnormal; and anti-angiogenic therapy is useful as an adjuvant, though, in general, its addition to the therapeutic armament prolongs life by only a few months [2,3]. Therefore, it is a good time to address some basic questions: What are tumor blood vessels, How do they form, and Why might their diversity be important therapeutically?

What Are Tumor Blood Vessels?

While it has long been recognized that tumor blood vessels are abnormal, angiogenic blood vessels are often spoken of as being of a single type. This is certainly not the case. Studies over the last decade have established that angiogenic tumor blood vessels are highly

Grant sponsor: U.S. Public Health Service; Grant numbers: HL-64402, P01 CA92644; Grant sponsor: National Foundation for Cancer Research; Grant sponsor: US Department of Defense; Grant numbers: PSOC U54CA143836-01, DOD W81XWH-05-1-0330; Grant sponsor: Susan G. Komen Foundation Postdoctoral Award; Grant number: PDF124906; Grant sponsor: National Cancer Institute Institutional Training; Grant number: T32 CA009043; Grant sponsor: Department of Defense Breast Cancer Research Program Concept Award; Grant number: BC023982; Grant sponsor: National Institutes of Health National Cancer Institute; Grant numbers: CA097214, CA122024, PS-OC U54; Grant sponsor: U.S. National Cancer Institute; Grant numbers: R01 CA113382, R01 CA109390.

*Correspondence to: Harold F. Dvorak, MD, Department of Pathology, Beth Israel Deaconess Medical Center, 330 Brookline Ave. RN227c, Boston, MA 02215. Fax: 617-667-2913.

E-mail: hdvorak@bidmc.harvard.edu

Received 2 June 2010; Accepted 16 July 2010

DOI 10.1002/jso.21709

Published online in Wiley Online Library (wileyonlinelibrary.com).

TABLE I. Classification of Angiogenic Tumor Blood Vessels

Vessel type	Vessel properties
Mother vessels	Large, thin-walled, hyperpermeable, lightly fenestrated pericyte-poor sinusoids that are engorged with red blood cells
Capillaries	Resemble normal capillaries as far as is known
Glomeruloid microvascular proliferations (GMP)	Poorly organized vascular structures that macroscopically resemble renal glomeruli. They are composed of endothelial cells and pericytes with minimal vascular lumens and reduplicated basement membranes
Vascular malformations (VM)	Mother vessels that have acquired an often asymmetric coat of smooth muscle cells and/or fibrous connective tissue. Resemble arterio-venous malformations found in other settings

heterogeneous and can be classified into at least four structurally and functionally distinct types (Table I).

How Do Angiogenic Tumor Blood Vessels Form?

Tumor angiogenesis falls into the general category of pathological angiogenesis, that is, the type of neovascular response induced by processes such as wound healing and chronic inflammation [5]. Further, it has been possible to induce surrogate forms of all of the types of angiogenic tumor blood vessels listed in Table I by expressing VEGF-A in mouse tissues with an adenoviral vector (Ad-VEGF-A¹⁶⁴) (Fig. 1). The first new blood vessel type to develop in tumors, as well as in healing wounds and chronic inflammation, is the “mother vessel” (MV) [6,7].

MVs arise from preexisting venules (and to a lesser extent from capillaries) and their properties are listed in Table I. The initial step in MV formation is degradation of venular basement membrane (VBM). VBM are rigid structures comprising a tightly woven meshwork of type IV collagen, laminin, entactin, perlecan, and heparan sulfate. VBM limits the expansion of the normal microvasculature to ~30% [8], whereas MVs have lumens that are 4–5 times those of the normal vessels from which they arise. Therefore, for microvessels to enlarge to become MV, their VBM must be degraded. Chang et al. [9] recently confirmed earlier observations that Ad-VEGF-A¹⁶⁴ and VEGF-A-expressing tumors induce VBM degradation and found that they did so

by upsetting the normal cathepsin–cysteine protease inhibitor (CPI) balance [9]. Cathepsins are members of the cysteine protease family and CPIs are a family of small proteins that serve as their endogenous inhibitors. Cathepsins B, S, and L were selectively upregulated in the pericytes of venules and capillaries as they were developing into MV, a process that began within a day or 2 after Ad-VEGF-A¹⁶⁴ or tumor cell injection into mouse tissues. Over the same time period, several CPIs were strikingly downregulated, thus freeing cathepsins from inhibition. On the other hand, the activity of matrix metalloproteases 2 and 9, proteases known to have important roles in tumor biology, actually declined during the course of MV formation. Together these data indicate that VEGF-A induces MV formation by upsetting the cathepsin–CPI balance in preexisting microvessels.

Degradation of the VBM has two important consequences. First, pericytes, having lost their VBM substrate, fall off, accounting for the death of pericytes associated with MV. Second, the underlying endothelium thins and expands to cover a now greatly enlarged surface area. These data indicate that the VBM and pericytes together serve as a restraint that limits the size of venules and capillaries. Further, they suggest that MV formation can result from events taking place entirely within the microvasculature itself, and that proteases, for example, secreted by tumor cells, are not necessary for MV formation. Remaining to be determined is the mechanism by which VEGF-A regulates the cathepsin–CPI axis.

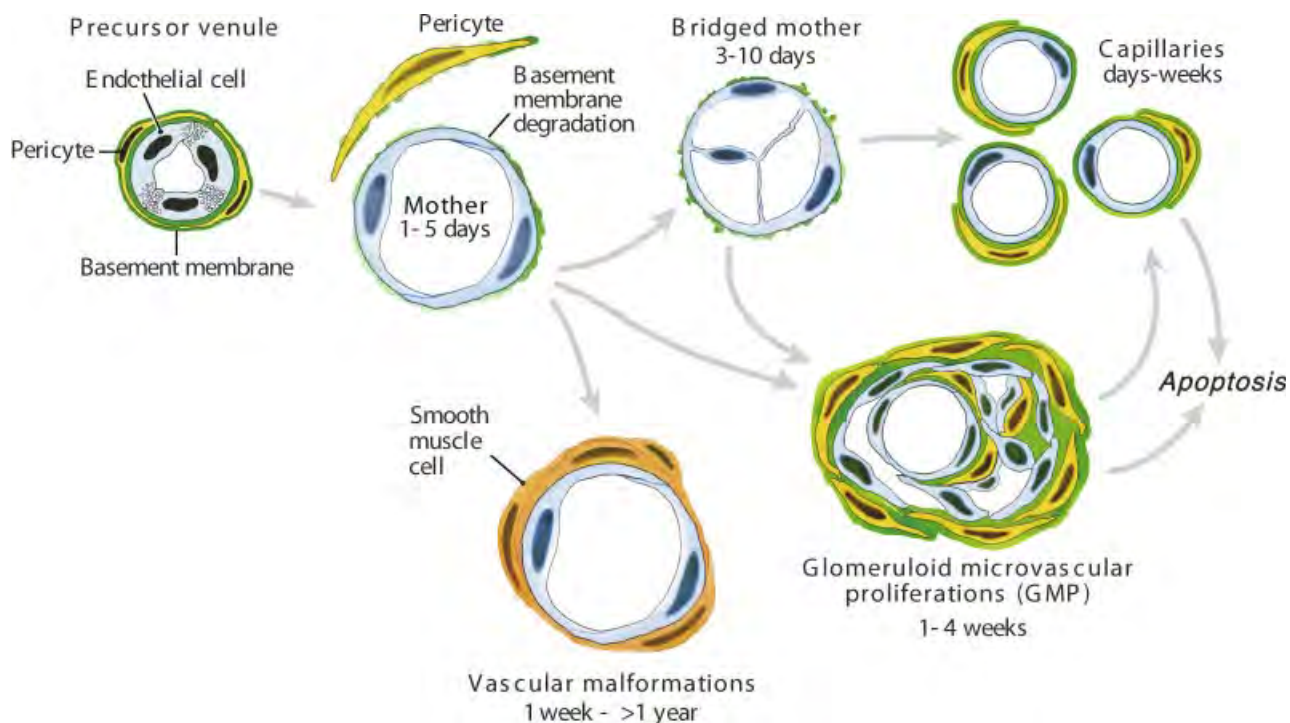


Fig. 1. Schematic diagram of tumor angiogenesis. Reproduced from Ref. [32].

Very little is known about the mechanisms by which MV evolve into the other types of angiogenic blood vessels (reviewed in Refs. [1,4,10]).

Why Is an Understanding of Tumor Blood Vessel Diversity Important Clinically?

Anti-VEGF therapy has been found to prolong the survival of some cancer patients, but it has not been as effective as was originally hoped for, based on studies in mouse cancer models. There are a number of possible reasons for this, for example, side effects that limit the use in cancer patients of anti-VEGF-A therapy at high doses; vascular normalization resulting from anti-angiogenic therapy [3]; neo-expression of growth factors other than VEGF-A, etc. However, another largely neglected and potentially important possibility is that the tumor vasculature is heterogeneous and that certain of the vessel subtypes listed in Table I have gained VEGF-A independence and no longer require VEGF-A for their maintenance.

To test this hypothesis, we have used the Ad-VEGF-A¹⁶⁴ system to generate tumor surrogate vessels of the several types listed in Table I in mice. Of particular interest are vessels that arise at later times as these are most likely to have lost their VEGF-A dependence. Our goal is to find new molecules on the surfaces of the endothelial cells that line such blood vessels and to gauge them for therapeutic potential. This approach has been promising, and we have recently identified one such potential target, the four transmembranes, tetraspanin-like protein, TM4SF1 [11]. TM4SF1 is highly expressed on the endothelial cell plasma membranes of smooth muscle coated blood vessels in several important human cancers. Knockdown of TM4SF1 inhibits division and migration of cultured endothelial cells and causes them to undergo senescence. Also, knockdown of this gene in vivo inhibited later stages of Ad-VEGF-A¹⁶⁴-induced angiogenesis. It will be of interest to determine whether antibodies under development that target this gene will be therapeutically effective in mouse and, more importantly, in human cancers.

BREAST CANCER AS A DISEASE OF ALTERED MECHANO-BIOLOGY (Valerie M. Weaver)

It has been known for some time that tumor and stromal cells talk to each other by secreting various cytokines (e.g., TGF- β) and other biochemical reagents. Less appreciated is the fact that tumor and stromal cells live in a microenvironment with which they interact by means of mechanical signaling. Cells in tissues are subject to a variety of forces including shear stress and compression and tension that result from their interaction with other cells or with the extracellular matrix. These mechanical forces are perceived and integrated in the cell at the molecular level through mechanically responsive sensors. Changes in these interactions may influence cell survival, motility, division, differentiation, and gene expression, for example, by regulating the activity of the RhoGTPases that modulate actomyosin contractility and actin dynamics. Integrins, by virtue of their extracellular interaction with the ECM and intracellular interactions with the cellular cytoskeleton, are prime examples of cellular mechano-transducers, and, upon activation, may induce signaling changes that lead to the formation of focal adhesions [12,13] (Fig. 2A). Thus, force-dependent activation of signaling cascades allows cells to respond quickly to a dynamic force environment, and the same pathways may also lead to sustained changes in cell behavior, for example, changes in gene expression, cell division, etc.

Loss of homeostasis is a hallmark of disease and therefore it is not surprising that cancers should be characterized by changes in tensional homeostasis. Tumors are often detected as a palpable "stiffening" or hardening of the tissue, and approaches such as magnetic resonance

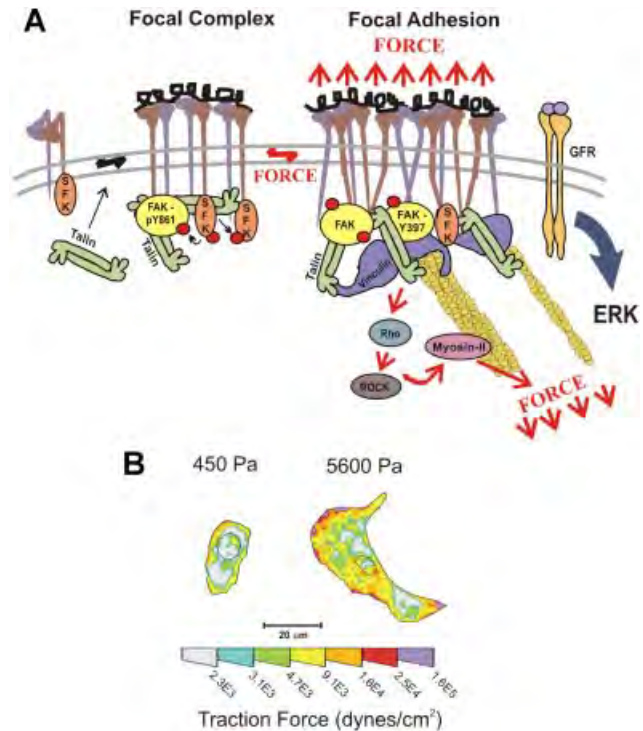


Fig. 2. **A:** The majority of integrins exist at the plasma membrane in a resting, inactive state in which they can be activated by inside-out or outside-in cues. With regard to outside-in activation, when cells encounter a mechanically rigid matrix or are exposed to an exogenous force, integrins become activated, which favors integrin oligomerization or clustering, talin 1 and p130Cas protein unfolding, vinculin-talin association, and Src and focal adhesion kinase (FAK) stimulation of RhoGTPase-dependent actomyosin contractility and actin remodeling. Focal adhesions mature with the recruitment of a repertoire of adhesion plaque proteins, including α -actinin to facilitate actin association, and adaptor proteins such as paxillin, which foster interactions between multiple signaling complexes to promote growth, migration and differentiation. **B:** Normal cells tune their contractility in response to matrix stiffness cues, but tumors exhibit altered tensional homeostasis. Cells exert actomyosin contractility and cytoskeleton-dependent force in response to matrix stiffness cues. These forces can be measured using traction force microscopy. Thus, non-malignant human mammary epithelial cells spread more and exert more force on a stiff matrix than on a soft matrix. Reproduced, with permission, from Refs. [12,14].

imaging elastography and sono-elastography have been developed to measure this property in order to enhance cancer detection. The palpable stiffening characteristic of breast and many other cancers is attributed to desmoplasia, the synthesis of abundant dense collagenous stroma that can occupy up to 80% of the tumor mass.

The crucial role of matrix compliance can be illustrated by studies in which mammary epithelium is grown in culture in matrices with different viscoelastic properties (Fig. 3) [14]. When grown in matrices comparable to those found in normal breast, epithelial cells proliferate until they form polarized mammary acinus-like structures with a central lumen and an external basement membrane. However, when the matrix is progressively stiffened, epithelial cell growth is enhanced, the cells lose their polarity, lose cell-cell junction proteins, and exhibit irregular cell shapes with detectable actin stress fibers. Thus, focal adhesion is increased along with increased adhesion signaling. Together, the stiffened matrix promotes epithelial cell transformation toward cancer.

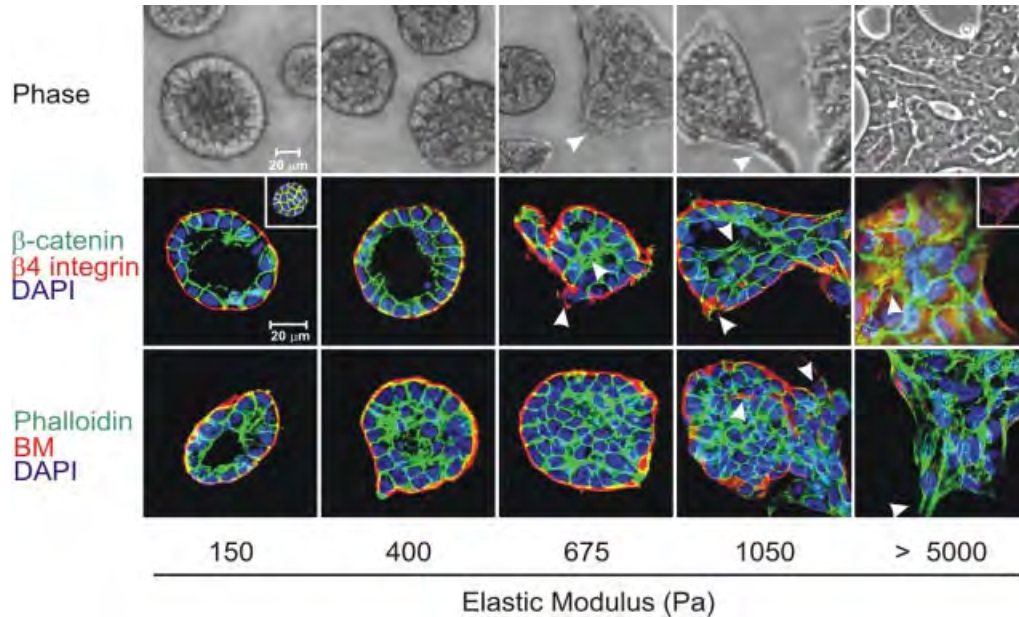


Fig. 3. Phase-contrast microscopy and confocal immunofluorescence images of non-malignant immortalized human mammary epithelial cell (HMEC; MCF10A) colonies interacting with a three-dimensional reconstituted basement membrane (BM)-laminated polyacrylamide gel of increasing stiffness (150–5,000 Pa) showing colony morphogenesis after 20 days of culture. On compliant gels with materials properties similar to that measured in the normal murine mammary gland (150 Pa) non-malignant MECs proliferate for 6–12 days to eventually form growth-arrested, polarized acini analogous to the terminal ductal lobular units observed at the end buds of the differentiated breast. These structures have intact adherens junctions and insoluble cell–cell localized β -catenin before (main images) and after (left inset) Triton extraction, and polarity, as shown by the basal localization of (α 6) β 4 integrin, the apical–lateral localization of cortical actin (Phalloidin), and the assembly of an endogenous laminin 5 basement membrane. Incremental stiffening of the basement membrane gel progressively compromises tissue morphogenesis and alters EGF-dependent growth of these cells. Thus, colony size progressively increases with matrix stiffening, lumen formation is compromised, cell–cell junctions are disrupted, as revealed by loss of cell–cell-associated β -catenin (right inset), and tissue polarity is inhibited, as indicated by disorganized (α 6) β 4 integrin localization and loss of the endogenous laminin 5 basement membrane. Interestingly, actin stress fibers were not observed in the structures until the stiffness of the matrix reached 5,000 Pa, as has been observed in murine breast tumors *in vivo*. The arrows indicate loss of the endogenous basement membrane and disruption of basal polarity. Reproduced from Refs. [12,14].

In breast cancer, tensional homeostasis is greatly altered. Breast cancers are characterized by increased tumor cell-generated force, increased compression force due to the solid state pressure exerted by the expanding tumor mass, matrix stiffening due to the desmoplastic response, and increased interstitial pressure due to a leaky vasculature, and poor lymphatic drainage. Transformed cells exhibit a vastly different intermediate filament profile. They also show compromised mechano-reciprocity such that they often exert abnormally high force in response to a compliant matrix; as a result, cell–cell junctions are altered, tissue polarity is compromised, and anchorage-independent survival and invasion are promoted. The increased cell-generated forces exhibited by tumor cells enhance their growth, survival, and invasion by promoting focal adhesion maturation and signaling through actomyosin contractility (Fig. 2B). The increased contractility of tumor cells and their associated stromal fibroblasts also induce tension-dependent matrix remodeling to promote the linear reorientation of collagen fibers surrounding the invasive front of the tumor.

The expanding tumor mass exerts compressive stress on the surrounding tissue extracellular matrix, vasculature, lymphatics, and interstitial space. Tumor-associated compression stress can, in turn, induce tumor angiogenesis by directly increasing expression of VEGF-A or by indirectly blocking the existing vasculature surrounding the tumor mass to induce hypoxia and thus VEGF-A expression. Compression also increases the interstitial pressure which may exceed ten times that of normal tissue; this increased pressure induces the accumulation of fluid from leaky blood vessels and impedes lymphatic clearance. Compression force can also shrink the interstitial space

surrounding the ductal structures, thereby increasing the local concentration of growth factors and cytokines that stimulate tumor cell growth. These changes in interstitial pressure can also impede the entry into tumors of chemotherapeutic drugs. In sum, tumor cells are exposed to a myriad of altered mechanical forces that dramatically modify their behavior and these findings directly implicate matrix changes in tumor evolution.

A topic of great recent interest, and one dealt with in greater detail in Dr. Tlsty's presentation, is that of the role of breast density and cancer incidence. Patients with increased breast density, as determined by mammography, have a four- to sixfold higher incidence of breast cancer. Dense breasts are characterized by increased collagen and other extracellular matrix components. Paradoxically, however, cancer incidence increases with age whereas breast density typically declines. However, although the postmenopausal breast has reduced collagen that which remains may have abnormal properties that promote carcinogenesis.

In sum, force is a critically important determinant of tissue development and its study has been much neglected. The ability of cells to sense, respond, and adapt appropriately to force contributes to disease, and particularly to cancer. Pathological changes in cells and in the architecture, topology, and material properties of the matrix microenvironment constitute a positive feedback loop that propels carcinogenesis. However, many questions still need to be resolved. Such questions include how the unique material properties of specific differentiated tissues are established and maintained, how cells coordinate their function and adaptation to external cues in the

microenvironment, and how physical signals might interface with and modulate the activity of biochemical signaling pathways. And, with specific regard to cancer: Does LOX-dependent collagen crosslinking stiffen the tissue and thus drive tumor progression? Would inhibiting LOX-dependent collagen crosslinking temper tissue desmoplasia, reduce mechano-transduction in mammary epithelium, and thereby reduce tumor incidence and delay tumor progression?

EPIGENETIC AND GENETIC EVENTS IN TUMOR PROGRESSION (Thea D. Tlsty)

It is well known that oncogenes and repressor genes play an important role in carcinogenesis and tumor progression. Less attention has been given to epigenetic events that affect these processes, that is, heritable changes in gene expression that occur without a change in DNA sequence. Epigenetic changes can result from methylation of DNA or of histones and from the action of small RNAs (e.g., microRNAs, PIWI RNAs, etc.). The active acquisition of epigenetic changes is a poorly understood but important process in development, differentiation, and also in cancer.

The mechanisms by which epigenetic changes occur are poorly understood. However, in recent years it has become clear that tumor cells live in a stromal microenvironment that is not passive, but rather one that can actively shape and modify tumor cell behavior. In particular, it is well known that tumor progression can be markedly affected by the cells and non-cellular elements of the stromal microenvironment in which they are embedded. Signals sent to tumor cells by the microenvironment can result in cell proliferation and in DNA methylation, centrosome abnormalities, telomeric dysfunction, and altered gene expression [15].

Recent work has dealt with the p16/pRB signaling pathway, a pathway that regulates the cell cycle and that is inactivated in many tumor cells [16]. When this pathway is suppressed, non-cancerous human epithelial cells in culture undergo dynamic epigenetic remodeling that results in the targeted methylation of a selected group of CpG islands. Repression of the p16/pRB pathway in primary human mammary epithelial cells activated an E2F-mediated increase in proteins that remodel chromatin and cause targeted de novo DNA methylation at a non-random collection of loci. Thus, repressing the p16/pRB pathway renders cells epigenetically plastic and results in DNA methylation in a deterministic (predictable) rather than a stochastic (random) pattern. Furthermore, the coordinated set of de novo DNA methylation events are preceded by, and dependent upon, the repression of gene expression. Thus, one can imagine that during cancer progression, tumor cells acquire epigenetic plasticity through repression of the p16/pRB pathway via mutations, deletions, or methylation, which then provide the potential for programming epigenetic events. These data show that p16, a commonly inactivated tumor suppressor gene, regulates DNA methylation and that epigenetic changes occur in preneoplastic cells. In sum, DNA methylation is an active and dynamic process, and chromatin remodeling and repression precede and are necessary for subsequent DNA hypermethylation. Finally, loss of p16 confers epigenetic plasticity, a silencing of genes important in differentiation.

To determine whether these findings were relevant to human cancer, the authors looked for p16-suppressed cells in human breast tissue. Using immunohistochemistry, her group found that normal breast tissue from cancer-free women contained foci of p16-suppressed cells, suggesting the presence of a premalignant program in these otherwise healthy women. This exciting finding directly demonstrates the relevance of p16 suppression to human cancer and offers a new marker of premalignancy [17,18].

Epithelial-to-mesenchymal transition (EMT) is a characteristic feature of epithelial cell tumor progression. EMT has been implicated

in tumor recurrence and is often associated with a poor prognosis in women with breast cancer. There is now evidence demonstrating a link between EMT, basal-like breast cancers, the stem-cell phenotype, and the acquisition of tumorigenic and metastatic potential. EMT is characterized by several molecular changes that include the loss of epithelial markers such as E-cadherin and ZO-1, and the induction of mesenchymal markers such as N-cadherin, fibronectin, vimentin, and Snail. Though alterations in E-cadherin expression can occur through multiple mechanisms, including loss of heterozygosity and mutational inactivation, E-cadherin is frequently silenced through aberrant DNA hypermethylation of its promoter. Interestingly, when E-cadherin is silenced through promoter DNA hypermethylation, mammary cell lines often exhibit a mesenchymal morphology through the coordinated induction of a set of genes involved in EMT. In contrast, when E-cadherin is inactivated by mutation, the cells continue to exhibit an epithelial morphology, and these genes are not induced [19]. This suggests that a program of molecular alterations leading to EMT, invasion, and metastasis can be modulated epigenetically. EMT has been shown to be induced in murine cells by oncogenic ras in cooperation with factors in serum. There is also evidence that exposing cells to serum induces a gene expression pattern that resembles that of a wounding response. This wound-response signature is strongly predictive of future invasive and metastatic behavior, both of which require EMT.

The next step was to determine whether immortalized human mammary epithelial cells with repressed p16INK4A and expressing oncogenic ras (vHMEC-ras) cells could be programmed by the microenvironment to acquire epigenetic changes associated with tumorigenic phenotypes such as EMT. vHMEC-ras cells were exposed to high (10%) and low (0.5%) concentrations of serum. When cultured in serum-rich media, thought to be typical of the tumor microenvironment, human vHMEC-ras cells, like murine cells, underwent phenotypic changes indicative of EMT [20]. This morphological transition was accompanied by increased motility, increased expression of fibronectin and N-cadherin, and reduced expression of E-cadherin. E-cadherin was silenced via de novo promoter DNA methylation. As described for the previous system, transcriptional repression was found to precede DNA hypermethylation. Also, additional genes underwent de novo promoter DNA hypermethylation, including estrogen receptor alpha, Twist, and CST6. Strikingly, these same genes are hypermethylated in human basal-like breast cancers that exhibit mesenchymal phenotypes and are associated with a poor prognosis but not in human luminal A, luminal B, etc. cancers.

In sum, these data indicate that cultured human cells can be programmed by their microenvironment to undergo phenotypic and gene expression changes associated with epigenetic alterations important in human tumor progression. They further indicate that cultured cells can provide valuable tools to elucidate malignant cell properties that are applicable to human cancer patients. A goal for the future is to use this information to create tools that address clinical questions, such as the development of prognostic biomarkers and therapeutic targets.

NOVEL FUNCTIONS OF VEGF AND PDGF SIGNALING CIRCUITS IN TUMOR ANGIOGENESIS AND INVASION (Gabriele Bergers)

Dr. Bergers presented work on two topics. The first dealt with the recruitment of pericyte progenitor cells from bone marrow and their differentiation into more mature pericytes in tumor blood vessels. By way of background, the normal microvasculature is composed of two types of cells, endothelial cells (the cells lining the blood vasculature) and pericytes, cells that surround and tightly envelop endothelial cells. Pericytes are thought to be necessary for the health of endothelial cells

and so of the blood microvasculature [21,22]. Tumors, however, include many blood vessels that lack, or have a reduced coating of pericytes, for example, MVs (see Dvorak presentation and Table I). Further, treating mice bearing the Rip1Tag2 tumor at later stages of growth with imatinib, a tyrosine kinase inhibitor that binds to the PDGF receptor (PDGFR) succeeded in regressing tumor vessels by causing pericytes to detach. These data emphasize the importance of pericytes in maintaining the tumor vasculature. However, the nature and source of tumor vessel pericytes have been little investigated. To address this question, the Bergers lab observed that, as in the developing vasculature, PDGFR β + cells enveloped the blood vessels of Rip1Tag2 tumors and that the PDGF ligands B and D for PDGFR β were expressed by tumor endothelial cells [23]. This suggested that a paracrine communication pathway between pericytes and endothelial cells might be operative in tumors, as in normal vascular development. Mature pericytes are known to express additional markers, namely, NG2, α SMA, and desmin. However, in tumors, not all tumor PDGFR β vessel enveloping cells bore these mature pericyte markers. Flow cytometry and immunohistochemical studies revealed three distinct types of such cells: PDGFR β +NG2- cells, PDGFR β +NG2+ cells, and PDGFR β -NG2+ cells. Thus, in Rip1Tag2 tumors, only a subset of PDGFR β + pericytes expressed mature pericyte markers and a subset of mature pericytes did not express detectable levels of PDGFR β likely reflecting distinct differentiation stages. Indeed, further work demonstrated that PDGFR β NG2- cells represent a population of progenitor pericytes, some of which are recruited from the bone marrow and bear markers (e.g., Sca1, CD45) characteristic of hematopoietic stem cells [23]. When PDGFR β cells were mixed with endothelial cells in three-dimensional cultures, endothelial cells formed tubes with pericytes attaching, particularly at branch points. In addition, these pericytes differentiated, acquiring markers of mature pericytes (NG2, α SMA, and desmin). These studies demonstrated that tumor blood vessel pericytes derive, at least in part from hematopoietic bone marrow progenitors and that progenitor pericytes undergo maturation when apposed to endothelial cells. Part of the maturation effect, but only that leading to α SMA expression, could be replicated by exposing pericyte progenitors to TGF- β .

A second series of studies demonstrated that VEGF is a negative regulator of cell invasion in the case of glioblastoma multiforme (GBM), rapidly growing and highly aggressive grade IV astrocytomas (brain tumors) [24]. GBM are characterized by zones of necrosis and hypoxia and, as a result, typically express high levels of HIF-1 and downstream angiogenic factors such as VEGF, angiopoietin-2, and SDF-1 α [25–27]. They disrupt the blood–brain barrier and are characterized by extensive edema and an influx of inflammatory cells. GBM spread with several distinct dispersion patterns: subpial spread, white matter infiltration, perivascular spread, and ventricular spread.

To investigate the functional significance of hypoxia and angiogenesis in astrocytoma progression, initial studies were performed with transformed astrocytes genetically engineered from murine primary culture astrocytes in which the hypoxia-responsive transcription factor HIF-1 α or its target gene, the angiogenic factor VEGF, was deleted [28]. Genetic deletion of VEGF blocked tumor angiogenesis and increased vascular cell apoptosis, but, paradoxically, increased tumor invasion. When HIF-1 α was knocked out in GBM cells, the new vessels that formed remained slim and regularly shaped, more closely resembling those of the normal brain vasculature. However, HIF-1 α k/o GBM adapted to their inability to grow new blood vessels by co-opting and moving along preexisting blood vessels, a phenomenon described as perivascular spread, and were actually more invasive than wild-type GBM cells [28].

Matrix metalloproteases (MMP), a large family of zinc-dependent endopeptidases, have been implicated in many aspects of tumor growth and progression. Of these, MMP-2 has been particularly implicated in tumor angiogenesis. To investigate the role of MMP-2 in GBM tumor

cell survival and invasion, genetically engineered MMP-2 knockout GBM cells were prepared and their growth properties studied in MMP-2 knockout (k/o) mice [29]. Wild-type GBM cells grew as invasive, highly angiogenic tumors with a leaky, tortuous vasculature and with hypoxic centers. In contrast, GBM-MMP-2k/o cells developed a markedly increased vasculature. Paradoxically, however, the tumor cells grew slower and were more prone to apoptosis and the mice exhibited a longer mean survival time. Apparently the dense and highly branched network of tumor blood vessels induced by these cells were not able to support tumor growth. In support of this hypothesis, tumor vessels exhibited substantially less VEGFR-2, pericytes were greatly reduced, and vessels were poorly perfused. Also, the pattern of tumor cell invasion was different in the absence of MMP-2. MMP-2k/o GBM grew more diffusely by migrating along preexisting blood vessels into the brain parenchyma, a pattern also observed when both HIF-1 and VEGF deficient GBM were implanted in brain (such tumors did not induce proper neovascularization). Apparently, MMP-2 acts as a negative regulator of vascular patterning and angiogenesis in GBM. Investigating the mechanisms for these findings, HIF-1 α expressed by GBM cells was found to induce SDF1 α , and, in this way recruit bone marrow-derived CD45+ myeloid cells containing Tie2+, VEGFR1+, CD11b+, and F4/80+ subpopulations, as well as endothelial and pericyte progenitor cells to promote neovascularization [29]. Further, MMP-9 activity of bone marrow derived CD45+ cells was found to be sufficient and essential to initiate angiogenesis by increasing VEGF bioavailability (releasing it from its bound state to matrix or cells). Conversely, in the absence of HIF-1 α , SDF1 α levels decreased and fewer bone-marrow-derived cells were recruited to tumors, thus decreasing MMP-9 and mobilization of VEGF.

Finally, it was found that VEGF is a direct and negative regulator of tumor cell invasion [29]. VEGF reduced the ability of VEGFR-expressing GBM cells to migrate and invade in vitro and in vivo. When VEGF activity was impaired, tumor cells invaded deep into the brain in the perivascular compartment. Further support for this finding has come from studies in which tumors were subjected to anti-angiogenesis therapies aimed at targeting the VEGF pathway. GBM and Rip1Tag2 tumors treated with tyrosine kinase inhibitors targeting VEGFR-2 showed initial vascular dropout and tumor stasis, only to be followed by a tumor adaptive-evasive response, mediated by other growth factors such as fibroblast growth factor and leading to augmented invasion and, in some cases, dissemination and distant metastasis [30,31]. Obviously these findings in animal models have implications for treating cancer patients with anti-angiogenic drugs, and particularly those targeting the VEGF pathway.

ACKNOWLEDGMENTS

This work was supported by U.S. Public Health Service grants HL-64402 and P01 CA92644, and by a contract from the National Foundation for Cancer Research (to H.F.D.); by PSOC U54CA143836-01 and DOD W81XWH-05-1-0330 from the US Department of Defense (to V.M.W.); and by U.S. National Cancer Institute grants R01 CA113382 and R01 CA109390 (to G.B.).

REFERENCES

1. Dvorak H: Tumor blood vessels. In: Aird W, editor. *Endothelial biomedicine*. Cambridge: Cambridge University Press; 2007; pp 1457–1478.
2. Hurwitz H, Fehrenbacher L, Novotny W, et al.: Bevacizumab plus irinotecan, fluorouracil, and leucovorin for metastatic colorectal cancer. *N Engl J Med* 2004;350:2335–2342.
3. Jain RK: Lessons from multidisciplinary translational trials on anti-angiogenic therapy of cancer. *Nat Rev Cancer* 2008;8: 309–316.

4. Nagy JA, Chang SH, Dvorak AM, et al.: Why are tumour blood vessels abnormal and why is it important to know? *Br J Cancer* 2009;100:865–869.
5. Dvorak HF: Rous–Whipple Award Lecture. How tumors make bad blood vessels and stroma. *Am J Pathol* 2003;162:1747–1757.
6. Paku S, Paweletz N: First steps of tumor-related angiogenesis. *Lab Invest* 1991;65:334–346.
7. Pettersson A, Nagy JA, Brown LF, et al.: Heterogeneity of the angiogenic response induced in different normal adult tissues by vascular permeability factor/vascular endothelial growth factor. *Lab Invest* 2000;80:99–115.
8. Swayne GT, Smaje LH, Bergel DH: Distensibility of single capillaries and venules in the rat and frog mesentery. *Int J Microcirc Clin Exp* 1989;8:25–42.
9. Chang SH, Kanasaki K, Gocheva V, et al.: VEGF-A induces angiogenesis by perturbing the cathepsin–cysteine protease inhibitor balance in venules, causing basement membrane degradation and mother vessel formation. *Cancer Res* 2009;69:4537–4544.
10. Nagy JA, Dvorak AM, Dvorak HF: VEGF-A and the induction of pathological angiogenesis. *Annu Rev Pathol* 2007;2:251–275.
11. Shih SC, Zukauskas A, Li D, et al.: The L6 protein TM4SF1 is critical for endothelial cell function and tumor angiogenesis. *Cancer Res* 2009;69:3272–3277.
12. Butcher DT, Alliston T, Weaver VM: A tense situation: Forcing tumour progression. *Nat Rev Cancer* 2009;9:108–122.
13. Engler AJ, Humbert PO, Wehrle-Haller B, et al.: Multiscale modeling of form and function. *Science* 2009;324:208–212.
14. Paszek MJ, Zahir N, Johnson KR, et al.: Tensional homeostasis and the malignant phenotype. *Cancer Cell* 2005;8:241–254.
15. Tlsty TD, Coussens LM: Tumor stroma and regulation of cancer development. *Annu Rev Pathol* 2006;1:119–150.
16. Reynolds PA, Sigaroudinia M, Zardo G, et al.: Tumor suppressor p16INK4A regulates polycomb-mediated DNA hypermethylation in human mammary epithelial cells. *J Biol Chem* 2006;281:24790–24802.
17. Crawford YG, Gauthier ML, Joubel A, et al.: Histologically normal human mammary epithelia with silenced p16(INK4a) overexpress COX-2, promoting a premalignant program. *Cancer Cell* 2004;5:263–273.
18. Holst CR, Nuovo GJ, Esteller M, et al.: Methylation of p16(INK4a) promoters occurs in vivo in histologically normal human mammary epithelia. *Cancer Res* 2003;63:1596–1601.
19. Lombaerts M, van Wezel T, Philippo K, et al.: E-cadherin transcriptional downregulation by promoter methylation but not mutation is related to epithelial-to-mesenchymal transition in breast cancer cell lines. *Br J Cancer* 2006;94:661–671.
20. Dumont N, Wilson MB, Crawford YG, et al.: Sustained induction of epithelial to mesenchymal transition activates DNA methylation of genes silenced in basal-like breast cancers. *Proc Natl Acad Sci USA* 2008;105:14867–14872.
21. Bergers G, Song S: The role of pericytes in blood-vessel formation and maintenance. *Neuro-Oncology* 2005;7:452–464.
22. Gerhardt H, Betsholtz C: Endothelial–pericyte interactions in angiogenesis. *Cell Tissue Res* 2003;314:15–23.
23. Song S, Ewald AJ, Stallcup W, et al.: PDGFRbeta+ perivascular progenitor cells in tumours regulate pericyte differentiation and vascular survival. *Nat Cell Biol* 2005;7:870–879.
24. Berger M, Wilson C: *The gliomas*. Philadelphia: W.B. Saunders; 1999.
25. Brat DJ, Castellano-Sanchez AA, Hunter SB, et al.: Pseudopalisades in glioblastoma are hypoxic, express extracellular matrix proteases, and are formed by an actively migrating cell population. *Cancer Res* 2004;64:920–927.
26. Du R, Lu KV, Petritsch C, et al.: HIF1alpha induces the recruitment of bone marrow-derived vascular modulatory cells to regulate tumor angiogenesis and invasion. *Cancer Cell* 2008;13:206–220.
27. Holash J, Thurston G, Rudge JS, et al.: Inhibitors of growth factor receptors, signaling pathways and angiogenesis as therapeutic molecular agents. *Cancer Metastasis Rev* 2006;25:243–252.
28. Blouw B, Song H, Tihan T, et al.: The hypoxic response of tumors is dependent on their microenvironment. *Cancer Cell* 2003;4:133–146.
29. Du R, Petritsch C, Lu K, et al.: Matrix metalloproteinase-2 regulates vascular patterning and growth affecting tumor cell survival and invasion in GBM. *Neuro-Oncology* 2008;10:254–264.
30. Casanovas O, Hicklin DJ, Bergers G, et al.: Drug resistance by evasion of antiangiogenic targeting of VEGF signaling in late-stage pancreatic islet tumors. *Cancer Cell* 2005;8:299–309.
31. Paez-Ribes M, Allen E, Hudock J, et al.: Antiangiogenic therapy elicits malignant progression of tumors to increased local invasion and distant metastasis. *Cancer Cell* 2009;15:220–231.
32. Nagy JA, Dvorak AM, Dvorak HF: VEGF-A and the induction of pathological angiogenesis. *Annu Rev Pathol Mech Dis* 2007;2:251–275.

DOD ABSTRACTS

AACR April 17th-21st 2010

Collagen remodeling and tissue mechanics at different mammary tumor development stages

Hongmei Yu¹ and Valerie M. Weaver^{1,2}

¹Department of Surgery and Center for Bioengineering and Tissue Regeneration, University of California at San Francisco, ²Departments of Anatomy and Bioengineering and Therapeutic Sciences, Eli and Edythe Broad Center of Regeneration Medicine and Stem Cell Research and Helen Diller Family Comprehensive Cancer Center, University of California, San Francisco, San Francisco, CA 94143.

Cross-linking of type I collagen is important in leading to tissue stiffening and collagen metabolism in breast cancer. We've shown breast cancer progression is strongly correlated with increased tissue stiffness and collagen remodeling; this ECM stiffness regulates cell proliferation, survival and polarity via integrin mediated focal adhesion maturation and cell-generated force in 3D culture models and in MMTV-Her2/Neu tumor malignant transformation. We now ask if matrix remodeling affects tumor formation, tumor stromal cell activation at specific stages of the highly-penetrant MMTV-PyMT mouse model. PyMT activates Ras, Src and PI3K signaling pathways at different tumor stages, which allows us to ask and test if matrix mechanics have specific roles at different tumor stages. To test our hypothesis, we inhibited Lysyl oxidase mediated collagen I cross-linking (beta-aminopropion, BAPN) in MMTV-PyMT mice at different ages, followed the tumor growth and tissue stiffness (mammary gland and lung) for 2, 4, 6, 8 weeks. We obtained high resolution quantification of tumor stiffness in vivo (~mm lesion) with a novel tissue diagnostic probe; and performed various imaging and biochemical analysis to assess collagen cross-linking, signaling pathways and cell types involved in tumor development. Our results showed that tissue stiffness starts increasing at hyperplastic stage and continues increasing as tumor progresses; BAPN treatment delays tissue stiffening, stromal cell activation and tumor progression and lung metastasis. We also found that primary tumors are affected when collagen cross-linking is inhibited at very early stage of tumorigenesis; and tumor metastasis is affected when collagen cross-linking is inhibited at late stages. These results suggest that collagen cross-linking and matrix stiffening may alter the recruitment and activation of different stromal cells required for tumor formation and tumor metastasis. Based on our previous results that tissue stiffness induced mechano-sensing and cross-talked with ErbB2 signaling pathway at PI3K level in MMTV-Her2/Neu model, we will test if signal pathways activated by PyMT are specifically collaborated with collagen modification and involved in tumor formation in PyMT models. These studies together will show that collagen cross-linking and tissue stiffness modulate multiple stages of cancer progression, and help us understand how mechano-sensing and mechano-transduction play roles in breast cancer progression.

BMES Oct 6th-9th 2010

Force Characterization of Tissue from Normal, Pre-invasive and Invasive Breast Cancer

Jose Lopez¹, Christopher DuFort¹, Hongmei Yu¹, Inkyung Kang¹, Irene Acerbi^{1,2}, Shelley Hwang³, Alfred Au³, and Valerie Weaver^{1,3,4,5}

¹Department of Surgery and Center for Bioengineering and Tissue Regeneration, University of California at San Francisco ²Unitat de Biofisica i Bioenginyeria, Universitat de Barcelona, Spain
³Institute for Regeneration Medicine, University of California San Francisco, ⁴Department of Bioengineering and Therapeutic Sciences, University of California at San Francisco,
⁵Department of Anatomy, University of California at San Francisco

Historically, cancer research has focused on understanding the genetic and biochemical regulation of tumor progression while the biomechanical influences have only recently been studied. Clear evidence has emerged indicating that mechanical forces are closely associated with tumor progression. In fact, biomechanical cues are integrated with biochemical and genetic cues at every step. To elucidate the role of biomechanical cues we have been studying the relationship between collagen remodeling and lysyloxidase (LOX)-dependent collagen cross-linking in breast tumor progression. We have shown that breast transformation is accompanied by elevated levels LOX, collagen I deposition, and significant collagen cross-linking as well as a pronounced stiffening of the breast and its surrounding extracellular matrix. Consistent with an increase in mechano-signaling, breast stromal cells and the mammary epithelium showed elevated levels of focal adhesions and enhanced integrin signaling. Subsequent studies demonstrated that increasing collagen cross-linking stiffened the extracellular matrix and disrupted mammary morphogenesis and promoted the invasion of a premalignant transformed mammary epithelium in culture and induced invasive breast cancer in vivo. To investigate how micro-environment stiffness may affect progression in human breast tumors, atomic force microscopy (AFM) was used to probe the mechanical properties of tissue from patients diagnosed with various stages of breast cancer. Using this technique we were able to assess the elastic modulus of the tissue focusing on the border between the tumor epithelium and the surrounding stroma. Preliminary data indicates that the extracellular matrix surrounding tumors have varying stiffness. These stiffer areas may be predictive of tumor type and invasiveness. Coupling these results with immunohistochemistry we will determine the nature of these mechanically distinct regions by drawing a correlation between stiffness and collagen cross-linking with localization of LOX. We will also determine how the tumor epithelium responds to mechanical cues by examining integrin activation and stress fiber formation.

***In Situ* Force Mapping of Breast Tissue Transformation.**

Jose I. Lopez¹, Inkyung Kang^{1,2}, Weon-Kyoo You³, Donald MacDonald³ and Valerie Weaver^{1,4,5}

¹Department of Surgery and Center for Bioengineering and Tissue Regeneration, University of California at San Francisco, San Francisco, CA 94143, ² Benaroya Research Institute at Virginia

Mason, Seattle, WA 98101, ³Department of Anatomy, University of California at San Francisco, San Francisco, CA 94143, ⁴Departments of Anatomy and Bioengineering and Therapeutic Sciences, Eli and Edythe Broad Center of Regeneration Medicine and Stem Cell Research and Helen Diller Family Comprehensive Cancer Center, University of California, San Francisco, San Francisco, CA 94143.

Understanding the role that mechanical force plays in regulating the transition of mammary tumor epithelium to malignancy *in vivo* is necessary in light of the expanding range of cellular processes that mechanical cues regulate *in vitro*. Here we explore the contribution of a variety of distinct tissue elements, including the tumor epithelium, vasculature and the extracellular matrix (ECM), to overall tissue stiffness as the mammary gland transforms from normal to malignant. We utilize atomic force microscopy (AFM) in conjunction with transgenic CFP fluorescent labeling, contrasting fluorescent labeling of the vasculature and a modified novel AFM *in situ* approach to explore the nature of the tumor biomechanical landscape in the relevant MMTV-PyMT transgenic mouse model of breast cancer. We find that the breast epithelium, the adjacent ECM and the tumor-associated vasculature all contribute to the increase in tissue rigidity observed during malignant progression. Importantly, by combining AFM mechanical characterization with traditional pathological examination, we note that ECM stiffening, mediated by an increase in collagen fiber deposition and altered fiber diameter, was the most consistent and sensitive biomechanical gauge and correlated best with tumor progression to malignancy. Furthermore, ECM stiffness and the associated collagen topology correlate well with tumor invasive fronts.

The Interplay Between Three Dimensional Microenvironment and Breast Cancer Invasion

L. Cassereau¹, J. I. Lopez², V. M. Weaver^{2, 3, 4}

¹ Bioengineering, University of California at Berkeley, Berkeley, CA, United States. ²Surgery and Center for Bioengineering and Tissue Regeneration, University of California at San Francisco, San Francisco, CA, United States. ³Institute for Regeneration Medicine, University of California at San Francisco, San Francisco, CA, United States. ⁴Bioengineering and Therapeutic Sciences, University of California at San Francisco, San Francisco, CA, United States.

Metastatic progression of breast cancer depends on tumor cells invading into the surrounding extracellular matrix (ECM), migrating to nearby blood vessels and lymphatics and then metastasizing and colonizing distant tissues. While much is known about the biochemical basis of tumor invasion, little is known about the role of biophysical cues to this process. Accordingly, we have begun an intensive study of how biomechanical and biochemical signals synergize to regulate tumor cell invasion with the ultimate goal of assisting with tumor prognosis and therapies aimed at curing this disease. In this respect, we have developed new approaches to explore the interplay between ECM topology and stiffness on breast tumor cell phenotype, motility and invasive behavior in tunable 3D scaffolds. We have been using chemically-modified silks in which fibril diameter, ligand composition, ECM concentration, topology and tension can

be accurately tuned and defined while still amenable to cell remodeling. We use fluorescently-tagged transgenic breast epithelial cells, topologically and tension-defined discontinuous 3D ECMs and spinning disc confocal microscopy imaging to monitor the interplay between a pre-malignant mammary tissue structure and a continuously evolving anisotropic ECM. We are using these discontinuous topologically and tension-defined ECMs and real time imaging of breast tumor invasion to assess the role of ECM remodeling on breast cancer metastasis in transgenic animals and clinical specimens.

ASCB Dec 11th-15th 2010

Cancer in Human Mammary Gland Shows Greatest Stiffness on Tumor Edge

Irene Acerbi^{1,2}, Alfred Au³, Jose Lopez^{1,2}, Chris DuFort^{1,2}, Shelley Hwang¹, Valerie M. Weaver^{1,2,4}

¹Department of Surgery, University of California, San Francisco, San Francisco, CA 94143.

²Center for Bioengineering and Tissue Regeneration, University of California, San Francisco, San Francisco, CA 94143. ³UCSF Carol Buck Breast Cancer Center, San Francisco.

⁴Departments of Anatomy and Bioengineering and Therapeutic Sciences, Eli and Edythe Broad Center of Regeneration Medicine and Stem Cell Research and Helen Diller Family Comprehensive Cancer Center, University of California San Francisco, San Francisco, CA 94143

Tumors are characteristically stiffer than normal tissue and changes to the extra cellular matrix (ECM) contribute to this phenotype. Previously, we investigated the relationship between collagen remodeling induced by lysyl oxidase (LOX), a collagen cross-linking protein, and breast tumor progression in mice (Levental, *et al.*, *Cell* 2009). These studies demonstrated that increased collagen cross-linking stiffened the ECM, disrupted mammary morphogenesis, promoted the invasion of a premalignant transformed epithelium in culture and induced invasive breast cancer *in vivo*. In the current study we determined whether malignant progression of human breast cancer is associated with collagen cross-linking and tissue stiffening and if so whether this could contribute to tumor progression. Towards this goal, a cohort of patients samples have been assembled that represent normal, benign, early non-invasive lesions and invasive breast tumors. Each sample has been stained using H&E to identify the tumor margins and atomic force microscopy (AFM) is being used to measure force maps adjacent to and surrounding the invasive tumor edge. Preliminary results indicate that tumor edges are stiffer (approximately 0.5-2 KPa) than the surrounding tissue. Moreover, data suggest that tumors exhibit 2-4 fold higher rigidity in the region adjacent to and that projects into the stroma. To explore the physiological basis for these findings we have been conducting immunohistochemical analysis of extracellular matrix deposition and modification. Studies suggest malignant transformation is accompanied by elevated deposition and linearization of collagen and increased expression of LOX. These results demonstrate the feasibility of obtaining high resolution AFM maps of human breast cancer tissue and implicate ECM

remodeling and stiffening in tumor progression. Because we noted significant orientation of collagen fibers and orientated stiffness regions our findings imply ECM stiffness could foster tumor progression by promoting the directed invasion of tumor cells into the stroma in a process termed durotaxis.

$\alpha 5\beta 1$ Integrin-Fibronectin interactions mediate force response of cells to the microenvironment

J. I. Lopez¹, Y. Miroshnikova^{2,1}, L. Cassereau^{2,1}, J. Lakins¹, V. Weaver^{1,2,3}

¹Surgery, UCSF, San Francisco, CA, United States. ²Bioengineering, UCSF, San Francisco, CA, United States. ³Anatomy, UCSF, San Francisco, CA, United States.

The importance of biomechanics in breast cancer progression is slowly becoming appreciated. Nevertheless, the molecular mechanisms whereby mechanical cues modulate cellular mechano-signaling to promote tumor progression remain ill-defined. We identified fibronectin (FN)-ligated $\alpha 5\beta 1$ integrin as a specific regulator of cellular mechano-responsiveness and tumor progression. We observed a specific increase in the expression and activity of $\alpha 5$ integrin in mammary epithelial cells (MECs) in response to oncogenic transformation. Gain of function and loss of function organotypic culture assays showed that $\alpha 5\beta 1$ integrin-fibronectin and not $\alpha 2\beta 1$ integrin-collagen interactions significantly enhance cell growth and survival, disrupt tissue polarity, perturb cell-cell adhesions and compromise basement membrane integrity. Xenograft manipulations and co culture assays demonstrated that fibronectin-ligated $\alpha 5\beta 1$ integrin promotes tumorigenesis and enhances angiogenesis. Upon further investigation we noted that fibronectin-ligation of $\alpha 5\beta 1$ integrin significantly increases breast cell migration and invasion and that this effect is potentiated when extracellular matrix (ECM) tension is higher. Indeed, fibronectin-ligated $\alpha 5\beta 1$ showed greatly enhanced gel contractility and stronger traction forces than collagen-ligated $\alpha 2\beta 1$ integrin. Experiments using polyacrylamide gels with tuned gradients of ECM stiffness revealed that fibronectin-ligated $\alpha 5\beta 1$ integrin fosters faster and more persistent cell migration than collagen-ligated $\alpha 2\beta 1$ integrin. Collectively, these observations suggest $\alpha 5\beta 1$ integrin-fibronectin interactions play a key role in breast tumor progression through their ability to sense and transduce mechanical cues. The findings also illustrate the dynamic interplay between oncogenic transformation and biochemical and biophysical aspects of the tissue microenvironment in tumorigenesis.

Deconstructing the 3rd Dimension: How matrix dimensionality promotes survival

C. Frantz¹, J. Friedland², J. Lakins¹, J.I. Lopez¹, J. Chernoff³, M. Schwartz⁴, L. C. Santy⁵, J. Alcaraz⁶, C. Chen², D. Boettiger², V.M. Weaver^{1,2}

¹ Department of Surgery and Center for Bioengineering and Tissue Regeneration, University of California, San Francisco, CA; ² Department of Bioengineering and Institute for Medicine and Engineering, University of Pennsylvania, Philadelphia, PA; ³ Fox Chase Cancer Center, Philadelphia, PA; ⁴ Department of Biochemistry, University of Virginia, Charlottesville, VA; ⁵

Department of Biochemistry and Molecular Biology, Penn State University, PA; ⁶ Facultat de Medicina, Universitat de Barcelona, Spain.

Survival of single non-spread cells in a three dimensional (3D) environment is crucial in the formation of embryonic bodies, during differentiation and dissemination of isolated tumor cells. However, information about the molecular mechanisms regulating cell survival have largely been deduced by studying the behavior of spread cells on two dimensional (2D) matrices. To clarify how non-spread cells might survive within a 3D microenvironment, we assessed the effect of cell shape and matrix spreading and integrin-dependent adhesion on the survival of isolated mammary epithelial cells (MECs) in 2D versus 3D. We showed that MEC viability is sustained by laminin ligation of $\alpha 6 \beta 4$ integrin and Rac-dependent Pak activity in round, non-spread MECs in 3D independent of ligand concentration, but not in 2D. Conversely, we determined that laminin-dependent growth and survival of MECs depends upon $\alpha 1$ integrin ligation and ERK and PI3Kinase activity in spread MECs in 2D, but not in 3D. Such differential survival mechanisms could be attributed to enhanced GTP loading of Rac and Arf6 and reduced Rac-dependent ROS and MMP activation in 3D. Experiments revealed that elevated Arf6 GTPase activity promotes MEC survival by enhancing Rac-Pak signaling and reducing Rac-NADPH-ROS production. Studies are in progress to determine GEFs and GAPs involved in Arf6 activation and to test whether matrix presentation could modulate Arf6-dependent cell fate by influencing membrane curvature, protein trafficking or actin remodeling.

The Interplay Between Three Dimensional Microenvironment and Breast Cancer Invasion

L. Cassereau¹, J. I. Lopez², V. M. Weaver^{2, 3, 4}

¹ Bioengineering, University of California at Berkeley, Berkeley, CA, United States. ² Surgery and Center for Bioengineering and Tissue Regeneration, University of California at San Francisco, San Francisco, CA, United States. ³ Institute for Regeneration Medicine, University of California at San Francisco, San Francisco, CA, United States. ⁴ Bioengineering and Therapeutic Sciences, University of California at San Francisco, San Francisco, CA, United States.

Metastatic progression of breast cancer depends on tumor cells invading into the surrounding extracellular matrix (ECM), migrating to nearby blood vessels and lymphatics and then metastasizing and colonizing distant tissues. While much is known about the biochemical basis of tumor invasion, little is known about the role of biophysical cues to this process. Accordingly, we have begun an intensive study of how biomechanical and biochemical signals synergize to regulate tumor cell invasion with the ultimate goal of assisting with tumor prognosis and therapies aimed at curing this disease. In this respect, we have developed new approaches to explore the interplay between ECM topology and stiffness on breast tumor cell phenotype, motility and invasive behavior in tunable 3D scaffolds. We have been using chemically-modified silks in which fibril diameter, ligand composition, ECM concentration, topology and tension can be accurately tuned and defined while still amenable to cell remodeling. We use fluorescently-tagged transgenic breast epithelial cells, topologically and tension-defined discontinuous 3D ECMs and spinning disc confocal microscopy imaging to monitor the interplay between a pre-

malignant mammary tissue structure and a continuously evolving anisotropic ECM. We are using these discontinuous topologically and tension-defined ECMs and real time imaging of breast tumor invasion to assess the role of ECM remodeling on breast cancer metastasis in transgenic animals and clinical specimens.

Engineering strategies to recapitulate epithelial morphogenesis in synthetic 3 dimensional matrix with tunable mechanical properties.

Miroshnikova, Y.A.^{1,2}, Jorgens, D.M.³, Auer, M.³, Spirio, L.⁴, Sieminski, A.L.¹, Weaver V.M.².

¹ Olin College Of Engineering, Needham, MA, ² University of California, San Francisco, San Francisco, CA, ³ University of California, Berkeley, Berkeley, CA, ⁴ PuraMatrix/ 3DM Inc., Cambridge, MA

The mechanical properties (i.e. stiffness) of the extracellular matrix (EC) influence cell fate and tissue morphogenesis and contribute to disease progression. Nevertheless, our understanding of the mechanisms by which ECM rigidity modulates cell behavior and fate remains rudimentary. While a number of two and three dimensional (2D and 3D) systems have been used to explore the effects of mechanical properties of the ECM on cell behaviors, these systems are typically limited by a lack of independent control of stiffness, fiber architecture, and adhesivity. Towards addressing this goal, biologically compatible systems are needed in which ECM stiffness can be modulated independently. Here we describe the use of ECM-adsorbed synthetic self-assembling peptide gels (SAPs; Puramatrix) to recapitulate normal epithelial acini morphogenesis and gene expression in a 3D context. Due to the viscoelastic range of these SAP gels and their ability to recreate native ECM fibril topology we were able to reconstitute a tumor-like behavior and gene expression phenotype in mammary epithelial cells while simultaneously maintaining constant ligand density and pore size. Accordingly, this SAP system presents the first tunable system capable of rigorously and independently assessing the interplay between ECM stiffness and cellular behavior in a 3D context.